ChemPubSoc Europe

DOI: 10.1002/slct.201803342

Chemistry SELECT Full Papers

Medicinal Chemistry & Drug Discovery

2-Aminobenzamide-Based Factor Xa Inhibitors with Novel Mono- and Bi-Aryls as S4 Binding Elements

Nirav R. Patel,[a] Dushyant V. Patel,[a] Ashish M. Kanhed,[a, c] Sagar P. Patel,[a] Kirti V. Patel,[a] Daniel K. Afosah,[b] Umesh R. Desai,[b] Rajshekhar Karpoormath,[c] and Mange Ram Yadav*[a]

Factor Xa, a key serine protease in the coagulation cascade, has attracted a great deal of attention as a target for developing new antithrombotic agents. A series of novel alkyl, benzyl, biphenyl and substituted piperazine derivatives as S4 binding elements have been synthesized as potential human factor Xa (FXa) inhibitors with 2-amino-5-chloropyridine as the S1 binding moiety. All the synthesized compounds were tested *in vitro* for FXa inhibitory activity by chromogenic substrate hydrolysis assay. The active compounds were selected to assess their *ex vivo* prothrombin time prolonging activity. Keeping in mind the promising *in vitro* and *ex vivo* profile of *N*-(5-chloropyridin-2-yl)-2-(4-(2-cyanophenyl)benzylamino)benzamide (**16f**), it was selected for further *in vivo* evaluation of its antithrombotic potential. Structure-activity relationship and molecular interaction analysis by the docking and dynamics studies within the series are discussed.

Introduction

Thrombosis is a leading contributor to global diseases like ischemic heart diseases, stroke and venous thromboembolism (VTE).[1] As per the impact report published by the International Society on Thrombosis and Hemostasis (ISTH), 1 in 4 deaths worldwide is due to thrombosis, and up to 60% of VTE are reported during hospitalization.[2] Due to several side effects and limitations of currently available antithrombotic drugs, extensive research efforts are required to develop an ideal orally active antithrombotic drug with a better safety profile. An ideal antithrombotic agent should suppress thrombosis without affecting normal hemostasis and should have good oral bioavailability, minimum bleeding risks and possesses specificity towards direct inhibition of an activated coagulation factor.[3]

To prevent or reduce clotting, currently there is a focus on certain vital enzymes which modulate the coagulation process. Over the last decade, two serine proteases, factor Xa (FXa) and factor IIa (FIIa or thrombin) attracted the attention of medicinal chemists. Out of these two, thrombin is responsible for fibrin formation and it also plays vital roles in several other physiological processes like platelet activation, platelet aggregation and development of new blood vessels. Compared to thrombin, inhibition of FXa is more specific and involves lower bleeding risks as it does not affect the existing levels of thrombin.[4] Several preclinical studies suggested that FXa could be a better target for anticoagulation therapy as compared to thrombin.[4b,5] One molecule of FXa is responsible for the generation of more than 1000 thrombin molecules.[6] Due to its upstream position in amplification cascade, inhibiting FXa could prove to be a better strategy than direct inhibition of thrombin. The latest results indicated that the use of indirect FXa inhibitors and recently approved direct FXa inhibitors had been associated with lower bleeding risks.[7] Thus, FXa is considered to be an attractive target for the development of antithrombotic drugs.

Currently U.S. Food and Drug Administration (FDA) has approved four orally active, selective FXa inhibitors, Rivaroxaban[8] (**1**), Apixaban[9] (**2**), Edoxaban[10] (**3**) and Betrixaban[11] (**4**) (Figure 1). These novel FXa inhibitors displayed higher specificity, better oral bioavailability and lesser food and drug interactions compared to the conventional anticoagulant agents.[12,13] However, they still have many drawbacks like drug-drug interactions,[13,14] narrow clinical indications[13,15,16] and lack of specific antidote for preventing bleeding.[17] These inhibitors are not recommended to the patients suffering from acute hepatic and renal impairment,[18,19] and patients with artificial heart valves.[20] So, there is a need to further develop novel and safer FXa inhibitors to advance their clinical use.

A large number of FXa inhibitors containing various scaffolds such as anthranilamide,[21] diamidobenzene, diaminocycloalkane, aminopiperidine,[22] pyrrolidine,[23] pyrazole,[24] oxazolidinone,[25] isoxazole,[26] piperazine, indole,[27] indazole,[28] dihydropyrazolopyridinone,[29] tetrahydroisoquinoline,[30] coumarin,[31] arylsulfonamidopiperidone[32] and amino acids (eg. glycine, proline)[33] have been reported by various research groups. Among these, anthranilamide and *cis*-diamine based

[a] *N. R. Patel, D. V. Patel, Dr. A. M. Kanhed, S. P. Patel, Dr. K. V. Patel, Prof. M. R. Yadav*
Faculty of Pharmacy, Kalabhavan Campus, The Maharaja Sayajirao University of Baroda, Vadodara-390001, Gujarat, India
E-mail: mryadav11@yahoo.co.in
[b] *D. K. Afosah, Dr. U. R. Desai*
Department of Medicinal Chemistry and Institute for Structrural Biology and Drug Discovery, Virginia Commonwealth University, Richmond, Virginia 23219, United States
[c] *Dr. A. M. Kanhed, Dr. R. Karpoormath*
Department of Pharmaceutical Chemistry, Discipline of Pharmaceutical Sciences, College of Health Sciences, University of KwaZulu-Natal (Westville), Durban 4000, South Africa.

Supporting information for this article is available on the WWW under https://doi.org/10.1002/slct.201803342

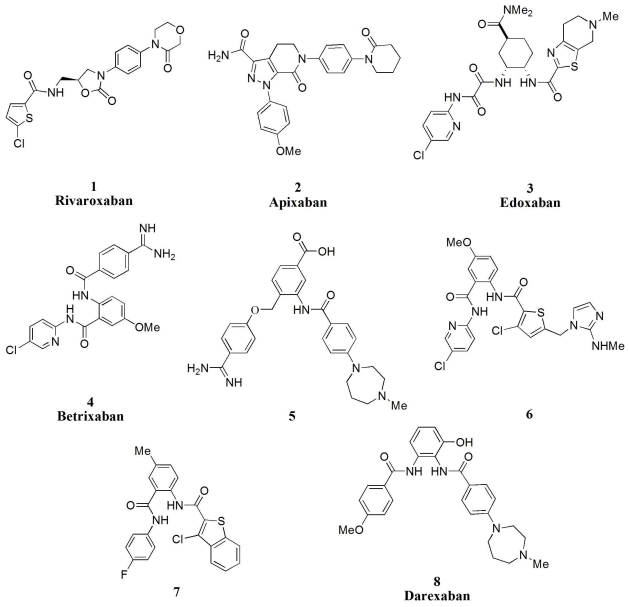

Figure 1. Some well-known FXa inhibitors.

FXa inhibitors have been explored extensively for developing orally active antithrombotic drugs. These vicinal diamide-based FXa inhibitors with U or V shape of the molecule demonstrated good binding to FXa. The benzamidine derivative **5** (Figure 1) with 1,2-disubstituted benzene scaffold and thiophene/benzothiophene substituted anthranilamides **6** and **7** (Figure 1) have been reported to inhibit human FXa with potent oral anticoagulant activity.[34,35] Darexaban, a 1,4-diazepanylbenzamide **8** (Figure 1) has been reported to be a potent orally active FXa inhibitor.[36] Favourable pharmacokinetic profile and metabolic stability with high potency promoted darexaban as a clinical candidate.

Inspired by the favourable biological profile of anthranilamide based FXa inhibitors, we selected betrixaban **4** as a lead molecule for further chemical modifications. It was planned to use anthranilamide as the central scaffold to connect it to the two different hydrophobic arms (S1 binding ligand and S4 binding ligand). The neutral haloaromatics, particularly the chlorinated ones have proven their worth as successful S1 binding ligands as they bind effectively to Tyr228 of S1 pocket by Cl-π interaction, improving selectivity and oral bioavailability.[37] The highly basic amidine group, initially used as successful S1 and S4 binding ligand, has been reported to be the culprit for poor oral bioavailabilty.[38]

To develop orally active antithrombotic agents, it was contemplated to introduce alkyls, benzyls, biphenyls or substituted piperazines as S4 binding ligands in the anthranilamide scaffold as the replacements of highly basic amidine group of betrixaban **4** and maintain the 5-chloro-2-pyridyl group as such, as the S1 binding ligand as represented in Figure 2.

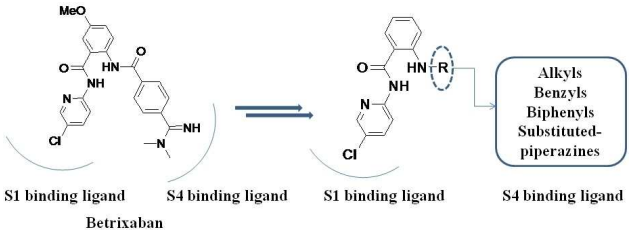

Figure 2. Anthranilamide derivatives possessing novel S4 binding ligands.

Results and discussion

Chemistry

The reported anthranilamide derivatives were synthesized by adopting Schemes **1**and **2**. The compounds **13a-13m** were prepared from commercially available isatoic anhydride in two steps. In the first step, isatoic anhydride **9** was reacted with alkyl/arylalkyl halides in presence of some organic base to obtain *N*-substituted isatoic anhydrides **10a-10l**.[39] The *N*-substituted isatoic anhydrides **10a-10l** were subjected to ring opening by reacting with 2-amino-5-chloropyridine to afford the desired substituted 2-amino-*N*-(5-chloropyridin-2-yl)benzamides **13a-13l**.

The synthetic routes for the preparation of compounds **15a-15f** and **16a-16i** are also illustrated in **Scheme I**. Commercially available 2-nitrobenzoic acid **11** was used as the starting material to obtain the targeted 2-aminobenzamide **13m**. Controlled condensation of 2-nitrobenzoic acid **11** with 2-amino-5-chloropyridine gave intermediate **12** which was reduced with $SnCl_2$ to get the aniline derivative **13m**. The 4-bromomethyl-1,1′-biphenyls **18a-18i**, prepared from **17a-17i** as per **Scheme II**, were used to obtain compounds **16a-16i**. Suzuki reaction was used to get biphenyls **17a-17i** from aryl halides and phenylboronic acids.[40] The key intermediate **13m** was reacted with chloroacetyl chloride to offer the intermediate **14**. The chloro group of the intermediate **14** was displaced by different substituted piperazines to get the desired piperazinyl compounds **15a-15f**.

Molecular modeling studies

To have a view of the molecular interactions of the synthesized compounds with the enzyme, docking studies were performed with FXa. All the synthesized compounds were docked in the active site of FXa. Docking of betrixaban **4** was also done as a standard. The docking scores are given in the supporting information. Compound **16f** offered the highest docking score which indicated its high binding interactions with the enzyme. The intermolecular interactions of the highest binding compound **16f** and betrixaban **4** as a standard drug are shown in Figure 3.

In betrixaban **4**, the pyridine ring occupied the S1 pocket, indicating a good lipophilic interaction. In addition to this, chloro group of pyridine and π-system of Tyr228 of S1 pocket exhibited a non-covalent lipophilic interaction. Interestingly,

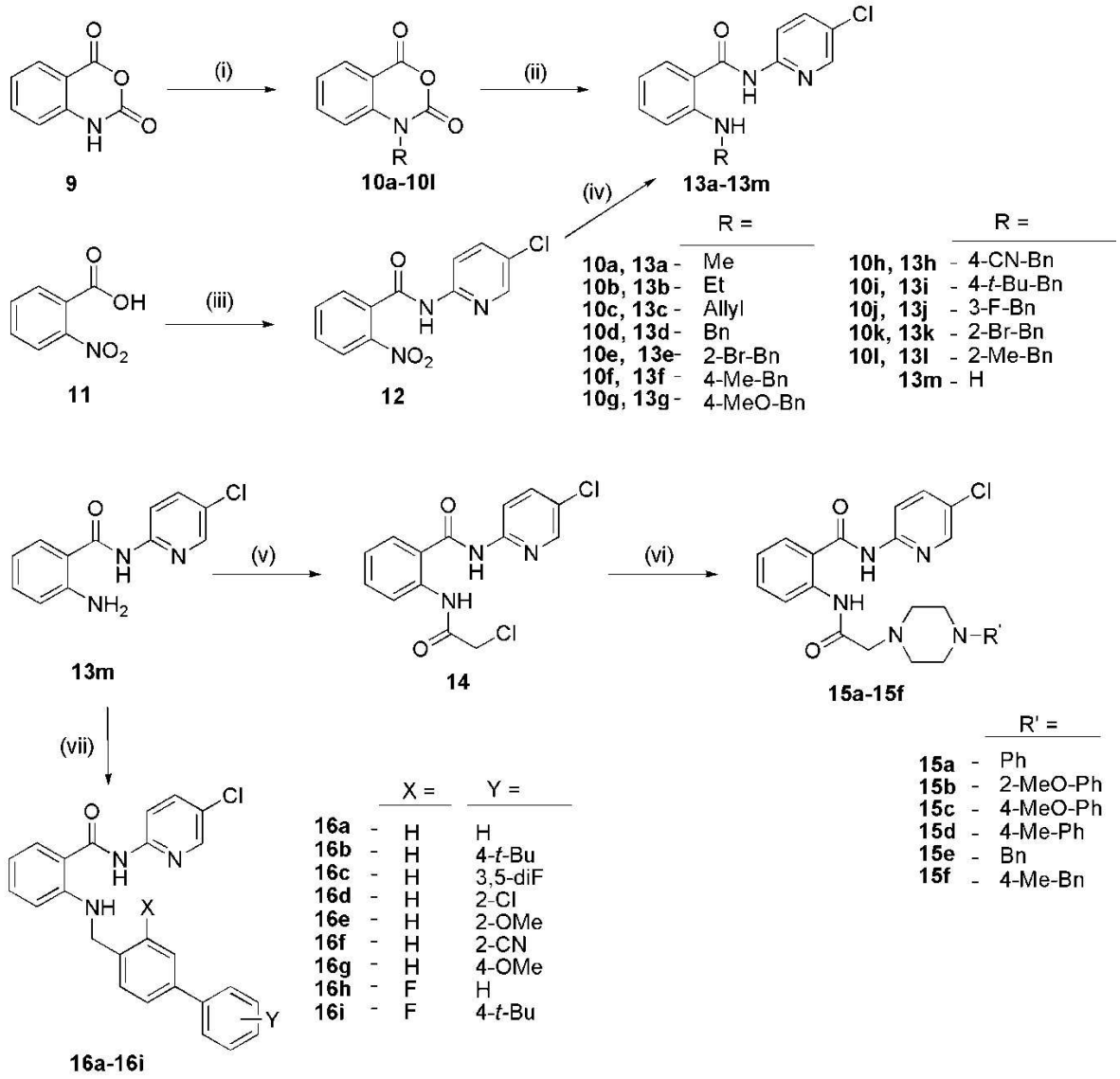

Scheme 1. Synthetic route for the preparation of compounds **15a-15f** and **16a-16i**. Reagents and conditions: (i) Alkyl/arylalkyl halide, DIPEA, DMA, rt; (ii) 2-Amino-5-chloropyridine, pot. *tert*-butoxide, THF, rt (Method A); (iii) 2-Amino-5-chloropyridine, $POCl_3$, dry pyridine, 0–5 °C, 3 hrs (iv) $SnCl_2.2H_2O$, EtOAc, reflux (for **13m**); (v) Chloroacetyl chloride, K_2CO_3, dry DCM, 0–5 °C; (vi) Substituted piperazines, DMF, 120 °C, 4–6 hrs (Method B);; (vii) K_2CO_3, DMF, **18a-18i**, 120 °C, 4–6 hrs (Method C).

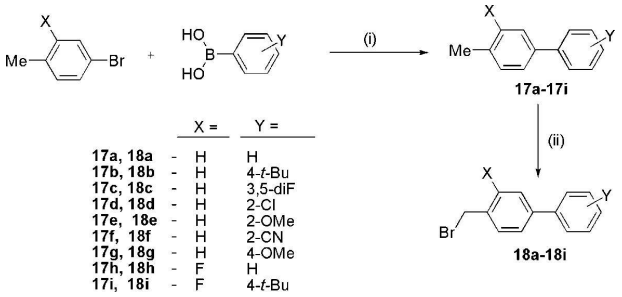

Scheme 2. Synthetic route for the preparation of compounds **18a-18i**. Reagents and conditions: (i) K_2CO_3, $Pd(OAc)_2$, PEG 400, H_2O, 50 °C, 30 mins (ii) *N*-Bromosuccinimide, AIBN, CCl_4, reflux, 20 h.

compound **16f** also demonstrated similar interactions and the chloro group of pyridine in compound **16f** was observed to be stabilized at 3.82 Å from the centroid of Tyr228 aromatic ring which indicated high stability between the ligand-enzyme complex. In case of betrixaban, –C=O of Gly219 (2.1 Å) and disulfide linkage of Cys191 and Cys220 (2.4 Å) displayed good hydrogen bonding interactions with the pyridine amide–NH to form a stable complex. Whereas in case of compound **16f**, the –C=O and -NH of the amide interacted with -NH of Gln192 (2.12 Å) and –C=O of Gly219 (1.92 Å), respectively by hydrogen bonding to form a stable complex. The aromatic ring of 2-aminobenzamide exhibited strong π-cation interactions with the Arg222. Generally the π-cation interaction is considered stronger than hydrogen bond or any other physical interac-

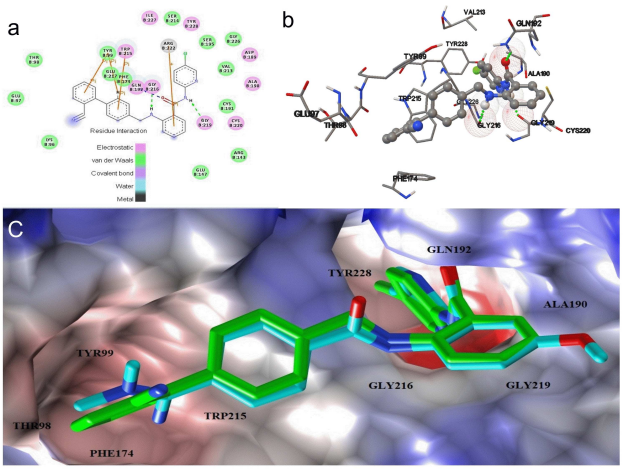

Figure 3. (a) 2D representation of interactions between compound **16f** and the active site of FXa enzyme. (b) Docking pose of compound **16f** within the active site of FXa. (c) Overlay of the 3D structures of compound **16f** and betrixaban **4** within the active site of FXa (PDB code: 4 A7I[41]). Color code: betrixaban = Cyan, **16f** = Green.

tions, and this has been observed here to impart ligand receptor stability. Further, the *ortho* substituted biphenyl group in compound **16f** exhibited excellent π-π interaction with Tyr99, Phe174 and Trp215 triad in the S4 pocket. From the obtained results we clearly get an idea that occupying S1 and S4 sites by specific lipophilic functionalities is of utmost importance for enhanced binding affinity of the ligands within the enzyme active site.

To check selectivity, we also performed docking of the most active compound **16f** with the Thrombin, FIXa and FXIa. For this purpose the protein structures were obtained from RCSB database (PDB code: 1SL3, 3CL5, 5QCK respectively). The docking scores suggest the selectivity of **16f** towards FXa over Thrombin, FIXa and FXIa.

Table 1. Docking score and IC_{50} values of Compound **16f**

Enzyme	Glide XP docking score	IC_{50} value (μM)[a]
FXa	-10.43	0.7 ± 0.2
Thrombin	-7.88	> 100
FIXa	-6.98	ND
FXIa	-8.07	ND

[a]Inhibitory activity against human FXa and FIIa. IC_{50} values shown are the mean of duplicate measurements. ND = Not Determined

Molecular dynamics simulations

In the molecular docking studies, compound **16f** exhibited highly favourable interactions within the active site of FXa. Thus, to confirm and validate the stability of the proposed complex of the active compound **16f** and FXa, molecular dynamics was performed. The dynamic stability of the ligand (**16f**) with FXa was studied in the complex over a period of 10 ns duration. Post dynamic analysis was carried out to understand stability of the ligand-receptor complex by average root mean square deviation (RMSD).[42] To examine the binding stability of the complex over the predefined period of time, RMSD–P, RMSF–P and RMSD–L (P = Protein; L = Ligand) were scrutinized to support the docking results. Initial pose of the ligand-receptor complex was considered as the reference frame to calculate these values. RMSD–P was calculated to understand the large scale movements in the protein in presence of the ligand in the active site. This gives insights into the structural conformation of the protein throughout the simulation time. The RMSD–P for FXa with ligand **16f** complex was observed in the range of 0.7 to 1.6 Å. This observation suggested that the presence of **16f** in the active site of FXa receptor has not influenced the stability of the protein backbone throughout the simulation run. To identify the stability of the ligand with respect to the protein and its binding site, the RMSD–L of **16f** was computed. The Lig fit on Prot RMSD–L for the ligand was observed in the range of 0.4 to 3.2 Å. Here, the major fluctuation was observed during first 1 ns duration and afterwards the ligand in the complex was quite stable with RMSD in the range of 0.4 to 1.8 Å with an average value of 1.1 Å. The average RMSD value observed here is significantly less than the RMSD–P, indicating that the ligand is stable inside the binding pocket and it has not diffused away from the active site during the entire simulation period. Further, the Lig fit on Lig RMSD was measured to understand the internal fluctuation of the ligand atoms. It was observed in the acceptable range of 0.3 to 1.3 Å and no deviation was observed during the study period (Figure 4a).

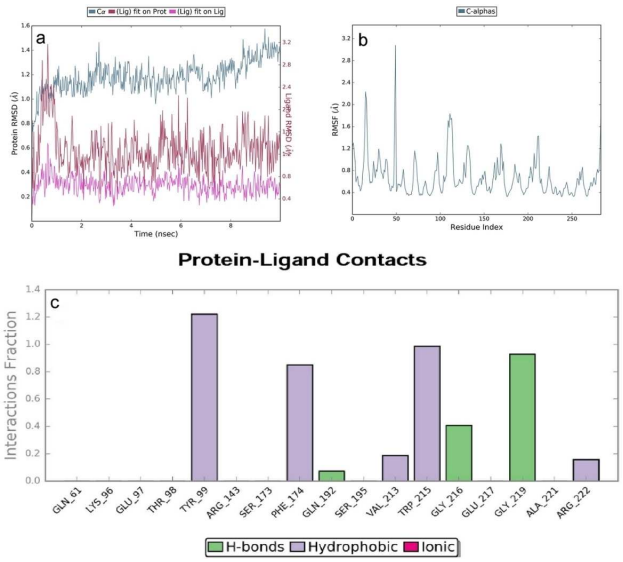

Figure 4. (a) RMSD–P, RMSD–L plot for FXa with **16f**; (b) RMSF–P for FXa with **16f**; (c) Ligand and receptor residue contact diagram for FXa with **16f**.

The structural integrity of the protein and the residual mobility of the ligand were quantified in terms of RMSF–P

(Figure 4b). For almost all residues including loop residues and the terminal residues of the protein in complexation with **16f**, in the active site, the RMSF–P was below 3.2 Å. In the protein ligand stability the interaction study was also evaluated over a period of time. In the docking study, the NH and C=O of the carboxamide group and NH of 2-aminobenzamide scaffold of compound **16f** form the H-bond with Gly219, Gln192 and Gly216 respectively. From simulation study it was confirmed that the amide NH and 2-amino -NH formed two H-bonds with Gly219 and Gly216. These were maintained stable over 92% and 29% of simulation time respectively with the respective amino acids. All these H-bonds were having distance within 2.5 Å, and donor angle of $\geq 120^{\circ}$ and acceptor angle of $\geq 90^{\circ}$. Further, the H-bond with Gln192 was not observed to be stable within these limits during the simulation time. Additionally, the amine –NH and amide –C=O of 2-aminobenzamide showed 23% stable intra-molecular H-bond over the total simulation period. Further, the MD study showed that the π-cation interaction between Arg222 and 2-aminobenzamide was stable only for approximately 20% of total duration of simulation. The hydrophobic interactions including π-π interaction with Tyr99, Phe174 and Trp215 played vital role in the stability of the ligand-receptor complex wherein all the residues were involved in hydrophobic interaction for more than 80% of the total simulation time (Figure 4c).

Biology

In vitro FXa and thrombin inhibition assays

In vitro enzyme inhibition assays for FXa and thrombin were performed for the synthesized compounds at a concentration of 100 μM by using a chromogenic substrate (Spectrozyme TH for thrombin and S-2222 for FXa) as per the previously reported procedure.[15a] The residual enzyme activity was determined from the change in the absorbance at 405 nm with hydrolysis of the substrate by the enzyme. Those compounds with less than 60% of the residual FXa activity were chosen for determination of their IC_{50} values. Compounds **13e-13g**, **13i-13k**, **15e** and **16a**, **16c-16f**, **16h** and **16i** showed inhibition of FXa in the preliminary screening (Figure 5). All the synthesized compounds showed more than 50% thrombin residual activity (Figure 6). All the selected compounds demonstrated good selectivity for FXa over thrombin (IC_{50} values of >100 μM). **Table 2** represents IC_{50} of compounds **13e-13g**, **13i-13k**, **15e** and **16a**, **16c-16f**, **16h** and **16i** against both the enzymes.

Ex vivo PT prolongation and clotting time

Compounds showing significant inhibition of the enzyme in the preliminary screening were evaluated further using *ex vivo* measurements of prothrombin time and clotting time. The PT prolonging activity and clotting time of compounds **13e-13g**, **13i-13k**, **15e** and **16a**, **16c-16f**, **16h** and **16i** along with control group and standard drug apixaban were determined at 2 h after oral administration in rat (30 mg/kg dose) and the data are shown in **Table 2**. Most of the tested compounds indicated slightly higher prolongation in prothrombin time than that of control (7.7 sec). Compounds **16c** (9.8 sec), **16d** (9.9 sec), **16f** (10.1 sec) and **13j** (9.9 sec) showed significant

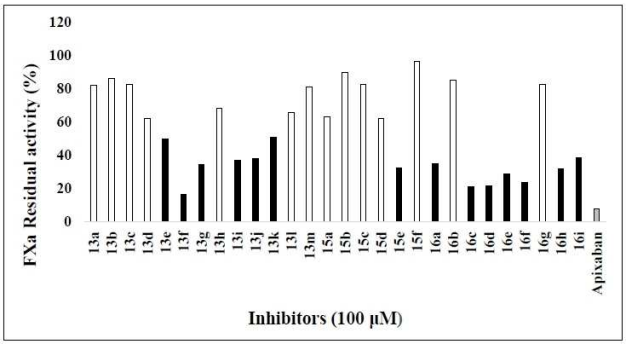

Figure 5. FXa residual activity (%) after treatment with the synthesized compounds. Experiments were performed at 100 μM in duplicate. Mean of % FXa residual activity values are represented (SE < 20%).

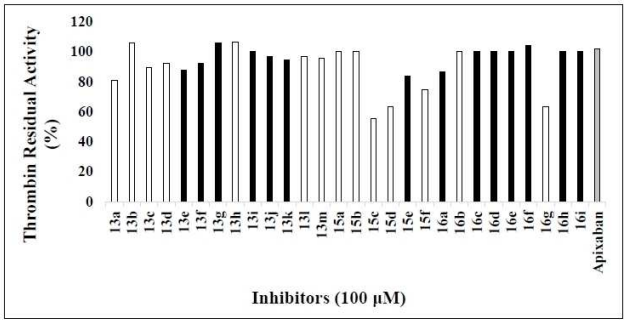

Figure 6. Thrombin residual activity (%) after treatment with the synthesized compounds. Experiments were performed at 100 μM in duplicate. Mean of % FXa residual activity values are represented (SE < 20%).

Table 2. IC_{50} values, PT time and Clotting time for the test compounds

Compound	IC_{50} value (μM)[a] FXa	Thrombin	PT time (sec)[b]	Clotting time (sec)[b]
13e	23.7 ± 3.4	>100	9.2	15
13f	18.4 ± 2.6	>100	8.7	30
13g	11.5 ± 1.3	>100	8.9	30
13i	41.0 ± 3.2	>100	8.6	30
13j	48.3 ± 2.9	>100	9.9	30
13k	23.2 ± 8.4	>100	9.4	37.5
15e	57.5 ± 8.6	>100	9.4	30
16a	35.3 ± 2.3	>100	8.8	35
16c	5.4 ± 1.0	>100	9.8	40
16d	1.3 ± 0.8	>100	9.9	40
16e	12.5 ± 2.2	>100	9.1	35
16f	**0.7 ± 0.2**	**>100**	**10.1**	**45**
16h	30.0 ± 6.4	>100	8.7	30
16i	52.5 ± 5.7	>100	9.5	35
Apixaban	0.35 ± 0.1	>100	12.8	60
Control	-	-	7.7	12.5

[a] IC_{50} values shown are the mean of duplicate or triplicate measurements. [b] The *ex vivo* PT time and Clotting time were determined 2 h after oral administration of the test compounds to rats at a dose of 30 mg/kg (n = 3).

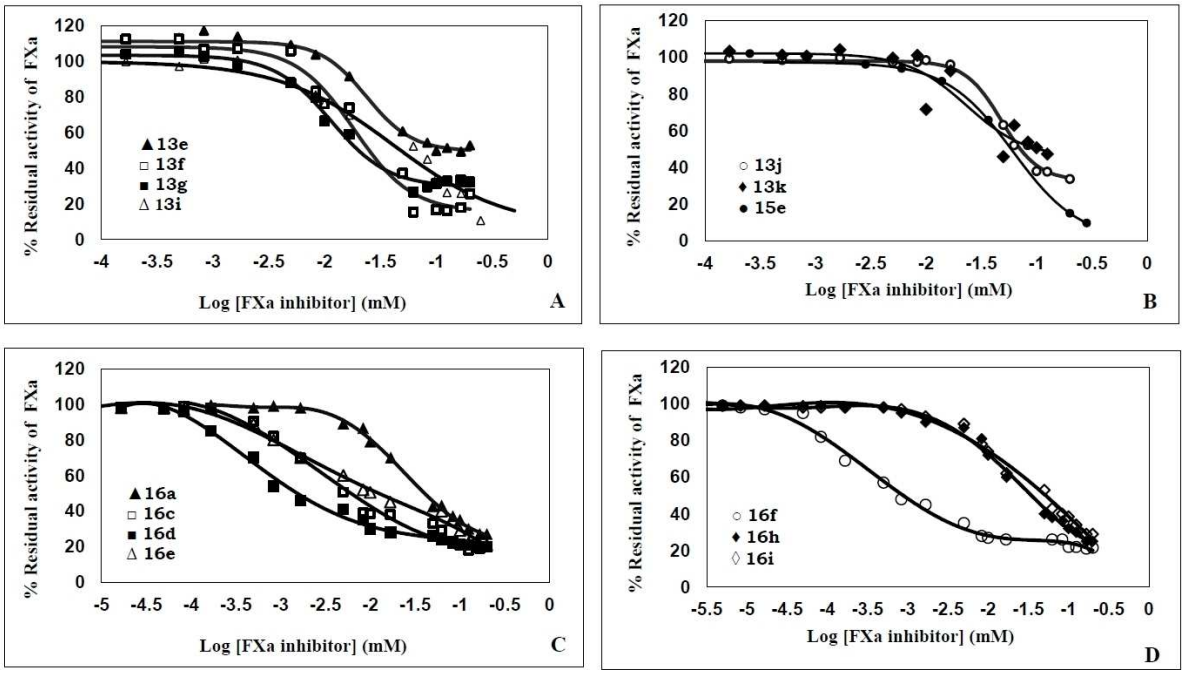

Figure 7. Direct inhibition of FXa by compounds **13e**, **13f**, **13g**, **13i** (A), **13j**, **13k**, **15e** (B), **16a**, **16c**, **16d**, **16e** (C) and **16f**, **16h**, **16i** (D). Solid lines represent sigmoidal fits to the data to obtain IC_{50} as described in experimental section. Experiments were performed in duplicate or triplicate (SE < 20%).

change in the prothrombin time. The selected test compounds also showed much higher clotting time than the control (12.5 sec). Compound **16f** (45 sec) exhibited significant change in clotting time offering the highest value among the selected compound. However, this was lesser than the standard drug apixaban (60 sec).

In vivo $FeCl_3$ induced arterial thrombosis

Based on *in vitro* FXa inhibitory activity and *ex vivo* PT prolongation time of compound **16f**, it was selected for *in vivo* evaluation of antithrombotic potential by $FeCl_3$ induced arterial thrombosis model in rats. The reduction in thrombus weight was considered as a preventive measure for *in vivo* efficacy of a compound. Compound **16f** reduced thrombus weight by 46% at 30 mg/kg in rats. In the case of standard drug (apixaban) at dose of 30 mg/kg, the reduction in thrombus weight was found to be 69%.

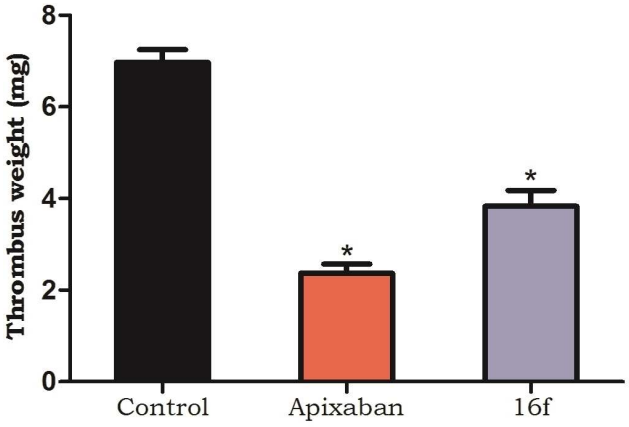

Figure 8. Effect of **16f** and apixaban (30 mg/kg) on thrombus weight ($FeCl_3$ induced arterial thrombosis model). Statistical analysis was performed by One way ANOVA using Graph-pad prism 5.0 *p < 0.01 vs. vehicle control. (n = 3)

Structure-activity relationships and interaction analysis

The effect of various S4 binding ligands on the anthranilamide scaffold has been studied with respect to antithrombotic activity of the synthesized compounds, retaining 2-amino-5-chloropyridine as the S1 binding moiety.

Simple alkyl substituted compounds **13a-13c** showed <50% inhibition of the enzyme in the initial screening. As S4 site is comprised of a cage of aromatic amino acids like Tyr99, Phe174 and Trp215, it was also observed in the computational binding analysis that simple aliphatic substituents did not exhibit good binding affinity in this region. This observation was supported by the fact that compounds containing substituted benzyl groups as the S4 moieties exhibited better activity, and favourable interactions with the enzyme in the docking study. Initially, benzyl groups were introduced to obtain compounds **13d-13l**. All the benzyl substituted compounds **13d-13l** showed low to moderate FXa inhibitory activity (IC_{50} = 10 to 50 μM). This was supported by the ligand-receptor binding analysis in terms of slightly improved hydrophobic and π-π stacking interactions. Compound **13g** with 4-methoxybenzyl group exhibited somewhat higher FXa inhib-

itory activity (IC_{50} = 11.5 μM) amongst the benzyl substituted compounds. Here, because of the 4-methoxy group, the π cloud of the aromatic ring was observed to be strong and it was reflected very well in the π-π interactions with the aromatic amino acids of the S4 binding pocket of the receptor. Compound **13j** containing 3-fluorobenzyl showed a moderate activity (IC_{50} = 48.3 μM). The orientation of the phenyl ring of the molecule in the molecular interactions with the receptor is a very important aspect as proven by the substituents on the *ortho* and *para* positions. In docking studies it was observed that, the *ortho* substituents on the aromatic ring were distorting the orientation of the benzyl ring because of the steric effects and hence in most of the cases, the π-π interactions were lacking or poor with the aromatic triad of Tyr99, Phe174 and Trp215 of the active site. The electron donating *para* substituents were found to be helping in both the ways by allowing proper orientation of the ring as well as by increasing the electron density.

Considering the favourable literature reports[43] on biphenyl derivatives, it was decided to synthesize substituted biphenyls as S4 binding ligands to get compounds **16a-16i**. Biphenyls were expected to show better activity. Except for compound **16b** and **16g**, the remaining biphenyl derivatives displayed more than 50% inhibition of the enzyme at 100 μM concentration. Poor activity of **16b** (*tert*-butyl group at *para* position) and **16g** (methoxy group at *para* position) could be rationalized using docking studies. In the receptor active site interactions of **16b** and **16g**, the *para* substituted hydrophobic groups were observed to be entering the polar and charged amino acids region like Glu97 and Thr98 and thus having unfavorable interactions. Compound **16a** without any substituents on both the rings exhibited an IC_{50} value of 35.0 μM. Substitution at 2-position of the proximal ring in compound **16h** resulted into slightly improved activity. Introduction of substituents on *ortho* position of the distal ring resulted into increased potency. For example, compounds **16d** (2-chloro) and **16e** (2-methoxy) demonstrated much improved FXa inhibitory activity with IC_{50} values of 1.3 μM and 12.5 μM respectively. Compound **16f** displayed the highest inhibition of the enzyme with an IC_{50} value of 0.7 μM. This improvement in activity was by the distal *ortho* substituent due to steric effect and could be explained by the docking study also. The orientation of the distal phenyl ring because of the presence of *ortho* substituent led to favourable orientation of the molecule for strong hydrophobic and π-π interactions with Tyr99, Phe174 and Trp215. Further substitution by 3,5 difluoro group in compound **16c** was found to offer an IC_{50} value of 5.4 μM. Incorporation of substituents at *para* position of the distal ring in compounds (**16b, 16g** and **16i**) was associated with decreased potency as explained above.

Further, substituted piperazines were introduced as the S4 binding moieties in place of biphenyls to obtain compounds **15a-15f**. Among the substituted piperazines, compound **15e** alone with benzylpiperazine group could offer moderate inhibition of the enzyme with an IC_{50} value of 57.5 μM.

Conclusion

A total of twenty-eight anthranilamide derivatives having some novel S4 binding moieties such as alkyls, benzyls, biphenyls and substituted piperazines were assessed to determine their effect on antithrombotic activity. Amongst the tested compounds, benzyl substituted derivative **13g** and the biphenyl derivatives **16c**, **16d** and **16f** showed significant inhibition of the enzyme with IC_{50} values of 11.5 μM, 5.4 μM, 1.3 μM and 0.7 μM respectively. The obtained results suggests that lipophilicity and aromaticity all alone do not play significant roles for good binding to the S4 pocket but steric and electronic effects of the functional groups are responsible for higher binding affinity. Compound **16f** is the 'best find' of the study offering high selectivity for FXa over thrombin, with IC_{50} value in submicromolar range and causing significant enhancement in the clotting time.

Supporting Information Summary

Details of experimental procedures for synthesis of compounds, biological evaluation and characterization data of compounds are provided in supporting information.

Acknowledgement

Nirav R. Patel gratefully acknowledges the University Grant Commission (UGC), New Delhi, for awarding Junior Research Fellowship (F. No. 25–1/2014-15(BSR)/7-129/2007/(BSR). Dushyant V. Patel is also thankful to DST-INSPIRE, New Delhi for awarding Research Fellowship (IF-150660). Authors also acknowledge the computational facility provided by Centre for High Performance Computing (CHPC), Cape Town, South Africa for molecular dynamics study.

Conflict of Interest

The authors declare no conflict of interest.

Keywords: Biphenyls · Factor Xa · FXa inhibitors · Thrombosis

[1] a) F. J. Vazquez, M. L. Posadas-Martinez, J. Vicens, F. Gonzalez Bernaldo de Quiros, D. H. Giunta, *Thromb J* **2013**, *11*, 16; b) G. E. Raskob, P. Angchaisuksiri, A. N. Blanco, H. Buller, A. Gallus, B. J. Hunt, E. M. Hylek, A. Kakkar, S. V. Konstantinides, M. McCumber, Y. Ozaki, A. Wendelboe, J. I. Weitz, *Arter Thromb Vasc Biol* **2014**, *34*, 2363–2371.
[2] https://www.isth.org (Accessed on 23rd November 2018)
[3] P. Stribys, *J Atr Fibrillation* **2016**, *9*, 79–83.
[4] a) T. Hara, A. Yokoyama, K. Tanabe, H. Ishihara, M. Iwamoto, *Thromb Haemost* **1995**, *74*, 635–639; b) Y. Morishima, K. Tanabe, Y. Terada, T. Hara, S. Kunitada, *Thromb Haemost* **1997**, *78*, 1366–1371.
[5] a) J. Graff, S. Harder, *Clin Pharmacokinet* **2013**, *52*, 243–254; b) M. Ufer, *Thromb Haemost* **2010**, *103*, 572–585.
[6] N. B. Norgard, J. J. DiNicolantonio, T. J. Topping, B. Wee, *Ther Adv Chronic Dis* **2012**, *3*, 123–136.
[7] a) K. P. Cabral, J. E. Ansell, *Vasc Health Risk Manag* **2015**, *11*, 117–123; b) M. Ieko, T. Tarumi, M. Takeda, S. Naito, T. Nakabayashi, T. Koike, *J Thromb Haemost* **2004**, *2*, 612–618; c) S. Li, B. Liu, D. Xu, Y. Xu, *PLoS ONE* **2014**, *9*, e95354; d) G. Wasserlauf, S. M. Grandi, K. B. Filion, M. J. Eisenberg, *Am J Cardiol* **2013**, *112*, 454–460.

[8] E. Perzborn, S. Roehrig, A. Straub, D. Kubitza, F. Misselwitz, *Nat Rev Drug Discov* **2011**, *10*, 61–75.
[9] M. Lassen, B. Davidson, A. Gallus, G. Pineo, J. Ansell, D. Deitchman, *J Thromb Haemost* **2007**, *5*, 2368–2375.
[10] G. Y. Lip, G. Agnelli, *Eur Heart J* **2014**, *35*, 1844–1855.
[11] A. T. Cohen, R. A. Harrington, S. Z. Goldhaber, *N Engl J Med* **2016**, *375*, 534–544.
[12] P. S. Rao, T. Burkart, *Blood Rev* **2017**, *31*, 205–211.
[13] Y. H. Mekaj, A. Y. Mekaj, S. B. Duci, *Ther Clin Risk Manag* **2015**, *11*, 967–977.
[14] P. Vranckx, M. Valgimigli, H. Heidbuchel, *Arrhythmia Electrophysiology Review* **2018**, *7*, 55–61.
[15] J. H. Alexander, R. D. Lopes, S. James, R. Kilaru, Y. He, P. Mohan, D. L. Bhatt, S. Goodman, F. W. Verheugt, M. Flather, *N Engl J Med* **2011**, *365*, 699–708.
[16] De Gottardi, A. J. Trebicka, C. Klinger, *Liver Int* **2017**, *37*, 694–699.
[17] Y. H. Chan, Y. H. Yeh, H. T. Tu *Oncotarget* **2017**, *8*, 98898–98917.
[18] J. Lutz, K. Jurk, H. Schinzel, *Int J Nephrol Renovasc Dis* **2017**, *10*, 135.
[19] J. Spinar, L. Spinarova, *Vnitr Lek* **2017**, *63*, 424–430.
[20] R. Trikha, P. R. Kowey, *Cardiology* **2017**, *136*, 115–124.
[21] a) D. Mendel, A. L. Marquart, S. Joseph, P. Waid, Y. K. Yee, A. L. Tebbe, A. M. Ratz, D. K. Herron, T. Goodson, J. J. Masters, J. B. Franciskovich, J. M. Tinsley, M. R. Wiley, L. C. Weir, J. A. Kyle, V. J. Klimkowski, G. F. Smith, R. D. Towner, L. L. Froelich, J. Buben, T. J. Craft, *Bioorg Med Chem Lett* **2007**, *17*, 4832–4836; b) J. Xing, L. Yang, H. Li, Q. Li, L. Zhao, X. Wang, Y. Zhang, M. Zhou, J. Zhou, H. Zhang, *Eur J Med Chem* **2015**, *95*, 388–399.
[22] Y. Imaeda, T. Kuroita, H. Sakamoto, T. Kawamoto, M. Tobisu, N. Konishi, K. Hiroe, M. Kawamura, T. Tanaka, K. Kubo, *J Med Chem* **2008**, *51*, 3422–3436.
[23] a) L. Anselm, D. W. Banner, J. Benz, K. G. Zbinden, J. Himber, H. Hilpert, W. Huber, B. Kuhn, J. L. Mary, M. B. Otteneder, N. Panday, F. Ricklin, M. Stahl, S. Thomi, W. Haap, *Bioorg Med Chem Lett* **2010**, *20*, 5313–5319; b) R. J. Young, C. Adams, M. Blows, D. Brown, C. L. Burns-Kurtis, C. Chan, L. Chaudry, M. A. Convery, D. E. Davies, A. M. Exall, G. Foster, J. D. Harling, E. Hortense, S. Irvine, W. R. Irving, S. Jackson, S. Kleanthous, A. J. Pateman, A. N. Patikis, T. J. Roethka, S. Senger, G. J. Stelman, J. R. Toomey, R. I. West, C. Whittaker, P. Zhou, N. S. Watson, *Bioorg Med Chem Lett* **2011**, *21*, 1582–1587.
[24] a) M. J. Orwat, J. X. Qiao, K. He, A. R. Rendina, J. M. Luettgen, K. A. Rossi, B. Xin, R. M. Knabb, R. R. Wexler, P. Y. Lam, D. J. Pinto, *Bioorg Med Chem Lett* **2014**, *24*, 3341–3345; b) M. L. Quan, D. J. Pinto, K. A. Rossi, S. Sheriff, R. S. Alexander, E. Amparo, K. Kish, R. M. Knabb, J. M. Luettgen, P. Morin, A. Smallwood, F. J. Woerner, R. R. Wexler, *Bioorg Med Chem Lett* **2010**, *20*, 1373–1377.
[25] a) T. Xue, S. Ding, B. Guo, Y. Zhou, P. Sun, H. Wang, W. Chu, G. Gong, Y. Wang, X. Chen, Y. Yang, *J Med Chem* **2014**, *57*, 7770–7791; b) Y. Zhao, M. Jiang, S. Zhou, S. Wu, X. Zhang, L. Ma, K. Zhang, P. Gong, *Eur J Med Chem* **2015**, *96*, 369–380.
[26] M. L. Quan, Q. Han, J. M. Fevig, P. Y. S. Lam, S. Bai, R. M. Knabb, J. M. Luettgen, P. C. Wong, R. R. Wexler, *Bioorg Med Chem Lett.* **2006**, *16*, 1795–1798.
[27] H. Matter, E. Defossa, U. Heinelt, P.-M. Blohm, D. Schneider, A. Müller, S. Herok, H. Schreuder, A. Liesum, V. Brachvogel, *J Med Chem* **2002**, *45*, 2749–2769.
[28] Y. K. Lee, D. J. Parks, T. Lu, T. V. Thieu, T. Markotan, W. Pan, D. F. McComsey, K. L. Milkiewicz, C. S. Crysler, N. Ninan, M. C. Abad, E. C. Giardino, B. E. Maryanoff, B. P. Damiano, M. R. Player, *J Med Chem* **2008**, *51*, 282–297.
[29] D. J. Pinto, M. J. Orwat, M. L. Quan, Q. Han, R. A. Galemmo, E. Amparo, B. Wells, C. Ellis, M. Y. He, R. S. Alexander, *Bioorg Med Chem Lett* **2006**, *16*, 4141–4147.
[30] a) R. A. Al-Horani, A. Y. Mehta, U. R. Desai, *Eur J Med Chem* **2012**, *54*, 771–783; b) N. S. Watson, C. Adams, D. Belton, D. Brown, C. L. Burns-Kurtis, L. Chaudry, C. Chan, M. A. Convery, D. E. Davies, A. M. Exall, J. D. Harling, S. Irvine, W. R. Irving, S. Kleanthous, I. M. McLay, A. J. Pateman, A. N. Patikis, T. J. Roethke, S. Senger, G. J. Stelman, J. R. Toomey, R. I. West, C. Whittaker, P. Zhou, R. J. Young, *Bioorg Med Chem Lett* **2011**, *21*, 1588–1592.
[31] K. M. Amin, N. M. Abdel Gawad, D. E. Abdel Rahman, M. K. El Ashry, *Bioorg Chem* **2014**, *52*, 31–43.
[32] Y. Shi, S. P. O'Connor, D. Sitkoff, J. Zhang, M. Shi, S. N. Bisaha, Y. Wang, C. Li, Z. Ruan, R. M. Lawrence, H. E. Klei, K. Kish, E. C. Liu, S. M. Seiler, L. Schweizer, T. E. Steinbacher, W. A. Schumacher, J. A. Robl, J. E. Macor, K. S. Atwal, P. D. Stein, *Bioorg Med Chem Lett* **2011**, *21*, 7516–7521.
[33] J. T. Kohrt, K. J. Filipski, W. L. Cody, C. F. Bigge, F. La, K. Welch, T. Dahring, J. W. Bryant, D. Leonard, G. Bolton, L. Narasimhan, E. Zhang, J. T. Peterson, S. Haarer, V. Sahasrabudhe, N. Janiczek, S. Desiraju, M. Hena, C. Fiakpui, N. Saraswat, R. Sharma, S. Sun, S. N. Maiti, R. Leadley, J. J. Edmunds, *Bioorg Med Chem* **2006**, *14*, 4379–4392.
[34] H. Koshio, F. Hirayama, T. Ishihara, R. Shiraki, T. Shigenaga, Y. Taniuchi, K. Sato, Y. Moritani, Y. Iwatsuki, S. Kaku, N. Katayama, T. Kawasaki, Y. Matsumoto, S. Sakamoto, S. Tsukamoto, *Bioorg Med Chem* **2005**, *13*, 1305–1323.
[35] M. J. Kochanny, M. Adler, E. Ewing, B. D. Griedel, E. Ho, R. Karanjawala, W. Lee, D. Lentz, A. M. Liang, M. M. Morrissey, G. B. Phillips, J. Post, K. L. Sacchi, S. T. Sakata, B. Subramanyam, R. Vergona, J. Walters, K. A. White, M. Whitlow, B. Ye, Z. Zhao, K. J. Shaw, *Bioorg Med Chem* **2007**, *15*, 2127–2146.
[36] F. Hirayama, H. Koshio, T. Ishihara, S. Hachiya, K. Sugasawa, Y. Koga, N. Seki, R. Shiraki, T. Shigenaga, Y. Iwatsuki, Y. Moritani, K. Mori, T. Kadokura, T. Kawasaki, Y. Matsumoto, S. Sakamoto, S. Tsukamoto, *J Med Chem* **2011**, *54*, 8051–8065.
[37] N. R. Patel, D. V. Patel, P. R. Murumkar, M. R. Yadav, *Eur J Med Chem* **2016**, *121*, 671–698.
[38] D. J. P. Pinto, J. M. Smallheer, D. L. Cheney, R. M. Knabb, R. R. Wexler, *J Med Chem* **2010**, *53*, 6243–6274.
[39] a) A. M. D'Souza, N. Spiccia, J. Basutto, P. Jokisz, L. S. Wong, A. G. Meyer, A. B. Holmes, J. M. White, J. H. Ryan, *Org Lett* **2011**, *13*, 486–489; b) J. Fensholdt, J. Thorhauge, B. Nørremark, Google Patents, **2011**; c) G. E. Hardtmann, G. Koletar, O. R. Pfister, *J Heterocycl Chem* **1975**, *12*, 565–572; d) A. A. Wube, F. Bucar, C. Hochfellner, M. Blunder, R. Bauer, A. Hüfner, *Eur J Med Chem* **2011**, *46*, 2091–2101; e) W.-Z. Zhang, N. Zhang, Y. Q. Sun, Y. W. Ding, X. B. Lu, *ACS Catal* **2017**, *7*, 8072–8076.
[40] a) M. de Candia, F. Liantonio, A. Carotti, R. De Cristofaro, C. Altomare, *J Med Chem* **2009**, *52*, 1018–1028; b) F. Fringuelli, R. Girotti, O. Piermatti, F. Pizzo, L. Vaccaro, *Org lett* **2006**, *8*, 5741–5744; c) L. Liu, Y. Zhang, Y. Wang, *J Org Chem* **2005**, *70*, 6122–6125; d) S. Pradhan, R. P. John, *New J Chem* **2015**, *39*, 5759–5766.
[41] M. Nazare, H. Matter, D. W. Will, M. Wagner, M. Urmann, J. Czech, H. Schreuder, A. Bauer, K. Ritter, V. Wehner *Angew Chem Int Ed* **2012**, *51*, 905.
[42] a) R. C. Dash, C. R. Maschinot, M. K. Hadden, *Biochim Biophys Acta Gen Subj* **2017**, *1861*, 168–177; b) R. C. Dash, A. M. Zaino, M. K. Hadden, *Biochim Biophys Acta Gene Regul Mech* **2018**, *1861*, 594–602.
[43] a) S. Maignan, J.-P. Guilloteau, Y. M. Choi-Sledeski, M. R. Becker, W. R. Ewing, H. W. Pauls, A. P. Spada, V. Mikol, *J Med Chem* **2003**, *46*, 685–690; b) J. Yang, G. Su, Y. Ren, Y. Chen, *Eur J Med Chem* **2015**, *101*, 41–51; c) M. Hammami, E. Rühmann, E. Maurer, A. Heine, M. Gütschow, G. Klebe, T. Steinmetzer, *Med Chem Comm* **2012**, *3*, 807–13.

Submitted: October 25, 2018
Accepted: January 4, 2019

European Journal of Medicinal Chemistry 121 (2016) 671–698

Contents lists available at ScienceDirect

European Journal of Medicinal Chemistry

journal homepage: http://www.elsevier.com/locate/ejmech

Review article

Contemporary developments in the discovery of selective factor Xa inhibitors: A review

Nirav R. Patel, Dushyant V. Patel, Prashant R. Murumkar, Mange Ram Yadav*

Faculty of Pharmacy, Kalabhavan Campus, The Maharaja Sayajirao University of Baroda, Vadodara 390001, Gujarat, India

ARTICLE INFO

Article history:
Received 22 February 2016
Received in revised form
25 April 2016
Accepted 19 May 2016
Available online 24 May 2016

Dedicated in the fond memory of Prof. Rajani Giridhar.

Keywords:
Thrombosis
Factor Xa
FXa inhibitors

ABSTRACT

Thrombosis is a leading cause of death in cardiovascular diseases such as myocardial infarction (MI), unstable angina and acute coronary syndrome (ACS) in the industrialized world. Venous thromboembolism is observed in about 1 million people every year in United States causing significant morbidity and mortality. Conventional antithrombotic therapy has been reported to have several disadvantages and limitations like inconvenience in oral administration, bleeding risks (heparin analogs), narrow therapeutic window and undesirable interactions with food and drugs (vitamin K antagonist-warfarin). The unmet medical demand for orally active safe anticoagulants has generated widespread interest among the medicinal chemists engaged in this field. To modulate blood coagulation, various enzymes involved in the coagulation process have received great attention as potential targets by various research groups for the development of oral anticoagulants. Among these enzymes, factor Xa (FXa) has remained the centre of attention in the last decade. Intensive research efforts have been made by various research groups for the development of small, safe and orally bioavailable FXa inhibitors. This review is an attempt to compile the research work of various researchers in the direction of development of FXa inhibitors reported since 2010 onward.

Contents

1. Introduction 672
 1.1. Hemostasis and thrombosis 672
 1.2. Blood coagulation 672
  1.2.1. The cascade model 672
  1.2.2. The cell-based model 672
 1.3. Structure of FXa 673
 1.4. Structural differences between FXa and thrombin 673
 1.5. Factor Xa as a promising target for the development of antithrombotic drugs 675
2. Designing strategies adopted for the development of FXa inhibitors 675
 2.1. P1 motifs used for designing of FXa inhibitors 675
  2.1.1. Amidine derivatives as P1 motifs 675
  2.1.2. Halo derivatives as P1 motifs 675
  2.1.3. Substituted benzenes as P1 motifs 675
 2.2. Central scaffolds used for attaching P1 and P4 motifs 676
 2.3. P4 motifs used for designing of FXa inhibitors 676
  2.3.1. Monoaryls as P4 motifs 676
  2.3.2. Biaryls as P4 motifs 676
  2.3.3. Miscellaneous groups as P4 motifs 676
  2.3.4. Pyrrolidine based FXa inhibitors 676

* Corresponding author.
E-mail address: mryadav11@yahoo.co.in (M.R. Yadav).

http://dx.doi.org/10.1016/j.ejmech.2016.05.039
0223-5234/

2.3.5. Oxazolidinone and isoxazole based FXa inhibitors 684
2.3.6. Anthranilamides and disubstituted benzenes as FXa inhibitors 686
2.3.7. Diamines as FXa inhibitors 688
2.3.8. Pyrazole based FXa inhibitors 689
2.3.9. Coumarins as FXa inhibitors 689
2.3.10. Arylsulfonamidopiperidone derivatives 690
2.3.11. Tetrahydroisoquinolines as FXa inhibitors 691
3. Conclusion 692
Acknowledgement 695
References 695

1. Introduction

Thrombosis is one of the leading causes of deaths in the cardiovascular diseases such as myocardial infarction (MI), unstable angina and acute coronary syndrome (ACS) in developed countries [1,2]. It is estimated that venous thromboembolism (VTE) afflicts about 1 million (1–2 per 1000) people every year in United States and about 0.1 million of them die of VTE [3]. More than one million individuals in Europe are affected by venous thromboembolic disorders each year that are responsible for at least 0.5 million deaths [4]. Thrombosis is obstruction of blood in the arterial and venous circulation. Depending upon the site of formation of thrombus, thrombosis is classified as arterial or venous thrombosis. Different types of antithrombotic drugs are used to treat both arterial and venous thrombosis depending on their pathological differences [5–11]. Arterial thrombosis is generally treated by antiplatelet agents because the condition is associated with platelet aggregation and activation induced by ruptured atherosclerotic plaque, leading to MI and ACS [12]. Obstruction of veins is in the form of deep vein thrombosis (DVT) or pulmonary embolism (PE) which can be treated by anticoagulant agents [13].

The current antithrombotic therapy includes vitamin K antagonists, coagulation enzymes' inhibitors and heparins such as unfractionated heparins (UFHs), low molecular weight heparins (LMWHs) or fractionated heparins [6,14–16]. Although these drugs have proved their efficacy in clinical practice but they have been found to be associated with several problems. Warfarin, a vitamin K antagonist is the most widely used antithrombotic drug. Unfortunately warfarin has a narrow therapeutic window, causes undesirable interactions with food and drugs and possesses risk of bleeding [17]. Debigatran etexilate, an oral thrombin inhibitor was found to have uncontrolled bleeding which could prove fatal [18]. Other anticoagulants like UFH, LMWHs, direct thrombin inhibitors (Argatroban, Hirudin derivatives) and indirect factor Xa (FXa) inhibitor (Fondaparinux) require parenteral administration which is responsible for clot formation at the site of injection limiting their use in clinical practice. Heparin analogs are associated with thrombocytopenia, immunological reactions and certain other serious side effects [19]. These shortcomings in the existing drugs motivate researchers to discover new orally bioavailable antithrombotic drugs with better safety profile.

1.1. Hemostasis and thrombosis

Hemostasis is a normal physiological process in which bleeding is prevented to minimize excessive blood loss [20]. Hemostasis maintains the integrity of circulatory system but it sometimes gets imbalanced, causing either thrombosis or hemorrhage. The balance between thrombosis and hemorrhagic condition is controlled in the body by the interactions between platelets and vascular membrane as well as coagulation factors and fibrinolytic system [21]. The hemostatic process involves three phases; primary hemostasis, coagulation and fibrinolysis. All the three processes are highly interrelated with each other and regulate blood fluidity in the vessels by maintaining vascular integrity and their openness [22]. The overstated response of hemostatic system causes vascular endothelial injury, arresting of blood flow and hypercoagulation, resulting into a pathological condition called thrombosis [23]. Primary hemostasis is initiated instantly due to vascular endothelial injury or damage and is associated with vasoconstriction to reduce blood loss from the site of injury, and the aggregation and activation of platelets to form a platelet plug [24]. Subsequently, secondary hemostasis starts which includes coagulation cascade resulting into formation of insoluble fibrin clot at the site of injury by complex interactions of clotting factors and fibrinolytic system [25]. Most of these clotting factors are trypsin-like serine proteases that are formed from their respective proenzymes or zymogens, synthesized by liver [2,26].

1.2. Blood coagulation

Blood coagulation, a complicated process, has been well explained in the literature [27–30]. There are two models which are used to explain the blood coagulation:

1.2.1. The cascade model

According to the cascade model [31,32], coagulation is regulated by two parallel pathways, the extrinsic and the intrinsic pathways, intersecting at the point of activation of FXa as illustrated in Fig. 1 [33]. After the activation of factor X, a common pathway begins with activation of prothrombin to thrombin which subsequently activates soluble fibrinogen to form insoluble fibrin. The polymerized fibrin and activated platelets form a stable clot at the site of injury [34].

1.2.2. The cell-based model

The cell based model explains the *in vivo* mechanism of blood coagulation in a better way that includes important interactions between the cells that are directly involved in hemostasis and the coagulation process. As per this model [35–37], coagulation consists of three phases: initiation, amplification and propagation as described in Fig. 2 [38]. Initiation takes place on the surface of the glycoprotein tissue factor (TF) which activates coagulation factor VII. The proteolytic complex of TF-VIIa activates factor IX and factor X. On the TF-exposed cells, FXa is responsible for generation of small amount of thrombin (FIIa) from prothrombin (FII). In amplification phase, the surface bound thrombin activates platelets along with factor V, factor XI, and factor VIII. FXIa plays a booster role in

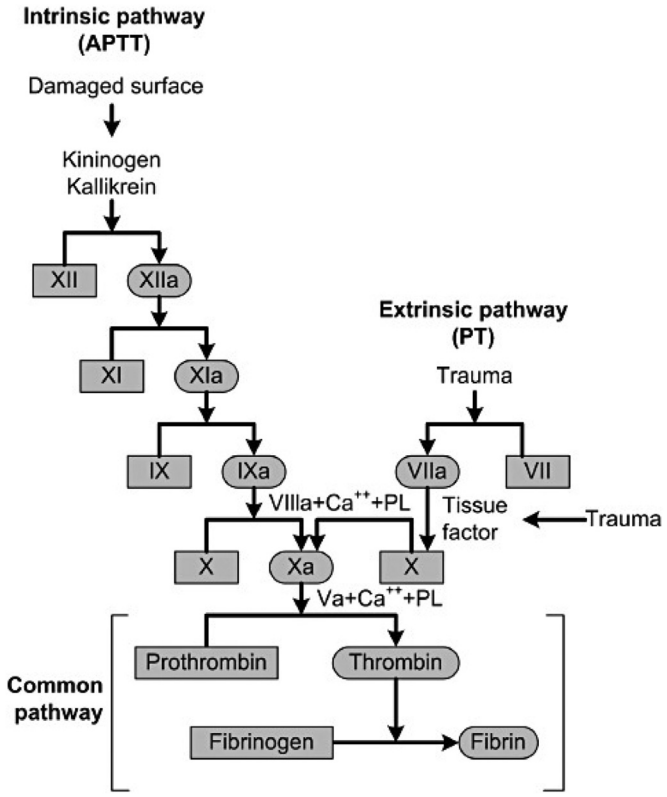

Fig. 1. The cascade model of coagulation (the feedback mechanisms are omitted for clarity). Used with permission from Adams, R. L. & Bird, R. J. *Nephrology*; 14, 2009, 462–470 (copyright© 2009, John Wiley & Sons Inc.).

generation of FIXa on the surface of the platelets and thus results in a thrombin burst. In propagation phase, the activated complexes FIXa-FVIIIa (termed as 'Xase') and FVa-FXa (termed as 'prothrombinase') are responsible for generation of FXa and thrombin respectively on the phospholipid surface of the activated platelets. In addition, the surface bound FXIa activates FIX to form more Xase and thus accelerates the generation of FXa which generates thrombin in association with FVa on the surface of the platelets. Finally, thrombin leads to proteolytic cleavage of the fibrinogen to fibrin.

1.3. Structure of FXa

FXa, a vitamin K-dependent serine protease has two chains of amino acids linked by a disulfide bridge [39]. The heavy chain consists of 303 amino acids and the light one of 139 amino acids. The catalytic triad in FXa is present in the heavy chain and comprises of Ser195, His57 and Asp102. The active site of FXa is identified as S1 and S4 subsites and the surrounding residues. The S1 subsite is a narrow pocket formed by Trp215-Gly216 on one side of the wall and Ala190-Cys191-Gln192 on the other side. The bottom of S1 pocket is lined by Asp189 and the side chain of Tyr228. Prothrombin, the natural substrate of FXa, interacts through ionic hydrogen bonding of the side chain of Arg to the Asp189 in S1 pocket (Fig. 3) [40]. In contrast to other serine proteases, access to the S2 pocket in FXa is blocked by Tyr99. The S4 binding pocket is an aromatic box formed by the side chains of Tyr99, Phe174 and Trp215. This binding site differs greatly from sites of other trypsin-like serine proteases. Highly selective inhibitors can be obtained by targeting the S4 pocket [41].

The nomenclature of binding pockets in the protease and its substrate (S1, S2 …, S1′, S2′ … and P1, P2 …, P1′, P2′ …) of a serine protease has been given by Schechter and Berger to simplify identification of the sites [42]. As per this nomenclature, a protein subsite indicated as S1 binds to the corresponding substrate amino acid indicated as P1. The cleavage point for the enzyme subsite is between S1′ and S1 and for the peptide substrate it is between P1′ and P1. In both the directions, the numbering of subsites is given from the cleavage point in ascending order (S1, S2, …, Sn increasing towards the N-terminus and S1′, S2′, …, Sn′ increasing towards the C-terminus) as shown in Fig. 4.

1.4. Structural differences between FXa and thrombin

Selectivity is an important issue for the development of FXa inhibitors. Due to structural similarities between both the enzymes, FXa inhibitors may also bind to thrombin. Hence, there is a need to address the selectivity issue for the development of newer FXa inhibitors by understanding structural differences between FXa and thrombin. Some research groups have resorted to molecular modeling techniques to obtain supportive results to understand the structural differences between both the enzymes and to sort out

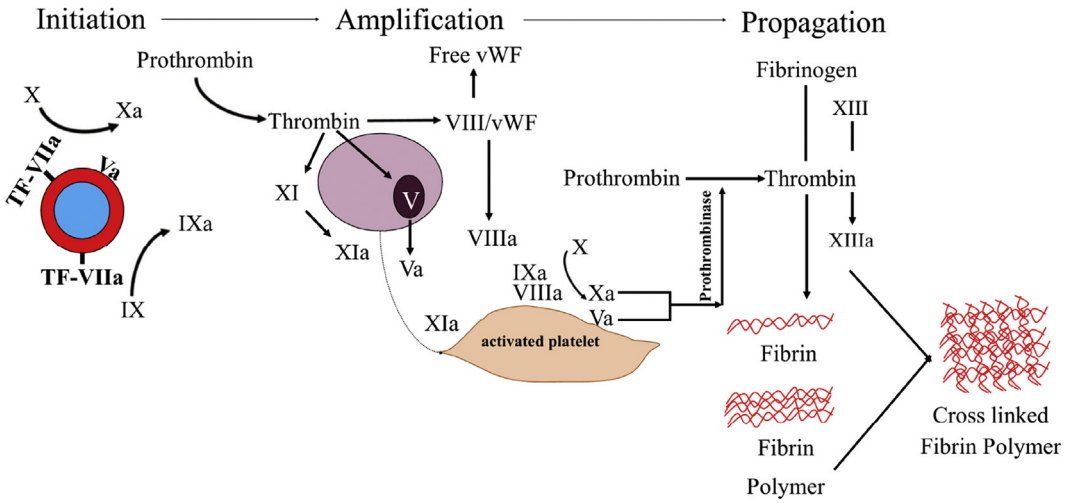

Fig. 2. Cell based model of coagulation.

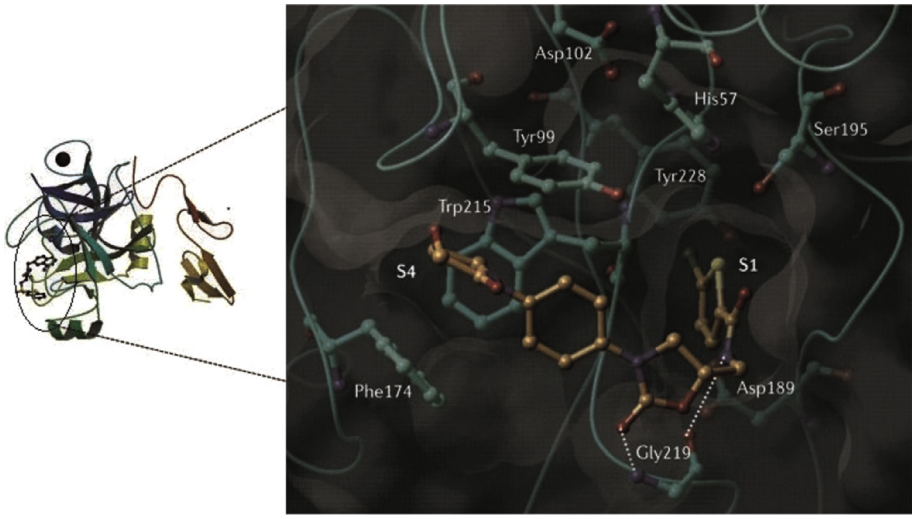

Fig. 3. X-ray crystal structure of FXa along with Rivaroxaban (PDB code: 2W26). Used with permission from Roehrig, S. et al. *J. Med. Chem.* 48, 2005, 5900–5908 (copyright© 2005, American Chemical Society).

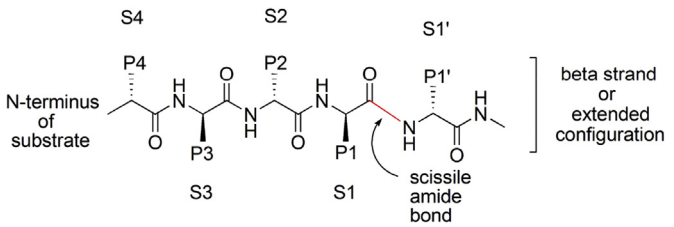

Fig. 4. Nomenclature for substrate/inhibitor residues and the corresponding binding sites in the enzyme.

the selectivity issue. There are different schools of thoughts as per literature regarding the selective binding of various inhibitors to FXa or to thrombin [43–47]. However, a more clear picture regarding the selectivity issue was given by Bhunia et al. [48] with the help of ligand and structure based modeling approaches. The most noticeable difference in thrombin from FXa (Fig. 5B) is the presence of D-pocket in thrombin (Fig. 5A), composed of Tyr60A-Pro60B-Pro60C-Trp60D residues [49]. This pocket in thrombin is considered as an important recognition site for the development of thrombin-selective inhibitors [48,50]. In both FXa and thrombin, the S1 pocket is highly similar to each other having two residues, Asp189 and Tyr228, and Cys191-Cys220 residues located at the bottom of the site. S1 pocket could be playing an important role toward potential inhibition of both the enzymes. The S1 pocket is about 12 Å deep, made up of two antiparallel β-sheets which form a partial roof by undergoing U-turn at the entry of S1-pocket. This partial roof was named as S2-pocket where the two amino acid residues namely Gly216 and Gly218 were found to play a critical role for potential inhibition of FXa whereas three amino acid residues (Gly216, Gly219 and Ser214) were found to play the same role

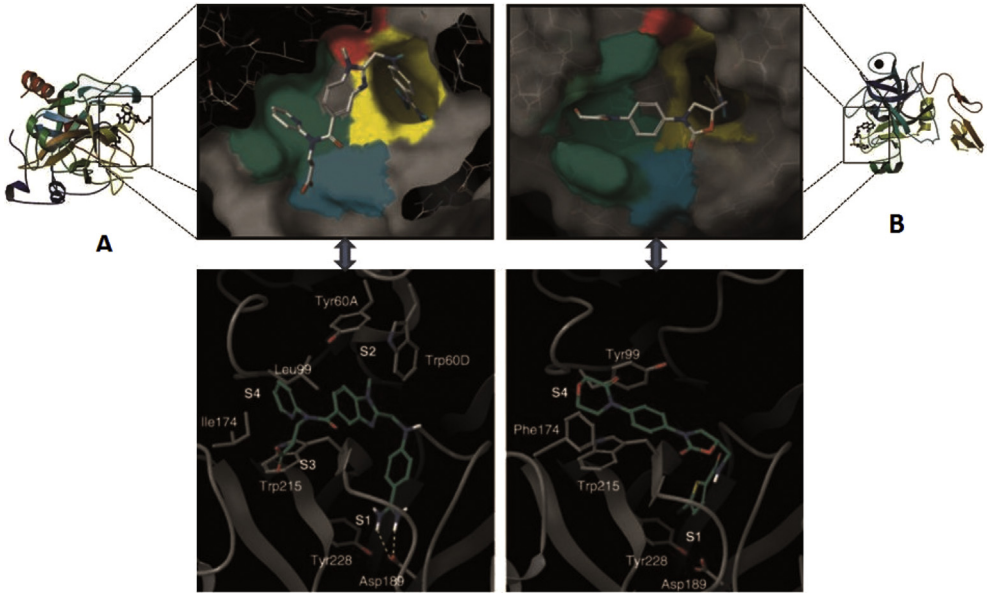

Fig. 5. Comparison of active site of (**A**) thrombin and (**B**) FXa. Top left: Thrombin complexed with Dabigatran (PDB code 1KTS) and Top right: FXa complexed with Rivaroxaban (PDB code 2W26). Used with permission from Straub et al. Angew. Chem. Int. Ed. Engl. 50, 2011, 4574–4590 (copyright© 2011, John Wiley & Sons Inc.).

in thrombin. Co-crystallization experiments have established the fact that these residues of S2 pocket are actually involved in forming H-bonds with the bound molecules. As far as amidine-based inhibitors are concerned, it has been reported that NH group of amidine formed strong H-bond with residual water located near Tyr228. In case of non-amidine based inhibitors, instead of interaction with the water residue, chloro group of the inhibitor is responsible to make strong bonding with Tyr228 in this pocket through van der Waals interactions. Additionally another molecular recognition site i.e. S3 pocket made up of Glu192 in thrombin and Gln192 in FXa called as esteric site, is present. Carboxylate group containing compounds interact more favorably with glutamine in FXa than with glutamate in thrombin. Differences in S4 pockets are more prominent between both of them. In thrombin this subsite is formed by leu99, Ile174 and Trp215 at the bottom while it is comparatively more symmetrically formed by the corresponding Tyr99 and Phe174 in FXa, which make an "aromatic box" along with Trp215 [49].

1.5. Factor Xa as a promising target for the development of antithrombotic drugs

Factor X, a vitamin K-dependent serine protease is secreted in blood as an inactive zymogen. This inactive form is converted into the active form FXa by the factor TF-VIIa complex through the extrinsic pathway or by factor IXa-VIIIa complex through the intrinsic pathway (Fig. 1). FXa is the key enzyme in the blood clotting pathway which converts prothrombin to thrombin. On the surface of the phospholipid membrane of activated platelets, FXa forms a complex with prothrombinase and factor Va in the presence of calcium ions [51]. Thus, FXa plays a central role in the enzymatic activation of blood coagulation cascade and controls hemostasis by regulating thrombin generation and formation of fibrin subsequently in both the models i.e. cascade model (Fig. 1) as well as the cell-based model (Fig. 2). Factor Xa is responsible for the propagation of coagulation process by converting prothrombin (Factor II) to thrombin (Factor IIa). One molecule of FXa is responsible for generation of more than 1000 thrombin molecules [52]. FXa thus plays a crucial amplifying role in the coagulation process.

Drug discovery programs for oral anticoagulants were initially focussed on developing strategies for inhibition of thrombin. But the available data supported the fact that FXa is a more important target than thrombin for the development of orally active small molecule anticoagulants [26]. Inhibition of FXa could prove to be more effective than direct inhibition of thrombin because of its upstream position from thrombin in the amplification cascade [53,54]. Selective inhibition of FXa has less bleeding risks because the pre-existing normal thrombin level, and activation and aggregation of platelets is not affected [55–58]. Several preclinical studies indicated that FXa inhibitors had a broader therapeutic window than direct thrombin inhibitors [59–62]. FXa has attracted substantial attention of medicinal chemists to develop novel antithrombotic drugs due to its pivotal role in coagulation cascade. U.S. Food and Drug Administration (FDA) has approved three orally active selective FXa inhibitors: Rivaroxaban **1** [63,64], Apixaban **2** [65] and Edoxaban **3** [66], while several others like Betrixaban **4** and Eribaxaban **5** are under different stages of clinical trials (Fig. 6) [30,67,68]. However, these FXa inhibitors have been reported to manifest many drawbacks like long half-life, drug-drug interactions [30,69], bleeding risks [70] and narrow clinical indications [71,72]. So, there is a need to develop novel potent FXa inhibitors as ideal oral anticoagulants with better safety and predictable pharmacokinetic profiles.

2. Designing strategies adopted for the development of FXa inhibitors

First crystal structure of FXa was reported in 1994 and till date 656 structures are available in protein data bank having 224 entries for Homosapiens [73]. After 2010 almost 33 entries of holo enzyme structures have been reported [74–86] with various inhibitors (Table 1; key terms used for search criterion "coagulation Fxa + Homosapiens + 2010–2015" in PDB). As per the inputs obtained from the enzymatic studies and the available crystallographic structure of FXa, three pharmacophore units i.e. P1 moiety, P4 moiety and a central scaffold are required to be present in potential FXa inhibitors. Availability of crystal structures of FXa bound to various inhibitors has enabled researchers to identify suitable chemical moieties capable of bonding to S1 and S4 pockets of FXa using structure based drug design approach for the designing of better FXa inhibitors. Going back to early days of developments, most of the FXa inhibitors were developed by using amidine grouping as P1 and P4 motif. But due to lack of oral bioavailability and nonselectivity of amidine-based FXa inhibitors, amidine was replaced by some nonbasic functional groups as P1 motifs. Initially, efforts were made to develop orally active selective FXa inhibitors having halo or other substituted benzenes as P1 motifs. Halo derivatives particularly chloro substituted moieties (5-chlorothiophen-2-yl moiety in Rivaroxaban **1**, 5-chloro-2-aminopyridine in Betrixaban **4** and Edoxaban **3**, and 4-chlorobezene in Eribaxaban **5**) and 4-methoxybenzenes (Apixaban **2** and Darexaban **88**) have proved to be successful P1 motifs. These neutral chlorinated P1 motifs bind effectively to Tyr228 of S1 pocket by C—Cl—π interaction and thus improve selectivity and oral bioavailability [76,87,88]. On the other side, amidine or bezamidine as P4 motifs were also replaced by bi- and mono-aryl motifs [75,86,89]. To connect the P1 and P4 moieties, various central scaffolds have been explored to form U/V or L shaped molecules [48,90–94]. Different P1, P4 and central scaffolds have been identified by various research groups to develop orally active selective FXa inhibitors [28,49,68,95–97]. Some of the preferred and frequently used P1 and P4 motifs, and the central scaffolds or linkers have been described below.

2.1. P1 motifs used for designing of FXa inhibitors

2.1.1. Amidine derivatives as P1 motifs

Amidines (Fig. 7) like acetamidine **6** [98], benzamidine **7** [99], naphthalene-2-carboxamidine **8** [100] have been reported as P1 motifs for the development of FXa inhibitors.

2.1.2. Halo derivatives as P1 motifs

Halogen containing homo/heteroaromatic groups (Fig. 8) like 2-chlorothiophene **9** [101], 4-chlorobenzene **10** [102], 5-chloropyridine **11** [103], 2-(5-chlorothien-2-yl)ethenyl **12** [104], 5-chlorobenzo[*b*]thiophene **13** [105], 6-chlorobenzo[*b*]thiophene **14**, 3,6-dichlorobenzo[*b*]thiophene **15**, 6-chloronaphthalene **16** [106,107], 7-chloroisoquinoline **17**, 6-chloro-4-quinolinone **18**, 6-chloro-4-quinazolinone **19**, 1-fluoronaphthalene **20** [84], 5-chloroindole **21** and 3-chloroindole (**22**, **23**) [84,108] have been reported to show favourable interaction with S1 pocket of FXa.

2.1.3. Substituted benzenes as P1 motifs

Substituted benzenes (Fig. 9) like 3-aminobenzo[*d*]isoxazole **24** [109], 3-aminoindazole **25**, 1-aminoisoquinoline **26**, 3-benzylamine **27**, 4-methoxybenzene **28** [110], 2-benzylamine **29** and 3-benzamide **30** [111] have been also reported as P1 motifs.

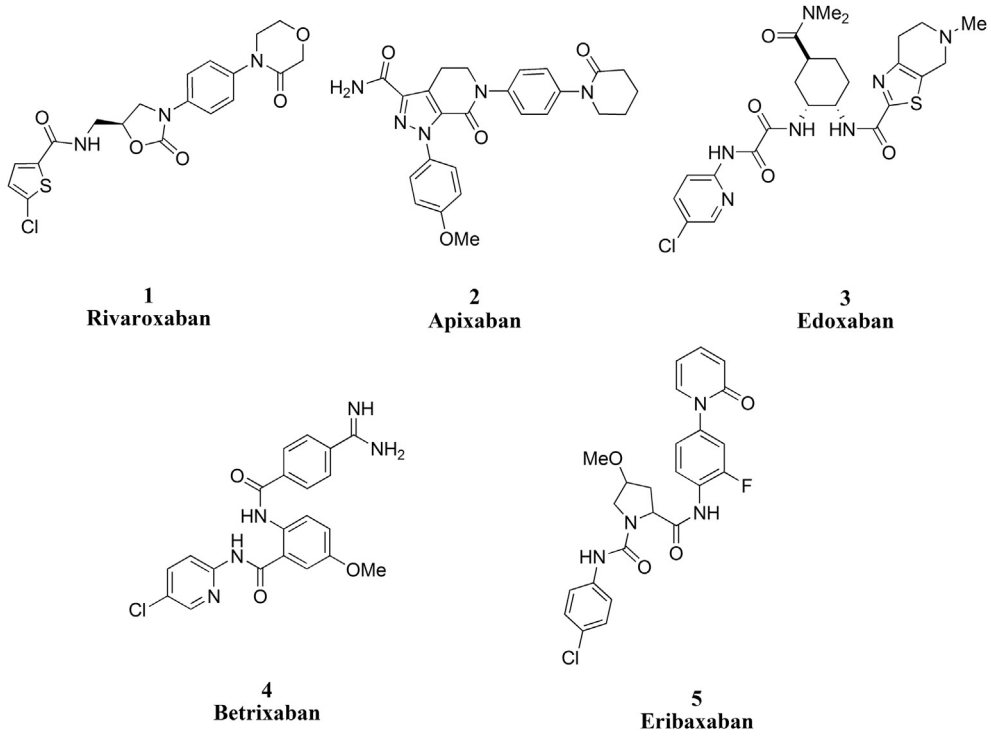

Fig. 6. Some well known FXa inhibitors (**1**–**5**).

2.2. Central scaffolds used for attaching P1 and P4 motifs

To connect both of the pharmacophores (P1 moiety and P4 moiety), several central scaffolds (Fig. 10) such as pyrazole **31** [112], oxazolidin-2-one **32** [94], pyrrolidin-2-one **33** [105], piperazine **34** and **35** [113], 4,5-dihydropyrazolo[3,4-*d*]pyrimidine-3-carboxamide **36** [114], 1,3-diazepan-2-one **37** [115], 4,5,6,7-tetrahydro-4-oxo-pyrazolo[4,3-*c*]pyridine-3-carboxamide **38** [116], pyrrolidine-1,2-dicarboxamide **39** [117], cyclohexane-1,2-diamine **40** [84], 2-aminobenzamide **41** [89,90,118,119] have been used for the development of FXa inhibitors.

2.3. P4 motifs used for designing of FXa inhibitors

2.3.1. Monoaryls as P4 motifs

Monoaryl groups (Fig. 11) like 1-phenylpiperidin-2-one **42** [118], 1-phenylpiperazine/morpholine/piperidine **43** [40], 4-(piperidin-1-yl)pyridine **44** [120], 4-phenylmorpholin-3-one **45** [64], 1-phenylpyrrolidin-2-one **46**, 2-(methanesulfonyl)benzene **47** [121], pyridin-2-one **48** [118], pyridine *N*-oxide **49** [122], 1-benzylpyrrolidine **50** [123], 2-(pyrrolidin-1-yl)methyl-1*H*-imidazole **51** [104] have been used as P4 motifs.

2.3.2. Biaryls as P4 motifs

Biaryls (Fig. 12) like substituted biphenyls **52**–**55** [124,125], 1-phenylpyridin-2(1*H*)-one **56** [118], 1-(3-fluorophenyl)-1*H*-imidazol-2-yl-*N*,*N*-dimethylmethanamine **57** [126] were reported as P4 motifs.

2.3.3. Miscellaneous groups as P4 motifs

Several other groups (Fig. 13) like piperidin-2-one **58**, morpholin-2-one **59** [121], *N*-methylpiperazine **60**, N-substituted 4*H*-imidazol-2-amine **61** [119], oxazolidin-2-one **62** [121], *N*,*N*-dimethylamidine **63** [103], 4,5,6,7-tetrahydro-5-methylthiazolo[5,4-*c*]pyridine **64** [122], 1*H*-pyrrolo[3,2-*c*]pyridine **65** [127], 1-(1-methylpiperidin-4-yl)piperazine **66** [128] have also been reported as P4 motifs.

Different research groups have designed molecules incorporating the above said pharmacophoric groups as FXa inhibitors. A large number of FXa inhibitors belonging to various chemical classes like arylpropanoic acid, arylsulfamoylacetic acid, isoxazoline, isoxazole, pyrazole, pyrrolidinone, aminopiperidine, lactam, piperazine, anthranilamide, disubstituted benzene, diaminocycloalkane and amino acids (glycine, proline and β-aminopropionate) have been reported previously [28,30,49]. In this report we have systemically described the developments in the field since 2010 onward on the basis of chemical classes to which they belong.

2.3.4. Pyrrolidine based FXa inhibitors

Glaxo Smith Kline has remained active in the development of FXa inhibitors (Fig. 14) [75]. Sulfonamidopyrrolidin-2-one containing compound **67** (FXa, $K_i = 4$ nM; $PT_{1.5X} = 1.2$ μM, $t_{1/2} = 0.7$ h, F = 75%), a clinical candidate, was used as a lead molecule for the development of novel FXa inhibitors. Structure and property based drug designing approach was utilized to design novel compounds having similar size, hydrophobicity and molecular weight as that of compound **67**. By considering pharmacokinetics data and structural properties, compounds were reported having different monoaryl motifs as S4 binding ligands. Compound **68a** (FXa, $K_i = 0.8$ nM; $PT_{1.5X} = 0.9$ μM), a mixture of two diastereomers **68b** and **68c**, having *N*,*N*-dimethylamino group as P4 motif and 2-(5-chlorothien-2-yl)ethenyl as P1 motif showed good anticoagulant activity and excellent inhibition of FXa. The individual isomers **68b** (FXa, $K_i = 2$ nM; $PT_{1.5X} = 0.7$ μM, $t_{1/2} = 1.3$ h, F = 54%) and **68c** (FXa, $K_i = 1$ nM; $PT_{1.5X} = 0.9$ μM, $t_{1/2} = 1.6$ h, F = 23%) showed similar profiles. Compound **69a** (FXa, $K_i = 0.8$ nM; $PT_{1.5X} = 2.9$ μM) was a mixture of two diastereomers **69b** and **69c** containing the same P4 *N*,*N*-dimethylamino motif as present in **68a**-**68c** with slightly more bulky 6-chloronaphthyl group as the P1 motif. The isomers **69b** (FXa, $K_i = 2$ nM) and **69c** (FXa, $K_i = 2$ nM) exhibited slightly reduced

Table 1
Crystal structures of FXa along with different inhibitors deposited in the PDB since 2010.

PDB Code	Resolution (Å)	Inhibitor	FXa Inhibition Ki (nM)	Reference
4BTI	2.3	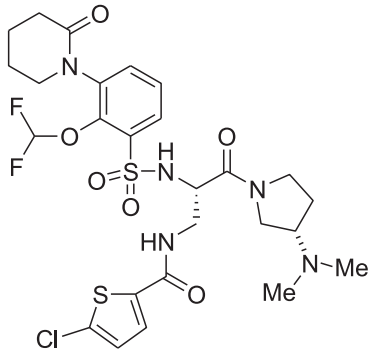	0.2	[76]
4BTT	2.59	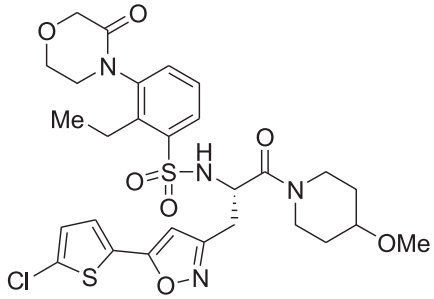	1.43 (IC_{50})	
4BTU	2.37	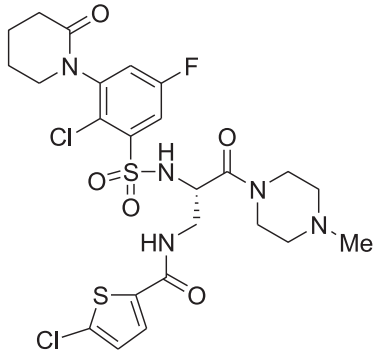	0.5 (IC_{50})	
3TK5	2.2	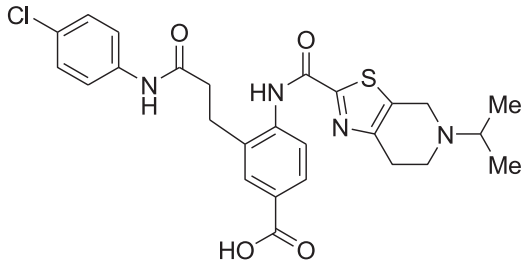	1.3 (IC_{50})	Deposition author(s): Suzuki, M., Mochiuki, A., Nagata, T., Takano, H., Kanno, H., Kishida, M., Ohta, T. Yet to be published
3TK6	1.8	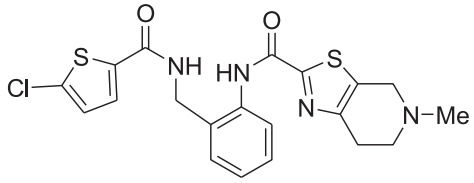	1.7 (IC_{50})	

(*continued on next page*)

Table 1 (*continued*)

PDB Code	Resolution (Å)	Inhibitor	FXa Inhibition Ki (nM)	Reference
4A7I	2.4	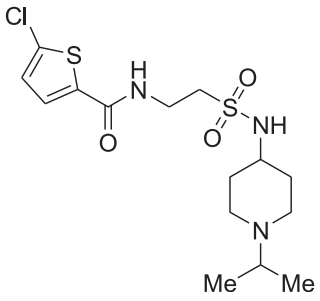	2	[78]
2Y5F	1.29	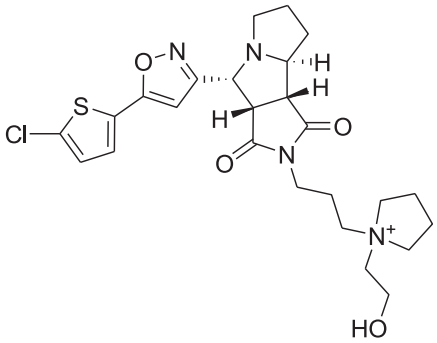	2	[81]
2Y5G	1.29	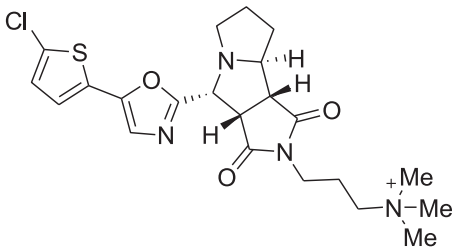	146	
2Y5H	1.33	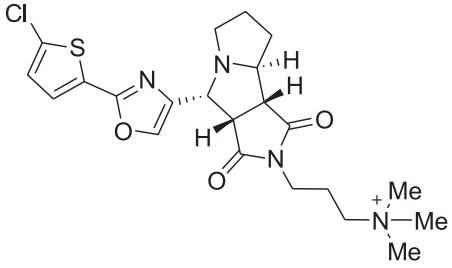	1620	
3Q3K	2.0	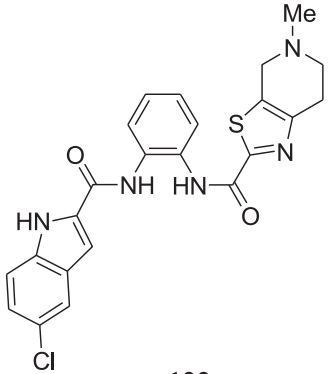	7.4 (IC_{50})	[85]

122

Table 1 (*continued*)

PDB Code	Resolution (Å)	Inhibitor	FXa Inhibition Ki (nM)	Reference
3SW2	2.42	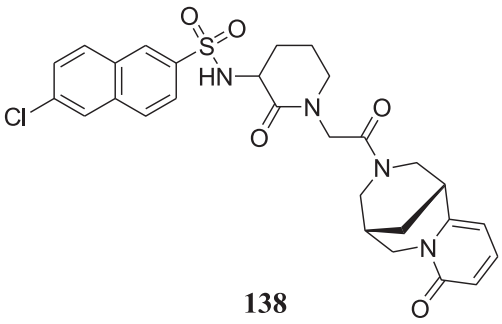 **138**	4.71 13 (IC_{50})	[82]
2Y7X	1.9	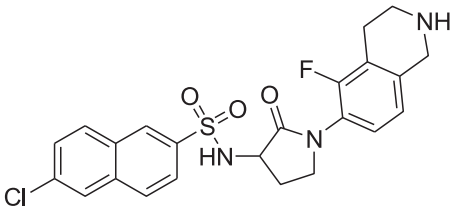 **74**	1	[83]
2Y7Z	1.84	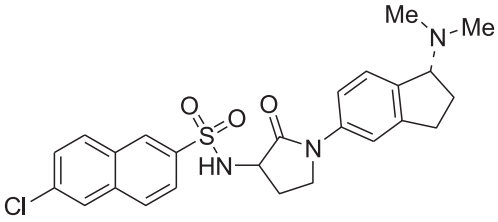 **72c (1*S*)**	2	[86]
2Y80	1.9	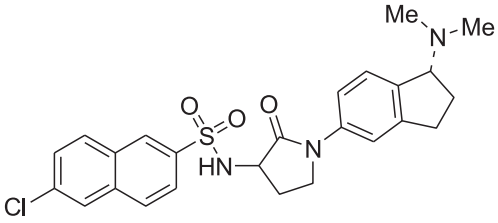 **72b (1*R*)**	9	
2Y81	1.7	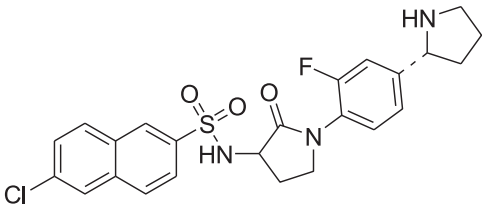 **73b (2*R*)**	2	

(*continued on next page*)

Table 1 (*continued*)

PDB Code	Resolution (Å)	Inhibitor	FXa Inhibition Ki (nM)	Reference
2Y82	2.2	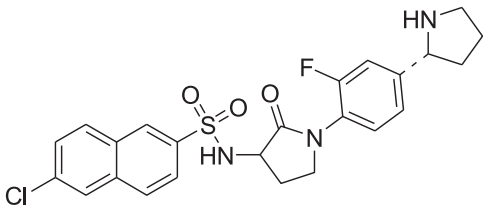 **73c (2*S*)**	4	
2WYG	1.88	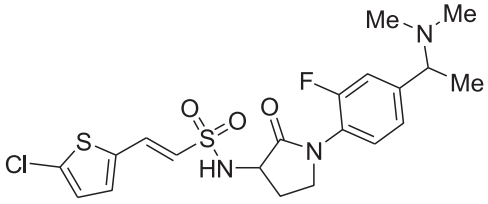 **68b (1*R*)**	2	[75]
2WYJ	2.38	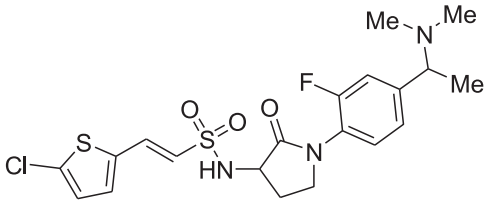 **68c (1*S*)**	1	
2XBV	1.66	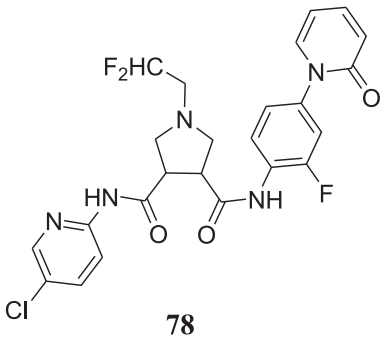 **78**	7	[74]
2XBW	1.72	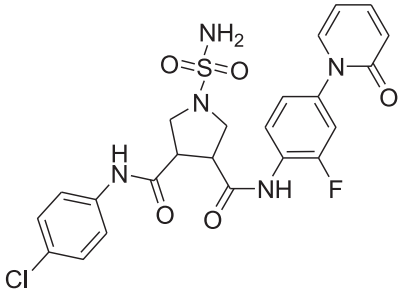	10	

Table 1 (*continued*)

PDB Code	Resolution (Å)	Inhibitor	FXa Inhibition Ki (nM)	Reference
2XBX	1.85	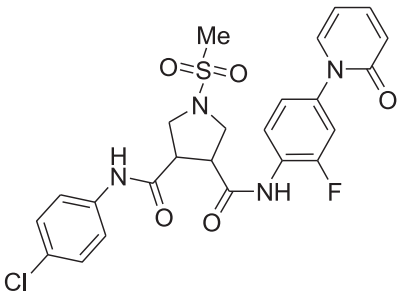	15	
2XBY	2.02	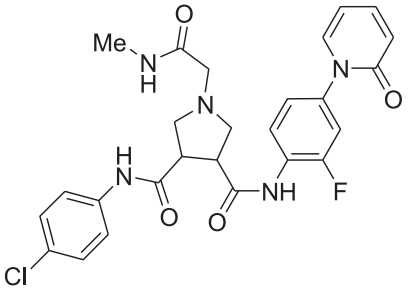	–	
2XC0	2.05	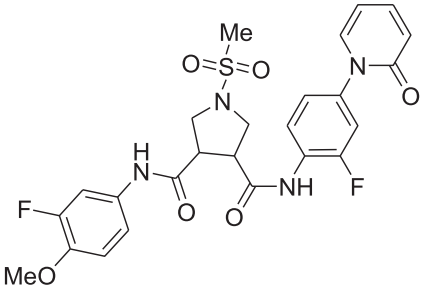	192	
2XC4	1.67	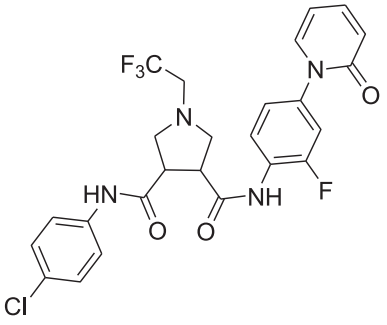	9	
2XC5	1.7	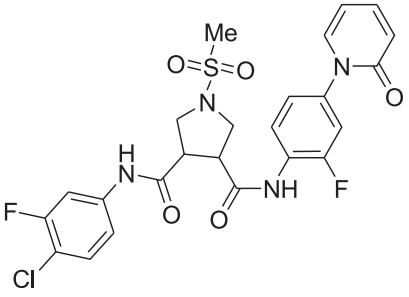	62	

(*continued on next page*)

Table 1 (*continued*)

PDB Code	Resolution (Å)	Inhibitor	FXa Inhibition Ki (nM)	Reference
3IIT	1.8	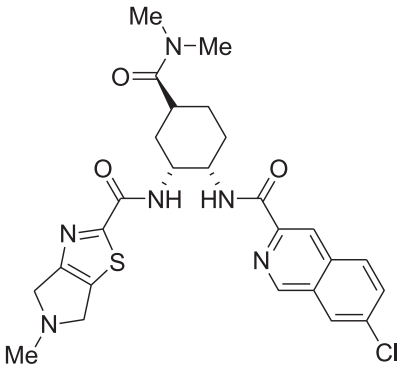	9.5 (IC_{50})	[84]
3M36	2.15	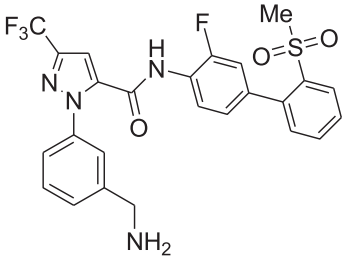 **124**	0.15–150	[79]
3M37	1.9	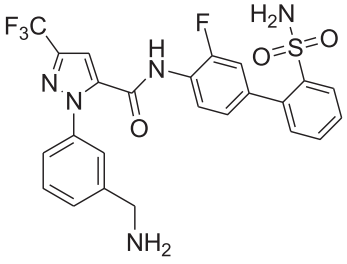	0.91–2.9	
3LIW	2.22	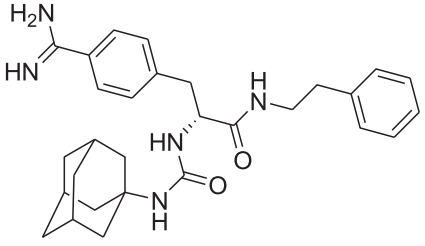	25	[77]
3KQB	2.25	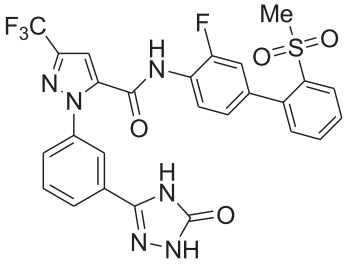 **125**	0.5	[80]

Table 1 (*continued*)

PDB Code	Resolution (Å)	Inhibitor	FXa Inhibition Ki (nM)	Reference
3KQC	2.2	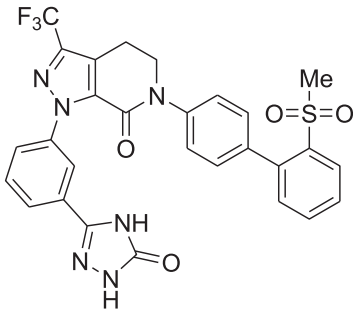	2.2	
3KQD	2.75	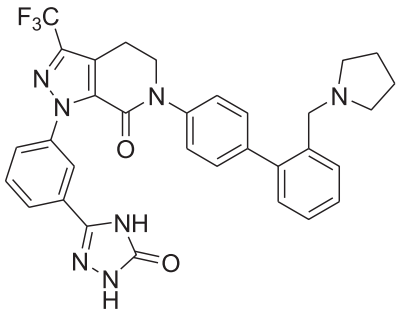	0.4	
3KQE	2.35	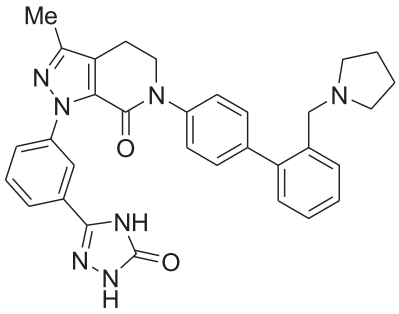	8.1	

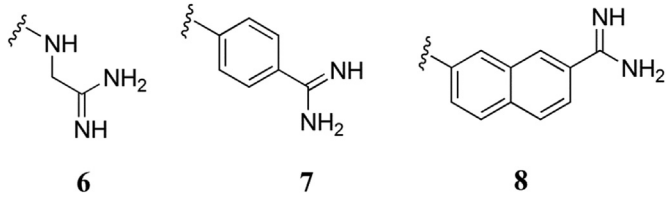

Fig. 7. Amidine derivatives (**6**–**8**) as P1 motifs.

anticoagulant activity ($PT_{1.5X}$ = 1.9 μM and 2.1 μM respectively) but somewhat improved pharmacokinetics profiles in terms of increased half-lives ($t_{1/2}$ = 2.6 h and 2.1 h respectively). *In vitro* metabolism of compounds **69b** and **69c** resulted into formation of demethylated analogs **70** (FXa, K_i = 4 nM; $PT_{1.5X}$ = 6.9 μM) and **71** (FXa, K_i = 2 nM; $PT_{1.5X}$ = 7.0 μM) with comparatively less potent anticoagulant activity.

To overcome the time dependent inhibition (TDI) of CYP3A4 in the α-methylbenzylamine (α-MBA) series, the GSK research group converted the benzylic amino group present in compounds **70** (TDI = 17 fold) and **71** (TDI = 8.5 fold) into cyclic structures like aminoindane **72** and phenylpyrrolidine **73** [86]. TDI of CYP3A4 was determined using diethoxyfluorescein (DEF) and 7BQ as substrates and expressed as fold decrease in the initial IC_{50} value. Among the reported compounds, the aminoindane derivatives showed significant time dependent P450 inhibition (TDI = 2.2 fold). Compounds **73a-73c** having phenylpyrrolidine as the P4 motif demonstrated comparable biological activity (FXa, K_i = 2–4 nM; $PT_{1.5X}$ = 4.5–8 μM) and pharmacokinetics profiles (plasma clearance 2.6–2.8 ml/min/kg, volumes of distribution 1.7–1.9 L/kg, half lives 7.5–10.2 h, oral bioavailability 25–38%) to the clinical candidate **67** (FXa, K_i = 4 nM; $PT_{1.5X}$ = 1.2 μM; Cl_p = 8 ml/min/kg; V_{ss} = 0.29 L/kg; $t_{1/2}$ = 0.7 h and F = 75%). Phenylpyrrolidine containing compound **73b** did not show TDI of CYP3A4 in the diethoxyfluorescein (DEF) assay (TDI = 1.7 fold in 7BQ assay). Tetrahydroisoquinoline (THIQ) derivatives **74** and **75** showed comparable selectivity for tissue plasminogen activator. Thus, to increase FXa selectivity, the compounds were modified by incorporating tetrahydro-2-benzazepine ring as the P4 motif resulting into compound **76** [83].

In efforts to find pyrrolidine based FXa inhibitors with improved pharmacokinetic profile like oral bioavailability and potency, exhaustive research was done on compounds having pyrrolidine scaffold **77** by researchers at Roche (Fig. 14) [74]. Efforts were made to optimize P1 component which showed favourable interactions with S_1 β-pocket. Among this series, compound **78** showed good oral

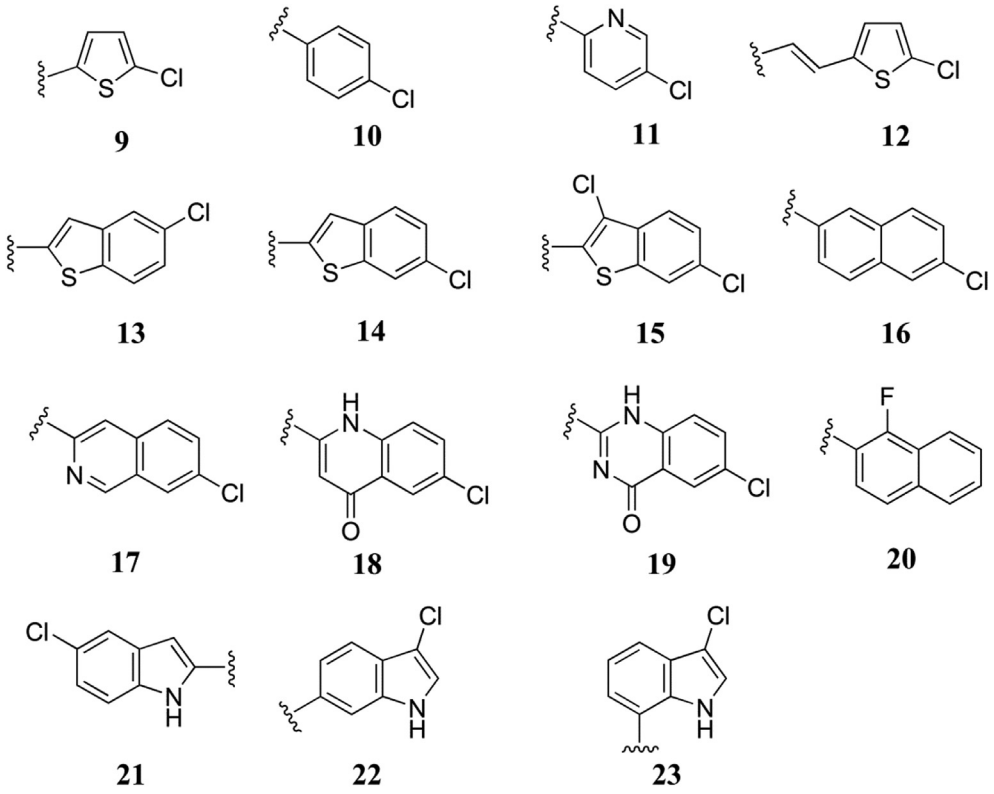

Fig. 8. Halo derivatives (**9**–**23**) as P1 motifs.

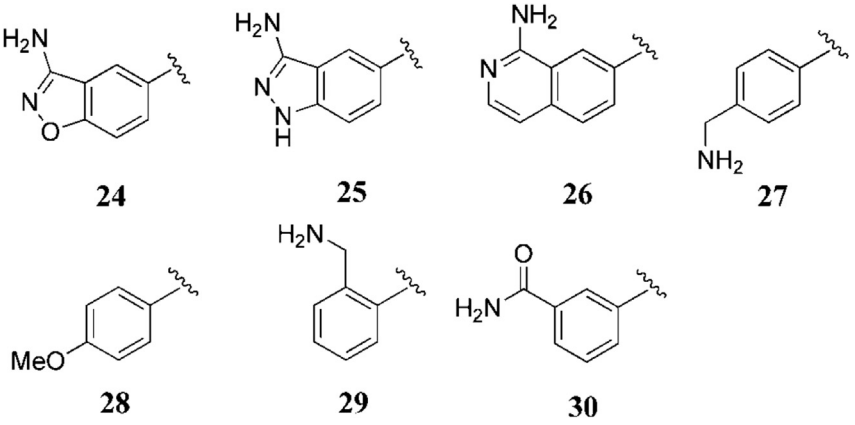

Fig. 9. Substituted benzenes (**24**–**30**) as P1 motifs.

bioavailability (F = 100% in rat and 65% in monkey), excellent selectivity (K_i for FXa = 7 nM, and for thrombin and other serine proteases K_i > 33 μM) and high anticoagulant activity (PT_{2X} = 1.5 μM). Compound **78** has been reported to be selected for clinical trials [74].

2.3.5. Oxazolidinone and isoxazole based FXa inhibitors

On the basis of the structure of the approved FXa inhibitor Rivaroxaban **1**, Xue et al. reported a novel series of fused [5,6,6] tricyclic oxazolidinones (Fig. 15) [121]. After studying the binding mode of Rivaroxaban **1** to human FXa, an additional linker was introduced to form a bridge between oxazolidine ring and phenyl ring without disturbing the structural planarity of the molecule. Structural modifications of both P1 and P4 groups and the linkers resulted into a novel series of FXa inhibitors. Further, SAR and pharmacokinetic studies in rats and dogs resulted into potent and highly selective FXa inhibiting compound **79** (FXa IC_{50} = 3.41 nM; Thrombin IC_{50} > 20 μM) exhibiting good oral bioavailability (F = 92% in dogs) and excellent efficacy in the *in vivo* models of thrombosis (AV-shunt, VT and arterial thrombosis). Compound **79** showed superior *in vivo* efficacy (ED_{50} = 2.97 mg/kg) to Rivaroxaban **1** (ED_{50} = 4.53 mg/kg) in arterial thrombosis model of rats [121].

Investigators at Shenyang Pharm. University have used oxazolidinone scaffold and different P4 motifs to develop a novel series of FXa inhibitors (Fig. 15) [94]. Replacement of morpholin-3-one, the S4 ligand of Rivaroxaban **1** with different motifs like pyrrole, indole and thiazole resulted into compounds having good FXa inhibitory activities. Compound **80** having pyrrole ring showed 98% inhibition

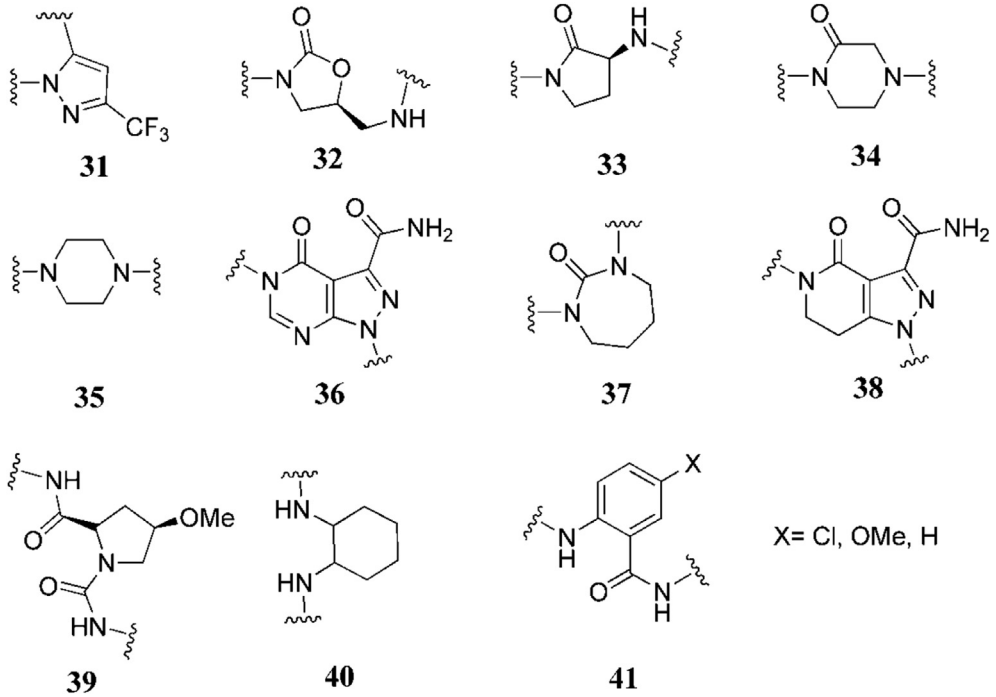

Fig. 10. Central scaffolds (**31**–**41**) used for designing of FXa inhibitors.

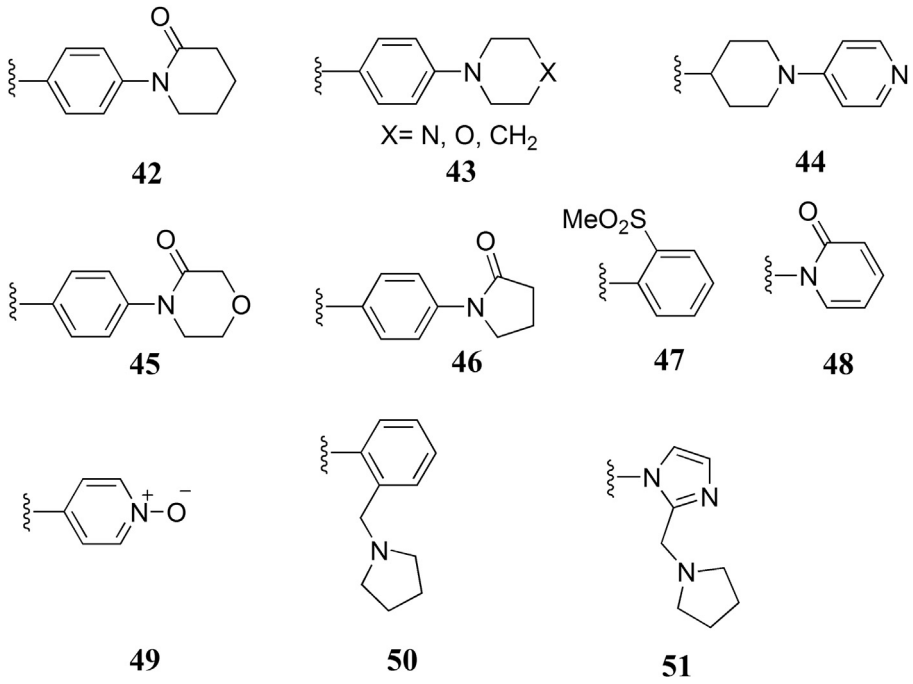

Fig. 11. Monoaryls (**42**–**51**) as P4 motifs.

at 0.1 μM, whereas thiazole containing compound **81** showed 91% inhibition at 0.1 μM. Indole based compound **82** showed 69% inhibition at 0.1 μM. Conversion of dimethylamino group of compound **80** ($PTCT_{2x}$ = 0.61 μM, $aPTTCT_{2x}$ = 1.20 μM) into diethylamino group led to the discovery of compound **83** ($PTCT_{2x}$ = 0.15 μM, $aPTTCT_{2x}$ = 0.30 μM) with an improved anticoagulant profile in human plasma.

With an assumption to prevent degradation of carboxamides into mutagenic anilines, Yang et al. sought to employ bicyclic isoxazole scaffold with different P1 and P4 groups (Fig. 15) [129]. Optimization of P1 and P4 moieties by attaching various substituents led to the discovery of compound **84** having high selectivity (FXa, IC_{50} = 0.013 μM; Thrombin, IC_{50} > 20 μM) and good anticoagulant effect in human plasma (PT_{2x} = 2.12 μM). Molecular docking studies of compound **84** showed π-π interaction of pyrimidinone ring with the phenyl ring of Tyr99 while the carbonyl

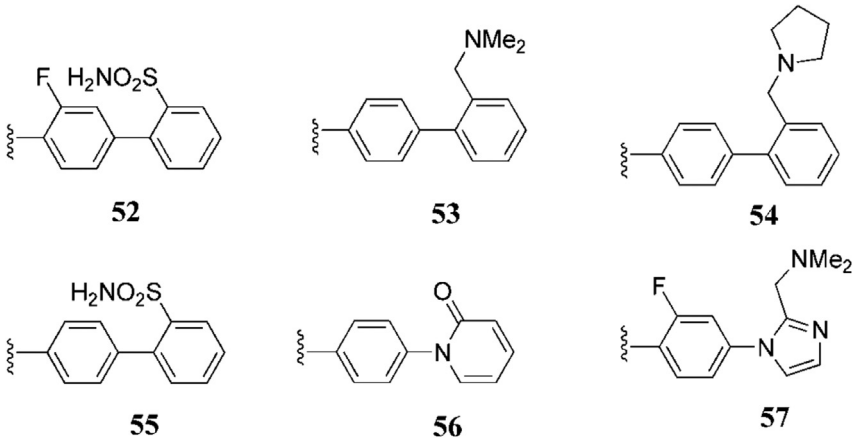

Fig. 12. Biaryls (**52**–**57**) as P4 motifs.

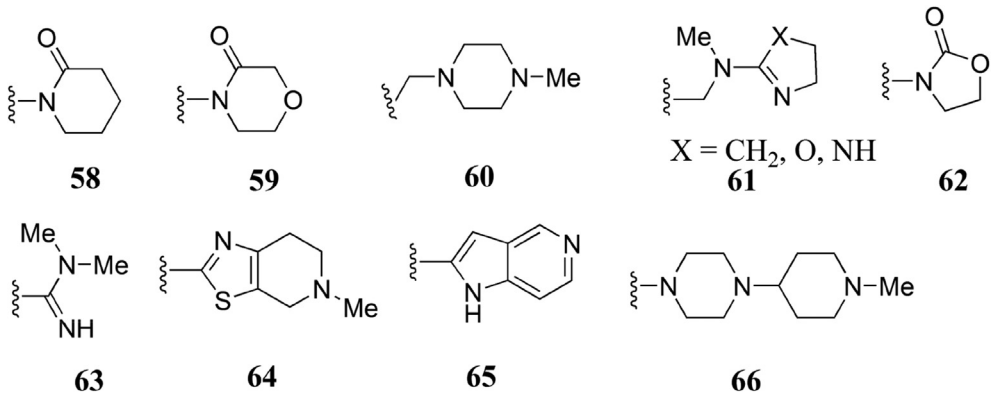

Fig. 13. Miscellaneous groups (**58**–**66**) as P4 motifs.

oxygen of P1 motif showed multiple hydrogen bonds with Ser214 and Trp215. Carbonyl oxygen of pyrimidinone ring showed H-bonding interaction with NH of Gly216 (Fig. 16).

2.3.6. Anthranilamides and disubstituted benzenes as FXa inhibitors

As an output of high-throughput screening (HTS) programme, researchers at Astellas Pharma disclosed compound **85** as a novel lead molecule (Fig. 17) [130]. Optimization of the lead compound **85** (IC_{50} = 6216 nM) by incorporating amidine group led to the development of compound **86**, as a highly selective and potent novel FXa inhibitor (IC_{50} = 8.6 nM, $PTCT_{2x}$ = 0.11 μM). With the aim to increase oral bioavailability, compound **86** was further optimized to a non-amidine group containing compound by substituting amidino group with methoxy group to get compound **87** (FXa, IC_{50} = 103 nM; $PTCT_{2x}$ = 2.8 μM). Introduction of a phenolic hydroxyl group at 3rd position of the central phenyl ring in compound **87** led to the discovery of Darexaban **88** with an improved FXa inhibitory activity (IC_{50} = 54.6 nM) and slightly reduced anticoagulant property ($PTCT_{2x}$ = 4.1 μM). Subsequent metabolic studies on compound **88** demonstrated formation of glucuronide conjugate **89** (FXa, IC_{50} = 28.6 nM; $PTCT_{2x}$ = 2.5 μM) as an active and stable metabolite of compound **88**. Compound **88** (FXa, K_i = 0.031 μM) and its metabolite **89** (FXa, K_i = 0.020 μM) showed higher selectivity for FXa over other serine proteses (K_i of **88** and **89** > 100 μM for FIIa) [130].

Ishihara et al. [131] reported a novel strategy for the discovery of orally active blood coagulation enzyme inhibitors (Fig. 17). The strategy was based on biotransformation of non-amidine inhibitors into more hydrophilic conjugates. Compound **90** (FXa, IC_{50} = 4 nM; $PTCT_{2x}$ = 0.31 μM) a phenol derivative, and the corresponding glucuronide **91** (FXa, IC_{50} = 4.9 nM; $PTCT_{2x}$ = 0.28 μM) showed comparable FXa inhibitory activity to the deshydroxy analog **92** (FXa, IC_{50} = 5.8 nM; $PTCT_{2x}$ = 0.22 μM). Both the compounds **90** and **91** demonstrated higher selectivity for FXa (FIIa, IC_{50} > 100 μM). Pharmacokinetics data indicated rapid transformation of compound **90** to its corresponding glucuronide **91** after oral administration. Thus, biotransformation of compound **90** into a highly hydrophilic conjugate **91** substantially improved its *ex vivo* anticoagulant activity.

Structural analog **93** of Darexaban **88** was also developed by the research group of Astellas Pharma (Fig. 17) [132]. Introduction of phenolic hydroxyl group at the 3rd position of the central phenyl ring of compound **93** (FXa, IC_{50} = 140 nM) resulted into compound **94** (FXa, IC_{50} = 150 nM, PT-prolongation value 1.97 fold after oral administration to mice with a dose of 100 mg/kg) and its corresponding glucuronide derivative **95** (FXa, IC_{50} = 66 nM). Incorporation of chloro group at 5th position of the central phenyl ring of compound **94** led to the identification of compound **96** with enhanced FXa inhibition potency (IC_{50} = 68 nM) and significant anticoagulant activity (PT-prolongation value 3.91 fold). Further structural modifications in the P1 moiety led to the identification of highly potent FXa inhibitor **97** (IC_{50} = 8.7 nM) with significant anticoagulant activity (PT-prolongation value 7.8 fold). The corresponding hydrophilic conjugate compound **98** (FXa, IC_{50} = 1.5 nM) exhibited approximately 40-fold higher activity than the corresponding glucuronide **95** (FXa, IC_{50} = 66 nM). Compound **98** also

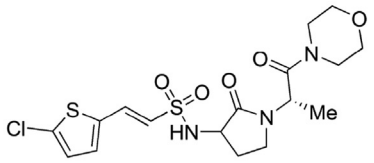

67

FXa, Ki= 4 nM
$PT_{1.5X}$ = 1.2 μM

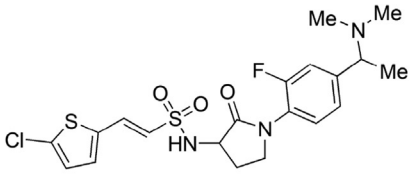

68a-68c

	FXa Ki (nM)	$PT_{1.5X}$ (μM)
68a	0.8	0.9
68b (1*R*)	2	0.7
68c (1*S*)	1	0.9

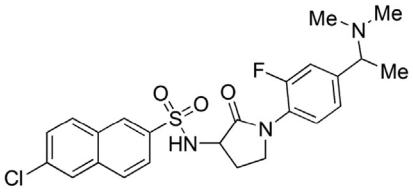

69a-69c

	FXa, Ki(nM)	$PT_{1.5X}$ (μM)
69a	0.8	2.9
69b (1*R*)	2	1.9
69c (1*S*)	2	2.1

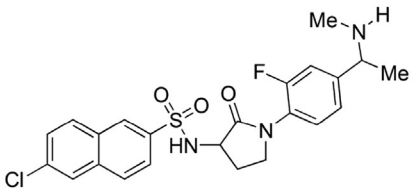

70,71

	FXa, Ki (nM)	$PT_{1.5X}$ (μM)
70 (1*R*)	4	6.9
71 (1*S*)	2	7.0

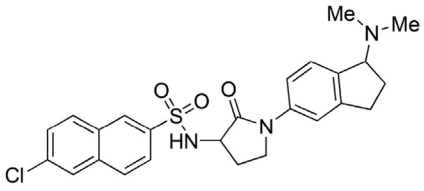

Aminoindanes 72a-72c

	FXa, Ki (nM)
72a	3
72b (1*R*)	9
72c (1*S*)	2

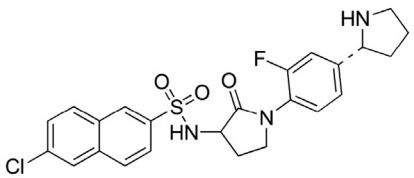

Phenylpyrrolidines 73a-73c

	FXa, Ki (nM)
73a	2
73b (2*R*)	2
73c (2*S*)	4

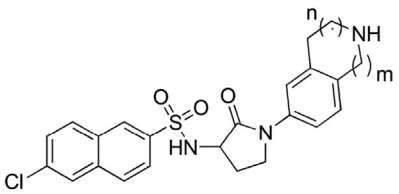

74-76

		FXa, Ki (nM)
74	(m, n = 1)	1
75	(m = 2, n = 1)	10
76	(m = 1, n = 2)	0.8

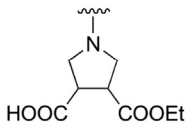

77

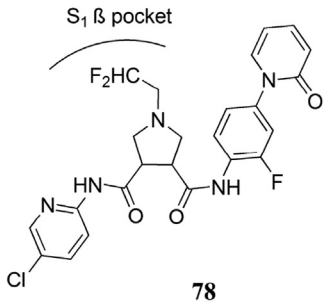

78

FXa, Ki= 7 nM
PT_{2X} = 1.5 μM

Fig. 14. Pyrrolidine based FXa inhibitors (**67**–**78**).

showed higher selectivity for FXa over thrombin (IC_{50} > 100 μM for thrombin).

Yang et al. [133] independently used 3,4-diaminobenzoyl scaffold with different P1 and P4 motifs (Fig. 18). Among the reported series of derivatives, compound **99** with 3,4-dimethoxyl group and compound **100** having 4-acetamido group as S1 binding ligands showed comparable FXa inhibitory activity (FXa, IC_{50} = 17.1 nM and 15.6 nM respectively) to Rivaroxaban **1** (FXa, IC_{50} = 14.4 nM). Compound **99** showed higher selectivity for FXa over other serine proteases like thrombin and trypsin ($IC_{50} \geq 100$ μM for thrombin). Compound **99** also exhibited excellent *in vivo* antithrombotic activity.

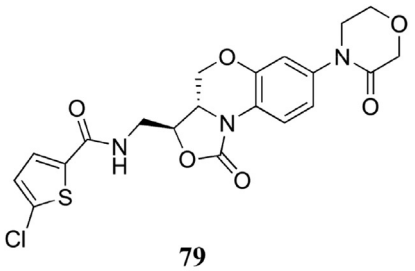

79

FXa, IC_{50} = 3.41 nM

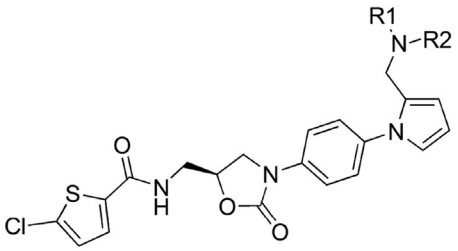

80, 83

	IC_{50} (nM)	% Inhibition (0.1 μM)	$PTCT_{2x}$ (μM)	$aPPTCT_{2x}$ (μM)
80 (R_1, R_2 = Me)	7.24	98	0.61	1.20
83 (R_1, R_2 = Et)	2.01	100	0.15	0.30

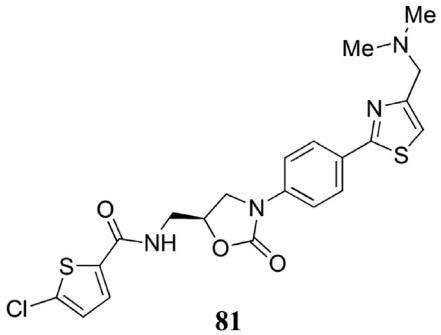

81

(91% Inhibition at 0.1 μM)

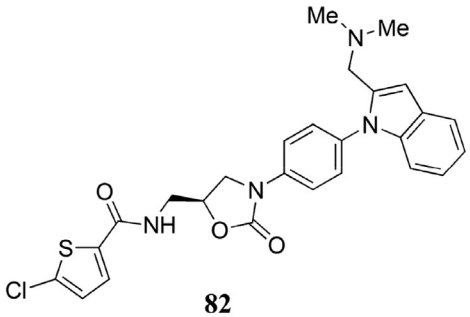

82

(69% Inhibition at 0.1 μM)

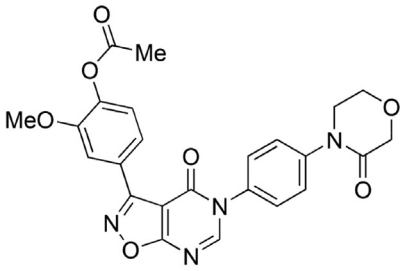

84

FXa, IC_{50} = 0.013 μM

PT_{2x} = 2.12 μM

Fig. 15. Oxazolidinone (**79**–**83**) and isoxazole **84** based FXa inhibitors.

Researchers at Zydus Research Centre reported some anthranilamide based compounds (Fig. 18) [134]. Replacement of the highly basic amidine group (S4 ligand) of Betrixaban **3** by neutral sulfoximine resulted into a series of active compounds. Compound **101** displayed 76% inhibition of FXa at 0.1 μM ($PTCT_{2x}$ = 7.2 μM). Effect of different substituents on nitrogen of sulfoximine group indicated that anticoagulant activity of a compound was a function of its potency, hydrophilicity and plasma-protein binding. Compound **102** bearing methoxyacetyl moiety on the nitrogen of sulfoximine group exhibited increased polarity and improved anticoagulant activity ($PTCT_{2x}$ = 3 μM). Replacement of methoxy group of compound **102** with different alkylamino substituents resulted into highly potent compound **103** (100% inhibition at 0.1 μM and $PTCT_{2x}$ = 0.68 μM). Compound **103** and its metabolite **104** were found to have higher selectivity for FXa (K_i = 1.1 and 1.5 respectively) over other related serine proteases (K_i of >20 μM for thrombin, trypsin and plasmin) and lesser effect on CYP3A4. Compound **103** demonstrated good *in vivo* antithrombotic activity.

Fragment based drug designing and virtual screening approaches were successfully applied by Xing et al. [135] to identify two hits **105** and **106** possessing FXa inhibitory activity (Fig. 18). Structural analogs of these two hits were prepared and evaluated for FXa inhibitory activity. Compound **107** was found as the most potent FXa inhibitor (FXa, IC_{50} = 23 nM) among the reported series of compounds having excellent selectivity (FIIa, IC_{50} = 48 μM) and potent anticoagulant activity (PT_{2x} = 8.7 μM).

2.3.7. Diamines as FXa inhibitors

As is the case with Edoxaban **3**, researchers at Daiichi Sankyo used diamine linker, 2-aminomethylphenylamine as a scaffold, for

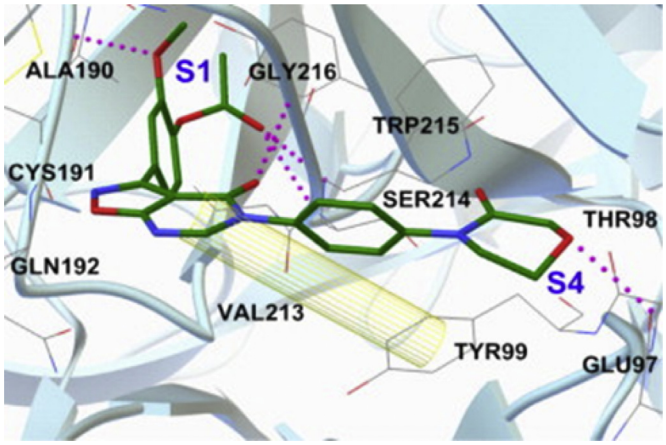

Fig. 16. Docking pose of compound **84** with FXa. Pink dotted lines indicate hydrogen bonds, and π-π interaction of the pyrimidone ring with the phenyl ring of Tyr99 is shown as yellow column. Used with permission from Yang et al. *Bioorg. Med. Chem. Lett.* 25, 2015, 492–495 (Copyright© 2014 Elsevier Ltd.). (For interpretation of the references to color in this figure legend, the reader is referred to the web version of this article.)

connecting S1 and S4 binding ligands (Fig. 19) [91]. Compound **108** (FXa, $IC_{50} = 1.7$ nM; $PTCT_{2x} = 0.50$ μM) was reported to show highly potent activity in rat and monkey models. Compound **108** was also found to have low aqueous solubility (17 μg/ml at pH 6.8) and moderate metabolic stability (53%) in human liver microsomes.

To overcome these issues, compound **108** was further modified by introduction of polar groups on the central phenyl ring resulting into compound **109** (FXa, $IC_{50} = 2$ nM; $PTCT_{2x} = 0.85$ μM) having good inhibitory activity in monkeys with higher solubility (>850 μg/ml at pH 6.8). Modifications of S4 binding ligands led to the discovery of *N*-isopropyl derivative **110** (FXa, $IC_{50} = 0.93$ nM; $PTCT_{2x} = 0.62$ μM) exhibiting higher inhibitory activity and metabolic stability (96%) than compound **109**. To reduce the risk of metabolic instability of thiophene moiety, investigators prepared phenypropionylamide derivatives and reported some potent compounds such as **111**–**113**. X-ray crystal structure of human FXa with compound **112** bound to it showed interactions of the chlorothiophene and thiazolopyridine groups with S1 and S4 pockets respectively. The central phenyl ring of compound **112** was observed near to the S1β-pocket. On the basis of interaction studies of compound **112** with FXa, researchers reported novel zwitterionic compounds such as **114**–**118** by attaching fluoro, chloro, trifluoromethyl, methoxy and ethoxy groups to the central phenyl ring of compound **112**. All these compounds **114**–**118** showed potent inhibitory activity and long duration of action after oral administration in monkeys. Compounds such as **110**, **112**, **113** and **115** displayed higher AUC values (605, 1368, 785 and 724 ngh/ml respectively) than compound **109** (AUC = 247 ngh/ml). The oral bioavailability of compounds **110**, **112** and **115** was found to be 51%, 67% and 52% respectively. Compounds **112** and **115** also showed small C_{max}/C_{24h} of 3.3 and 3.9 respectively [136].

Daiichi Sankyo researchers discovered alternative scaffolds to cyclohexanediamine present in Edoxaban **3**, such as ethylenediamine and phenylenediamine (Fig. 19) [85]. Unsubstituted ethylenediamine derivative **119** (FXa, $IC_{50} = 221$ nM; $PTCT_{2x} = 18$ μM) with chloroindole as the S1 binding ligand and thiazolotetrahydropyridine as the S4 binding ligand showed moderate FXa inhibitory activity. Introduction of methyl acetate group on C-1 position of ethylenediamine in *S* configuration resulted into compound **120** (FXa, $IC_{50} = 70$ nM; $PTCT_{2x} = 6.5$ μM) with improved FXa inhibitory activity. Replacement of methoxy group of **120** with dimethylamino group resulted into compound **121** (FXa, $IC_{50} = 47$ nM; $PTCT_{2x} = 3.2$ μM) with modest FXa inhibitory activity. Phenylenediamine as a new scaffold was also identified by this group. Compound **122** (FXa, $IC_{50} = 7.4$ nM) having phenylenediamine as the spacer and the same P1 and P4 groups as present in compound **119**, demonstrated strong FXa inhibitory activity. Substitution of carboxylic function at the 4th position of phenylenediamine increased the inhibitory activity against FXa. Compound **123** showed magnificent FXa inhibitory potency (FXa, $IC_{50} = 2.2$ nM) and good anticoagulant activity ($PTCT_{2x} = 3.9$ μM) along with improved solubility (71 μg/ml at pH 1.2 and 362 μg/ml at pH 6.8). Compound **123** showed 91% *ex vivo* FXa inhibitory activity after intravenous administration in rats, and high metabolic stability but low permeability.

2.3.8. Pyrazole based FXa inhibitors

Development of pyrazole based FXa inhibitors has been considered as an interesting approach due to the success of Apixaban **2**. During extensive efforts to develop a conceivable back up to Apixaban, Bristol-Myers Squibb researchers discovered phenyltriazolinone containing compounds having excellent affinity for FXa (Fig. 20) [80]. Efforts were made to replace benzylamine group (P1 moiety) in compound **124** with different heterocyclic analogs resulting into compound **125** having phenyltriazolinone as S1 binding ligand with high affinity for FXa ($K_i = 0.5$ nM). Introduction of phenyltriazolinone to the bicyclic pyrazole scaffold of Apixaban **2** resulted into compound **126** with good selectivity (FXa, $K_i = 0.25$ nM; FIIa, $K_i > 6000$ nM) and comparable anticoagulant activity (PT $EC_{2x} = 4.4$ μM) to Apixaban **2** (FXa, $K_i = 0.08$ nM; PT $EC_{2x} = 3.8$ μM). X-ray crystal studies of compounds bound to the human FXa enzyme indicated that phenyltriazolinone motif was accommodated in S1 pocket of FXa due to re-orientation of a side chain of Asp 189. Efforts have also been made by this group to identify different P4 moieties by replacing the lactam ring of Apixaban [137]. Compound **127** bearing a neutral hydroxymethyl group as a P4 motif showed good FXa affinity (FXa, $K_i = 0.66$ nM; FIIa, $K_i = 2578$ nM) and moderate anticoagulant activity (PT $EC_{2x} = 3.8$ μM) along with good pharmacokinetic profile in dogs (clearance value of 0.98 L/kg/h, V_{dss} value of 3.02 L/kg, $t_{1/2}$ value of 4.95 h and F value of 50%). Compound **128** with methylsulfone as the P4 moiety exhibited high FXa affinity, good anticoagulant activity (FXa, $K_i = 0.48$ nM; PT $EC_{2x} = 3.90$ μM) and a favourable pharmacokinetic profile (clearance = 0.32 L/kg/h, $V_{dss} = 0.51$ L/kg, $t_{1/2} = 1.70$ h and F = 79%).

2.3.9. Coumarins as FXa inhibitors

As coumarin derivatives were known to possess anticoagulant activity, Amin et al. [138] employed coumarin as a scaffold to develop novel FXa inhibitors with favourable biological profiles (Fig. 21). A novel series of amidino derivatives was found to exhibit prothrombin time comparable to warfarin (PT = 42.3 s). Compound **129** was found to be the most potent one with a PT value of 36.5 s. Substitution on the nitrogen of amidine in compound **129** with hydroxyl group resulted into compound **130** with good anticoagulant activity (PT = 26.0 s). Some novel compounds containing heterocyclic moieties substituted at 6-position of the coumarin ring were also reported. Cyclization of amidoxime group of compound **130** led to identification of the most potent anticoagulant compound **131** with a PT value of 42.3 s similar to warfarin. Compounds having pyrazole **132** and coumarinyloxadiazole **133** showed good anticoagulant activity with PT values of 38.5 s and 37.8 s respectively.

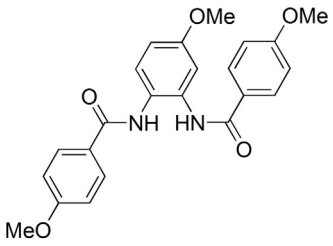

85

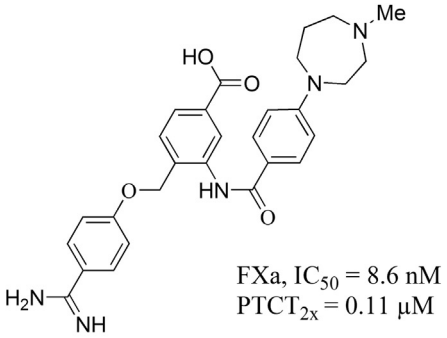

FXa, IC_{50} = 8.6 nM
$PTCT_{2x}$ = 0.11 μM

86

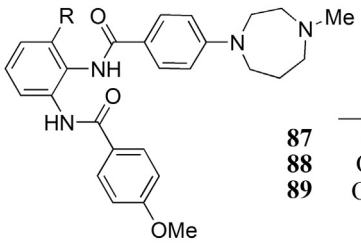

	R	FXa, IC_{50} (nM)	$PTCT_2$ (μM)
87	H	103	2.8
88	OH	54.6	4.1
89	OGlu	28.6	2.5

87-89

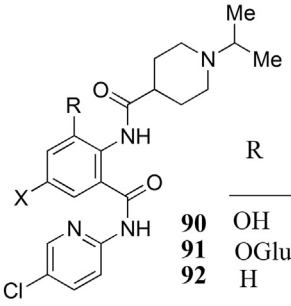

	R	X	FXa, IC_{50} (nM)	$PTCT_2$ (μM)
90	OH	Br	4.0	0.31
91	OGlu	Br	4.9	0.28
92	H	Cl	5.8	0.22

OGlu =

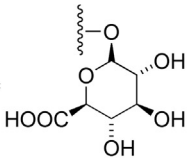

90-92

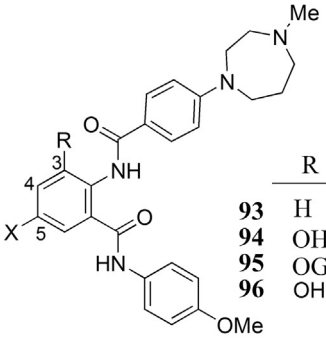

	R	X	IC_{50} (nM)
93	H	H	140
94	OH	H	150
95	OGlu	H	66
96	OH	Cl	68

93-96

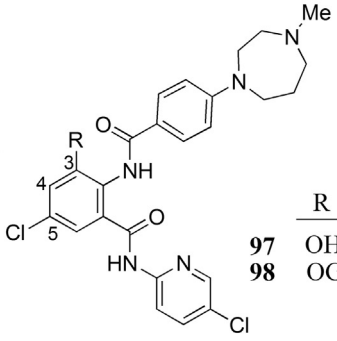

	R	IC_{50} (nM)
97	OH	8.7
98	OGlu	1.5

97, 98

Fig. 17. Disubstituted benzenes (**85**–**89**) and anthranilamides (**90**–**98**) reported by Astellas Pharma.

2.3.10. Arylsulfonamidopiperidone derivatives

Researchers at Bristol-Myers Squibb reported a novel series of compounds **134**–**138** having the arylsulfonamide-valerolactam scaffold (Fig. 22) [82]. Benzofuran sulfonamidopiperidin-2-one **134** (FXa, IC_{50} = 1110 nM) with pyrrolidine as the P4 moiety was modified utilizing different aromatic rings as the P1 moiety. Among the series, compound **135** with 6-chloro-2-naphthyl as the P1 moiety showed good FXa inhibitory (IC_{50} = 32 nM) and anticoagulant (PT EC_{2x} = 12 μM) activities. Replacement of the P4 pyrrolidine moiety of compound **135** with the 3,7-diazabicyclo [3.3.1]nonan-3-yl group and cytisine resulted into more potent compounds **136** (FXa, IC_{50} = 22 nM; PT EC_{2x} = 3.5 μM) and **138** (FXa, IC_{50} = 13 nM; PT EC_{2x} = 4.1 μM) respectively. X-ray crystal structure of compound **138** in the bound form to human FXa revealed that the 6-chloro-2-naphthyl group binds to the S1 pocket, with the acylcytisine group occupying the S4 pocket. Derivatization

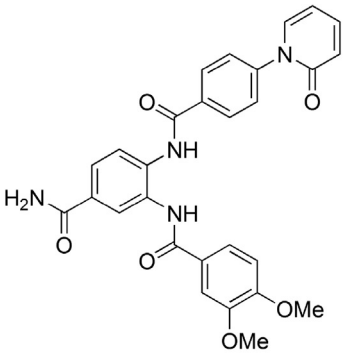

99
FXa, IC_{50} = 17.1 nM

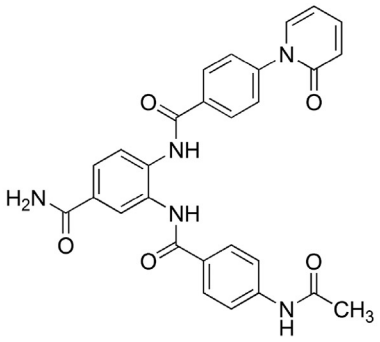

100
FXa, IC_{50} = 15.6 nM

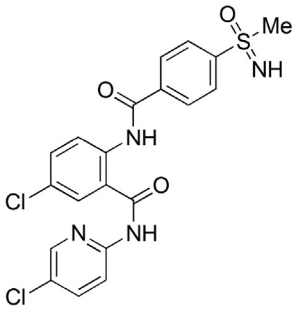

101
76 % Inhibition at 0.1 μM
$PTCT_2$ = 7.2 μM

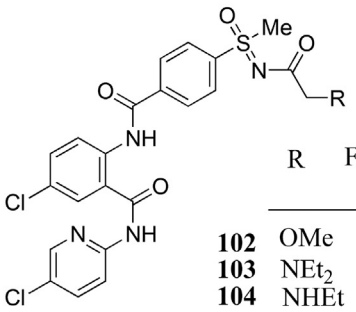

	R	FXa, IC_{50} (nM)	$PTCT_2$ (μM)
102	OMe	-	3.0
103	NEt_2	2.1	0.68
104	NHEt	2.7	0.81

102-104

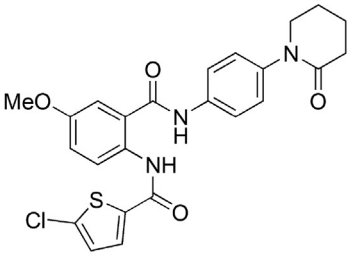

105

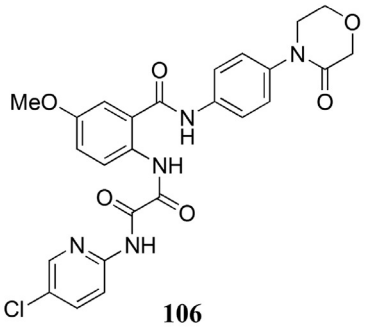

106

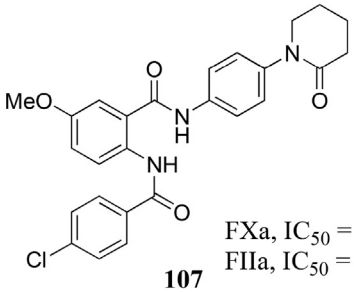

107
FXa, IC_{50} = 23 nM
FIIa, IC_{50} = 48 μM

Fig. 18. Diamidobenzenes (**99**, **100**) reported by Yang et al., anthranilamides (**101**–**107**) reported by Zydus Research Centre and Xing et al.

of NH group of 3,7-diazabicyclo[3.3.1]nonan-3-yl of compound **136** resulted into the formation of the most potent compound **137** (FXa, IC_{50} 7 nM; PT EC_{2x} = 1.7 μM) of the series.

2.3.11. Tetrahydroisoquinolines as FXa inhibitors

Al-Horani et al. [139] discovered tetrahydroisoquinoline as a novel scaffold having two hydrophobic arms which are the structural requirements for inhibition of FXa (Fig. 23). Compound **139** was identified as a novel hit from the molecular modeling studies of FXa inhibitors. Replacement of piperidone ring of **139** (FXa, IC_{50} = 56 μM) with morpholin-3-one resulted into compound **140** (FXa, IC_{50} = 36 μM) with somewhat improved activity. The *p*-chlorophenylacetyl group as the P1 moiety in compound **141** (IC_{50} = 1.3 μM) showed a high affinity for FXa. Further optimization of the structure led to discovery of dicarboxamide **142** (IC_{50} = 0.27 μM) as a highly efficacious FXa inhibitor with a K_i value

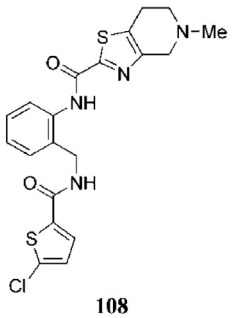

108
FXa, IC_{50} = 1.7 nM
$PTCT_2$ = 0.50 μM

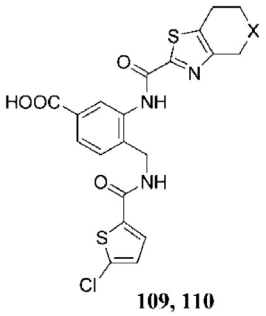

109, 110
109 X = N-Me; FXa, IC_{50} = 2 nM; $PTCT_2$ = 0.85 μM
110 X = N-Pr; FXa, IC_{50} = 0.93 nM; $PTCT_2$ = 0.62 μM

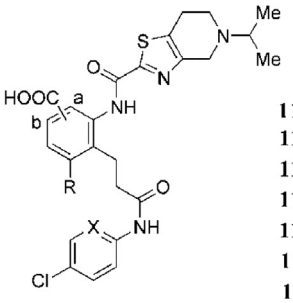

	R	X	FXa, IC_{50} (nM)	$PTCT_2$ (μM)
111	H	CH	1.5	0.77
112	H	CH	1.3	0.77
113	H	N	2.3	0.72
114	F	CH	0.8	0.62
115	Cl	CH	0.38	0.73
116	CF_3	CH	0.48	0.79
117	OMe	CH	0.54	0.5
118	OEt	CH	0.74	0.76

111-118
111 COOH at position 'a'
112-118 COOH at position 'b'

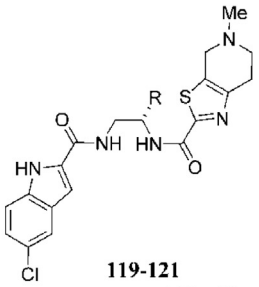

119-121

	R	FXa, IC_{50} (nM)	$PTCT_2$ (μM)
119	H	221	18
120	CH_2-CO-OMe	70	6.5
121	CH_2-CO-NMe_2	47	3.2

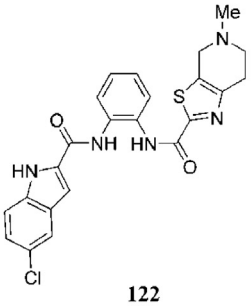

122
FXa, IC_{50} = 7.4 nM

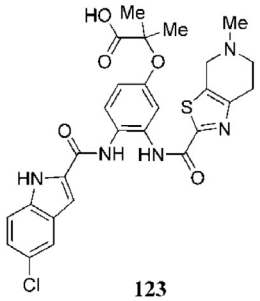

123
FXa, IC_{50} = 2.2 nM;
$PTCT_2$ = 3.9 μM

Fig. 19. Diamines (**108**–**123**) as FXa inhibitors.

of 135 nM, PT value of 17.1 μM and aPTT value of 20.2 μM in human plasma. Compound **142** showed 1852 fold higher selectivity for FXa inhibition over other serine proteases.

3. Conclusion

Discovery of an ideal orally active antithrombotic drug has remained elusive till date. Research efforts in this direction led to the discovery of numerous coagulation enzyme inhibitors including various thrombin and FXa inhibitors. Several preclinical studies have highlighted the importance of FXa as a better and effective target than thrombin because of its upstream position in the coagulation cascade. In addition to this, FXa inhibitors are reported to show nil or less bleeding risks. Better safety and superior efficacy have also been reported with FXa inhibitors over thrombin inhibitors. All these facts elevated the importance of FXa as an ideal target for the development of orally active antithrombotic agents. For the development of selective FXa inhibitors, the crystal structures of both the enzymes (FXa and thrombin) have been used. Since both these enzymes have high degree of structural similarity, computer aided drug designing techniques have been utilized to sort out the selectivity issue and to understand the structural differences in the active sites of the two enzymes. A better description of the selectivity issue has been given by Bhunia et al. [48] by taking different classes of selective thrombin, FXa and FXa-thrombin dual inhibitors into consideration.

In the current review, we have systematically discussed FXa inhibitors reported by various research groups. Majority of the structural changes are reportedly carried out in three pharmacophoric units i.e. P1 moiety, P4 moiety and the central scaffold of the

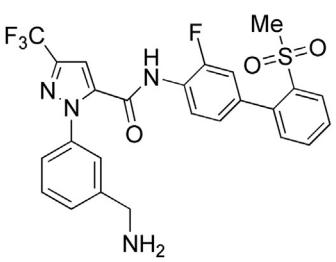

124
FXa, K_i = 0.15 nM

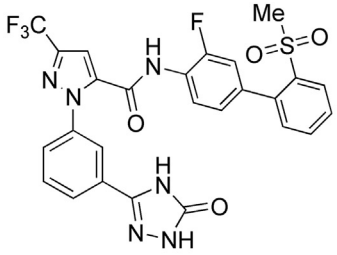

125
FXa, K_i = 0.5 nM

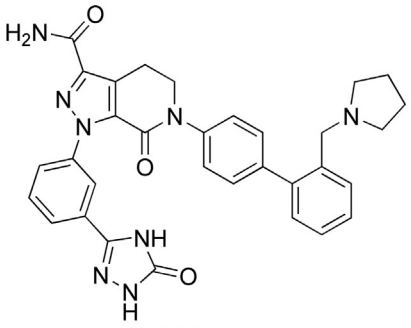

126
FXa, K_i = 0.25 nM

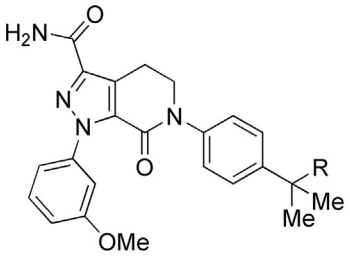

127, 128
127 R = CH_2OH; FXa, K_i = 0.66 nM
128 R = SO_2Me; FXa, K_i = 0.48 nM

Fig. 20. Pyrazole based FXa inhibitors (**124**–**128**).

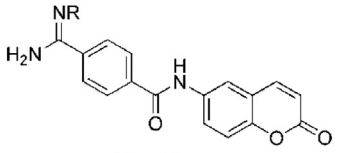

129, 130
129 R = H; PT value 36.5 sec
130 R = OH; PT value 26 sec

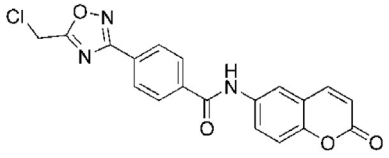

131
PT value 42.3 sec

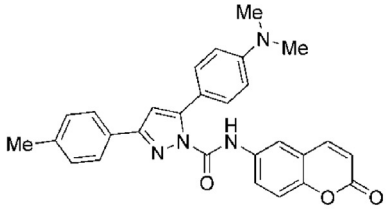

132
PT value 38.5 sec

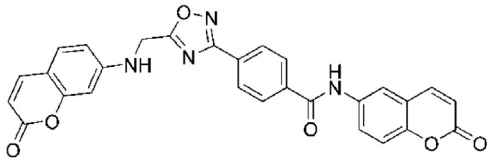

133
PT value 37.8 sec

Fig. 21. Coumarins (**129**–**133**) as FXa inhibitors.

inhibitors. The inhibitors have been classified on the basis of chemical classes as pyrrolidine, oxazolidinone, isoxazole, anthranilamide, diamidobenzene, diamine, pyrazole, coumarin, arylsulfonamidopiperidone and tetrahydroisoquinoline based compounds reported since 2010 onward. Although a large number of compounds possess potent FXa inhibitory activity as discussed in this review, none of these compounds has entered clinical trials successfully because of their poor oral bioavailability. However, a few of the compounds (**78**, **88**) are reported to have been selected for further clinical development. Whether these would cross the bar of clinical trials and hit the market, is a big question. Compound **78** showed an effective FXa inhibition (FXa K_i = 7 nM) and good oral bioavailability (F = 100% in rat and 65% in monkey) [74].

On the basis of binding modes of the active compounds, it could be concluded that 4-methoxyphenyl group in compounds **88** and **94**, haloaromatics like 4-chlorophenyl in compound **107**, 5-

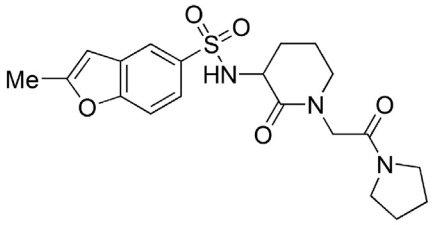

134
FXa, IC_{50} = 1110 nM

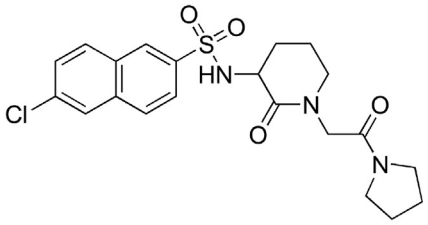

135
FXa, IC_{50} = 32 nM
EC_{2xPT} = 12 μM

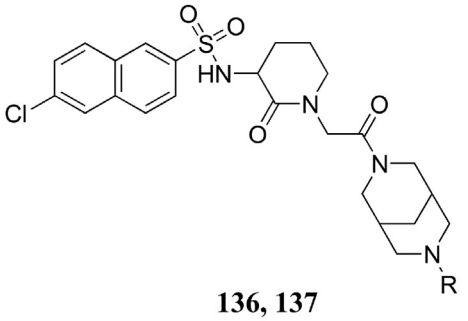

136, 137

	R	FXa, IC_{50} (nM)	PT EC_{2x} (μM)
136	H	22	3.5
137	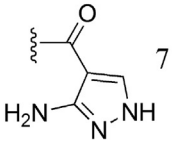	7	1.7

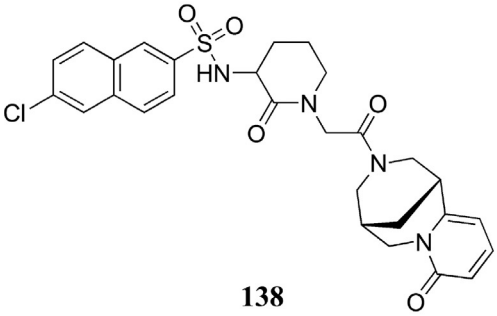

138
FXa, IC_{50} = 13 nM
PT EC_{2x} = 4.1 μM

Fig. 22. Arylsulfonamidopiperidones (**134**–**138**) as FXa inhibitors.

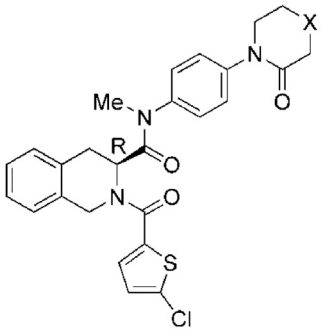

139, 140
139 X = CH_2; FXa, IC_{50} = 56 μM
140 X = O; FXa, IC_{50} = 36 μM

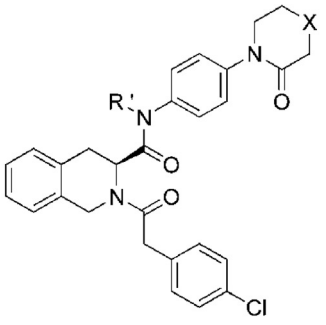

141, 142
141 R' = CH_3, X = CH_2; FXa, IC_{50} = 1.3 μM
142 R' = H, X = O; FXa, IC_{50} = 0.27μM; K_i = 135 nM

Fig. 23. Tetrahydroisoquinolines (**139**–**142**) as FXa inhibitors.

chloropyridine in compound **78** and 2-chlorothiophene in compounds **79** and **81** have showed good affinities for S1 pocket. Monoaryl motifs like 1-phenylpiperidin-2-one in compound **107**, 1-phenylmorpholin-2-one in compounds **79** and **84**, biaryl motifs like substituted biphenyls in compounds **124**–**126** and 1-phenylpyridin-2(1*H*)-one in compounds **78**, **99** and **100** have showed good affinity towards S4 pocket. It can also be concluded that to maintain the desired U/V or L shaped skeletal frame of the compounds, selection of a suitable central scaffold or linker is the key to the development of potent and selective FXa inhibitors. It is hoped that this review would be helpful to the researchers for the development of selective orally active new FXa inhibitors suitable

for the treatment of various thrombotic conditions involved in various cardiovascular complications.

Acknowledgement

Nirav R. Patel is thankful to the University Grant Commission (UGC), New Delhi, for awarding Junior Research Fellowship (F. No. 25-1/2014-15(BSR)/7-129/2007/(BSR).

References

[1] http://www.who.int/mediacentre/factsheets/fs317/en/ (accessed on 21.04.16).
[2] H.E. Achneck, B. Sileshi, A. Parikh, C.A. Milano, I.J. Welsby, J.H. Lawson, Pathophysiology of bleeding and clotting in the cardiac surgery patient: from vascular endothelium to circulatory assist device surface, Circulation 122 (2010) 2068–2077.
[3] http://www.cdc.gov/ncbddd/dvt/data.html (accessed on 21.04.16).
[4] A.T. Cohen, G. Agnelli, F.A. Anderson, J.I. Arcelus, D. Bergqvist, J.G. Brecht, I.A. Greer, J.A. Heit, J.L. Hutchinson, A.K. Kakkar, D. Mottier, E. Oger, M.M. Samama, M. Spannagl, Venous thromboembolism (VTE) in Europe. The number of VTE events and associated morbidity and mortality, Thromb. Haemost. 98 (2007) 756–764.
[5] P. Alonso-Coello, S. Bellmunt, C. McGorrian, S.S. Anand, R. Guzman, M.H. Criqui, E.A. Akl, P. Olav Vandvik, M.G. Lansberg, G.H. Guyatt, F.A. Spencer, Antithrombotic therapy in peripheral artery disease: antithrombotic therapy and prevention of thrombosis, 9th ed: American college of chest physicians evidence-based clinical practice guidelines, Chest 141 (2012) 669S–690S.
[6] J. Fareed, Antithrombotic therapy in 2014: making headway in anticoagulant and antiplatelet therapy, Nat. Rev. Cardiol. 12 (2015) 70–71.
[7] C. Kearon, E.A. Akl, A.J. Comerota, P. Prandoni, H. Bounameaux, S.Z. Goldhaber, M.E. Nelson, P.S. Wells, M.K. Gould, F. Dentali, M. Crowther, S.R. Kahn, Antithrombotic therapy for VTE disease: antithrombotic therapy and prevention of thrombosis, 9th ed: American college of chest physicians evidence-based clinical practice guidelines, Chest 141 (2012) 419S–494S.
[8] W.M. Lijfering, L.E. Flinterman, J.P. Vandenbroucke, F.R. Rosendaal, S.C. Cannegieter, Relationship between venous and arterial thrombosis: a review of the literature from a causal perspective, in: Seminars in Thrombosis and Hemostasis, 2011, p. 885.
[9] J.I. Weitz, J.W. Eikelboom, M.M. Samama, New antithrombotic drugs: antithrombotic therapy and prevention of thrombosis, 9th ed: American college of chest physicians evidence-based clinical practice guidelines, Chest 141 (2012) 120S–151S.
[10] X.-Z. Yang, W.-H. Yang, Y.-G. Xu, X.-J. Diao, G.-W. He, G.-Q. Gong, Synthesis and antithrombotic evaluation of novel dabigatran prodrugs containing a cleavable moiety with anti-platelet activity, Eur. J. Med. Chem. 57 (2012) 21–28.
[11] J.J. You, D.E. Singer, P.A. Howard, D.A. Lane, M.H. Eckman, M.C. Fang, E.M. Hylek, S. Schulman, A.S. Go, M. Hughes, F.A. Spencer, W.J. Manning, J.L. Halperin, G.Y.H. Lip, Antithrombotic therapy for atrial fibrillation: antithrombotic therapy and prevention of thrombosis, 9th ed: American college of chest physicians evidence-based clinical practice guidelines, Chest 141 (2012) 531S–575S.
[12] G. Lippi, M. Franchini, G. Targher, Arterial thrombus formation in cardiovascular disease, Nat. Rev. Cardiol. 8 (2011) 502–512.
[13] S.J. McRae, J.S. Ginsberg, Initial treatment of venous thromboembolism, Circulation 110 (2004) I-3–I-9.
[14] D.E. Becker, Antithrombotic drugs: pharmacology and implications for dental practice, Anesth. Prog. 60 (2013) 72–80.
[15] J.L. Mega, T. Simon, Pharmacology of antithrombotic drugs: an assessment of oral antiplatelet and anticoagulant treatments, Lancet 386 (2015) 281–291.
[16] M.M. Shahpouri, S. Mousavi, F. Khorvash, S.M. Mousavi, T. Hoseini, Anticoagulant therapy for ischemic stroke: a review of literature, J. Res. Med. Sci. 17 (2012) 396–401.
[17] P.D. Stein, D. Grandison, T.A. Hua, P.M. Slettehaugh, J.W. Henry, P. Turlapaty, R. Kerwin, Therapeutic level of oral anticoagulation with warfarin in patients with mechanical prosthetic heart valves: review of literature and recommendations based on international normalized ratio, Postgrad. Med. J. 70 (Suppl. 1) (1994) S72–S83.
[18] S.A. Spinler, V.J. Willey, A patient's guide to taking dabigatran etexilate, Circulation 124 (2011) 209–211.
[19] D.B. Blossom, A.J. Kallen, P.R. Patel, A. Elward, L. Robinson, G. Gao, R. Langer, K.M. Perkins, J.L. Jaeger, K.M. Kurkjian, M. Jones, S.F. Schillie, N. Shehab, D. Ketterer, G. Venkataraman, T.K. Kishimoto, Z. Shriver, A.W. McMahon, K.F. Austen, S. Kozlowski, A. Srinivasan, G. Turabelidze, C.V. Gould, M.J. Arduino, R. Sasisekharan, Outbreak of adverse reactions associated with contaminated heparin, N. Engl. J. Med. 359 (2008) 2674–2684.
[20] G. Lippi, E.J. Favaloro, M. Franchini, G.C. Guidi, Milestones and perspectives in coagulation and hemostasis, Semin. Thromb. Hemost. 35 (2009) 9–22.
[21] S. Palta, R. Saroa, A. Palta, Overview of the coagulation system, Indian J. Anaesth. 58 (2014) 515–523.
[22] D. Lasne, B. Jude, S. Susen, From normal to pathological hemostasis, Can. J. Anaesth. 53 (2006) S2–S11.
[23] G. Lippi, M. Franchini, Pathogenesis of venous thromboembolism: when the cup runneth over, Semin. Thromb. Hemost. 34 (2008) 747–761.
[24] C.H. van Ommen, M. Peters, Clinical practice: the bleeding child. Part I: primary hemostatic disorders, Eur. J. Pediatr. 171 (2012) 1–10.
[25] A.J. Gale, Current understanding of hemostasis, Toxicol. Pathol. 39 (2011) 273–280.
[26] J. Ansell, Factor Xa or thrombin: is factor Xa a better target? J. Thromb. Haemost. 5 (2007) 60–64.
[27] E.W. Davie, O.D. Ratnoff, Waterfall sequence for intrinsic blood clotting, Science 145 (1964) 1310–1312.
[28] Y.K. Lee, M.R. Player, Developments in factor Xa inhibitors for the treatment of thromboembolic disorders, Med. Res. Rev. 31 (2011) 202–283.
[29] N. Mackman, R.E. Tilley, N.S. Key, Role of the extrinsic pathway of blood coagulation in hemostasis and thrombosis, Arterioscler. Thromb. Vasc. Biol. 27 (2007) 1687–1693.
[30] D.J. Pinto, J.M. Smallheer, D.L. Cheney, R.M. Knabb, R.R. Wexler, Factor Xa inhibitors: next-generation antithrombotic agents, J. Med. Chem. 53 (2010) 6243–6274.
[31] R.G. Macfarlane, An enzyme cascade in the blood clotting mechanism, and its function as a biochemical amplifier, Nature 202 (1964) 498–499.
[32] E.A. Beck, The chemistry of blood coagulation: a summary by Paul Morawitz, Thromb. Haemost. 37 (1977) (1905) 376–379.
[33] R.L. Adams, R.J. Bird, Review article: coagulation cascade and therapeutics update: relevance to nephrology. Part 1: overview of coagulation, thrombophilias and history of anticoagulants, Nephrology (Carlton Vic.) 14 (2009) 462–470.
[34] J.P. Riddel, B.E. Aouizerat, C. Miaskowski, D.P. Lillicrap, Theories of blood coagulation, J. Pediatr. Oncol. Nurs. 24 (2007) 123–131.
[35] E.W. Davie, K. Fujikawa, W. Kisiel, The coagulation cascade: initiation, maintenance, and regulation, Biochemistry 30 (1991) 10363–10370.
[36] R. De Caterina, S. Husted, L. Wallentin, G. Agnelli, F. Bachmann, C. Baigent, J. Jespersen, S.D. Kristensen, G. Montalescot, A. Siegbahn, F.W. Verheugt, J. Weitz, Anticoagulants in heart disease: current status and perspectives, Eur. Heart. J. 28 (2007) 880–913.
[37] M.M. Hoffman, D.M. Monroe, Rethinking the coagulation cascade, Curr. Hematol. Rep. 4 (2005) 391–396.
[38] R. De Caterina, S. Husted, L. Wallentin, F. Andreotti, H. Arnesen, F. Bachmann, C. Baigent, K. Huber, J. Jespersen, S.D. Kristensen, G.Y.H. Lip, J. Morais, L.H. Rasmussen, A. Siegbahn, F.W.A. Verheugt, J.I. Weitz, General mechanisms of coagulation and targets of anticoagulants (Section I). Position paper of the ESC working group on thrombosis – task force on anticoagulants in heart disease, Thromb. Haemost. 109 (2013) 569–579.
[39] K. Padmanabhan, K. Padmanabhan, A. Tulinsky, C.H. Park, W. Bode, R. Huber, D. Blankenship, A. Cardin, W. Kisiel, Structure of human des (1-45) factor Xa at 2· 2 Å resolution, J. Mol. Biol. 232 (1993) 947–966.
[40] S. Roehrig, A. Straub, J. Pohlmann, T. Lampe, J. Pernerstorfer, K.H. Schlemmer, P. Reinemer, E. Perzborn, Discovery of the novel antithrombotic agent 5-chloro-N-({(5S)-2-oxo-3-[4-(3-oxomorpholin-4-yl)phenyl]-1,3-oxazolidin-5-yl}methyl)thiophene-2-arboxamide (BAY 59-7939): an oral, direct factor Xa inhibitor, J. Med. Chem. 48 (2005) 5900–5908.
[41] S. Maignan, V. Mikol, The use of 3D structural data in the design of specific factor Xa inhibitors, Curr. Top. Med. Chem. 1 (2001) 161–174.
[42] I. Schechter, A. Berger, On the active site of proteases. III. Mapping the active site of papain; specific peptide inhibitors of papain, Biochem. Biophys. Res. Commun. 32 (1968) 898–902.
[43] W. Bode, P. Schwager, The refined crystal structure of bovine β-trypsin at 1 8 Å resolution: II. Crystallographic refinement, calcium binding site, benzamidine binding site and active site at pH 7 0, J. Mol. Bio. 98 (1975) 693–717.
[44] W. Bode, D. Turk, A. Karshikov, The refined 1.9-Å X-ray crystal structure of d-Phe-Pro-Arg chloromethylketone-inhibited human α-thrombin: structure analysis, overall structure, electrostatic properties, detailed active-site geometry, and structure-function relationships, Protein Sci. 1 (1992) 426–471.
[45] H. Brandstetter, A. Kühne, W. Bode, R. Huber, W. von der Saal, K. Wirthensohn, R.A. Engh, X-ray structure of active site-inhibited clotting factor Xa implications for drug design and substrate recognition, J. Biol. Chem. 271 (1996) 29988–29992.
[46] F. Dullweber, M.T. Stubbs, Đ. Musil, J. Stürzebecher, G. Klebe, Factorising ligand affinity: a combined thermodynamic and crystallographic study of trypsin and thrombin inhibition†, J. Mol. Bio. 313 (2001) 593–614.
[47] S. Katakura, T. Nagahara, T. Hara, S. Kunitada, M. Iwamoto, Molecular model of an interaction between factor Xa and DX-9065a, a novel factor Xa inhibitor: contribution of the acetimidoylpyrrolidine moiety of the inhibitor to potency and selectivity for serine proteases, Eur. J. Med. Chem. 30 (1995) 387–394.
[48] S.S. Bhunia, K.K. Roy, A.K. Saxena, Profiling the structural determinants for the selectivity of representative factor-Xa and thrombin inhibitors using combined ligand-based and structure-based approaches, J. Chem. Inf. Model. 51 (2011) 1966–1985.
[49] A. Straub, S. Roehrig, A. Hillisch, Oral, direct thrombin and factor Xa inhibitors: the replacement for warfarin, leeches, and pig intestines? Angew. Chem. Int. Ed. Engl. 50 (2011) 4574–4590.
[50] M.T. Stubbs, R. Huber, W. Bode, Crystal structures of factor Xa specific

inhibitors in complex with trypsin: structural grounds for inhibition of factor Xa and selectivity against thrombin, FEBS Lett. 375 (1995) 103–107.
[51] S. Krishnaswamy, K.G. Mann, M.E. Nesheim, The prothrombinase-catalyzed activation of prothrombin proceeds through the intermediate meizothrombin in an ordered, sequential reaction, J. Biol. Chem. 261 (1986) 8977–8984.
[52] N.B. Norgard, J.J. DiNicolantonio, T.J. Topping, B. Wee, Novel anticoagulants in atrial fibrillation stroke prevention, Ther. Adv. Chronic Dis. 3 (2012) 123–136.
[53] B. Kaiser, Visions & reflections factor Xa - a promising target for drug development, Cell. Mol. Life Sci. 59 (2002) 189–192.
[54] J.M. Walenga, W.P. Jeske, D. Hoppensteadt, J. Fareed, Factor Xa inhibitors: today and beyond, Curr. Opin. Investig. Drugs 4 (2003) 272–281.
[55] M. Ieko, T. Tarumi, M. Takeda, S. Naito, T. Nakabayashi, T. Koike, Synthetic selective inhibitors of coagulation factor Xa strongly inhibit thrombin generation without affecting initial thrombin forming time necessary for platelet activation in hemostasis, J. Thromb. Haemost. 2 (2004) 612–618.
[56] G. Liwei, M. Shutao, Advances in inhibitors of FXa, Curr. Drug Targets 16 (2015) 1207–1232.
[57] K.G. Mann, S. Butenas, K. Brummel, The dynamics of thrombin formation, Arterioscler, Thromb. Vasc. Biol. 23 (2003) 17–25.
[58] Y. Morishima, K. Tanabe, Y. Terada, T. Hara, S. Kunitada, Antithrombotic and hemorrhagic effects of DX-9065a, a direct and selective factor Xa inhibitor: comparison with a direct thrombin inhibitor and antithrombin III-dependent anticoagulants, Thromb. Haemost. 78 (1997) 1366–1371.
[59] J. Graff, S. Harder, Anticoagulant therapy with the oral direct factor Xa inhibitors rivaroxaban, apixaban and edoxaban and the thrombin inhibitor dabigatran etexilate in patients with hepatic impairment, Clin. Pharmacokinet. 52 (2013) 243–254.
[60] J.P. Ordovas Baines, E. Climent Grana, A. Jover Botella, I. Valero Garcia, Pharmacokinetics and pharmacodynamics of the new oral anticoagulants dabigatran and rivaroxaban, Farm. Hosp. organo Of. expr. Cient. Soc. Espanola Farm. Hosp. 33 (2009) 125–133.
[61] M. Ufer, Comparative efficacy and safety of the novel oral anticoagulants dabigatran, rivaroxaban and apixaban in preclinical and clinical development, Thromb. Haemost. 103 (2010) 572–585.
[62] P. Wong, E. Crain, C. Watson, B. Xin, Favorable therapeutic index of the direct factor Xa inhibitors, apixaban and rivaroxaban, compared with the thrombin inhibitor dabigatran in rabbits, Thromb. Haemost. 7 (2009) 1313–1320.
[63] J.S. Paikin, J.J. Manolakos, J.W. Eikelboom, Rivaroxaban for Stroke Prevention in Atrial Fibrillation: a Critical Review of the ROCKET AF Trial, 2012.
[64] E. Perzborn, S. Roehrig, A. Straub, D. Kubitza, F. Misselwitz, The discovery and development of rivaroxaban, an oral, direct factor Xa inhibitor, Nat. Rev. Drug Discov. 10 (2011) 61–75.
[65] M. Lassen, B. Davidson, A. Gallus, G. Pineo, J. Ansell, D. Deitchman, The efficacy and safety of apixaban, an oral, direct factor Xa inhibitor, as thromboprophylaxis in patients following total knee replacement1, J. Thromb. Haemost. 5 (2007) 2368–2375.
[66] D.A. Parasrampuria, T. Marbury, N. Matsushima, S. Chen, P.K. Wickremasingha, L. He, V. Dishy, K.S. Brown, Pharmacokinetics, safety, and tolerability of edoxaban in end-stage renal disease subjects undergoing haemodialysis, Thromb. Haemost. 113 (2015) 719–727.
[67] N.C. Chan, J. Hirsh, J.S. Ginsberg, J.W. Eikelboom, Betrixaban (PRT054021): pharmacology, dose selection and clinical studies, Future Cardiol. 10 (2014) 43–52.
[68] D.J. Pinto, M.J. Orwat, M.L. Quan, Q. Han, R.A. Galemmo, E. Amparo, B. Wells, C. Ellis, M.Y. He, R.S. Alexander, 1-[3-Aminobenzisoxazol-5′-yl]-3-trifluoromethyl-6-[2′-(3-(R)-hydroxy-N-pyrrolidinyl) methyl-[1, 1′]-biphen-4-yl]-1, 4, 5, 6-tetrahydropyrazolo-[3, 4-c]-pyridin-7-one (BMS-740808) a highly potent, selective, efficacious, and orally bioavailable inhibitor of blood coagulation factor Xa, Bioorg. Med. Chem. Lett. 16 (2006) 4141–4147.
[69] N.C. Chan, V. Bhagirath, J.W. Eikelboom, Profile of betrixaban and its potential in the prevention and treatment of venous thromboembolism, Vasc. Health Risk Manag. 11 (2015) 343–351.
[70] S. Li, B. Liu, D. Xu, Y. Xu, Bleeding risk and mortality of edoxaban: a pooled meta-analysis of randomized controlled trials, PLoS One 9 (2014) e95354.
[71] J.H. Alexander, R.D. Lopes, S. James, R. Kilaru, Y. He, P. Mohan, D.L. Bhatt, S. Goodman, F.W. Verheugt, M. Flather, Apixaban with antiplatelet therapy after acute coronary syndrome, N. Engl. J. Med. 365 (2011) 699–708.
[72] J.L. Mega, E. Braunwald, S.D. Wiviott, J.-P. Bassand, D.L. Bhatt, C. Bode, P. Burton, M. Cohen, N. Cook-Bruns, K.A. Fox, Rivaroxaban in patients with a recent acute coronary syndrome, N. Engl. J. Med. 366 (2012) 9–19.
[73] http://www.rcsb.org/pdb/results/results.do?qrid=69FC3F8F&tabtoshow=Current (accessed on 13.04.16).
[74] L. Anselm, D.W. Banner, J. Benz, K.G. Zbinden, J. Himber, H. Hilpert, W. Huber, B. Kuhn, J.L. Mary, M.B. Otteneder, N. Panday, F. Ricklin, M. Stahl, S. Thomi, W. Haap, Discovery of a factor Xa inhibitor (3R,4R)-1-(2,2-difluoro-ethyl)-pyrrolidine-3,4-dicarboxylic acid 3-[(5-chloro-pyridin-2-yl)-amide] 4-[[2-fluoro-4-(2-oxo-2H-pyridin-1-yl)-phenyl]-amide] as a clinical candidate, Bioorg. Med. Chem. Lett. 20 (2010) 5313–5319.
[75] S. Kleanthous, A.D. Borthwick, D. Brown, C.L. Burns-Kurtis, M. Campbell, L. Chaudry, C. Chan, M.-O. Clarte, M.A. Convery, J.D. Harling, E. Hortense, W.R. Irving, S. Irvine, A.J. Pateman, A.N. Patikis, I.L. Pinto, D.R. Pollard, T.J. Roethka, S. Senger, G.P. Shah, G.J. Stelman, J.R. Toomey, N.S. Watson, R.I. West, C. Whittaker, P. Zhou, R.J. Young, Structure and property based design of factor Xa inhibitors: pyrrolidin-2-ones with monoaryl P4 motifs, Bioorg. Med. Chem. Lett. 20 (2010) 618–622.
[76] J. Meneyrol, M. Follmann, G. Lassalle, V. Wehner, G. Barre, T. Rousseaux, J.-M. Altenburger, F. Petit, Z. Bocskei, H. Schreuder, N. Alet, J.-P. Herault, L. Millet, F. Dol, P. Florian, P. Schaeffer, F. Sadoun, S. Klieber, C. Briot, F. Bono, J.-M. Herbert, 5-Chlorothiophene-2-carboxylic acid [(S)-2-[2-methyl-3-(2-oxopyrrolidin-1-yl)benzenesulfonylamino]-3-(4-methylpiperazin-1-yl)-3-oxopropyl]amide (SAR107375), a selective and potent orally active dual thrombin and factor Xa inhibitor, J. Med. Chem. 56 (2013) 9441–9456.
[77] M.M. Mueller, S. Sperl, J. Sturzebecher, W. Bode, L. Moroder, (R)-3-Amidinophenylalanine-derived inhibitors of factor Xa with a novel active-site binding mode, Biol. Chem. 383 (2002) 1185–1191.
[78] M. Nazare, H. Matter, D.W. Will, M. Wagner, M. Urmann, J. Czech, H. Schreuder, A. Bauer, K. Ritter, V. Wehner, Fragment deconstruction of small, potent factor Xa inhibitors: exploring the superadditivity energetics of fragment linking in protein-ligand complexes, Angew. Chem. 51 (2012) 905–911.
[79] J.R. Pruitt, D.J. Pinto, R.A. Galemmo Jr., R.S. Alexander, K.A. Rossi, B.L. Wells, S. Drummond, L.L. Bostrom, D. Burdick, R. Bruckner, H. Chen, A. Smallwood, P.C. Wong, M.R. Wright, S. Bai, J.M. Luettgen, R.M. Knabb, P.Y. Lam, R.R. Wexler, Discovery of 1-(2-aminomethylphenyl)-3-trifluoromethyl-N-[3-fluoro-2'-(aminosulfonyl)[1,1'-biphenyl)]-4-yl]-1H-pyrazole-5-carboxyamide (DPC602), a potent, selective, and orally bioavailable factor Xa inhibitor(1), J. Med. Chem. 46 (2003) 5298–5315.
[80] M.L. Quan, D.J. Pinto, K.A. Rossi, S. Sheriff, R.S. Alexander, E. Amparo, K. Kish, R.M. Knabb, J.M. Luettgen, P. Morin, A. Smallwood, F.J. Woerner, R.R. Wexler, Phenyltriazolinones as potent factor Xa inhibitors, Bioorg. Med. Chem. Lett. 20 (2010) 1373–1377.
[81] L.M. Salonen, M.C. Holland, P.S. Kaib, W. Haap, J. Benz, J.L. Mary, O. Kuster, W.B. Schweizer, D.W. Banner, F. Diederich, Molecular recognition at the active site of factor Xa: cation-pi interactions, stacking on planar peptide surfaces, and replacement of structural water, Chem. Weinheim Bergstrasse Ger. 18 (2012) 213–222.
[82] Y. Shi, S.P. O'Connor, D. Sitkoff, J. Zhang, M. Shi, S.N. Bisaha, Y. Wang, C. Li, Z. Ruan, R.M. Lawrence, H.E. Klei, K. Kish, E.C. Liu, S.M. Seiler, L. Schweizer, T.E. Steinbacher, W.A. Schumacher, J.A. Robl, J.E. Macor, K.S. Atwal, P.D. Stein, Arylsulfonamidopiperidone derivatives as a novel class of factor Xa inhibitors, Bioorg. Med. Chem. Lett. 21 (2011) 7516–7521.
[83] N.S. Watson, C. Adams, D. Belton, D. Brown, C.L. Burns-Kurtis, L. Chaudry, C. Chan, M.A. Convery, D.E. Davies, A.M. Exall, J.D. Harling, S. Irvine, W.R. Irving, S. Kleanthous, I.M. McLay, A.J. Pateman, A.N. Patikis, T.J. Roethke, S. Senger, G.J. Stelman, J.R. Toomey, R.I. West, C. Whittaker, P. Zhou, R.J. Young, The discovery of potent and long-acting oral factor Xa inhibitors with tetrahydroisoquinoline and benzazepine P4 motifs, Bioorg. Med. Chem. Lett. 21 (2011) 1588–1592.
[84] K. Yoshikawa, S. Kobayashi, Y. Nakamoto, N. Haginoya, S. Komoriya, T. Yoshino, T. Nagata, A. Mochizuki, K. Watanabe, M. Suzuki, H. Kanno, T. Ohta, Design, synthesis, and SAR of cis-1,2-diaminocyclohexane derivatives as potent factor Xa inhibitors. Part II: exploration of 6-6 fused rings as alternative S1 moieties, Bioorg. Med. Chem. 17 (2009) 8221–8233.
[85] K. Yoshikawa, T. Yoshino, Y. Yokomizo, K. Uoto, H. Naito, K. Kawakami, A. Mochizuki, T. Nagata, M. Suzuki, H. Kanno, M. Takemura, T. Ohta, Design, synthesis and SAR of novel ethylenediamine and phenylenediamine derivatives as factor Xa inhibitors, Bioorg. Med. Chem. Lett. 21 (2011) 2133–2140.
[86] R.J. Young, C. Adams, M. Blows, D. Brown, C.L. Burns-Kurtis, C. Chan, L. Chaudry, M.A. Convery, D.E. Davies, A.M. Exall, G. Foster, J.D. Harling, E. Hortense, S. Irvine, W.R. Irving, S. Jackson, S. Kleanthous, A.J. Pateman, A.N. Patikis, T.J. Roethka, S. Senger, G.J. Stelman, J.R. Toomey, R.I. West, C. Whittaker, P. Zhou, N.S. Watson, Structure and property based design of factor Xa inhibitors: pyrrolidin-2-ones with aminoindane and phenylpyrrolidine P4 motifs, Bioorg. Med. Chem. Lett. 21 (2011) 1582–1587.
[87] Y.M. Choi-Sledeski, R. Kearney, G. Poli, H. Pauls, C. Gardner, Y. Gong, M. Becker, R. Davis, A. Spada, G. Liang, V. Chu, K. Brown, D. Collussi, R. Leadley, S. Rebello, P. Moxey, S. Morgan, R. Bentley, C. Kasiewski, S. Maignan, J.-P. Guilloteau, V. Mikol, Discovery of an orally efficacious inhibitor of coagulation factor Xa which incorporates a neutral P1 ligand, J. Med. Chem. 46 (2003) 681–684.
[88] H. Matter, M. Nazare, S. Gussregen, D.W. Will, H. Schreuder, A. Bauer, M. Urmann, K. Ritter, M. Wagner, V. Wehner, Evidence for C-Cl/C-Br...pi interactions as an important contribution to protein-ligand binding affinity, Angew. Chem. Int. Ed. Engl. 48 (2009) 2911–2916.
[89] P. Zhang, L. Bao, J.F. Zuckett, E.A. Goldman, Z.J. Jia, A. Arfsten, S. Edwards, U. Sinha, A. Hutchaleelaha, G. Park, J.L. Lambing, S.J. Hollenbach, R.M. Scarborough, B.Y. Zhu, Design, synthesis, and SAR of anthranilamide-based factor Xa inhibitors incorporating substituted biphenyl P4 motifs, Bioorg. Med. Chem. Lett. 14 (2004) 983–987.
[90] D. Mendel, A.L. Marquart, S. Joseph, P. Waid, Y.K. Yee, A.L. Tebbe, A.M. Ratz, D.K. Herron, T. Goodson, J.J. Masters, J.B. Franciskovich, J.M. Tinsley, M.R. Wiley, L.C. Weir, J.A. Kyle, V.J. Klimkowski, G.F. Smith, R.D. Towner, L.L. Froelich, J. Buben, T.J. Craft, Anthranilamide inhibitors of factor Xa, Bioorg. Med. Chem. Lett. 17 (2007) 4832–4836.
[91] A. Mochizuki, T. Nagata, H. Kanno, M. Suzuki, T. Ohta, 2-aminomethylphenylamine as a novel scaffold for factor Xa inhibitor,

Bioorg. Med. Chem. 19 (2011) 1623–1642.
[92] T. Nagata, T. Yoshino, N. Haginoya, K. Yoshikawa, Y. Isobe, T. Furugohri, H. Kanno, Cycloalkanediamine derivatives as novel blood coagulation factor Xa inhibitors, Bioorg. Med. Chem. Lett. 17 (2007) 4683–4688.
[93] R. Rai, P. Sprengeler, K. Elrod, W. Young, Perspectives on factor Xa inhibition, Curr. Med. Chem. 8 (2001) 101–119.
[94] Y. Zhao, M. Jiang, S. Zhou, S. Wu, X. Zhang, L. Ma, K. Zhang, P. Gong, Design, synthesis and structure-activity relationship of oxazolidinone derivatives containing novel S4 ligand as FXa inhibitors, Eur. J. Med. Chem. 96 (2015) 369–380.
[95] M. de Candia, G. Lopopolo, C. Altomare, Novel factor Xa inhibitors: a patent review, Expert Opin. Ther. Pat. 19 (2009) 1535–1580.
[96] J.M.W. Fevig, R.R. Wexler, Anticoagulants: thrombin and factor Xa inhibitors, in: In Annual Reports in Medicinal Chemistry, Academic Press:, London, 1999, pp. 81–100.
[97] U.J.P. Ries, H.W.M. Priepke, Factor Xa inhibitors: a review of the recent patent literature, IDrugs 3 (2000) 1509–1524.
[98] J.L. Collins, B.G. Shearer, J.A. Oplinger, S. Lee, E.P. Garvey, M. Salter, C. Duffy, T.C. Burnette, E.S. Furfine, N-Phenylamidines as selective inhibitors of human neuronal nitric oxide synthase: structure–activity studies and demonstration of *in vivo* activity, J. Med. Chem. 41 (1998) 2858–2871.
[99] B. Gabriel, M.T. Stubbs, A. Bergner, J. Hauptmann, W. Bode, J. Sturzebecher, L. Moroder, Design of benzamidine-type inhibitors of factor Xa, J. Med. Chem. 41 (1998) 4240–4250.
[100] Y. Taniuchi, Y. Sakai, N. Hisamichi, M. Kayama, Y. Mano, K. Sato, F. Hirayama, H. Koshio, Y. Matsumoto, T. Kawasaki, Biochemical and pharmacological characterization of YM-60828, a newly synthesized and orally active inhibitor of human factor Xa, Thromb. Haemost. 79 (1998) 543–548.
[101] G. Lopopolo, M. de Candia, L. Panza, M.R. Romano, M.D. Lograno, F. Campagna, C. Altomare, β-D-Glucosyl conjugates of highly potent inhibitors of blood coagulation factor Xa bearing 2-chorothiophene as a P1 potif, ChemMedChem 7 (2012) 1669–1677.
[102] J.T. Kohrt, C.F. Bigge, J.W. Bryant, A. Casimiro-Garcia, L. Chi, W.L. Cody, T. Dahring, D.A. Dudley, K.J. Filipski, S. Haarer, R. Heemstra, N. Janiczek, L. Narasimhan, T. McClanahan, J.T. Peterson, V. Sahasrabudhe, R. Schaum, C.A. Van Huis, K.M. Welch, E. Zhang, R.J. Leadley, J.J. Edmunds, The discovery of (2R,4R)-N-(4-chlorophenyl)-N- (2-fluoro-4-(2-oxopyridin-1(2H)-yl) phenyl)-4-methoxypyrrolidine-1,2-dicarboxamide (PD 0348292), an orally efficacious factor Xa inhibitor, Chem. Biol. Drug Des. 70 (2007) 100–112.
[103] P. Zhang, W. Huang, L. Wang, L. Bao, Z.J. Jia, S.M. Bauer, E.A. Goldman, G.D. Probst, Y. Song, T. Su, J. Fan, Y. Wu, W. Li, J. Woolfrey, U. Sinha, P.W. Wong, S.T. Edwards, A.E. Arfsten, L.A. Clizbe, J. Kanter, A. Pandey, G. Park, A. Hutchaleelaha, J.L. Lambing, S.J. Hollenbach, R.M. Scarborough, B.Y. Zhu, Discovery of betrixaban (PRT054021), N-(5-chloropyridin-2-yl)-2-(4-(N,N-dimethylcarbamimidoyl)benzamido)-5-methoxybenz amide, a highly potent, selective, and orally efficacious factor Xa inhibitor, Bioorg. Med. Chem. Lett. 19 (2009) 2179–2185.
[104] R.J. Young, A.D. Borthwick, D. Brown, C.L. Burns-Kurtis, M. Campbell, C. Chan, M. Charbaut, M.A. Convery, H. Diallo, E. Hortense, W.R. Irving, H.A. Kelly, N.P. King, S. Kleanthous, A.M. Mason, A.J. Pateman, A.N. Patikis, I.L. Pinto, D.R. Pollard, S. Senger, G.P. Shah, J.R. Toomey, N.S. Watson, H.E. Weston, P. Zhou, Structure and property based design of factor Xa inhibitors: biaryl pyrrolidin-2-ones incorporating basic heterocyclic motifs, Bioorg. Med. Chem. Lett. 18 (2008) 28–33.
[105] R.J. Young, A.D. Borthwick, D. Brown, C.L. Burns-Kurtis, M. Campbell, C. Chan, M. Charbaut, C.-w. Chung, M.A. Convery, H.A. Kelly, N. Paul King, S. Kleanthous, A.M. Mason, A.J. Pateman, A.N. Patikis, I.L. Pinto, D.R. Pollard, S. Senger, G.P. Shah, J.R. Toomey, N.S. Watson, H.E. Weston, Structure and property based design of factor Xa inhibitors: pyrrolidin-2-ones with biaryl P4 motifs, Bioorg. Med. Chem. Lett. 18 (2008) 23–27.
[106] N. Haginoya, S. Kobayashi, S. Komoriya, T. Yoshino, M. Suzuki, T. Shimada, K. Watanabe, Y. Hirokawa, T. Furugori, T. Nagahara, Synthesis and conformational analysis of a non-amidine factor Xa inhibitor that incorporates 5-methyl-4,5,6,7-tetrahydrothiazolo[5,4-c]pyridine as S4 binding element, J. Med. Chem. 47 (2004) 5167–5182.
[107] Y. Imaeda, T. Miyawaki, H. Sakamoto, F. Itoh, N. Konishi, K. Hiroe, M. Kawamura, T. Tanaka, K. Kubo, Discovery of sulfonylalkylamides: a new class of orally active factor Xa inhibitors, Bioorg. Med. Chem. 16 (2008) 2243–2260.
[108] T. Nagata, T. Yoshino, N. Haginoya, K. Yoshikawa, M. Nagamochi, S. Kobayashi, S. Komoriya, A. Yokomizo, R. Muto, M. Yamaguchi, K. Osanai, M. Suzuki, H. Kanno, Discovery of N-[(1R,2S,5S)-2-{[(5-chloroindol-2-yl) carbonyl]amino}-5-(dimethylcarbamoyl)cyclohexyl]-5-methyl-4,5,6,7-tetrahydrothiazolo[5,4-c]pyridine-2-carboxamide hydrochloride: a novel, potent and orally active direct inhibitor of factor Xa, Bioorg. Med. Chem. 17 (2009) 1193–1206.
[109] M.L. Quan, P.Y.S. Lam, Q. Han, D.J.P. Pinto, M.Y. He, R. Li, C.D. Ellis, C.G. Clark, C.A. Teleha, J.-H. Sun, R.S. Alexander, S. Bai, J.M. Luettgen, R.M. Knabb, P.C. Wong, R.R. Wexler, Discovery of 1-(3'-Aminobenzisoxazol-5'-yl)-3-trifluoromethyl-N-[2-fluoro-4- [(2'-dimethylaminomethyl)imidazol-1-yl] phenyl]-1H-pyrazole-5-carboxyamide hydrochloride (Razaxaban), a highly potent, selective, and orally bioavailable factor Xa inhibitor, J. Med. Chem. 48 (2005) 1729–1744.
[110] P.Y.S. Lam, C.G. Clark, R. Li, D.J.P. Pinto, M.J. Orwat, R.A. Galemmo, J.M. Fevig, C.A. Teleha, R.S. Alexander, A.M. Smallwood, K.A. Rossi, M.R. Wright, S.A. Bai, K. He, J.M. Luettgen, P.C. Wong, R.M. Knabb, R.R. Wexler, Structure-based design of novel guanidine/benzamidine mimics: potent and orally bioavailable factor Xa inhibitors as novel anticoagulants, J. Med. Chem. 46 (2003) 4405–4418.
[111] D.J. Pinto, R.A. Galemmo Jr., M.L. Quan, M.J. Orwat, C. Clark, R. Li, B. Wells, F. Woerner, R.S. Alexander, K.A. Rossi, A. Smallwood, P.C. Wong, J.M. Luettgen, A.R. Rendina, R.M. Knabb, K. He, R.R. Wexler, P.Y. Lam, Discovery of potent, efficacious, and orally bioavailable inhibitors of blood coagulation factor Xa with neutral P1 moieties, Bioorg. Med. Chem. Lett. 16 (2006) 5584–5589.
[112] J.X. Qiao, X. Cheng, J.M. Smallheer, R.A. Galemmo, S. Drummond, D.J. Pinto, D.L. Cheney, K. He, P.C. Wong, J.M. Luettgen, R.M. Knabb, R.R. Wexler, P.Y. Lam, Pyrazole-based factor Xa inhibitors containing N-arylpiperidinyl P4 residues, Bioorg. Med. Chem. Lett. 17 (2007) 1432–1437.
[113] A.W. Faull, Aminoheterocyclic compounds with antithrombotic/anticoagulant effect, in: Google Patents, 2000.
[114] Y.-L. Li, J.M. Fevig, J. Cacciola, J. Buriak Jr., K.A. Rossi, J. Jona, R.M. Knabb, J.M. Luettgen, P.C. Wong, S.A. Bai, R.R. Wexler, P.Y.S. Lam, Preparation of 1-(3-aminobenzo[d]isoxazol-5-yl)-1H-pyrazolo[4,3-d]pyrimidin-7(6H)-ones as potent, selective, and efficacious inhibitors of coagulation factor Xa, Bioorg. Med. Chem. Lett. 16 (2006) 5176–5182.
[115] R.A. Galemmo Jr., T.P. Maduskuie, C. Dominguez, K.A. Rossi, R.M. Knabb, R.R. Wexler, P.F.W. Stouten, The de novo design and synthesis of cyclic urea inhibitors of factor Xa: initial sar studies, Bioorg. Med. Chem. Lett. 8 (1998) 2705–2710.
[116] D.J. Pinto, M.J. Orwat, S. Koch, K.A. Rossi, R.S. Alexander, A. Smallwood, P.C. Wong, A.R. Rendina, J.M. Luettgen, R.M. Knabb, K. He, B. Xin, R.R. Wexler, P.Y. Lam, Discovery of 1-(4-methoxyphenyl)-7-oxo-6-(4-(2-oxopiperidin-1-yl)phenyl)-4,5,6,7-tetrahydro-1H -pyrazolo[3,4-c]pyridine-3-carboxamide (apixaban, BMS-562247), a highly potent, selective, efficacious, and orally bioavailable inhibitor of blood coagulation factor Xa, J. Med. Chem. 50 (2007) 5339–5356.
[117] C.A. Van Huis, C.F. Bigge, A. Casimiro-Garcia, W.L. Cody, D.A. Dudley, K.J. Filipski, R.J. Heemstra, J.T. Kohrt, L.S. Narasimhan, R.P. Schaum, E. Zhang, J.W. Bryant, S. Haarer, N. Janiczek, R.J. Leadley Jr., T. McClanahan, J. Thomas Peterson, K.M. Welch, J.J. Edmunds, Structure-based drug design of pyrrolidine-1, 2-dicarboxamides as a novel series of orally bioavailable factor Xa inhibitors, Chem. Biol. Drug Des. 69 (2007) 444–450.
[118] J.R. Corte, T. Fang, D.J. Pinto, W. Han, Z. Hu, X.J. Jiang, Y.L. Li, J.F. Gauuan, M. Hadden, D. Orton, A.R. Rendina, J.M. Luettgen, P.C. Wong, K. He, P.E. Morin, C.H. Chang, D.L. Cheney, R.M. Knabb, R.R. Wexler, P.Y. Lam, Structure-activity relationships of anthranilamide-based factor Xa inhibitors containing piperidinone and pyridinone P4 moieties, Bioorg. Med. Chem. Lett. 18 (2008) 2845–2849.
[119] B. Ye, D.O. Arnaiz, Y.-L. Chou, B.D. Griedel, R. Karanjawala, W. Lee, M.M. Morrissey, K.L. Sacchi, S.T. Sakata, K.J. Shaw, Thiophene-anthranilamides as highly potent and orally available factor Xa inhibitors 1, J. Med. Chem. 50 (2007) 2967–2980.
[120] H. Nishida, Y. Miyazaki, T. Mukaihira, H. Shimada, K. Suzuki, F. Saitoh, M. Mizuno, T. Matsusue, A. Okamoto, Y. Hosaka, Synthesis and evaluation of 1-arylsulfonyl-3-piperazinone derivatives as factor Xa inhibitors III. Effect of ring opening of piperazinone moiety on inhibition, Chem. Pharm. Bull. 52 (2004) 459–462.
[121] T. Xue, S. Ding, B. Guo, Y. Zhou, P. Sun, H. Wang, W. Chu, G. Gong, Y. Wang, X. Chen, Y. Yang, Design, synthesis, and structure-activity and structure-pharmacokinetic relationship studies of novel [6,6,5] tricyclic fused oxazolidinones leading to the discovery of a potent, selective, and orally bioavailable FXa inhibitor, J. Med. Chem. 57 (2014) 7770–7791.
[122] S. Komoriya, S. Kobayashi, K. Osanai, T. Yoshino, T. Nagata, N. Haginoya, Y. Nakamoto, A. Mochizuki, T. Nagahara, M. Suzuki, Design, synthesis, and biological activity of novel factor Xa inhibitors: improving metabolic stability by S1 and S4 ligand modification, Bioorg. Med. Chem. 14 (2006) 1309–1330.
[123] J.M. Fevig, J. Cacciola, J. Buriak Jr., K.A. Rossi, R.M. Knabb, J.M. Luettgen, P.C. Wong, S.A. Bai, R.R. Wexler, P.Y.S. Lam, Preparation of 1-(4-methoxyphenyl)-1H-pyrazolo[4,3-d]pyrimidin-7(6H)-ones as potent, selective and bioavailable inhibitors of coagulation factor Xa, Bioorg. Med. Chem. Lett. 16 (2006) 3755–3760.
[124] M.L. Quan, Q. Han, J.M. Fevig, P.Y.S. Lam, S. Bai, R.M. Knabb, J.M. Luettgen, P.C. Wong, R.R. Wexler, Aminobenzisoxazoles with biaryl P4 moieties as potent, selective, and orally bioavailable factor Xa inhibitors, Bioorg. Med. Chem. Lett. 16 (2006) 1795–1798.
[125] P. Zhang, L. Bao, J.F. Zuckett, E.A. Goldman, Z.J. Jia, A. Arfsten, S. Edwards, U. Sinha, A. Hutchaleelaha, G. Park, J.L. Lambing, S.J. Hollenbach, R.M. Scarborough, B.-Y. Zhu, Design, synthesis, and SAR of anthranilamide-based factor Xa inhibitors incorporating substituted biphenyl P4 motifs, Bioorg. Med. Chem. Lett. 14 (2004) 983–987.
[126] M.L. Quan, P.Y. Lam, Q. Han, D.J. Pinto, M.Y. He, R. Li, C.D. Ellis, C.G. Clark, C.A. Teleha, J.H. Sun, R.S. Alexander, S. Bai, J.M. Luettgen, R.M. Knabb, P.C. Wong, R.R. Wexler, Discovery of 1-(3′-aminobenzisoxazol-5′-yl)-3-trifluoromethyl-N-[2-fluoro-4- [(2′-dimethylaminomethyl)imidazol-1-yl] phenyl]-1H-pyrazole-5-carboxyamide hydrochloride (razaxaban), a highly potent, selective, and orally bioavailable factor Xa inhibitor, J. Med. Chem. 48 (2005) 1729–1744.
[127] Y.M. Choi-Sledeski, R. Kearney, G. Poli, H. Pauls, C. Gardner, Y. Gong, M. Becker, R. Davis, A. Spada, G. Liang, V. Chu, K. Brown, D. Collussi,

R. Leadley Jr., S. Rebello, P. Moxey, S. Morgan, R. Bentley, C. Kasiewski, S. Maignan, J.P. Guilloteau, V. Mikol, Discovery of an orally efficacious inhibitor of coagulation factor Xa which incorporates a neutral P1 ligand, J. Med. Chem. 46 (2003) 681–684.

[128] A.G. Turpie, Oral, direct factor Xa inhibitors in development for the prevention and treatment of thromboembolic diseases, Arterioscler. Thromb. Vasc. Biol. 27 (2007) 1238–1247.

[129] J. Yang, G. Su, Y. Ren, Y. Chen, Design, synthesis and evaluation of isoxazolo [5,4-d]pyrimidin-4(5H)-one derivatives as antithrombotic agents, Bioorg. Med. Chem. Lett. 25 (2015) 492–495.

[130] F. Hirayama, H. Koshio, T. Ishihara, S. Hachiya, K. Sugasawa, Y. Koga, N. Seki, R. Shiraki, T. Shigenaga, Y. Iwatsuki, Y. Moritani, K. Mori, T. Kadokura, T. Kawasaki, Y. Matsumoto, S. Sakamoto, S. Tsukamoto, Discovery of N-[2-hydroxy-6-(4-methoxybenzamido)phenyl]-4- (4-methyl-1,4-diazepan-1-yl) benzamide (darexaban, YM150) as a potent and orally available factor Xa inhibitor, J. Med. Chem. 54 (2011) 8051–8065.

[131] T. Ishihara, Y. Koga, K. Mori, K. Sugasawa, Y. Iwatsuki, F. Hirayama, Novel strategy to boost oral anticoagulant activity of blood coagulation enzyme inhibitors based on biotransformation into hydrophilic conjugates, Bioorg. Med. Chem. 22 (2014) 6324–6332.

[132] T. Ishihara, Y. Koga, Y. Iwatsuki, F. Hirayama, Identification of potent orally active factor Xa inhibitors based on conjugation strategy and application of predictable fragment recommender system, Bioorg. Med. Chem. 23 (2015) 277–289.

[133] J. Yang, G. Su, Y. Ren, Y. Chen, Synthesis of 3,4-diaminobenzoyl derivatives as factor Xa inhibitors, Eur. J. Med. Chem. 101 (2015) 41–51.

[134] V. Pandya, M. Jain, G. Chakrabarti, H. Soni, B. Parmar, B. Chaugule, J. Patel, T. Jarag, J. Joshi, N. Joshi, A. Rath, V. Unadkat, B. Sharma, H. Ajani, J. Kumar, K.V. Sairam, H. Patel, P. Patel, Synthesis and structure-activity relationship of potent, selective and orally active anthranilamide-based factor Xa inhibitors: application of weakly basic sulfoximine group as novel S4 binding element, Eur. J. Med. Chem. 58 (2012) 136–152.

[135] J. Xing, L. Yang, H. Li, Q. Li, L. Zhao, X. Wang, Y. Zhang, M. Zhou, J. Zhou, H. Zhang, Identification of anthranilamide derivatives as potential factor Xa inhibitors: drug design, synthesis and biological evaluation, Eur. J. Med. Chem. 95 (2015) 388–399.

[136] A. Mochizuki, T. Nagata, H. Kanno, D. Takano, M. Kishida, M. Suzuki, T. Ohta, Orally active zwitterionic factor Xa inhibitors with long duration of action, Bioorg. Med. Chem. Lett. 21 (2011) 7337–7343.

[137] M.J. Orwat, J.X. Qiao, K. He, A.R. Rendina, J.M. Luettgen, K.A. Rossi, B. Xin, R.M. Knabb, R.R. Wexler, P.Y. Lam, D.J. Pinto, Orally bioavailable factor Xa inhibitors containing alpha-substituted gem-dimethyl P4 moieties, Bioorg. Med. Chem. Lett. 24 (2014) 3341–3345.

[138] K.M. Amin, N.M. Abdel Gawad, D.E. Abdel Rahman, M.K. El Ashry, New series of 6-substituted coumarin derivatives as effective factor Xa inhibitors: synthesis, in vivo antithrombotic evaluation and molecular docking, Bioorg. Chem. 52 (2014) 31–43.

[139] R.A. Al-Horani, A.Y. Mehta, U.R. Desai, Potent direct inhibitors of factor Xa based on the tetrahydroisoquinoline scaffold, Eur. J. Med. Chem. 54 (2012) 771–783.

Bioorganic Chemistry 101 (2020) 103977

Contents lists available at ScienceDirect

Bioorganic Chemistry

journal homepage: www.elsevier.com/locate/bioorg

Novel carbazole-stilbene hybrids as multifunctional anti-Alzheimer agents

Dushyant V. Patel[a], Nirav R. Patel[a], Ashish M. Kanhed[b], Divya M. Teli[c], Kishan B. Patel[a], Prashant D. Joshi[a], Sagar P. Patel[a], Pallav M. Gandhi[a], Bharat N. Chaudhary[a], Navnit K. Prajapati[a], Kirti V. Patel[a], Mange Ram Yadav[a,*,1]

[a] Faculty of Pharmacy, Kalabhavan Campus, The Maharaja Sayajirao University of Baroda, Vadodara 390001, Gujarat, India
[b] Shobhaben Pratapbhai Patel – School of Pharmacy & Technology Management, SVKM's NMIMS University, Vile Parle, Mumbai 400056, India
[c] Department of Pharmaceutical Chemistry, L. M. College of Pharmacy, Navrangpura, Ahmedabad 380009, Gujarat, India

ARTICLE INFO

Keywords:
Alzheimer's disease
MTDL
Acetylcholinesterase
Butyrylcholinesterase
Aβ aggregation
Metal chelation
Carbazole
Stilbene

ABSTRACT

Molecules capable of engaging with multiple targets associated with pathological condition of Alzheimer's disease have proved to be potential anti-Alzheimer's agents. In our goal to develop multitarget-directed ligands for the treatment of Alzheimer's disease, a novel series of carbazole-based stilbene derivatives were designed by the fusion of carbazole ring with stilbene scaffold. The designed compounds were synthesized and evaluated for their anti-AD activities including cholinesterase inhibition, Aβ aggregation inhibition, antioxidant and metal chelation properties. Amongst them, (*E*)-1-(4-(2-(9-ethyl-9*H*-carbazol-3-yl)vinyl)phenyl)-3-(2-(pyrrolidin-1-yl)ethyl)thiourea (**50**) appeared to be the best candidate with good inhibitory activities against AChE (IC_{50} value of 2.64 μM) and BuChE (IC_{50} value of 1.29 μM), and significant inhibition of self-mediated $A\beta_{1-42}$ aggregation (51.29% at 25 μM concentration). The metal chelation study showed that compound (**50**) possessed specific copper ion chelating property. Additionally, compound (**50**) exhibited moderate antioxidant activity. To understand the binding mode of **50**, molecular docking studies were performed, and the results indicated strong non-covalent interactions of **50** with the enzymes in the active sites of AChE, BuChE as well as of the $A\beta_{1-42}$ peptide. Additionally, it showed promising *in silico* ADMET properties. Putting together, these findings evidently showed compound (**50**) as a potential multitarget-directed ligand in the course of developing novel anti-AD drugs.

1. Introduction

Alzheimer's disease (AD) is an age-related devastating neurodegenerative disorder, characterized by slow and inexorable memory loss that begins many years before the symptoms emerge [1]. It is the most common type of senile dementia with prevalence of 50 million people worldwide. By 2050, it is estimated that the number will rise to 150 million if no preventative means are made available [2]. The two major hallmarks of AD are the accumulation of beta-amyloid (Aβ) plaques outside the neurons and the twisted strands of tau protein inside the neurons in the brain. Although the etiology of AD is very complex and not fully resolved, several factors like deficit of acetylcholine (ACh) [3], abnormal Aβ deposition and accumulation [4], tau hyperphosphorylation [5], oxidative stress [6], and dyshomeostasis of biometals [7] are considered to play notable roles in the pathophysiology of AD. Currently, four drugs are approved for the treatment of AD namely: donepezil, rivastigmine, galantamine and memantine [8]. They only give symptomatic relief to the patient while none of the drugs available today stops the damage and destruction of neurons that make the AD fatal.

The cholinergic hypothesis reveals that the cognitive deficit associated with AD is due to cholinergic system dysfunction, mainly due to the declining levels of ACh in the brain [3,9]. ACh is rapidly hydrolyzed by acetylcholinesterase (AChE) and butyrylcholinesterase (BuChE) in the brain. Therefore, ChE inhibition is a useful strategy to increase ACh levels within the brain [10]. Besides its catalytic role, AChE also plays proaggregatory role by accelerating Aβ peptide aggregation and deposition into the fibrils. It is reported that AChE binds through peripheral anionic site (PAS) to non-amyloidogenic form of Aβ, acting as a pathological chaperone inducing conformational changes in

Abbreviations: ACh, acetylcholine; AChE, acetylcholinesterase; AD, Alzheimer's disease; APP, amyloid precursor protein; Aβ, beta-amyloid; BuChE, butyrylcholinesterase; 8-HQ, 8-hydroxyquinoline; MTDLs, multi-target directed ligands; PAS, peripheral anionic site; RMSD, root-mean-square deviation; RNS, reactive nitrogen species; ROS, reactive oxygen species; ThT, thioflavin T; XP, extra precision

* Corresponding author.
E-mail address: mryadav11@yahoo.co.in (M.R. Yadav).
[1] Current Position: Director (R & D), Parul University, Limbda, Waghodia Road, Vadodara, Gujarat, India.

https://doi.org/10.1016/j.bioorg.2020.103977
Received 6 May 2020; Received in revised form 20 May 2020; Accepted 24 May 2020
Available online 26 May 2020

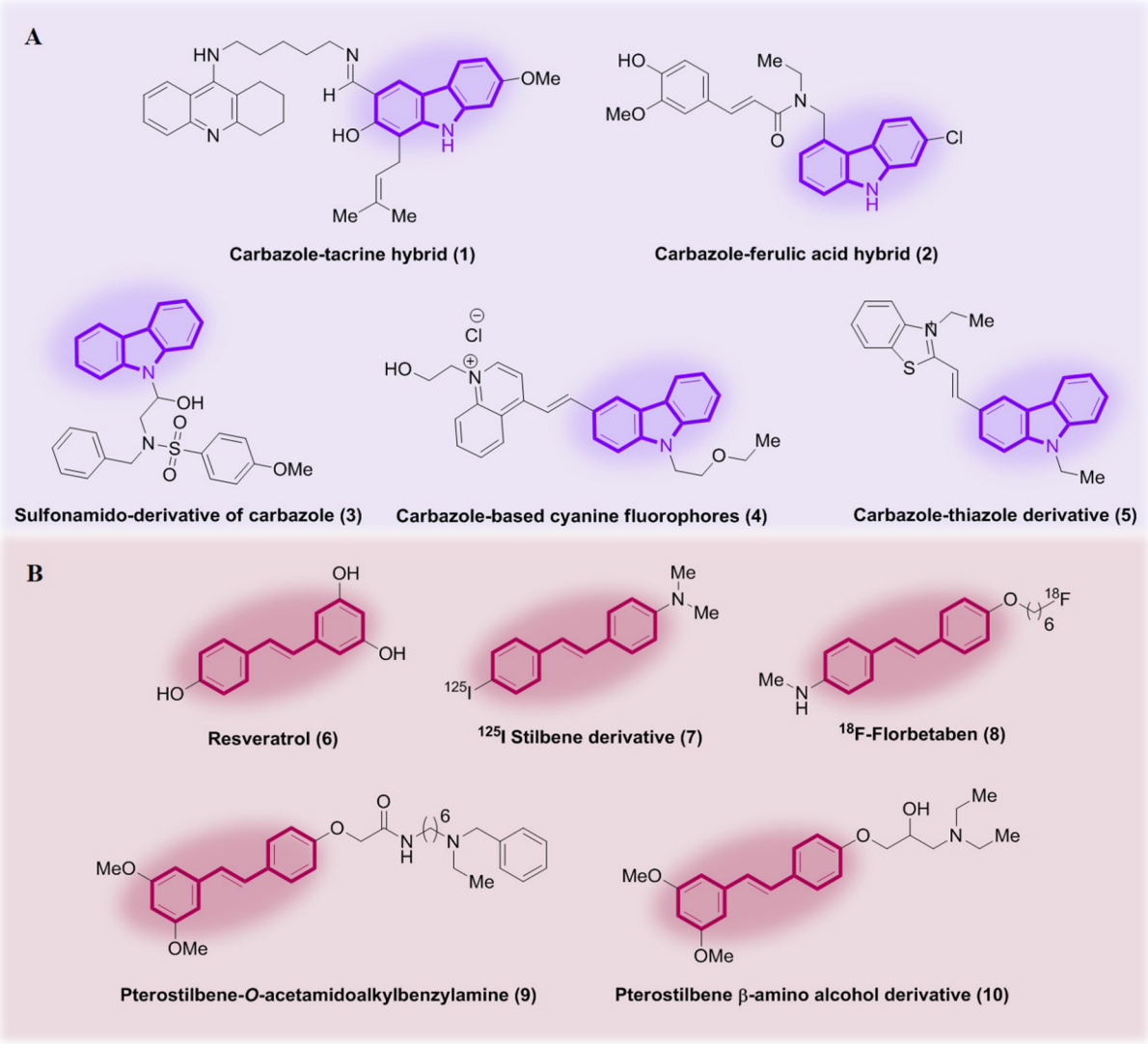

Fig. 1. Chemical structures of some previously reported (A) carbazole-based compounds (**1–5**) and (B) stilbene-based compounds (**6–10**) as anti-AD agents.

amyloidogenic form of Aβ with subsequent Aβ fibril formation [11]. In a healthy brain, AChE plays a major role in the hydrolysis of ACh. As the disease progresses, AChE level decreases, but BuChE level increases up to 40 to 90% in the hippocampus and temporal cortex region of the brain [12]. BuChE plays several roles both in neural and non-neural functioning. Clinical data suggested that high cortical levels of BuChE were associated with some important AD hallmarks, such as the extracellular deposition of the Aβ and aggregation of hyperphosphorylated tau protein [13]. This attests to the crucial role played by both the cholinesterases and the imperative to develop multi-targeted directed ligands (MTDLs) which could act on both of these ChEs.

Amyloid hypothesis states that Aβ plaques in the brain play a critical role in AD pathogenesis [14,15]. The plaques consist of aggregated oligomeric Aβ of variable lengths which are produced by sequential cleavage of the amyloid precursor protein (APP) by β- and γ-secretase. These aggregates initiate pathogenic cascade and eventually lead to neuronal loss and dementia [16]. The Aβ plaques generated from $A\beta_{1\text{-}42}$ are neurotoxic which continuously activate inflammatory mediators, such as TNF-α and IL-6. Furthermore, $A\beta_{1\text{-}42}$ itself can serve as an oxygen-free radical donor that produces reactive oxygen species and directly affects the normal physiological functions of neurocytes [17]. Hence, the inhibition of $A\beta_{1\text{-}42}$ aggregation could serve as a rational approach for the treatment of AD.

Recent research indicates that oxidative stress is an event that precedes the appearance of other hallmarks of AD. The subtle equilibrium between oxidants/antioxidants disturbed by inequity between generation and scavenging of free radicals cause oxidative stress [18]. By pathological oxidation–reduction steps, reactive oxygen species (ROS) and reactive nitrogen species (RNS) can denature biomolecules like proteins, lipids and nucleic acids. This can induce tissue damage through necrosis and apoptosis [19]. Thus, anti-oxidants endowed with additional pharmacological properties are thought to offer a hope to combat this complex disease, in which free radicals are important culprits but not the sole drivers.

Likewise, dyshomeostasis of metal ions such as iron, zinc, and copper, clearly occur in AD brains. The elevated concentrations of metal ions hasten the formation of Aβ aggregates and neurofibrillary tangles, which activate neurotoxic pathways and promote inflammation, leading to dysfunction and death of brain cells [20,21]. Additionally, redox-active metal ions, Cu (I/II), and Fe(II/III) associated with Aβ, were demonstrated to generate ROS under physiological conditions through Fenton-like reactions [22]. The overproduction of ROS leads to oxidative stress and eventually neuronal death in AD patients. Therefore, Aβ aggregation and ROS production induced by metal ions can be modulated by metal chelators, which highlights metal-ion chelation therapy as a promising AD treatment. However, non-selective metal chelators are likely to exhibit adverse side effects which is liable to limit their long-term clinical use.

In continuation of our research for unraveling potential novel MTDLs to combat AD, a series of novel carbazole-based stilbene derivatives as multifunctional anti-AD agents are presented here. Herein, we report the designing, synthesis and anti-AD activities of these novel compounds including cholinesterase inhibition, Aβ aggregation inhibition, antioxidant and metal chelation properties. Molecular modeling studies were also performed to know the binding mode of these compounds with the target proteins. ADMET properties of the synthesized compounds were also predicted using *in silico* methods.

2. Rationale of designing

The multifactorial nature of AD demands assaulting its key pathological hallmarks using MTDLs. Although ChEIs provide only symptomatic and transient benefits to the patients, they still remain the drugs of choice. Neurotoxic Aβ plaques, metal ion dyshomeostasis and oxidative stress play crucial roles in the pathogenesis of AD. However, targeting these factors all alone might not be enough to combat such a highly complex pathological disease like AD. So, cholinesterase inhibitors endowed with additional Aβ aggregation inhibitory, metal chelating and antioxidant activities could prove to be the competent candidates to confront this multifaceted disease.

Carbazole is an important nitrogen-containing heterocycle present widely in many phytochemicals with a range of biological activities [23]. It has been reported that the carbazole derivatives possess cholinesterase inhibitory [24], Aβ aggregation inhibitory [25], ROS scavenging, and neuron protective activities against oxidative damage [26]. Recently, various hybrid molecules having the carbazole scaffold and some other biologically active moieties have been developed as potential MTDLs for AD, like carbazole-tacrine hybrid (**1**) [27], carbazole-ferulic acid hybrid (**2**) [24] and carbazole-thiazole hybrid (**5**) [28] (Fig. 1). A plethora of biological activities associated with carbazole makes it an interesting privileged scaffold in the search for new anti-AD agents. Resveratrol (3,5,4′-trihydroxy-*trans*-stilbene) (**6**) is a naturally occurring stilbene derivative possessing multiple anti-AD properties i.e. Aβ aggregation inhibitory [29], neuroprotective [30] and antioxidant activities [31]. Several stilbene derivatives with encouraging Aβ binding abilities have been developed as Aβ imaging probes and Aβ aggregation inhibitors during the last two decades (Fig. 1) [32]. In combination with other bioactive moieties, these stilbene hybrids showed cholinesterase inhibitory, metal chelating, Aβ aggregation inhibitory, and free radical scavenging activities [33–35]. A central lipophilic scaffold with a terminal amine group is the salient feature of most of the reported stilbene derivatives which could have an impact on their anti-AD properties.

A combination of pharmacophoric moieties having different activities offering some novel hybrids have brought new hope for the treatment of AD. By molecular hybridization approach, a fusion of one pharmacophore to other results into a highly integrated scaffold with lower molecular weight. Here, a carbazole based stilbene scaffold was generated by the fusion of carbazole ring with a stilbene scaffold. We have previously reported substituted triazinoindole derivatives as anti-AD agents, in which pyrrolidine and piperidine side chains played an indispensable role in offering cholinesterase inhibitory activity [36]. Herein, we have designed two series of carbazole based stilbene derivatives in which the heterocyclic amines were linked with the designed scaffold using linkers endowed with additional anti-AD property (Fig. 2).

3. Results and discussion

3.1. Chemistry

Based on the attachment of the heterocyclic amines through suitable linkers on either of the two sites of the designed scaffold, these carbazole based stilbene derivatives have been divided into two series i.e. Series-1, wherein the attachment of the linker was to the carbazole ring and Series-2, in which the attachment was to the phenyl ring of the stilbene moiety (Fig. 2). Synthesis of the designed carbazole derivatives of Series 1 has been depicted in Schemes 1 and 2. The synthetic route for the required key intermediate (*E*)-9-ethyl-6-styryl-9*H*-carbazol-3-amine (**16**) from the commercially available carbazole (**11**) is outlined in Scheme 1. Ethylation of carbazole (**11**) by ethyl bromide in the presence of aqueous NaOH solution in DMSO afforded *N*-ethylcarbazole (**12**) in excellent yield. Mono-formylation of *N*-ethylcarbazole (**12**) by Vilsmeier-Haack formylation using DMF and phosphorus oxychloride generated 9-ethyl-3-formylcarbazole (**13**). Treatment of **13** with concentrated nitric acid gave the nitro derivative (**14**), which was reacted with benzyltriphenylphosphonium bromide under Wittig reaction condition to yield a mixture of *cis*- and *trans*-stilbenes. This isomeric mixture was converted to a single *trans* isomer (**15**) by performing the reaction with catalytic amounts of iodine in toluene. Reduction of the nitro group in (*E*)-9-ethyl-3-nitro-6-styryl-9*H*-carbazole (**15**) by stannous chloride offered the key amine intermediate (**16**).

N-(9-Ethyl-3-styryl-9*H*-carbazole-6-yl)aminoalkylamide derivatives (**20–25**) have been synthesized in two steps as shown in Scheme 2. Reaction of the amine intermediate (**16**) with the respective acid chlorides in presence of K_2CO_3 in acetone yielded the amide intermediates (**17–19**), which were further linked with alicyclic amines to offer the designed *N*-(9-ethyl-3-styryl-9*H*-carbazole-6-yl)aminoalkylamides (**20–25**).

Synthetic route for the designed (*E*)-1-(9-ethyl-6-styryl-9*H*-carbazol-3-yl)aminoalkylurea derivatives (**26–31**) is shown in Scheme 2. The amine intermediate (**16**) was reacted with *p*-nitrophenyl chloroformate in the presence of triethylamine, followed by reaction with alicyclic amines and aminoalkylamines yielded the designed (*E*)-1-(9-ethyl-6-styryl-9*H*-carbazol-3-yl)aminoalkylurea derivatives (**26–31**).

Synthesis of the designed carbazole derivatives of **Series 2** has been outlined in Schemes 3 and 4. Synthetic route for the required key intermediate (*E*)-4-(2-(9-ethyl-9*H*-carbazol-3-yl)vinyl)aniline (**34**) from 9-ethyl-9*H*-carbazole-3-carbaldehyde (**13**) is shown in Scheme 3. The reaction of **13** with 4-nitrophenylacetic acid (**32**) in the presence of piperidine under microwave conditions afforded the *trans* nitro stilbene derivative (**33**) as the sole product, configuration of which was confirmed by XRD. Reduction of the nitro group in compound (**33**) by stannous chloride yielded the desired amine intermediate (**34**).

(*E*)-*N*-(4-(2-(9-Ethyl-9*H*-carbazol-3-yl)vinyl)phenyl)aminoalkylamide derivatives (**38–43**) have been synthesized in a way similar to compounds (**20–25**) in two steps as shown in Scheme 4. Reaction of the amine intermediate (**34**) with the respective acid chlorides offered the amide intermediates (**35–37**), which were further reacted with alicyclic amines to afford the designed (*E*)-*N*-(4-(2-(9-ethyl-9*H*-carbazol-3-yl)vinyl)phenyl)aminoalkylamides (**38–43**).

Synthesis of the designed urea derivatives (**44–49**) and thiourea derivatives (**50–52**) was performed as depicted in Scheme 4. Reaction of the amine intermediate (**34**) with *p*-nitrophenyl chloroformate in the presence of triethylamine, followed by reaction with aminoalkylamines afforded the designed urea derivatives (**44–49**). Similarly, reaction of the amine intermediate (**34**) with thiocarbonyldiimidazole followed by reaction with the respective aminoalkylamines afforded the designed thiourea derivatives (**50–52**).

3.2. Biological evaluation

3.2.1. In vitro cholinesterase inhibition studies

Anti-cholinesterase activity has been confirmed in the tested compounds using the previously reported *in vitro* Ellman's assay [36–38]. The obtained IC_{50} values of the compounds for both AChE and BuChE enzymes and their selectivity indices (SI) are summarized in Tables 1 and 2. All the compounds (**20–31, 38–52**) offered IC_{50} values in the range of 1.84–6.63 μM for AChE and 1.02–5.01 μM for BuChE.

The inhibitory potential of the compounds from **Series 1** having a

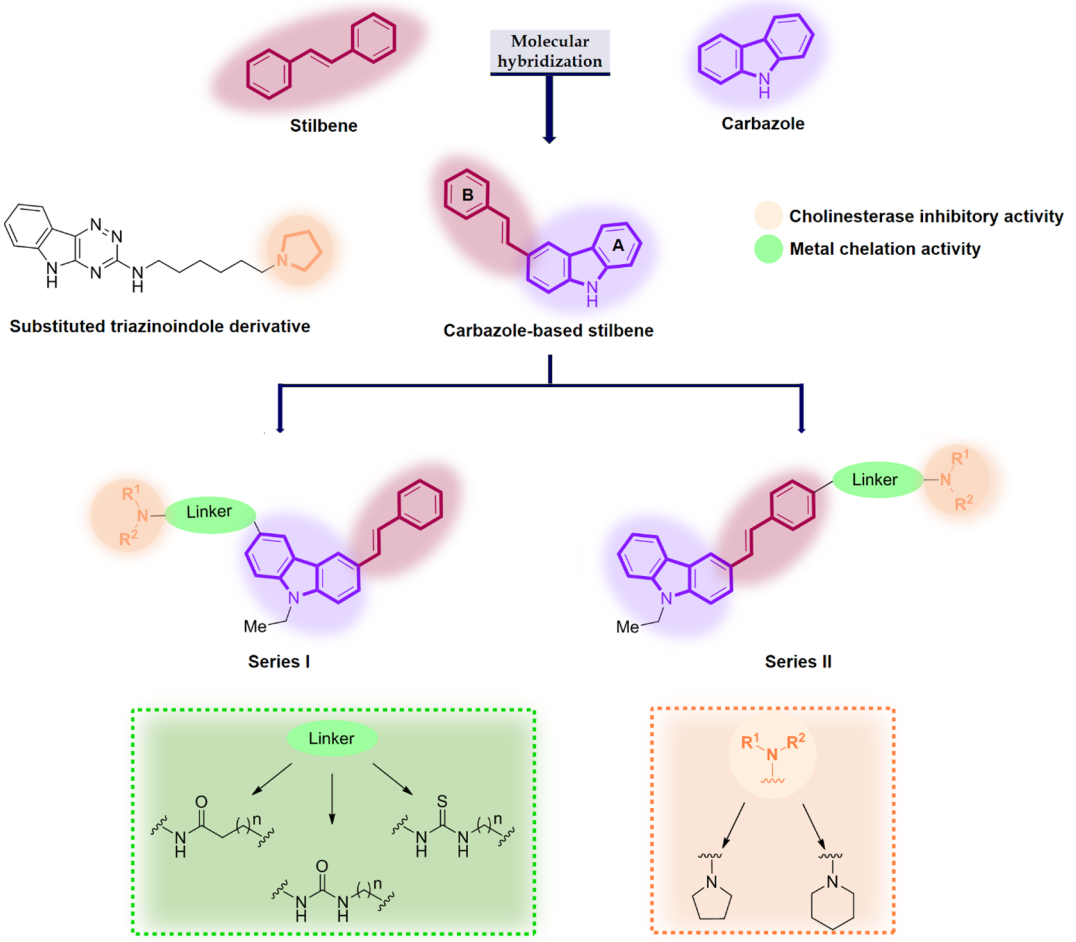

Fig. 2. Molecular hybridization approach used to design carbazole-based stilbene derivatives.

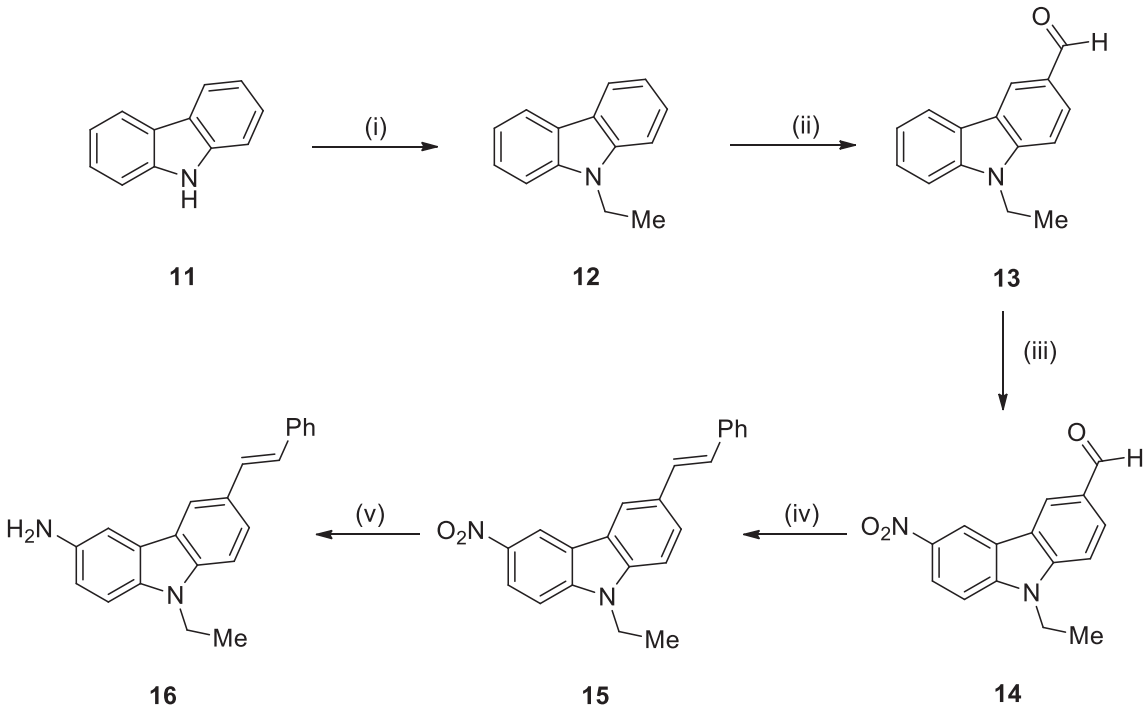

Scheme 1. Synthesis of the key intermediate (*E*)-9-ethyl-6-styryl-9*H*-carbazol-3-amine (**16**). Reagents and conditions: (i) EtBr, NaOH, DMSO, RT; (ii) $POCl_3$, DMF, $CHCl_3$; (iii) conc. HNO_3, AcOH; (iv) (a) benzyltriphenylphosphonium bromide, LiOH, IPA, reflux, (b) I_2, toluene, reflux; (v) $SnCl_2$, THF, MeOH, reflux.

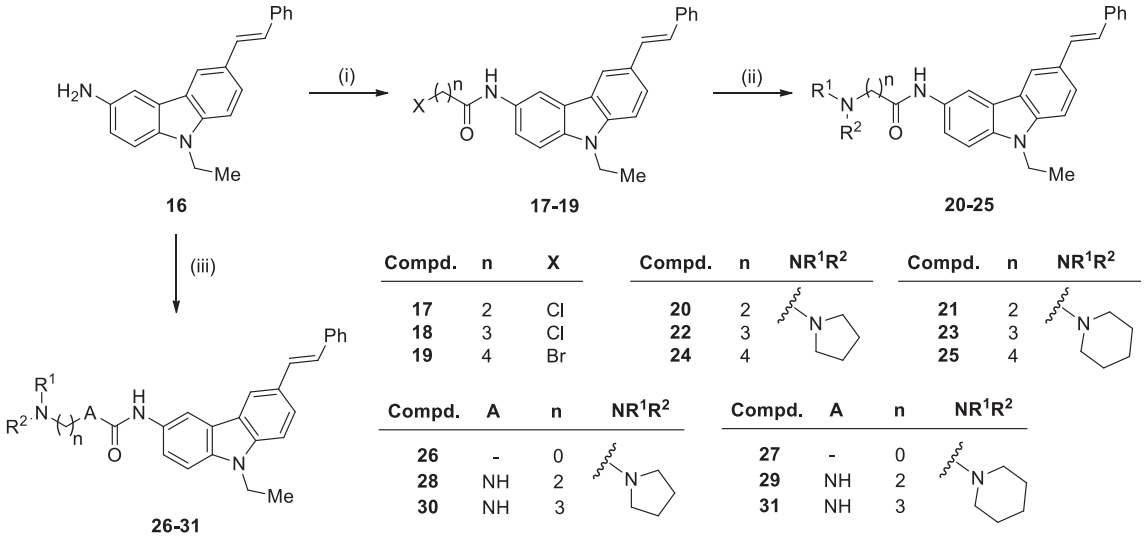

Scheme 2. Synthetic route for the synthesis of compounds (**20–31**). Reagents and conditions: (i) acid chloride, K_2CO_3, acetone; (ii) NHR^1R^2, THF, reflux; (iii) (a) *p*-nitrophenyl chloroformate, TEA, DCM:THF (1:1), 0 °C to RT, (b) pyrrolidine/piperidine/aminoalkylamines, RT.

side chain attached to the carbazole (ring A) has been shown in Table 1. It was observed that changing the length of the carbon chain affected the inhibitory activity. A comparative analysis of the inhibitory potential of compounds (**21**, **23** and **25**) having a piperidine ring, revealed that compound (**25**, n = 4) showed comparatively better AChE inhibitory activity (IC_{50} value of 1.84 μM) while compound (**21**, n = 3) and compound (**23**, n = 2) showed slightly poorer AChE inhibitory activities (IC_{50} values of 3.54 and 4.59 μM, respectively) (Table 1). A similar activity pattern was also observed for the compounds (**20**, **22** and **24**) having a pyrrolidine ring. Among these compounds, **21** (n = 2) showed better BuChE inhibition (IC_{50} value of 1.40 μM) in comparison to the other two derivatives. When the pyrrolidinyl (compound **26**) and piperidinyl (compound **27**) moieties were attached directly (n = 0, Table 1) to form urea derivatives, the inhibitory activities against both the enzymes decreased notably. Due to direct attachment, these compounds lost their basic centers, which are seemingly indispensable for cation-π interaction with the enzymes. Compounds (**26** and **27**) showed inhibitory activities (AChE; IC_{50} = 6.63 μM and 5.99 μM, respectively and BuChE; IC_{50} = 4.48 μM and 5.01 μM, respectively). There was no significant change observed in inhibitory activities when the amide linkers (compounds **20–25**) were substituted with urea linkers (compounds **28–31**) (Table 1).

Shifting the chain from the carbazole (ring A, Fig. 2) to the phenyl ring (ring B) of stilbene preserved the ChEs inhibitory potency (Table 2). A comparative analysis of the inhibitory potential of compounds (**38**, **40** and **42**) having a pyrrolidine ring, revealed that compound (**40**, n = 2) showed the best profile of AChE and BuChE inhibitory activities (IC_{50} values of 2.36 μM and 1.46 μM, respectively) while compound (**38**, n = 1) and compound (**42**, n = 3) showed slightly lower AChE and BuChE inhibitory activities. A similar activity pattern was also observed for the compounds (**39**, **41,** and **43**). Among these, compound (**41**, n = 2) showed the highest AChE and BuChE inhibitory activities (IC_{50} values of 2.25 μM and 1.74 μM, respectively).

All the urea derivatives (**46–49**) showed good ChEs inhibition, whereas compounds (**44** and **45**) in which the heterocyclic amine was directly attached (n = 0) to form urea showed moderate inhibitory

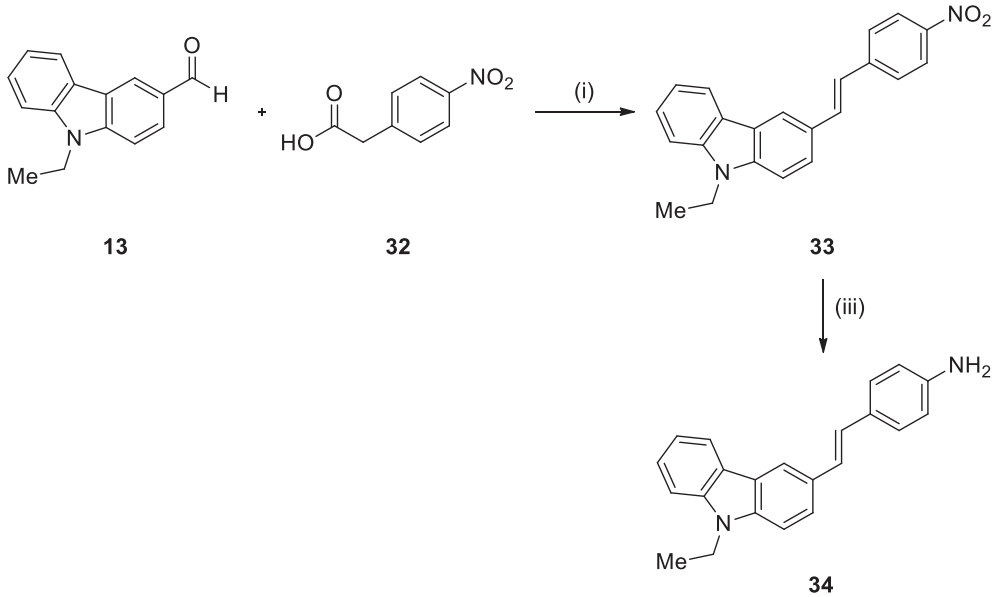

Scheme 3. Synthesis of the key intermediate (*E*)-4-(2-(9-ethyl-9*H*-carbazol-3-yl)vinyl)aniline (**34**). Reagents and conditions: (i) Piperidine, MW; (ii) $SnCl_2$, THF, MeOH, reflux.

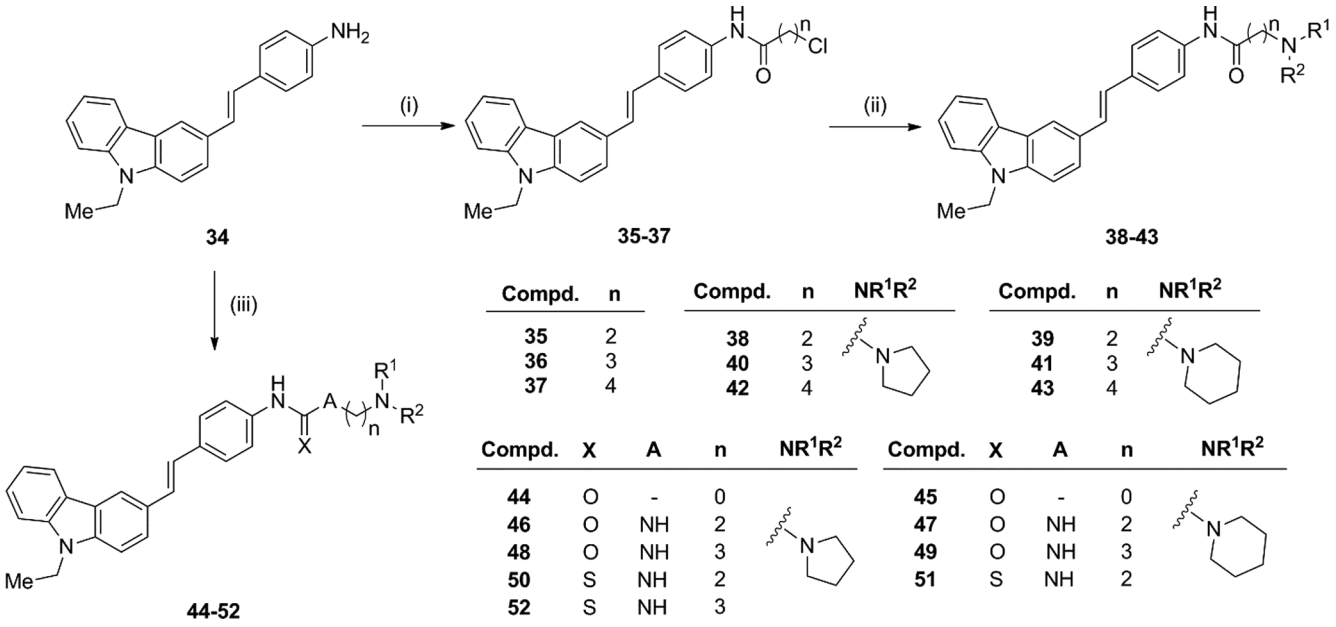

Scheme 4. Synthetic route for the synthesis of compounds (**38–52**). Reagents and conditions: (i) Acid chloride, K_2CO_3, acetone; (ii) NHR^1R^2, THF, reflux; (iii) For **44–49** (a) *p*-nitrophenyl chloroformate, TEA, DCM:THF (1:1), 0 °C to RT, (b) pyrrolidine/piperidine/aminoalkylamines, RT; For **50–52** (a) thiocarbonyldiimidazole, DCM:THF (1:1), 0 °C to RT; (b) aminoalkylamines, RT.

activities (AChE; IC_{50} = 16.22 μM and 12.37 μM, respectively) and (BuChE; IC_{50} = 11.65 μM and 8.58 μM, respectively). There was no significant change observed in AChE inhibitory activities when the amide linkers (compounds **42** and **43**) were substituted with urea linkers (compounds **46** and **47**) whereas the BuChE inhibitory activity was observed to be increased by two fold. All the thiourea derivatives (**50–52**) showed the best ChEs inhibitory activities profile amongst all of the derivatives. Among them, compound (**50**) was conferred with the highest AChE and BuChE inhibitory activities (n = 2, IC_{50} value of 2.64 μM and 1.29 μM, respectively).

3.2.2. Self-mediated $A\beta_{1-42}$ aggregation inhibition study

Aβ Peptides present in the extracellular amyloid plaques are produced by sequential cleavage of APP by β- and γ-secretases. $A\beta_{1-40}$ and $A\beta_{1-42}$ are the two main isoforms of Aβ peptides present in the plaques. $A\beta_{1-40}$ is the predominant product in the proteolytic cleavage, whereas $A\beta_{1-42}$ is more fibrillogenic in nature [39,40]. So, $A\beta_{1-42}$ was chosen for the Aβ aggregation inhibition study. The potential of the compounds to inhibit self-mediated $A\beta_{1-42}$ aggregation was assessed using Thioflavin T (ThT) fluorescence assay. Curcumin was used as a positive control in this assay. Percentage inhibitions of self-mediated $A\beta_{1-42}$ aggregation of all the tested compounds at 25 μM concentrations are listed in Tables 1 and 2. All the tested compounds showed good $A\beta_{1-42}$ aggregation inhibition ranging from 38.9 to 55.79%. Amongst them, compound (**47**) showed the best $A\beta_{1-42}$ aggregation inhibition (55.79%) at 25 μM concentration.

3.2.3. Antioxidant activity

The antioxidant activity of the compounds was evaluated by their ability to reduce DPPH· radical (purple) to DPPHH (yellow) and the corresponding radical-scavenging potential was assessed by a decrease in the absorbance at 517 nm [36]. Ascorbic acid was employed as a positive control in this assay. All the test compounds displayed moderate free radical scavenging activity (Tables 1 and 2). Amongst the thiourea derivatives (compounds **50–52**) showed moderate free radical scavenging activity (IC_{50} values 86.13 μM, 91.72 μM and 90.33 μM, respectively) compared to ascorbic acid (IC_{50} value of 13.9 μM) whereas tacrine and donepezil (IC_{50} values > 500 μM) were found to be practically devoid of significant free radical scavenging activity at this concentration.

3.2.4. Metal chelation study

High levels, and at the same time deregulation of biometal ions, such as Cu^{2+}, Zn^{2+}, and Fe^{2+}, are closely involved in the pathogenesis of AD [41]. Thus, the potential of compounds to form chelates with these biometals present in the brain of AD patients is like adding a feather in the cap of ideal MTDLs to treat AD patients.

The ability of the test compound to chelate biometals was assessed using UV–vis spectrophotometric assay [42]. The results demonstrated that when $CuSO_4$ was added to a solution of compound (**50**), its maximum absorbance at 343 nm decreased dramatically, indicating the formation of ligand-Cu^{2+} complex (Fig. 3**A**). There were insignificant changes in the positions and values of absorbance when $FeSO_4$, $FeCl_3$, $ZnCl_2$ or $AlCl_3$ were added into the solution of the test compound, suggesting that the test compound (**50**) had poor chelating abilities for Fe^{2+}, Fe^{3+}, Zn^{2+}, and Al^{3+}. The test compound (**50**) was also assessed for its binding ability to other biologically significant metal ions, such as Mg^{2+} and Ca^{2+} wherein the compound (**50**) exhibited very poor/no binding to these metal ions. 8-Hydroxyquinoline (HQ) was selected as a positive control to validate the assay protocol. There were significant changes in the positions and values of absorbance when metal ion solutions were added into the solution of HQ, confirming the nonselective metal-chelating abilities of HQ (Fig. 3**B**).

The above results and comparison of Fig. 3**A** and Fig. 3**B** evinced that the target compound (**50**) could selectively chelate Cu^{2+}. This high specificity for a particular metal ion is of prime importance in the design of a metal chelator to avoid chaotic binding to other critical biometal ions, the depletion of which can lead to allied side effects.

3.3. Computational studies

3.3.1. Docking studies of compound (50) with target proteins

To understand the molecular interactions and binding mode of the most active compound (**50**) with the ChEs, docking studies were carried out within the active sites of *Tc*AChE (PDB code: 2CKM) and *h*BuChE (PDB code: 4BDS) [43].

In the docking study of **50** with AChE, orientation of the compound along with the active site was found to be similar to that of donepezil,

Table 1
*In vitro h*AChE, *Eq*BuChE and self-induced Aβ aggregation inhibitory activities and DPPH radical scavenging activity of compounds (**20–31**).

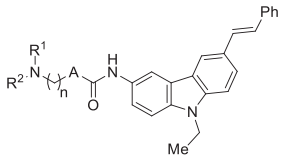

20-31

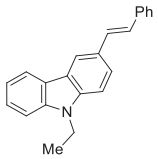

(CS-1)

Compd	A	n	R^1R^2N	IC_{50} ± SEM (μM)		SI[c]	Aβ1-42 aggregation Inhibition (%)[d] at 25 μM	RP of DPPH[e] IC_{50} ± SEM (μM) or% inhibition at 100 μM
				*h*AChE[a]	*Eq*BuChE[b]			
20	–	2		3.00 ± 0.52	1.53 ± 0.31	0.51	42.72 ± 0.31	144.61 ± 2.32 (35.46%)
21	–	2		4.69 ± 0.25	1.40 ± 0.22	0.29	52.08 ± 0.64	135.42 ± 2.05 (39.31%)
22	–	3		2.91 ± 0.14	1.51 ± 0.35	0.52	53.92 ± 0.28	145.02 ± 3.61 (36.15%)
23	–	3		3.54 ± 0.56	2.56 ± 0.29	0.72	49.88 ± 0.15	122.41 ± 3.20 (41.63%)
24	–	4		2.63 ± 0.31	3.17 ± 0.43	1.20	46.72 ± 0.33	134.63 ± 1.29 (38.11%)
25	–	4		1.84 ± 0.27	2.51 ± 0.19	1.36	48.09 ± 0.54	138.18 ± 1.53 (36.97%)
26	–	–		6.63 ± 0.54	4.48 ± 0.15	0.67	17.58 ± 0.42	nd
27	–	–		5.99 ± 0.07	5.01 ± 1.02	0.83	21.55 ± 0.62	nd
28	–NH	2		2.65 ± 0.32	1.70 ± 0.18	0.64	52.29 ± 0.34	104.28 ± 3.87 (48.94%)
29	–NH	2		3.79 ± 0.41	1.99 ± 0.21	0.52	50.08 ± 0.47	110.42 ± 2.62 (47.54%)
30	–NH	3		4.54 ± 0.52	3.19 ± 0.35	0.70	54.94 ± 0.76	123.62 ± 3.53 (42.49%)
31	–NH	3		3.57 ± 0.29	1.02 ± 0.18	0.28	54.35 ± 0.38	118.58 ± 3.20 (45.62%)
CS-1[f]				> 100	> 100	–	27.53 ± 0.93	> 500
Tacrine				0.056 ± 0.01	0.008 ± 0.00	0.14	nd	> 500
Donepezil				0.023 ± 0.01	1.87 ± 0.08	81.3	nd	> 500
Curcumin				nd	nd	–	20.43 ± 0.72 μM (IC_{50})	nd
Ascorbic acid				nd	nd	–	nd	13.91 ± 1.33 (98.25%)

[a] AChE from human erythrocytes.
[b] BuChE from equine serum, IC_{50} = 50% inhibitory concentration (means ± SEM of three experiments).
[c] Selectivity index = IC_{50} (BuChE)/IC_{50} (AChE).
[d] $A\beta_{1\text{-}42}$ peptide/inhibitor 1:1 with 25 μM inhibitor concentration.
[e] RP of DPPH (%) = reduction percentage of DPPH.
[f] CS-1 (carbazole-stilbene without amine side chain, supporting information).

extending from the active site amino acid residue Trp84 to the peripheral site amino acid residue Tyr70. Binding to the dual sites having such an interaction with these amino acids is crucial to display a strong affinity to the enzyme. In the classical binding mode, the tricyclic scaffold without an amine side chain is generally positioned near the CAS but in case of compound (**50**) an inverted binding mode is observed where instead of the aromatic scaffold, the protonated tertiary amine is positioned in the CAS, deep in the binding gorge. Pyrrolidinylethyl thiourea part of the compound (**50**) was observed interacting with the CAS of the active site gorge, whereas the *N*-ethylcarbazole moiety of the scaffold was found to be interacting with the receptor active site in PAS of the gorge (Fig. 4). In PAS, the aromatic carbazole moiety exhibited very strong π-π interactions with Tyr70 and Tyr334 (*h*AChE: Tyr72 and Tyr341). The phenyl ring of compound (**50**) was observed to be stabilized comfortably in the active site of the enzyme by forming hydrophobic interactions with the aromatic amino acids Tyr116, Phe330 and Phe331 (*h*AChE: Tyr119, Tyr337 and Phe338). Stability to the ligand-receptor complex in CAS is mainly observed because of hydrogen bonding, cation-π interaction and salt bridge. The –NH of thiourea group interacted with Tyr130 (*h*AChE: Tyr133) by forming a stable hydrogen bond. In addition to this, at physiological *p*H, the protonated nitrogen of pyrrolidine moiety exhibited strong cation-π interaction with Trp84 (*h*AChE: Trp86) along with a hydrogen bonding and salt bridge interactions with Glu199 (*h*AChE: Glu202).

The binding mode of **50** with the BuChE enzyme indicated that it also occupied a large catalytic cavity of BuChE (Fig. 5). Carbazole ring was found to be stabilized in the hydrophobic pocket of nonpolar amino acid residues Ala277, Val280, Pro285 and Leu286. The phenyl ring stabilized the ligand-receptor complex by forming stable π-π interaction with Tyr332 residue. Hydrogen bond between the –NH of thiourea and Tyr332 residue imparted stability to the ligand-receptor complex. Further stability to this complex was also provided by the protonated nitrogen of pyrrolidine by forming cation-π interaction with Trp82 residue of the active site.

To understand the binding interaction of compound (**50**) with $A\beta_{1\text{-}}$

Table 2
*In vitro h*AChE, *Eq*BuChE and self-induced Aβ aggregation inhibitory activities and DPPH radical scavenging activity of compounds (**38–52**).

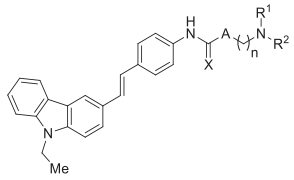

(38-52)

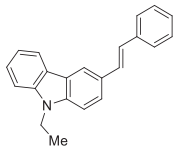

(CS-1)

Compd	X	A	n	R^1R^2N	IC_{50} ± SEM (μM)		SI[c]	Aβ1-42 aggregation Inhibition (%)[d]	RP of DPPH[e] IC_{50} ± SEM (μM) or % inhibition at 100 μM
					*h*AChE[a]	*Eq*BuChE[b]			
38	O	–	1		2.98 ± 0.78	2.49 ± 0.65	0.84	51.14 ± 0.31	132.42 ± 1.17 (42.34%)
39	O	–	1		3.52 ± 0.87	2.72 ± 0.98	0.79	45.17 ± 0.64	146.28 ± 3.21 (35.46%)
40	O	–	2		2.36 ± 0.20	1.46 ± 0.42	0.62	54.27 ± 0.28	189.10 ± 2.26 (30.15%)
41	O	–	2		2.25 ± 0.31	1.74 ± 0.19	0.77	51.92 ± 0.15	178.51 ± 3.66 (25.81%)
42	O	–	3		4.77 ± 0.61	4.76 ± 1.03	0.99	53.08 ± 0.33	126.43 ± 2.27 (41.34%)
43	O	–	3		3.29 ± 1.09	2.11 ± 0.69	0.64	49.78 ± 0.54	118.58 ± 1.12 (42.91%)
44	O	–	–		16.22 ± 1.03	11.65 ± 0.51	0.68	42.84 ± 0.82	nd
45	O	–	–		12.37 ± 0.87	8.58 ± 1.02	0.69	44.15 ± 0.67	nd
46	O	–NH	2		4.71 ± 1.05	2.32 ± 0.97	0.49	38.90 ± 0.85	161.45 ± 1.46 (13.67%)
47	O	–NH	2		3.13 ± 0.71	1.20 ± 0.57	0.38	55.79 ± 0.78	97.36 ± 1.46 (51.19%)
48	O	–NH	3		3.04 ± 0.43	1.92 ± 0.25	0.63	53.86 ± 0.66	106.01 ± 1.39 (45.95%)
49	O	–NH	3		2.94 ± 0.98	1.98 ± 0.84	0.67	54.06 ± 0.49	134.70 ± 1.17 (41.98%)
50	**S**	**–NH**	**2**		**2.64 ± 0.41**	**1.29 ± 0.10**	**0.49**	**51.29 ± 0.42**	**86.13 ± 1.23 (72.36%)**
51	S	–NH	2		3.41 ± 0.25	1.72 ± 0.25	0.50	53.24 ± 0.44	91.72 ± 3.43 (66.36%)
52	S	–NH	3		3.19 ± 0.34	1.32 ± 0.17	0.41	53.29 ± 0.62	90.33 ± 1.20 (70.36%)
CS-1[f]					> 100	> 100	–	27.53 ± 0.93	> 500
Tacrine					0.056 ± 0.01	0.008 ± 0.00	0.14	nd	> 500
Donepezil					0.023 ± 0.01	1.87 ± 0.08	81.3	nd	> 500
Curcumin					nd	nd	–	20.43 ± 0.72 μM (IC_{50})	nd
Ascorbic acid					nd	nd	–	nd	13.91 ± 1.33 (98.25%)

[a] AChE from human erythrocytes.
[b] BuChE from equine serum, IC_{50} = 50% inhibitory concentration (means ± SEM of three experiments).
[c] Selectivity index = IC_{50} (BuChE)/IC_{50} (AChE).
[d] $A\beta_{1\text{-}42}$ peptide/inhibitor 1:1 with 25 μM inhibitor concentration.
[e] RP of DPPH (%) = reduction percentage of DPPH.
[f] CS-1 (carbazole-stilbene without amine side chain, supporting information).

$_{42}$, a blind docking study was performed using the X-ray crystal structure of human $A\beta_{1\text{-}42}$ (PDB code: 1IYT) [44]. The important regions involved in Aβ aggregation include the *N*-terminal region, central hydrophobic core (Leu17-Ala21), hinge regions (Arg5-Ser8 and Glu22-Asn27) and the hydrophobic region (Ile32-Ala42). The hydrophobic core around Leu17-Ala21 residues plays a crucial role in the β-sheet formation. In this study, the most stable ligand-receptor complex offered promising interactions (Fig. 6). Compound (**50**) was observed to be aligned with the chain of $A\beta_{1\text{-}42}$. The carbazole ring showed stable interaction with Phe19 residue, whereas both the –NH of thiourea group were observed to be interacting strongly with Asp7 residue by forming hydrogen bonding. Further, the protonated nitrogen of pyrrolidine established stable salt bridge interactions with Asp7 and Glu11 residues. Along with this interaction, the ligand-receptor stability was further supported by hydrogen bonding of the nitrogen of pyrrolidine with Asp7 residue of the active site. As hydrogen bondings, salt bridges and hydrophobic interactions of $A\beta_{1\text{-}42}$ monomers represent a crucial factor governing their aggregation, binding of **50** with $A\beta_{1\text{-}42}$ monomers by π-π interactions and hydrogen bondings suggests that compound (**50**) could inhibit Aβ aggregation by blocking intermolecular interactions among multiple Aβ monomers. It needs to be specified that this docking is only a predictive tool, the real binding mode and interaction of compound (**50**) with $A\beta_{1\text{-}42}$ has not been verified practically.

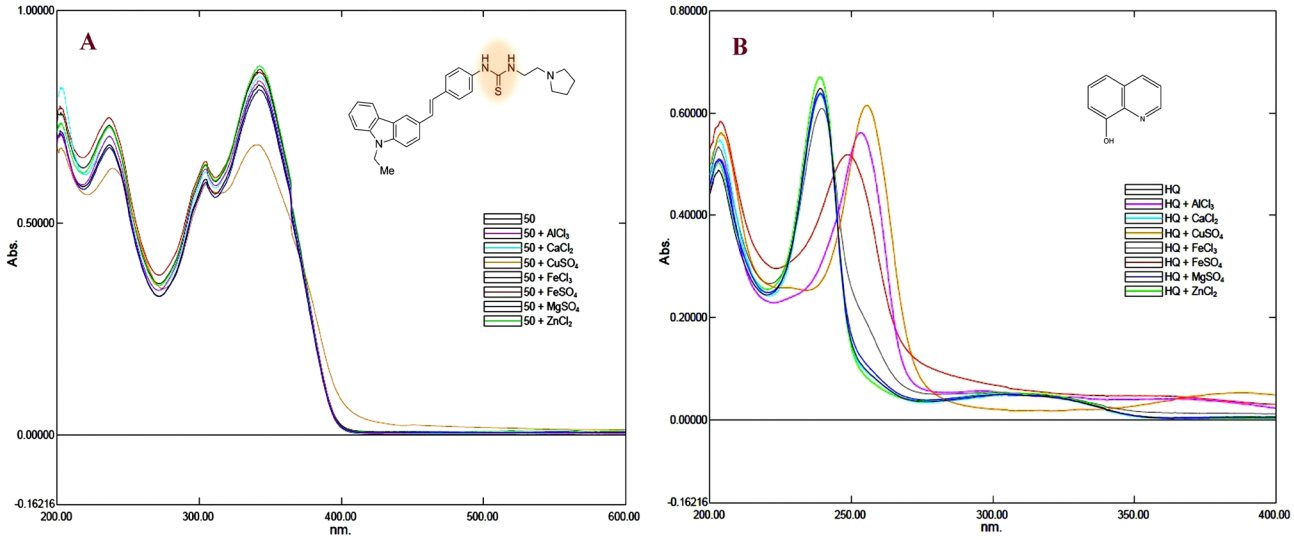

Fig. 3. Metal chelation study of compound (**50**) and HQ. UV–vis spectra of (A) compound (**50**) and (B) HQ (25 μM) alone and in the presence of $CuSO_4$ (25 μM), $ZnCl_2$ (25 μM), $FeSO_4$ (25 μM), $FeCl_3$ (25 μM), $AlCl_3$ (25 μM) $MgSO_4$ (25 μM) and $CaCl_2$ (25 μM) in methanol at room temperature.

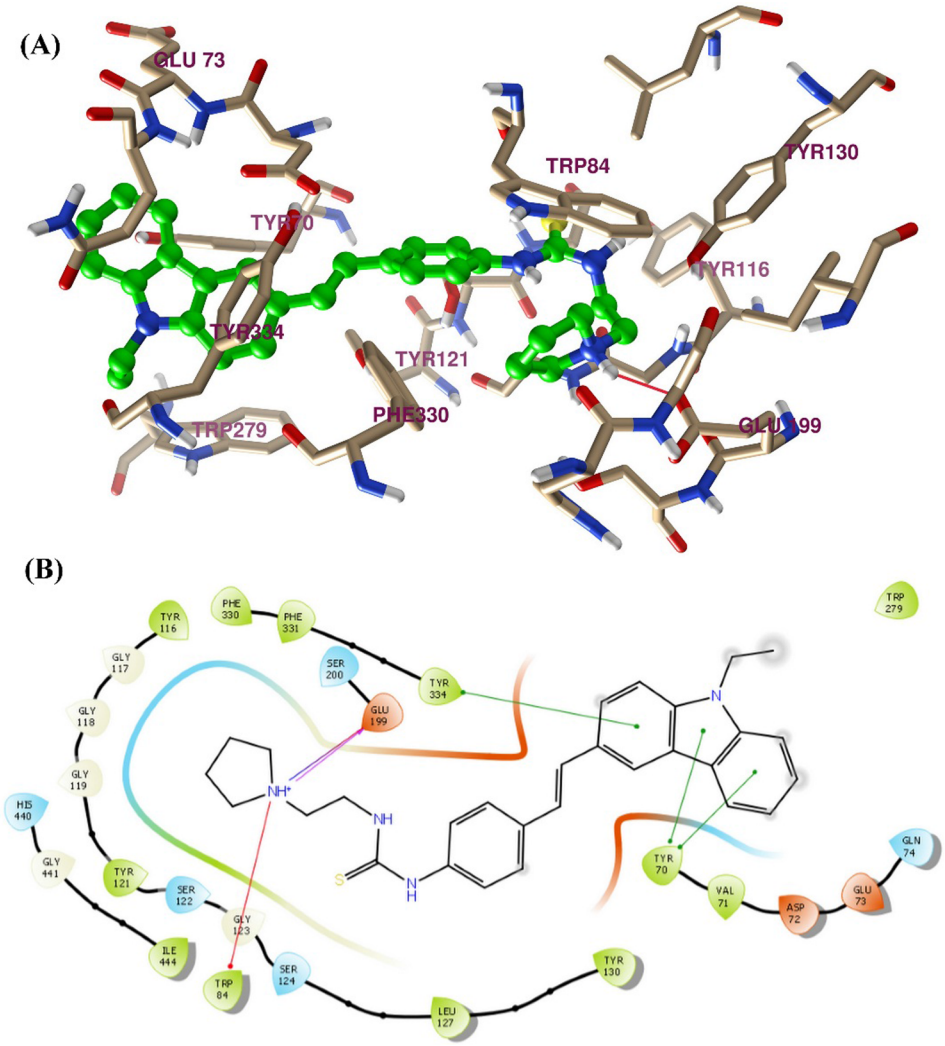

Fig. 4. Docking model of compound (**50**) with *Tc*AChE (PDB ID: 2CKM). (A) Binding mode of **50** in the active site of *Tc*AChE. The ligand is shown as green balls and sticks. AChE residues are shown as atom type colour sticks. Hydrogen bonds formed between the ligand and the receptor are indicated by red lines. (B) Ligand interaction diagram of **50** with *Tc*AChE.

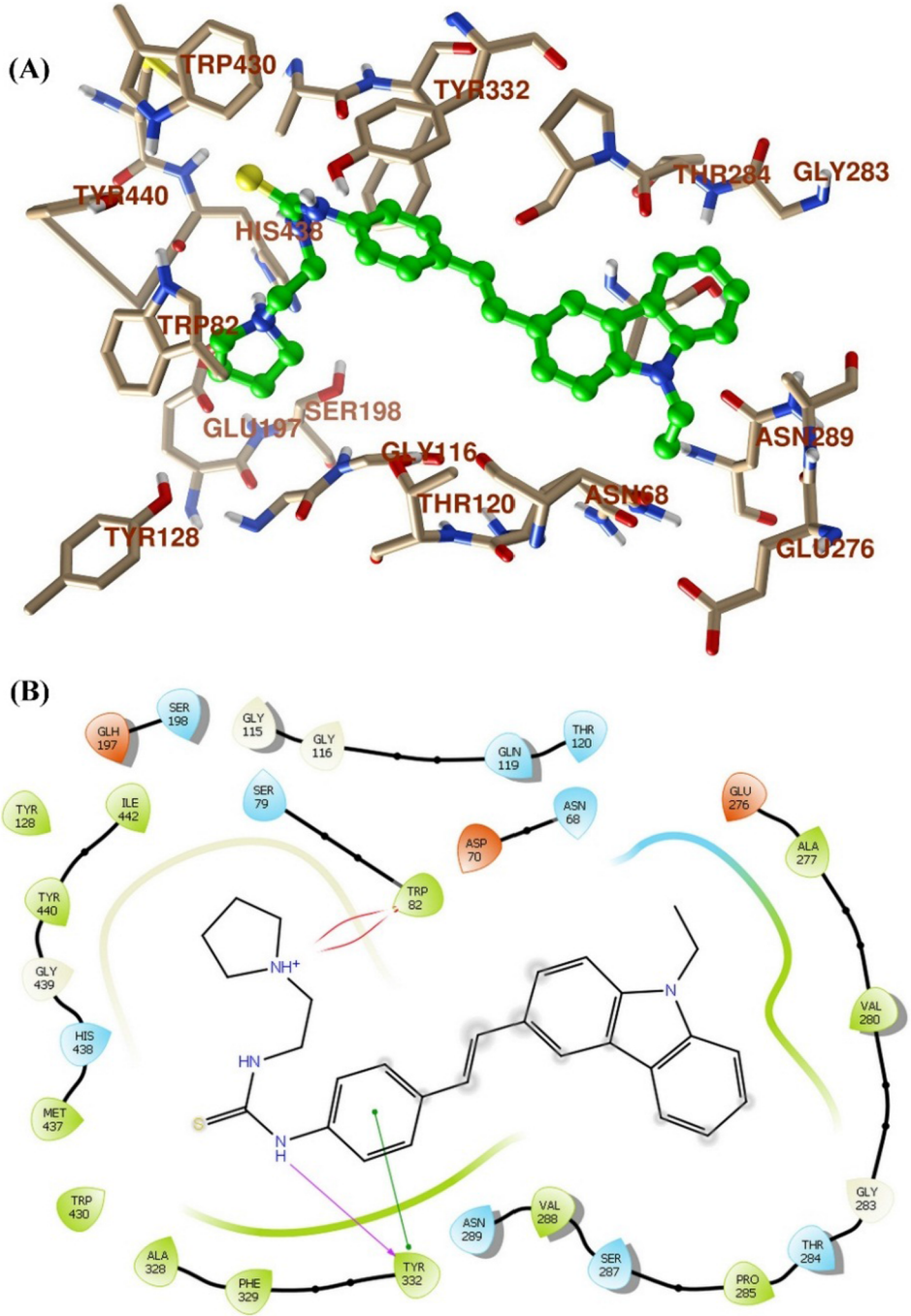

Fig. 5. Docking model of compound (**50**) with *h*BuChE (PDB ID: 4BDS). (A) Binding mode of **50** in the active site of *h*BuChE. Ligand is shown as green balls and sticks. *h*BuChE residues are shown as atom type colour sticks. (B) Ligand interaction diagram of **50** with *h*BuChE.

3.3.2. In silico physicochemical and pharmacokinetics parameters prediction

For considering any synthesized compound as a therapeutically important molecule, it should not only be biologically active but should also be endowed with desirable physico-chemical land pharmacokinetic properties. Approximately 40% of the drug candidates failed in the clinical trials due to the unacceptable ADME (absorption, distribution, metabolism, and excretion) properties [45]. The *in silico* prediction of the ADME properties during the drug development process is a useful strategy to identify these physicochemical and pharmacokinetic liabilities and to identify and reject those compounds that are suspected to withstand the rigors of the later stages of drug developments. Due to the significant progress made in the field of computational sciences in recent times, *in silico* prediction of ADMET parameters becomes relatively simple and reliable. The virtual physicochemical and pharmacokinetic parameters like Lipinski's parameters, NRB, PSA, QPPCaco, QPPMDCK, CNS, QPlogBB, QPlogKhsa were predicted for compound (**50**) with QikProp module (Table 3) [46].

Lipinski's rule-of-five states that most of the "drug-like" molecules should have molecular weight ≤ 500, number of hydrogen bond acceptors ≤ 10, number of hydrogen bond donors ≤ 5 and LogP ≤ 5 [47]. Poor absorption or permeation is more likely to be the case when molecules violate more than one of these rules. Compound (**50**) satisfied all these parameters offering values in the given acceptable ranges except for $QPlogP_{o/w}$ (value > 5). Compounds (**50**) violates only one limit of the Lipinski's rule-of-five, making it as a promising

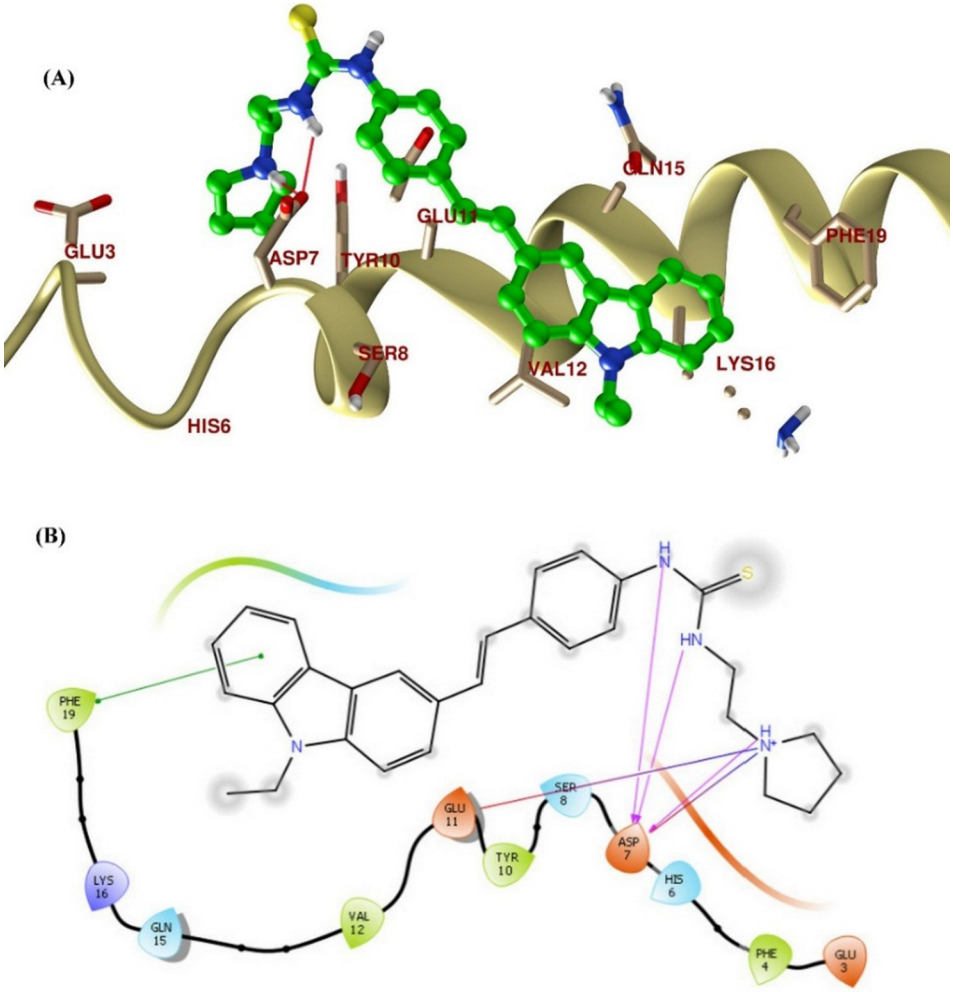

Fig. 6. Docking model of compound (**50**) with $A\beta_{1-42}$ (PDB code 1IYT): (A) Binding mode of **50** with $A\beta_{1-42}$. Ligand is shown as green balls and sticks. $A\beta_{1-42}$ is shown as cartoon. Hydrogen bonds formed between the ligand and the receptor are indicated by red lines. (B) Ligand interaction diagram of **50** with *h*BuChE.

lead as a drug candidate. The number of rotatable bond (NRB) and topological polar surface area (TPSA) are the two key parameters introduced by Veber [48]. NRB is a simple topological parameter that indicates molecular flexibility. It is an important descriptor for oral bioavailability of drugs. The compound could have 0–8 rotatable bonds or less than 7 linear chains outside rings for good oral bioavailability. TPSA is another important descriptor that is well correlated with passive transport through membranes and therefore, it allows the prediction of bioavailability and penetration through blood–brain barrier (BBB) and drug absorption, including intestinal absorption [49]. The mean value of a TPSA is 40.5 $Å^2$ (range 4.63–108 $Å^2$) for the marketed CNS drugs. Compound (**50**) possesses eight rotatable bonds and a TPSA value of 38.55 $Å^2$ [50]. QPCaco-2 value relates to the oral absorption of a drug. It shows apparent permeability through gut-blood barrier. Values above 500 predict high oral absorption which has been attained by compound (**50**). Good oral bioavailability of compound (**50**) is also supported by the predicted human oral absorption percent (% HOA) value. Brain/blood partition coefficient (QPlogBB), CNS, *n*-octanol − water partition coefficient (QPlogPo/w), and apparent MDCK cell permeability (QPPMDCK) all predict the ability of the compound to cross the BBB. Compound (**50**) is predicted to be CNS active as it possesses a CNS value as 1 and QPlogBB value as 0.219. QPPMDCK value is predicted apparent MDCK cell permeability in nm/s. It is recognized as a good mimic for the BBB [51]. A QPPMDCK value higher than 25 is viewed as good, and the compound (**50**) has shown considerably high value. The QPlogKhsa value predicts the binding of the compound with human serum albumin. Compound (**50**) showed a slightly higher value than the recommended QPlogKhsa values. #Star shows the number of parameters with values that fall outside the 95% range of similar values for known drugs. A larger number of #stars suggests that the compound is less druglike than the compound with few #stars. The value of #star for compound (**50**) suggests its drug-likeness. Further, a compound having a tertiary nitrogen-containing moiety, which is a common feature in many CNS active drugs, normally exhibits a higher degree of brain permeation [50]. As discussed above, the compound (**50**) is predicted to possess a good pharmacokinetic profile, which highlights its biological significance.

4. Conclusion

By molecular hybridization approach, a combination of carbazole and stilbene rings resulted in (*E*)-3-styryl-9*H*-carbazole scaffold. Modifications by attaching alicyclic amines with different linkers to the (*E*)-3-styryl-9*H*-carbazole scaffold resulted in a novel series of anti-AD agents. Among the series, compound (**50**) having pyrrolidine moiety and thiourea linker showed the most promising inhibitory activities against AChE (IC_{50} value of 2.64 μM) and BuChE (IC_{50} value of 1.29 μM). Compound (**50**) exhibited a significant self-mediated $A\beta_{1-42}$ aggregation inhibition (51.29% at 25 μM concentration). It also displayed specific metal (Cu^{2+}) chelating ability and moderate antioxidant activity. Molecular modeling studies indicated significant interactions between this most potent compound (**50**) with PAS as well as

Table 3
Predicted ADMET parameters of compound (50) and donepezil.[a]

Parameter	Limit	50	Donepezil
MW	130–725	468.659	379.498
HBA	2–20	4.5	5.5
HBD	0–6	2	0
NRB	0–8	8	6
QPlogP$_{o/w}$	−2 to 6.5	7.002	4.242
PSA	7 to 200	38.55	46.234
Volume	500–2000	1571.159	1248.451
ReFG	0–2	0	0
SASA	300 to 1000	878.316	681.675
Rule of Five(violation)	0–1	1	0
CNS	–	1	1
QPPMDCK	–	1284.443	589.289
QPlogBB	−3 to 1.2	0.219	0.223
QPPCaco	–	1235.258	1070.771
QPlogKhsa	−1.5 to 1.5	1.58	0.516
QPlogS	−6.5 to 0.5	−8.12	−4.059
% HOA	0–100	100	100
#star	0–5	4	0

[a] MW: molecular weight, HBA: hydrogen-bond acceptor atoms, HBD: hydrogen-bond donor atoms, NRB: number of rotatable bonds, QPlogP$_{o/w}$: Predicted octanol/water partition coefficient, PSA: polar surface area, #rtvFG: number of reactive functional groups; SASA: total solvent accessible surface area, CNS: predicted central nervous system activity on a −2 (inactive) to + 2 (active) scale, QPPMDCK: Predicted apparent MDCK cell permeability in nm/s, QPlogBB: brain/blood partition coefficient, QPPCaco: Caco-2 cell permeability in nm/s, QPlogKhsa: binding to human serum albumin, QPlogS: predicted aqueous solubility, % HOA: human oral absorption on 0–100% scale, #star: number of parameters with values that fall outside the 95% range of similar values for known drugs.

CAS sites of both the enzymes as well as with A$\beta_{1\text{-}42}$ peptide. Additionally, compound (**50**) exhibited favorable *in silico* ADMET properties. All these results suggest that compound (**50**) could be a leading candidate with a high potential for further development as a novel anti-AD drug.

5. Experimental

General: All of the commercial reagents and solvents required during the synthesis of the compounds were procured from Sigma-Aldrich, Spectrochem, S. d. fine chemicals and Avra chemicals, and were purified by general laboratory techniques whenever needed. Reaction monitoring was carried out by thin-layer chromatography (TLC), using silica gel precoated plates (60F254, Merck, 0.25 mm thickness) and visualizing in ultraviolet (UV) light (λ = 254 nm) or in an iodine chamber. Compounds were purified by flash column chromatography with a Teledyne ISCO CombiFlash Rf system using RediSep Rf columns. Yields reported here are unoptimized. Melting points were determined in glass capillary tubes using a silicon oil-bath type melting point apparatus (Veego) and the reported melting points are uncorrected. The IR spectra were recorded on a Bruker ALPHA-T (Germany) FT-IR spectrophotometer for all the reported compounds and are consistent with the assigned structures. ^{1}H NMR and ^{13}C NMR spectra were recorded on a Bruker Advance-II 400 MHz spectrometer in $CDCl_3$ or DMSO-d_6 solvents. Chemical shifts (δ) are expressed in parts per million (ppm) relative to the standard TMS, and the peak patterns are indicated as s (singlet), d (doublet), t (triplet), m (multiplet), and br (broad signal). Mass spectra were recorded using a Thermo Fisher mass spectrometer with an ESI ion source. LCMS analyses were performed on WATERS-2690 with QDA-Mass detector and electrospray ionization. LCMS method is described in the Supporting Information. Elemental analyses were performed on a Thermo Fisher FLASH 2000 organic elemental analyzer. The elemental compositions of the compounds were within ± 0.4% range of the calculated values.

5.1. Chemistry

5.1.1. 9-Ethyl-9H-carbazole (12)

To a rapidly stirring solution of carbazole **1** (0.5 g, 2.99 mmole) in DMSO (10 mL), a few drops of aqueous sodium hydroxide (0.25 g) were added and stirred for 5 min. To it ethyl iodide (0.3 mL, 3.58 mmole) was added slowly. The reaction mixture was stirred for further 4–5 hrs to complete the reaction. After completion of the reaction, the reaction mixture was poured in crushed ice, and the solid precipitate so obtained was collected and washed with water to remove the residual solvent and dried to obtain the titled compound (**12**) (0.54 g, 94%), m.p. 64–66 °C (lit [52] m.p. 67–69 °C); IR (KBr, cm^{-1}): 3049, 2978, 2869, 1596, 1018, 753, 700; MS (*m/z*): 196.3 [M + H]$^{+}$.

5.1.2. 9-Ethyl-9H-carbazole-3-carbaldehyde (13)

Phosphorus oxychloride (0.47 mL, 5.12 mmol) was added, over a period of 10 min to an ice cooled stirred solution of 9-ethyl-9*H*-carbazole (**12**) (1.0 g, 5.13 mmol) and dimethylformamide (0.38 mL, 5.12 mmol) in 10 mL of chloroform. The resulting reaction mixture was refluxed for overnight. The reaction mixture was then poured into crushed ice. After warming to RT the resulting product was extracted into chloroform and the organic phase was washed with water and brine, dried over magnesium sulphate and evaporated at reduced pressure. The obtained residue was purified by column chromatography on silica gel using petroleum ether-ethyl acetate (15%) to obtain the titled compound (**13**) (0.96 g, 88%), m.p. 84–86 °C (lit [53] m.p. 84–86 °C); IR (KBr, cm^{-1}): 2971, 2929, 2822, 2743, 1679, 1588, 620; ^{1}H NMR (DMSO-d_6): δ 10.12 (s, 1H, –C*H*O), 8.64 (s, 1H, Ar*H*), 8.18 (d, J = 8 Hz, 1H, Ar*H*), 8.04 (d, J = 8 Hz, 1H, Ar*H*), 7.37–7.58 (m, 4H, Ar*H*), 4.43 (q, J = 7.2 Hz, 2H, –NCH_2CH$_3$), 1.49 (t, J = 7.2 Hz, 3H, –NCH$_2$CH_3); MS (*m/z*): 224 [M + H]$^{+}$.

5.1.3. 9-Ethyl-6-nitro-9H-carbazole-3-carbaldehyde (14)

Nitric acid (0.44 mL) was added drop-wise to a stirring solution of 9-ethyl-9*H*-carbazole-3-carbaldehyde (**13**) (1.0 g, 4.47 mmol) in acetic acid (10 mL) under cold conditions. After completion of addition, the reaction mixture was further stirred for additional 1 h. The solid so precipitated was collected by filtration and washed with acetic acid (10 mL). Excess acetic acid was removed by washing with water. The solid so obtained was dried to obtain greenish colored compound (**14**) (1.1 g, 92%); m.p. 241–243 °C (lit [54] m.p. 247–248 °C); IR (KBr, cm^{-1}): 3081, 2967, 2870, 2822, 2728, 1685, 1591, 1021, 752; ^{1}H NMR ($CDCl_3$): δ 10.16 (s, 1H, –C*H*O), 9.09 (d, J = 2.4 Hz, 1H, Ar*H*), 8.69 (d, J = 1.2 Hz, 1H, Ar*H*), 8.47 (dd, J = 2.4 Hz, 9.2 Hz, 1H, Ar*H*), 8.15 (dd, J = 1.6, 8.4 Hz, 1H, Ar*H*), 7.61 (d, J = 8.4 Hz, 1H, Ar*H*), 7.53 (d, J = 9.2 Hz, 1H, Ar*H*), 4.68 (q, J = 7.2 Hz, 2H, –NCH_2CH$_3$), 1.54 (t, J = 7.2 Hz, 3H, –NCH$_2$CH_3); MS (*m/z*): 269 [M + H]$^{+}$.

5.1.4. (E)-9-Ethyl-3-nitro-6-styryl-9H-carbazole (15)

To a stirred solution of benzyltriphenylphosphonium bromide (2.4 g, 5.58 mmol) in isopropyl alcohol (25 mL), lithium hydroxide (0.18 g, 7.44 mmol) was added. The reaction mixture was stirred further for 30 min at room temperature. To it 9-ethyl-6-nitro-9*H*-carbazole-3-carbaldehyde **14** (1.0 g, 3.72 mmol) was added in small portions over a period of a few minutes. The resulting reaction mixture was heated to 80 °C for 5–6 h. Progress of the reaction was monitored by TLC. After completion of the reaction, the solid so precipitated was collected by filtration and washed with isopropyl alcohol (15 mL). The obtained solid contained mixture of *cis* and *trans* isomers. This isomeric mixture was dissolved in benzene (50 mL) and catalytic amount of iodine was added to it. The reaction mixture was heated to 70 °C for 4–5 h. Conversion of the isomeric mixture to a single *trans* isomer product was confirmed by TLC. After completion of the reaction, the organic phase was washed with aqueous sodium thiosulfate solution (10%) to quench the remaining quantity of iodine. The organic layer was collected, washed with water and brine, dried over sodium sulfate,

filtered and evaporated to give the titled compound (**15**) as yellow solid. (Yield: 0.99 g, 78.5%); m.p. 151–154 °C; IR (KBr, cm^{-1}): 2986, 2939, 1592, 1482, 1315, 1088, 804, 748; ^{1}H NMR ($CDCl_3$): δ 9.00 (d, J = 2 Hz, 1H, Ar*H*), 8.36–8.39 (dd, J = 7.2 Hz, 2 Hz, 1H, Ar*H*), 8.23 (s, 1H, Ar*H*), 7.74–7.76 (m,1H, Ar*H*), 7.57–7.59 (m, 2H, Ar*H*), 7.16–7.45 (m, 5H, Ar*H,* 2H, vinylic-*H*), 4.40 (q, J = 7.2 Hz, 2H, –NCH_2CH$_3$), 1.48 (t, J = 7.2 Hz, 3H, –NCH$_2$CH_3); MS (*m/z*) : 343 $[M + H]^+$.

5.1.5. (E)-9-Ethyl-6-styryl-9H-carbazol-3-amine (16)

To a solution of (*E*)-9-ethyl-3-nitro-6-styryl-9*H*-carbazole **15** (1.0 g, 2.92 mmol) in 1:1 THF/MeOH mixture (50 mL), stannous chloride (1.10 g, 5.84 mmol) was added in small portions over a period of a few minutes. After completion of addition, the reaction mixture was refluxed for 6–7 hrs. Progress of reaction was monitored by TLC. After completion of the reaction, *p*H of the mixture was adjusted to eight with NaOH solution (10%), and then extracted with ethyl acetate (20 mL × 3). The collected organic layer was washed with water and brine, dried over magnesium sulfate, filtered and evaporated to give crude product. It was further purified by recrystallization with methanol to give yellowish green colored crystals of the titled compound (**16**). (Yield: 0.7 g, 77%); m.p. 132–134 °C; IR (KBr, cm^{-1}): 3401, 3304, 3053, 3023, 2971, 2933, 1592, 1491, 797, 688; ^{1}H NMR (DMSO-d_6): δ 8.15 (s, 1H, Ar*H*), 7.65–7.67 (m, 1H, Ar*H*), 7.57–7.59 (m, 2H, Ar*H*), 7.23–7.48 (m, 5H, Ar*H*, 2H, vinylic-*H*), 7.12–7.16 (m, 1H, Ar*H*), 6.94–6.96 (m, 1H, Ar*H*), 4.31–4.33 (m, 2H, –NCH_2CH$_3$), 1.42 (t, 3H, –NCH$_2$CH_3); MS (*m/z*) : 313.5 $[M + H]^+$.

5.1.6. General method for the synthesis of (E)-N-(9-ethyl-6-styryl-9H-carbazol-3-yl)alkylamides (17–19)

Method A: To a stirring solution of 9-ethyl-6-styryl-9*H*-carbazole-3-amine **16** (1.0 g, 3.20 mmol) in dry acetone (25 mL), potassium carbonate (1.12 g, 7.98 mmol) was added. To it, respective acid chloride (4.8 mmol) was added dropwise under cold conditions. After completion of addition, the reaction mixture was kept on stirring for additional 1 h. The progress of the reaction was monitored by TLC. After completion of the starting material, the reaction mixture was poured into ice-cold water and extracted with ethyl acetate (20 mL × 3). The organic layer was washed with saturated sodium bicarbonate solution followed by water and brine, dried over sodium sulfate, and evaporated to yield the title compound.

5.1.6.1. (E)-3-Chloro-N-(9-ethyl-3-styryl-9H-carbazol-6-yl)propanamide (17). The title compound (**17**) was synthesized from compound (**16**) (1.0 g, 3.20 mmol) and 3-chloropropionyl chloride (0.47 mL, 4.8 mmol) following **Method A** (yield: 0.96 g, 74%). Brown colored solid; m.p. 154–156 °C; IR (KBr, cm^{-1}): 3297, 3024, 2972, 1652, 1595, 1554, 1231, 799, 699; MS (*m/z*): 403.6 $[M]^+$, 405.6 $[M + 2]^+$.

5.1.6.2. (E)-4-Chloro-N-(9-ethyl-3-styryl-9H-carbazol-6-yl)butanamide (18). The title compound (**18**) was synthesized from compound (**16**) (1.0 g, 3.20 mmol) and 4-chlorobutyryl chloride (0.53 mL, 4.8 mmol) following **Method A** (yield: 0.99 g, 74%). Brown colored solid; m.p. 161–163 °C; IR (KBr, cm^{-1}): 3291, 3118, 2969, 1648, 1542, 1486, 1229, 956, 799, 692; MS (*m/z*): 417.3 $[M]^+$, 419.3 $[M + 2]^+$.

5.1.6.3. (E)-5-Bromo-N-(9-ethyl-3-styryl-9H-carbazol-6-yl)pentanamide (19). The title compound (**19**) was synthesized from compound (**16**) (1.0 g, 3.20 mmol) and 5-bromovaleryl chloride (0.96 g, 4.8 mmol) following **Method A** (yield: 0.90 g, 72%). Brown colored solid; m.p. 147–150 °C; IR (KBr, cm^{-1}): 3288, 3025, 2967, 1647, 1593, 1540, 1486, 793; MS (*m/z*): 476.4 $[M + H]^+$, 477.4 $[M + 2]^+$.

5.1.7. General procedure for the synthesis of (E)-N-(9-ethyl-6-styryl-9H-carbazol-3-yl) aminoalkylamide (20–25)

Method B: Pyrrolidine/piperidine (5 equiv.) was added to a solution of (*E*)-*N*-(9-ethyl-6-styryl-9*H*-carbazol-3-yl)alkylamides (**17–19**, 0.5 g) in THF (10 mL). The reaction mixture was refluxed under nitrogen atmosphere till completion of the reaction as judged by TLC. The reaction mixture was then evaporated under reduced pressure and the residue was dissolved in 20 mL of water and extracted with ethyl acetate (20 mL × 3). The combined organic phase was then dried and evaporated to obtain the crude product, which was further purified by column chromatography using a mixture of chloroform and methanol as eluent to obtain off-white colored compound.

5.1.7.1. (E)-N-(9-Ethyl-6-styryl-9H-carbazol-3-yl)-3-(pyrrolidin-1-yl) propanamide (20). The title compound (**20**) was synthesized from compound (**17**) (0.5 g, 1.24 mmol) and pyrrolidine (0.5 mL, 6.20 mmol) following **Method B** (yield: 0.36 g, 67%). Brown colored solid; m.p. 129–131 °C; IR (KBr, cm^{-1}): 3366, 3056, 3018, 2966, 1596, 1488, 1229, 963, 806, 791; ^{1}H NMR (DMSO-d_6): δ 10.11 (s, 1H, –N*H*CO), 8.53 (d, 1H, Ar*H*), 8.31 (d, 1H, Ar*H*), 7.72–7.74 (dd, 1H, Ar*H*), 7.22–7.63 (m, 8H, Ar*H* and 2H, vinylic-*H*), 4.41 (q, J = 7.2 Hz, 2H, –NCH_2CH$_3$), 2.76 (t, 2H, –NHCOCH_2), 2.45–2.54 (m, 6H, –NCH_2CH$_2$), 1.68–1.71 (m, 4H, –NCH$_2$CH_2), 1.30 (t, J = 7.2 Hz, 3H, –NCH$_2$CH_3); LCMS (*m/z*): 438.26 $[M + H]^+$, Purity: nearly 100%.

5.1.7.2. (E)-N-(9-Ethyl-6-styryl-9H-carbazol-3-yl)-3-(piperidin-1-yl) propanamide (21). The title compound (**21**) was synthesized from compound (**17**) (0.5 g, 1.24 mmol) and piperidine (0.61 mL, 6.20 mmol) following **Method B** (yield: 0.38 g, 67%). Off-white solid; m.p. 148–151 °C; IR (KBr, cm^{-1}): 3309, 3023, 2967, 1690, 1587, 1520, 1478, 1233, 749; ^{1}H NMR (DMSO-d_6): δ 10.20 (s, 1H, –N*H*CO), 8.53 (d, 1H, Ar*H*), 8.30 (d, 1H, Ar*H*), 7.73 (dd, 1H, Ar*H*), 7.45–7.63 (m, 3H, Ar*H*, 2H, vinylic-*H*), 7.36–7.41 (m, 3H, Ar*H*), 7.24–7.30 (m, 2H, Ar*H*), 4.40 (q, J = 7.2 Hz, 2H, –NCH_2CH$_3$), 2.64 (t, 2H, –NHCOCH_2), 2.48–2.52 (m, 4H, –NCH_2CH$_2$), 2.35–2.42 (m, 2H, –NCH_2CH$_2$), 1.49–1.55 (m, 4H, –NCH$_2$CH_2), 1.39–1.40 (m, 2H, –CH_2) and 1.30 (t, J = 7.2 Hz, 3H, –NCH$_2$CH_3); LCMS (*m/z*): 452.16 $[M + H]^+$, Purity: 98.58%.

5.1.7.3. (E)-N-(9-Ethyl-6-styryl-9H-carbazol-3-yl)-4-(pyrrolidin-1-yl) butanamide (22). The title compound (**22**) was synthesized from compound (**18**) (0.5 g, 1.20 mmol) and pyrrolidine (0.5 mL, 6.20 mmol) following **Method B** (yield: 0.34 g, 63%). Off-white solid; m.p. 127–130 °C; IR (KBr, cm^{-1}): 3292, 3118, 3027, 2961, 2876, 2795, 1651, 1596, 1532, 1486, 1305 and 797; ^{1}H NMR (DMSO-d_6): δ 9.94 (s, 1H, –N*H*CO), 8.53 (d, 1H, Ar*H*), 8.30 (s, 1H, Ar*H*), 7.72–7.74 (dd, 1H, Ar*H*), 7.24–7.63 (m, 8H, Ar*H,* 2H, vinylic-*H*), 4.41 (q, J = 7.2 Hz, 2H, –NCH_2CH$_3$), 2.37–2.46 (m, 6H, –NCH_2CH$_2$, 2H, –NHCOCH_2), 1.78–1.82 (m, 2H, –NCH$_2$CH_2), 1.66–1.69 (m, 4H, –NCH$_2$CH_2) and 1.30 (t, J = 7.2 Hz, 3H, –NCH$_2$CH_3); LCMS (*m/z*): 452.26 $[M + H]^+$, Purity: nearly 100%.

5.1.7.4. N-(9-Ethyl-3-styryl-9H-carbazol-6-yl)-4-(piperidin-1-yl) butanamide (23). The title compound (**23**) was synthesized from compound (**18**) (0.5 g, 1.20 mmol) and piperidine (0.59 mL, 6.00 mmol) following **Method B** (yield: 0.38 g, 70%). Off-white solid; m.p. 114–118 °C; IR (KBr, cm^{-1}): 3286, 3117, 3025, 2928, 2770, 1644, 1594, 1536, 1486, 1152, 791, 691; ^{1}H NMR (DMSO-d_6): δ 9.89 (s, 1H, –N*H*CO), 8.35 (d, 1H, Ar*H*), 8.15–8.18 (m, 1H, Ar*H*), 7.70 (dd, 1H, Ar*H*), 7.17–7.62 (m, 8H, Ar*H,* 2H, vinylic-*H*), 4.44 (q, J = 7.2 Hz, 2H, –NCH_2CH$_3$), 2.24–2.34 (m, 6H, –NCH_2CH$_2$, 2H, –NHCOCH_2), 1.69–1.77 (m, 2H, –NCH$_2$CH_2), 1.44–1.50 (m, 4H, –NCH$_2$CH_2), 1.35–1.38 (m, 3H, –NCH$_2$CH$_2$CH_2), 1.32 (t, J = 7.2 Hz, 3H, –NCH$_2$CH_3); LCMS (*m/z*): 466.4 $[M + H]^+$, Purity: nearly 100%.

5.1.7.5. (E)-N-(9-Ethyl-6-styryl-9H-carbazol-3-yl)-5-(pyrrolidin-1-yl) pentanamide (24). The title compound (**24**) was synthesized from compound (**19**) (0.5 g, 1.05 mmol) and pyrrolidine (0.43 mL, 5.25 mmol) following **Method B** (yield: 0.34 g, 63%). Off-white solid; m.p. 161–164 °C; IR (KBr, cm^{-1}): 3289, 3026, 2962, 2933,

1648, 1596, 1484, 1082, 796 and 687; ^{1}H NMR (DMSO-d_6): δ 9.91 (s, 1H, –N*H*CO), 8.52 (d, 1H, Ar*H*), 8.30 (s, 1H, Ar*H*), 7.73 (dd, 1H, Ar*H*), 7.24–7.63 (m, 8H, Ar*H,* 2H, vinylic-*H*), 4.40 (q, *J* = 7.2 Hz, 2H, –NC*H*$_2$CH$_3$), 2.34–2.42 (m, 6H, –NC*H*$_2$, 2H, –NHCOC*H*$_2$), 1.65–1.69 (m, 6H, –NCH$_2$C*H*$_2$), 1.49–1.52 (m, 2H, –C*H*$_2$) and 1.30 (t, *J* = 7.2 Hz, 3H, –NCH$_2$C*H*$_3$; LCMS (*m/z*): 466.26 [M + H]$^+$, Purity: nearly 100%.

5.1.7.6. (E)-N-(9-Ethyl-6-styryl-9H-carbazol-3-yl)-5-(piperidin-1-yl) pentanamide (25). The title compound (**25**) was synthesized from compound (**19**) (0.5 g, 1.05 mmol) and piperidine (0.45 mL, 5.25 mmol) following **Method B** (yield: 0.36 g, 66%). Off-white solid; m.p. 159–161 °C; IR (KBr, cm^{-1}): 3290, 3025, 2929, 2856, 1647, 1540, 1487, 1228, 799 and 689; ^{1}H NMR (DMSO-d_6): δ 9.91 (s, 1H, –N*H*CO), 8.52 (d, 1H, Ar*H*), 8.30 (d, 1H, Ar*H*), 7.73 (dd, 1H, Ar*H*), 7.22–7.63 (m, 8H, Ar*H*, 2H, vinylic-*H*), 4.41 (q, *J* = 7.2 Hz, 2H, –NC*H*$_2$CH$_3$), 2.23–2.37 (m, 6H, –NC*H*$_2$CH$_2$, 2H, –NHCOC*H*$_2$), 1.61–1.65 (m, 2H, –NHCOCH$_2$C*H*$_2$), 1.45–1.49 (m, 6H, –NCH$_2$C*H*$_2$), 1.35–1.37 (m, 2H, –NCH$_2$CH$_2$ C*H*$_2$) and 1.30 (t, *J* = 7.2 Hz, 3H, –NCH$_2$C*H*$_3$); LCMS (*m/z*): 480.17 [M + H]$^+$, Purity: 98.79%.

5.1.8. General method for the synthesis of (E)-1-(9-ethyl-6-styryl-9H-carbazol-3-yl)aminoalkylurea (26–31)

Method C: To a stirring solution of (*E*)-9-ethyl-6-styryl-9*H*-carbazol-3-amine **16** (1.0 g, 3.20 mmol) and triethylamine (0.5 mL, 3.52 mmol) in dry THF (20 mL), 4-nitrophenyl chloroformate (0.71 g, 3.52 mmol) in dry THF (10 mL) was added dropwise at 0–5 °C over a period of 15 min. The resulting reaction mixture was allowed to stir at room temperature for 2 h. Progress of the reaction was monitored by TLC. After complete consumption of the starting material, the respective amine (4.0 mmol) was added to the reaction mixture and the reaction was further stirred for 30 min. After completion of the reaction, the solvent was recovered at reduced pressure. The residues so obtained was triturated with chilled methanol (20 mL), filtered and dried to obtain the title compound.

5.1.8.1. (E)-N-(9-Ethyl-6-styryl-9H-carbazol-3-yl)pyrrolidine-1-carboxamide (26). The title compound was synthesized from compound (**16**) (1.0 g, 3.20 mmol) and pyrrolidine (0.33 mL, 4.00 mmol) as per **Method C** (yield: 1.02 g, 78%). Off-white solid; m.p. 193–195 °C; IR (KBr, cm^{-1}): 3313, 3058, 3023, 2960, 2868, 1635, 1551, 1481, 1151, 956, 801 and 691; ^{1}H NMR (DMSO-d_6): δ 8.29–8.27 (m, 2H, Ar*H*), 8.14 (s, 1H, –N*H*CO), 7.70–7.72 (m, 1H, Ar*H*), 7.61–7.63 (m, 2H, Ar*H*), 7.55–7.57 (m, 1H, Ar*H*), 7.21–7.52 (m, 5H, Ar*H*, 2H, vinylic-*H*), 4.40 (q, *J* = 7.2 Hz, 2H, –NC*H*$_2$CH$_3$), 3.39–3.43 (m, 4H, –NC*H*$_2$CH$_2$), 1.86–1.90 (m, 4H, –NCH$_2$C*H*$_2$) and 1.31 (t, *J* = 7.2 Hz, 3H, –NCH$_2$C*H*$_3$); LCMS (*m/z*): 410.30 [M + H]$^+$, Purity: nearly 100%

5.1.8.2. (E)-N-(9-Ethyl-6-styryl-9H-carbazol-3-yl)piperidine-1-carboxamide (27). The title compound was synthesized from compound (**16**) (1.0 g, 3.20 mmol) and piperidine (0.40 mL, 4.00 mmol) as per **Method C** (yield: 1.08 g, 82%). Off-white solid; m.p. 217–219 °C; IR (KBr, cm^{-1}): 3346, 3026, 2929, 2847, 1627, 1532, 1486, 1232, 1140, 860 and 750; ^{1}H NMR (DMSO-d_6): δ 8.47 (s, 1H, –N*H*CO), 8.26–8.29 (m, 2H, Ar*H*), 7.69–7.72 (m, 1H, Ar*H*), 7.61–7.63 (m, 2H, Ar*H*), 7.55–7.57 (m, 1H, Ar*H*), 7.22–7.49 (m, 5H, Ar*H*, 2H, vinylic-*H*), 4.40 (q, *J* = 7.2 Hz, 2H, –NC*H*$_2$CH$_3$), 3.45–3.48 (m, 4H, –NC*H*$_2$CH$_2$), 1.52–1.60 (m, 6H, –NCH$_2$ C*H*$_2$C*H*$_2$) and 1.30 (t, *J* = 7.2 Hz, 3H, –NCH$_2$C*H*$_3$); LCMS (*m/z*): 424.25 [M + H]$^+$, Purity: nearly 100%.

5.1.8.3. (E)-1-(9-Ethyl-6-styryl-9H-carbazol-3-yl)-3-(2-(pyrrolidin-1-yl) ethyl)urea (28). The title compound was synthesized from compound (**16**) (1.0 g, 3.20 mmol) and 2-(aminoethyl)pyrrolidine (0.40 mL, 4.00 mmol) as per **Method C** (yield: 1.03 g, 75%). Off-white solid; m.p. 176–178 °C; IR (KBr, cm^{-1}): 3322, 3022, 2961, 2872, 1630, 1562, 1486, 1132, 952, 799 and 691; ^{1}H NMR (DMSO-d_6): δ 10.23 (s, 1H, –N*H*CO), 8.52 (s, 1H, –N*H*CO) 8.31 (s, 1H, Ar*H*), 7.24–7.57 (m, 10*H*, Ar*H*, 2H, vinylic-*H*), 4.41 (q, *J* = 7.2 Hz, 2H, –NC*H*$_2$CH$_3$), 2.62–2.67 (m, 2H, –NH*CH*$_2$), 2.35–2.45 (m, 6H, –NC*H*$_2$) and 1.31 (t, *J* = 7.2 Hz, 3H, –NCH$_2$C*H*$_3$); LCMS (*m/z*): 453.3 [M + H]$^+$, Purity: nearly 100%.

5.1.8.4. (E)-1-(9-Ethyl-6-styryl-9H-carbazol-3-yl)-3-(2-(piperidin-1-yl) ethyl)urea (29). The title compound was synthesized from compound (**16**) (1.0 g, 3.20 mmol) and 2-(aminoethyl)piperidine (0.57 mL, 4.00 mmol) as per **Method C** (yield: 1.06 g, 71%). Off-white solid; m.p. 187–189 °C; IR (KBr, cm^{-1}): 3325, 3024, 2932, 2777, 1635, 1561, 1484, 1137, 952, 796 and 748; ^{1}H NMR (DMSO-d_6): δ 8.61 (s, 1H, –N*H*CO), 8.29 (s, 1H, Ar*H*), 7.21–7.71 (m, 9H, Ar*H*, 2H, vinylic-*H*), 6.01 (bs, 1H, –N*H*CO), 4.39 (q, *J* = 7.2 Hz, 2H, –NC*H*$_2$), 3.22–3.24 (m, 2H, –NH*CH*$_2$), 2.35–2.39 (m, 6H, –NC*H*$_2$), 1.50–1.52 (m, 4H, –NCH$_2$C*H*$_2$), 1.40–1.39 (m, 2H, –NCH$_2$CH$_2$C*H*$_2$) and 1.29 (t, *J* = 7.2 Hz, 3H, –NCH$_2$C*H*$_3$); LCMS (*m/z*): 467.26 [M + H]$^+$, Purity: 99.59%.

5.1.8.5. (E)-1-(9-Ethyl-6-styryl-9H-carbazol-3-yl)-3-(3-(pyrrolidin-1-yl) propyl)urea (30). The title compound was synthesized from compound (**16**) (1.0 g, 3.20 mmol) and 3-(aminopropyl)pyrrolidine (0.51 g, 4.00 mmol) as per **Method C** (yield: 1.1 g, 75%). Off-white solid; m.p. 164–166 °C; IR (KBr, cm^{-1}): 3304, 3024, 2962, 2873, 1628, 1590, 1486, 1150, 957, 800 and 692; ^{1}H NMR (DMSO-d_6): δ 8.43 (s, 1H, –N*H*CO), 8.26–8.28 (m, 2H, Ar*H*), 7.21–7.71 (m, 9H, Ar*H*, 2H, vinylic-*H*), 6.18 (t, 1H, –N*H*CO), 4.39 (q, *J* = 7.2 Hz, 2H, –NC*H*$_2$), 3.14–3.19 (m, 2H, –NH*CH*$_2$), 2.52–2.55 (m, 6H, –NC*H*$_2$), 1.62–1.74 (m, 6H, –NCH$_2$C*H*$_2$) and 1.29 (t, *J* = 7.2 Hz, 3H, –NCH$_2$C*H*$_3$); LCMS (*m/z*): 467.26 [M + H]$^+$, Purity: nearly 100%.

5.1.8.6. (E)-1-(9-Ethyl-6-styryl-9H-carbazol-3-yl)-3-(3-(piperidin-1-yl) propyl)urea (31). The title compound was synthesized from compound (**16**) (1.0 g, 3.20 mmol) 3-(aminopropyl)piperidine (0.57 g, 4.00 mmol) as per **Method C** (yield: 1.2 g, 79%). Off-white solid; m.p. 168–170 °C; IR (KBr, cm^{-1}): 3289, 3024, 2927, 1645, 1595, 1485, 1285, 1083, 951, 798 and 688; ^{1}H NMR (DMSO-d_6): δ 8.36 (s, 1H, –N*H*CO), 8.26–8.29 (m, 2H, Ar*H*), 7.21–7.71 (m, 9H, Ar*H*, 2H, vinylic-*H*), 6.01 (t, 1H, –N*H*CO), 4.39 (q, *J* = 7.2 Hz, 2H, –NC*H*$_2$CH$_3$), 3.11–3.16 (m, 2H, –NH*CH*$_2$), 2.27–2.33 (m, 6H, –NC*H*$_2$CH$_2$), 1.57–1.64 (m, 4H, –NCH$_2$C*H*$_2$), 1.46–1.51 (m, 4H, –NCH$_2$C*H*$_2$), 1.34–1.39 (m, 2H, –C*H*$_2$) and 1.30 (t, *J* = 7.2 Hz, 3H, –NCH$_2$C*H*$_3$); LCMS (*m/z*): 481.4 [M + H]$^+$, Purity: nearly 100%.

5.1.9. 2-(4-Nitrophenyl)acetic acid (32)

A mixture of concentrated nitric acid (1.47 mL) and an equal volume of concentrated sulphuric acid (1.47 mL) was placed in a two neck flask fitted with a thermometer and a dropping funnel. The mixture was cooled to 10 °C in ice bath and benzyl cyanide (1.0 g, 8.53 mmol) was run at such a rate that the temperature was maintained around 10 °C and did not rise above 20 °C. The solution was further stirred for 1 h at room temperature and then poured into crushed ice. The mass was filtered under vacuum and pressed well to remove as much oil as possible. The crude product was recrystallize from methanol to obtain 2-(4-nitrophenyl)acetonitrile (yield:1.21 g, 88%); m.p. 110–112 °C (lit. [55] m.p. 113–115 °C); IR (KBr, cm^{-1}): 3117, 3054, 2943, 2851, 2253, 1517, 1345, 1107, 732. A solution of sulphuric acid (50%) was prepared by adding concentrated sulphuric acid cautiously to water. Two third of the sulphuric acid was added into a round bottom flask containing 2-(4-nitrophenyl)acetonitrile (1.0 g) and the nitrile adhering to the walls of the flask was washed down with the remaining acid. The content was boiled under reflux for 15 min and diluted with 25 mL of ice-cold water. The resulting pale yellow solid mass was filtered, washed, decolorized and recrystallized from hot water to yield titled compound (**32**) (yield: 0.87 g, 78%); m.p. 148–150 °C (lit [55] m.p. 151–152 °C); IR (KBr, cm^{-1}): 3450, 3084, 2931, 2847, 1708, 1514, 1346, 951, 709.

5.1.10. (E)-9-Ethyl-3-(4-nitrostyryl)-9H-carbazole (33)

A mixture of 2-(4-nitrophenyl)acetic acid (**32**, 1.63 g, 8.96 mmol) and 9-ethyl-9*H*-carbazole-3-carbaldehyde (**13**, 1.0 g, 4.47 mmol) in the presence of piperidine (1.33 mL, 13.44 mmol) was irradiated under microwave at 800 W in a microwave reactor. Reaction progress was monitored by TLC. After completion of reaction, the reaction mixture was cooled and methanol (15 mL) was added to it. The solid so obtained was filtered and dried to obtain the orange colored crystals of the titled compound (**33**) [56]. (Yield:1.25 g, 82%); m.p. 215–217 °C; IR (KBr, cm^{-1}): 3048, 2976, 1621, 1593, 1505, 1333 and 749; ^{1}H NMR (DMSO-d_6): δ 8.49 (s, 1H, Ar*H*), 8.24 (d, 2H, Ar*H*), 8.18 (d, 1H, Ar*H*), 7.86 (d, 2H, Ar*H*), 7.81–7.83 (m, 1H, Ar*H*), 7.62–7.74 (m, 3H, Ar*H*), 7.42–7.50 (m, 1H, Ar*H,* 1H, vinylic-*H*), 7.22–7.26 (m, 1H, Vinylic-*H*), 4.46 (q, J = 7.2 Hz, 2H, –NCH_2) and 1.32 (t, J = 7.2 Hz, 3H, –NCH$_2$CH_3); MS (m/z): 343 $[M + H]^+$.

5.1.11. (E)-4-(2-(9-Ethyl-9H-carbazol-3-yl)vinyl)aniline (34)

To a solution of (*E*)-9-ethyl-3-(4-nitrostyryl)-9*H*-carbazole (**33**) (1.0 g, 2.92 mmol) in tetrahydrofuran: methanol (1:1) mixture (50 mL), stannous chloride (1.11 g, 5.84 mmol) was added in portion. After completion of addition, the reaction mixture was refluxed for 6–7 hrs. Progress of reaction was monitored by TLC. After completion of the reaction, *p*H of the mixture was adjusted to basic with aqueous NaOH solution (10%), and then extracted with ethyl acetate (20 mL × 3). The collected organic layer was washed with water and brine, dried and evaporated to give crude product, which was further purified by re-crystallization with methanol to give white colored crystals of the titled compound (**34**). (Yield: 0.88 g, 92%); m.p. 162–164 °C; IR (KBr, cm^{-1}): 3417, 3368, 3029, 2966, 2926, 1615, 1513, 958, 819 and 748; ^{1}H NMR (DMSO-d_6): δ 8.26 (s, 1H, Ar*H*), 8.14–8.16 (m, 1H, Ar*H*), 7.62–7.65 (m, 1H, Ar*H*), 7.54–7.59 (m, 2H, Ar*H*), 7.41–7.48 (m, 1H, Ar*H*), 7.27–7.30 (m, 2H, Ar*H*), 7.17–7.21 (m, 1H, Ar*H*), 7.05–7.07 (m, 2H, vinylic-*H*), 6.56–6.59 (m, 2H, Ar*H*), 5.20 (bs, 2H, –NH_2), 4.42 (q, J = 7.2 Hz, 2H, –NCH_2CH$_3$) and 1.31 (t, J = 7.2 Hz, 3H, –NCH$_2$CH_3); MS (m/z) : 313 $[M + H]^+$.

5.1.12. (E)-2-Chloro-N-(4-(2-(9-ethyl-9H-carbazol-3-yl)vinyl)phenyl) acetamide (35)

The title compound was synthesized from compound (**34**) (1.0 g, 3.20 mmol) and 2-chloroacetyl chloride (0.38 mL, 4.8 mmol) following **Method A** (yield: 0.91 g, 71%). Brown colored solid; m.p. 207–209 °C; IR (KBr, cm^{-1}): 3249, 3038, 2974, 1664, 1593 and 738; MS (m/z): 388.2 $[M]^+$, 390.2 $[M + 2]^+$.

5.1.13. (E)-3-Chloro-N-(4-(2-(9-ethyl-9H-carbazol-3yl)vinyl)phenyl) propanamide (36)

The title compound was synthesized from compound (**34**) (1.0 g, 3.20 mmol) and 3-chloropropionyl chloride (0.46 mL, 4.8 mmol) following **Method A** (yield: 0.87 g, 65%). Brown colored solid; m.p. 219–222 °C; IR (KBr, cm^{-1}): 3273, 3036, 2970, 1644, 1594 and 744; MS (m/z): 403.3 $[M]^+$, 405.3 $[M + 2]^+$.

5.1.14. (E)-4-Chloro-N-(4-(2-(9-ethyl-9H-carbazol-3-yl)vinyl)phenyl) butanamide (37)

The title compound was synthesized from compound (**34**) (1.0 g, 3.20 mmol) and 4-chlorobutyryl chloride (0.54 mL, 4.8 mmol) following **Method A** (yield: 0.88 g, 66%). Brown colored solid; m.p. 193–195 °C; IR (KBr, cm^{-1}): 3295, 3028, 2968, 1653, 1589 and 746; MS (m/z): 417.3 $[M]^+$, 419.3 $[M + 2]^+$.

5.1.15. (E)-N-(4-(2-(9-Ethyl-9H-carbazol-3-yl)vinyl)phenyl)-2-(pyrrolidin-1-yl)acetamide (38)

The title compound was synthesized from compound (**35**) (0.5 g, 1.05 mmol) and pyrrolidine (0.54 mL, 6.45 mmol) following **Method B** (yield: 0.35 g, 65%). Off-white solid; m.p. 120–122 °C; IR (KBr, cm^{-1}): 3306, 3022, 2867, 1691, 1584, 1521, 1233 and 749; ^{1}H NMR (DMSO-d_6): δ 9.76 (s, 1H, –N*H*CO), 8.37 (s, 1H, Ar*H*), 8.17 (d, 1H, Ar*H*), 7.67–7.72 (m, 3H, Ar*H*), 7.54–7.60 (m, 4H, Ar*H*), 7.43–7.47 (m, 1H, Ar*H*), 7.31–7.35 (m, 1H, Ar*H*), 7.19–7.23 (m, 2H, Vinylic-*H*), 4.43 (q, J = 7.2 Hz, 2H, –NCH_2), 3.25 (s, 2H, –NHCOCH_2), 2.56–2.61 (m, 4H, –NCH_2), 1.69–1.81 (m, 4H, –NCH$_2$CH_2) and 1.31 (t, J = 7.2 Hz, 3H, –NCH$_2$CH_3); ^{13}C NMR (DMSO-d_6): 169.00, 140.33, 139.66, 138.15, 133.32, 128.85, 128.61, 126.85, 126.34, 125.69, 125.01, 123.03, 122.71, 120.87, 120.10, 119.38, 118.78, 109.78, 109.73, 59.97, 54.20, 37.53, 23.95, 14.21; LCMS (m/z): 424.25 $[M + H]^+$, Purity: 99.71%.

5.1.16. (E)-N-(4-(2-(9-Ethyl-9H-carbazol-3-yl)vinyl)phenyl)-2-(piperidin-1-yl)acetamide (39)

The title compound was synthesized from compound (**35**) (0.5 g, 1.05 mmol) and piperidine (0.64 mL, 6.45 mmol) following **Method B** (yield: 0.33 g, 60%). Off-white solid; m.p. 131–134 °C; IR (KBr, cm^{-1}): 3326, 3016, 2938, 2795, 1693, 1582, 1516, 1231, 815 and 749; ^{1}H NMR (DMSO-d_6): δ 9.72 (s, 1H, –N*H*CO), 8.37 (d, 1H, Ar*H*), 8.17 (d, 1H, Ar*H*), 7.55–7.70 (m, 7H, Ar*H*), 7.43–7.47 (m, 1H, Ar*H*), 7.31–7.35 (m, 1H, Ar*H*), 7.19–7.23 (m, 2H, vinylic-*H*), 4.43 (q, J = 7.2 Hz, 2H, –NCH_2CH$_3$), 3.07 (s, 2H, –NHCOCH_2), 2.46–2.49 (m, 4H, –NCH_2CH$_2$), 1.54–1.60 (m, 4H, –NCH$_2$CH_2), 1.37–1.42 (m, 2H, –NCH$_2$CH$_2$CH_2) and 1.32 (t, J = 7.2 Hz, 3H, –NCH$_2$CH_3); ^{13}C NMR (DMSO-d_6): 168.96, 140.44, 139.67, 138.00, 133.39, 128.84, 128.64, 126.89, 126.34, 125.67, 125.01, 123.04, 122.72, 120.87, 120.04, 119.39, 118.80, 109.79, 109.73, 63.16, 54.57, 37.52, 25.95, 24.03 and 14.21; LCMS (m/z): 438.26 $[M + H]^+$, Purity: 99.81%.

5.1.17. (E)-N-(4-(2-(9-Ethyl-9H-carbazol-3-yl)vinyl)phenyl)-3-(pyrrolidin1yl)propanamide (40)

The title compound was synthesized from compound (**36**) (0.5 g, 1.24 mmol) and pyrrolidine (0.52 mL, 6.20 mmol) following **Method B** (yield: 0.32 g, 60%). Off-white solid; m.p. 158–160 °C; IR (KBr, cm^{-1}): 3281, 3175, 3102, 3025, 2963, 2930, 1653, 1595 and 745; ^{1}H NMR (DMSO-d_6): δ 10.14 (s, 1H, –N*H*CO), 8.36 (s, 1H, Ar*H*), 8.17 (d, 1H, Ar*H*), 7.69–7.72 (m, 1H, Ar*H*), 7.53–7.63 (m, 6H, Ar*H*), 7.43–7.47 (m, 1H, Ar*H*), 7.29–7.33 (m, 1H, Ar*H*), 7.18–7.23 (m, 2H, vinylic-*H*) 4.43 (q, J = 7.2 Hz, 2H, –NCH_2CH$_3$), 2.71 (t, 2H, –NHCOCH_2), 2.46–2.50 (m, 6H, –CH_2 , –NCH_2CH$_2$), 1.66–1.69 (m, 4H, –NCH$_2$CH_2),1.31 (t, J = 7.2 Hz, 3H, –NCH$_2$CH_3); ^{13}C NMR (DMSO-d_6): 170.57, 140.43, 139.65, 138.77, 133.01, 128.88, 128.46, 126.94, 126.33, 125.74, 124.99, 123.04, 122.71, 120.88, 119.66, 119.38, 118.77, 109.77, 109.71, 53.88, 52.04, 37.52, 36.64, 23.65 and 14.20; LCMS (m/z): 438.21 $[M + H]^+$, Purity: nearly 100%.

5.1.18. (E)-N-(4-(2-(9-Ethyl-9H-carbazol-3-yl)vinyl)phenyl)-3-(piperidin-1-yl)propananamide (41)

The title compound was synthesized from compound (**36**) (0.5 g, 1.24 mmol) and piperidine (0.61 mL, 6.20 mmol) following **Method B** (yield: 0.32 g, 58%). Off-white solid; m.p. 173–176 °C; IR (KBr, cm^{-1}): 3018, 2974, 2931, 2839, 2799, 1683, 1595, 1537, 817 and 747; ^{1}H NMR (DMSO-d_6): δ 10.24 (s, 1H, –N*H*CO), 8.36 (s, 1H, Ar*H*), 8.17 (d, 1H, Ar*H*), 7.70–7.72 (m, 1H, Ar*H*), 7.53–7.61 (m, 6H, Ar*H*), 7.44–7.48 (m, 1H, Ar*H*), 7.30–7.34 (m, 1H, Ar*H*), 7.18–7.22 (m, 2H, vinylic-*H*), 4.44 (q, J = 7.2 Hz, 2H, –NCH_2CH$_3$), 2.58–2.61 (m, 2H, –NHCOCH_2), 2.45–2.49 (m, 2H, –NCH_2), 2.37–2.40 (m, 4H, –NCH_2), 1.49–1.52 (m, 4H, –NCH$_2$CH_2), 1.36–1.41 (m, 2H, –NCH$_2$CH$_2$CH_2) and 1.32 (t, J = 7.2 Hz, 3H, –NCH$_2$CH_3); ^{13}C NMR (DMSO-d_6): 170.70, 140.43, 196.65, 138.73, 133.0, 128.8, 128.47, 126.96, 126.34, 125.73, 125.01, 123.03, 122.71, 120.88, 119.63, 119.37, 118.75, 109.78, 109.72, 54.93, 54.13, 37.52, 34.57, 26.10, 24.48 and 14.21; LCMS (m/z): 452.21 $[M + H]^+$, Purity: nearly 100%.

5.1.19. (E)-N-(4-(2-(9-Ethyl-9H-carbazol-3-yl)vinyl)phenyl)-4-(pyrrolidin-1yl)butanamide (42)

The title compound was synthesized from compound (**37**) (0.5 g, 1.20 mmol) and pyrrolidine (0.50 mL, 6.0 mmol) following **Method B**

(yield: 0.32 g, 60%). Off-white solid; m.p. 179–181 °C; IR (KBr, cm^{-1}): 33294, 3023, 2960, 2874, 2791, 1657, 1523, 818 and 745; ^{1}H NMR (DMSO-d_6): δ 9.96 (s, 1H, –N*H*CO), 8.36 (d, 1H, Ar*H*), 8.17 (d, 1H, Ar*H*), 7.71 (dd, 1H, Ar*H*), 7.59–7.63 (m, 4H, Ar*H*), 7.53–7.55 (m, 2H, Ar*H*), 7.46–7.48 (m, 1H, Ar*H*), 7.29–7.33 (m, 1H, Ar*H*), 7.18–7.23 (m, 2H, vinylic-*H*), 4.44 (q, J = 7.2 Hz, 2H, –NCH_2CH$_3$), 2.34–2.42 (m, 2H, –NHCOCH_2, 6H, –NCH_2CH$_2$), 1.73–1.77 (m, 2H, –NCH$_2$CH_2), 1.65–1.68 (m, 4H, –NCH$_2$CH_2) and 1.32 (t, J = 7.2 Hz, 3H, –NCH$_2$CH_3); ^{13}C NMR (DMSO-d_6): 171.59, 140.43, 139.64, 138.87, 132.90, 128.89, 128.40, 126.90, 126.33, 125.76, 124.99, 123.03, 122.71, 120.88, 119.65, 119.37, 118.75, 109.78, 109.72, 55.63, 54.00, 37.52, 35.00, 24.85, 23.60 and 14.20; LCMS (m/z): 452.21 [M + H]$^+$, Purity: 99.05%.

5.1.20. (E)-N-(4-(2-(9-Ethyl-9H-carbazol-3-yl)vinyl)phenyl)-4-(piperidin-1-yl)butanamide (43)

The title compound was synthesized from compound (**37**) (0.5 g, 1.20 mmol) and piperidine (0.59 mL, 6.0 mmol) following **Method B** (yield: 0.35 g, 63%). Off-white solid; m.p. 173–176 °C; IR (KBr, cm^{-1}): 3296, 3023, 2928, 2850, 1657, 1594, 1523, 1409, 961, 858 and 745; ^{1}H NMR (DMSO-d_6): δ 9.93 (s, 1H, –N*H*CO), 8.36 (d, 1H, Ar*H*), 8.17 (d, 1H, Ar*H*), 7.71 (dd, 1H, Ar*H*), 7.58–7.63 (m, 4H, Ar*H*), 7.44–7.54 (m, 3H, Ar*H*), 7.29–7.33 (m, 1H, Ar*H*), 7.18–7.21 (m, 2H, vinylic-*H*), 4.44 (q, J = 7.2 Hz, 2H,–NCH_2CH$_3$), 2.24–2.44 (m, 2H, –NHCOCH_2, 6H, –NCH_2CH$_2$), 1.72–1.75 (m, 2H, –NCH$_2$CH_2), 1.44–1.50 (m, 4H, –NCH$_2$CH_2), 1.33–1.36 (m, 2H, –CH_2) and 1.31 (t, J = 7.2 Hz, 3H, –NCH$_2$CH_3); ^{13}C NMR (DMSO-d_6): 171.61, 140.43, 139.64, 138.88, 132.87, 128.90, 128.39, 126.89, 126.34, 125.77, 124.99, 123.03, 122.71, 120.88, 119.65, 119.37, 118.74, 109.78, 109.72, 58.54, 54.52, 37.52, 34.99, 26.08, 24.66, 22.85 and 14.21; LCMS (m/z): 466.21 [M + H]$^+$, Purity: 99.88%.

5.1.21. (E)-N-(4-(2-(9-Ethyl-9H-carbazol-3-yl)vinyl)phenyl)pyrrolidine-1-carboxamide (44)

The title compound was synthesized from compound (**34**) (1.0 g, 3.20 mmol) and pyrrolidine (0.33 mL, 4.00 mmol) following **Method C** (yield: 0.76 g, 58%). Off-white solid; m.p. 144–146 °C; IR (KBr, cm^{-1}): 3334, 3018, 2974, 2873, 1630, 1522, 1234, 965 and 753; ^{1}H NMR (DMSO-d_6): δ 8.23 (d, 1H, Ar*H*), 8.15 (d, 1H, Ar*H*), 7.67–7.69 (dd, 1H, Ar*H*), 7.38–7.52 (m, 7H, Ar*H*), 7.10–7.47 (m, 1H, Ar*H,* 2H, vinylic-*H*), 6.28 (bs, 1H, –N*H*CO), 4.39 (q, J = 7.2 Hz, 2H, –NCH_2), 3.48–3.52 (m, 4H, –NCH_2), 1.98–2.02 (m, 4H, –NCH$_2$CH_2) and 1.46 (t, J = 7.2 Hz, 3H, –NCH$_2$CH_3); ^{13}C NMR (DMSO-d_6): 140.39, 131.58, 129.01, 127.68, 126.64, 126.37, 125.97, 124.92, 123.00, 122.66, 120.89, 120.11, 120.01, 119.38, 118.61, 109.76, 109.68, 46.17, 37.51, 25.46 and 14.16; MS (m/z): 410.3 [M + H]$^+$.

5.1.22. (E)-N-(4-(2-(9-Ethyl-9H-carbazol-3-yl)vinyl)phenyl)piperidine-1-carboxamide (45)

The title compound was synthesized from compound (**34**) (1.0 g, 3.20 mmol) and piperidine (0.40 mL, 4.00 mmol) following **Method C** (yield: 0.58 g, 55%). Off-white solid; m.p. 214–216 °C; IR (KBr, cm^{-1}): 3305, 3026, 2972, 2931, 2854, 1633, 1589, 1515, 1234, 951 and 746; ^{1}H NMR (DMSO-d_6): δ 8.24 (s, 1H, Ar*H*), 8.15 (d, 1H, Ar*H*), 7.67–7.69 (m, 1H, Ar*H*), 7.39–7.52 (m, 8H, Ar*H*), 7.24–7.27 (m, 1H, Ar*H,* 2H, vinylic-*H*), 7.10–7.14 (m, 1H, Ar*H*), 6.47 (bs, 1H, –N*H*CO), 4.39 (q, J = 7.2 Hz, 2H,–NCH_2CH$_3$), 3.49–3.51 (m, 4H, –NCH_2), 1.64–1.71 (m, 6H, –NCH$_2$CH_2) and 1.46 (t, J = 7.2 Hz, 3H, –NCH$_2$CH_3); ^{13}C NMR (DMSO-d_6): 155.26, 140.41, 140.38, 139.55, 131.51, 129.05, 127.65, 126.61, 126.32, 126.00, 124.92, 123.02, 122.70, 120.87, 120.09, 119.35, 118.59, 109.76, 109.70, 45.17, 37.51, 26.00, 24.58 and 14.20; MS (m/z): 424.3 [M + H]$^+$.

5.1.23. (E)-1-(4-(2-(9-Ethyl-9H-carbazol-3-yl)vinyl)phenyl)-3-(2-(pyrrolidin-1-yl)-ethyl)urea (46)

The title compound was synthesized from compound (**34**) (1.0 g, 3.20 mmol) and 2-(aminoethyl) pyrrolidine (0.40 mL, 4.00 mmol) following **Method C** (yield: 0.88 g, 60%). Off-white solid; m.p. > 250 °C; IR (KBr, cm^{-1}): 3299, 3025, 2969, 2931, 1645, 1593, 1234, 960 and 743; ^{1}H NMR (DMSO-d_6): δ 8.73 (s, 1H, –N*H*CONH), 8.34 (s, 1H, Ar*H*), 8.17 (d, 1H, Ar*H*), 7.69 (d, 1H, Ar*H*), 7.56–7.60 (m, 2H, Ar*H*), 7.41–7.50 (m, 5H, Ar*H*), 7.15–7.27 (m, 1H, Ar*H,* 2H, vinylic-*H*), 6.15 (t, 1H, –NHCON*H*), 4.42 (q, J = 7.2 Hz, 2H, –NCH_2), 3.20–3.24 (m, 2H, –NHCONHCH_2), 2.43–2.49 (m, 6H, –NCH_2), 1.66–1.72 (m, 4H, –NCH$_2$CH_2) and 1.31 (t, J = 7.2 Hz, 3H, –NCH$_2$CH_3); ^{13}C NMR (DMSO-d_6): 155.64, 140.43, 139.60, 139.03, 132.00, 129.10, 127.94, 127.40, 127.03, 125.86, 124.98, 123.03, 122.71, 120.89, 119.37, 118.87, 118.68, 118.14, 109.78, 55.83, 53.97, 38.06, 37.52, 23.61 and 14.02; LCMS (m/z): 453.16 [M + H]$^+$, Purity: nearly 100%.

5.1.24. (E)-1-(4-(2-(9-Ethyl-9H-carbazol-3-yl)vinyl)phenyl)-3-(2-(piperidin-1-yl)-ethyl)urea (47)

The title compound was synthesized from compound (**34**) (1.0 g, 3.20 mmol) and 2-(aminoethyl) piperidine (0.57 mL, 4.00 mmol) following **Method C** (yield: 0.89 g, 60%). Off-white solid; m.p. 213–216 °C; IR (KBr, cm^{-1}): 3307, 3023, 2962, 2853, 1641, 1581,1237, 962 and 743; ^{1}H NMR (DMSO-d_6): δ 8.22 (d, 1H, Ar*H*), 8.13 (d, 1H, Ar*H*), 7.67 (dd, 1H, Ar*H*), 7.10–7.54 (m, 10*H*, Ar*H*, 2H, vinylic-*H*), 6.0 (bs, 1H, –NHCON*H*), 4.37 (q, J = 7.2 Hz, 2H, –NCH_2CH$_3$), 3.43–3.47 (m, 2H, –NHCONHCH_2); 2.50–2.69 (m, 6H, –NCH_2), 1.70–1.76 (m, 4H, –NCH$_2$CH_2), 1.51–1.59 (m, 2H, –NCH$_2$CH$_2$CH_2) and 1.45 (t, J = 7.2 Hz, 3H, –NCH$_2$CH_3); ^{13}C NMR (DMSO-d_6): 155.54, 140.41, 140.19, 139.53, 131.02, 129.07, 127.41, 127.41, 126.31, 126.00, 124.90, 123.02, 122.71, 120.88, 119.34, 118.56, 118.18, 109.76, 109.70, 58.60, 54.50, 37.51, 36.92, 26.01, 24.57 and 14.02; LCMS (m/z): 467.21 [M + H]$^+$, Purity: 99.88%.

5.1.25. (E)-1-(4-(2-(9-Ethyl-9H-carbazol-3-yl)vinyl)phenyl)-3-(3-(pyrrolidin-1-yl)-propyl)urea (48)

The title compound was synthesized from compound (**34**) (1.0 g, 3.20 mmol) and 3-(aminopropyl)pyrrolidine (0.51 g, 4.00 mmol) following **Method C** (yield: 0.97 g, 65%). Off-white solid; m.p. 215–217 °C; IR (KBr, cm^{-1}): 3322, 3022, 2982, 2803, 1634, 1588, 1235, 959 and 745; ^{1}H NMR (DMSO-d_6): δ 8.74 (s, 1H, –N*H*CONH), 8.34 (d, 1H, Ar*H*), 8.17 (d, 1H, Ar*H*),7.69 (dd, 1H, Ar*H*), 7.57–7.60 (m, 2H, Ar*H*), 7.40–7.49 (m, 5H, Ar*H*), 7.15–7.27 (m, 1H, Ar*H,* 2H, vinylic-*H*), 6.07 (t, 1H, –NHCON*H*), 4.44 (q, J = 7.2 Hz, 2H, –NCH_2CH$_3$), 3.17–3.22 (m, 2H, –NHCH_2), 2.33–2.36 (m, 6H, –NCH_2), 1.49–1.54 (m, 4H, –NCH$_2$CH_2), 1.36–1.42 (m, 2H, –CH_2) and 1.31 (t, J = 7.2 Hz, 3H, –NCH$_2$CH_3); ^{13}C NMR (DMSO-d_6): 155.64, 140.41, 140.18, 139.58, 131.03, 129.07, 127.42, 127.01, 126.31, 126.00, 124.89, 123.02, 122.71, 120.87, 119.34, 118.57, 118.26, 109.75, 109.69, 54.09, 53.75, 38.06, 37.51, 29.51, 23.56 and 14.20; LCMS (m/z): 467.21 [M + H]$^+$, Purity: 97.38%

5.1.26. (E)-1-(4-(2-(9-Ethyl-9H-carbazol-3-yl)vinyl)phenyl)-3-(3-(piperidin-1-yl)-propyl)urea (49)

The title compound was synthesized from compound (**34**) (1.0 g, 3.20 mmol) and 3-(aminopropyl) piperidine (0.57 g, 4.00 mmol) following **Method C** (yield: 1.0 g, 67%). Off-white solid; m.p. 206–207 °C; IR (KBr, cm^{-1}): 3308, 3027, 2961, 2870, 1641, 1591, 1233, 959 and 745; ^{1}H NMR (DMSO-d_6): δ 8.53 (s, 1H, –N*H*CONH), 8.34 (d, 1H, Ar*H*), 8.17 (d, 1H, Ar*H*), 7.69 (dd, 1H, Ar*H*), 7.58–7.60 (m, 2H, Ar*H*), 7.41–7.49 (m, 5H, Ar*H*), 7.15–7.27 (m, 1H, Ar*H,* 2H, vinylic-*H*), 6.17 (t, 1H, –NHCON*H*), 4.43 (q, J = 7.2 Hz, 2H, –NCH_2CH$_3$), 3.08–3.13 (m, 2H, –NHCH_2), 2.23–2.29 (m, 6H, –NCH_2), 1.55–1.59 (m, 2H, –NHCH$_2$CH_2), 1.46–1.51 (m, 4H, –NCH$_2$CH_2), 1.35–1.40 (m, 2H, –NCH$_2$CH$_2$CH_2) and 1.31 (t, J = 7.2 Hz, 3H, –NCH$_2$CH_3); ^{13}C NMR (DMSO-d_6): 155.64, 140.41, 140.19, 139.52, 131.03, 129.07, 127.41, 127.01, 126.30, 126.00, 124.88, 123.03, 122.71, 120.87, 119.34, 118.58, 118.28, 109.74, 109.63, 56.64, 54.57, 38.09, 37.50, 27.52, 26.01, 24.62 and 14.19; LCMS (m/z): 481.17 [M + H]$^+$, Purity: nearly 100%.

5.1.27. General method for the synthesis of (E)-1-(9-ethyl-6-styryl-9H-carbazol-3-yl)-3-(aminoalkyl)thiourea (50–52)

Method D. To a stirring solution of **34** (1.0 g, 3.20 mmol) and triethylamine (0.5 mL, 3.52 mmol) in dry 1:1 THF/DCM mixture (20 mL), thiocarbonyldiimidazole (0.63 g, 3.52 mmol) in 1:1 THF/DCM mixture (10 mL) was added drop wise at 0–5 °C over a period of 15 min. The resulting reaction mixture was allowed to stir at room temperature for 2 hrs. Progress of the reaction was monitored by TLC. After complete consumption of the starting material, the appropriate amine (4 mmol) was added to the reaction mixture and the reaction was further stirred for 30 min. After the completion of the reaction, the solvent was removed at reduced pressure. The residue so obtained was triturated with chilled methanol (20 mL). The solid was collected by filtration, washed again with chilled methanol (10 mL) and dried to the give titled compound [57].

5.1.27.1. (E)-1-(4-(2-(9-Ethyl-9H-carbazol-3-yl)vinyl)phenyl)-3-(2-(pyrrolidin-1-yl)ethyl)thiourea (50). The title compound was synthesized from compound (**34**) (1.0 g, 3.20 mmol) and 2-(aminoethyl) pyrrolidine (0.40 mL, 4.00 mmol) following **Method D** (yield: 1.13 g, 74%). Light yellow solid; m.p. 114–116 °C; IR (KBr, cm^{-1}): 3248, 3026, 2966, 2804, 1597, 1512, 1480, 1339, 1057, 961 and 746; ^{1}H NMR (DMSO-d_6): δ 9.71 (s, 1H, -N*H*CSNH), 8.36 (d, 1H, Ar*H*), 8.17 (d, 1H, Ar*H*), 7.69–7.73 (m, 1H, Ar*H*), 7.54–7.61 (m, 4H, Ar*H*), 7.41–7.48 (m, 3H, Ar*H*), 7.19–7.32 (m, 1H, Ar*H,* 2H, vinylic-*H*), 4.44 (q, J = 7.2 Hz, 2H, –NCH_2CH$_3$), 3.54–3.61 (m, 2H, –NHCH_2), 2.61 (t, 2H, –NCH_2CH$_2$), 2.47–2.51 (m, 4H, –NCH_2CH$_2$), 1.74–1.67 (m, 4H, –NCH$_2$CH_2) and 1.30 (t, J = 7.2 Hz, 3H, –NCH$_2$CH_3); ^{13}C NMR (DMSO-d_6): 139.96, 139.22, 133.43, 128.48, 128.32, 126.27, 125.90, 125.10, 124.62, 122.55, 122.23, 120.44, 118.94, 118.39, 109.35, 109.30, 53.43, 42.90, 37.06, 23.20 and 13.77; LCMS (*m/z*): 469.3 [M + H]$^+$, Purity: nearly 100%.

5.1.27.2. (E)-1-(4-(2-(9-Ethyl-9H-carbazol-3-yl)vinyl)phenyl)-3-(2-(piperidin-1-yl)ethyl)thiourea (51). The title compound was synthesized from compound (**34**) (1.0 g, 3.20 mmol) and 2-(aminoethyl) piperidine (0.57 mL, 4.00 mmol) following **Method D** (yield: 1.08 g, 70%). Light yellow solid; m.p. 183–185 °C; IR (KBr, cm^{-1}): 3290, 3029, 2934, 2846, 2801, 1599, 1513, 1478, 1236, 961, 821 and 750; ^{1}H NMR (DMSO-d_6): δ 9.72 (s, 1H, -N*H*CSNH), 8.37 (d, 1H,Ar*H*), 8.17 (d, 1H, Ar*H*), 7.71–7.73 (m, 1H, Ar*H*), 7.55–7.61 (m, 5H, Ar*H*), 7.43–7.48 (m, 3H, Ar*H*), 7.19–7.37 (m, 1H, Ar*H,* 2H, vinylic-*H*), 4.44 (q, J = 7.2 Hz, 2H, –NCH_2CH$_3$), 3.52–3.58 (m, 2H, –NHCH_2), 2.47 (t, 2H, –NCH_2CH$_2$), 2.33–2.38 (m, 4H, –NCH_2CH$_2$), 1.45–1.52 (m, 2H, –NCH$_2$CH_2), 1.34–1.41 (m, 2H, –NCH$_2$CH$_2$CH_2) and 1.30 (t, J = 7.2 Hz, 3H, –NCH$_2$CH_3); ^{13}C NMR (DMSO-d_6): 139.96, 139.24, 133.61, 128.59, 128.30, 126.41, 125.91, 125.06, 124.64, 122.85, 122.55, 122.23, 120.44, 118.95, 118.42, 109.35, 109.30, 53.87, 41.20, 37.06, 25.63, 24.08 and 13.76; LCMS (*m/z*): 483.4 [M + H]$^+$, Purity: nearly 100%.

5.1.27.3. (E)-1-(4-(2-(9-Ethyl-9H-carbazol-3-yl)vinyl)phenyl)-3-(3-(pyrrolidin-1-yl)-propyl)thiourea (52). The title compound was synthesized from compound (**34**) (1.0 g, 3.20 mmol) and 3-(aminopropyl)pyrrolidine (0.51 g, 4.00 mmol) following **Method D** (yield: 1.11 g, 72%). Light yellow solid; m.p. 188–190 °C; IR (KBr, cm^{-1}): 3186, 2967, 2871, 2816, 1594, 1524, 1307, 1236, 958 and 747; ^{1}H NMR (DMSO-d_6): δ 9.55 (s, 1H, -N*H*CSNH), 8.37 (d, 1H, Ar*H*), 8.17 (d, 1H, Ar*H*), 7.96–8.00 (m, 1H, Ar*H*), 7.71–7.73 (m, 1H, Ar*H*), 7.55–7.60 (m, 4H, Ar*H*), 7.19–7.47 (m, 3H, Ar*H,* 2H, vinylic-*H*), 4.44 (q, J = 7.2 Hz, 2H, –NCH_2CH$_3$), 3.51–3.55 (m, 2H, –NHCH_2), 2.37–2.45 (m, 6H, –NCH_2), 1.66–1.75 (m, 2H, –NCH$_2$CH_2), 1.55–1.59 (m, 4H, –NCH$_2$CH_2) and 1.32 (t, J = 7.2 Hz, 3H, –NCH$_2$CH_3); ^{13}C NMR (DMSO-d_6): 179.9, 139.96, 139.24, 133.69, 128.60, 128.29, 126.40, 125.04, 124.64, 123.09, 122.55, 122.23, 120.44, 118.95, 118.42, 109.35, 109.30, 53.59, 37.06, 27.34, 23.03 and 13.77; LCMS (*m/z*): 483.4 [M + H]$^+$, Purity: nearly 100%.

5.2. Biology

5.2.1. In vitro cholinesterase inhibition studies

The ability of the test compounds to inhibit ChEs was evaluated using Ellman's method as presented in our earlier report [36–38]. All the experiments were performed in 50 mM Tris-HCl buffer (*p*H = 8). Five different concentrations (0.001–100 μM) of each test compound were used to determine the enzyme inhibition activity. Briefly, 10 μL of the test or standard compounds and 50 μL of AChE (0.22 U/mL) or 50 μL of BuChE (0.06 U/mL) were incubated in 96-well plates at room temperature for 30 min. Further, 30 μL of the substrate ATCI (15 mM) or BTCI (15 mM) was added and the solution was incubated additionally for 30 min. Finally, 160 μL of DTNB (1.5 mM) was added to it, and the absorbance at 415 nm wavelength was measured using the microplate reader 680 XR (BIO-RAD, India). The IC_{50} values were calculated from the absorbance obtained for various concentrations of the test and the standard compounds. All determinations were carried out in triplicate.

5.2.2. Antioxidant activity

The antioxidant potential of the compounds was estimated using spectrophotometric DPPH assay as described earlier [36]. In brief, 10 μL of the test compound (10, 20, 50, 100 and 200 μM in methanol) was mixed with 20 μL of DPPH (10 mM in methanol) in a 96-well plate. Finally, the volume was adjusted to 200 μL using methanol. After a 30 s incubation at room temperature with protection from light, the absorbance was recorded using a microplate reader 680 XR (BIORAD, India) at 520 nm wavelength. The free radical scavenging activity was determined as the reduction percentage (RP) of DPPH using the equation $RP = 100[(A_0 - A_C)/A_0]$, where A_0 is the untreated DPPH absorbance and A_C is the absorbance value for the added sample concentration C. Ascorbic acid was used as the standard antioxidant.

5.2.3. Self-induced $A\beta_{1\text{-}42}$ aggregation inhibition study

The potential of carbazole-based stilbene derivatives to inhibit self-mediated $A\beta_{1\text{-}42}$ aggregation was evaluated by a thioflavin T (ThT)-based fluorescence assay [58]. 1,1,1,3,3,3-Hexafluoro-2-propanol (HFIP)-pretreated $A\beta_{1-42}$ peptide (Sigma Aldrich) was resolubilized with a 50 mM phosphate buffer (pH = 7.4) to get a stable stock solution (100 μM). The assay was performed in Costar, clear-bottom, black-surround 96-well plates. For the experiment, the $A\beta_{1-42}$ stock solution was additionally diluted to 50 μM (by a 50 mM phosphate buffer, *p*H = 7.4) before use. A mixture of the peptide (10 μL) with or without the test compounds (10 μL) at 25 μM and 50 μM final concentrations were incubated at 37 °C temperature for 48 h with frequent shaking. Blank readings using 50 mM phosphate buffer (*p*H = 7.4) instead of a peptide with or without test compounds were also taken. After incubation, the samples were diluted with 180 μL of thioflavin T (5 μM, in 50 mM glycine-NaOH buffer, *p*H = 8). The fluorescence intensities were measured on a SpectraMax iD3 multi-mode microplate reader with 446 nm excitation wavelength and 490 nm emission wavelengths. Each test compound was examined in duplicate. The fluorescence intensities were compared and the percent inhibition due to the presence of the test compound was calculated by the following equation, % inhibition = $(1\text{-}IF_i/IF_0) \times 100$, where IF_i and IF_0 are the fluorescence intensities obtained for $A\beta_{1\text{-}42}$ in the presence and the absence of test compound, respectively.

5.2.4. Metal-chelating study

The metal chelating ability of the selected compound was assessed using UV spectrophotometry [42]. The absorption spectra of compound (**50**) and 8-hydroxyquinoline (25 μM, final concentration) alone or in the presence of $CuSO_4$, $ZnCl_2$, $FeSO_4$, $FeCl_3$, $AlCl_3$, $MgSO_4$ or $CaCl_2$ (25 μM, final concentration) for 30 min were recorded at room temperature at wavelengths ranging from 200 to 600 nm.

5.3. Computational studies

5.3.1. Docking studies of compound (50) with ChEs

Docking studies were carried out with Glide module of Schrodinger Suite. It offers grid-based ligand docking and explores the promising interactions between ligand molecules and a protein. The 3D crystallographic structures of AChE (PDB code: 2CKM, 1B41) and of BuChE (PDB code: 4BDS) were retrieved from the RCSB Protein Data Bank and prepared for docking by the Protein Preparation Wizard of Schrödinger. The grid was generated on the active site of the respective protein structure. For the validation of the generated grids for docking studies, the cocrystallized molecules in the 3D structures of *Tc*AChE and *h*BuChE (PDB code: 2CKM and 4BDS, respectively) were knocked out of the binding sites. The knocked-out molecules were built within Maestro using the Build module, energy minimized, and redocked into the active sites of the grids. Very similar interactions were observed between the redocked molecules and the enzymes as was the case with the original cocrystallized ligands. The root-mean-square deviation (RMSD) values of the redocked ligands with those of the original orientations in co-crystallized forms in 2CKM and 4BDS were observed to be 0.40 and 0.26 Å, respectively. The 3D structure of the ligand molecule (**50**) was built within Maestro using the Build module, and a single low energy conformation search was carried out for it using the OPLS_2005 force field at physiological *p*H conditions using the LigPrep module of Schrödinger, keeping all parameters at standard values [59]. Docking calculations for the minimized 3D ligand structure were carried out in extra precision (XP) mode within the active sites of the protein structures [60]. Docking protocol was validated by comparing the interactions of the docked conformer of donepezil in the active site of AChE with the reported literature.

5.3.2. Docking studies of compound (50) with $A\beta_{1\text{-}42}$

The docking studies were carried out by using AutoDock4.2 [61,62]. $A\beta_{1\text{-}42}$ peptide structure was obtained from RCSB (PDB Code: 1IYT) and was cleaned and prepared for docking in AutoDock. The docking study of compound (**50**) was carried out by the blind docking method. Grid was generated over the entire protein structure, and the ligand under study was allowed to interact with the entire sequence to know the most stable/possible interactions between the ligand and the target protein. For the ligand-receptor complex, 10 docking experiments were carried out using the Lamarckian genetic algorithm. The maximum number of energy evaluations of 25 million was applied for each docking experiment. All the 3D docking images were generated using Chimera tool [63].

5.3.3. In silico prediction of physicochemical and pharmacokinetics parameters

In silico prediction of physicochemical and pharmacokinetic properties was carried out using the QikProp module of Schrodinger Suite [46]. The structures of the ligand molecules built for the docking studies were employed to determine the various physicochemical and pharmacokinetic descriptors. The major descriptors that were analyzed in this study were Lipinski's rule of five, the number of rotatable bonds, polar surface area, total solvent-accessible surface area, central nervous system permeability, apparent MDCK cell permeability, Caco-2 cell permeability, brain/blood partition coefficient, human serum albumin binding, aqueous solubility, and percent human-oral absorption.

Author contributions

M.R.Y. conceived and designed the study. D.V.P. and N.R.P. performed synthesis and collected data. A.M.K. designed and performed computational studies. D.M.T., K.B.P. and P.D.J. contributed reagents and materials and assisted in synthesis and data collection. K.V.P. drafted the biological evaluation studies. S.P.P., P.M.G., and B.N.C. carried out biological studies and collected data. N.K.P. assisted in the synthesis and data interpretation. D.V.P., N.R.P. and A.M.K. wrote the manuscript. All authors have given approval to the final version of the manuscript.

Declaration of Competing Interest

The authors declare that they have no known competing financial interests or personal relationships that could have appeared to influence the work reported in this paper.

Acknowledgements

Dushyant V. Patel gratefully acknowledges the DST-INSPIRE, New Delhi for awarding Research Fellowship (IF-150660). Nirav R. Patel is thankful to the UGC, New Delhi, for awarding Senior Research Fellowship [F. No. 25-1/2014-15(BSR)/7-129/2007/(BSR)]. The authors thank Dr. Kapil Juvale, SPPSPTM, NMIMS University, Mumbai, for providing SpectramMax iD3 multi-mode microplate reader to perform $A\beta_{1\text{-}42}$ aggregation study.

Appendix A. Supplementary material

Supplementary data to this article can be found online at https://doi.org/10.1016/j.bioorg.2020.103977.

References

[1] M. Goedert, M.G. Spillantini, A century of Alzheimer's disease, Science 314 (2006) 777–781.
[2] Alzheimer's Disease International. (2019, April 10). World Alzheimer report 2019: Attitudes to dementia. Retrieved from https://www.alz.co.uk/research/world-report-2019.
[3] V.N. Talesa, Acetylcholinesterase in Alzheimer's disease, Mech. Ageing Dev. 122 (2001) 1961–1969.
[4] D.J. Selkoe, Folding proteins in fatal ways, Nature 426 (2003) 900–904.
[5] R.B. Maccioni, G. Farías, I. Morales, L. Navarrete, The revitalized tau hypothesis on Alzheimer's disease, Arch. Med. Res. 41 (2010) 226–231.
[6] D.J. Bonda, X. Wang, G. Perry, A. Nunomura, M. Tabaton, X. Zhu, M.A. Smith, Oxidative stress in Alzheimer disease: a possibility for prevention, Neuropharmacology 59 (2010) 290–294.
[7] M.A. Greenough, J. Camakaris, A.I. Bush, Metal dyshomeostasis and oxidative stress in Alzheimer's disease, Neurochem. Int. 62 (2013) 540–555.
[8] E. Scarpini, P. Scheltens, H. Feldman, Treatment of Alzheimer's disease: Current status and new perspectives, Lancet Neurol. 2 (2003) 539–547.
[9] R.T. Bartus, R.L. Dean, M.J. Pontecorvo, C. Flicker, The cholinergic hypothesis: a historical overview, current perspective, and future directions, Ann. N. Y. Acad. Sci. 444 (1985) 332–358.
[10] P.E. Gold, Acetylcholine modulation of neural systems involved in learning and memory, Neurobiol. Learn. Mem. 80 (2003) 194–210.
[11] U. Holzgrabe, P. Kapková, V. Alptüzün, J. Scheiber, E. Kugelmann, Targeting acetylcholinesterase to treat neurodegeneration, Expert Opin. Ther. Targets. 11 (2007) 161–179.
[12] J. Hartmann, C. Kiewert, E.G. Duysen, O. Lockridge, N.H. Greig, J. Klein, Excessive hippocampal acetylcholine levels in acetylcholinesterase- deficient mice are moderated by butyrylcholinesterase activity, J. Neurochem. 100 (2007) 1421–1429.
[13] N.H. Greig, D.K. Lahiri, K. Sambamurti, Butyrylcholinesterase: an important new target in Alzheimer's disease therapy, Int. Psychogeriatrics. 14 (2002) 77–91.
[14] F. Durst, C. Tropea, The amyloid hypothesis of Alzheimer's disease at 25 years, EMBO Mol. Med. 8 (2016) 595–608.
[15] J. Hardy, The amyloid hypothesis for Alzheimer's disease: a critical reappraisal, J. Neurochem. 110 (2009) 1129–1134.
[16] R.J. O'Brein, P.C. Wong, Amyloid precursor protein processing and Alzheimer's disease, Annu. Rev. Neurosci. 34 (2015) 185–204.
[17] C. Cheignon, M. Tomas, D. Bonnefont-Rousselot, P. Faller, C. Hureau, F. Collin, Oxidative stress and the amyloid beta peptide in Alzheimer's disease, Redox Biol. 14 (2018) 450–464.
[18] V. Lobo, A. Patil, A. Phatak, N. Chandra, Free radicals, antioxidants and functional foods: Impact on human health, Pharmacogn. Rev. 4 (2010) 118–126.
[19] D. Poljuha, I. Šola, J. Bilić, S. Dudaš, T. Bilušić, J. Markić, G. Rusak, Oxidative stress and neurodegenerative diseases: a review of upstream and downstream antioxidant therapeutic options, Eur. Food Res. Technol. 241 (2015) 65–74.
[20] Y. Liu, M. Nguyen, A. Robert, B. Meunier, Metal ions in Alzheimer's disease: a key role or not ? Acc. Chem. Res. 52 (2019) 2026–2035.
[21] A.I. Bush, The metallobiology of Alzheimer's disease, Trends Neurosci. 26 (2003) 207–214.
[22] F. Collin, Chemical basis of reactive oxygen species reactivity and involvement in neurodegenerative diseases, Int. J. Mol. Sci. 20 (2019) E2407.

[23] L.S. Tsutsumi, D. Gündisch, D. Sun, Carbazole scaffold in medicinal chemistry and natural products: a review from 2010–2015, Curr. Top. Med. Chem. 16 (2016) 1290–1313.
[24] L. Fang, M. Chen, Z. Liu, X. Fang, S. Gou, L. Chen, Ferulic acid-carbazole hybrid compounds: combination of cholinesterase inhibition, antioxidant and neuroprotection as multifunctional anti-Alzheimer agents, Bioorganic Med. Chem. 24 (2016) 886–893.
[25] W. Yang, Y. Wong, O.T.W. Ng, L.P. Bai, D.W.J. Kwong, Y. Ke, Z.H. Jiang, H.W. Li, K.K.L. Yung, M.S. Wong, Inhibition of beta-amyloid peptide aggregation by multifunctional carbazole-based fluorophores, Angew. Chemie. 124 (2012) 1840–1846.
[26] N. Naik, H.V. Kumar, H. Swetha, Synthesis and evaluation of novel carbazole derivatives as free radical scavengers, Bulg. Chem. Commun. 42 (2010) 40–45.
[27] S. Thiratmatrakul, C. Yenjai, P. Waiwut, O. Vajragupta, P. Reubroycharoen, M. Tohda, C. Boonyarat, Synthesis, biological evaluation and molecular modeling study of novel tacrine-carbazole hybrids as potential multifunctional agents for the treatment of Alzheimer's disease, Eur. J. Med. Chem. 75 (2014) 21–30.
[28] C. Saengkhae, M. Salerno, D. Adès, A. Siove, L. Le Moyec, V. Migonney, A. Garnier-Suillerot, Ability of carbazole salts, inhibitors of Alzheimer β-amyloid fibril formation, to cross cellular membranes, Eur. J. Pharmacol. 559 (2007) 124–131.
[29] H.T.T. Phan, K. Samarat, Y. Takamur, A.F. Azo-Oussou, Y. Nakazono, M.C. Vestergaard, Polyphenols modulate alzheimer's amyloid beta aggregation in a structure-dependent manner, Nutrients. 11 (2019) 756.
[30] N. Singh, M. Agrawal, S. Doré, Neuroprotective properties and mechanisms of resveratrol in in vitro and in vivo experimental cerebral stroke models, ACS Chem. Neurosci. 4 (2013) 1151–1162.
[31] N.A.M. Azman, M.H. Gordon, M. Skowyra, F. Segovia, M.P. Almajano, Antioxidant properties of resveratrol: a structure-activity insight, J. Sci. Food Agric. 95 (2015) 210–218.
[32] M.C. Hong, Y.K. Kim, J.Y. Choi, S.Q. Yang, H. Rhee, Y.H. Ryu, T.H. Choi, G.J. Cheon, G.I. An, H.Y. Kim, Y. Kim, D.J. Kim, J.S. Lee, Y.T. Chang, K.C. Lee, Synthesis and evaluation of stilbene derivatives as a potential imaging agent of amyloid plaques, Bioorg. Med. Chem. 18 (2010) 7724–7730.
[33] X. Zhang, Y. Wang, S. nan Wang, Q. he Chen, Y. lin Tu, X. hong Yang, J. kao Chen, J. wu Yan, R. biao Pi, Y. Wang, Discovery of a novel multifunctional carbazole–aminoquinoline dimer for Alzheimer's disease: copper selective chelation, anti-amyloid aggregation, and neuroprotection, Med. Chem. Res. 27 (2018) 777–784.
[34] C. Lu, Y. Guo, J. Li, M. Yao, Q. Liao, Z. Xie, X. Li, Design, synthesis, and evaluation of resveratrol derivatives as Aß1-42 aggregation inhibitors, antioxidants, and neuroprotective agents, Bioorganic Med. Chem. Lett. 22 (2012) 7683–7687.
[35] C.L. Xia, N. Wang, Q.L. Guo, Z.Q. Liu, J.Q. Wu, S.L. Huang, T.M. Ou, J.H. Tan, H.G. Wang, D. Li, Z.S. Huang, Design, synthesis and evaluation of 2-arylethenyl-N-methylquinolinium derivatives as effective multifunctional agents for Alzheimer's disease treatment, Eur. J. Med. Chem. 130 (2017) 139–153.
[36] D.V. Patel, N.R. Patel, A.M. Kanhed, S.P. Patel, A. Sinha, D.D. Kansara, A.R. Mecwan, S.B. Patel, P.N. Upadhyay, K.B. Patel, D.B. Shah, N.K. Prajapati, P.R. Murumkar, K.V. Patel, M.R. Yadav, Novel multitarget directed triazinoindole derivatives as anti-Alzheimer agents, ACS Chem. Neurosci. 10 (2019) 3635–3661.
[37] A. Sinha, R.S. Tamboli, B. Seth, A.M. Kanhed, S.K. Tiwari, S. Agarwal, S. Nair, R. Giridhar, R.K. Chaturvedi, M.R. Yadav, Correction to: neuroprotective role of novel triazine derivatives by activating Wnt/β catenin signaling pathway in rodent models of Alzheimer's disease, Mol. Neurobiol. 56 (2019) 7246–7248.
[38] A.M. Kanhed, A. Sinha, J. Machhi, A. Tripathi, Z.S. Parikh, P.P. Pillai, R. Giridhar, M.R. Yadav, Discovery of isoalloxazine derivatives as a new class of potential anti-Alzheimer agents and their synthesis, Bioorg. Chem. 61 (2015) 7–12.
[39] Y.R. Chen, C.G. Glabe, Distinct early folding and aggregation properties of Alzheimer amyloid-β peptides $A\beta_{40}$ and $A\beta_{42}$: stable trimer or tetramer formation by $A\beta_{42}$, J. Biol. Chem. 281 (2006) 24414–24422.
[40] G. Bitan, S.S. Vollers, D.B. Teplow, Elucidation of primary structure elements controlling early amyloid β-protein oligomerization, J. Biol. Chem. 278 (2003) 34882–34889.
[41] M.G. Savelieff, S. Lee, Y. Liu, M.H. Lim, Untangling amyloid-β, tau, and metals in Alzheimer's disease, ACS Chem. Biol. 8 (2013) 856–865.
[42] Z. Wang, Y. Wang, B. Wang, W. Li, L. Huang, X. Li, Design, synthesis, and evaluation of orally available clioquinol-moracin M hybrids as multitarget-directed ligands for cognitive improvement in a rat model of neurodegeneration in Alzheimer's disease, J. Med. Chem. 58 (2015) 8616–8637.
[43] Protein Data Bank, www.rcsb.org/pdb/home/home.do.
[44] O. Crescenzi, S. Tomaselli, R. Guerrini, S. Salvadori, A.M. D'Ursi, P.A. Temussi, D. Picone, Solution structure of the Alzheimer amyloid β-peptide (1–42) in an apolar microenvironment: Similarity with a virus fusion domain, Eur. J. Biochem. 269 (2002) 5642–5648.
[45] J. Wang, L. Urban, The impact of early ADME profiling on drug discovery and development strategy, Drug Discov. World. 73–86 (2004).
[46] QikProp version 3.2 (2009) Schrödinger, LLC, New York, NY.
[47] A.L. Christiphor, L. Franco, W.D. Beryl, J.F. Paul, Experimental and computational approaches to estimate solubility and permeability in drug discovery and development settings, Adv. Drug Deliv. Rev. 23 (2019) 3–25.
[48] D.F. Veber, S.R. Johnson, H.Y. Cheng, B.R. Smith, K.W. Ward, K.D. Kopple, Molecular properties that influence the oral bioavailability of drug candidates, J. Med. Chem. 45 (2002) 2615–2623.
[49] J. Kelder, P.D.J. Grootenhuis, D.M. Bayada, L.P.C. Delbressine, J.P. Ploemen, Polar molecular surface as a dominating determinant for oral absorption and brain penetration of drugs, Pharm. Res. 16 (1999) 1514–1519.
[50] H. Pajouhesh, G.R. Lenz, Medicinal chemical properties of successful central nervous system drugs, NeuroRx. 2 (2005) 541–553.
[51] Q. Wang, J.D. Rager, K. Weinstein, P.S. Kardos, G.L. Dobson, J. Li, I.J. Hidalgo, Evaluation of the MDR-MDCK cell line as a permeability screen for the blood-brain barrier, Int. J. Pharm. 288 (2005) 349–359.
[52] D. Li, P. Wu, D. Guo, Y. Yu, H. Xiao, X. Jiang, Synthesis and luminescence properties of novel carbazolyl-containing amino alcohol Schiff bases, Res. Chem. Intermed. 41 (2015) 2591–2601.
[53] K.S. Vadagaonkar, C.J. Yang, W.H. Zeng, J.H. Chen, B.N. Patil, P. Chetti, L.Y. Chen, A.C. Chaskar, Triazolopyridine hybrids as bipolar host materials for green phosphorescent organic light-emitting diodes (OLEDs), Dye. Pigment. 160 (2019) 301–314.
[54] R. Nagarajan, D. Muralidharan, P.T. Perumal, A new and facile method for the synthesis of nitrocarbazoles by urea nitrate, Synth. Commun. 34 (2004) 1259–1264.
[55] G. Robertson, R. *p*-Nitrophenylacetic acid, Org. Synth. 2 (1922) 59.
[56] M.J. Cen, Y. Wang, Y.W. He, Microwave assistant synthesis of trans-4-nitrostilbene derivatives in solvent free condition, Eur. J. Chem. 8 (2017) 13–14.
[57] T.K. Venkatachalam, F.M. Uckun, Synthesis of substituted heterocyclic thiourea compounds, Synth. Commun. 37 (2007) 3667–3675.
[58] S.Y. Li, X.B. Wang, S.S. Xie, N. Jiang, K.D.G. Wang, H.Q. Yao, H. Bin Sun, L.Y. Kong, Multifunctional tacrine-flavonoid hybrids with cholinergic, β-amyloid-reducing, and metal chelating properties for the treatment of Alzheimer's disease, Eur. J. Med. Chem. 69 (2013) 632–646.
[59] LigPrep Version 2.3 (2009) Schrödinger. LLC, New York, NY.
[60] Glide version 5.5 (2009) Schrödinger, LLC, New York, NY.
[61] G.M. Morris, R. Huey, W. Lindstrom, M.F. Sanner, R.K. Belew, D.S. Goodsell, A.J. Olson, AutoDock4 and AutoDockTools4: Automated docking with selective receptor flexibility, J. Comput. Chem. 16 (2009) 2785–2791.
[62] M.F. Sanner, Python: A programming language for software integration and development, J. Mol. Graph. Model. 17 (1999) 57–61.
[63] E.F. Pettersen, T.D. Goddard, C.C. Huang, G.S. Couch, D.M. Greenblatt, E.C. Meng, T.E. Ferrin, UCSF Chimera - a visualization system for exploratory research and analysis, J. Comput. Chem. 13 (2004) 1605–1612.

ACS Chemical Neuroscience
Cite This: ACS Chem. Neurosci. 2019, 10, 3635−3661
Research Article
pubs.acs.org/chemneuro

Novel Multitarget Directed Triazinoindole Derivatives as Anti-Alzheimer Agents

Dushyant V. Patel, Nirav R. Patel, Ashish M. Kanhed, Sagar P. Patel, Anshuman Sinha, Deep D. Kansara, Annie R. Mecwan, Sarvangee B. Patel, Pragnesh N. Upadhyay, Kishan B. Patel, Dharti B. Shah, Navnit K. Prajapati, Prashant R. Murumkar, Kirti V. Patel, and Mange Ram Yadav*

Faculty of Pharmacy, Kalabhavan Campus, The Maharaja Sayajirao University of Baroda, Vadodara-390001 Gujarat, India

Supporting Information

ABSTRACT: The multifaceted nature of Alzheimer's disease (AD) demands treatment with multitarget-directed ligands (MTDLs) to confront the key pathological aberrations. A novel series of triazinoindole derivatives were designed and synthesized. In vitro studies revealed that all the compounds showed moderate to good anticholinesterase activity; the most active compound **23e** showed an IC_{50} value of 0.56 ± 0.02 μM for AChE and an IC_{50} value of 1.17 ± 0.09 μM for BuChE. These derivatives are also endowed with potent antioxidant activity. To understand the plausible binding mode of the compound **23e**, molecular docking studies and molecular dynamics simulation studies were performed, and the results indicated significant interactions of **23e** within the active sites of AChE as well as BuChE. Compound **23e** successfully diminished H_2O_2-induced oxidative stress in SH-SY5Y cells and displayed excellent neuroprotective activity against H_2O_2 as well as Aβ-induced toxicity in SH-SY5Y cells in a concentration dependent manner. Furthermore, it did not show any significant toxicity in neuronal SH-SY5Y cells in the cytotoxicity assay. Compound **23e** did not show any acute toxicity in rats at doses up to 2000 mg/kg, and it significantly reversed scopolamine-induced memory deficit in mice model. Additionally, compound **23e** showed notable in silico ADMET properties. Taken collectively, these findings project compound **23e** as a potential balanced MTDL in the evolution process of novel anti-AD drugs.

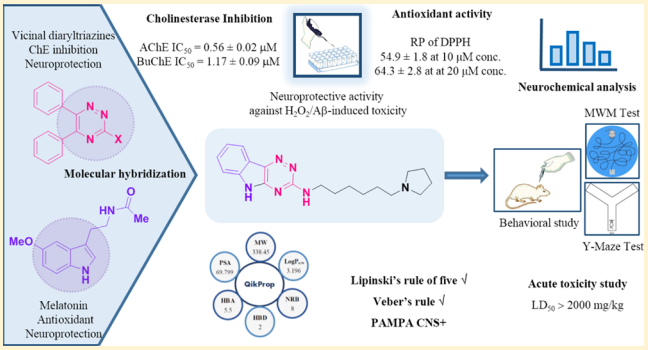

KEYWORDS: *Alzheimer's disease, MTDL, anticholinesterase, antioxidant, neuroprotection, triazinoindole*

INTRODUCTION

Alzheimer's disease (AD) is an irrevocable age-related neurodegenerative disorder clinically identified by progressive deterioration in memory, cognitive deficit, abnormal behavior, and incoherent language.[1] It is the most prominent form of dementia. More than 50 million people are suffering from it worldwide, and the number will significantly rise up to 152 million by 2050 if no cure or preventive measures are found.[2] This burgeoning number of people suffering from AD, in both developed and developing countries, has drawn the attention of medicinal chemists to accelerate research on drug discovery in this area.

The etiology of AD is still enigmatic. Different factors, like low levels of neurotransmitter acetylcholine (ACh),[3] aggregation of the β-amyloid peptide,[4,5] accumulation of hyperphosphorylated tau protein,[6,7] dyshomeostasis of biometals,[8] oxidative stress,[9] mitochondrial dysfunction,[10] and neuroinflammation,[11−13] are proposed to play pivotal roles in the pathogenesis of AD. To combat AD-like diseases having a complex etiology, development of multitarget-directed ligands (MTDLs) is recognized as one of the most assuring drug discovery approaches.[14−17] Drugs acting on a single target even though they have high affinity and selectivity for their targets might not influence the mysterious etiology of the disease satisfactorily. An MTDL having moderate but balanced affinities for the targets can still exert more beneficial effects compared to a single-targeted molecule. Concurrent effects on several therapeutic targets make MTDLs superior in altering the complex equilibrium of the cellular network.[18,19] A mild and balanced activity on multiple therapeutic targets might secure higher safety and reduce the risk of therapeutic resistance.[20]

After perusal of current research in this field, we focused our attention on inhibition of cholinesterase and antioxidant potential of new chemical entities (NCEs) as the core objectives of anti-AD drug design. Two types of cholinesterase enzymes (ChEs), namely, acetylcholinesterase (AChE) (EC 3.1.1.7) and butyrylcholinesterase (BuChE) (EC 3.1.1.8), are

Received: April 13, 2019
Accepted: July 16, 2019
Published: July 16, 2019

DOI: 10.1021/acschemneuro.9b00226
ACS Chem. Neurosci. 2019, 10, 3635−3661

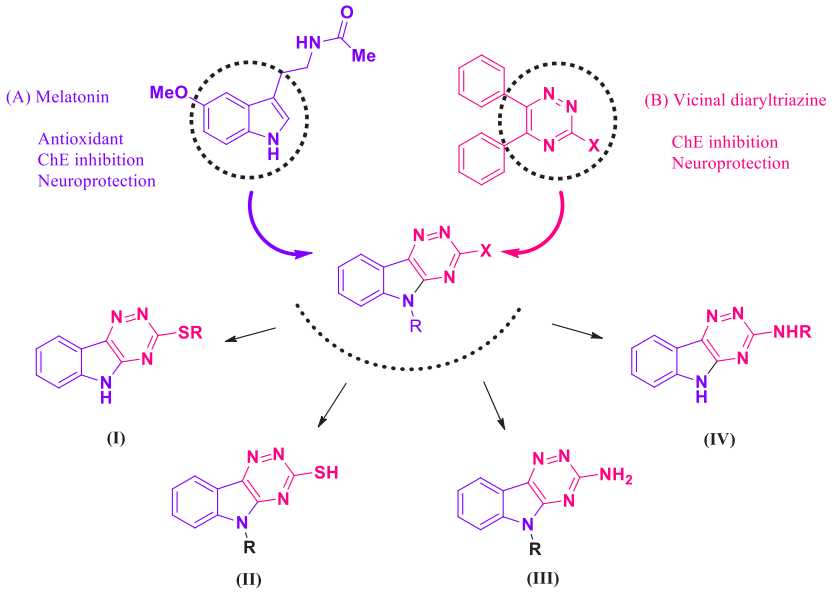

Figure 1. Molecular hybridization approach to design triazinoindole derivatives.

found in the central nervous system. Both of these enzymes belong to the carboxylesterase family of enzymes and play an important role in cholinergic transmission through hydrolysis of the neurotransmitter ACh. Although AChE and BuChE are produced by different genes, they are highly homologous with more than 65% similarity in their active sites.[21,22] AChE has two major binding subsites, a peripheral anionic site (PAS) and a catalytic active site (CAS).[23] The CAS of the enzyme is actively involved in the maintenance of cholinergic neurotransmission. PAS is involved in the formation of β-amyloid fibrils that are associated with plaque deposition.[24,25] AChE inhibitors blocking both CAS and PAS simultaneously could alleviate the cognitive defect in AD patients by elevating ACh levels, and they have also been endowed with disease modifying ability by inhibiting amyloid plaque formation.[26] In healthy brains, AChE is more active than BuChE and can hydrolyze about 80% of ACh. Current studies have demonstrated that, as the disease progresses, the ability of BuChE increases by 40−90%, and that of AChE declines in the hippocampus and temporal cortex areas of the brain.[27−29] BuChE plays several roles both in neural and non-neural functioning. Clinical data suggested that the high cortical levels of BuChE were associated with some important AD hallmarks, such as extracellular deposition of the Aβ and aggregation of hyperphosphorylated tau protein.[21,30,31] This reflects the important role played by both cholinesterases and the necessity to develop MTDLs which could act on both of these ChEs.[32]

Recent research has emphasized the significance of oxidative stress in the fundamental molecular mechanism of AD.[8,9] Oxidative stress occurs when there is an inequity between the formation and quenching of free radicals formed from oxygen species. These reactive oxygen species (ROS) are regarded as the other major etiological factor of AD, since the role of the ROS in the formation of both amyloid plaques and neurofibrillary tangles is confirmed.[33] Through pathological oxidation−reduction steps, ROS can denature biomolecules like proteins, lipids, and nucleic acids. This can cause tissue damage through necrosis and apoptosis.[34] Thus, oxidative stress plays a central role in the pathogenesis of AD, leading to neuronal dysfunction and cell death.[35]

Considering the facts that inhibition of AChE provides a symptomatic treatment to AD, increased levels of BuChE are observed in the brains of AD patients, and the ROS system plays a vital role in neurodegeneration, a series of triazinoindole derivatives were designed, synthesized, and evaluated in the current report for their multifactorial anti-AD activities, including cholinesterase inhibitory activity, antioxidant activity, cytoprotective effect against H_2O_2/Aβ-induced cell injury, and acute toxicity in animal models. The in silico ADMET properties of the synthesized derivatives were predicted and the structure−activity relationship (SAR) of these novel derivatives has been discussed. Molecular modeling studies were performed to offer an insight into the binding mode of the derivatives with the target proteins, and these findings were supported by the time dependent stability analysis of the ligand−receptor complex of the most active ligand and the receptor under study, by means of molecular dynamics simulations.

DESIGNING ASPECTS

To combat a disease like AD having complex etiology, development of MTDLs has been recognized as one of the most assuring drug discovery approaches. In spite of considerable research on new targets available for AD treatment, the cholinesterase inhibitors still remain the drugs of choice, although they provide symptomatic and transient benefits to the patients. Oxidative stress plays an important role in pathogenesis of AD. However, antioxidant molecules alone might not be enough to treat such a highly complex pathological disease like AD.[36] So dual cholinesterase inhibitors endowed with additional antioxidant and neuroprotective properties could increase the chances of combating AD successfully.

The indole ring is prodigiously present in many natural compounds possessing invaluable medicinal and biological properties.[37,38] Melatonin is an indole ring containing pineal neurohormone whose levels decrease during aging, especially in AD patients.[39−41] It is endowed with strong free radical scavenging properties.[42] The high reactivity of melatonin with ROS is apparently due to its electron-rich indole ring, acting as

DOI: 10.1021/acschemneuro.9b00226
ACS Chem. Neurosci. 2019, 10, 3635−3661

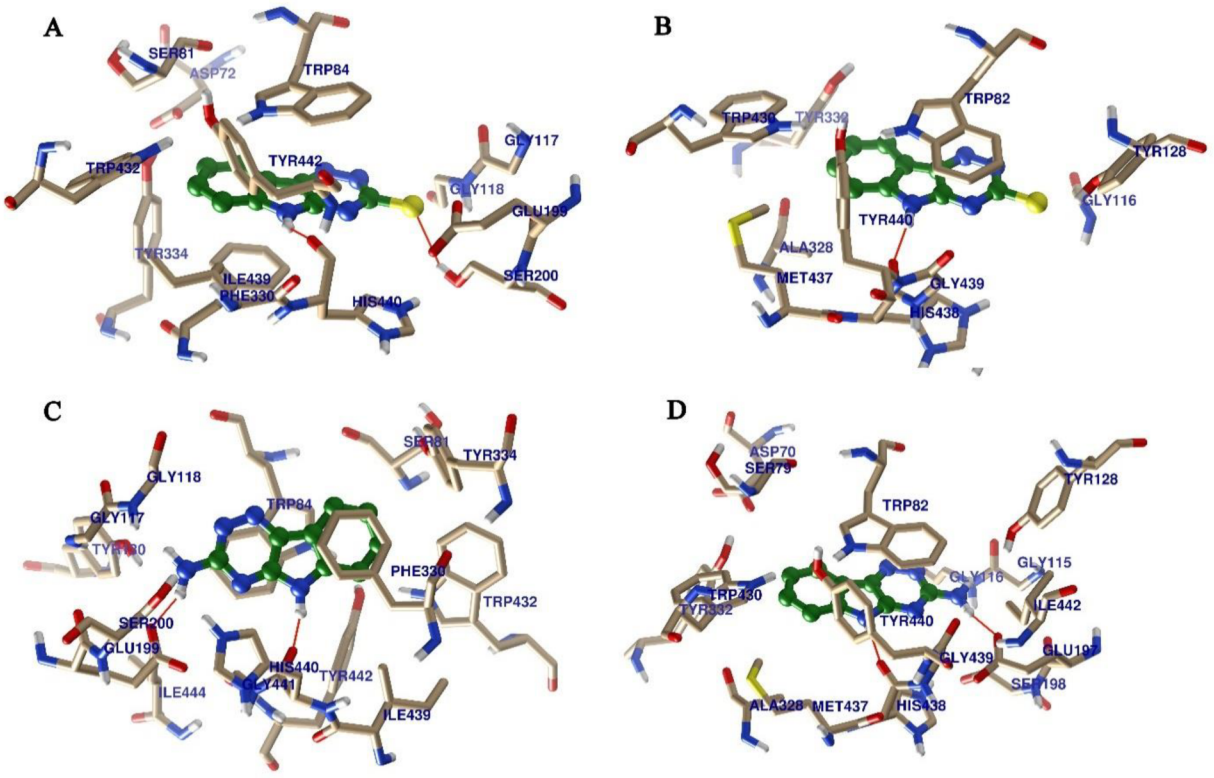

Figure 2. Interaction of 5*H*-[1,2,4]triazino[5,6-*b*]indole-3-thiol with (A) AChE and (B) BuChE; and 5*H* [1,2,4]triazino[5,6-*b*]indol-3-amine with (C) AChE and (D) BuChE.

Scheme 1. Synthesis of Compounds 2, 3a−3l, and 5a−5k[a]

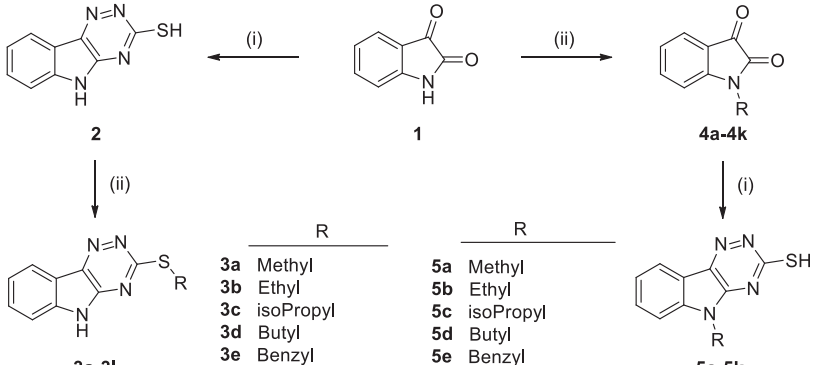

[a]Reagents and conditions: (i) Thiosemicarbazide, K_2CO_3, H_2O, reflux, overnight; (ii) alkyl/substituted benzyl halides, K_2CO_3, DMF.

an electron donor. Recent studies have also shown that melatonin offers protective effects against Aβ-induced apoptosis,[43] glutamate-induced excitotoxicity,[44] and nitric oxide toxicity,[45] decreases neurofilament hyperphosphorylation, and augments learning and memory in rats. In recent years, many indole based hybrids, e.g., tacrine−melatonin hybrids,[46] donepezil−chromone−melatonin hybrids,[47] melatonin−*N*,*N*-dibenzyl(*N*-methyl)amine hybrids,[48] and carbamate derivatives of indolines,[49] have been designed to act as multifunctional agents for the treatment of AD. Furthermore, the indole moiety is present in several central nervous system (CNS)-active drugs like rizatriptan and oxypertine. Thus, the indole ring offers a privileged scaffold for CNS-active drugs which could augment the search for new therapeutics for AD. The 1,2,4-triazine nucleus is another important structural system present in several biologically active compounds.[50] The significance of triazines in neuropharmacology is explored progressively for their potential anti-AD,[51−54] antianxiety,[55] antiepileptic,[56] and antidepressant[57] activities. Some triazine derivatives have been reported to be potent neuroprotective

DOI: 10.1021/acschemneuro.9b00226
ACS Chem. Neurosci. 2019, 10, 3635−3661

Scheme 2. Synthesis of Compounds 7a−7j and 10a−10j[a]

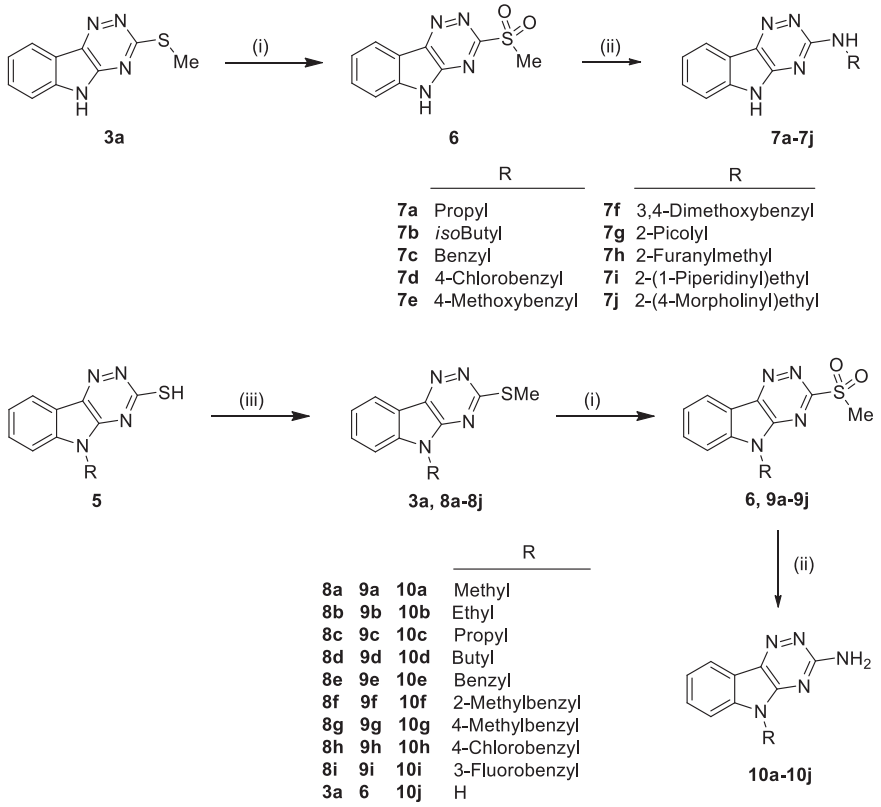

[a]Reagents and conditions: (i) *m*CPBA, DCM, 0 °C to RT; (ii) amines/ammonia, THF, reflux; (iii) MeI, K_2CO_3, DMF.

agents against H_2O_2-induced cell death in the PC12 cell line.[58] In the recent past, our research group reported substituted diaryltriazines as potential anti-AD entities.[59] Reports of remarkable biological activities associated with the indole ring and the 1,2,4-triazine nucleus prompted us to fuse these two privileged scaffolds into a single moiety which could potentially offer multiple favorable activities for the treatment of AD.

Different 5*H*-[1,2,4]triazino[5,6-*b*]indole-3-thiol and 5*H*-[1,2,4]triazino[5,6-*b*]indol-3-amine derivatives were designed by following a rational hybridization approach (Figure 1). The molecular interactions of the designed derivatives were evaluated theoretically by means of docking the designed compounds within the active site of AChE and BuChE. Both of the designed scaffolds showed promising binding affinities within the active sites of AChE as well as BuChE (Figure 2). The 5*H*-[1,2,4]triazino[5,6-*b*]indole-3-thiol scaffold showed stability within the CAS of AChE (docking score: −7.96) by forming $\pi-\pi$ interactions with Trp84 and Phe330 and hydrogen bonding with His440, while the same scaffold in the active site of BuChE (docking score: −7.21) exhibited $\pi-\pi$ interactions with Trp82, Trp430, and His438 along with hydrogen bonding with His438. Another designed scaffold 5*H*-[1,2,4]triazino[5,6-*b*]indol-3-amine showed similar $\pi-\pi$ interactions but offering higher binding affinities with AChE (docking score: −8.89) and BuChE (docking score: −7.22) enzymes due to additional strong hydrogen bonding caused by the 3-amino group. During the in vitro enzyme inhibition study, 5*H*-[1,2,4]triazino[5,6-*b*]indole-3-thiol showed 11.26 μM and 55.81 μM inhibitory activity (IC_{50}) against AChE and BuChE respectively, whereas 5*H*-[1,2,4]triazino[5,6-*b*]indol-3-amine was found to possess IC_{50} values of 9.76 μM and 51.25 μM against AChE and BuChE, respectively. On the basis of these moderately promising activities of the designed scaffolds, modifications were carried out by incorporating various alkyl/benzyl substituents to understand the SAR and to come up with some potential leads. Accordingly, compounds of the four series (**I**−**IV**), as shown in Figure 1, were synthesized and discussed here in this work.

RESULTS AND DISCUSSION

Chemistry. Compounds **2**, **3a**−**3l**, and **5a**−**5k** were synthesized as depicted in Scheme 1. Compound **2** was obtained by condensation of commercially available isatin (**1**) with thiosemicarbazide in aqueous potassium carbonate solution at reflux conditions. The clear liquid obtained was acidified by glacial acetic acid to get the condensed product **2**. Alkylation or benzylation of compound **2** with the corresponding alkyl/benzyl halides gave thio-substituted compounds **3a**−**3l**. Similarly, N-substituted 1,2,4-triazino-[5,6-*b*]indole-3-thiol derivatives **5a**−**5k** were synthesized by condensation of the N-substituted isatins **4a**−**4k** with thiosemicarbazide. N-Alkylation or N−benzylation of the isatins was achieved with the corresponding alkyl/benzyl halides in the presence of potassium carbonate in DMF.

When the substituted isatins were subjected to cyclization reaction with aminoguanidine instead of thiosemicarbazide, uncyclized N-substituted isatin-3-aminoguanylhydrazones were obtained instead of the 5-substituted [1,2,4]triazino[5,6-*b*]indol-3-amine derivatives. All efforts made to cyclize these N-substituted isatin-3-aminoguanylhydrazones to get 5-substituted [1,2,4]triazino[5,6-*b*]indol-3-amine derivatives failed,

DOI: 10.1021/acschemneuro.9b00226
ACS Chem. Neurosci. 2019, 10, 3635−3661

Scheme 3. Synthesis of Compounds 21a−23h[a]

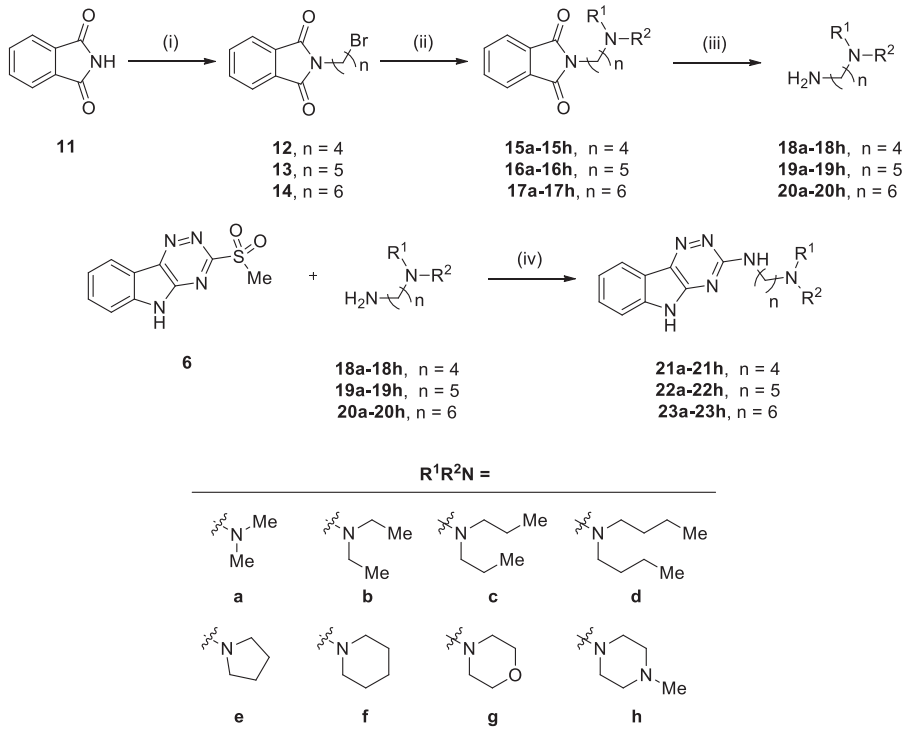

[a]Reagents and conditions: (i) $Br(CH_2)_nBr$, K_2CO_3, TEBAC, acetone, RT; (ii) HNR^1R^2, TEA, MeOH, reflux; (iii) $NH_2NH_2.H_2O$, MeOH, reflux; (iv) THF, reflux.

and only the noncyclized starting compounds were obtained. In one attempt, cyclization of *N*-benzylisatin-3-aminoguanylhydrazone in the presence of a strong base and diethylene glycol as a polar protic solvent, the hydrolyzed product, i.e., 2-(benzylamino)benzoic acid, was isolated.

In an alternative approach, the desired amino derivatives were synthesized from the thiol derivatives. The thiol derivatives were first methylated, and the methylthio derivatives were treated with various amines.[60] Unfortunately, the thiomethyl derivatives failed to react with the amines. So the thiomethyl group at the C-3 position was converted to sulfone, as it has more electron withdrawing ability compared to the parent thiomethyl group. This was achieved by oxidizing the thiomethyl group by *meta*-chloroperbenzoic acid (*m*CPBA) to sulfone. When these sulfone derivatives were reacted with amines in THF under refluxing conditions, the sulfone group was substituted by the amino group, offering the desired substituted [1,2,4]triazino[5,6-*b*]indol-3-amine derivatives **7a−7j**. Similarly, compounds **5** were methylated and further oxidized to the corresponding sulfone compounds **9a−9j**. These sulfone compounds were reacted with ammonia to obtain the desired 5-substituted [1,2,4]triazino[5,6-*b*]indol-3-amine derivatives **10a−10j** (Scheme 2).

The aminoalkylamines **18a−20h** required for the synthesis of compounds **21a−23h** were prepared through Gabriel synthesis using phthalimide as the starting material. Phthalimide (**11**) was reacted with dibromoalkanes to form *N*-(bromoalkyl)phthalimides **12−14**. The desired basic amines (**a−h**;R^1R^2NH) were reacted with *N*-(bromoalkyl)-phthalimides **12−14** to yield compounds **15a−17h**. Hydrazinolysis of compounds **15a−17h** in methanol offered the desired aminoalkylamines **18a−20h** in 67−87% yields. These aminoalkylamines **18a−20h** were reacted with compound **6** as discussed previously to obtain the desired final products **21a−23h** (Scheme 3).

Biological Evaluation. *Inhibition Studies on AChE and BuChE.* The potential of the synthesized compounds to inhibit cholinesterases (ChEs) was evaluated in vitro using a spectrophotometric method of Ellman et al. using donepezil and tacrine as reference drugs as previously reported by our group.[59,61,62] The obtained IC_{50} values of the compounds for the two enzymes and their selectivity over each other are summarized in Tables 1−3. All of the tested compounds showed IC_{50} values for both of the enzymes in micromolar to submicromolar ranges. Compounds **23e** and **23f** exhibited the highest inhibition of AChE (IC_{50} values of 0.56 and 0.67 μM, respectively) and BuChE (IC_{50} values of 1.17 and 0.84 μM, respectively).

Structure−Activity Relationships. To validate our design rationale, initially compound **2** was prepared and evaluated for its cholinesterase inhibitory potential. To our delight, as shown in Table 1. Compound **2** exhibited good inhibitory activity (AChE, IC_{50} = 11.26 μM; BuChE, IC_{50} = 55.81 μM). This encouraging result of the lead scaffold prompted us to explore various substituents on thiol sulfur and the nitrogen of the indole ring to frame a structure−activity relationship. Introducing alkyl substituents on the indole ring as in compounds **5a−5d** increased the inhibitory activity. Among them, compound **5d** with the butyl chain showed the most potent inhibitory activity (AChE, IC_{50} = 5.36 μM; BuChE, IC_{50} = 14.26 μM). Incorporation of benzyl and substituted benzyls at the NH of the indole ring decreased the AChE inhibitory activity except for compounds **5g** and **5k**. Compound **5g** and **5k** having 3-fluorobenzyl and 4-methylbenzyl groups, respectively, showed potent inhibitory activities. The thio-substituted compounds **3a−3l** offered IC_{50}

DOI: 10.1021/acschemneuro.9b00226
ACS Chem. Neurosci. 2019, 10, 3635−3661

Table 1. In Vitro Inhibition of AChE and BuChE, and Selectivity Index (SI) of Compounds 2, 3a−3l, and 5a−5k

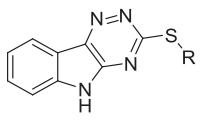

(2, 3a-3l)

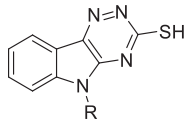

(5a-5k)

Compd	R	IC$_{50}$ ± SEM (μM)		SI[c]	Compd	R	IC$_{50}$± SEM(μM)		SI[c]
		AChE[a]	BuChE[b]				AChE[a]	BuChE[b]	
2		11.26 ± 1.24	55.81 ± 2.12	4.96	5a		7.33 ± 0.82	58.61 ± 1.23	7.99
3a		12.62 ± 1.45	55.24 ± 2.04	4.37	5b		8.50 ± 0.77	91.62 ± 2.76	10.9
3b		16.01 ± 1.42	48.40 ± 1.93	3.02	5c		6.16 ± 0.53	35.28 ± 3.01	5.72
3c		10.03 ± 0.83	33.69 ± 1.76	3.35	5d		5.36 ± 0.46	14.26 ± 1.29	2.66
3d	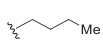	12.28 ± 1.66	40.08 ± 1.51	3.26	5e		8.05 ± 0.78	75.29 ± 2.82	9.35
3e		20.33 ± 1.47	42.05 ± 1.68	2.07	5f		15.35 ± 1.02	22.01 ± 1.34	1.43
3f		9.88 ± 0.75	76.50 ± 2.51	7.74	5g		5.52 ± 0.40	70.22 ± 2.56	12.7
3g		19.16 ± 1.43	84.96 ± 2.02	4.43	5h		15.73 ± 0.98	23.47 ± 1.76	1.49
3h	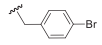	17.49 ± 1.32	51.93 ± 2.95	2.97	5i	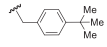	13.97 ± 0.93	18.24 ± 1.11	1.30
3i	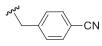	19.02 ± 1.65	75.99 ± 2.77	3.99	5j	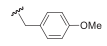	13.21 ± 1.52	19.02 ± 1.34	1.44
3j	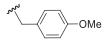	9.64 ± 0.87	46.74 ± 2.69	4.84	5k		5.73 ± 0.51	2.97 ± 0.90	0.52
3k	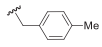	15.52 ± 1.37	49.34 ± 2.85	3.18	Tacrine		0.056 ± 0.01	0.008 ± 0.00	0.14
3l		9.93 ± 0.92	61.42 ± 2.13	6.18	Donepezil		0.023 ± 0.01	1.87 ± 0.08	81.3

[a]AChE from human erythrocytes; IC$_{50}$, 50% inhibitory concentration (means ± SEM of three experiments). [b]BuChE from equine serum. [c]Selectivity index = IC$_{50}$ (BuChE)/IC$_{50}$ (AChE).

values for AChE in the range of 9−20 μM. The presence of various substituents on the thiol group did not influence the activity significantly in comparison to the lead compound **2**. The inhibitory activity was retained as such when the thiol group was replaced with an amino group (Table 2). When the *N*-propyl moiety in compound **7a** was replaced with 2-(1-piperidinyl)ethyl (compound **7i**) and 2-(4-morpholinyl)ethyl (compound **7j**) moieties, inhibitory activities against both the enzymes increased notably. Compounds **7i** and **7j** showed inhibitory activities for AChE (IC$_{50}$ = 6.16, 6.61 μM, respectively) and BuChE (IC$_{50}$ = 20.53, 9.14 μM, respectively).

Joining of the tricyclic triazinoindole moiety with cyclic amines like piperidine and morpholine through two carbon atom spacers improved AChE inhibition dramatically compared to the simple alkyl/benzyl substituted triazinoindole derivatives. Based on this observation, we planned to study the effect of the attached basic amines and the length of the linker on the cholinesterase inhibitory activity of the resulting compounds. As indicated in Table 3, all the compounds **21a−23h** exhibited good inhibitory activity against both the enzymes with IC$_{50}$ values ranging from 0.564 to 36.7 μM for AChE and from 0.341 to 32.19 μM for BuChE. These results suggested that the presence of heterocyclic amines is particularly important for the ChE inhibitory activity as all the compounds bearing pyrrolidino, piperidino, morpholino, and *N*-methylpiperazino moieties exhibited strong ChE inhibition. The pyrrolidino moiety appeared to be a better choice over other amines, as compounds **21e**, **22e**, and **23e** bearing a pyrrolidino moiety exhibited higher activity than the rest of the compounds having other amines as attachments (Figure 3).

It has been observed that changing the length of the carbon chain also potentially affected the inhibitory activity. A comparative analysis of the inhibitory potential of compounds **21e**, **22e**, and **23e**, having a pyrrolidine ring as heterocyclic amine, revealed that compound **23e** (n = 6, IC$_{50}$ value of 0.564 μM) exhibited the highest AChE inhibitory activity while compound **21e** (n = 4, IC$_{50}$ value of 2.690 μM) and compound **22e** (n = 5, IC$_{50}$ value of 0.853 ± 0.02 μM) showed 5-fold and 1.5-fold decrease in AChE inhibitory activities in comparison to compound **23e** (Figure 3). However, their inhibitory

DOI: 10.1021/acschemneuro.9b00226
ACS Chem. Neurosci. 2019, 10, 3635−3661

Table 2. In Vitro Inhibition of AChE and BuChE, and Selectivity Index (SI) of Compounds 7a−7j and 10a−10j

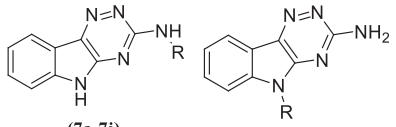

(7a-7j) (10a-10j)

Compd	R	IC_{50}± SEM (μM)		SI[c]	Compd	R	IC_{50}± SEM (μM)		SI[c]
		AChE[a]	BuChE[b]				AChE[a]	BuChE[b]	
7a		11.07 ± 0.86	52.19 ± 2.01	4.71	10a		7.81 ± 1.01	52.23 ± 1.76	6.69
7b		9.21 ± 0.54	61.23 ± 1.12	6.64	10b		8.13 ± 1.32	29.42 ± 1.21	3.62
7c		8.06 ± 0.75	56.41 ± 1.65	6.99	10c		10.12 ± 1.16	32.78 ± 1.47	3.24
7d	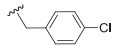	41.22 ± 1.83	9.09 ± 0.65	0.22	10d	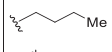	9.26 ± 0.82	16.02 ± 1.10	1.73
7e	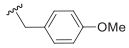	36.63 ± 1.22	67.32 ± 1.32	1.84	10e		20.57 ± 1.34	24.87 ± 1.38	1.21
7f	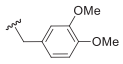	10.75 ± 0.62	13.12 ± 1.02	1.22	10f		17.23 ± 1.22	32.72 ± 1.32	1.90
7g		14.71 ± 1.37	26.08 ± 1.21	1.77	10g	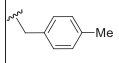	22.09 ± 1.78	22.64 ± 1.49	1.02
7h		20.22 ± 1.21	33.02 ± 1.65	1.63	10h	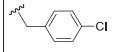	24.63 ± 2.01	29.45 ± 1.62	1.20
7i	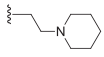	6.16 ± 0.53	20.53 ± 2.01	3.33	10i	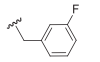	20.22 ± 1.25	25.32 ± 1.23	1.25
7j	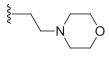	6.61 ± 0.69	9.14 ± 0.54	1.38	10j		9.76 ± 1.25	51.25 ± 1.32	5.25

[a]AChE from human erythrocytes; IC_{50}, 50% inhibitory concentration (means ± SEM of three experiments). [b]BuChE from equine serum. [c]Selectivity index = IC_{50} (BuChE)/IC_{50} (AChE).

activity against BuChE was slightly lower than that against AChE, which might be due to the conformational differences between the structures of these two enzymes.[63] Compound **23e** (IC_{50} value of 1.178 μM) exhibited an acceptable level of BuChE inhibitory activity, while compound **21e** (IC_{50} value of 5.893 μM) and compound **22e** (IC_{50} value of 17.01 μM) showed 5-fold and 14-fold decrease in BuChE inhibitory activities. Compounds **23e** (SI value of 2.09) and **23f** (SI value of 1.25) have more balanced activity on both cholinesterase enzymes than donepezil (SI value of 81.3) and tacrine (SI value of 0.14).

Antioxidant Activity [1,1-Diphenyl-2-picrylhydrazyl (DPPH) Radical Scavenging Activity]. The DPPH radical scavenging assay is commonly used as a rapid and reliable method to assess the antioxidant/free radical scavenging potential of compounds.[64] DPPH is a stable free radical that can accept a hydrogen radical or an electron to become a stable molecule. The antioxidant activity of the selected compounds was estimated by their ability to reduce DPPH·radical (purple color) to DPPHH (yellow) and the corresponding radical-scavenging potential was evaluated by the decrease in the absorbance at 517 nm.[65] Only those compounds having IC_{50} values (AChE) less than 5 μM were selected for this study. Ascorbic acid was used as the positive control in this assay. All the test compounds exhibited notable free radical scavenging activity ranging 40−55% and 56−70% at 10 and 20 μM concentrations, respectively (Table 4).

Compound **23e** showed better free radical scavenging activity (54.9% and 64.3% at 10 and 20 μM concentrations, respectively) compared to ascorbic acid (36.5% and 61.8% at 10 and 20 μM concentrations, respectively), whereas tacrine and donepezil were found to be devoid of significant free radical scavenging activity at these concentrations.

Assessment of Cytotoxicity and Neuroprotection Offered by the Synthesized Compounds. To ascertain the therapeutic potential of the synthesized compounds, their effect on cell viability and neuroprotective ability against oxidative stress were assessed using the human neuroblastoma SH-SY5Y cell line. Only those compounds having IC_{50} values (AChE) less than 5 μM were selected for these studies. For the assessment of cytotoxicity of the test compounds, cells were exposed to significantly high concentrations of the test compounds (40 and 80 μM) for 24 h, followed by determination of the cell viability using MTT assay. Even at such high concentrations, all the test compounds caused negligible cell death (Table 5).

The neuroprotective potential of the selected compounds against the oxidative stress induced by exogenous toxins (H_2O_2 or $A\beta_{1-42}$) was evaluated. H_2O_2-induced toxicity is due to the oxidative damage to the neuronal cells,[66] while the Aβ-induced toxicity is more complex, involving generation of reactive

DOI: 10.1021/acschemneuro.9b00226
ACS Chem. Neurosci. 2019, 10, 3635−3661

Table 3. In Vitro Inhibition of AChE and BuChE, and Selectivity Index (SI) of Compounds 21a−23h

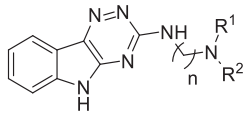

(21a-23h)

Compd	n	R^1R^2N	IC_{50}± SEM (μM)		SI[c]	Compd	n	R^1R^2N	IC_{50}± SEM (μM)		SI[c]
			AChE[a]	BuChE[b]					AChE[a]	BuChE[b]	
21a	4		33.70 ± 1.12	6.39 ± 0.22	0.19	**22e**	5		0.85 ± 0.05	17.01 ± 0.40	20.0
21b	4		6.31 ± 0.43	11.09 ± 0.27	1.75	**22f**	5		0.96 ± 0.04	2.77 ± 0.05	2.89
21c	4		2.47 ± 0.11	8.05 ± 0.51	3.26	**22g**	5		18.58 ± 0.41	6.74 ± 0.21	0.36
21d	4		20.70 ± 0.76	0.47 ± 0.03	0.02	**22h**	5		1.65 ± 0.11	29.19 ± 1.10	17.7
21e	4		2.69 ± 0.08	5.89 ± 0.70	2.19	**23a**	6		1.25 ± 0.09	4.43 ± 0.27	3.54
21f	4		3.17 ± 0.10	18.01± 1.31	5.68	**23b**	6		2.40 ± 0.11	12.70 ± 0.42	5.29
21g	4		15.01 ± 0.54	1.92 ± 0.15	0.13	**23c**	6		1.48 ± 0.08	3.43 ± 0.24	2.32
21h	4		2.61 ± 0.07	32.19 ± 1.02	12.3	**23d**	6		1.43 ± 0.07	4.01 ± 0.32	2.80
22a	5		3.58 ± 0.28	23.24 ± 0.67	6.49	**23e**	**6**		**0.56 ± 0.02**	**1.17 ± 0.09**	**2.09**
22b	5		6.79 ± 0.22	0.34 ± 0.03	0.05	**23f**	6		0.67 ± 0.02	0.84 ± 0.03	1.25
22c	5		2.77 ± 0.07	0.48 ± 0.03	0.17	**23g**	6		4.16 ± 0.15	23.65 ± 1.38	5.69
22d	5		2.76 ± 0.18	0.38 ± 0.05	0.14	**23h**	6		0.79 ± 0.04	3.92 ± 0.21	4.96

[a]AChE from human erythrocytes; IC_{50}, 50% inhibitory concentration (means ± SEM of three experiments). [b]BuChE from equine serum. [c]Selectivity Index = IC_{50} (BuChE)/IC_{50} (AChE).

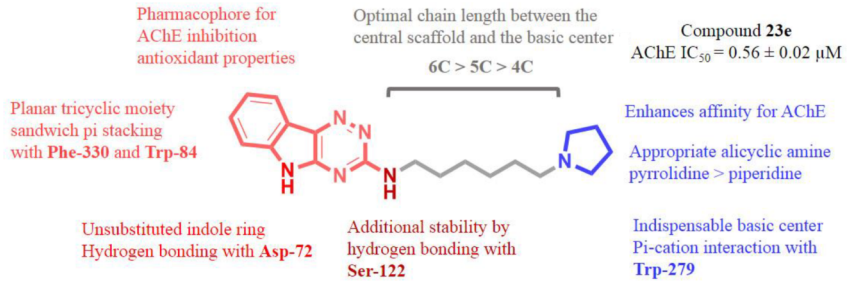

Figure 3. Important structural features of compound **23e**.

oxygen species, interleukin-1, interleukin-6, TNF-α like damaging cytokines' release, and mitochondrial dysfunction.[33,67]

In this study, when the cells were exposed to H_2O_2 (100 μM) and Aβ_{1-42} (25 μM) separately, notable toxicities to cells were observed and the cell viability declined to nearly 55% and 52%, respectively. To assess the neuroprotective potential of the test compounds against these toxic insults, the cells were pretreated with the test compounds (10 and 20 μM) for 2 h followed by treatment with the insults for 24 h. The selected derivatives exhibited a significant neuroprotective effect at 10 and 20 μM concentrations. For comparison, the cells were coincubated with compound **23e**, compound **23f**, donepezil, and tacrine at different concentrations. Compound **23e** offered significant protection to the cells against the toxic insults (Figure 4). The results suggested that these compounds possessed the ability to protect neuronal cells against oxidative-stress-associated cell death.

DOI: 10.1021/acschemneuro.9b00226
ACS Chem. Neurosci. 2019, 10, 3635−3661

Table 4. DPPH Radical Scavenging Activity of the Compounds[a]

compd	RP of DPPH (%)[b]	
	10 μM	20 μM
21c	45.5 ± 3.1	57.3 ± 2.9
21e	52.1 ± 2.4	63.1 ± 2.3
21f	51.5 ± 1.6	62.7 ± 1.7
21h	53.7 ± 2.7	65.4 ± 1.3
22a	43.2 ± 3.3	60.2 ± 2.7
22c	44.3 ± 2.4	59.4 ± 3.1
22d	46.7 ± 1.9	60.7 ± 3.3
22e	53.2 ± 2.4	62.4 ± 2.5
22f	52.8 ± 2.9	60.7 ± 2.9
22h	54.1 ± 1.7	65.1 ± 2.1
23a	44.1 ± 3.4	61.3 ± 2.3
23b	43.7 ± 2.5	60.3 ± 3.4
23c	42.7 ± 3.7	58.4 ± 3.1
23d	47.3 ± 2.0	59.6 ± 2.2
23e	**54.9 ± 1.8**	**64.3 ± 2.8**
23f	54.3 ± 2.1	66.4 ± 2.4
23g	56.7 ± 1.6	67.3 ± 1.7
23h	55.1 ± 3.4	64.2 ± 1.9
tacrine	3.4 ± 0.4	6.4 ± 0.3
donepezil	4.5 ± 0.6	4.9 ± 1.2
ascorbic acid	36.5 ± 2.9	61.8 ± 3.2

[a]Data are expressed as mean ± SE (three independent experiments) [b]RP of DPPH (%) = reduction percentage of DPPH.

In Vitro Blood-Brain Barrier (BBB) Permeation Assay. The BBB permeability is a primary criterion for the development of novel CNS active agents. The ability of triazinoindole derivatives to penetrate into the brain was assessed using a parallel artificial membrane permeation assay (PAMPA), in a similar manner as described by Di and co-workers.[68,69] This assay is used to predict the passive diffusion of a molecule through the BBB. The BBB permeability (P_e) of the most active compounds **23e** and **23f** was determined through a porcine brain lipid. The assay was validated by comparing the experimental permeability values [P_e(exp)] of seven commercial drugs with the reported permeability values [P_e(ref)], offering a linear relationship i.e., $P_e(\text{exp}) = 1.16\ P_e(\text{ref}) + 0.1668$ ($R^2 = 0.9781$) (see the Supporting Information, Figure S1). From this equation and considering the limits for BBB permeation established by Di et al.,[68] it was concluded that compounds with P_e(exp) greater than 4.8×10^{-6} cm s^{-1} (see the Supporting Information, Table S2) were capable of crossing the BBB. Both compounds **23e** and **23f** showed permeability values above this limit (Table 6). Therefore, P_e(exp) suggested a high potential of the compounds to cross the BBB by passive diffusion.

Computational Studies. *Docking Studies.* To have an idea of the binding mode of compound **23e** with the cholinesterase enzymes, docking studies were performed within the active sites of *Torpedo californica* AChE (*Tc*AChE) and human BuChE (*h*BuChE). To validate the generated grids for docking studies, the cocrystallized molecules in the 3D structures of *Tc*AChE and *h*BuChE (PDB code: 2CKM and 4BDS, respectively) were initially knocked out of the binding sites. The knocked out molecules were constructed fresh, energy minimized, and redocked into the active sites of the grids. Very similar interactions were observed between the redocked molecules and the enzymes as was the case with the original cocrystallized ligands. The root-mean-square deviation (RMSD) values of the redocked ligands with those of the original orientations in cocrystallized forms in 2CKM and 4BDS were observed to be 0.40 and 0.26 Å, respectively.

It is well-known that AChE has a dumbbell shaped active site gorge composed of two active sites: the CAS at the bottom and the PAS at the lip. The CAS pocket looks like a vessel, and

Table 5. Cell viability and Neuroprotective Action of the Selected Test Compounds against H_2O_2 and Aβ_{1-42} Induced Toxicity in the Human Neuroblastoma SH-SY5Y Cell Line[a]

compd	cell viability (%)		neuroprotection (%) (against H_2O_2)		neuroprotection (%) (against Aβ_{1-42})	
	40 μM	80 μM	10 μM	20 μM	10 μM	20 μM
21c	92.4 ± 2.2	90.3 ± 1.8	34.4 ± 2.7	48.9 ± 2.3	37.5 ± 2.1	56.2 ± 1.9
21e	93.0 ± 1.5	91.2 ± 2.1	39.8 ± 1.9	53.2 ± 3.2	40.3 ± 2.5	57.5 ± 2.2
21f	91.9 ± 2.4	87.1 ± 3.3	41.7 ± 1.3	55.4 ± 1.9	42.1 ± 1.9	60.7 ± 1.4
21h	91.3 ± 3.2	85.7 ± 2.4	37.2 ± 2.8	50.3 ± 2.9	41.5 ± 2.7	59.0 ± 1.5
22a	92.2 ± 3.1	90.5 ± 1.9	30.4 ± 3.6	46.5 ± 2.3	39.4 ± 3.1	57.3 ± 2.2
22c	92.4 ± 2.5	89.8 ± 3.1	31.8 ± 3.5	48.4 ± 2.2	38.1 ± 2.8	56.2 ± 2.9
22d	90.4 ± 3.3	87.1 ± 2.2	33.5 ± 2.9.	48.7 ± 3.1	38.5 ± 2.5	59.5 ± 2.3
22e	93.1 ± 2.7	90.6 ± 1.5	41.8 ± 3.5	54.3 ± 1.7	43.7 ± 3.1	60.1 ± 3.4
22f	93.9 ± 3.2	92.2 ± 1.9	43.4 ± 2.2	55.6 ± 2.1	41.4 ± 2.4	62.4 ± 1.9
22h	90.5 ± 3.7	86.4 ± 2.9	41.2 ± 2.7.	50.2 ± 2.8	40.3 ± 1.9	58.7 ± 2.1
23a	92.4 ± 3.2	89.3 ± 2.5	32.7 ± 3.4	43.5 ± 2.6	37.1 ± 2.3	59.3 ± 3.3
23b	93.2 ± 2.1	91.7 ± 1.9	31.2 ± 2.5	40.4 ± 3.6	37.7 ± 3.1	57.2 ± 3.4
23c	94.3 ± 2.2	91.1 ± 3.2	35.3 ± 1.4	46.1 ± 2.0	39.1 ± 2.6	57.5 ± 2.3
23d	91.4 ± 2.8	87.4 ± 2.3	34.2 ± 3.5	49.5 ± 2.7	38.8 ± 1.9	58.3 ± 2.9
23e	**94.9 ± 3.2**	**92.3 ± 1.5**	**42.5 ± 2.1**	**53.7 ± 1.3**	**44.5 ± 2.1**	**62.6 ± 1.9**
23f	94.5 ± 2.1	91.8 ± 2.8	44.8 ± 1.7	54.5 ± 2.4	43.2 ± 2.5	63.6 ± 2.2
23g	92.1 ± 2.7	89.7 ± 1.9	40.3 ± 1.8	52.3 ± 2.2	45.3 ± 2.2	61.4 ± 3.3
23h	91.4 ± 3.2	85.4 ± 2.7	41.2 ± 1.4	51.6 ± 2.5	42.7 ± 3.1	62.5 ± 2.5
tacrine	90.1 ± 1.8	88.1 ± 2.4	51.0 ± 3.4	70.4 ± 3.2	40.5 ± 2.3	58.7 ± 2.7
donepezil	92.4 ± 2.5	90.7 ± 1.2	53.4 ± 3.1	72.1 ± 2.7	47.2 ± 2.1	65.1 ± 1.8

[a]Data are expressed as Mean ± SE (three independent experiments).

DOI: 10.1021/acschemneuro.9b00226
ACS Chem. Neurosci. 2019, 10, 3635−3661

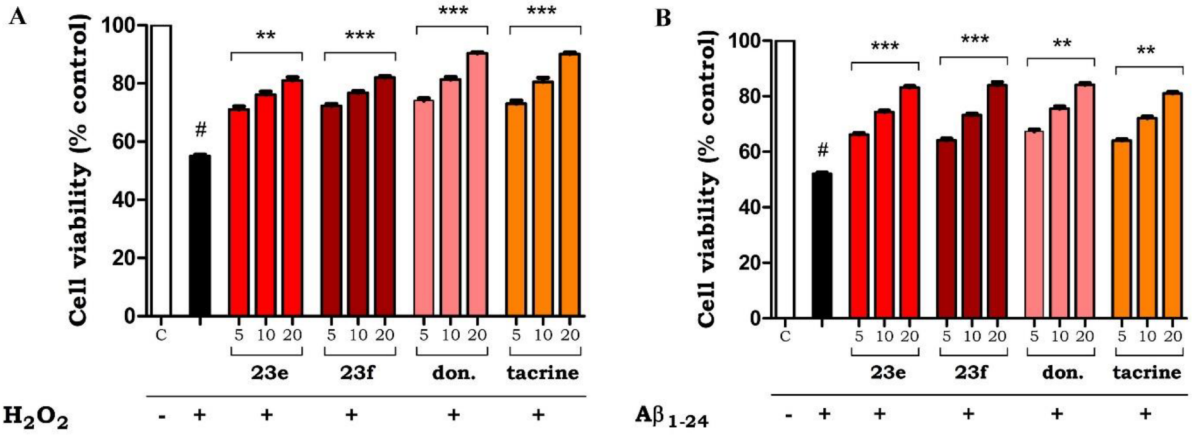

Figure 4. Protective effects of compound **23e**, compound **23f**, donepezil, and tacrine against H_2O_2 and Aβ_{1-42}-induced cytotoxicity in SH-SY5Y cells. Determination of the viability of SH-SY5Y cells by the MTT assay after treatment with (A) H_2O_2 (100 μM) and (B) Aβ_{1-42}(25 μM) in the absence or presence of the indicated concentrations of compounds **23e** and **23f** and the standard drugs. Data are expressed as mean ± SD of three experiments, and each includes triplicate sets. #$p < 0.05$ vs control; **$p < 0.01$, ***$p < 0.001$ vs H_2O_2/Aβ_{1-42} alone.

Table 6. Permeability (P_e, 10^{-6} cm s^{-1}) of Compounds 23e and 23f and Donepezil in the PAMPA-BBB Permeation Assay with Their Predicted Penetration into the CNS[a]

compd	P_e (10^{-6} cm s^{-1})	prediction
23e	11.3 ± 1.8	CNS+
23f	12.5 ± 1.2	CNS+
donepezil	14.3 ± 1.7	CNS+

[a]Data are expressed as mean ± SEM of three independent experiments.

on its bottom lies Trp84 which is crucial for binding of both the substrates to the inhibitors. Moreover, halfway up the gorge is a narrow tunnel where some crucial amino acid residues such as Phe330 and Tyr-334 stabilize the enzyme–inhibitor complex. At the entrance of the gorge exists the PAS, which is mainly built up by Trp279 and Tyr70 residues. The docking interactions of compound **23e** were studied in the active site of the AChE of *Tc*AChE, and then *Tc*AChE was humanized with *h*AChE to know the human sequence interacting with compound **23e**.

The interaction view of compound **23e** with AChE is represented in Figure 5A. As presented, compound **23e** was stacked well in the groove formed by Trp84, Trp279, and Phe330 (*h*AChE: Trp86, Trp284, and Tyr337) amino acid residues. It has orientation along the active site gorge similar to the reference compound donepezil, extending from the active site amino acid residue Trp84 to the peripheral site amino acid residue Trp279. Ligand interactions with these two amino acids are important to elicit a strong inhibitory effect by the dual binding site inhibitors. The hydrophobic planar nature of the tricyclic scaffold allows the creation of a more favorable sandwich type $\pi-\pi$ stacking with Trp84 and Phe330 (*h*AChE: Trp86 and Tyr337). The −NH group of the indole ring exhibited hydrogen bonding with Gly80 (*h*AChE: Gly82). The −NH group at the third position of the triazine ring showed hydrogen bonding with Ser122 (*h*AChE: Ser125). The nitrogen atom of the pyrrolidine ring could be protonated at physiological pH. The protonated nitrogen showed strong cation$-\pi$ interaction with Trp279 (*h*AChE Trp284). This interaction is particularly important as Trp279 plays a prominent role in deposition of beta-amyloid plaques.[24]

The binding mode of compound **23e** with BuChE revealed that it also occupied the large catalytic cavity of BuChE (Figure 5B). The aromatic ring of the tricyclic moiety was observed to be interacting with Trp231 and Phe329 residues by $\pi-\pi$ stacking. π–Alkyl interaction was observed between the aromatic ring of the scaffold and Leu286. Further, the −NH group on the third position added stability to the ligand–receptor complex by forming a hydrogen bond with Ser287. Additionally, salt bridge between −NH of the pyrrolidine and Asp70, and cation$-\pi$ interaction between the nitrogen of

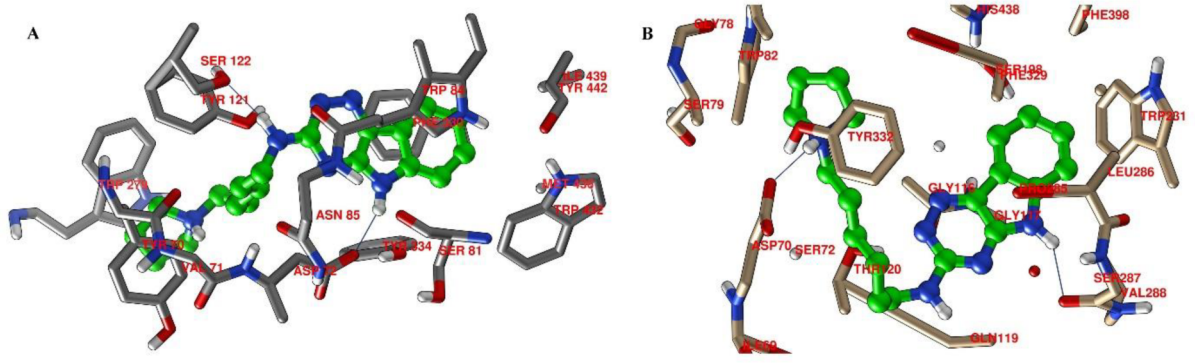

Figure 5. Docking interactions of compound **23e** in the active sites of (A) AChE and (B) BuChE.

DOI: 10.1021/acschemneuro.9b00226
ACS Chem. Neurosci. 2019, 10, 3635–3661

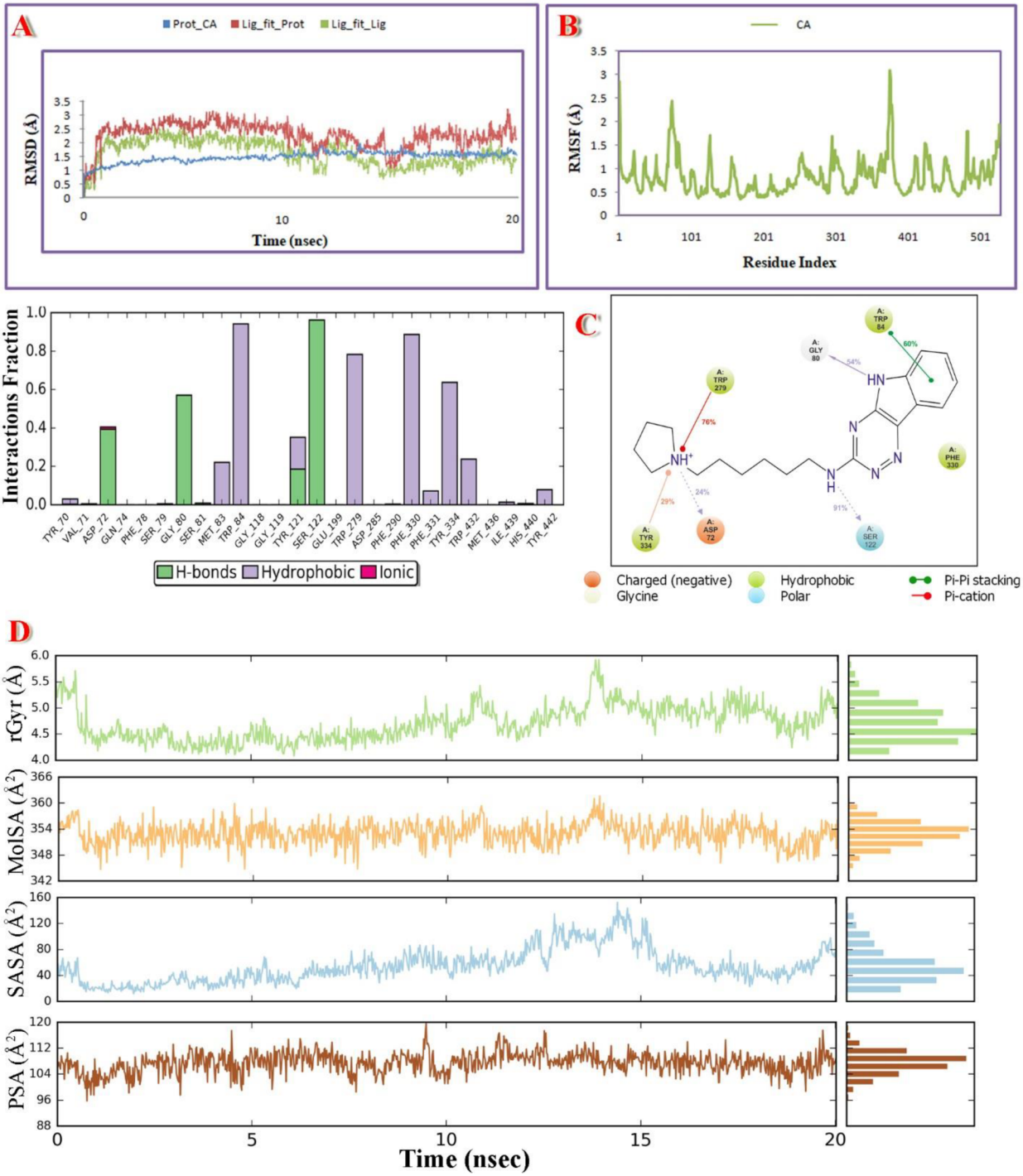

Figure 6. (A) RMSD-P and RMSD-L plots for AChE with **23e**. (B) RMSF-P plot for AChE with **23e**. (C) Ligand and receptor residue contact diagram for AChE with **23e**. (D) rGyr, MolSA, SASA, and PSA for **23e** with AChE.

pyrrolidine and Trp82 provided stability to the ligand−receptor complex.

Molecular Dynamics Simulations. In the molecular docking studies, compound **23e** exhibited very good interactions within the active sites of the AChE and BuChE enzymes. Thus, to confirm, validate, and understand the time dependent interactions of the active compound **23e** with the AChE and BuChE enzymes and the stability of the ligand−receptor complex, a molecular dynamics study was performed. The binding stability of the ligand−receptor complex was studied for a duration of 20 ns to check its time dependent stability. In order to observe the binding stability of the complex over a period of time, certain parameters like RMSD-P, RMSF-P, and RMSD-L (P = protein; L = ligand) were scrutinized to support the results of the docking study. The initial pose of the ligand−receptor complex was considered as the reference frame to calculate these values. The RMSD-P is essentially studied to understand the level of movements of various atoms/groups in the enzyme when the ligand is present in the active site of the receptor. This provides insight into the

DOI: 10.1021/acschemneuro.9b00226
ACS Chem. Neurosci. 2019, 10, 3635−3661

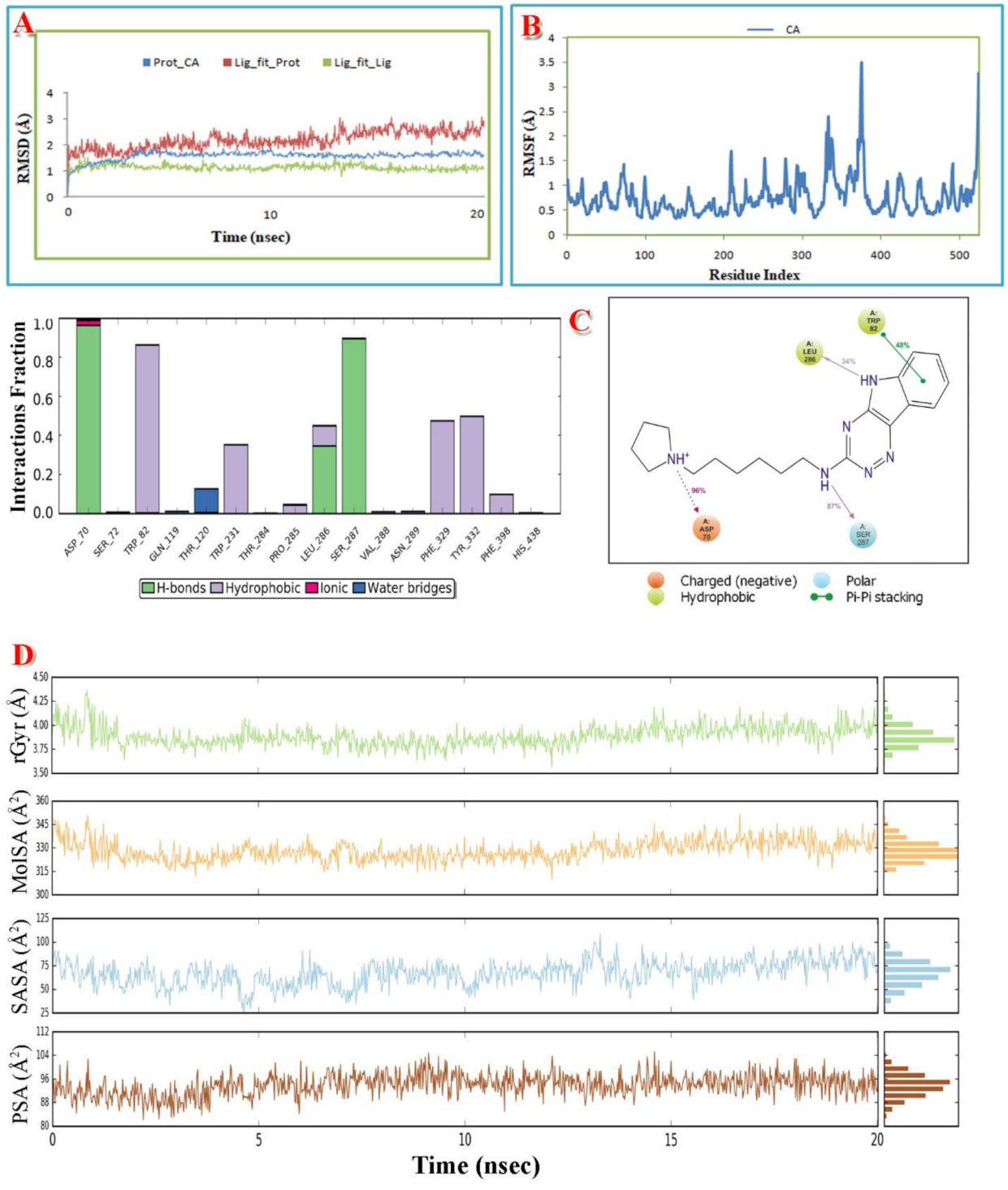

Figure 7. (A) RMSD-P and RMSD-L plots for BuChE with **23e**. (B) RMSF-P plot for BuChE with **23e**. (C) Ligand and receptor residue contact diagram for BuChE with **23e**. (D) rGyr, MolSA, SASA, and PSA for **23e** with BuChE.

structural conformations of the enzyme over a given period of simulation. The RMSD-P for AChE in the ligand−receptor complex was found to be in the range of 0.7−2.0 Å. This finding explained that the presence of **23e** in the active site of the AChE has not prejudiced the stability of the protein backbone all the way throughout the simulation period. To recognize the stability of the ligand with respect to the receptor and its active binding site, the RMSD-L of **23e** was determined. The "Lig fit" on Prot RMSD-L for ligand was observed in the range of 0.8−3.2 Å. The "Lig fit Prot" is the RMSD of a ligand when the protein−ligand complex is first aligned on the reference protein backbone and then the RMSD of the ligand heavy atoms is determined. Here, despite having a large number of rotatable bonds in the ligand, the RMSD value is not observed to be significantly higher than the protein RMSD, suggesting that the compound **23e** is stable within the binding site and does not diffuse away from the active site during the entire course of simulation period. Additionally, the

DOI: 10.1021/acschemneuro.9b00226
ACS Chem. Neurosci. 2019, 10, 3635−3661

Table 7. Predicted ADMET Indicators of Compound 23e, Compound 23f, Donepezil, and Tacrine[a]

parameter	limit	23e	23f	donepezil	tacrine
MW	130−725	338.455	352.481	379.498	198.267
HBA	2−20	5.5	5.5	5.5	2
HBD	0−6	2	2	0	1.5
NRB	0−8	8	8	6	1
$QPlogP_{o/w}$	−2 to 6.5	3.196	3.455	4.242	2.536
PSA	7 to 200	69.799	71.149	46.234	33.825
volume	500−2000	1180.047	1225.635	1248.451	701.299
ReFG	0−2	0	0	0	0
SASA	300 to 1000	679.568	701.805	681.675	425.06
rule of five (violation)	0−1	0	0	0	0
CNS		1	1	1	1
QPPMDCK		122.099	111.307	589.289	1602.036
QPlogBB	−3 to 1.2	−0.628	−0.686	0.223	0.047
QPPCaco		249.594	229.114	1070.771	2965.755
QPlogKhSa	−1.5 to 1.5	0.36	0.476	0.516	0.049
QPlogS	−6.5 to 0.5	−4.034	−4.419	−4.059	−3.036
% HOA	0−100	88.567	89.416	100	100
#star	0−5	0	0	0	0

[a]MW, molecular weight; HBA, hydrogen-bond acceptor atoms; HBD, hydrogen-bond donor atoms; $QPlogP_{o/w}$, predicted octanol/water partition coefficient; PSA, polar surface area; ReFG, number of reactive functional groups; SASA, total solvent accessible surface area; CNS, predicted central nervous system activity on a −2 (inactive) to +2 (active) scale; QPPMDCK, predicted apparent MDCK cell permeability in nm/s; QPPCaco, caco-2 cell permeability in nm/s; QPlogBB, brain/blood partition coefficient; QPlogKhsa, binding to human serum albumin; QPlogS, predicted aqueous solubility; % HOA, human oral absorption on 0−100% scale; #star: number of parameters with values that fall outside the 95% range of similar values for known drugs.

Lig fit on Lig RMSD was calculated to comprehend the internal fluctuation of the ligand atoms, and it was observed in the acceptable range of 0.4−2.4 Å (Figure 6A).

The structural integrity of the receptor and the residual mobility of the ligand were quantified in terms of RMSF-P (Figure 6B). For all the residues, including the loop as well as the terminal residues of the protein, with the compound **23e** in the active site, the RMSF-P was below 3.2 Å. The protein−ligand stability interaction study was also performed over a period of time to evaluate the interaction stability. In the docking studies, the H-bond was observed between −NH of the indole and −NH of the 3-amino group of compound **23e** with Gly80 and Ser122 (*h*AChE: Gly82 and Ser125) residues, respectively. From the MD simulation study, it was established that the two −NH groups of compound **23e** formed H-bonds with Gly80 and Ser122. These were observed to be stable over 54% and 91% of the simulation time with Gly80 and Ser122, respectively. Further, the salt bridge between the protonated pyrrolidine and Asp72 (*h*AChE: Asp74) was observed to be stable for around 24% of the simulation time. All these H-bond strengths were with H-bond distances of 2.5 Å or less and donor angles of ≥120° and acceptor angles of ≥90°. The cation−π interactions between the protonated pyrrolidine and Trp279 and Tyr334 (*h*AChE: Trp284 and Tyr341) were also found to be stable over 76% and 29% of the entire simulation time, respectively. Further, strong hydrophobic interactions of compound **23e** with Trp-84, Trp-279, and Phe-330 played a vital role in providing stability to the ligand−receptor complex where all these hydrophobic interactions were observed for more than 60% of the total simulation time (Figure 6C). The other ligand parameters like radius of gyration (rGyr), molecular surface area (MolSA), solvent-accessible surface area (SASA), and polar surface area (PSA) were observed in the acceptable range as shown in Figure 6D.

Similarly, the molecular dynamics study of compound **23e** with BuChE was also performed, and this also indicated good stability of ligand−receptor complex. The RMSD-P was in the range of 0.8−1.9 Å, whereas the RMSD-L "Lig fit" on Prot was observed to be between 1.2 and 3.2 Å which was not alarmingly higher than the RMSD-P. The "Lig fit" on the ligand was observed in the 0.4−1.8 Å range (Figure 7A). The protein fluctuation value RMSF-P was observed below 3.6 Å (Figure 7B). The ligand−receptor interaction analysis elucidated the stability of ligand−receptor complex by supporting the H-bonding between −NH of the indole and −NH at the third position of compound **23e** with protein residues Leu286 and Ser287, respectively. These were observed to be stable over 34% and 87% of simulation time, respectively. The protonated pyrrolidine formed a stable salt bridge with Asp70 over 96% of the simulation time period. The residues Trp82, Trp231, Leu286, Phe329, and Tyr332 were positively contributing toward the stability of the complex by hydrophobic interactions (Figure 7C). The other ligand parameters like rGyr, MolSA, SASA, and PSA were also observed in the acceptable range (Figure 7D). These observations from the molecular dynamics study strongly supported the observations made in the docking studies.

In Silico Prediction of Physicochemical and Pharmacokinetics Parameters. On account of poor ADME (absorption, distribution, metabolism, and excretion) properties, approximately 4 drug candidates out of 10 fail in clinical trials. These late-stage failures significantly contribute to the enhancement of development cost for the drugs. Hence, we need to resort to ADME predictions as a part of the drug development process to have an idea of the ADME properties during clinical trials.[70] Due to significant developments in the field of computational chemistry in recent times, virtual prediction of ADME properties becomes relatively easy and also reliable. For the most active compounds **23e** and **23f** along with donepezil and

DOI: 10.1021/acschemneuro.9b00226
ACS Chem. Neurosci. 2019, 10, 3635−3661

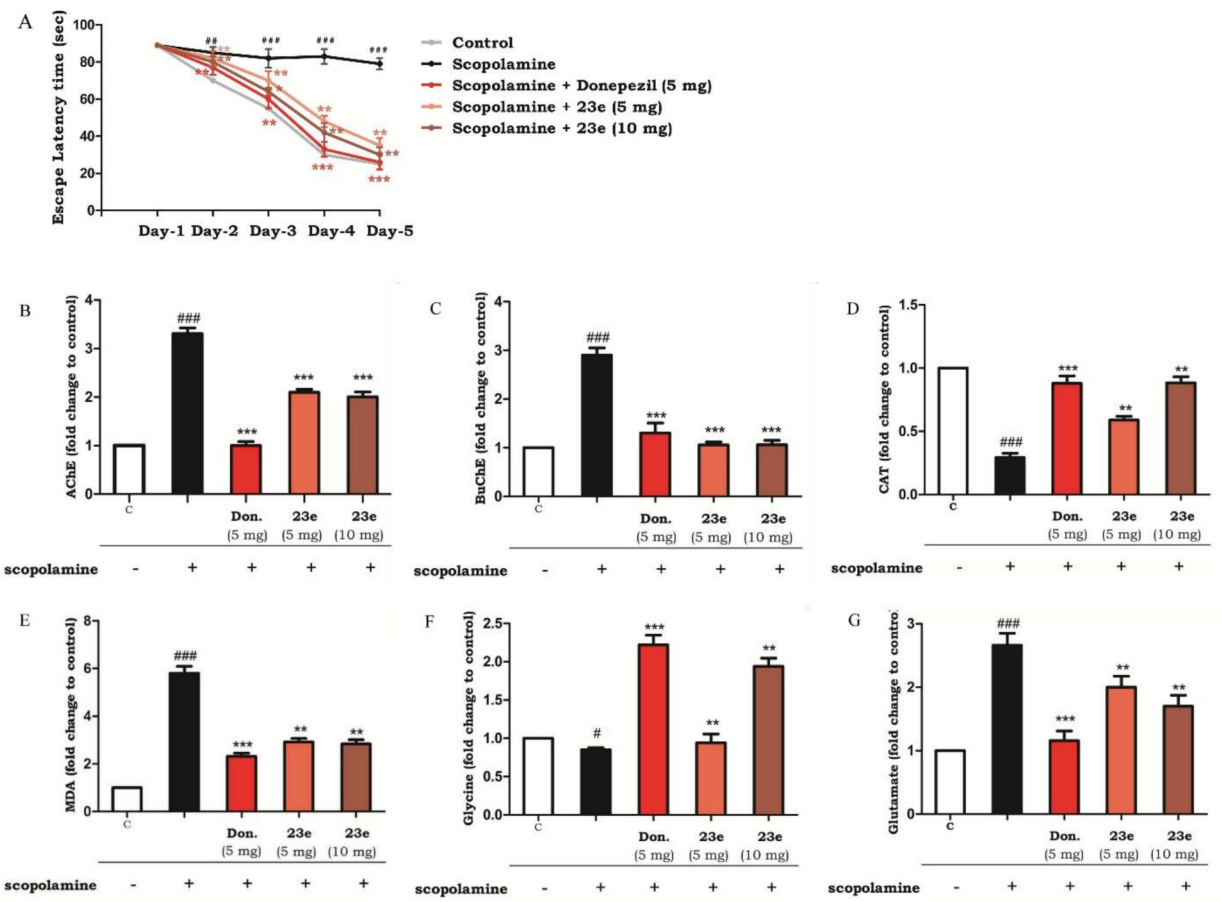

Figure 8. MWM test, ex vivo anticholinesterase and antioxidant activities, and neurotransmitter levels in scopolamine- induced amnesic brain. Data are expressed as mean ± SEM (n = 7): $^{###}p < 0.001$, $^{\#}p < 0.05$ vs vehicle-treated control group; $^{***}p < 0.001$, $^{**}p < 0.01$, vs scopolamine-treated control group. C = vehicle-treated control group.

tacrine as reference drugs, pharmacokinetics profile indicators like Lipinski's parameter, QPlog$P_{o/w}$, PSA, QPPMDCK, QPlogBB, QPPCaco, and QPLogKhsa were predicted with QikProp module (Table 7).[71]

According to Lipinski's rule of five,[72] most "druglike" molecules have LogP ≤ 5, molecular weight ≤ 500, number of hydrogen bond acceptors ≤ 10, and number of hydrogen bond donors ≤ 5. According to this rule, poor absorption or permeation is more likely when molecules violate more than one of these rules. Compounds **23e** and **23f** do not break Lipinski's rule of five at all, predicting them to be promising drug candidates. The number of rotatable bonds and topological polar surface area (TPSA) are the two other important parameters introduced by Veber and co-workers.[73] Number of rotatable bonds is the simple topological parameter for molecular flexibility. It has been shown to be a very good descriptor for oral bioavailability of drugs. For oral bioavailability, a molecule should have less than seven atoms in linear chains outside the rings or eight rotatable bonds. TPSA value is another key descriptor that was shown to equate well with passive molecular diffusion through membranes and therefore, allows prediction of drug absorption, including intestinal absorption, bioavailability, and BBB penetration.[74] The mean TPSA value for the marketed CNS drugs is 40.5 Å^2 with a range of 4.63−108 Å^2.[75] Compounds **23e** and **23f** possess eight rotatable bonds each and TPSA values of 69.8 and 71.2 Å^2, respectively. QPCaco-2 is indicative of the oral absorption of a drug. It assesses the apparent gut-blood barrier permeability. Values above 500 predict high oral absorption which is obtained for both the compound **23e** and **23f**. Similarly, human oral absorption percent (% HOA) values also support prediction of good oral bioavailability of the test compounds. Brain/blood partition coefficient (QPlogBB), n-octanol−water partition coefficient (QPlog$P_{o/w}$), apparent MDCK cell permeability (QPPMDCK), and CNS predict the ability of a compound to cross the BBB, a mandatory criterion for CNS active drugs. Typically, drugs which penetrate the BBB through passive diffusion should have n-octanol−water partition coefficient (log$P_{o/w}$) values of ∼3.[76] The QPPMDCK predicts the apparent MDCK cell permeability in nanometers per second. MDCK (Madin-Darby canine kidney) cell permeability is considered to be a good mimic for the BBB.[77] A value of QPPMDCK above 25 is considered as good, and almost all the test ligands have shown considerably high values. The test ligands are predicted to be CNS active as they have a value of CNS as 1. The QPlogKhsa value predicts the binding of CNS active drug with human serum albumin. Compound **23e** and **23f** showed compliance with the recommended values, indicating that these compounds would have low serum albumin binding and the unbound fraction would have access to the putative receptor drug target. #star denotes the number of parameters with values that fall outside the 95% range of similar values for known drugs. A large number of #stars indicates that the

DOI: 10.1021/acschemneuro.9b00226
ACS Chem. Neurosci. 2019, 10, 3635−3661

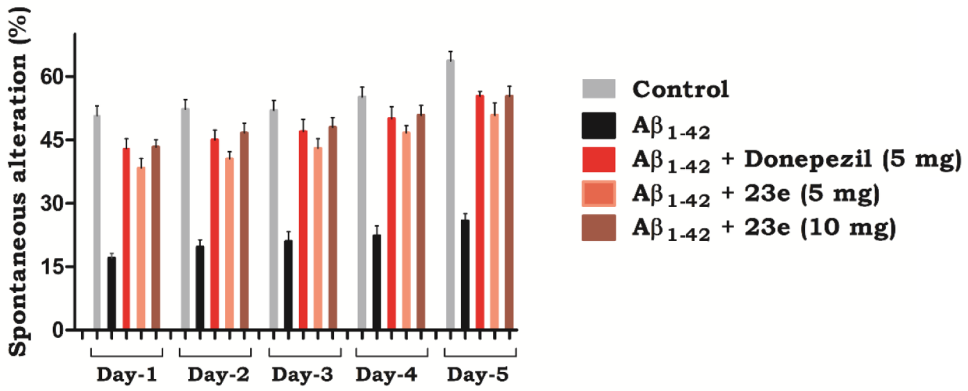

Figure 9. Compound **23e** improved immediate working memory in rats which received icv injection of Aβ_{1-42} in the Y-maze test.

molecule is less druglike than the molecule with few #stars. Values of #star for compound **23e** and **23f** indicate their drug-likeness. Additionally, a compound possessing a tertiary nitrogen containing moiety, which is a common feature in many CNS acting drugs, shows a higher degree of brain permeation.[75] Thus, it can be claimed that compounds **23e** and **23f** are predicted to possess good pharmacokinetics profile, which would enhance their biological significance.

Assessment of Cognitive Improvement in an Animal Model of AD. *Morris Water Maze (MWM) Test.* To determine the effect of compound **23e** on cognitive improvement, an animal model of scopolamine-induced amnesia in rodents was adopted.[78−80] Scopolamine blocks the cholinergic pathway distinctly by antagonizing the muscarinic receptors, offering a typical AD model to explore the role of cholinergic system in cognition.

The Morris water maze learning test was utilized to assess the hippocampal-dependent spatial learning ability of the animals. This test assesses the reference or long-term memory by observing the escape latency.[81] During the last 5 days of the treatment period, escape latency time (ELT) was recorded for the animals of the experimental groups. The ELT was significantly prolonged (Figure 8A) by scopolamine treatment (1.4 mg/kg, ip). In the donepezil (5 mg/kg, po)-treated group, ELT was considerably shortened as compared to the scopolamine-treated control group. Compound **23e** (5 and 10 mg/kg, po) significantly reduced ELT as compared to the scopolamine-treated control group. This result revealed that the animals retained the previous memory in the Morris water maze test, showing spatial memory improvement.

Neurochemical Analysis. After completion of the MWM test, the effects of scopolamine and compound **23e** on cholinesterase levels and oxidant stress parameters in brain were assessed. Scopolamine treatment significantly increases the cholinesterase levels in the brain. The effect of compound **23e** on the brain cholinesterase levels was assessed in mice using Ellman's method. The inflated levels of AChE (Figure 8B) and BuChE (Figure 8C) were significantly attenuated by compound **23e** at a dose equivalent to that of donepezil. Malondialdehyde (MDA), catalase (CAT), glutamate, and glycine levels in the brain were assessed in order to further perceive the antiamnesic effects of compound **23e**. Estimation of the lipid peroxidation products in the brain homogenate samples was carried out by thiobarbituric acid reactive substances (TBARS) assay, which estimates the MDA, a byproduct of lipid peroxidation by measuring the absorbance at 532 nm. The scopolamine-treated group showed elevated MDA levels (Figure 8C) in comparison to the vehicle-treated control group. Treatment of compound **23e** to the amnesic mice appreciably attenuated the increase in MDA levels in the brain (Figure 8C) as compared to the scopolamine-treated group. CAT is an important antioxidant defense system responsible for the decomposition of hydrogen peroxide to water and oxygen. Scopolamine treatment significantly reduced the CAT levels (Figure 8D) in the brains of the treated animals compared to the vehicle-treated control group animals. However, treatment of the amnesic mice with compound **23e** elevated the CAT levels considerably (Figure 8D). These results revealed the antioxidant potential of the test compound **23e**.

Disturbances in the balance between glutamate (excitatory neurotransmitter) and glycine (inhibitory neurotransmitter) system leads to the development of pathological features observed in AD.[82] Apart from the role in signal transmission and plasticity, glutamate also takes part in the regulation of survival or apoptosis induction of brain cells. This system is counter balanced by glycine signaling to ensure normal brain functioning by maintaining equilibrium between these inhibitory and excitatory activities. Scopolamine-treated group showed reduced levels of glycine (Figure 8F) compared to the vehicle-treated control group. The reduced level of glycine is also associated with impairment in the cognitive functions.[83,84] Treatment of the amnesic mice with compound **23e** increased the glycine levels (Figure 8F) as compared to the scopolamine-treated group. The elevated levels of glycine could improve the NMDA receptor hypofunction which is helpful in reviving cognitive function and memory. Furthermore, the scopolamine-treated group showed elevated levels of glutamate (Figure 8G) compared to the vehicle-treated control group. The elevated level of glutamate is alarming to the neuronal cells.[85,86] It causes the triggering of calcium-dependent intracellular pathways, generating highly reactive free radical species, and surging the oxidative stress which ultimately leads to cell death.[87] Treatment of the amnesic mice with compound **23e** decreased the glutamate levels (Figure 8G) as compared to the scopolamine-treated group. This might provide protection against excitotoxicity induced by elevated levels of glutamate.

Y-Maze Test. The animal model of Aβ_{1-42}-induced AD in rodents was used to assess the effect of compound **23e** on learning and memory. In this model, animals were subjected to intracerebroventricular (icv) injection of Aβ_{1-42} in the

DOI: 10.1021/acschemneuro.9b00226
ACS Chem. Neurosci. 2019, 10, 3635−3661

hippocampal region of the brain. Impairment of the working memory in the animals was assessed using the Y-maze test.[59,88] The spontaneous alteration in the behavior of the animals was considered to reflect short-term or spatial working memory. As shown in Figure 9, spontaneous alternations in Aβ_{1-42}-treated rats were significantly lowered over the vehicle-treated control rats. Donepezil, used as a reference standard, could considerably increase spontaneous alternation behavior compared to the Aβ_{1-42}-treated group. Further, the lowered spontaneous alternations induced by Aβ_{1-42} were significantly reversed by compound **23e** at both 5 mg/kg and 10 mg/kg dose levels (Figure 9).

Results of these behavioral studies and neurochemical analysis in scopolamine-induced amnesia and Aβ-induced AD models revealed that compound **23e** possessed the ability to reverse the reference and working memory-deficit as well as manage the oxidative stress-induced dementia.

Acute Toxicity Study. For the development of a NCE as a drug, determination of its acute toxicity is considered to be an important criterion. Acute toxicity of compound **23e**, the most promising candidate of the current study, was determined according to OECD 423 guidelines.[89] Wistar female rats were dosed with compound **23e** at a dose of 2000 mg/kg (n = 3 per group) by oral administration. After administration of the compound, the animals were monitored continuously for the first 4 h for any abnormal behavior and mortality. Later on the animals were intermittently observed for the next 24 h and occasionally for 14 days for any sign of delayed effects. All the animals survived in the duration of the study period and appeared healthy in terms of fur sleekness, water and food consumption, and body weight. On the 15th day, all the animals were sacrificed for macroscopic examination of the heart, liver, and kidneys for any damage. No damage was observed in these organs. The results from the study showed that rats treated with compound **23e** did not produce any acute toxicity or mortality immediately or during the post-treatment period. Therefore, compound **23e** can be considered to be nontoxic and well tolerated at doses up to 2000 mg/kg.

CONCLUSION

Encouraged by the therapeutic potential of the MTDLs as anti-AD agents, we intended to amalgamate two different activities, cholinesterase inhibition and antioxidant activity, in a single scaffold to enhance the potential of anti-AD drug therapy. Combination of the indole ring and the 1,2,4-triazine nucleus by a molecular hybridization approach resulted in a triazinoindole scaffold. Incorporation of various substituents in the triazinoindole scaffold resulted in a novel series of anti-AD agents showing good in vitro cholinesterase inhibitory and antioxidant activities. Among these compounds, the most active compound **23e** showed IC_{50} values of 0.56 μM for AChE and 1.17 μM for BuChE (SI value of 2.09). Molecular modeling studies indicated significant interactions between the most potent compound **23e** with PAS as well as CAS sites of both the enzymes. Results from the docking studies were further validated by time dependent molecular dynamics study. Compound **23e** displayed excellent neuroprotective activity against H_2O_2 as well as Aβ-induced toxicity in SH-SY5Y cells in a concentration dependent manner. Further, it did not show any significant toxicity in neuronal SH-SY5Y cells in the cytotoxicity assay. Compound **23e** showed high permeability in PAMPA-BBB assay. The overall ideology to develop efficacious MTDLs is to have the proof of concept by performing in vivo studies, which would provide relevance to the results obtained in in vitro studies. Keeping in mind the excellent in vitro profile of compound **23e**, it was selected for further in vivo evaluation of its anti-AD efficacy in animal models. Compound **23e** was able to successfully reverse the cognitive impairment in both MWM and Y-Maze tests. Restoration of CAT and MDA levels to their normal values supports the antioxidant potential of compound **23e**. Additionally compound **23e** is endowed with the capability to restore the memory deficit through increasing glycine levels and decreasing glutamate levels in scopolamine-treated animals. It did not show any acute toxicity in rats at a dose of 2000 mg/kg. In addition, compound **23e** was predicted in silico to possess notable ADMET properties. Taken together, these findings project compound **23e** as a well-balanced potential MTDL for further development as a novel anti-AD drug.

METHODS

General. All of the commercial reagents and solvents required for synthesis of the compounds were purchased from Spectrochem, Sigma-Aldrich, S. d. fine chemicals, and Avra chemicals and were purified by general laboratory techniques whenever needed. Reaction monitoring was assessed by thin layer chromatography (TLC), using silica gel precoated plates ($60F_{254}$, Merck, 0.25 mm thickness) and visualizing in ultraviolet (UV) light (λ = 254 nm) or in an iodine chamber. Chromatographic purification was performed by flash column chromatography with a Teledyne ISCO CombiFlash Rf system using RediSep Rf columns. Yields reported here are unoptimized. Melting points were determined in glass capillary tubes using a silicon oil-bath type melting point apparatus (Veego) or by differential scanning calorimetry (DSC) using a Shimadzu DSC-60 instrument, and melting points are uncorrected. The purity of the compounds was accessed by HPLC, with all the compounds exhibiting a ≥95% purity level. HPLC purity determination methods are described in the Supporting Information. The IR spectra were recorded on a Bruker ALPHA-T (Germany) FT-IR spectrophotometer for all the reported compounds and are consistent with the assigned structures. ^{1}H NMR and ^{13}C NMR spectra were recorded on a Bruker Advance-II 400 MHz spectrometer in $CDCl_3$ or DMSO-d_6 solvents. Chemical shifts (δ) are expressed in parts per million (ppm) relative to the standard TMS, and the peak patterns are indicated as s (singlet), d (doublet), t (triplet), m (multiplet), and br (broad signal). Mass spectra were recorded using a Thermo Fisher mass spectrometer with an EI ion source. Elemental analyses were performed on a Thermo Fisher FLASH 2000 organic elemental analyzer. The elemental compositions of the compounds were within ±0.4% range of the calculated values. All the procedures performed on the animals during this work were in accordance with CPCSEA established guidelines and regulations and were reviewed and approved by IAEC (Institutional Animal Ethics Committee) (Approval No. MSU/IAEC/2016-17/1636).

Chemistry. *5H-[1,2,4]Triazino[5,6-b]indole-3-thiol (**2**). General Procedure A.* To a stirred suspension of isatin (**1**) (1 g, 6.5 mmol) in aqueous potassium carbonate (1.34 g in 50 mL water) was added thiosemicarbazide (592 mg, 6.5 mmol). The mixture was refluxed for 16 h. After cooling down to room temperature, the solution was acidified with glacial acetic acid and left overnight. The obtained precipitate was filtered and washed with a mixture of water/acetic acid (24:1 v/v). The resulting solid was triturated with hot DMF, filtered, and dried to yield compound **2** as a pale yellow solid. Yield 92%; mp >350 °C (lit.[90] mp > 350 °C); IR (KBr, cm^{-1}): 3410, 3038, 1609, 1427, 1345, 1160; ^{1}H NMR ($CDCl_3$): δ 14.58 (br, 1H, −S*H*), 12.35 (br, 1H, −N*H*), 7.98 (d, 1H, Ar*H*), 7.62−7.58 (m, 1H, Ar*H*), 7.43 (d, 1H, Ar*H*), 7.35−7.31 (m, 1H, Ar*H*); MS (m/z): 203 (M + H)$^+$; RP-HPLC (method A) purity: 98.6%, t_R = 3.58 min.

*Synthesis of 3-Substituted Thio-5H-[1,2,4]triazino[5,6-b]indole (**3a−3l**). General Procedure B.* To a suspension of 5*H*-[1,2,4]-

DOI: 10.1021/acschemneuro.9b00226
ACS Chem. Neurosci. 2019, 10, 3635−3661

triazino[5,6-*b*]indole-3-thiol (**2**) (1g, 4.95 mmol) in DMF (20 mL), potassium carbonate (1.02 g, 7.42 mmol) and alkyl/aryl-alkyl bromide (4.95 mmol) were added. The reaction mixture was allowed to stir at 60 °C for 6−8 h. After completion of the reaction, the reaction mixture was poured into crushed ice. The precipitated product so formed was filtered, washed with water and recrystallized to yield the titled compounds **3a**−**3l**.

*3-Methylthio-5H-[1,2,4]triazino[5,6-b]indole (**3a**).* Greenish yellow solid; yield 69%; mp 306.73 °C (DSC); IR (KBr, cm^{-1}): 3204, 3056, 2801, 1604, 1342, 1184; ^{1}H NMR (DMSO-d_6): δ 12.62 (br, 1H, −N*H*), 8.28 (d, 1H, Ar*H*), 7.67−7.64 (m, 1H, Ar*H*), 7.55 (d, 1H, Ar*H*), 7.42−7.39 (m, 1H, Ar*H*), 2.66 (s, 3H, $-CH_3$); ^{13}C NMR (DMSO-d_6): δ 168.1, 147.2, 141.3, 140.8, 131.3, 122.9, 121.9, 118.2, 113.2, 13.9; MS (*m*/*z*): 216 $(M)^+$; RP-HPLC (method A) purity: 99.5%, t_R = 8.23 min.

*3-Ethylthio-5H-[1,2,4]triazino[5,6-b]indole (**3b**).* Yellow solid, yield 69%; mp 287.45 °C (DSC); IR (KBr, cm^{-1}): 3210, 3059, 2802, 1606, 1336, 1187; ^{1}H NMR (DMSO-d_6): δ 12.57 (br, 1H, −N*H*), 8.28 (d, 1H, Ar*H*), 7.68−7.64 (m, 1H, Ar*H*), 7.55 (d, 1H, Ar*H*), 7.42−7.39 (m, 1H, Ar*H*), 3.27 (q, *J* = 7.3 Hz, 2H, $-SCH_2$), 1.43 (t, *J* = 7.3 Hz, 3H, $-CH_2CH_3$); ^{13}C NMR (DMSO-d_6): δ 167.7, 147.2, 141.3, 140.8, 131.3, 122.9, 121.9, 118.2, 113.2, 24.3, 15.1; MS (*m*/*z*): 230 $(M)^+$; RP-HPLC (method A) purity: 98.8%, t_R = 5.92 min.

*3-Isopropylthio-5H-[1,2,4]triazino[5,6-b]indole (**3c**).* Light yellow solid; yield 67%; mp 282.63 °C (DSC); IR (KBr, cm^{-1}): 3200, 3058, 2865, 2800, 1603, 1339, 1182; ^{1}H NMR (DMSO-d_6): δ 12.53 (br, 1H, −N*H*), 8.28 (d, 1H, Ar*H*), 7.66−7.62 (m, 1H, Ar*H*), 7.54 (d, 1H, Ar*H*), 7.42−7.38 (m, 1H, Ar*H*), 4.13−4.06 (m, 1H, −SC*H*), 1.47 (d, 6H, $-CH_3$); ^{13}C NMR (DMSO-d_6): δ 167.8, 147.2, 141.3, 140.8, 131.3, 122.9, 121.9, 118.2, 113.2, 35.7, 23.3; MS (*m*/*z*): 244 $(M)^+$; RP-HPLC (method A) purity: 97.4%, t_R = 4.72 min.

*3-Butylthio-5H-[1,2,4]triazino[5,6-b]indole (**3d**).* Light yellow solid; yield 68%; mp 262.83 °C (DSC); IR (KBr, cm^{-1}): 3209, 3057, 2867, 2800, 1606, 1336, 1187; ^{1}H NMR (DMSO-d_6): δ 12.57 (br, 1H, −N*H*), 8.27 (d, 1H, Ar*H*), 7.66−7.62 (m, 1H, Ar*H*), 7.54 (d, 1H, Ar*H*), 7.41−7.37 (m, 1H, Ar*H*), 3.27 (t, 2H, $-SCH_2$), 1.80−1.72 (m, 2H, $-SCH_2CH_2$), 1.55−1.45 (m, 2H, $-CH_2CH_3$), 0.97 (t, 3H, $-CH_2CH_3$); ^{13}C NMR (DMSO-d_6): δ 167.8, 147.2, 141.4, 140.7, 131.3, 122.9, 121.9, 118.2, 113.2, 31.4, 30.1, 22.0, 14.1; MS (*m*/*z*): 258 $(M)^+$; RP-HPLC (method B) purity: 98.5%, t_R = 13.32 min.

*3-Benzylthio-5H-[1,2,4]triazino[5,6-b]indole (**3e**).* Yellow solid; yield 70%; mp 275.15 °C (DSC); IR (KBr, cm^{-1}): 3203, 3055, 2930, 2797, 1600, 1338, 1180, 752; ^{1}H NMR (DMSO-d_6): δ 12.54 (br, 1H, −N*H*), 8.29 (d, 1H, Ar*H*), 7.67−7.63 (m, 1H, Ar*H*), 7.56 (d, 1H, Ar*H*), 7.50 (d, 2H, Ar*H*), 7.43−7.39 (m, 1H, Ar*H*), 7.33−7.29 (m, 2H, Ar*H*), 7.26−7.22 (m, 1H, Ar*H*), 4.56 (s, 2H, $-CH_2$); ^{13}C NMR (DMSO-d_6): δ 167.2, 147.1, 141.6, 140.8, 138.1, 131.4, 129.6, 128.9, 127.7, 123.1, 122.0, 118.2, 113.2, 34.6; MS (*m*/*z*): 292 $(M)^+$; RP-HPLC (method B) purity: 99.2%, t_R = 14.23 min.

*3-(2-Methylbenzylthio)-5H-[1,2,4]triazino[5,6-b]indole (**3f**).* Yellow solid; yield 66%; mp 254.96 °C (DSC); IR (KBr, cm^{-1}): 3201, 3059, 2969, 2801, 1600, 1340, 1175, 771, 747; ^{1}H NMR (DMSO-d_6): δ 12.53 (br, 1H, −N*H*), 8.27 (d, 1H, Ar*H*), 7.66−7.61 (m, 1H, Ar*H*), 7.53−7.51 (m, 1H, Ar*H*), 7.47−7.45 (m, 1H, Ar*H*), 7.41−7.37 (m, 1H, Ar*H*), 7.19−7.10 (m, 3H, Ar*H*), 4.54 (s, 2H, $-SCH_2$), 2.42 (s, 3H, $ArCH_3$); MS (*m*/*z*): 306.09 $(M)^+$; RP-HPLC (method B) purity: 98.8%, t_R = 20.89 min.

*3-(3-Fluorobenzylthio)-5H-[1,2,4]triazino[5,6-b]indole (**3g**).* Light yellow solid; yield 71%; mp 262.80 °C; IR (KBr, cm^{-1}): 3210, 3059, 2944, 2802, 1606, 1335, 1182, 884, 755; ^{1}H NMR (DMSO-d_6): δ 12.55 (br, 1H, −N*H*), 8.29 (d, 1H, Ar*H*), 7.67−7.63 (m, 1H, Ar*H*), 7.56 (d, 1H, Ar*H*), 7.43−7.39 (m, 1H, Ar*H*), 7.35−7.29 (m, 3H, Ar*H*), 7.03−6.98 (m, 1H, Ar*H*), 4.57 (s, 2H, $-SCH_2$); ^{13}C NMR (DMSO-d_6): δ 166.9, 163.5, 161.6, 147.1, 141.7, 140.9, 131.5, 130.9, 125.7, 123.0, 122.0, 118.1, 116.4, 114.6, 113.3, 33.9; MS (*m*/*z*): 309.99 $(M)^+$; RP-HPLC (method B) purity: 97.5%, t_R = 16.89 min.

*3-(4-Bromobenzylthio)-5H-[1,2,4]triazino[5,6-b]indole (**3h**).* Yellow solid; yield 74%; mp 294.73 °C (DSC); IR (KBr, cm^{-1}): 3203, 3054, 2965, 2798, 1603, 1340, 1180, 752; ^{1}H NMR (DMSO-d_6): δ 12.62 (br, 1H, −N*H*), 8.30 (d, 1H, Ar*H*), 7.71−7.67 (m, 1H, Ar*H*), 7.58 (d, 1H, Ar*H*), 7.45−7.38 (m, 3H, Ar*H*), 7.14−7.12 (m, 2H, Ar*H*), 4.51 (s, 2H, $-SCH_2$), 2.26 (s, 3H, $-CH_3$); ^{13}C NMR (DMSO-d_6): δ 166.4, 146.6, 141.2, 140.3, 137.4, 131.2, 130.9, 122.5, 121.5, 120.2, 117.6, 112.7, 33.2; MS (*m*/*z*): 371 $(M)^+$; RP-HPLC (method B) purity: 98.3%, t_R = 24.1 min.

*3-(4-Cyanobenzylthio)-5H-[1,2,4]triazino[5,6-b]indole (**3i**).* Brownish solid; yield 76%; mp 288.48 °C (DSC); IR (KBr, cm^{-1}): 3200, 3151, 2978, 2226, 1599, 1179, 743; ^{1}H NMR (DMSO-d_6): δ 12.62 (br, 1H, −N*H*), 8.29 (d, 1H, Ar*H*), 7.78−7.66 (m, 5H, Ar*H*), 7.57 (d, 1H, Ar*H*), 7.44−7.40 (m, 1H, Ar*H*), 4.63 (s, 2H, $-SCH_2$); ^{13}C NMR (DMSO-d_6): δ 166.6, 147.1, 144.6, 141.8, 140.9, 132.8, 131.5, 130.6, 123.0, 122.0, 119.3, 118.0, 113.3, 110.3, 34.0; MS (*m*/*z*): 317.09 $(M)^+$; RP-HPLC (method B) purity: 99.8%, t_R = 11.0 min.

*3-(4-Methoxybenzylthio)-5H-[1,2,4]triazino[5,6-b]indole (**3j**).* Light yellow solid; yield 64%; mp 254.93 °C (DSC); IR (KBr, cm^{-1}): 3054, 2961, 2931, 2834, 1609, 1250, 1178, 753; ^{1}H NMR (DMSO-d_6): δ 12.57 (br, 1H, −N*H*), 8.29 (d, 1H, Ar*H*), 7.68−7.64 (m, 1H, Ar*H*), 7.56 (d, 1H, Ar*H*), 7.46−7.38 (m, 3H, Ar*H*), 6.87−6.82 (m, 2H, Ar*H*), 4.50 (s, 2H, $-SCH_2$), 3.73 (s, 3H, $-OCH_3$); MS (*m*/*z*): 322.09 $(M)^+$; RP-HPLC (method B) purity: 98.4%, t_R = 15.17 min.

*3-(4-Methylbenzylthio)-5H-[1,2,4]triazino[5,6-b]indole (**3k**).* Yellow solid; yield 72%; mp 290.38 °C (DSC); IR (KBr, cm^{-1}): 3202, 3052, 2964, 2798, 1604, 1340, 1181, 751; ^{1}H NMR (DMSO-d_6): δ 12.62 (br, 1H, −N*H*), 8.30 (d, 1H, Ar*H*),7.71−7.67 (m, 1H, Ar*H*), 7.58 (d, 1H, Ar*H*), 7.45−7.38 (m, 3H, Ar*H*), 7.14−7.12 (m, 2H, Ar*H*), 4.51 (s, 2H, $-SCH_2$), 2.26 (s, 3H, $-CH_3$); ^{13}C NMR (DMSO-d_6): δ 166.8, 146.6, 141.0, 140.3, 136.4, 134.3, 130.8, 128.9, 122.4, 121.4, 117.6, 112.7, 33.8, 20.7; MS (*m*/*z*): 306.19 $(M)^+$; RP-HPLC (method B) purity: 98.5%, t_R = 20.69 min.

*3-Phenethylthio-5H-[1,2,4]triazino[5,6-b]indole (**3l**).* Yellow solid; yield 74%; mp 246.05 °C (DSC); IR (KBr, cm^{-1}): 3204, 3058, 2965, 2801, 1606, 1334, 1186, 751, 695; ^{1}H NMR (DMSO-d_6): δ 12.55 (br, 1H, −N*H*), 8.30 (d, 1H, Ar*H*), 7.69−7.64 (m, 1H, Ar*H*), 7.57 (d, 1H, Ar*H*), 7.44−7.40 (m, 1H, Ar*H*), 7.36−7.30 (m, 4H, Ar*H*), 7.26−7.20 (m, 1H, Ar*H*), 3.53−3.49 (m, 2H, $-SCH_2CH_2$), 3.10−3.06 (m, 2H, $-SCH_2CH_2$); ^{13}C NMR (DMSO-d_6): δ 167.5, 147.2, 141.4, 140.7, 131.3, 129.2, 128.9, 126.9, 122.9, 121.9, 118.2, 113.2, 35.5, 31.9; MS (*m*/*z*): 306.19 $(M)^+$; RP-HPLC (method B) purity: 98.3%, t_R = 17.89 min.

*Synthesis of 5-Substituted 5H-[1,2,4]Triazino[5,6-b]indole-3-thiol Derivatives (**5a**−**5k**).* Following General Procedure A, 5-substituted 5*H*-[1,2,4]triazino[5,6-*b*]indole-3-thiol derivatives **5a**−**5k** were synthesized by condensation of N_1-substituted isatins with thiosemicarbazide. The obtained solids were recrystallized to yield the titled compounds.

*5-Methyl[1,2,4]triazino[5,6-b]indole-3-thiol (**5a**).* Pale yellow solid; yield 68%; mp 290.34 °C (DSC); IR (KBr, cm^{-1}): 2975, 1601, 1566, 1362, 1139, 750; ^{1}H NMR (DMSO-d_6): δ 14.61 (bs, 1H, −S*H*), 8.02 (d, 1H, Ar*H*), 7.71−7.67 (m, 1H, Ar*H*), 7.59 (d, 1H, Ar*H*), 7.41−7.37 (m, 1H, Ar*H*), 3.70 (s, 3H,$-CH_3$); MS (*m*/*z*): 217.20 $(M + H)^+$; RP-HPLC (method A) purity: 99.8%, t_R = 6.69 min.

*5-Ethyl[1,2,4]triazino[5,6-b]indole-3-thiol (**5b**).* Yellow solid; yield 73%; mp 304.17 °C (DSC); IR (KBr, cm^{-1}): 2855, 1574, 1347, 1143, 743; ^{1}H NMR (DMSO-d_6): δ 14.61 (bs, 1H, −S*H*), 8.03 (d, 1H, Ar*H*), 7.71−7.63 (m, 2H, Ar*H*), 7.41−7.37 (m, 1H, Ar*H*), 4.27 (q, *J* = 7.2 Hz, 2H, $-NCH_2CH_3$), 1.37 (t, *J* = 7.2 Hz, 3H, $-NCH_2CH_3$); ^{13}C NMR (DMSO-d_6): δ 179.0, 147.6, 143.2, 135.3, 131.8, 123.5, 121.8, 117.5, 111.6, 35.9, 12.9; MS (*m*/*z*): 231.10 $(M + H)^+$; RP-HPLC (method A) purity: 99.6%, t_R = 4.50 min.

*5-Isopropyl[1,2,4]triazino[5,6-b]indole-3-thiol (**5c**).* Yellow solid; yield 66%; mp 307.01 °C (DSC); IR (KBr, cm^{-1}): 2941, 1602, 1559, 1349, 1146, 742; ^{1}H NMR (DMSO-d_6): δ 14.73 (bs, 1H, −S*H*), 8.05 (d, 1H, Ar*H*), 7.80 (d, 1H, Ar*H*), 7.70−7.65 (m, 1H, Ar*H*), 7.41−7.37 (m, 1H, Ar*H*), 5.08−5.05 (m, 1H, −NC*H*), 1.60 (d, 6H, $-CH_3$); ^{13}C NMR (DMSO-d_6): δ 178.8, 147.7, 142.6, 135.3, 131.7, 123.8, 121.9, 117.9, 112.9, 45.8, 19.5; MS (*m*/*z*): 245.20 $(M + H)^+$; RP-HPLC (method A) purity: 98.9%, t_R = 9.74 min.

DOI: 10.1021/acschemneuro.9b00226
ACS Chem. Neurosci. 2019, 10, 3635−3661

*5-Butyl[1,2,4]triazino[5,6-b]indole-3-thiol (**5d**).* Yellow solid; yield 71%; mp 274.32 °C (DSC); IR (KBr, cm^{-1}): 2925, 1603, 1561, 1330, 1137, 757; ^1H NMR (DMSO-d_6): δ 14.42 (bs, 1H, −S*H*), 7.86 (d, 1H, Ar*H*), 7.53−7.52 (m, 2H, Ar*H*), 7.24−7.20 (m, 1H, Ar*H*), 4.01 (t, 2H, $-NCH_2$), 1.59−1.53 (m, 2H, $-NCH_2CH_2$), 1.20−1.14 (m, 2H, $-CH_2CH_3$), 0.74 (t, 3H, $-CH_2CH_3$); ^{13}C NMR (DMSO-d_6): δ 179.0, 147.9, 143.6, 135.2, 131.8, 123.4, 121.8, 117.4, 111.8, 42.9, 29.6, 19.6, 13.7; MS (*m*/*z*): 259.20 $(M + H)^+$; RP-HPLC (method B) purity: 99.8%, t_R = 14.49 min.

*5-Benzyl[1,2,4]triazino[5,6-b]indole-3-thiol (**5e**).* Light yellow solid; yield 69%; mp 293.24 °C (DSC); IR (KBr, cm^{-1}): 2841, 1599, 1569, 1163, 744; ^1H NMR (DMSO-d_6): δ 14.73 (bs, 1H,−S*H*), 8.02 (d, 1H, Ar*H*), 7.60−7.56 (m, 1H, Ar*H*), 7.43 (d, 1H, Ar*H*), 7.38−7.25 (m, 6H, Ar*H*), 5.47 (s, 2H, $-NCH_2$); ^{13}C NMR (DMSO-d_6): δ 179.3, 148.4, 143.3, 135.4, 131.8, 128.8, 127.8, 127.3, 123.7, 121.9, 117.6, 111.9, 44.0; MS (*m*/*z*): 291.68 $(M)^+$; RP-HPLC (method A) purity: 98.6%, t_R = 6.46 min.

*5-(2-Bromobenzyl)[1,2,4]triazino[5,6-b]indole-3-thiol (**5f**).* Yellow solid; yield 84%; mp 298.92 °C (DSC); IR (KBr, cm^{-1}): 2980, 2889, 1575, 1180, 748; ^1H NMR (DMSO-d_6): δ 14.72 (bs, 1H, −S*H*), 8.09 (d, 1H, Ar*H*), 7.72−7.70 (m, 1H, Ar*H*), 7.63−7.59 (m, 1H, Ar*H*), 7.43−7.39 (m, 1H, Ar*H*), 7.35 (d, 1H, Ar*H*), 7.27−7.22 (m, 2H, Ar*H*), 6.93−6.91 (m, 1H, Ar*H*), 5.45 (s, 2H, $-NCH_2$); MS (*m*/*z*): 370.09 $(M)^+$, 372 $(M + 2)^+$; RP-HPLC (method B) purity: 99.8%, t_R = 17.49 min.

*5-(3-Fluorobenzyl)[1,2,4]triazino[5,6-b]indole-3-thiol (**5g**).* Yellow solid; yield 64%; mp 282.15 °C (DSC); IR (KBr, cm^{-1}): 2925, 1597, 1571, 1349, 1146, 745; ^1H NMR (DMSO-d_6): δ 14.71 (bs, 1H, −S*H*), 8.19 (s, 1H, Ar*H*), 8.04 (d, 1H, Ar*H*), 7.62−7.58 (m, 1H, Ar*H*), 7.46 (d, 1H, Ar*H*), 7.40−7.33 (m, 1H, Ar*H*), 7.19 (d, 2H, Ar*H*), 7.08−7.03 (m, 2H, Ar*H*), 5.48 (s, 2H, $-NCH_2$); MS (*m*/*z*): 311.20 $(M + H)^+$; RP-HPLC (method A) purity: 95.7%, t_R = 3.84 min.

*5-(4-Chlorobenzyl)[1,2,4]triazino[5,6-b]indole-3-thiol (**5h**).* Yellow solid; yield 76%; mp 300.43 °C (DSC); IR (KBr, cm^{-1}): 2980, 2885, 1571, 1377, 1141, 754; ^1H NMR (DMSO-d_6): δ 14.69 (bs, 1H, −S*H*), 8.04 (d, 1H, Ar−*H*), 7.63−7.59 (m, 1H, Ar−*H*), 7.48 (d, 1H, Ar−*H*), 7.41−7.35 (m, 5H, Ar−*H*), 5.45 (s, 2H, $-NCH_2$); MS (*m*/*z*): 325.99 $(M)^+$, 328 $(M + 2)^+$; RP-HPLC (method B) purity: 98.3%, t_R = 13.65 min.

*5-(4-tert-Butylbenzyl)[1,2,4]triazino[5,6-b]indole-3-thiol (**5i**).* Yellow solid; yield 81%; mp 249.58 °C (DSC); IR (KBr, cm^{-1}): 3236, 3145, 2970, 2900, 1606, 1465, 1334, 1140; ^1H NMR (DMSO-d_6): δ 12.46 (bs, 1H, −S*H*), 7.73−7.72 (m, 1H, Ar*H*), 7.34−7.27 (m, 5H, Ar*H*), 7.12−7.08 (m, 1H, Ar*H*), 7.02−7.00 (m, 1H, Ar*H*), 4.91 (s, 2H, $-NCH_2$), 1.26 (s, 9H, $-CH_3$); MS (*m*/*z*): 350.09 $(M + H)^+$; RP-HPLC (method A) purity: 99.6%, t_R = 4.31 min.

*5-(4-Methoxybenzyl)[1,2,4]triazino[5,6-b]indole-3-thiol (**5j**).* Yellow solid; yield 78%; mp >250 °C (decomposition); IR (KBr, cm^{-1}): 2980, 1608, 1346, 1246, 759; ^1H NMR (DMSO-d_6): δ 14.63 (bs, 1H, −S*H*), 7.57−7.53 (m, 2H, Ar*H*), 7.34−7.32 (m, 2H, Ar*H*), 7.12−7.08 (m, 1H, Ar*H*), 6.98−6.96 (m, 1H, Ar*H*), 6.88−6.86 (m, 2H, Ar*H*), 4.84 (s, 2H, $-NCH_2$), 3.73 (s, 3H, $-OCH_3$); MS (*m*/*z*): 321.09 $(M)^+$; RP-HPLC (method B) purity: 97.0%, t_R = 18.95 min.

*5-(4-Methylbenzyl)[1,2,4]triazino[5,6-b]indole-3-thiol (**5k**).* Yellow solid; yield 72%; mp 292.88 °C (DSC); IR (KBr, cm^{-1}): 2924, 1599, 1572, 1347, 1145, 752; ^1H NMR (DMSO-d_6): δ 14.69 (bs, 1H, −S*H*), 8.03 (d, 1H, Ar*H*), 7.61−7.57 (m, 1H, Ar*H*), 7.45 (d, 1H, Ar*H*), 7.38−7.34 (m, 1H, Ar*H*), 7.25 (d, 2H, Ar*H*), 7.12 (d, 2H, Ar*H*), 5.41 (s, 2H, $-NCH_2$), 2.27 (s, 3H, $-CH_3$); ^{13}C NMR (DMSO-d_6): δ 179.3, 148.3, 143.3, 137.1, 135.4, 132.4, 132.8, 129.3, 127.3, 123.7, 121.9, 117.6, 112.0, 43.9, 20.7; MS (*m*/*z*): 307.20 $(M + H)^+$; RP-HPLC (method A) purity: 99.3%, t_R = 5.89 min.

*3-(Methylsulfonyl)-5H-[1,2,4]triazino[5,6-b]indole (**6**). General Procedure C.* To a stirred solution of 3-(methythio)-5*H*-[1,2,4]-triazino[5,6-*b*]indole (**5a**) (1 g, 4.62 mmol) in anhydrous methylene chloride (20 mL) at 0 °C, *m*CPBA (80−85% tech solid, 1.79 g, 10.40 mmol) was added as a solid in small portions over a period of a few minutes. The resulting reaction mixture was stirred at room temperature with the exclusion of moisture for 24 h. The progress of the reaction was monitored by TLC. After completion of the reaction, the organic phase was washed several times with saturated sodium bicarbonate solution and then with the brine solution. The collected organic phase was dried over anhydrous magnesium sulfate, filtered, and evaporated to give light yellowish solid. Yield 72%; mp 232−234 °C; IR (KBr, cm^{-1}): 3447, 3307, 1621, 1591, 1297, 1090, 758; ^1H NMR (DMSO-d_6): δ 13.25 (bs, 1H, N*H*), 8.45 (d, 1H, Ar*H*), 7.77−7.81 (m, 1H, Ar*H*), 7.68 (d, 1H, Ar*H*), 7.49−7.53 (m, 1H, Ar*H*), 3.50 (s, 3H, SO_2CH_3);MS (*m*/*z*): 249 $[M + H]^+$.

*Synthesis of N-Substituted 5H-[1,2,4]Triazino[5,6-b]indol-3-amine Derivatives (**7a**−**7j**). General Procedure D.* To 3-(methylsulfonyl)-5*H*-[1,2,4]triazino[5,6-*b*]indole (**6**) (0.5 g, 2.014 mmol) in THF (20 mL), an appropriate amine (10 mmol) was added and refluxed on a water-bath for approximately 4 h. Progress of the reaction was monitored by TLC. After completion of the reaction, the reaction mixture was poured into ice cold water (20 mL). The aqueous phase was extracted with ethyl acetate (3 × 30 mL), the organic layer was combined and washed with sodium bicarbonate solution (5%) and brine, and the collected organic layer was dried over anhydrous sodium sulfate and evaporated to give a crude product which was further purified by flash chromatography.

*N-Propyl-5H-[1,2,4]triazino[5,6-b]indol-3-amine (**7a**).* Yellow solid; yield 70%; mp 252−253 °C; IR (KBr, cm^{-1}): 3447, 3060, 2963, 1614, 1533, 1459, 1393, 749; ^1H NMR (DMSO-d_6): δ 11.73 (bs, 1H, N*H*), 8.07 (d, 1H, Ar−*H*), 7.44−7.22 (m, 3H, Ar−*H*, 1H, −N*H*), 3.40−3.37 (m, 2H, $-NHCH_2$), 1.69−1.64 (m, 2H, $-CH_2CH_3$), 0.97 (t, 3H, $-CH_2CH_3$); ^{13}C NMR (DMSO-d_6): δ 161.7, 149.0, 139.5, 128.5, 121.9, 119.9, 119.7, 116.2, 112.3, 43.0, 22.6, 11.9; MS (*m*/*z*): 228.1 $[M + H]^+$; RP-HPLC (method C) purity: 96.1%, t_R = 4.65 min.

*N-Isobutyl-5H-[1,2,4]triazino[5,6-b]indol-3-amine (**7b**).* Yellow solid; yield 82%; mp 243−245 °C; IR (KBr, cm^{-1}): 3429, 3069, 2960, 1609, 1524, 1467, 750; ^1H NMR (DMSO-d_6): δ 11.81 (bs, 1H, N*H*), 8.08 (d, 1H, Ar−*H*), 7.45−7.25 (m, 3H, Ar−*H*), 3.24 (m, 2H, $-NHCH_2$), 2.02−1.95 (m, 1H, −C*H*), 0.94 (d, 6H, CH_3); ^{13}C NMR (DMSO-d_6): δ 161.7, 149.0, 139.5, 128.5, 121.9, 119.9, 119.7, 116.2, 112.3, 49.4, 28.1, 20.8; MS (*m*/*z*): 242.1 $[M + H]^+$; RP-HPLC (method C) purity: 96.7%, t_R = 3.39 min.

*N-Benzyl-5H-[1,2,4]triazino[5,6-b]indol-3-amine (**7c**).* Yellow solid; yield 81%; mp 294 °C (DSC); IR (KBr, cm^{-1}): 3440, 3076, 2966, 1606, 1528, 694; ^1H NMR (DMSO-d_6): δ 11.79 (bs, 1H, N*H*), 8.08 (d, 1H, Ar−*H*), 7.45−7.18 (m, 8H, Ar−*H*), 4.67 (d, 2H, $-NHCH_2$); ^{13}C NMR (DMSO-d_6): δ 161.7, 148.9, 140.5, 139.6, 128.9, 128.7, 127.5, 127.2, 122.0, 120.0, 119.6, 116.2, 112.3, 44.4; MS (*m*/*z*): 276.1 $[M + H]^+$; RP-HPLC (method C) purity: 96.9%, t_R = 7.32 min.

*N-(4-Chlorobenzyl)-5H-[1,2,4]triazino[5,6-b]indol-3-amine (**7d**).* Yellow solid; yield 68%, mp 218−220 °C; IR (KBr, cm^{-1}): 3414, 3062, 2921, 1620, 1592, 1092, 758; ^1H NMR (DMSO-d_6): δ 11.82 (bs, 1H, −N*H*), 8.07 (d, 1H, Ar−*H*), 7.46−7.24 (m, 7H, Ar−*H*, 1H, −N*H*), 4.63 (d, 2H, $-NHCH_2$); ^{13}C NMR (DMSO-d_6): δ 161.5, 149.0, 139.6, 139.0, 131.6, 129.3, 128.8, 128.7, 122.4, 120.1, 119.5, 116.0, 112.4, 43.9; MS (*m*/*z*): 310.1 $[M + H]^+$; RP-HPLC (method C) purity: 96.4%, t_R = 5.94 min.

*N-(4-Methoxybenzyl)-5H-[1,2,4]triazino[5,6-b]indol-3-amine (**7e**).* Yellow solid; yield 75%; mp 241−243 °C; IR (KBr, cm^{-1}): 3371, 3058, 2961, 1610, 756; ^1H NMR (DMSO-d_6): δ 11.83 (bs, 1H, −N*H*), 8.06 (d, 1H, Ar−*H*), 7.96 (bs, 1H, −N*H*), 7.46−7.24 (m, 5H, Ar−*H*), 6.86−6.82 (m, 2H, Ar−*H*), 4.57 (d, 2H, $-NHCH_2$), 3.73 (s, 3H, OCH_3); MS (*m*/*z*): 306.1 $[M + H]^+$; RP-HPLC (method C) purity: 97.3%, t_R = 4.11 min.

*N-(3,4-Dimethoxybenzyl)-5H-[1,2,4]triazino[5,6-b]indol-3-amine (**7f**).* Yellow solid; yield 70%; mp 201−203 °C; IR (KBr, cm^{-1}): 3374, 1615, 1518, 806; ^1H NMR (DMSO-d_6): δ 8.07 (d, 1H, Ar−*H*), 7.46−6.82 (m, 6H, Ar−*H*, 1H, −N*H*), 4.57 (d, 2H, $-NHCH_2$), 3.76 (s, 3H, $-OCH_3$), 3.74 (s, 3H, $-OCH_3$); ^{13}C NMR (DMSO-d_6): δ 161.2, 149.1, 148.9, 148.2, 139.7, 132.9, 128.7, 122.0, 120.1, 119.7, 116.0, 112.4, 112.5, 111.9; MS (*m*/*z*): 336.1 $[M + H]^+$; RP-HPLC (method C) purity: 97.7%, t_R = 3.63 min.

DOI: 10.1021/acschemneuro.9b00226
ACS Chem. Neurosci. 2019, 10, 3635−3661

*N-(2-Picolyl)-5H-[1,2,4]triazino[5,6-b]indol-3-amine (**7g**).* Brownish yellow solid; yield 82%; mp 241−243 °C; IR (KBr, cm^{-1}): 3396, 3069, 2972, 1615, 1562, 750; ^{1}H NMR (DMSO-d_6): δ 11.79 (bs, 1H, −N*H*), 8.52 (d, 1H, Ar−*H*), 8.13−7.18 (m, 7H, Ar−*H*, 1H, −N*H*), 4.77 (d, 2H, −NHCH_2); ^{13}C NMR (DMSO-d_6): δ 159.8, 149.3, 148.9, 139.6, 137.2, 137.1, 128.8, 122.5, 121.1, 120.9, 120.2, 119.5, 116.0, 112.4, 46.5; MS (*m*/*z*): 277.1 [M + H]$^+$; RP-HPLC (method C) purity: 98.3%, t_R = 3.36 min.

*N-((Furan-2-yl)methyl)-5H-[1,2,4]triazino[5,6-b]indol-3-amine (**7h**).* Yellow solid; yield 63%; mp 234−236 °C.IR (KBr, cm^{-1}): 3406, 3118, 2967, 1615, 1559, 751; ^{1}H NMR (DMSO-d_6): δ 11.83 (bs, 1H, −N*H*), 8.12−8.08 (m, 1H, Ar−*H*), 7.92−6.26 (m, 6H, Ar−*H*, 1H, −N*H*), 4.64 (d, 2H, −NHCH_2); ^{13}C NMR (DMSO-d_6): δ 155.8, 153.5, 148.9, 142.5, 139.7, 128.8, 122.1, 120.9, 120.2, 119.5, 116.0, 110.9, 107.3, 38.3; MS (*m*/*z*): 266.1 [M + H]$^+$; RP-HPLC (method C) purity: 98.0%, t_R = 3.55 min.

*N-(2-(Piperidin-1-yl)ethyl)-5H-[1,2,4]triazino[5,6-b]indol-3-amine (**7i**).* Yellow solid; yield 69%; mp 217−219 °C; IR (KBr, cm^{-1}): 3399, 3231, 3113, 1618, 1524, 1126, 1092, 754; ^{1}H NMR (DMSO-d_6): δ 11.84 (bs, 1H, −N*H*), 8.07 (d, 1H, Ar−*H*), 7.46−7.24 (m, 3H, Ar−*H*, 1H, −N*H*), 3.52−3.50 (m, 2H, −NHCH_2CH$_3$), 2.55−2.52 (m, 2H, CH_2), 2.43−2.40 (m, 4H, −NCH_2), 1.55−1.51 (m, 4H, −CH_2), 1.42−1.41 (m, 2H, −CH_2); ^{13}C NMR (DMSO-d_6): δ 155.8, 149.0, 139.5, 128.4, 122.0, 120.0, 119.7, 116.0, 112.3, 57.9, 54.6, 41.4, 26.0, 24.5; MS (*m*/*z*): 297.1 [M + H]$^+$; RP-HPLC (method D) purity: 98.5%, t_R = 5.33 min.

*N-(2-Morpholinoethyl)-5H-[1,2,4]triazino[5,6-b]indol-3-amine (**7j**).* Yellow solid, yield 68%; mp >270 °C; IR (KBr, cm^{-1}): 3337, 3070, 2967, 1607, 1526, 1132, 757; ^{1}H NMR (DMSO-d_6): δ 11.74 (s, 1H, −N*H*), 8.08 (d, 1H, Ar−*H*), 7.45−7.03 (m, 3H, Ar−*H*, 1H, −N*H*), 3.64−3.62 (m, 4H, -OCH_2), 3.57−3.55 (m, 2H, −NHCH_2), 2.62−2.59 (m, 2H, −NCH_2), 2.49−2.47 (m, 4H, −NCH_2); ^{13}C NMR (DMSO-d_6): δ 161.7, 149.0, 139.5, 128.6, 122.0, 120.0, 119.6, 116.2, 112.4, 66.7, 57.7, 53.8, 38.3; MS (*m*/*z*): 299.2 [M + H]$^+$; RP-HPLC (method D) purity: 99.1%, t_R = 4.55 min.

*Synthesis of 5-substituted-3-(methylthio)-5H-[1,2,4]triazino[5,6-b]indole derivatives (**8a**−**8i**).* Following the General Procedure B, 5-substituted 3-(methylthio)-5*H*-[1,2,4]triazino[5,6-*b*]indole derivatives **8a**−**8i** were synthesized by methylation of the respective thiol derivatives **7** with methyl iodide.

*5-Methyl-3-(methylthio)-5H-[1,2,4]triazino[5,6-b]indole (**8a**).* Greenish yellow solid; yield 85%; mp 160−162 °C; IR (KBr, cm^{-1}): 3052, 3022, 2968, 2925, 1578, 1179, 1072, 762; MS (*m*/*z*): 231 [M + H]$^+$.

*5-Ethyl-3-(methylthio)-5H-[1,2,4]triazino[5,6-b]indole (**8b**).* Yellow solid; yield 82%; mp 148−150 °C; IR (KBr, cm^{-1}): 3054, 2970, 2928, 2872, 1580, 1188, 1078, 749; MS (*m*/*z*): 245 [M + H]$^+$.

*5-Propyl-3-(methylthio)-5H-[1,2,4]triazino[5,6-b]indole (**8c**).* Light yellow solid; yield 80%; mp 128−130 °C; IR (KBr, cm^{-1}): 3053, 3026, 2966, 2924, 1575, 1190, 1073, 746; MS (*m*/*z*): 259 [M + H]$^+$.

*5-Butyl-3-(methylthio)-5H-[1,2,4]triazino[5,6-b]indole (**8d**).* Light yellow solid; yield 84%; mp 140−142 °C; IR (KBr, cm^{-1}): 3054, 2953, 2925, 1578, 1187, 1075, 742; MS (*m*/*z*): 273 [M + H]$^+$.

*5-Benzyl-3-(methylthio)-5H-[1,2,4]triazino[5,6-b]indole (**8e**).* Yellow solid; yield 87%; mp 168−170 °C; IR (KBr, cm^{-1}): 3058, 3028, 2955, 2923, 1578, 1186, 1074, 745, 694; MS (*m*/*z*): 307 [M + H]$^+$.

*5-(2-Methylbenzyl)-3-(methylthio)-5H-[1,2,4]triazino[5,6-b]-indole (**8f**).* Light yellow solid; yield 82%; mp 161−163 °C; IR (KBr, cm^{-1}): 3059, 3029, 2974, 2924, 1574, 1181, 1073, 748; MS (*m*/*z*): 321 [M + H]$^+$.

*5-(4-Methylbenzyl)-3-(methylthio)-5H-[1,2,4]triazino[5,6-b]-indole (**8g**).* Light yellow solid; yield 81%; mp 195−197 °C; IR (KBr, cm^{-1}): 3056, 2922, 1581, 1182, 1083, 749; MS (*m*/*z*): 321 [M + H]$^+$.

*5-(4-Chlorobenzyl)-3-(methylthio)-5H-[1,2,4]triazino[5,6-b]-indole (**8h**).* Light yellow solid; yield 79%; mp 181−183 °C; IR (KBr, cm^{-1}): 3059, 3026, 2927, 1583, 1184, 1088, 748; MS (*m*/*z*): 341 [M + H]$^+$.

*5-(4-Fluorobenzyl)-3-(methylthio)-5H-[1,2,4]triazino[5,6-b]-indole (**8i**).* Light yellow solid; yield 85%; mp 176−178 °C; IR (KBr, cm^{-1}): 3055, 2924, 1581, 1185, 1078, 751; MS (*m*/*z*): 325 [M + H]$^+$.

*Synthesis of 5-Substituted 3-(Methylsulfonyl)-5H-[1,2,4]triazino-[5,6-b]indole Derivatives (**9a**−**9i**).* Following the General Procedure C, 5-substituted-3-(methylsulfonyl)-5*H*-[1,2,4]triazino[5,6-*b*]indole derivatives **9a**−**9i** were synthesized by oxidation of respective thiomethyl derivatives **8a**−**8i** with *m*CPBA. The obtained product was used in the next step without further purification.

*Synthesis of 5-substituted-5H-[1,2,4]triazino[5,6-b]indol-3-amine derivatives (**10a**−**10j**).* Following the General Procedure D, 5-substituted-5*H*-[1,2,4]triazino[5,6-*b*]indol-3-amine derivatives **10a**−**10j** were synthesized by reaction of respective sulfone derivatives **9a**−**9f** and **6** with aqueous ammonia. The obtained solids were purified by flash chromatography to yield the titled compounds **10a**−**10j**.

*5-Methyl-5H-[1,2,4]triazino[5,6-b]indol-3-amine (**10a**).* Light brown solid; yield 64%; mp >270 °C; IR (KBr, cm^{-1}): 3383, 3307, 3212, 1549,1106,770; ^{1}H NMR (DMSO-d_6): δ 8.09 (d, 1H, Ar*H*), 7.60 (d, 1H, Ar*H*), 7.54−7.50 (m, 1H, Ar*H*), 7.35−7.31 (m, 1H, Ar*H*), 7.26 (bs, 2H, −NH_2), 3.72 (s, 3H, −NCH_3), MS (*m*/*z*): 200 [M + H]$^+$; RP-HPLC (method C) purity: 95.2%, t_R = 4.32 min.

*5-Ethyl-5H-[1,2,4]triazino[5,6-b]indol-3-amine (**10b**).* Brown solid; yield 67%; mp >270 °C; IR (KBr, cm^{-1}): 3384, 3308, 3211, 2937, 1549, 1019, 755; ^{1}H NMR (DMSO-d_6): δ 8.02 (d, 1H, Ar*H*), 7.71−7.62 (m, 2H, Ar*H*), 7.41−7.37 (m, 1H, Ar*H*), 6.84 (bs, 2H, −NH_2), 4.30−4.24 (m, 2H, −NCH_2CH$_3$), 1.82−1.76 (m, 3H, −NCH$_2$CH_3), MS (*m*/*z*): 214.2 [M + H]$^+$; RP-HPLC (method C) purity: 99.0%, t_R = 4.68 min.

*5-Propyl-5H-[1,2,4]triazino[5,6-b]indol-3-amine (**10c**).* Greenish yellow solid; yield 67%; mp 265−267 °C; IR (KBr, cm^{-1}): 3384,3308, 3212, 2938, 1588, 1105, 755; ^{1}H NMR (DMSO-d_6): δ 8.11 (d, 1H, Ar*H*), 7.65 (d, 1H, Ar*H*), 7.52−7.48 (m, 1H, Ar*H*), 7.34−7.30 (m, 1H, Ar*H*), 7.27 (bs, 2H, −NH_2), 4.21 (t, 2H, −NCH_2), 1.85−1.78 (m, 2H, −CH_2CH$_3$), 0.90 (t, 3H, −CH$_2$CH_3); MS (*m*/*z*): 229 [M + H]$^+$; RP-HPLC (method C) purity: 99.1%, t_R = 4.88 min.

*5-Butyl-5H-[1,2,4]triazino[5,6-b]indol-3-amine (**10d**).* Light brown solid; yield 70%; mp 208−210 °C; IR (KBr, cm^{-1}): 3377, 3298, 3210, 2961, 1525, 1035, 741; ^{1}H NMR (DMSO-d_6): δ 8.10 (d, 1H, Ar*H*), 7.52−7.51 (m, 2H, Ar*H*), 7.31−7.27 (m, 1H, Ar*H*), 6.90 (bs, 2H, −NH_2), 4.22−4.19 (m, 2H, −NCH_2), 1.81−1.74 (m, 2H, −NCH$_2$CH_2), 1.36−1.30 (m, 2H, −CH_2CH$_3$), 0.92 (t, 3H, −CH$_2$CH_3); MS (*m*/*z*): 242.3 [M + H]$^+$; RP-HPLC (method C) purity: 98.0%, t_R = 5.65 min.

*5-Benzyl-5H-[1,2,4]triazino[5,6-b]indol-3-amine (**10e**).* Reddish brown solid; yield 68%; mp 265−267 °C; IR (KBr, cm^{-1}): 3396, 3329, 3029, 2929, 1542, 1030, 746; ^{1}H NMR (DMSO-d_6): δ 8.14−7.93 (m, 1H, Ar*H*), 7.49−7.22 (m, 8H, Ar*H*), 5.45 (s, 2H, −NCH_2); MS (*m*/*z*): 276.2 [M + H]$^+$; RP-HPLC (method C) purity: 99.1%, t_R = 8.92 min.

*5-(2-Methylbenzyl)-5H-[1,2,4]triazino[5,6-b]indol-3-amine (**10f**).* Yellow solid; yield 71%; mp 253−254 °C; IR (KBr, cm^{-1}): 3462, 3334, 3009, 2922, 1553, 1107, 744; ^{1}H NMR (CDCl$_3$): δ 8.40 (d, 1H, Ar*H*), 7.44−7.35 (m, 2H, Ar*H*), 7.28−7.20 (m, 2H, Ar*H*), 7.13 (d, 1H, Ar*H*), 7.09−7.06 (m, 1H, Ar*H*), 6.72 (d, 1H, Ar*H*), 5.44 (bs, 2H, −NH_2), 5.21 (s, 2H, −NCH_2), 2.44 (s, 3H, −CH_3); MS (*m*/*z*): 290 [M + H]$^+$; RP-HPLC (method C) purity: 95.9%, t_R = 5.54 min.

*5-(4-Methylbenzyl)-5H-[1,2,4]triazino[5,6-b]indol-3-amine (**10g**).* Yellow solid; yield 64%; mp 245−247 °C; IR (KBr, cm^{-1}): 3471, 3271, 3057, 2963, 1536, 1098, 743; ^{1}H NMR (DMSO-d_6) δ 7.95−7.93 (m, 1H, Ar*H*), 7.55−7.14 (m, 5H, Ar*H*), 6.90−6.88 (m, 2H, Ar*H*), 5.27 (s, 2H, −NCH_2), 3.72 (s, 3H, −CH_3); MS (*m*/*z*): 290.2 [M + H]$^+$; RP-HPLC (method C) purity: 96.6%, t_R = 5.73 min.

*5-(4-Chlorobenzyl)-5H-[1,2,4]triazino[5,6-b]indol-3-amine (**10h**).* Light brown solid; yield 67%; mp 215−217 °C; IR (KBr, cm^{-1}): 3417, 3298, 2925, 1540, 1039, 746; ^{1}H NMR (CDCl$_3$) δ 8.39 (d, 1H, Ar*H*), 7.47−7.43 (m, 1H, Ar*H*), 7.39−7.26 (m, 6H, Ar*H*), 5.47 (s, 2H, −NCH_2), 5.16 (bs, 2H, −NH_2);; MS (*m*/*z*): 310 [M + H]$^+$; RP-HPLC (method C) purity: 97.4%, t_R = 5.99 min.

*5-(3-Fluorobenzyl)-5H-[1,2,4]triazino[5,6-b]indol-3-amine (**10i**).* Brown solid; yield 59%; mp 230−232 °C; IR (KBr, cm^{-1}): 3418, 3299, 2924, 1550, 1039, 748; ^{1}H NMR (DMSO-d_6): δ 7.96−7.94 (m, 1H, Ar*H*), 7.55−7.46 (m, 4H, Ar*H*), 7.32−7.30 (m, 1H, Ar*H*), 7.18−

DOI: 10.1021/acschemneuro.9b00226
ACS Chem. Neurosci. 2019, 10, 3635−3661

7.16 (m, 2H, ArH), 5.33 (s, 2H, $-NCH_2$); MS (m/z): 294 $[M + H]^+$; RP-HPLC (method C) purity: 97.4%, t_R = 6.93 min.

*5H-[1,2,4]Triazino[5,6-b]indol-3-amine (**10j**).* Light brown solid; yield 52%; mp >270 °C; IR (KBr, cm^{-1}): 3383, 3307, 3212, 1558, 1021,755; ^1H NMR (DMSO-d_6) δ 8.30 (d, 1H, ArH), 7.67−7.63 (m, 1H, ArH), 7.56 (d, 1H, ArH), 7.43−7.39 (m, 1H, ArH), 6.90 (bs, 2H, $-NH_2$), MS (m/z): 186.09 $[M + H]^+$; RP-HPLC (method C) purity: 98.7%, t_R = 3.45 min.

*General Procedure for the Synthesis of N-(Bromoalkyl)-phthalimides (**12−14**).* Phthalimide (1 g, 6.80 mmol), potassium carbonate (3.76 g, 27.2 mmol), and benzyltriethylammonium chloride (154 mg, 0.68 mmol) were suspended in acetone (50 mL). Dibromoalkane (27.2 mmol) was added to the suspension and the reaction mixture was stirred at room temperature for 24 h. The solvent was evaporated under vacuum and the residue was dissolved in water (50 mL) and dichloromethane (50 mL). The organic layer was separated, and the aqueous solution was further extracted with dichloromethane (50 mL × 2). The combined organic solution was dried over sodium sulfate, filtered, and concentrated. The crude product was purified by column chromatography to provide *N*-(bromoalkyl)phthalimides as colorless solids. Melting point data for **12−14** were in accordance with the literature values.[91]

*N-(Bromobutyl)phthalimides (**12**).* White solid; yield 95%, mp 75−78 °C; IR (KBr, cm^{-1}): 2988, 2862, 1768, 1712, 1610, 717.

*N-(Bromopentyl)phthalimides (**13**).* White solid; yield 96%, mp 61−63 °C; IR (KBr, cm^{-1}): 2932, 2862, 1769, 1710, 1613, 717.

*N-(Bromohexyl)phthalimides (**14**).* White solid; yield 94%, mp 57−59 °C; IR (KBr, cm^{-1}): 2983, 2927, 2860, 1764, 1704, 1610, 720.

*General Procedure for the Synthesis of N,N-(Disubstitutedamino)alkylamines (**18a−20h**).* To a solution of *N*-(bromoalkyl)phthalimide (4 mmol) in methanol (50 mL), secondary amines (4.8 mmol) and triethylamine (0.7 mL, 4.8 mmol) were added. The reaction mixture was refluxed overnight. After completion of the reaction, the solvent was removed under reduced pressure. The residue was dissolved in chloroform and washed with water and brine. The collected organic layer was dried over magnesium sulfate, filtered, and evaporated under reduced pressure to give yellowish brown oils which were used in next step without further purification. The phthalimides thus obtained were dissolved in methanol, and hydrazine monohydrate (0.8 mL, 16 mmol) was added dropwise. The mixture was refluxed for about 4 h. The reaction mixture was cooled to room temperature, the insoluble phthalhydrazide was filtered off, and the filtrate was evaporated under reduced pressure. The obtained oil was dissolved in chloroform and filtered to remove some more phthalhydrazide (this procedure was repeated until complete disappearance of phthalhydrazide was observed). The filtrate was concentrated to give pure product as viscous yellowish oil which was used as such without further purification.

*Synthesis of N-Substituted 5H-[1,2,4]Triazino[5,6-b]indol-3-amine derivatives (**21a−23h**).* Following the General Procedure D, N-substituted 5*H*-[1,2,4]triazino[5,6-*b*]indol-3-amine derivatives **21a−23h** were synthesized by reacting compound **6** with the respective amines **18a−20h**. The obtained solids were purified by flash chromatography to yield the titled compounds **21a−23h**.

*N-(4-(Dimethylamino)butyl)-5H-[1,2,4]triazino[5,6-b]indol-3-amine (**21a**).* Yellow solid; yield 67%; mp 161−163 °C; IR (KBr, cm^{-1}): 3443, 3327, 3048, 2944, 1615, 1463, 1393, 742; ^1H NMR (DMSO-d_6): δ 11.75 (bs, 1H, NH), 8.09−8.07 (m, 1H, ArH), 7.46−7.39 (m, 2H, ArH), 7.27−7.23 (m, 1H, ArH), 3.50−3.49 (m, 2H, $-NHCH_2$), 2.80−2.78 (m, 2H, $-NCH_2$), 2.563 (s, 6H, $-NCH_3$), 1.80−1.82 (m, 2H, $-NHCH_2CH_2$), 1.68−1.75 (m, 2H, $-CH_2$); ^{13}C NMR (DMSO-d_6): δ 155.9, 149.0, 139.6, 128.6, 122.1, 120.03, 119.6, 116.1, 112.4, 56.9, 46.1, 42.6, 26.3, 26.2; MS (m/z): 285.1 $[M + H]^+$; RP-HPLC (method D) purity: 98.1%, t_R = 3.45 min.

*N-(4-(Diethylamino)butyl)-5H-[1,2,4]triazino[5,6-b]indol-3-amine (**21b**).* Yellow solid; yield 69%; mp 190−192 °C; IR (KBr, cm^{-1}): 3442, 3336, 2966, 1616, 1461, 1391, 748; ^1H NMR ($CDCl_3$): δ 8.24 (d, 1H, ArH), 7.48−7.44 (m, 1H, ArH), 7.36 (d, 1H, ArH), 7.33−7.29 (m, 1H, ArH),6.04 (bs, 1H, −NH), 3.55−3.50 (m, 2H, $-NHCH_2$), 2.51−2.42 (m, 6H, $-NCH_2$), 1.74−1.54 (m, 4H, $-CH_2CH_2$), 1.05 (t, 6H, CH_3); MS (m/z): 313.3 $[M + H]^+$; RP-HPLC (method D) purity: 97.4%, t_R = 3.43 min.

*N-(4-(Dipropylamino)butyl)-5H-[1,2,4]triazino[5,6-b]indol-3-amine (**21c**).* Yellow solid; yield 69%; mp 198−200 °C; IR (KBr, cm^{-1}): 3444, 3333, 3003, 2956, 1615, 1461, 1390, 746; ^1H NMR (DMSO-d_6): δ 11.72 (bs, 1H, NH), 8.06 (d, 1H, ArH), 7.44−7.36 (m, 2H, ArH), 7.26−7.22 (m, 1H, ArH), 2.55−2.54 (m, 2H, $-NHCH_2$), 2.41−2.38 (m, 2H, $-NCH_2$), 2.32 (t, 4H, $-NCH_2$), 1.66−1.62 (m, 2H, $-NHCH_2CH_2$), 1.51−1.48 (m, 2H, $-CH_2$), 1.44−1.35 (m, 4H, $-CH_2CH_3$), 0.84 (t, J = 7.3 Hz, 6H, $-CH_3$); ^{13}C NMR (DMSO-d_6): δ 155.8, 149.1, 139.5, 128.5, 121.9, 119.9, 119.7, 116.2, 112.3, 56.0, 53.8, 41.1, 27.3, 24.8, 20., 12.3; MS (m/z): 341.1 $[M + H]^+$; RP-HPLC (method D) purity: 97.6%, t_R = 3.72 min.

*N-(4-(Dibutylamino)butyl)-5H-[1,2,4]triazino[5,6-b]indol-3-amine (**21d**).* Yellow solid; yield 64%; mp 180−182 °C; IR (KBr, cm^{-1}): 3442, 3222, 3003, 2955, 1614, 1460, 1388, 743; ^1H NMR ($CDCl_3$): δ 8.25 (d, 1H, ArH), 7.48−7.44 (m, 1H, ArH), 7.39 (d, 1H, ArH), 7.33−7.29 (m, 1H, ArH), 5.89 (bs, 1H, NH), 3.55−3.50 (m, 2H, $-NHCH_2$), 2.54−2.50 (m, 2H, $-NCH_2$), 2.48−2.40 (m, 4H, $-NCH_2$), 1.73−1.66 (m, 2H, $-NHCH_2CH_2$), 1.63−1.56 (m, 2H, $-NCH_2CH_2$), 1.47−1.40 (m, 4H, $-NCH_2CH_2$), 1.33−1.24 (m, 4H, $-CH_2CH_3$), 0.89 (t, 6H, $-CH_3$); ^{13}C NMR (DMSO-d_6): δ155.9, 149.1, 139.5, 128.4, 121.9, 119.9, 119.7, 116.2, 112.3, 53.6, 53.8, 41.1, 29.4, 27.3, 24.8, 20.5, 14.3; MS (m/z): 369.2 $[M + H]^+$; RP-HPLC (method D) purity: 96.2%, t_R = 3.51 min.

*N-(4-(Pyrrolidin-1-yl)butyl)-5H-[1,2,4]triazino[5,6-b]indol-3-amine (**21e**).* Yellow solid; yield 71%; mp 220−222 °C; IR (KBr, cm^{-1}): 3434, 3219, 3000, 2934, 1617, 1459, 1382, 745; ^1H NMR (DMSO-d_6): δ 8.06 (d, 1H, ArH), 7.44−7.36 (m, 2H, ArH), 7.26−7.22 (m, 1H, ArH), 3.41−3.34 (m, 2H, $-NHCH_2$), 2.47−2.43 (m, 6H, $-NCH_2$), 1.71−1.64 (m, 6H, $-NCH_2CH_2$), 1.59−1.54 (m, 2H, CH_2); MS (m/z): 311.3 $[M + H]^+$; RP-HPLC (method D) purity: 97.6%, t_R = 3.42 min.

*N-(4-(Piperidin-1-yl)butyl)-5H-[1,2,4]triazino[5,6-b]indol-3-amine (**21f**).* Yellow solid; yield 66%; mp 199−201 °C; IR (KBr, cm^{-1}): 3445, 3326, 3061, 2933, 1660, 1460, 1393, 748; ^1H NMR (DMSO-d_6): δ 11.74 (bs, 1H, NH), 8.06 (d, 1H, ArH), 7.44−7.22 (m, 3H, ArH), 3.41−3.40 (m, 2H, $-NHCH_2$), 2.32−2.26 (m, 6H, $-NCH_2$), 1.66−1.59 (m, 2H, $-NHCH_2CH_2$), 1.58−1.49 (m, 6H, $-NCH_2CH_2$), 1.40−1.39 (m, 2H, $-CH_2$); ^{13}C NMR (DMSO-d_6): δ 155.78, 149.05, 139.54, 128.44, 121.9, 119.9, 119.7, 116.1, 112.3, 58.8, 54.5, 41.2, 27.4, 26.0, 24.7, 24.4; MS (m/z): 325.1 $[M + H]^+$; RP-HPLC (method D) purity: 98.2%, t_R = 3.43 min.

*N-(4-Morpholinobutyl)-5H-[1,2,4]triazino[5,6-b]indol-3-amine (**21g**).* Yellow solid; yield, 63%; mp 191−193 °C; IR (KBr, cm^{-1}): 3430, 3222, 3007, 2944, 1612, 1457, 1387, 747; ^1H NMR (DMSO-d_6): δ 11.63 (bs, 1H, NH), 8.07 (d, 1H, ArH), 7.447.36 (m, 2H, ArH), 7.26−7.22 (m, 1H, ArH), 3.65−3.62 (m, 4H, -OCH_2), 3.46−3.44 (m, 2H, $-NHCH_2$), 2.39−2.32 (m, 6H, $-NCH_2$), 1.71−1.62 (m, 2H, $-CH_2$), 1.71−1.54 (m, 4H, $-CH_2$); ^{13}C NMR (DMSO-d_6): δ155.8, 149.1, 139.5, 128.5, 121.9, 119.9, 119.7, 116.2, 112.3, 66.7, 58.5, 53.8, 41.1, 27.2, 24.0; MS (m/z): 327.3 $[M + H]^+$; RP-HPLC (method D) purity: 97.2%, t_R = 3.49 min.

*N-(4-(4-Methylpiperazin-1-yl)butyl)-5H-[1,2,4]triazino[5,6-b]-indol-3-amine (**21h**).* Yellow solid; yield 65%; mp 175−177 °C; IR (KBr, cm^{-1}): 3425, 3222, 3052, 2935, 1615, 1457, 1389, 741; ^1H NMR (DMSO-d_6): δ 11.68 (bs, 1H, −NH), 8.03 (d, 1H, ArH), 7.41−7.32 (m, 2H, ArH), 7.23−7.19 (m, 1H, ArH), 3.39−3.38 (m, 2H, $-NHCH_2$), 2.31−2.27 (m, 10H, $-NCH_2$), 2.15 (s, 3H, $-NCH_3$), 1.64−1.59 (m, 2H, $-NHCH_2CH_2$), 1.55−1.48 (m, 2H, $-CH_2$); ^{13}C NMR (DMSO-d_6): δ 155.9, 149.1, 139.6, 128.5, 121.9, 119.9, 119.7, 116.2, 112.3, 58.0, 55.2, 53.2, 46.2, 41.2, 27.2, 24.4; MS (m/z): 340.3 $[M + H]^+$; RP-HPLC (method D) purity: 99.5%, t_R = 3.45 min.

*N-(5-(Dimethylamino)pentyl)-5H-[1,2,4]triazino[5,6-b]indol-3-amine (**22a**).* Yellow solid; yield 62%; mp 198−200 °C; IR (KBr, cm^{-1}): 3222, 3111, 3007, 2945, 1612, 1457, 748; ^1H NMR (DMSO-d_6): δ 8.10−8.05 (m, 1H, ArH), 7.44−7.35 (m, 2H, ArH), 7.26−7.21 (m, 1H, ArH), 3.35−3.30 (m, 2H, $-NHCH_2$), 2.20 (t, 2H, $-NCH_2$), 2.135 (s, 6H, $-NCH_3$), 1.68−1.60 (m, 2H, $-NHCH_2CH_2$), 1.46−1.34 (m, 4H, $-CH_2$); ^{13}C NMR (DMSO-d_6): δ 155.9, 149.0, 139.5,

DOI: 10.1021/acschemneuro.9b00226
ACS Chem. Neurosci. 2019, 10, 3635−3661

128.4, 121.9, 119.9, 119.7, 116.2, 112.3, 59.6, 45.7, 41.2, 29.2, 27.4, 24.9; MS (m/z): 299.3 $[M + H]^+$; RP-HPLC (method D) purity: 97.8%, t_R = 3.20 min.

*N-(5-(Diethylamino)pentyl)-5H-[1,2,4]triazino[5,6-b]indol-3-amine (**22b**).* Yellow solid; yield 70%; mp 191−193 °C; IR (KBr, cm^{-1}): 3442, 3333, 3059, 2967, 1615, 1460, 1370, 745; ^1H NMR (DMSO-d_6): δ 11.62 (bs, 1H, N*H*), 8.06−8.02 (m, 1H, Ar*H*), 7.37−7.32 (m, 2H, Ar*H*), 7.23−7.19 (m, 1H, Ar*H*), 3.36−3.29 (m, 2H, −NHCH_2), 2.44−2.39 (m, 4H, −NCH_2), 2.34 (t, 2H, −NCH_2), 1.63−1.57 (m, 2H, −NHCH$_2$CH_2), 1.41−1.30 (m, 4H, −CH_2), 0.92 (t, 6H, −CH_3); ^{13}C NMR (DMSO-d_6): δ 155.9, 149.0, 139.5, 128.4, 121.9, 119.9, 119.7, 116.2, 112.3, 52.7, 46.7, 41.2, 29.3, 26.9, 24.9, 12.2; MS (m/z): 327.1 $[M + H]^+$; RP-HPLC (method D) purity: 98.40%, t_R = 4.18 min.

*N-(5-(Dipropylamino)pentyl)-5H-[1,2,4]triazino[5,6-b]indol-3-amine (**22c**).* Yellow solid; yield 66%; mp 200−202 °C; IR (KBr, cm^{-1}): 3443, 3329, 3057, 2956, 1614, 1461, 1390, 747; ^1H NMR ($CDCl_3$): δ 8.25 (d, 1H, Ar*H*), 7.49−7.45 (m, 1H, Ar*H*), 7.37 (d, 1H, Ar*H*), 7.33−7.30 (m, 1H, Ar*H*), 5.54 (bs, 1H, −N*H*), 3.54−3.49 (m, 2H, −NHCH_2), 2.47−2.38 (m, 6H, −NCH_2), 1.71−1.66 (m, 2H, −NHCH$_2$CH_2), 1.55−1.39 (m, 8H, −CH_2), 0.86 (t, 6H, −CH_3); ^{13}C NMR (DMSO-d_6): δ 155.9, 149.1, 139.6, 128.4, 121.9, 119.9, 119.7, 116.2, 112.3, 56.1 53.9, 41.1, 29.2, 27.1, 24.9, 20.4, 12.2; MS (m/z): 355.3 $[M + H]^+$; RP-HPLC (method D) purity: 99.2%, t_R = 5.0 min.

*N-(5-(Dibutylamino)pentyl)-5H-[1,2,4]triazino[5,6-b]indol-3-amine (**22d**).* Yellow solid; yield 72%; mp 184−186 °C; IR (KBr, cm^{-1}): 3444, 3332, 3059, 2931, 1614, 1460, 1390, 746; ^1H NMR ($CDCl_3$): δ 8.18 (d, 1H, Ar*H*), 7.41−7.37 (m, 1H, Ar*H*), 7.31−7.29 (m, 1H, Ar*H*), 7.25−7.22 (m, 1H, Ar*H*), 5.54 (bs, 1H, −N*H*), 3.40−3.36 (m, 2H, −NHCH_2), 2.41−2.36 (m, 6H, −NCH_2), 1.63−1.54 (m, 2H, −NHCH$_2$CH_2), 1.48−1.44 (m, 2H, −CH_2), 1.39−1.33 (m, 6H, −NCH$_2$CH_2), 1.25−1.20 (m, 4H, −CH_2), 0.82 (t, 7.3 Hz, 6H, −CH_3); ^{13}C NMR (DMSO-d_6): δ 155.8, 149.0, 139.5, 128.4, 121.9, 119.9, 119.7, 116.1, 112.3, 53.9, 53.6, 41.2, 29.4, 29.2, 27.0, 24.9, 20.5, 14.4; MS (m/z): 383.2 $[M + H]^+$; RP-HPLC (method D) purity: 98.8%, t_R = 3.07 min.

*N-(5-(Pyrrolidin-1-yl)pentyl)-5H-[1,2,4]triazino[5,6-b]indol-3-amine (**22e**).* Yellow solid; yield 73%; mp 191−193 °C; IR (KBr, cm^{-1}): 3459, 3306, 3059, 2937, 1615, 1456, 1383, 743; ^1H NMR (DMSO-d_6): δ 11.66 (bs, 1H, −N*H*), 8.06−8.02 (m, 1H, Ar*H*), 7.37−7.32 (m, 2H, Ar*H*), 7.22−7.18 (m, 1H, Ar*H*), 3.38−3.37 (m, 2H, −NHCH_2), 2.39−2.34 (m, 6H, NCH_2), 1.68−1.57 (m, 6H, −NCH$_2$CH_2), 1.51−1.44 (m, 2H, −CH_2), 1.41−1.34 (m, 2H, −CH_2); ^{13}C NMR (DMSO-d_6): δ 155.8, 149.1, 139.5, 128.5, 121.9, 119.7, 119.6, 116.2, 112.2, 53.2, 54.1, 41.1, 29.3, 28.7, 25.0, 23.5; MS (m/z): 325.4 $[M + H]^+$; RP-HPLC (method D) purity: 98.3%, t_R = 2.84 min.

*N-(5-(Piperidin-1-yl)pentyl)-5H-[1,2,4]triazino[5,6-b]indol-3-amine (**22f**).* Yellow solid; yield 63%; mp 196−198 °C; IR (KBr, cm^{-1}): 3423, 3223, 3007, 2935, 1614, 1455, 1383, 741; ^1H NMR (DMSO-d_6): δ 11.58 (bs, 1H, −N*H*), 8.04 (d, 1H, Ar*H*), 7.43−7.39 (m, 1H, Ar*H*), 7.35 (d, 1H, Ar*H*), 7.25−7.21 (m, 1H, Ar*H*), 3.41−3.40 (m, 2H, −NHCH_2), 2.27−2.18 (m, 6H, −NCH_2), 1.64−1.59 (m, 2H, −NHCH$_2$CH_2), 1.49−1.41 (m, 6H, −NCH$_2$CH_2), 1.37−1.34 (m, 4H, −CH_2); ^{13}C NMR (DMSO-d_6): δ 155.9, 149.1, 139.6, 128.5, 121.9, 119.9, 119.7, 116.2, 112.3, 59.2, 54.6, 41.2, 29.3, 26.7, 26.1, 25.0, 24.7; MS (m/z): 339.3 $[M + H]^+$; RP-HPLC (method D) purity: 96.8%, t_R = 5.43 min.

*N-(5-Morpholinopentyl)-5H-[1,2,4]triazino[5,6-b]indol-3-amine (**22g**).* Yellow solid; yield 62%; mp 199−201 °C; IR (KBr, cm^{-1}): 3426, 3222, 3050, 2925, 1613, 1455, 1384, 749; ^1H NMR (DMSO-d_6): δ 11.41 (bs, 1H, −N*H*), 8.03 (d, 1H, Ar*H*), 7.40−7.32 (m, 2H, Ar*H*) 7.22−7.18 (m, 1H, Ar*H*), 3.56−3.54 (m, 4H, −OCH_2), 3.39−3.37 (m, 2H, NHCH_2), 2.32−2.29 (m, 4H, −NCH_2), 2.27−2.24 (m, 2H, −NCH_2), 1.65−1.58 (m, 2H, −NHCH$_2$CH_2), 1.50−1.43 (m, 2H, −CH_2), 1.40−1.32 (m, 2H, −CH_2); ^{13}C NMR (DMSO-d_6): δ 155.8, 149.1, 139.5, 128.4, 122.0, 119.9, 119.7, 116.1, 112.3, 66.7, 58.8, 53.9, 41.1, 29.2, 26.2, 24.9; MS (m/z): 341.1 $[M + H]$+; RP-HPLC (method D) purity: 98.5%, t_R = 3.20 min.

*N-(5-(4-Methylpiperazin-1-yl)pentyl)-5H-[1,2,4]triazino[5,6-b]-indol-3-amine (**22h**).* Yellow solid; yield 68%; mp 162−164 °C; IR (KBr, cm^{-1}): 3439, 3234, 3061, 2931, 1614, 1460, 1389, 745; ^1H NMR ($CDCl_3$): δ 9.76 (bs, 1H, −N*H*), 8.25 (d, 1H, Ar*H*), 7.49−7.44 (m, 2H, Ar*H*), 7.37−7.31 (m, 1H, Ar*H*), 5.57 (bs, 1H, −NH), 3.53−3.47 (m, 2H, −NHCH_2), 2.60−2.42 (m, 6H, −NCH_2), 2.39−2.35 (m, 4H, −NCH_2), 2.29 (s, 3H, −NCH_3), 1.72−1.65 (m, 2H, −NHCH$_2$CH_2), 1.62−1.53 (m, 2H, −NCH$_2$CH_2), 1.46−1.37 (m, 2H, −CH_2); ^{13}C NMR (DMSO-d_6): δ 155.6, 149.1, 139.7, 128.5, 121.9, 119.9, 119.3, 116.2, 112.3, 58.4, 55.2, 53.2, 46.2, 41.1, 29.2, 26.6, 24.9; MS (m/z): 354.3 $[M + H]^+$; RP-HPLC (method D) purity: 98.4%, t_R = 3.13 min.

*N-(6-(Dimethylamino)hexyl)-5H-[1,2,4]triazino[5,6-b]indol-3-amine (**23a**).* Yellow solid; yield 69%; mp 180−182 °C; IR (KBr, cm^{-1}): 3321, 3223, 3058, 2937, 1615, 1462, 1386, 744; ^1H NMR (DMSO-d_6) δ 11.76 (bs, 1H, −N*H*), 8.06 (d, 1H, Ar*H*), 7.43−7.36 (m, 2H, Ar*H*), 7.27−7.25 (m, 1H, Ar*H*), 3.39−3.32 (m, 2H, −NHCH_2), 2.19 (t, 2H, −NCH_2), 2.11 (s, 6H, −NCH_3), 1.62−1.61 (m, 2H, −NHCH$_2$CH_2), 1.43−1.32 (m, 6H, −CH_2); ^{13}C NMR (DMSO-d_6): δ 155.7, 149.1, 139.5, 128.4, 121.9, 119.9, 119.7, 116.1, 112.3, 59.6, 45.6, 41.1, 29.3, 27.5, 27.1, 26.9; MS (m/z): 313.1 $[M + H]^+$; RP-HPLC (method D) purity: 99.8%, t_R = 3.52 min.

*N-(6-(Diethylamino)hexyl)-5H-[1,2,4]triazino[5,6-b]indol-3-amine (**23b**).* Yellow solid; yield 71%; mp 170−172 °C; IR (KBr, cm^{-1}): 3443, 3333, 3060, 2929, 1614, 1461, 1374, 747; ^1H NMR ($CDCl_3$): δ 8.25 (d, 1H, Ar*H*), 7.47−7.35 (m, 3H, Ar*H*), 5.75 (bs, 1H, −N*H*), 3.50−3.43 (m, 2H, −NHCH_2), 2.65−2.59 (m, 4H, −NCH_2), 2.52−2.48 (m, 2H, NCH_2), 1.71−1.60 (m, 4H, −CH_2), 1.46−1.37 (m, 4H, −CH_2), 1.07−1.03 (m, 6H, −CH_3); ^{13}C NMR (DMSO-d_6): δ 155.9, 149.1, 139.6, 128.4, 121.9, 119.9, 119.7, 116.2, 112.3, 52.6, 46.7, 41.2, 29.3, 27.3, 27.2, 26.9, 12.04; MS (m/z): 341.1 $[M + H]^+$; RP-HPLC (method D) purity: 99.5%, t_R = 4.7 min.

*N-(6-(Dipropylamino)hexyl)-5H-[1,2,4]triazino[5,6-b]indol-3-amine (**23c**).* Yellow solid; yield 65%; mp 195−197 °C; IR (KBr, cm^{-1}): 3445, 3332, 3060, 2929, 1614, 1461, 1374, 747; ^1H NMR (DMSO-d_6): 11.669 (bs, 1H, −N*H*), 8.03 (d, 1H, Ar*H*), 7.40−7.38 (m, 1H, Ar*H*), 7.35−7.33 (m, 1H, Ar*H*),7.24−7.20 (m, 1H, Ar*H*),3.33−3.31 (m, 2H, −NHCH_2), 2.32−2.24 (m, 6H, −NCH_2), 1.62−1.58 (m, 2H, −NHCH$_2$CH_2), 1.39−1.29 (m, 10H, −CH_2), 0.80 (t, 6H, −CH_3); ^{13}C NMR (DMSO-d_6): δ 155.8, 149.1, 139.6, 128.5, 121.9, 119.9, 119.7, 116.2, 112.3, 56.1, 53.9, 41.1, 29.3, 27.2, 27.1, 26.9, 20.4, 12.3; MS (m/z): 369.1 $[M + H]^+$; RP-HPLC (method D) purity: 99.1%, t_R = 9.72 min.

*N-(6-(Dibutylamino)hexyl)-5H-[1,2,4]triazino[5,6-b]indol-3-amine (**23d**).* Yellow solid; yield 68%; mp 192−194 °C; IR (KBr, cm^{-1}): 3445, 3322, 3058, 2955, 1615, 1461, 1391, 747; ^1H NMR (DMSO-d_6): δ 11.74 (bs, 1H, N*H*), 8.09−8.07 (m, 1H, Ar*H*), 7.40−7.24 (m, 3H, Ar*H*), 3.42−3.40 (m, 2H, −NHCH_2), 2.54−2.33 (m, 6H, −NCH_2), 1.68−1.58 (m, 2H, −NHCH$_2$CH_2), 1.44−1.24 (m, 14H, −CH_2), 0.98−0.82 (m, 6H, −CH_3); ^{13}C NMR (DMSO-d_6): δ 155.8, 149.1, 139.6, 128.4, 121.9, 119.9, 119.7, 116.1, 112.3, 53.9, 53.6, 41.2, 29.4, 29.3, 27.2, 26.9, 26.0, 20.5, 14.4; MS (m/z): 397.2 $[M + H]^+$; RP-HPLC (method D) purity: 98.6%, t_R = 8.67 min.

*N-(6-(Pyrrolidin-1-yl)hexyl)-5H-[1,2,4]triazino[5,6-b]indol-3-amine (**23e**).* Yellow solid; yield 73%; mp 177−179 °C; IR (KBr, cm^{-1}): 3442, 3330, 3058, 2930, 1614, 1458, 743; ^1H NMR (DMSO-d_6): δ 11.66 (bs, 1H, −N*H*), 8.05−8.01 (m, 1H, Ar*H*), 7.37−7.32 (m, 2H, Ar*H*), 7.21−7.17 (m, 1H, Ar*H*), 3.36−3.34 (m, 2H, −NHCH_2), 2.38−2.32 (m, 6H, −NCH_2), 1.66−1.57 (m, 6H, −NCH$_2$CH_2), 1.45−1.40 (m, 2H, −NHCH$_2$CH_2), 1.38−1.30 (m, 4H, −CH_2); ^{13}C NMR (DMSO-d_6): δ 155.8, 149.0, 139.6, 128.5, 121.9, 119.9, 119.7, 116.1, 112.3, 56.2, 54.1, 41.2, 29.3, 28.9, 27.4, 26.9, 23.5; MS (m/z): 339.1 $[M + H]^+$; RP-HPLC (method D) purity: 97.5%, t_R = 4.35 min.

*N-(6-(Piperidin-1-yl)hexyl)-5H-[1,2,4]triazino[5,6-b]indol-3-amine (**23f**).* Yellow solid; yield 70%; mp 178−180 °C; IR (KBr, cm^{-1}): 3445, 3322, 3058, 2955, 1615, 1461, 1391, 747; ^1H NMR (DMSO-d_6): δ 11.68 (bs, 1H, −N*H*), 8.07 (d, 1H, Ar*H*), 7.44−7.35 (m, 2H, Ar*H*), 7.26−7.22 (m, 1H, Ar*H*), 3.42−3.32 (m, 2H, −NHCH_2), 2.31−2.21 (m, 6H, −NCH_2), 1.68−1.61 (m, 2H, −NHCH$_2$CH_2), 1.52−1.48 (m, 6H, −CH_2), 1.39−1.32 (m, 6H,

DOI: 10.1021/acschemneuro.9b00226
ACS Chem. Neurosci. 2019, 10, 3635−3661

$-CH_2$); ^{13}C NMR (DMSO-d_6): δ 155.8, 149.0, 139.5, 128.4, 121.9, 119.9, 119.7, 116.1, 112.3, 59.1, 54.6, 41.1, 29.3, 27.3, 26.9, 26.8, 26.1, 24.7; MS (m/z): 353.1 $[M + H]^+$; RP-HPLC (method D) purity: 97.1%, t_R = 4.66 min.

*N-(6-Morpholinohexyl)-5H-[1,2,4]triazino[5,6-b]indol-3-amine (**23g**).* Yellow solid; yield 65%; mp 163−165 °C; IR (KBr, cm^{-1}): 3460, 3334, 3057, 2931, 1614, 1459, 1392, 748; ^1H NMR ($CDCl_3$): δ 9.20 (bs, 1H, −N*H*), 8.25 (d, 1H, Ar*H*), 7.49−7.46 (m, 1H, Ar−*H*), 7.41−7.38 (m, 1H, Ar*H*), 7.34−7.31 (m, 1H, Ar*H*), 5.70 (bs, 1H, N*H*), 3.75−3.72 (m, 4H, -OCH_2), 3.50−3.53 (m, 2H, −NHCH_2), 2.48−2.42 (m, 4H, −NCH_2), 2.36−2.33 (m, 2H, −NCH_2), 1.70−1.66 (m, 4H, −NHCH$_2$CH_2), 1.54−1.51 (m, 2H, −CH_2), 1.41−1.38 (m, 4H, −CH_2); ^{13}C NMR (DMSO-d_6): δ 155.9, 149.1, 139.6, 128.5, 121.9, 119.9, 119.7, 116.2, 112.3, 66.6, 58.7, 53.8, 41.1, 29.3, 27.1, 26.9, 26.8; MS (m/z): 355.1 $[M + H]^+$; RP-HPLC (method D) purity: 98.9%, t_R = 3.7 min.

*N-(6-(4-Methylpiperazin-1-yl)hexyl)-5H-[1,2,4]triazino[5,6-b]-indol-3 amine (**23h**).* Yellow solid; yield 67%; mp 160−162 °C; IR (KBr, cm^{-1}): 3460, 3336, 3056, 2928, 1614, 1459, 1391, 747; ^1H NMR (DMSO-d_6): δ 11.71(bs, 1H, −N*H*), 8.03 (d, 1H, Ar*H*), 7.41−7.33 (m, 2H, Ar*H*), 7.23−7.19 (m, 1H, Ar*H*), 3.36−3.34 (m, 2H, −NHCH_2), 2.32−2.28 (m, 6H, −NCH_2), 2.24−2.20 (m, 2H, −NCH_2), 2.13 (s, 3H, −NCH_3), 1.62−1.56 (m, 2H, −NHCH$_2$CH_2), 1.42−1.29 (m, 6H, −CH_2); ^{13}C NMR (DMSO-d_6): δ 155.1, 149.1, 139.6, 128.5, 121.9, 119.9, 119.7, 116.4, 112.3, 58.3, 55.2, 53.2, 46.2, 41.1, 29.3, 27.2, 26.9, 26.8; MS (m/z): 368.1 $[M + H]^+$; RP-HPLC (method D) purity: 99.1%, t_R = 3.26 min.

Biology. *Inhibition Studies on AChE and BuChE.* The potential of the test compounds to inhibit ChEs was assessed using the Ellman's method as detailed in our earlier report.[59,61,62] Human AChE (product number C1682), equine serum BuChE (product number C1057), 5,5′-dithiobis(2-nitrobenzoic acid) (DTNB, product number D8130), acetylthiocholine iodide (ATCI, product number A5751), and butyrylthiocholine iodide (BTCI, product number B3253) were purchased from Sigma-Aldrich. Donepezil hydrochloride and tacrine hydrochloride hydrate were used as standard drugs. All the experiments were carried out in 50 mM Tris-HCl buffer at pH 8. Five different concentrations (0.001−100 μM) of each test compound were used to determine the enzyme inhibition activity. Briefly, 50 μL of AChE (0.22 U/mL) or 50 μL of BuChE (0.06 U/mL) and 10 μL of the test or standard compounds were incubated in 96-well plates at room temperature for 30 min. Further, 30 μL of the substrate, namely, ATCI (15 mM) or BTCI (15 mM), was added, and the solution was incubated for additional 30 min. Finally, 160 μL of DTNB (1.5 mM) was added to it, and the absorbance was measured at 415 nm wavelength using the microplate reader 680 XR (BIO-RAD, India). The IC_{50} values were determined from the absorbance obtained for various concentrations of the test and the standard compounds. The IC_{50} value recounts the concentration of the drug required to inhibit the enzyme activity by 50%. All determinations were performed in triplicate and at least in three independent runs.

Antioxidant Activity [1,1-Diphenyl-2-picrylhydrazyl (DPPH) Radical Scavenging Activity]. The spectrophotometric DPPH assay was carried out as described earlier.[61] Concentrations of the selected test compounds that exhibited promising neuroprotective effects against H_2O_2 insult were selected for the DPPH assay. In brief, 10 μL of a test compound (10 and 20 μM, in Tris-HCl buffer, pH 7.4) was mixed with 20 μL of DPPH (10 mM in methanol) in a 96-well plate. Finally, the volume was adjusted to 200 μL using methanol. After a 30 s incubation at room temperature protected from light, the absorbance was noted at 520 nm wavelength using a microplate reader 680 XR (BIORAD, India). The free radical scavenging activity was determined as the reduction percentage (RP) of DPPH using the equation RP = $100[(A_0 - A_C)/A_0]$, where A_0 is the untreated DPPH absorbance and A_C is the absorbance value for the added sample concentration C. Ascorbic acid was used as the standard antioxidant.

Cell Culture Studies. The human neuroblastoma SH-SY5Y cell line was procured from the National Centre for Cell Science (NCCS) (Pune, India). Cells were routinely cultured in Dulbecco's modified Eagle's medium (DMEM) supplemented with 10% fetal bovine serum (FBS), 1 mM glutamine, 50 U/mL penicillin, and 50 μg/mL streptomycin (reagents from Gibco) at 37 °C in a humidified incubator at 5% CO_2. All cells used in the study were of the low passage number (<15).

Determination of Cell Viability and Neuroprotection. To determine the cytotoxicity of the selected test compounds, 3-(4,5-dimethylthiazol-2-yl)-2,5-diphenyltetrazolium bromide (MTT) assay was performed. SH-SY5Y cells were seeded in 96-well plate at a density of 5×10^4 cells per well. After 24 h, the medium was replaced with relatively higher concentrations of test compounds (40 μM and 80 μM) for another 24 h at 37 °C. After the incubation period, the cell viability was determined using MTT assay. In another set of experiments, the test compounds were assessed for their ability to protect SH-SY5Y cells against oxidative damage induced by H_2O_2 and Aβ_{1-42}. Cells were exposed to the test compounds at relatively low concentrations (5, 10, and 20 μM) and incubated for 2 h. After the incubation period, the test compounds were replaced with a medium containing cytotoxic insult, i.e., H_2O_2 (100 μM) or Aβ_{1-42} (25 μM) and left for an additional 24 h period. Thereafter, the cell viability was assessed using MTT assay. Briefly, the medium was replaced with 80 μL of fresh medium and 20 μL of MTT (0.5 mg/mL, final concentration; Sigma) in PBS. After 4 h, MTT was removed and the crystals of formazan were dissolved in DMSO. Formazan concentrations were quantified at 570 nm with 630 nm reference wavelengths using a microplate reader 680 XR (BIO-RAD, India). Percentage protection against H_2O_2 and Aβ_{1-42} insults was calculated by considering absorbance of the control cells as 100% of the cell viability.

In Vitro Blood-Brain Barrier Permeation Assay. The PAMPA assay was performed to predict the BBB permeation of the most active compounds **23e** and **23f**. The donor microplates (PVDF membrane, pore size 0.45 μm) and the acceptor microplates were obtained from the Millipore. Porcine brain lipid (PBL) was purchased from Avanti Polar Lipids. The filter surface of the donor microplate was first impregnated with 4 μL of porcine brain lipid (20 mg in 1 mL dodecane). The acceptor microplate was filled with 200 μL of phosphate buffer saline (PBS)/ethanol (70:30). The test compounds (5 mg/mL) were dissolved in DMSO and diluted with PBS/ethanol (70:30) to get a final concentration of 100 μg/mL. 200 μL of the solution was filled in the donor well and the donor plate was carefully placed on the acceptor plate to form a sandwich and incubated for 120 min at 25 °C. After the incubation period, the donor plate was removed and the concentration of the test compounds in the acceptor wells was determined using UV spectrophotometry. Each sample was analyzed at five different wavelengths, in four wells, and at least in three independent runs. The results are expressed as mean ± SEM. P_e was calculated using the following equation:

$$P_e = -\left(\frac{V_d V_a}{(V_d + V_a)At}\right) \ln\left(1 - \frac{(\text{drug})_{\text{acceptor}}}{(\text{drug})_{\text{equilibrium}}}\right)$$

where V_d and V_a are the volumes in the donor well and acceptor well, respectively, A is the filter area, t is the permeation time, $(\text{drug})_{\text{acceptor}}$ is the concentration of the test compound in the acceptor well, and $(\text{drug})_{\text{equilibrium}}$ is the theoretical equilibrium concentration.

In the experiment, seven commercial drugs of known BBB permeability were included to validate the analysis set (Table S1, Supporting Information). A plot of the P_e(exp) versus P_e(ref) values gave a strong linear correlation, P_e(exp) = 1.16 P_e(ref) + 0.1668 (R^2 = 0.9781) (Figure S277, Supporting Information).

Assessment of Cognitive Improvement in an Animal Model of AD. *Morris Water Maze Test.* Adult male Swiss Albino mice (20−25 g) were divided into five groups of seven animals each as per the given treatment (normal control, vehicle-treated control, donepezil at 5 mg/kg, compound **23e** at 5 and 10 mg/kg). Scopolamine hydrochloride (1.4 mg/kg)[79,80] was dissolved in saline and administered intraperitoneally (ip) to the animals of all groups except the vehicle-treated control group, which received an equal volume of saline. Donepezil at 5 mg/kg and compound **23e** at 5 and 10 mg/kg in 0.5% CMC were administered orally 30 min prior to administration

DOI: 10.1021/acschemneuro.9b00226
ACS Chem. Neurosci. 2019, 10, 3635−3661

of scopolamine to the respective experimental group animals. All these treatments were continued for 14 consecutive days. During the last 5 days of the treatment period, spatial learning and memory were assessed using the Morris water maze (MWM) test.[59,79]

A maze consisting of a circular pool (65 cm diameter; 30 cm height) was filled with water (26 ± 1 °C) up to 20 cm depth. The inside walls of the pool were painted black. The pool was divided into four quadrants, and the escape platform was placed 1 cm below the water surface in the middle of any one quadrant. Experiments on the individual animals were carried out to determine the time required by the animal to reach the hidden platform (i.e., escape latency time, ELT) which assesses the spatial learning and memory. All of the experiments were carried out in a soundproof room and supervised by a blind observer.

Neurochemical Analysis. After completing the MWM test, the animals were sacrificed and the whole brain was isolated from the skull and homogenized in a glass Teflon homogenizer in 12.5 mM sodium phosphate buffer (pH 7). The homogenates were centrifuged at 15 000 rpm for 15 min at 4 °C. The supernatants were utilized for estimations of different biochemical parameters. The cholinergic biomarkers AChE and BuChE were estimated in the mice brain using Ellman's method. A volume of 100 μL of the supernatant was incubated with 2.7 mL of phosphate buffer and 100 μL of freshly prepared ATCI or BTCI (15 mM) for 5 min. Finally, 100 μL of DTNB (1.5 mM) was added, and the absorbance was noted at 415 nm wavelength spectrophotometrically.

MDA, an indicator of lipid peroxidation, was estimated using the thiobarbituric acid reacting substance (TBARS) method as described earlier.[61] MDA reacted with thiobarbituric acid in acidic medium at high temperature and formed a red complex TBARS which was analyzed spectrophotometrically. Briefly, 200 μL of the supernatant was mixed with 1 mL of 50% trichloroacetic acid in 0.1 M HCl and 1 mL of 26 mM thiobarbituric acid. After vortex mixing, samples were heated at 95 °C for 20 min. Later on the samples were centrifuged at 15000 rpm for 10 min and the supernatants were read at 532 nm wavelength.

Catalase (CAT) is an enzyme mediating breakdown of H_2O_2, a toxic form of oxygen metabolite into oxygen and water. CAT activity was determined following the method described by Sinha et al.[59] Briefly, 100 μL of the supernatant was mixed with 150 μL of 0.01 M phosphate buffer (pH 7). Reaction was started by the addition of 250 μL of H_2O_2 (0.16 M), the medium was incubated at 37 °C for 1 min, and the reaction was stopped by the addition of 1 mL of dichromate/acetic acid reagent (5% $K_2Cr_2O_7$/glacial acetic acid; 1:3 v/v). The reaction mixture was immediately kept in a boiling water bath for 15 min and resulted in the development of a green color. Finally, the mixture was analyzed at 570 nm wavelength spectrophotometrically.

In order to extract glycine and glutamate, 10 μL aliquots of hypothalamus homogenate were thawed and then mixed with 0.17 M perchloric acid (10% w/v). The mixture was left for 20 min at 4 °C. The resulting supernatant was decanted in a separate Eppendorf tube and centrifuged at 4 °C for 20 min at 15 000 rpm. After centrifugation, the supernatant fraction was separated and maintained at −70 °C until determination of free amino acids by HPLC coupled with an electrochemical detector (model no. Waters 2465, Waters Corporation, Milford, MA). Mobile phase was prepared by dissolving monosodium phosphate (0.1 M), EDTA (0.5 mM) and potassium chloride (2 mM) in HPLC grade methanol (25% v/v), diluted with distillated water. The solution pH was adjusted to 4.5. The mobile phase was filtered twice and degassed in an ultrasonic bath for 20 min, before circulation in the HPLC system. Analysis was performed on a Welchrom C18 column with 1.2 mL/min flow rate, 3000 psi pressure, and 850 mV working potential of the detector. The internal standards were prepared by mixing 200 μL of 1 mM stock of glycine/glutamate in 200 μL of pooled supernatant and diluted with 600 μL of mobile phase. It was used with an equimolar concentration of derivatizing agent [22 mg of *o*-phthalaldehyde dissolved in 500 μL of absolute ethanol, 500 μL of 1 M sodium sulfite, and 900 μL of 0.1 M tetraborate buffer, adjusted to pH 10.4 with 5 M sodium hydroxide] to make final concentrations of 2, 1, 0.5, 0.4, 0.2, and 0.1 μmol/L, and 200 μL of which was injected into the HPLC column. The sample solutions were prepared by diluting 200 μL of homogenate in 800 μLof mobile phase; 10 μL of it was mixed with 10 μL of derivatizing agent and diluted in 880 μL of mobile phase. The concentration of neurotransmitter in the brain was estimated by comparing the area with the calibration curve.[92]

Y-Maze Test. Adult male Wistar rats (150−200 g) were divided into five experimental groups of seven animals each as per the given treatment: (normal control, vehicle-treated control, donepezil at 5 mg/kg, and compound **23e** at 5 and 10 mg/kg). The animals were anesthetized with ketamine (100 mg/kg, ip) and xylazine (30 mg/kg, ip) and mounted in a stereotaxic apparatus (Stoelting). All of the groups (except the vehicle-treated control group which received an equal volume of normal saline) were injected with 2 μL of $A\beta_{1-42}$ (4 μM/μL in normal saline) unilaterally at the following coordinates: −4.0 mm anteroposterior, −2.5 mm mediolateral, and −3.5 mm dorsoventral from bregma. Donepezil at 5 mg/kg and compound **23e** at 5 and 10 mg/kg in 0.1% CMC were administered perorally to the respective experimental group animals for 15 consecutive days after 5 days of surgical recovery.[59] The Y-maze test was adopted for the assessment of immediate working memory. The test was performed during the last 5 days of the treatment period in the animals which were subjected to icv injection of $A\beta_{1-42}$. Each animal from the treated groups was kept at the end of any one arm of the maze and allowed to explore all the three arms. The sequence and the number of arm entries were recorded visually for each rat over a period of 5 min. An actual "alteration" was defined as entries in all three arms in consecutive choices (i.e., ABC, BCA, or CAB but not BAB). Repeat arm entry was considered as a sign of memory impairment. The number of arm entries indicated locomotor activity. The "alteration score" for each rat was calculated using the equation:

$$\%\ \text{spontaneous alteration performance} = [\text{no. of altered entries}/\text{no. of repeated entries}] \times 100$$

Acute Toxicity Study. Wistar female rats (200−250 g) were used to determine the acute toxicity of the test compound **23e**. During the experiment, animals were maintained with free access of food and water ad libitum. Compound **23e** was suspended in 0.5% CMC−Na and given orally to the experimental groups. After administration of the test compound, the animals were observed continuously for the first 4 h for any abnormal behavior and mortality. Afterward, the animals were observed intermittently for the next 24 h and occasionally for 14 consecutive days after administration of compound **23e**. After 14 days, the animals were sacrificed and examined macroscopically for possible damage to the heart, liver, and kidneys.

Computational Studies. *Docking Studies.* Docking studies were performed with Glide module of Schrodinger Suite. Glide is projected for screening of probable ligands based on binding mode and affinity for a given receptor molecule. It performs grid-based ligand docking and searches for promising interactions between ligand molecules and a macromolecule, typically a protein. The 3D structures of ligand molecules were built within Maestro[93] using the Build module, and a single low energy conformation search was carried out for all molecules under study using the OPLS_2005 force field at physiological pH conditions using the LigPrep module of Schrödinger, keeping all parameters at standard values. The 3D crystallographic structures of AChE (PDB code: 2CKM, 1B41) and of BuChE (PDB code: 4BDS) were obtained from the RCSB Protein Data Bank[94] and prepared for docking with the protein preparation wizard of Schrödinger. The grid was generated on the active site of the respective receptor structure and was validated by redocking the preexisting cocrystallized ligand structures. Docking calculations for the minimized 3D ligand structures were performed in extra precision (XP) mode within the active sites of the receptor structures. This docking protocol was validated by comparing the interactions of the docked conformer of donepezil in the active site of AChE with the reported literature.[95]

DOI: 10.1021/acschemneuro.9b00226
ACS Chem. Neurosci. 2019, 10, 3635−3661

Molecular Dynamics Simulations. Maestro−Desmond (based on the OPLS-2005 force field) was used to perform the molecular dynamics simulation study of the molecule **23e**.[96−98] To begin, the system was solvated with the TIP3P water model in an orthorhombic box of 10 Å^3 and neutralized by Na^+ ions for AChE and by Cl^- ions for BuChE. The long-range electrostatic interactions were studied by smooth particle-mesh Ewald (PME) approximation, and the nonbonded interactions were analyzed by using a MSHAKE algorithm with a cutoff of 9 Å. The default "six step relaxation protocol" was followed to relax the system, which was involved with both restrained as well as unrestrained minimizations (2 steps) chased by the equilibration processes (4 steps). The productive MD was carried out for 20 ns with the NPT ensemble at 300 K and 1 atm pressure using a Nosé−Hoover thermostat and Martyna−Tuckerman−Klein barostat. The coordinates and energies were noted at every 10 and 1.2 ps, respectively. The ligand−protein complex stability was analyzed by determining the root-mean-square deviation of the protein (RMSD-P), root-mean-square fluctuation of the protein (RMSF-P), root-mean-square deviation of the ligand (RMSD-L), molecular surface area (MolSA), solvent-accessible surface area (SASA), radius-of-gyration (rGyr), and polar surface area (PSA).

In Silico Prediction of Physicochemical and Pharmacokinetics Parameters. In silico prediction of physicochemical and pharmacokinetic properties was carried out with QikProp program v 3.5 (Schrodinger LLC, New York).[71] The structures of the ligand molecules were built within Maestro using the Build module, and a single low energy conformation search was carried out for all molecules under study using OPLS_2005 force field at physiological pH condition using LigPrep module of Schrödinger. These structures were used for Qik-Prop to determine various physicochemical and pharmacokinetic descriptors. There were 51 properties predicted by the software. The major descriptors that were considered in this study were Lipinski's rule of five (Rule of 5); NRB, number of rotatable bonds; PSA, polar surface area; SASA, total solvent accessible surface area; CNS, predicted central nervous system activity; QPPMDCK, predicted apparent MDCK cell permeability; QPPCaco, Caco-2 cell permeability in nm/s; QPlogBB, brain/blood partition coefficient; QPlogKhsa, binding to human serum albumin; QPlogS, predicted aqueous solubility; and percent human-oral Absorption, human oral absorption.

■ ASSOCIATED CONTENT

Supporting Information

The Supporting Information is available free of charge on the ACS Publications website at DOI: 10.1021/acschemneuro.9b00226.

HPLC methods, spectral data of synthesized compounds, and in vitro blood-brain barrier permeation assay data (PDF)

Docking pose of compound **23e** within AChE (PDB)

Docking pose of compound **23e** within BuChE (PDB)

■ AUTHOR INFORMATION

Corresponding Author

*Tel.: +91 265 2434187. Fax: +91 265 2418927. E-mail: mryadav11@yahoo.co.in.

Author Contributions

D.V.P., N.R.P., and A.M.K. performed synthesis and collected data. D.D.K., S.B.P., P.N.U., K.B.P., and D.B.S. contributed reagents and materials and assisted in synthesis and data collection. A.M.K. designed and performed computational studies. K.V.P. drafted the biological evaluation studies. S.P.P., A.S., and A.R.M. performed biological studies and collected data. P.R.M. and N.K.P. helped in synthesis and data interpretation. D.V.P. and N.R.P. wrote the manuscript. M.R.Y. conceived and designed the study and approved the final version of the manuscript.

Funding

M.R.Y. is thankful to the University Grant Commission (UGC), New Delhi, for providing UGC-BSR Faculty Fellowship [No. F.18-1/2011(BSR)]. D.V.P. gratefully acknowledges the DST-INSPIRE, New Delhi for awarding Research Fellowship (IF-150660). N.R.P. is thankful to the UGC, New Delhi, for awarding Senior Research Fellowship [F. No. 25-1/2014-15(BSR)/7-129/2007/(BSR)].

Notes

The authors declare no competing financial interest.

■ ACKNOWLEDGMENTS

The authors are thankful to Bharat Senta for his generous help in carrying out HPLC analysis of final compounds.

■ ABBREVIATIONS USED

ACh, acetylcholine; AChE, acetylcholinesterase; AD, Alzheimer's disease; ADME, absorption, distribution, metabolism, and excretion; ATCI, acetylthiocholine iodide; BBB, blood-brain barrier; BTCI, butyrylthiocholine iodide; BuChE, butyrylcholinesterase; CAS, catalytic active site; CAT, catalase; ChEs, cholinesterases; DMEM, Dulbecco's modified Eagle's medium; DPPH, 1,1-diphenyl-2-picrylhydrazyl; DSC, differential scanning calorimetry; DTNB, 5,5′-dithiobis(2-nitrobenzoic acid); ELT, escape latency time; FBS, fetal bovine serum; % HOA, human oral absorption percent; IAEC, institutional animal ethics committee; mCPBA, *meta*-chloroperbenzoic acid; MDA, malondialdehyde; MolSA, molecular surface area; MTDLs, multitarget-directed ligands; MTT, 3-(4,5-dimethylthiazol-2-yl)-2,5-diphenyltetrazolium bromide; MWM, Morris water maze; NCE, new chemical entity; NRB, number of rotatable bonds; PAMPA, parallel artificial membrane permeation assay; PAS, peripheral anionic site; PBL, porcine brain lipid; PBS, phosphate buffer saline; PSA, polar surface area; rGyr, radius of gyration; RMSD-L, root-mean-square deviation of the ligand; RMSD-P, root-mean-square deviation of the protein; RMSF-P, root-mean-square fluctuation of the protein; ROS, reactive oxygen species; SASA, solvent-accessible surface area; SI, selectivity index; TBARS, thiobarbituric acid reactive substances; THF, tetrahydrofuran; TLC, thin layer chromatography; TPSA, topological polar surface area; UV, ultraviolet; XP, extra precision

■ REFERENCES

(1) Scheltens, P., Blennow, K., Breteler, M. M. B., de Strooper, B., Frisoni, G. B., Salloway, S., and Van der Flier, W. M. (2016) Alzheimer's disease. *Lancet 388*, 505−517.

(2) Patterson, C. (2018) *World Alzheimer Report 2018: The State of the Art of Dementia Research: New Frontiers*, pp 32− 36, Alzheimer's Disease International, London.

(3) Talesa, V. N. (2001) Acetylcholinesterase in Alzheimer's disease. *Mech. Ageing Dev. 122*, 1961−1969.

(4) Selkoe, D. J. (2003) Folding proteins in fatal ways. *Nature 426*, 900.

(5) Hardy, J. A., and Higgins, G. A. (1992) Alzheimer's disease: the amyloid cascade hypothesis. *Science 256*, 184.

(6) Maccioni, R. B., Farías, G., Morales, I., and Navarrete, L. (2010) The revitalized tau hypothesis on Alzheimer's disease. *Arch. Med. Res. 41*, 226−231.

(7) Chu, D., and Liu, F. (2019) Pathological changes of tau related to Alzheimer's Disease. *ACS Chem. Neurosci. 10*, 931−944.

DOI: 10.1021/acschemneuro.9b00226
ACS Chem. Neurosci. 2019, 10, 3635−3661

(8) Greenough, M. A., Camakaris, J., and Bush, A. I. (2013) Metal dyshomeostasis and oxidative stress in Alzheimer's disease. *Neurochem. Int. 62*, 540−555.
(9) Bonda, D. J., Wang, X., Perry, G., Nunomura, A., Tabaton, M., Zhu, X., and Smith, M. A. (2010) Oxidative stress in Alzheimer disease: a possibility for prevention. *Neuropharmacology 59*, 290−294.
(10) Maruszak, A., and Żekanowski, C. (2011) Mitochondrial dysfunction and Alzheimer's disease. *Prog. Neuro-Psychopharmacol. Biol. Psychiatry 35*, 320−330.
(11) Heneka, M. T., Carson, M. J., El Khoury, J., Landreth, G. E., Brosseron, F., Feinstein, D. L., Jacobs, A. H., Wyss-Coray, T., Vitorica, J., Ransohoff, R. M., et al. (2015) Neuroinflammation in Alzheimer's disease. *Lancet Neurol. 14*, 388−405.
(12) Fu, W. Y., Wang, X., and Ip, N. Y. (2019) Targeting neuroinflammation as a therapeutic strategy for alzheimer's disease: mechanisms, drug candidates, and new opportunities. *ACS Chem. Neurosci. 10*, 872−879.
(13) Del Pino, J., Marco-Contelles, J., Lopez-Munoz, F., Romero, A., and Ramos, E. (2018) Neuroinflammation signaling modulated by Ass234, a multitarget small molecule for Alzheimer's disease therapy. *ACS Chem. Neurosci. 9*, 2880−2885.
(14) Agis-Torres, A., Sollhuber, M., Fernandez, M., and Sanchez-Montero, J. (2014) Multi-target-directed ligands and other therapeutic strategies in the search of a real solution for Alzheimer's disease. *Curr. Neuropharmacol. 12*, 2−36.
(15) Bajda, M., Guzior, N., Ignasik, M., and Malawska, B. (2011) Multi-target-directed ligands in Alzheimer's disease treatment. *Curr. Med. Chem. 18*, 4949−4975.
(16) Oset-Gasque, M. J., and Marco-Contelles, J. (2018) Alzheimer's disease, the "one-molecule, one-target" paradigm, and the multitarget directed ligand approach. *ACS Chem. Neurosci. 9*, 401−403.
(17) Wang, T., Liu, X. H., Guan, J., Ge, S., Wu, M. B., Lin, J. P., and Yang, L. R. (2019) Advancement of multi-target drug discoveries and promising applications in the field of Alzheimer's disease. *Eur. J. Med. Chem. 169*, 200−223.
(18) Csermely, P., Agoston, V., and Pongor, S. (2005) The efficiency of multi-target drugs: the network approach might help drug design. *Trends Pharmacol. Sci. 26*, 178−182.
(19) Morphy, J. R. (2012) The challenges of multi-target lead optimization. In *Designing Multi-Target Drugs* (Morphy, J. R., and Harris, C. J., Eds.), pp 141−154, Royal Society of Chemistry.
(20) Cavalli, A., Bolognesi, M. L., Minarini, A., Rosini, M., Tumiatti, V., Recanatini, M., and Melchiorre, C. (2008) Multi-target-directed ligands to combat neurodegenerative diseases. *J. Med. Chem. 51*, 347−372.
(21) Greig, N. H., Lahiri, D. K., and Sambamurti, K. (2002) Butyrylcholinesterase: an important new target in Alzheimer's disease therapy. *Int. Psychogeriatr. 14*, 77−91.
(22) Jing, L., Wu, G., Kang, D., Zhou, Z., Song, Y., Liu, X., and Zhan, P. (2019) Contemporary medicinal-chemistry strategies for the discovery of selective butyrylcholinesterase inhibitors. *Drug Discovery Today 24*, 629−635.
(23) Sussman, J. L., Harel, M., Frolow, F., Oefner, C., Goldman, A., Toker, L., and Silman, I. (1991) Atomic structure of acetylcholinesterase from Torpedo californica: a prototypic acetylcholine-binding protein. *Science 253*, 872−879.
(24) De Ferrari, G. V., Canales, M. A., Shin, I., Weiner, L. M., Silman, I., and Inestrosa, N. C. (2001) A structural motif of acetylcholinesterase that promotes amyloid β-peptide fibril formation. *Biochemistry 40*, 10447−10457.
(25) Dinamarca, M. C., Sagal, J. P., Quintanilla, R. A., Godoy, J. A., Arrázola, M. S., and Inestrosa, N. C. (2010) Amyloid-β-Acetylcholinesterase complexes potentiate neurodegenerative changes induced by the Aβ peptide. Implications for the pathogenesis of Alzheimer's disease. *Mol. Neurodegener. 5*, 4.
(26) Wang, Y., Wang, H., and Chen, H. (2016) AChE inhibition-based multi-target-directed ligands, a novel pharmacological approach for the symptomatic and disease-modifying therapy of Alzheimer's disease. *Curr. Neuropharmacol. 14*, 364−375.
(27) Hartmann, J., Kiewert, C., Duysen, E. G., Lockridge, O., Greig, N. H., and Klein, J. (2007) Excessive hippocampal acetylcholine levels in acetylcholinesterase-deficient mice are moderated by butyrylcholinesterase activity. *J. Neurochem. 100*, 1421−1429.
(28) Arendt, T., Bigl, V., Walther, F., and Sonntag, M. (1984) Decreased ratio of CSF acetylcholinesterase to butyrylcholinesterase activity in Alzheimer's disease. *Lancet 323*, 173.
(29) Kosak, U., Brus, B., Knez, D., Zakelj, S., Trontelj, J., Pislar, A., Sink, R., Jukic, M., Zivin, M., Podkowa, A., et al. (2018) The magic of crystal structure-based inhibitor optimization: development of a butyrylcholinesterase inhibitor with picomolar affinity and in vivo activity. *J. Med. Chem. 61*, 119−139.
(30) Geula, C., and Mesulam, M. (1995) Cholinesterases and the pathology of Alzheimer disease. *Alzheimer Dis. Assoc. Disord. 9*, 23.
(31) Guillozet, A., Mesulam, M. M., Smiley, J., and Mash, D. (1997) Butyrylcholinesterase in the life cycle of amyloid plaques. *Ann. Neurol. 42*, 909−918.
(32) Mishra, P., Kumar, A., and Panda, G. (2019) Anti-cholinesterase hybrids as multi-target-directed ligands against Alzheimer's disease (1998−2018). *Bioorg. Med. Chem. 27*, 895−930.
(33) Jakob-Roetne, R., and Jacobsen, H. (2009) Alzheimer's disease: from pathology to therapeutic approaches. *Angew. Chem., Int. Ed. 48*, 3030−3059.
(34) Uttara, B., Singh, A. V., Zamboni, P., and Mahajan, R. (2009) Oxidative stress and neurodegenerative diseases: a review of upstream and downstream antioxidant therapeutic options. *Curr. Neuropharmacol. 7*, 65−74.
(35) Zhao, Y., and Zhao, B. (2013) Oxidative stress and the pathogenesis of Alzheimer's disease. *Oxid. Med. Cell. Longevity 2013*, 316523.
(36) Mecocci, P., and Polidori, M. C. (2012) Antioxidant clinical trials in mild cognitive impairment and Alzheimer's disease. *Biochim. Biophys. Acta, Mol. Basis Dis. 1822*, 631−638.
(37) Sharma, V., Kumar, P., and Pathak, D. (2010) Biological importance of the indole nucleus in recent years: a comprehensive review. *J. Heterocycl. Chem. 47*, 491−502.
(38) Kaushik, N., Kaushik, N., Attri, P., Kumar, N., Kim, C., Verma, A., and Choi, E. (2013) Biomedical importance of indoles. *Molecules 18*, 6620−6662.
(39) Zhou, J. N., Liu, R. Y., Kamphorst, W., Hofman, M. A., and Swaab, D. F. (2003) Early neuropathological Alzheimer's changes in aged individuals are accompanied by decreased cerebrospinal fluid melatonin levels. *J. Pineal Res. 35*, 125−130.
(40) Wu, Y. H., Feenstra, M. G., Zhou, J. N., Liu, R. Y., Toranõ, J. S., Van Kan, H. J., Fischer, D. F., Ravid, R., and Swaab, D. F. (2003) Molecular changes underlying reduced pineal melatonin levels in Alzheimer disease: alterations in preclinical and clinical stages. *J. Clin. Endocrinol. Metab. 88*, 5898−5906.
(41) Wu, Y. H., and Swaab, D. F. (2005) The human pineal gland and melatonin in aging and Alzheimer's disease. *J. Pineal Res. 38*, 145−152.
(42) Pandi-Perumal, S. R., Srinivasan, V., Maestroni, G., Cardinali, D., Poeggeler, B., and Hardeland, R. (2006) Melatonin: Nature's most versatile biological signal. *FEBS J. 273*, 2813−2838.
(43) Feng, Z., and Zhang, J. T. (2004) Melatonin reduces amyloid β-induced apoptosis in pheochromocytoma (PC12) cells. *J. Pineal Res. 37*, 257−266.
(44) Espinar, A., García-Oliva, A., Isorna, E. M., Quesada, A., Prada, F. A., and Guerrero, J. M. (2000) Neuroprotection by melatonin from glutamate-induced excitotoxicity during development of the cerebellum in the chick embryo. *J. Pineal Res. 28*, 81−88.
(45) Aydogan, S., Yerer, M. B., and Goktas, A. (2006) Melatonin and nitric oxide. *J. Endocrinol. Invest. 29*, 281−287.
(46) Rodríguez-Franco, M. I., Fernández-Bachiller, M. I., Pérez, C., Hernández-Ledesma, B., and Bartolomé, B. (2006) Novel tacrine-melatonin hybrids as dual-acting drugs for Alzheimer disease, with improved acetylcholinesterase inhibitory and antioxidant properties. *J. Med. Chem. 49*, 459−462.

DOI: 10.1021/acschemneuro.9b00226
ACS Chem. Neurosci. 2019, 10, 3635−3661

(47) Pachon-Angona, I., Refouvelet, B., Andrýs, R., Martin, H., Luzet, V., Iriepa, I., Moraleda, I., Diez-Iriepa, D., Oset-Gasque, M. J., Marco-Contelles, J., et al. (2019) Donepezil-chromone-melatonin hybrids as promising agents for Alzheimer's disease therapy. *J. Enzyme Inhib. Med. Chem. 34*, 479−489.
(48) Lopez-Iglesias, B., Pérez, C. N., Morales-Garcia, J. A., Alonso-Gil, S., Pérez-Castillo, A., Romero, A., López, M. G., Villarroya, M., Conde, S., and Rodríguez-Franco, M. I. (2014) New melatonin-*N*, *N*-dibenzyl (*N*-methyl) amine hybrids: Potent neurogenic agents with antioxidant, cholinergic, and neuroprotective properties as innovative drugs for Alzheimer's disease. *J. Med. Chem. 57*, 3773−3785.
(49) Yanovsky, I., Finkin-Groner, E., Zaikin, A., Lerman, L., Shalom, H., Zeeli, S., Weill, T., Ginsburg, I., Nudelman, A., and Weinstock, M. (2012) Carbamate derivatives of indolines as cholinesterase inhibitors and antioxidants for the treatment of Alzheimer's disease. *J. Med. Chem. 55*, 10700−10715.
(50) Kumar, R., Sirohi, T., Singh, H., Yadav, R., Roy, R., Chaudhary, A., and Pandeya, S. (2014) 1,2,4-triazine analogs as novel class of therapeutic agents. *Mini-Rev. Med. Chem. 14*, 168−207.
(51) Irannejad, H., Amini, M., Khodagholi, F., Ansari, N., Tusi, S. K., Sharifzadeh, M., and Shafiee, A. (2010) Synthesis and in vitro evaluation of novel 1,2,4-triazine derivatives as neuroprotective agents. *Bioorg. Med. Chem. 18*, 4224−4230.
(52) Veloso, A. J., Chow, A. M., Dhar, D., Tang, D. W., Ganesh, H. V., Mikhaylichenko, S., Brown, I. R., and Kerman, K. (2013) Biological activity of sym-triazines with acetylcholine-like substitutions as multitarget modulators of Alzheimer's disease. *ACS Chem. Neurosci. 4*, 924−929.
(53) Veloso, A. J., Dhar, D., Chow, A. M., Zhang, B., Tang, D. W., Ganesh, H. V., Mikhaylichenko, S., Brown, I. R., and Kerman, K. (2013) sym-Triazines for directed multitarget modulation of cholinesterases and amyloid-β in Alzheimer's disease. *ACS Chem. Neurosci. 4*, 339−349.
(54) Tripathi, P. N., Srivastava, P., Sharma, P., Tripathi, M. K., Seth, A., Tripathi, A., Rai, S. N., Singh, S. P., and Shrivastava, S. K. (2019) Biphenyl-3-oxo-1,2,4-triazine linked piperazine derivatives as potential cholinesterase inhibitors with anti-oxidant property to improve the learning and memory. *Bioorg. Chem. 85*, 82−96.
(55) Russell, M. G., Carling, R. W., Street, L. J., Hallett, D. J., Goodacre, S., Mezzogori, E., Reader, M., Cook, S. M., Bromidge, F. A., Newman, R., et al. (2006) Discovery of imidazo[1,2-*b*][1,2,4]-triazines as GABAA α2/3 subtype selective agonists for the treatment of anxiety. *J. Med. Chem. 49*, 1235−1238.
(56) Leach, M. J., Marden, C. M., and Miller, A. A. (1986) Pharmacological studies on lamotrigine, a novel potential antiepileptic drug. *Epilepsia 27*, 490−497.
(57) Misra, U., Hitkari, A., Saxena, A., Gurtu, S., and Shanker, K. (1996) Biologically active indolylmethyl-1,3,4-oxadiazoles, 1,3,4-thiadiazoles, 4*H*-1,3,4-triazoles and 1,2,4-triazines. *Eur. J. Med. Chem. 31*, 629−634.
(58) Ansari, N., Khodagholi, F., Ramin, M., Amini, M., Irannejad, H., Dargahi, L., and Amirabad, A. D. (2010) Inhibition of LPS-induced apoptosis in differentiated-PC12 cells by new triazine derivatives through NF-κB-mediated suppression of COX-2. *Neurochem. Int. 57*, 958−968.
(59) Sinha, A., Tamboli, R. S., Seth, B., Kanhed, A. M., Tiwari, S. K., Agarwal, S., Nair, S., Giridhar, R., Chaturvedi, R. K., and Yadav, M. R. (2015) Neuroprotective role of novel triazine derivatives by activating Wnt/β catenin signaling pathway in rodent models of Alzheimer's disease. *Mol. Neurobiol. 52*, 638−652.
(60) Tamboli, R. S., Giridhar, R., Gandhi, H. P., Kanhed, A. M., Mande, H. M., and Yadav, M. R. (2016) Design, green synthesis and pharmacological evaluation of novel 5,6-diaryl-1,2,4-triazines bearing 3-morpholinoethylamine moiety as potential antithrombotic agents. *J. Enzyme Inhib. Med. Chem. 31*, 704−713.
(61) Shidore, M., Machhi, J., Shingala, K., Murumkar, P., Sharma, M. K., Agrawal, N., Tripathi, A., Parikh, Z., Pillai, P., and Yadav, M. R. (2016) Benzylpiperidine-linked diarylthiazoles as potential anti-Alzheimer's agents: synthesis and biological evaluation. *J. Med. Chem. 59*, 5823−5846.
(62) Kanhed, A. M., Sinha, A., Machhi, J., Tripathi, A., Parikh, Z. S., Pillai, P. P., Giridhar, R., and Yadav, M. R. (2015) Discovery of isoalloxazine derivatives as a new class of potential anti-Alzheimer agents and their synthesis. *Bioorg. Chem. 61*, 7−12.
(63) Saxena, A., Redman, A. M., Jiang, X., Lockridge, O., and Doctor, B. (1997) Differences in active site gorge dimensions of cholinesterases revealed by binding of inhibitors to human butyrylcholinesterase. *Biochemistry 36*, 14642−14651.
(64) Kedare, S. B., and Singh, R. (2011) Genesis and development of DPPH method of antioxidant assay. *J. Food Sci. Technol. 48*, 412−422.
(65) Mathew, M., and Subramanian, S. (2014) In vitro screening for anti-cholinesterase and antioxidant activity of methanolic extracts of ayurvedic medicinal plants used for cognitive disorders. *PLoS One 9*, No. e86804.
(66) Porcal, W., Hernández, P., González, M., Ferreira, A., Olea-Azar, C., Cerecetto, H., and Castro, A. (2008) Heteroarylnitrones as drugs for neurodegenerative diseases: synthesis, neuroprotective properties, and free radical scavenger properties. *J. Med. Chem. 51*, 6150−6159.
(67) Dahlgren, K. N., Manelli, A. M., Stine, W. B., Baker, L. K., Krafft, G. A., and LaDu, M. J. (2002) Oligomeric and fibrillar species of amyloid-β peptides differentially affect neuronal viability. *J. Biol. Chem. 277*, 32046−32053.
(68) Di, L., Kerns, E. H., Fan, K., McConnell, O. J., and Carter, G. T. (2003) High throughput artificial membrane permeability assay for blood−brain barrier. *Eur. J. Med. Chem. 38*, 223−232.
(69) Di, L., Kerns, E. H., Bezar, I. F., Petusky, S. L., and Huang, Y. (2009) Comparison of blood−brain barrier permeability assays: in situ brain perfusion, MDR1-MDCKII and PAMPA-BBB. *J. Pharm. Sci. 98*, 1980−1991.
(70) Wang, J., and Urban, L. (2004) The impact of early ADME profiling on drug discovery and development strategy. *Drug Discovery World 5*, 73−86.
(71) *QikProp*, version 3.5, Schrödinger, LLC, New York, 2012.
(72) Lipinski, C. A., Lombardo, F., Dominy, B. W., and Feeney, P. J. (1997) Experimental and computational approaches to estimate solubility and permeability in drug discovery and development settings. *Adv. Drug Delivery Rev. 23*, 3−25.
(73) Veber, D. F., Johnson, S. R., Cheng, H. Y., Smith, B. R., Ward, K. W., and Kopple, K. D. (2002) Molecular properties that influence the oral bioavailability of drug candidates. *J. Med. Chem. 45*, 2615−2623.
(74) Kelder, J., Grootenhuis, P. D., Bayada, D. M., Delbressine, L. P., and Ploemen, J. P. (1999) Polar molecular surface as a dominating determinant for oral absorption and brain penetration of drugs. *Pharm. Res. 16*, 1514−1519.
(75) Pajouhesh, H., and Lenz, G. R. (2005) Medicinal chemical properties of successful central nervous system drugs. *NeuroRx 2*, 541−553.
(76) Waterhouse, R. N. (2003) Determination of lipophilicity and its use as a predictor of blood-brain barrier penetration of molecular imaging agents. *Mol. Imaging Biol. 5*, 376−389.
(77) Wang, Q., Rager, J. D., Weinstein, K., Kardos, P. S., Dobson, G. L., Li, J., and Hidalgo, I. J. (2005) Evaluation of the MDR-MDCK cell line as a permeability screen for the blood-brain barrier. *Int. J. Pharm. 288*, 349−359.
(78) Chen, J., Long, Y., Han, M., Wang, T., Chen, Q., and Wang, R. (2008) Water-soluble derivative of propolis mitigates scopolamine-induced learning and memory impairment in mice. *Pharmacol., Biochem. Behav. 90*, 441−446.
(79) Lee, M. R., Yun, B. S., Park, S. Y., Ly, S. Y., Kim, S. N., Han, B. H., and Sung, C. K. (2010) Anti-amnesic effect of Chong−Myung−Tang on scopolamine-induced memory impairments in mice. *J. Ethnopharmacol. 132*, 70−74.
(80) Goverdhan, P., Sravanthi, A., and Mamatha, T. (2012) Neuroprotective effects of meloxicam and selegiline in scopolamine-

DOI: 10.1021/acschemneuro.9b00226
ACS Chem. Neurosci. 2019, 10, 3635−3661

induced cognitive impairment and oxidative stress. *Int. J. Alzheimer's Dis. 2012*, 1−8.
(81) Morris, R. (1984) Developments of a water-maze procedure for studying spatial learning in the rat. *J. Neurosci. Methods 11*, 47−60.
(82) Chumakov, I., Nabirotchkin, S., Cholet, N., Milet, A., Boucard, A., Toulorge, D., Pereira, Y., Graudens, E., Traoré, S., Foucquier, J., et al. (2015) Combining two repurposed drugs as a promising approach for Alzheimer's disease therapy. *Sci. Rep. 5*, 7608.
(83) Rosenbrock, H., Giovannini, R., Schmid, B., Kramer, G., Arban, R., Dorner-Ciossek, C., and Wunderlich, G. (2016) Improving cognitive function in rodents via increasing glycine levels in brain by the novel glycine transporter-1 inhibitor BI 425809. *Alzheimer's Dementia 12*, 1018.
(84) Rosenbrock, H., Desch, M., Kleiner, O., Dorner-Ciossek, C., Schmid, B., Keller, S., Schlecker, C., Moschetti, V., Goetz, S., Liesenfeld, K. H., et al. (2018) Evaluation of pharmacokinetics and pharmacodynamics of BI 425809, a novel GlyT1 inhibitor: translational studies. *Clin. Transl. Sci. 11*, 616−623.
(85) Camacho, A., and Massieu, L. (2006) Role of glutamate transporters in the clearance and release of glutamate during ischemia and its relation to neuronal death. *Arch. Med. Res. 37*, 11−18.
(86) Sattler, R., and Rothstein, J. (2006) Regulation and dysregulation of glutamate transporters. In *Neurotransmitter Transporters. Handbook of Experimental Pharmacology* (Sitte, H. H., and Freissmuth, M., Eds.), Vol. *175*, pp 277−303, Springer, Berlin, Heidelberg.
(87) Mattson, M. P. (2007) Calcium and neurodegeneration. *Aging Cell 6*, 337−350.
(88) Yan, J. J., Cho, J. Y., Kim, H. S., Kim, K. L., Jung, J. S., Huh, S. O., Suh, H. W., Kim, Y. H., and Song, D. K. (2001) Protection against *β*-amyloid peptide toxicity in vivo with long-term administration of ferulic acid. *Br. J. Pharmacol. 133*, 89−96.
(89) OECD (2002) *Test No. 423: Acute Oral toxicity - Acute Toxic Class Method*.
(90) El Ashry, E. S. H., Ramadan, E. S., Hamid, H. M., and Hagar, M. (2004) Microwave irradiation for accelerating each step for the synthesis of 1,2,4-triazino [5,6-*b*]indole-3-thiols and their derivatives from isatin and 5-chloroisatin. *Synlett 2004*, 723−725.
(91) Hou, D. R., Cheng, H. Y., and Wang, E. C. (2004) Efficient syntheses of oncinotine and neooncinotine. *J. Org. Chem. 69*, 6094−6099.
(92) Monge-Acuna, A. A., and Fornaguera-Trías, J. (2009) A high performance liquid chromatography method with electrochemical detection of gamma-aminobutyric acid, glutamate and glutamine in rat brain homogenates. *J. Neurosci. Methods 183* (2), 176−181.
(93) *Maestro*, version 9.0, Schrodinger, LLC, New York, 2009.
(94) Protein Data Bank, www.rcsb.org/pdb/home/home.do (accessed Jan. 09, 2019).
(95) Cheung, J., Rudolph, M. J., Burshteyn, F., Cassidy, M. S., Gary, E. N., Love, J., Franklin, M. C., and Height, J. J. (2012) Structures of human acetylcholinesterase in complex with pharmacologically important ligands. *J. Med. Chem. 55*, 10282−10286.
(96) Patel, N. R., Patel, D. V., Kanhed, A. M., Patel, S. P., Patel, K. V., Afosah, D., Desai, U. R., Karpoormath, R., and Yadav, M. R. (2019) 2-Aminobenzamide-based factor Xa inhibitors with novel mono-and bi-aryls as S4 binding elements. *Chemistry Select 4*, 802−809.
(97) Bowers, K. J., Chow, D. E., Xu, H., Dror, R. O., Eastwood, M. P., Gregersen, B. A., Klepeis, J. L., Kolossvary, I., Moraes, M. A., and Sacerdoti, F. D. (2006) *Scalable algorithms for molecular dynamics simulations on commodity clusters*, SC 2006 Conference, Proceedings of the ACM/IEEE, pp 43−43, IEEE.
(98) Tuckerman, M., Berne, B. J., and Martyna, G. J. (1992) Reversible multiple time scale molecular dynamics. *J. Chem. Phys. 97*, 1990−2001.

DOI: 10.1021/acschemneuro.9b00226
ACS Chem. Neurosci. 2019, 10, 3635−3661

ChemPubSoc Europe

DOI: 10.1002/slct.201803237

Chemistry SELECT Full Papers

Sustainable Chemistry

Improved Rapid and Green Synthesis of *N*-Aryl Piperazine Hydrochlorides Using Synergistic Coupling of Hydrated Task Specific Ionic Liquid ([Bbim]OH) and Microwave Irradiation

Riyaj S. Tamboli[+],[a] Mahesh M. Shidore[+],[a] Radha Charan Dash,[b] Ashish M. Kanhed,[a] Nirav R. Patel,[a] Shailesh R. Shah,[c] and Mangeram R. Yadav*[a]

Dedicated to fond memory of Late Prof. Rajani Giridhar

An improved and rapid green synthesis of *N*-alkyl/aryl piperazine hydrochlorides using synergistic coupling of hydrated Task Specific Ionic Liquid ([Bbim]OH) and Microwave Irradiation (MWI) has been described. The protocol worked well with good yields for electron withdrawing as well as electron donating groups in aryl amines to provide the respective aryl piperazine hydrochlorides. Presence of other labile groups like hydroxyl and thiol in the aryl amines remained unaffected. The said TSIL could be reused upto five cycles without an appreciable loss of the catalytic activity. It is proposed that [Bbim]OH along with a water molecule is able to catalyse the reaction due to symphoria. The proposed mechanism is supported by DFT and molecular dynamics studies. The use of hydrated TSIL like ([Bbim]OH) as reaction media may open new gates in green organic syntheses.

Introduction

N-Aryl piperazines are used as important intermediates for the synthesis[1] of biologically active ligands for modulating serotonin, dopamine and monoamine transport in neuroscience.[2–4] They are important structural components of many drugs used in the treatment of neurodegenerative diseases like Alzheimer's and Parkinson's.[5,6]

N-Aryl piperazines are reported to be synthesized in the literature by two common approaches. In the first approach, piperazine ring is attached directly to the aryl ring while in the second approach anilines are cyclized with mustard like compounds. In the first approach, some well established syntheses utilize Pd or Ni catalyzed reactions *e.g.* Buchwald-Hartwig reaction,[7] Cu mediated Ullmann reaction,[8a] nucleophilic substitution reaction through benzyne intermediates[8b] and use of transition metal complexes.[9] All these protocols have one or the other disadvantage like formation of undesired diarylated products, harsh reaction conditions, formation of more than one regioisomers, need for activation of the reactants by resins[10] or metals, use of monoprotected diamines,[11a–c] excessive use of reagents,[12a] special catalytic systems like Ni/bipyridine,[12b] Pd/BINAP[11d] *etc.* which make these methods commercially uneconomical. Base-mediated reaction of anilines with *N,N-bis*(2-bromoethyl)amine in methanol was developed by Prelog in 1930's as an alternative approach.[13] Modifications have been done subsequently in this protocol by substituting the solvent and the base but practical problems like longer reaction times, existence of substrate specific reactivity (electron rich and electron deficient anilines showing huge differences in yields), high temperature conditions and low reaction yields *etc.* still persisted. An interesting synthesis by intramolecular ring opening of 2-oxazolidinone derivatives has also been reported.[14] Some alternative protocols were also developed like the use of diglyme and catalytic iodine,[15] diethylene glycol monomethyl ether (DEGMME),[16a] basic alumina,[16b,c] microwave assisted synthesis in PEG,[17a,b] use of corrosive hydrochloric acid,[17c] resin immobilization with metal complexes[18] and Wang resin;[19] but all of them suffer from one or the other above-mentioned problems. The electro-deficient and sterically-hindered anilines have rarely been used as reactants in these protocols due to

[a] *Dr. R. S. Tamboli,[+] Dr. M. M. Shidore,[+] Dr. A. M. Kanhed, N. R. Patel, Prof. M. R. Yadav*
Faculty of Pharmacy, Kalabhavan Campus,
The Maharaja Sayajirao University of Baroda, Vadodara-390001, Gujarat, India
Tel.: +91 265 2434187
fax: +91 265 2418927
E-mail: mryadav11@yahoo.co.in
[b] *Dr. R. C. Dash*
Visiting research associate,
Faculty of Pharmacy, Kalabhavan Campus,
The Maharaja Sayajirao University of Baroda, Vadodara 390 001, Gujarat, India
[c] *Dr. S. R. Shah*
Department of Chemistry,
Faculty of Science, Sayajiganj,
The Maharaja Sayajirao University of Baroda, Vadodara 390 001, Gujarat, India
[+] *Both are first authors*

Supporting information for this article is available on the WWW under https://doi.org/10.1002/slct.201803237

lack of high driving force for such reactions resulting into lower yields. To the best of our knowledge, an ionic liquid promoted microwave assisted synthesis of aryl piperazine hydrochloride salts in a single shot has not been reported till date.

Varma *et. al* and Chilin *et. al* have reported *N*-heterocyclization and *N*-alkylation under aqueous conditions using microwave irradiation.[20a–c] Water is the most preferable green solvent. However, many drawbacks like the lack of recyclability, formation of contaminated waste water, need of high pressure tubes for performing reactions including operational hazards, use of temperatures above critical point of water and the lack of selectivity are responsible for its limited industrial use in the reactions.

Recently, task specific ionic liquids (TSILs) have attracted a great deal of attention due to their high polarity, boiling points and thermal stability over a wide range of temperatures, high solubility for a variety of substrates and reactants and non-volatility to afford pollution-free synthetic protocols.[21] Interestingly TSILs have exhibited versatile qualities as catalysts in controlling the reaction rates and in offering selectivity.[22] After the successful use of chloroaluminate anion,[23a] a number of imidazolium-based ionic liquids have been developed[23b–e] with a variety of anionic species which are moisture insensitive unlike chloroaluminates.

Microwave assisted organic synthesis (MAOS)[24] has also been established as one of the green techniques for Multi-Component Reactions (MCR). The synergistic coupling of ILs and MAOS has been explored as an eco-friendly technology in organic syntheses.[25] As part of our ongoing program to develop green protocols for the synthesis of medicinally active compounds,[26] we reported synthesis of diaryltriazines catalyzed by an ionic liquid.[26b] Herein, we report an unprecedented catalysis offered by a new hydrated task-specific ionic liquid, Dibutylimidazolium Hydroxide [Bblm]OH, in cyclization reactions to obtain arylated and alkylated piperazines under microwave irradiation conditions.

Results and discussion

In our efforts to develop small molecules as CNS-active agents, we were in need of substituted *N*-aryl piperazines. It was envisaged to synthesize *N*-aryl piperazines from the corresponding anilines. Using the Prelog's protocol,[13] the reactions were first carried out in low boiling alcohols using excess anilines, resulting into poor yields. To modify these conditions higher boiling solvents like *n*-butanol,[27a] 2-butoxyethanol,[27b] chlorobenzene,[27c,d] DMF[20a] and toluene[20a] were employed at elevated temperatures in presence of K_2CO_3 as an acid scavenger offering poor to moderate yields with other undesirable features like longer reaction times and cumbersome isolation procedures. The common organic solvents (polar or nonpolar) yielded low to modest yields (Table 1; entries 1–6). Their volatile nature would still pose environmental problems. Hence, it was thought to replace these reaction conditions with ecofriendly conditions by the combined synergy of MAOS and ILs.

Table 1. Use of different solvents, bases and catalysts for the synthesis of phenylpiperazine free base by conventional oil bath heating procedure

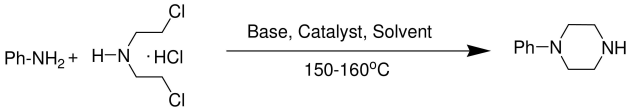

Entry	Base	Catalyst	Solvent	Yield [%][a]
1	K_2CO_3	-	Chlorobenzene	52
2	Na_2CO_3	-	Ethanol	30
3	K_2CO_3	-	*n*-Butanol	16
4	-	I_2	Diglyme	65
5	-	-	DEGMME[b]	79
6	-	Pd/ Ni	-	75
7	-	-	[Bblm]Br	NP[c]
8	-	[Hblm]BF_4	DMF	NP[c]
9	-	[Bblm]Br	DMF	NP[c]
10	-	[Hblm]BF_4	DMSO	NP[c]
11	-	[Bblm]Br	DMSO	Traces

[a] Isolated yields based on aniline as the starting material. [b] Diethylene glycol monomethyl ether. [c] No product formation as observed on TLC.

Initial experiments were performed between aniline and *N,N-bis*(2-chloroethyl)amine hydrochloride by using either neat dibutylimidazolium bromide [Bblm]Br or catalytic amounts of acidic ILs like 1-n-butylimidazolium tetrafluoroborate [Hblm]BF_4 or [Bblm]Br in DMF/DMSO (1:10)[26b,28] at 120 °C for durations upto several hours. *N,N-Bis*(2-chloroethyl)amine hydrochloride salt was preferred as the alkylating agent over the free bromo derivative as it has several advantages[29a–c,30a,b] and avoids the formation of aziridinium ion as reported earlier.[30c] Unexpectedly, none of the reactions proceeded and the starting materials only were recovered back except for the formation of traces of the product in one case (Table 1; entries 7–10 vs entry 11).

Then the same reaction was performed in ionic liquids alone without any added solvent under microwave irradiation for different time periods and temperatures, using a monomode microwave reactor (Table 2). At this stage it was thought

Table 2. Use of different ILs and DEGMME for the synthesis of phenylpiperazine HCl salt by microwave irradiation.

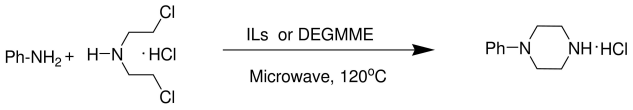

Entry	Solvent	Yield [%][a]	Time [min]
1	DEGMME[b]	80	18
2	[Bmlm]Br	20	>60
3	[Bmlm]OH	25	>60
4	[Hblm]BF_4	NP[c]	>60
5	[Bblm]BF_4	61	55
6	[Bblm]Br	80	07
7	[Bblm]OH	**92**	**03**

[a] Isolated yields based on aniline as the starting material (substrate). [b] Diethylene glycol monomethyl ether. [c] No product formation as observed on TLC.

to tune the basicity of the ionic liquid so that it would not breakdown the HCl salt into the free piperazine base. The commercially available 1-butyl-3-methylimidazolium bromide [BmIm]Br failed to give the product beyond 20% yield after 60 min of microwave irradiation (Table 2; entry 2). The previously reported 1-butyl-3-methylimidazolium hydroxide [BmIm]OH[31a,b] also did not give results upto our expectations even after 50 min of microwave irradiation (Table 2; entry 3). Further use of this IL was ruled out because of its relatively high basicity (pH *9.3*) and insufficient catalytic power. So, it was decided to prepare a new ionic liquid which would have lower basicity. This could offer three advantages - catalyze the reaction, trap the generated hydrogen chloride gas and would not break the amine hydrochloride salt as a product resulting into easy isolation of the desired product. Out of the ILs synthesized in the laboratory, [BbIm]OH was identified to be the most suitable one as its *p*H was found to be moderately basic (*p*H about *8.6*) hence, it was used in further synthetic protocols. Contrary to the literature reports,[12] the initial ratio of the substrate, the reactant and the ionic liquid was kept as 1:1:1. With [BbIm]OH as the ionic liquid the best results were obtained with this ratio, at a temperature of 120 °C in 3 min (Table 2, entry 7) offering excellent yield (92%) of the isolated product as the hydrochloride salt. The same experiment was performed with DEGMME (Table 2; entry 1) as a control solvent, but it failed to offer yields beyond 80% under these experimental conditions using even longer reaction time (18 min vs 3 min).

After identifying [BbIm]OH to be a better IL, different molar ratios of [BbIm]OH with the reactant *i.e. N,N-bis*(2-chloroethyl) amine hydrochloride (1:1, 1:1.5, 1:2, 1:3 respectively) were also tried but none of the higher ratios offered significantly better yields or caused reduction in reaction time (Table 3; entries 1–4). Higher substrate (*i.e.* aniline) ratio was also tried showing marginal increase in the yield (Table 3; entry 5). It is worthy to note that none of the reported byproducts[29] was formed in these experiments under microwave irradiation conditions.

Table 3. Effect of different proportions of the catalyst, i.e. [BbIm]OH to one equivalent of the reactant i.e. *N,N-bis*(2-chloroethyl)amine hydrochloride on the reaction time and yield of the product, i.e.phenylpiperazine hydrochloride by microwave irradiation at 120 °C.

Entry	Eq. of [BbIm]OH	Time [min]	Yield [%][a]
1	**1.0**	**05**	**92**
2	1.5	05	92
3	2.0	05	93
4	3.0	05	93
5	1.0	05	94[b]

[a] Isolated yield based on aniline as the starting material. [b] aniline used: 3 times.

Parallel experiments were also performed by using conventional heating on oil bath for the reaction of substituted anilines with *N,N-bis*(2-chloroethyl)amine hydrochloride in DEGMME as a control solvent to demonstrate the superiority of microwave irradiation over conventional heating. These reactions took much longer reaction times (8-20 hrs) and offered low to moderately good yields (15-87%) by conventional heating. Microwave irradiation showed a clear advantage by improving the overall yields and shortening the reaction times from hours to a few minutes. The IL protocol (using the reactant, substrate and TSIL in equimolar ratios) was adopted for a variety of aromatic amines having various substituents differing in electronic and steric properties (Table 4; entries 1–12). A previous study showed that these reactions were highly substrate specific[32a] and depended on steric as well as electronic factors.[27a,32b] To our pleasant surprise, all of the reactions got completed with excellent yields and high purity levels within a short span of time. This protocol was adopted uniformly for various types of anilines offering slight differences in product yields and reaction times. But noteworthy differences were not observed in the yields for *p*-fluoroaniline, *m*-nitroaniline and *p*-toluidine (Table 4; entries 3, 4 and 6 resp.) indicating that the reactions were insignificantly affected by the electronic characters of the substituents. The protocol was found to be equally valid for naphthylamine and *p*-aminobenzoic acid (Table 4; entries 8 and 10). The di- and tri-substituted anilines were also smoothly converted into their respective aryl piperazines in good yields (Table 4; entries 5 and 9).

The reaction of *p*-aminophenol (Table 5; entry 1) demonstrated chemoselectively ceasing the hydroxyl group unaffected furnishing the *N*-substituted piperazine as the sole product from the reaction, showing that the amino group was selectively activated under these reaction conditions. In a similar manner, reaction of equimolar quantities of *p*-aminothiophenol and *N,N-bis*(2-chloroethyl)amine hydrochloride resulted in chemoselective formation of 4-(piperazin-1-yl)benzenethiol hydrochloride salt in 90% yield within 12 min of microwave irradiation (Table 5; entry 3). When two or more equivalents of *N,N-bis*(2-chloroethyl)amine hydrochloride were used for this reaction, the thiol group also got alkyalted additionally (Table 5; entry 4).

Low solubility of hydrochloride salts (the reactant and the products both) in common organic solvents is one of the major stumbling blocks in these reactions. Contrary to this, high solubility of these salts in TSIL became one of the greatest advantages of this protocol. The low solubility/insolubility of HCl salts of the formed products in common organic solvents proved ideal for isolation and from purity points of view for the products. Not even a single protocol describing the direct *in situ* synthesis of arylpiperazines as hydrochloride salts in a single step could be located in the literature. It became evident from the elemental analyses and proton NMR spectra of the products that none of the products formed in these reactions in TSIL is a free base. All of the compounds showed a characteristic singlet (for bases) or two singlets (for two protons, N*H.H*Cl salt form) in the range of δ 8–10 (Supporting Information for ^{1}H NMR).

Very easy isolation of the products from the reaction media was an important aspect of the study. All of the previously reported methods for the preparation of aryl piperazines were

Table 4. Synthesis of aryl piperazine hydrochlorides/free bases using different aryl amines using [Bbim]OH or DEGMME as solvents

Entry	Aryl amine	DEGMME[a]				[Bbim]OH[b]	
		Conventional Heating[c]		Microwave Method[d]		Microwave Method[d]	
		Yield [%][e]	Time [hrs]	Yield [%][e]	Time [min]	Yield [%][e,f]	Time [min]
1	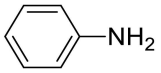	79	11	86	18	92	03
2	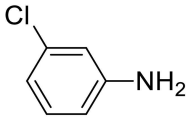	67	10	**75**	6	**85**	6.5
3	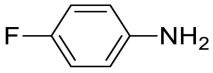	87	7.5	90	12	95	03
4	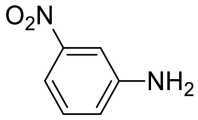	80	12	85	14	90	3.5
5	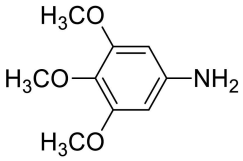	75	08	**79**	8	**90**	2.5
6	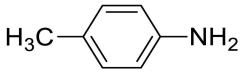	80	09	85	6	90	03
7	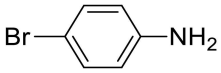	80	7.5	85	13	90	2.5
8	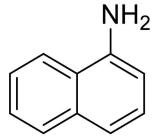	60	9.5	**69**	10	**80**	05
9	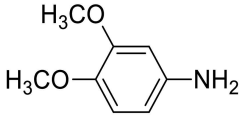	60	09	**74**	12	**85**	3.5
10	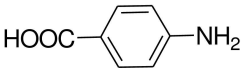	NA[g]	-	**70**	10	**90**	05
11	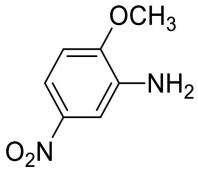	NA[g]	-	NP[h]	60	**62**	10
12	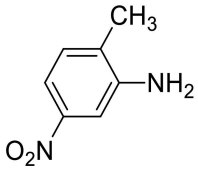	NA[g]	-	NP[h]	60	**65**	05

[a] Diethylene glycol monomethyl ether. [b] [Bbim]OH: 1 eq. [c] Oil bath heating at 150–160 °C and product is isolated as free base. [d] CEM monomode open vessel microwave reactor at standard operating conditions with 120 °C and 150 W. [e] Isolated yields based on aniline as the starting material. [f] product obtained as hydrochloride salt. [g] Not performed by conventional heating. [h] No product formation as observed on TLC.

plagued with cumbersome isolation procedures. In this protocol, after completion of the reaction, the reaction mixture was quenched with a small quantity of CH_2Cl_2 (1-2 ml) and 2–3 drops of methanol to precipitate out the HCl salt and the precipitated salt was washed free from the TSIL with diethyl ether. The salt so separated out was collected as such and was found to be pure enough for all practical purposes. The CH_2Cl_2 washings were combined and evaporated in rotary evaporator

Table 5. Synthesis of *N*-alkyl/aryl piperazine hydrochlorides using microwave irradiation[a]

Entry	Alkyl/Aryl amine (Ratio with respect to the mustard)	Product	DEGMME[b] Yield [%][d]	Time [min]	[Bblm]OH[c] Yield [%][d]	Time [min]
1	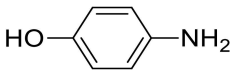	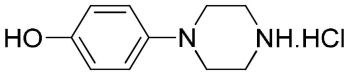	91	08	95	1.5
2	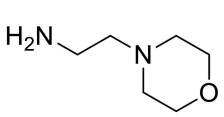	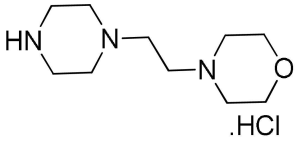	77	10	90	05
3	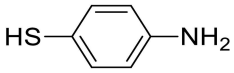	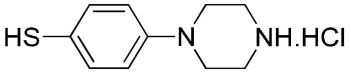	NA[e]	-	90	12
4	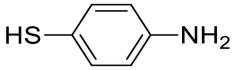	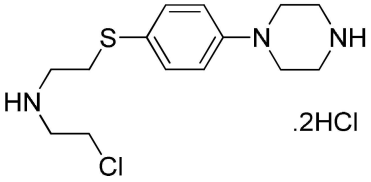	NA[e]	-	87	14

[a] CEM monomode open vessel microwave reactor at standard operating conditions at 120 °C and 150 W. [b] Diethylene glycol monomethyl ether. [c] [Bblm]OH: 1 eq. [d] Isolated yields based on aniline as the starting material. [e] Not performed.

to remove the volatiles and subsequently washed with diethyl ether to offer the TSIL which was reused for subsequent reactions upto five cycles with a marginal loss of catalytic activity (Table 6; entries 1–6). The DSC and TGA studies suggested that the TSIL was not degraded upto 170 °C. FTIR and PMR of the recycled TSIL suggested a little degradation but it could be reused several times as such or after treatment with potassium hydroxide (see preparation of [Bblm]OH). Consequently, it could be considered as a green synthetic protocol ideally suited particularly for industrial application.

Table 6. Use of recycled [Bblm]OH for the synthesis of phenylpiperazine hydrochloride by microwave irradiation

Entry	Cycle[a]	Time [min]	Yield [%][b]	*p*H[c]
1	0	-	-	*8.601*
2	1	03	92	*4.169*
3	2	03	91	*3.505*
4	3	3.5	90	*3.421*
5	4	04	90	*3.368*
6	5	4.5	88	*2.805*

[a] Recovered IL was used. [b] Isolated yield based on aniline as the starting material. [c] Mean of three experiments after the cycle.[33a]

By this time it became amply clear that [Bblm]OH is acting as a catalyst as well as a reaction medium (Table 2). It has been reported in literature[23a,31c,d] that the acidic C_2-H in imidazolium-based ionic liquids influences the reaction kinetics. It was planned to synthesize C_2-Me derivative of [Bblm]OH and evaluate its role in these cyclization reactions. But all our attempts failed to prepare the desired ionic liquid (*i.e.* 1,3-dibutyl-2-methylimidazolium hydroxide) in sufficiently pure form. So, a C_2-Me substituted ionic liquid *i.e.* 1-butyl-2,3-dimethyl imidazolium hydroxide [BmmIm]OH was prepared from [BmmIm]BF_4 (synthesized[33b] as well as procured from Sigma-Aldrich). Both of these ionic liquids ([BmmIm]BF_4 and [BmmIm]OH) were used for the cyclization reaction between aniline and *N,N-bis*(2-chloroethyl)amine hydrochloride (Table 7).

Table 7. Screening of C_2-H substituted and other hydrated/nonhydrated ionic liquids for the synthesis of phenylpiperazine hydrochloride by microwave irradiation.

Entry	Solvent/catalyst [% of water content]	Yield [%][a]	Time [min]
1	[BmmIm]OH [3]	NP[b]	60
2	[BmmIm]BF_4 [0.01]	NP[b]	60
3	[Bblm]BF_4 [3]	61	55
4	[Bblm]$OH_{0.65}Br_{0.35}$ [10]	90	04
5	[Bblm]OH.H_2O (dried at 50 °C for 5 hr) [12]	91	04
6	[Bblm]OH.H_2O (dried at 90 °C for 10 hrs) [10]	92	3.5
7	[Bblm]OH (with 50 µl of water in 0.2 g) [10]	86	08
8	[Bblm]OH (with equivalent w/v water) [50]	82	11

[a] Isolated yields based on aniline as the starting material. [b] No product formation as observed on TLC.

To our surprise, the reaction did not get completed even after 60 min of microwave irradiation and the monoalkylated aniline only was obtained as the product in both the cases instead of the desired cyclized product. This was a significant finding as the use of [BmIm]OH in earlier experiments had offered the desired cyclized product (Table 2, entry 3) although in much lower yields. Another interesting observation was made during

the synthesis of [BmmIm]OH from [BmmIm]BF_4 and KOH in presence and absence of air. In both the cases it was observed that the colour of the reaction mixture started turning from colourless to pale yellow to yellow to orange to ultimately dark brown (Figure S1-S3). This observation was in stark contrast to the earlier observation wherein formation of carbene was stipulated.[34a] Because in this case, the C_2 position was already blocked by a methyl group and there was no chance of carbene formation and further degradation of the ionic liquid through the carbene.

It was evident from our experiments that the *N*,*N*′-dibutyl group, an acidic C_2-H component in the cationic moiety, and hydroxide as the anion offered the best results, although bromide as anion also offered moderate yields of the desired cyclized product (Table 2, entry 6). The so called [BbIm]$OH_{0.65}Br_{0.35}$ IL was also prepared by the reported[34b] ion exchange method and used for catalyzing the cyclization reaction, offering yields almost at par with [BbIm]OH (Table 7, entry 4).

All of the experiments performed above underlined the importance of *N*,*N*′-dibutyl group, the acidic C_2-H and the hydroxide anion in catalyzing the cyclization reaction but they did not exclude the involvement of a carbene species in the catalysis. Considering the controversy on [BmIm]OH as a basic ionic liquid or a neutral carbene,[34a,c] it was planned to include different proportions of water in the IL and observe the effect of water on the product yield. It has been reported that the presence of water reverses/prevents carbene formation.[34a] Two batches of [BbIm]OH.H_2O were prepared from the reaction between [BbIm]Br and lithium hydroxide monohydrate (LiOH.H_2O). One batch was dried at 50 °C and the other at 90 °C *in vacuo* for 10 hrs and the water contents determined for both the batches (Table 7). No noteworthy differences were observed in the product yields obtained from the reactions utilizing the two batches of the ILs. Two other batches of the previously synthesized [BbIm]OH (having water contents about 7%) were diluted with water, one contained 10% w/v water while the other had 50% w/v water contents. Both of these batches when used in the cyclization reaction offered the desired product in somewhat lowered yields with enhanced period of microwave exposure.

It is hypothesized that the alkyl chains attached to imidazolium moiety in the ionic liquid might also affect the catalytic power in this reaction. To ensure the effect of various alkyl groups with varying chain length attached to the imidazolium scaffold, we further prepared symmetrical ionic liquids having dimethyl, diethyl, dipropyl, dipentyl and didodecyl chains (Table 8). Interestingly, none of them showed noteworthy decrease in reaction times. The time taken for completion of the reaction varied from 25 min to more than 60 min (Table 8; entries 1–10). These observations highlighted the role of an optimum chain length of the alkyl groups for catalytic activity, making [BbIm]OH as a true task specific ionic liquid for synthesizing aryl piperazines from anilines.

It is worthy to note that repeated use of the same batch of [BbIm]OH upto five cycles reduced the *p*H of the TSIL from the original value of *8.6* to *2.8* but still it did not cause a significant decrease in the product yield (Table 6).

Table 8. Screening of symmetrical ionic liquids of different chain lengths for the synthesis of phenylpiperazine hydrochloride by microwave irradiation.

Entry	Ionic Liquid[a]	Time taken [min]
1	[MmIm]Br	>60
2	[EeIm]Br	50
3	[DipropylIm]Br	30
4	[DipentylIm]Br	>60
5	[DidodecylIm]Br	>60
6	[MmIm]OH	>60
7	[EeIm]OH	30
8	[DipropylIm]OH	25
9	[DipentylIm]OH	>60
10	[DidodecylIm]OH	>60

[a] All bromide ILs were prepared according to earlier reported procedures[35]. The respective hydroxyl ILs were prepared as per literature report[31a].

Taking all the above observations into consideration, a possible mechanism is proposed for the catalyzing role played by [BbIm]OH in offering the cyclized products in high yield. It is proposed to be a classical case of symphoria wherein the dibutylimidazolium cation containing the acidic C_2-H, the hydroxide ion, a water molecule, an aniline molecule and *N*,*N*-*bis*(2-chloroethyl)amine hydrochloride, all are placed in a three dimensional cage-type structure (Figure 1a). The *N*,*N*′-dibutyl chains due to high perturbation provide enough space above and below the flat imidazolium cation wherein the *bis*chloroethyl group of the amine gets positioned in such a way that electrostatic interaction occurs between the positively charged nitrogens of the imidazolium ring and the electronegative chlorines. Both the chloro groups are further stabilized by partial ionic interactions with the acidic hydrogen attached to C_2 of imidazolium ring. Due to the partial ionic interactions among the hydroxide ion, water molecule and the two hydrogens of aniline, the nitrogen atom of aniline is brought close to the two partially positive carbons of the 2-chloroethyl groups (Figure 1a). It is already reported[31a,36] that the acidic C_2-H, hydroxide ion and water in the cage increase the nucleophilicity of nitrogen of the amines. Due to the symphoria, all of the reacting species are so well placed strategically that the nitrogen of the aniline attacks both the electrophilic carbons simultaneously and both the halogens are captured by both hydrogens of the aniline to eject out two HCl molecules, and offers the aryl piperazine as hydrochloride salt (Figure 1b). It is to be noted that although hydroxide ion is proposed to be fitting ideally into the cage but its position can also be taken up by an anion like bromide or chloride. Water molecule plays a vital role in the cage and ultimately in the whole catalytic process as such. It may be noted that even the most highly dried IL used in these reactions contained about 7% of water contents. This proposed mechanism has been supported by computational studies.

To support the postulated reaction mechanism, the DFT and molecular dynamics (MD) studies have been carried out.

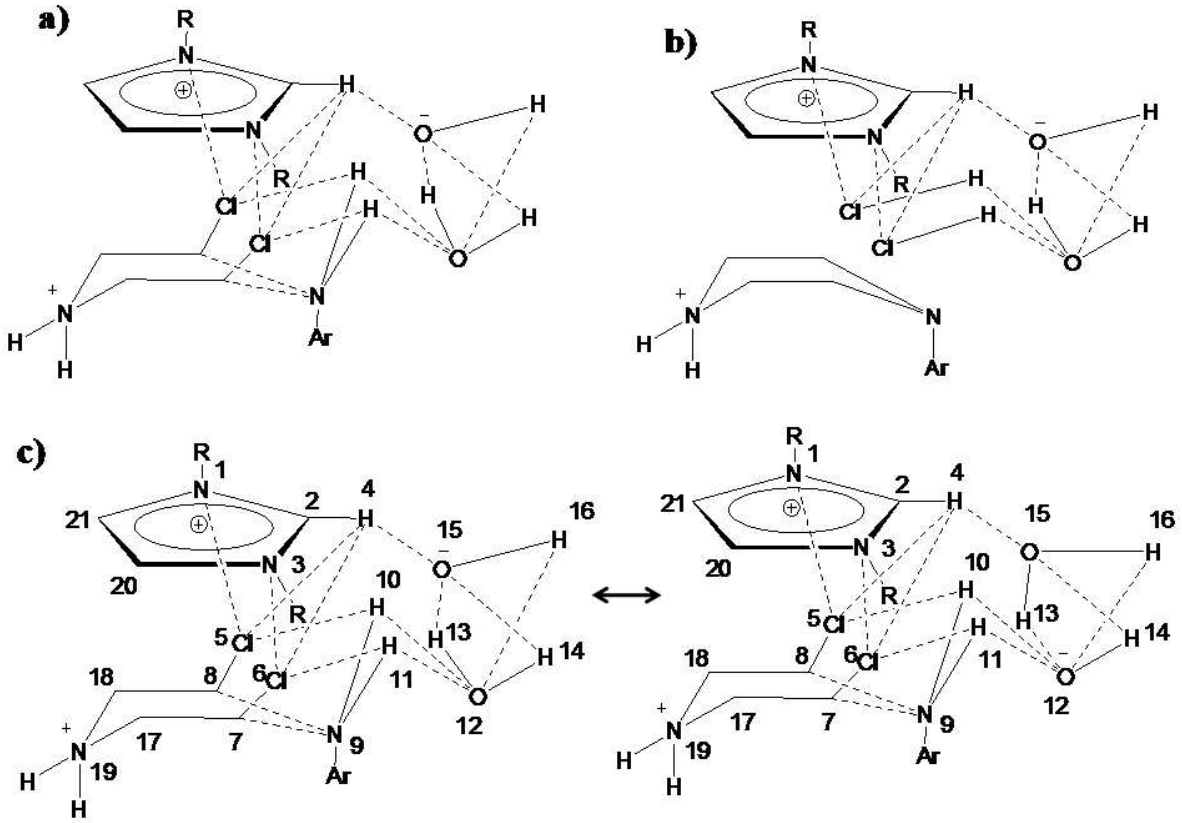

Figure 1. (a) A postulated mechanism of catalysis involving symphoria. **(b)** Formation of aryl piperazine hydrochloride salt and trapping of the formed HCl. **(c)** Numbering of atoms indicated in the computational study.

Though the classical MD method is convenient it provides limited information about chemical reactions. It offers limited insight into the reaction in revealing the development of reaction regions and chemical groups during certain time intervals. Analyses of the radial distribution function (RDF) and spatial distribution function (SDF) provide information about the way in which the (desired) chemical groups or atoms (which are of interest for the reaction) in a system are radially and spatially distributed around each other. The RDF calculations take into account the volume available to the system and the total number of particles or atoms, *i.e.* the density, as well as the number of available atoms of the type for which the RDF is calculated. RDF can be calculated easily by counting the number of atoms present in each concentric spherical shell surrounding a fixed reference atom. If atoms in a system are distributed completely randomly or uniformly, then such counts would grow in direct proportionality to the volume of the shells, whereas their density in each shell would be a constant. In other words, the radial distribution function in such a situation is simply a constant. If a system possessed strong interactions between atoms leading to their distribution at different relative distances, then such density would vary from shell to shell, resulting in a radial distribution function with peaks and other distinctive features. The radial distribution function (RDF) *g(r)* is calculated using the given equation:

$$g(\mathrm{r}) = \lim_{\mathrm{dr}\to 0} \frac{p(r)}{4\pi\ \left(N_{pair}/V\right)\mathrm{r}^2\mathrm{dr}}$$

where **r** is the distance between a pair of particles, **p**(**r**) is the average number of atom pairs found at a distance between **r** and **r** + **dr**, **V** is the total volume of the system, and $\mathbf{N_{pair}}$ is the number of unique pairs of atoms where one atom is from each of two sets.

Considering the difference in the system densities, the RDF analyses provide the distances where the first pairs are found (X-axis in RDF plot), versus the values found for the RDF (Y-axis in RDF plot). RDF values for different systems are not comparable due to the different available volumes. As per our hypothesized mechanism of the reaction, the radial and spatial distribution functions were evaluated for the (i) Cl_5 and Cl_6 of *bis*-chloroethylamine around N_1 and N_3 imidazolium nitrogens (ii) distribution of C_7 and C_8 of *bis*-chloroethylamine around N_9 of aniline (iii) Cl_5 and Cl_6 of *bis*-chloroethylamine around H_{10} and H_{11} of aniline and (iv) H_4 of imidazolium with water and hydroxide ion.

The RDF of the chlorine Cl_5 and Cl_6 of the *bis*-chloroethylamine around the N_1 and N_3 of the imidazolium ring were calculated from an MD simulation as shown in Figure 2. From this figure it is clear that the distribution of both the chlorine atoms of *bis*-chloroethylamine around the nitrogen atoms of the imidazoline ring is similar. At shorter distances (less than

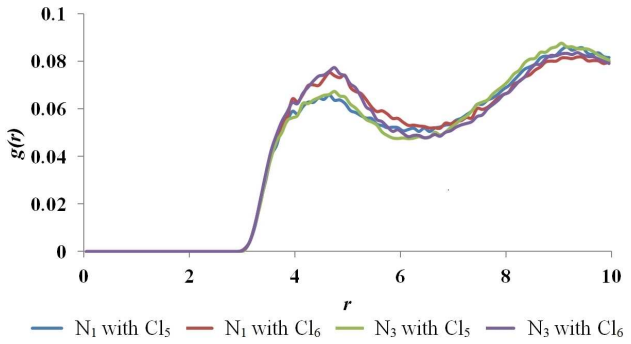

Figure 2. RDF of the chlorine Cl_5 and Cl_6 of the *bis*-chloroethylamine around N_1 and N_3 of the imidazolium ring

atomic diameter) r = 2.85 Å, *g*(r) is zero. This is due to the strong repulsive forces between the set of atoms under study. For RDF between the N_1 with chlorine Cl_5 the first (and large) peak occurs at 4.35 Å, with g(r) having a value of about 0.075. This means that it is 0.075 times more likely that the two molecules would be found at this separation. The radial distribution function then falls and passes through a minimum value around *r* = 6.45 Å. The chances of finding two atoms with this separation are less. Similar readings were observed in case of N_3 of imidazolium with Cl_5 and Cl_6 of *bis*-chloroethylamine. From these observations it is confirmed that the two chlorine atoms are uniformly interacting with the two nitrogen atoms of the imidazolium ion. The resulting RDF was further supported by SDF results. From Figure 3, it can be clearly observed that

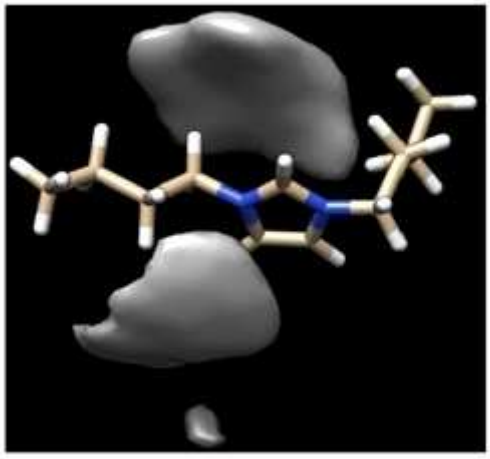

Figure 3. Spatial distribution of chlorine atoms of *bis*-chloroethylamine around imidazolium ring

the distribution of the two chlorine atoms of *bis*-chloroethylamine is equal around the nitrogen atoms of the imidazolium. This supports our hypothesis as the two butyl chains cause enough perturbations above and below the plane of imidazolium ring so that the chlorine atoms (Cl_5 and Cl_6) can easily align on one side of the plane of the ring to interact with both the positively charged nitrogens of the imidazolium ring.

Further, the RDF of C_7 and C_8 of *bis*-chloroethylamine around N_9 of aniline is described in Figure 4. Here a strong

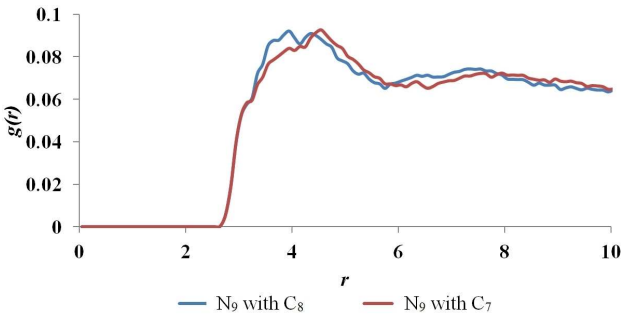

Figure 4. RDF of C_7 and C_8 of *bis*-chloroethylamine around N_9 of aniline

columbic interaction between these atoms was observed. In case of the two carbon atoms the g(r) is zero till *r* = 2.55 Å, and at 4.55 Å there is increase in density of the carbon around the nitrogen of aniline with *g(r)* 0.092. Here both the carbon atoms were found to be interacting with the nitrogen of the aniline uniformly. The SDF study (Figure 5) clearly showed a uniform

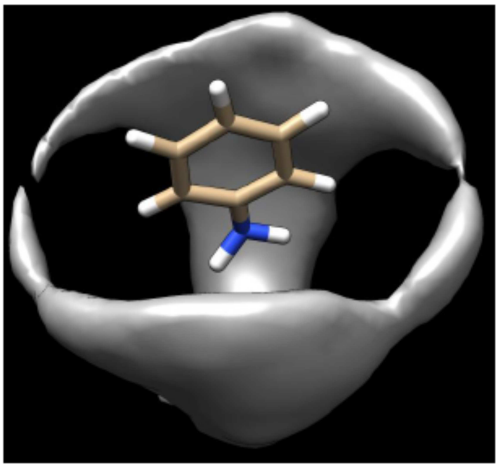

Figure 5. Spatial distributions of C_7 and C_8 of *bis*-chloroethylamine around N_9 of aniline

distribution of carbon atoms concentrating mainly on the partially negatively charged nitrogen atom of the aniline ring. The empty region around the hydrogen atoms of the -NH_2 group represents the absence of any interactions.

The distribution of two chlorine atoms of *bis*-chloroethylamine around the hydrogen atoms of the -NH_2 group is represented in Figure 6. Both the chlorine atoms showed similar distribution function around H_{10} and H_{11} of the aniline at 4.15 Å. After 4.15 Å the density of the chlorine atoms almost remains constant till 10 Å. In Figure 7 the first probable density

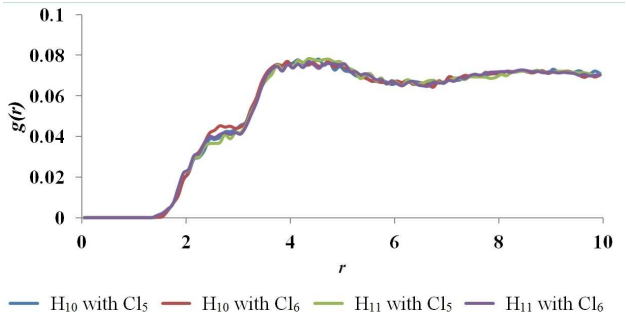

Figure 6. RDF of chlorine Cl_5 and Cl_6 of the *bis*-chloroethylamine around H_{10} and H_{11} of -NH_2 group of the aniline

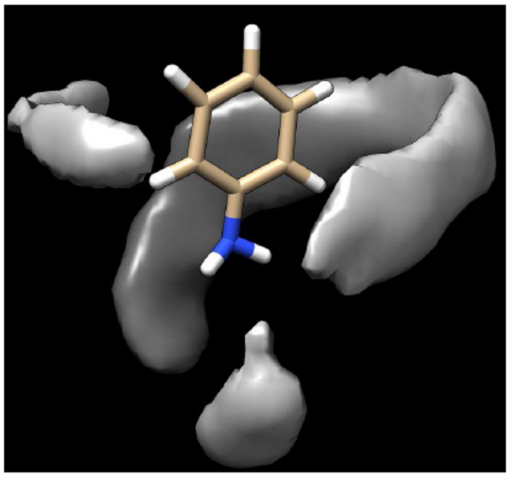

Figure 7. Spatial distribution of chlorine Cl_5 and Cl_6 of the *bis*-chloroethylamine around H_{10} and H_{11} of -NH_2 group of the aniline

regions of the two chlorines around the -NH_2 group are shown. This spatial distribution function explained the distribution of chlorine atoms concentrating mainly around the -NH_2 group and along the symmetry of aromatic ring of aniline which could reveal the columbic interactions between the charged groups.

Figure 8 represents the distribution of water molecule around the acidic proton (H_4) of the imidazolium ring. The

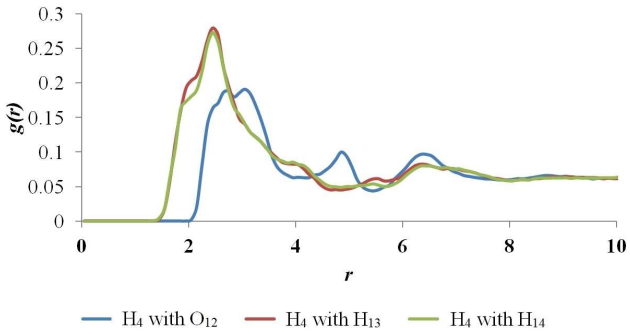

Figure 8. RDF of water molecule around the acidic proton (H_4) of the imidazolium ring

distribution of hydrogen of water around the acidic proton of the imidazolium ring is comparatively higher than the oxygen which may reveal the orientation of the water. The distribution of the H atoms around the acidic proton is high at distance 2.45 Å with *g(r)* 0.26 while the oxygen atom shows maximum *g (r)* 0.187 at 2.75 Å. In Figure 9 the SDF of water around the

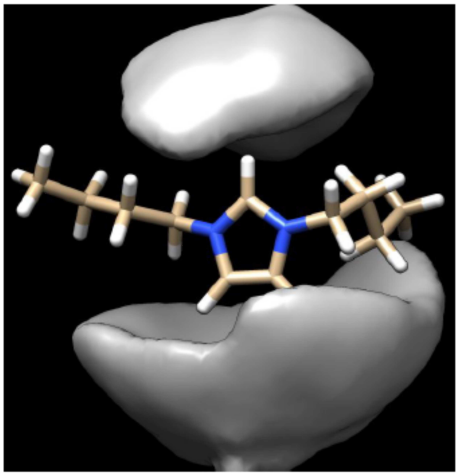

Figure 9. Spatial distribution of water molecule around the acidic proton (H_4) of the imidazolium ring

imidazolium ring is shown which explains the distribution of water molecules mainly concentrated in two zones around the H atoms of the imidazolium ring. This represents a strong association of water molecule with H atoms of the imidazolium ring.

The role of hydroxide ion was found out to be much less considerable in this computational study. Hydroxyl anion may strengthen the role of water by inter-converting into each other, which might be responsible for higher yields of the products in presence of hydroxyl ionic liquids. This entire computational study broadly supports the proposed reaction mechanism.

Conclusion

Total avoidance of volatile organic solvents, time consuming extraction procedures, easy recovery of products without aqueous workup (important in this case because highly hygroscopic salts were formed in this study) and recyclability of ionic liquid are the greener advantages of our protocol. The investigated hydrated TSIL, [Bbim]OH offers an interesting alternative to synthesize aryl/alkyl piperazine hydrochlorides. A plausible reaction mechanism has also been proposed for the TSIL which has been supported by MD simulations of the reaction as computed by DFT.

Supporting Information Summary

Details of experimental procedures for synthesis and characterization data of compounds and other related information are provided in supporting information.

Acknowledgements

The authors are thankful to AICTE for providing NDF to RST and to UGC for BSR-RFSMS to NRP, AMK and MMS. The authors acknowledge the BRAF-CDAC, Pune for software facilities.

Conflict of Interest

The authors declare no conflict of interest.

Keywords: *N*-Aryl piperazines · Green chemistry · Imidazolium · Microwave Irradiation (MWI) · Task Specific Ionic Liquid (TSIL)

[1] a) J. S. Nakhla, J. P. Wolfe, *Org. Lett.* **2007**, *9*, 3279–3282; b) M. Hepperle, J. Eckert, D. Gala, L. Shen, C. A. Evans, A. Goodman, *Tetrahedron Lett.* **2002**, *43*, 3359–3363; c) M. Nishiyama, T. Yamamoto, Y. Koie, *Tetrahedron Lett.* **1998**, *39*, 617–620.

[2] a) P. Chaudhary, R. Kumar, A. K. Verma, D. Singh, V. Yadav, A. K. Chhillar, G. L. Sharma, R. Chandra, *Bioorg. Med. Chem.* **2006**, *14*, 1819–1826. b) P. Chaudhary, S. Nimesh, V. Yadav, A. K. Verma, R. Kumar, *Eur. J. Med. Chem.* **2007**, *42*, 471–476. c) J. P. Feighner, W. F. Boyer, *Psychopathology* **1989**, *22*, 21–26.

[3] a) A. B. Reitz, D. J. Bennett, P. S. Blum, E. E. Codd, C. A. Maryanoff, M. E. Ortegon, M. J. Renzi, M. K. Scott, R. P. Shank, J. L. Vaught, *J. Med. Chem.* **1994**, *37*, 1060–1062. b) M. K. Scott, E. W. Baxter, D. J. Bennett, R. E. Boyd, P. S. Blum, E. E. Codd, M. J. Kukla, E. Malloy, B. E. Maryanoff, C. A. Maryanoff, *J. Med. Chem.* **1995**, *38*, 4198–4210. c) A. B. Reitz, E. W. Baxter, D. J. Bennett, E. E. Codd, A. D. Jordan, E. A. Malloy, B. E. Maryanoff, M. E. McDonnell, M. E. Ortegon, M. J. Renzi, *J. Med. Chem.* **1995**, *38*, 4211–4222.

[4] a) R. Perrone, F. Berardi, N. A. Colabufo, E. Lacivita, M. Leopoldo, V. Tortorella, *J. Med. Chem.* **2003**, *46*, 646–649; b) E. Lacivita, D. Patarnello, N. Stroth, A. Caroli, M. Niso, M. Contino, P. De Giorgio, P. Di Pilato, N. A. Colabufo, F. Berardi, R. Perrone, P. Svenningsson, P. B. Hedlund, M. Leopoldo, *J. Med. Chem.* **2012**, *55*, 6375–6380; c) M. Leopoldo, E. Lacivita, P. De Giorgio, C. Fracasso, S. Guzzetti, S. Caccia, M. Contino, N. A. Colabufo, F. Berardi, R. Perrone, *J. Med. Chem.* **2008**, *51*, 5813–5822; d) M. L. López-Rodríguez, M. J. Morcillo, T. K. Rovat, E. Fernández, B. Vicente, A. M. Sanz, M. Hernández, L. Orensanz, *J. Med. Chem.* **1999**, *42*, 36–49; e) M. Murasaki, S. Miura, *Prog. Neuro-Psychopharmacol. Biol. Psychiatry* **1992**, *16*, 833–845.

[5] R. F. Squires, E. Saederup, *Neurochem. Res.* **1993**, *18*, 787–793.

[6] a) A. Zhang, J. L. Neumeyer, R. J. Baldessarini, *Chem. Rev.* **2007**, *107*, 274–302; b) N. Ye, J. L. Neumeyer, R. J. Baldessarini, X. Zhen, A. Zhang, *Chem. Rev.* **2013**, *113,* PR123-178.

[7] a) J. F. Hartwig, *Angew. Chem. Int. Ed. Engl.* **1998**, *37*, 2046–2067; b) J. P. Wolfe, S. Wagaw, J. F. Marcoux, S. L. Buchwald, *Acc. Chem. Res.* **1998**, *31*, 805–818; c) C. C. Mauger, G. A. Mignani, *Aldrichimica Acta* **2006**, *39*, 17; d) S. H. Zhao, A. K. Miller, J. Berger, L. A. Flippin, *Tetrahedron Lett.* **1996**, *37*, 4463–4466.

[8] a) J. Lindley, *Tetrahedron* **1984**, *40*, 1433–145; b) H. Heaney, *Chem. Rev.* **1962**, *62*, 81–97.

[9] a) A. J. Pearson, A. M. Gelormini, M. A. Fox, D. Watkins, *J. Org. Chem.* **1996**, *61*, 1297–1305; b) M. Perez, P. Potier, S. Halazy, *Tetrahedron Lett.* **1996**, *37*, 8487–8488.

[10] a) J. M. Salvino, B. Gerard, H. F. Ye, B. Sauvagnat, R. E. Dolle, *J. Comb. Chem.* **2003**, *5*, 260–266; b) C. Macleod, B. I. Martinez-Teipel, W. M. Barker, R. E. Dolle, *J. Comb. Chem.* **2006**, *8*, 132–140.

[11] a) M. Hepperle, J. Eckert, D. Gala, *Tetrahedron Lett.* **1999**, *40*, 5655–5659; b) W. ten Hoeve, C. G. Kruse, J. M. Luteyn, J. R. G. Thiecke, *J. Org. Chem.* **1993**, *58*, 5101–5106; c) J. A. Bender, N. A. Meanwell, T. Wang, *Tetrahedron* **2002**, *58*, 3111–3128; d) M. Hepperle, J. Eckert, D. Gala, L. Shen, A. C. Evans, A. Goodman, *Tetrahedron Lett.* **2002**, *43*, 3359–3363.

[12] a) E. Brenner, R. Schneider, Y. Fort, *Tetrahedron* **2002**, *58*, 6913–6924; b) E. Brenner, R. Schneider, Y. Fort, *Tetrahedron* **1999**, *55*, 12829–12845.

[13] a) V. Prelog, Z. Blazek, *Collect. Czech. Chem. Commun.* **1934**, *6*, 211–224; b) V. Prelog, G. J. Driza, *Collect. Czech. Chem. Commun.* **1933**, *5*, 497–502.

[14] G. S. Poindexter, M. A. Bruce, K. L. LeBoulluec, I. Moncovic, *Tetrahedron Lett.* **1994**, *35*, 7331–7334.

[15] T. R. Elworthy, A. P. D. W. Ford, G. W. Bantle, D. J. Jr. Morgans, R. S. Ozer, W. S. Palmer, D. B. Repke, M. Romero, L. Sandoval, E. B. Sjogren, F. X. Talamas, A. Vazquez, H. Wu, N. F. Arredondo, D. R. Blue Jr., A. DeSousa, L. M. Gross, M. S. Kava, J. D. Lesnick, R. L. Vimont, T. J. Williams, Q. M. Zhu, J. R. Pfister, D. E. Clarke, *J. Med. Chem.* **1997**, *40*, 2674–2687.

[16] a) K. G. Liu, A. J. Robichaud, *Tetrahedron Lett.* **2005**, *46*, 7921–7922; b) E. Mishani, C. S. Dence, T. J. McCarthy, M. J. Welch, *Tetrahedron Lett.* **1996**, *37*, 319; c) P. K. Ambre, C. L. Viswanathan, A. A. Juvekar, *Indian Drugs* **2002**, *39*, 195–203.

[17] a) P. C. Pan, C. M. Sun, *Tetrahedron Lett.* **1998**, *39*, 9505–9508; b) J. S. D. Kumar, V. J. Majo, S. C. Hsiung, M. S. Millak, K. P. Liu, H. Tamir, J. Prabhakaran, N. R. Simpson, R. L. Van Heertum, J. J. Mann, R. V. Parsey, *J. Med. Chem.* **2006**, *49*, 125; c) C. P. Pollard, L. G. MacDowell, *J. Am. Chem. Soc.* **1934**, *56*, 2199.

[18] a) T. Ruhland, K. S. Bang, K. J. Andersen, *Org. Chem.* **2002**, *67*, 5257–5268; b) L. K. Rasmussen, M. Begtrup, T. Ruhland, *J. Org. Chem.* **2004**, *69*, 6890–6893.

[19] a) C. Migihashi, F. Sato, *J. Heterocycl. Chem.* **2003**, *40*, 143–147; b) A. A. Macdonald, S. H. DeWitt, E. M. Hogan, R. Ramage, *Tetrahedron Lett.* **1996**, *37*, 4815–4818; c) A. Ganesan, Wang Resin. e-EROS Encyclopedia of Reagents for Organic Synthesis, 2003, DOI: 10.1002/047084289X.rn00168.

[20] a) Y. Ju, R. S. Varma, *J. Org. Chem.* **2006**, *71*, 135–141; b) Y. Ju, R. S. Varma, *Org. Lett.* **2005**, *7*, 2409–2411; c) G. Marzaro, A. Guiotto, A. Chilin, *Green Chem.* **2009**, *11*, 774–776.

[21] a) N. V. Plechkova, K. R. Seddon, *Chem. Soc. Rev.* **2008**, *37*, 123–150; b) P. Walden, *Bull. Acad. Imp. Sci. St.-Petersbourg*, **1914**, *1800*, 405–422; c) R. A. Sheldon, *Green Chem.* **2007**, *9*, 1273–1283; d) W. L. Hough, M. Smiglak, H. Rodríguez, R. P. Swatloski, S. K. Spear, D. T. Daly, J. Pernak, J. E. Grisel, R. D. Carliss, M. D. Soutullo, J. H. Davis Jr., R. D. Rogers, *New J. Chem.* **2007**, *31*, 1429–1436; e) T. Welton, *Chem. Rev.* **1999**, *99,* 2071–2084.

[22] a) P. J. Dyson, T. J. Geldbach, *Electrochem. Soc. Interface* **2007**, *16*, 50–53; b) K. R. Seddon, *J. Chem. Technol. Biotechnol.* **1997**, *68*, 351–356; c) C. M. Gordon, *Appl. Catal. A* **2001**, *222*, 101–117; d) H. O. Bourbigou, L. Magna, *J. Mol. Catal. A.* **2002**, *182*, 419–437; e) J. Dupont, R. F. de Souza, P. A. Z. Suarez, *Chem. Rev.* **2002**, *102*, 3667–3692; f) T. Welton, *Coord. Chem. Rev.* **2004**, *248*, 2459–2477; g) V. I. Parvulescu, C. Hardacre, *Chem. Rev.* **2007**, *107*, 2615–2665.

[23] a) J. A. Boon, J. A. Levinsky, J. I. Pflug, J. S. Wilkes, *J. Org. Chem.* **1986**, *51*, 480–483; b) T. L. Greaves, C. J. Drummond, *Chem. Rev.* **2008**, *108*, 206–237; c) J. C. Plaquevent, J. Levillain, F. Guillen, C. Malhiac, A. C. Gaumont *Chem. Rev.* **2008**, *108*, 5035–5060; d) M. A. P. Martins, C. P. Frizzo, D. N. Moreira, N. Zanatta, H. G. Bonacorso, *Chem. Rev.* **2008**, *108*, 2015–2050; e) S. S. Palimkar, S. A. Siddiqui, T. Daniel, R. J. Lahoti, K. V. Srinivasan, *J. Org. Chem.* **2003**, *68*, 9371–9378.

[24] a) A. Domling, W. Wang, K. Wang, *Chem. Rev.* **2012**, *112*, 3083–3135; b) P. Lidström, J. Tierney, B. Wathey, J. Westman, *Tetrahedron* **2001**, *57*, 9225–9283; c) C. O. Kappe, *Chem. Soc. Rev.* **2008**, *37*, 1127–1139; d) C. O. Kappe, D. Dallinger, *Nat. Rev. Drug Discovery* **2006**, *5*, 51; e) C. O. Kappe, *Angew. Chem. Int. Ed.* **2004**, *43*, 6250–6284.

[25] a) R. M. Palou, *J. Mex. Chem. Soc.* **2007**, *51*, 252–264; b) B. Major, I. Kelemen-Horv'ath, Z. Csan'adi, K. B'elafi-Bak'o, L. Gubicz, *Green Chem.* **2009**, *11*, 614–616. c) I. Guryanov, A. M. Lo'pez, G. Scorrano, M. Maggini, M. Carraro, M. Prato, T. Da Ros, M. Bonchio, *Chem. Commun.* **2009**, 3940–3942; d) L. C. Henderson, N. Byrne, *Green Chem.* **2011**, *13*, 813–816; e) A. S. Chaudhari, Y. S. Parab, V. Patil, N. Sekar, S. R. Shukla, *RSC Adv.* **2012**, *2*, 12112–12117.

[26] a) A. Sinha, R. S. Tamboli, B. Seth, A. M. Kanhed, S. Tiwari, S. Agarwal, S. Nair, R. Giridhar, R. K. Chaturvedi, M. R. Yadav, *Mol. Neurobiol.* **2015**, *52*, 638–652; b) R. S. Tamboli, R. Giridhar, H. Mande, S. R. Shah, M. R. Yadav, *Synth. Commun.* **2014**, *44*, 2192–2204; c) R. Giridhar, R. S. Tamboli, R. Ramajayam, D. G. Prajapati, M. R. Yadav, *Eur. J. Med. Chem.* **2012**, *50*,

428–432; d) R. Ramajayam, R. Giridhar, M. R. Yadav, R. Balaraman, H. Djaballah, D. Shum, C. Radu, *Eur. J. Med. Chem.* **2008**, *43*, 2004–2010; e) S. T. Shirude, P. J. Patel, R. Giridhar, M. R. Yadav, *Indian J. Chem.* **2006**, *45B*, 1080–1085.

[27] a) G. E. Martin, R. J. Elgin Jr., J. R. Mathiasen, C. B. Davis, J. M. Kesslick, W. J. Baldy, R. P. Shank, D. L. DiStefano, C. L. Fedde, M. K. Scott, *J. Med. Chem.* **1989**, *32*, 1052–1056; b) K. Brewster, D. B. Coult, R. M. Pinder, *Chim. Ther.* **1972**, *87*; c) L. Orus, J. Martinez, S. Perez, A. M. Oficialdegui, J. C. del Castillo, M. Mourelle, B. Lasheras, J. del Rio, A. Monge, *Pharmazie* **2002**, *8*, 515–518; d) L. Orus, S. Perez-Silanes, A. M. Oficialdegui, J. Martinez-Esparza, J. C. Del Castillo, M. Mourelle, T. Langer, S. Guccione, G. Donzella, E. M. Krovat, K. Poptodorov, B. Lasheras, S. Ballaz, I. Hervias, R. Tordera, J. Del Rio, A. Monge, *J. Med. Chem.* **2002**, *45*, 4128–4139.

[28] a) S. N. Dighe, R. V. Bhattad, R. R. Kulkarni, K. S. Jain, K. V. Srinivasan, *Synapse* **2010**, *40*, 3522–3527; b) S. N. Dighe, K. S. Jain, K. V. Srinivasan, *Tetrahedron Lett.* **2009**, *50*, 6139–6142; c) M. K. Kathiravan, R. Jalnapurkar, T. S. Chitre, R. S. Tamboli, K. V. Srinivasan, *Green Sustainable Chem.* **2011**, *1*, 12.

[29] a) C. B. Singh, V. Kavala, A. K. Samal, B. K. Patel, *Eur. J. Org. Chem.* **2007**, *8*, 1369-1377. (Described 10% of dialkylated product from the aqueous reaction of arylamine with alkyl halide in 1:1.1 ratio); b) In ref. 13; Prelog described 6% of *N*-(2-(2-(*p*-toluidino)ethylamino)ethyl)-4-methylbenzenamine hydrobromide as the byproduct; c) In ref. 20a; Varma *et al.* also suggested that side reactions were observed in DMF but did not isolate the side products.

[30] a) I. Sircar, S. J. Haleen, S. E. Burke, H. Barth, *J. Med. Chem.* **1992**, *35*, 4442–4449; b) R. Ratouis, J. R. Boissier, C. Dumont, *J. Med. Chem.* **1965**, *8*, 104–107; c) P. J. Foley, R. S. Neale, *J. Chem. Eng. Data* **1968**, *13*, 593–595.

[31] a) B. C. Ranu, S. Banerjee, *Org. Lett.* **2005**, *7*, 3049; b) J. M. Xu, B. K. Liu, W. B. Wu, C. Qian, Q. Wu, X. F. Lin, *J. Org. Chem.* **2006**, *71*, 3991–3993; c) A. Aggarwal, N. L. Lancaster, A. R. Sethi, T. Welton, *Green Chem.* **2002**, *4*, 517–520; d) J. Ross, J. Xiao, *Chem. Eur. J.* **2003**, *9*, 4900–4906.

[32] a) J. A. Kiritsy, D. K. Yung, D. E. Mahony, *J. Med. Chem.* **1978**, *21*, 1301–1307; b) R. Gao, D. J. Canney, *J. Org. Chem.* **2010**, *75*, 7451–7453.

[33] a) E. Ennis, S. T. Handy, *Molecules* **2009**, *14*, 2235–2245; b) X. Cui, S. Zhang, F. Shi, Q. Zhang, X. Ma, L. Lu, Y. Deng, *ChemSusChem* **2010**, *3*, 1043–1047.

[34] a) A. K. L. Yuen, A. F. Masters, T. Maschmeyer, *Catal. Today* **2013**, *200*, 9–16; b) P. S. Wheatley, P. K. Allan, S. J. Teat, S. E. Ashbrook, R. E. Morris, *Chem. Sci.* **2010**, *1*, 483–487; c) O. Hollóczki, D. S. Firaha, J. Friedrich, M. Brehm, R. Cybik, M. Wild, A. Stark, B. Kirchner, *J. Phys. Chem. B.* **2013**, *117*, 5898–5907.

[35] a) S. V. Dzyuba, R. A. Bartsch, *Chem. Commun.* **2001**, 1466–1467; b) R. Rohini, C. K. Lee, J. T. Lu, I. J. B. Lin, *J. Chin. Chem. Soc.* **2013**, *60*, 745-754; c) R. S. Varma, V. V. Namboodiri, *Chem. Commun.* **2001**, 643–644; d) B. M. Khadilkar, G. L. Rebeiro, *Org. Process Res. Dev.* **2002**, *6*, 826–828; e) M. Deetlefs, K. R. Seddon, *Green Chem.* **2003**, *5*, 181–186 and references cited therein.

[36] a) F. D'Anna, V. Frenna, R. Noto, V. Pace, D. Spinelli, *J. Org. Chem.* **2006**, *71*, 5144–5150; b) A. Caley, B. W. McCann, O. Acevedo, *J. Phys. Chem. B.* **2015**, *119*, 743–752; c) L. Crowhurst, N. L. Lancaster, J. M. P. Arlandis, T. Welton, *J. Am. Chem. Soc.* **2004**, *126*, 11549–11555; d) M. Mečiarová, Š. Toma, P. Kotrusz, *Org. Biomol. Chem.* **2006**, *4*, 1420–1424.

Submitted: October 16, 2018
Accepted: January 11, 2019

FULL PAPERS

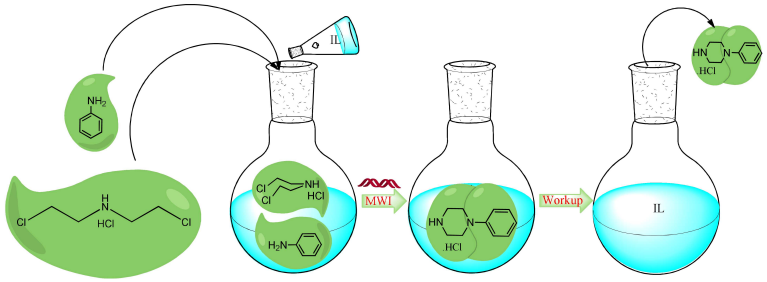

The hydrated Task Specific Ionic Liquid ([Bbim]OH) has been synthesized and utilized for an improved and rapid green synthesis of *N*-alkyl/aryl piperazine hydrochlorides under microwave irradiation (MWI).

*Dr. R. S. Tamboli, Dr. M. M. Shidore, Dr. R. C. Dash, Dr. A. M. Kanhed, N. R. Patel, Dr. S. R. Shah, Prof. M. R. Yadav**

1 – 12

Improved Rapid and Green Synthesis of *N*-Aryl Piperazine Hydrochlorides Using Synergistic Coupling of Hydrated Task Specific Ionic Liquid ([Bbim]OH) and Microwave Irradiation

Synthesis and Biological Activities of Vicinal Diaryl Furans

Chapter · January 2018

DOI: 10.1016/B978-0-08-102237-5.00007-9

2 authors:

Nirav R. Patel

11 PUBLICATIONS **28** CITATIONS

SEE PROFILE

Dushyant Patel

The Maharaja Sayajirao University of Baroda

10 PUBLICATIONS **28** CITATIONS

SEE PROFILE

CHAPTER

7

Synthesis and Biological Activities of Vicinal Diaryl Furans

Nirav R. Patel, Dushyant V. Patel

The Maharaja Sayajirao University of Baroda, Vadodara, India

Abstract

Furans are considered an influential part of heterocyclic systems due to their interesting biological properties. Vicinal diaryl furans have shown significant biological activities such as anti-inflammatory, anticancer, antioxidant, and antifungal. Rofecoxib, a selective COX-2 inhibitor belonging to this class was previously approved by the FDA, but withdrawn later on due to its toxicity. Efforts have been made in this chapter to describe the general methods for the synthesis of vicinal diaryl furans and to elaborate the biological significance of these derivatives as reported in the literature.

Keywords: Vicinal diaryl furan, Rofecoxib, Anti-inflammatory, Anti-cancer, Antioxidant, Antifungal, COX-2 inhibitors, LOX inhibitors

Heterocyclic compounds are widely distributed in nature. Furan (**1**) (Fig. 7.1) is a five-membered aromatic ring with one oxygen atom. Ether oxygen in furan imparts polarity and hydrogen bond acceptor potential to the molecule. It is soluble in alcohol, ether, and acetone but slightly soluble in water. The presence of furan ring in various compounds attributes interesting biological features to them.

The concept of bioisosterism has given special significance to furan derivatives in the field of medicinal chemistry. Furan is electronically and sterically similar to benzene and other heterocyclic rings such as pyrrole and thiophene. As a result, furan analogs of this biologically active ring system exhibit similar activities. The high reactivity of furan ring offers substitution in the ring even at much mild reaction conditions. The presence of oxygen heteroatom has the potential to alter the metabolic fate of the resulting molecules. Thus, the furan derivatives are less likely to be vulnerable to toxic effects showing a better therapeutic profile.

The furan ring skeleton is present in numerous medicinal agents (**2**–**7**) possessing a variety of activities such as analgesic, antibacterial, anticonvulsant, antifungal, anti-inflammatory, antihyperglycemic, antitumor, antiviral, etc. Some prominent drugs containing furan ring includes rofecoxib (**2**), dantrolene (**3**), prazosin (**4**), ranitidine (**5**), nitrofurantoin (**6**), and furosemide (**7**) (Fig. 7.2).

https://doi.org/10.1016/B978-0-08-102237-5.00007-9

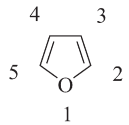

1

FIG. 7.1 Structure of a furan (**1**).

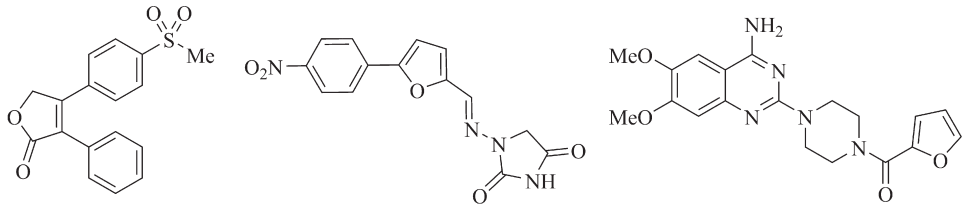

2, Rofecoxib **3, Dantrolene** **4, Prazosin**

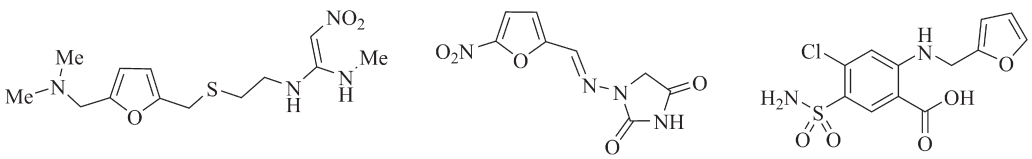

5, Ranitidine **6, Nitrofurantoin** **7, Furosemide**

FIG. 7.2 Structures of furan-containing drugs (**2–7**).

In the last 2 decades, vicinal diaryl heterocycles have gained enormous attention due to the expanding horizon of their biological profile. Various heterocycles have been incorporated into the vicinal diaryl scaffold and the resulting compounds have been evaluated for their biological effects. Vicinal diaryl furan derivatives have been reported in the literature by various research groups possessing biological activities such as antioxidant, anti-inflammatory, anticancer, etc. In this chapter, we discus vicinal diaryl furans and their derivatives along with their medicinal significance.

7.1 SYNTHESIS OF VICINAL DIARYL FURANS

A number of well-established methods for the synthesis of vicinal diaryl furans have been described in the literature. Some of the general synthetic routes to prepare vicinal diaryl furans are described below.

7.1.1 Synthesis of Diaryl Furans by Dehydration of 1,4-Diketones

The Stetter reaction of aldehydes with chalcones (**8**) is reported to give 1,4-diketones (**9**), which on acid-catalyzed dehydration converts to diaryl furans (**10**) (Fig. 7.3) (Stetter and Kuhlmann, 2004).

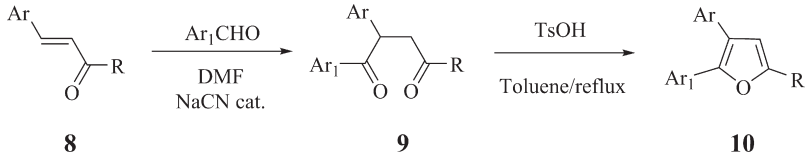

FIG. 7.3 Synthesis of vicinal diaryl furans (**10**) from 1,4-diketones.

7.1.2 Synthesis of Diaryl Furans by Intramolecular Aldol Condensation

Reaction of substituted phenylacetic acid (**11**) with the monobromo derivative of acetophenone (**12**) gives 2-oxo-2-phenylethyl 2-phenylacetate derivative (**13**). Intramolecular aldol condensation of compound (**13**) forms the lactone ring. α, β-Unsaturated lactone (**14**) on reduction with DIBAL-H gives the furan derivative (**15**) (Fig. 7.4) (Pirali et al., 2006).

7.1.3 Synthesis of Diaryl Furanones by Condensation Reaction

When substituted benzaldehyde is coupled to lithium acetylide (**16**), it results in the formation of diol (**17**). Oxidation of the benzylic hydroxyl group by manganese dioxide (MnO_2) gives the corresponding ketone (**18**), which is cyclized by diethylamine to 5-aryl-2, 2-dialkyl-3(2*H*)-furanone (**19**). The bromination of acetic acid results in the corresponding bromo derivative (**20**), which on Suzuki coupling with the relevant arylboronic acid resulted in the diaryl compound (**21**) (Fig. 7.5) (Shin et al., 2001).

7.1.4 Synthesis of Diaryl Furan-2,5-Diones From Benzoylformic Acid

The condensation reaction between benzoylformic acid (**22**) and phenylacetic acid (**23**) in the presence of acetic anhydride under reflux conditions results in the formation of compound (**24**) (Fig. 7.6) (Fields et al., 1990).

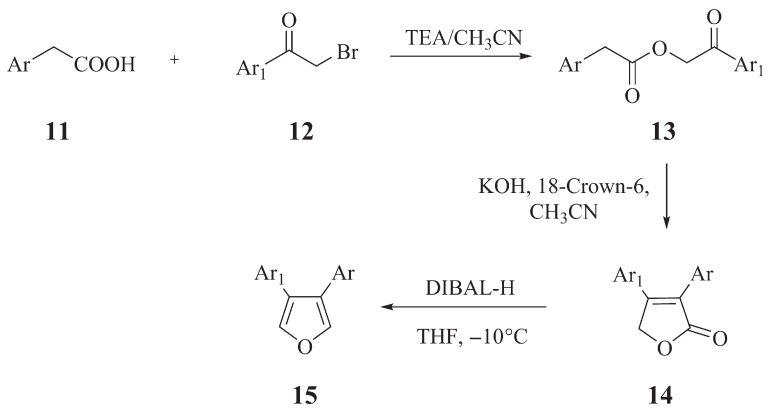

FIG. 7.4 Synthesis of 3,4-diaryl furans (**15**) by intramolecular aldol condensation.

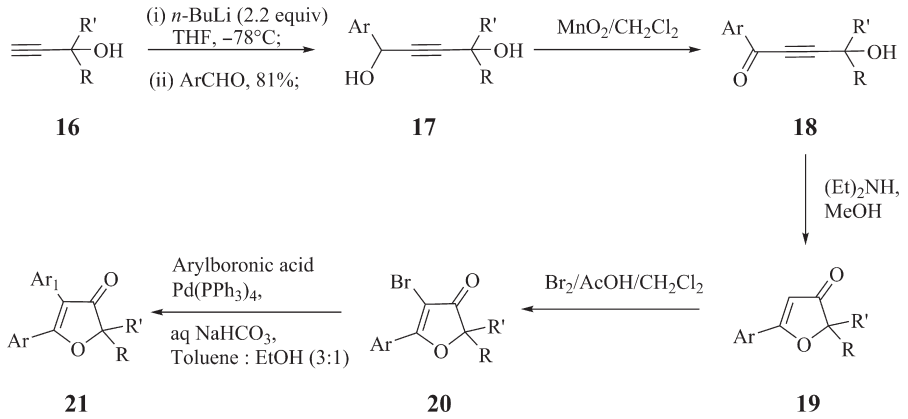

FIG. 7.5 Synthesis of vicinal diarylfuranone derivatives (**21**).

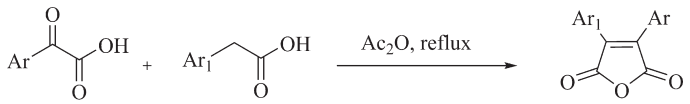

FIG. 7.6 Synthesis of 3,4-diaryl furan-2,5-diones (**24**).

7.1.5 Synthesis of Diaryl Hydroxyfuranones From Aryl Pyruvates

The reaction of methyl arylpyruvates (**25**) with benzaldehyde (**26**) and 1,5-diazabicyclo [5.4.0]undecene (DBU) in DMF gives diaryl hydroxyfuranone (**27**) (Fig. 7.7) (Weber et al., 2002).

In another method, (Z)-3-aryl-2-hydroxypropenoic acid (**29**) is obtained by acidic hydrolysis of 4-benzylideneoxazol-5(4*H*)-one (**28**) which is synthesized from substituted benzaldehde by Erlenmeyer synthesis (Bailly et al., 2004). Methylation of the acid (**29**) by methyl iodide in the presence of DBU gives methyl arylpyruvates (**30**) (Namiki et al., 1988). On condensation with an appropriate benzaldehyde, methyl arylpyruvate **(30)** afforded the corresponding hydroxyfuranone derivative **(31)** (Fig. 7.8) (Weber et al., 2002).

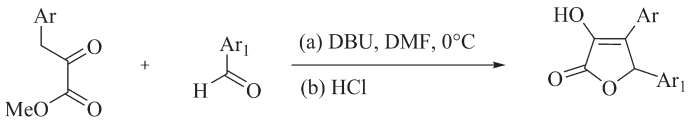

FIG. 7.7 Synthesis of 4,5-diaryl hydroxyfuranones (**27**).

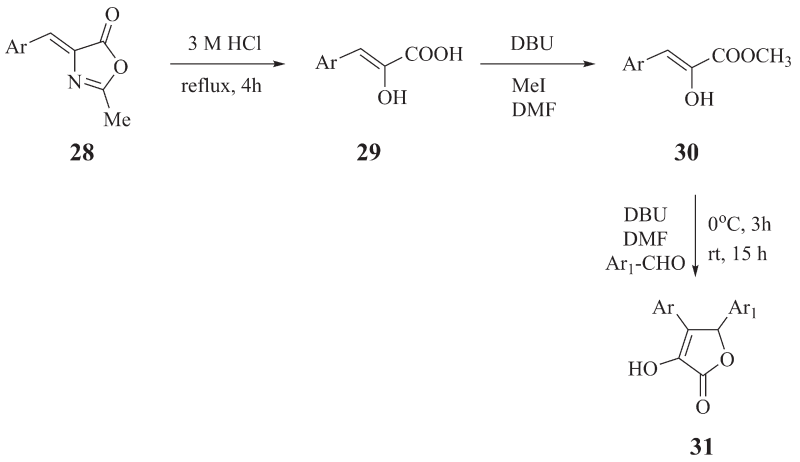

FIG. 7.8 Synthesis of vicinal diaryl furanones (**31**).

7.2 VICINAL DIARYL FURANS AS COX-2 INHIBITORS

More than 4 decades ago, it was proposed that the nonsteroidal anti-inflammatory drugs (NSAIDs) act by inhibiting the prostaglandins (PGs) biosynthesis via the cyclooxygenase (COX) enzyme (Vane, 1971). Vane was bestowed with Nobel Prize in Medicine for this work. Some 20 years after this discovery, in around 1990, it was discovered that there were two COX isoforms, namely cyclooxygenase-1 (COX-1) and cyclooxygenase-2 (COX-2) (Fu et al., 1990). COX-1 is expressed constitutively in several tissues including the kidneys, platelets, and the gastrointestinal (GI) tract, and is involved in the normal physiological homeostasis such as GI integrity, renal function, and vascular dilation. Interruption of COX-1 activity elicits gastrointestinal toxicity such as perforation of the gut, ulceration, and bleeding (Smith and Dewitt, 1996). COX-2 is induced by inflammatory stimulus that causes inflammation (Dubois et al., 1998).

Traditional NSAIDs, for example, aspirin, diclofenac, ibuprofen, naproxen, piroxicam, etc. inhibit both COX isoforms that account for their anti-inflammatory effect as well as their undesired effect of GI toxicity (Dannhardt and Kiefer, 2001). So selectively inhibiting COX-2 over COX-1 was considered a favorable approach for the management of inflammation and inflammation-mediated disorders as it lowered GI toxicity in comparison to the traditional NSAIDs (Cannon and Breedveld, 2001).

The underlying endeavors for the evolution of selective COX-2 inhibitors were being made by the Merck research group by keeping in mind that these inhibitors would have the potential to open up a new era of novel NSAIDs having better therapeutic properties and lesser side effects like gastropathy. A number of tricyclic 4-methylsulfonylphenyl class of compounds were reported by the researchers at that time taking **DuP 697** (**32**) (Fig. 7.9), as a lead from that study (Gans et al., 1990). It was known beforehand that replacing the methylsulfonyl group by a sulfonamide group enhanced the oral bioavailability but at the same time, it dramatically increased COX-1 inhibitory activity thereby deteriorating the selectivity indices of the resulting compounds. The presence of a bromo or a methyl group in the central scaffold also increased the COX-1 inhibitory activity (Leblanc et al., 1995; Gauthier

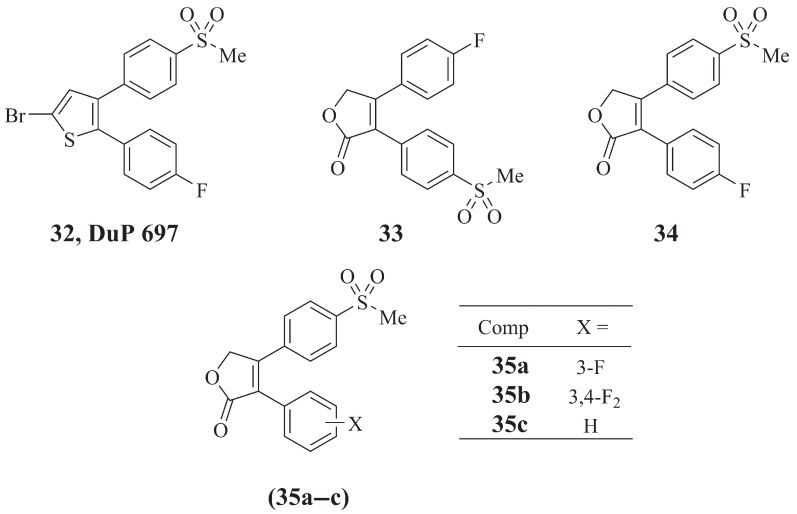

Comp	X =
35a	3-F
35b	3,4-F_2
35c	H

FIG. 7.9 COX inhibitors (**32–35**) reported by the MERCK research group.

et al., 1996). By considering these aspects, Merck researchers planned to consolidate the following structural modifications into the designed selective COX-2 inhibitors for the improvement in their oral absorption without compromising the selectivity ratio: (1) utilizing the methylsulfone rather than the sulfonamide group to increase COX-2 selectivity; (2) replacement of the bulky bromo substituent in **DuP 697** (**32**) to increase COX-2 selectivity; and (3) replacing the central thiophene scaffold with a new heterocycle to address the oral absorption issue.

In light of these points, the thiophene scaffold was substituted by a lactone ring. The methylsulfone moiety was retained for augmenting COX-2 selectivity. The two isomeric lactone derivatives (**33** and **34**) (Fig. 7.9) were synthesized and out of the two, compound **(33)** was found to be inactive, whereas compound (**34**) was observed to possess noteworthy COX-2 inhibitory activity. Compound (**34**) showed potent COX-2 inhibitory activity comparable to indomethacin; however, it was a much poorer inhibitor of COX-1.

Likewise with other reported vicinal diaryl COX-2 inhibitors, it was observed that compounds with the *p*-substituted phenyl rings at the C-3 position of the furan showed improved COX-1 inhibition raising the selectivity issue. Compound (**34**) was a more potent COX-1 inhibitor than compound (**35c**) (Fig. 7.9). Moreover, the presence of substituent at the third position (e.g., **35a**) or at both third and fourth positions (e.g., **35b**) (Fig. 7.9) led to a decrease in COX-1 inhibitory activity, whereas the COX-2 inhibitory activity of the compounds (**35a** and **35b**) remained unaffected. It was observed that these changes did not significantly influence their COX-2 inhibitory activities. The lower phenyl ring (at the C-3 position) was replaced by some heterocycles, but these compounds exhibited a reduction in COX-2 inhibitory activity. From these results, it was conceded that the active site of the COX-1 enzyme is sterically more challenging compared with the active site of COX-2, which made it more challenging toward the changes in the substitution pattern (Mancini et al., 1994).

Among so many compounds synthesized and screened, rofecoxib (**35c**) was identified to be an orally active, potent, and selective COX-2 inhibitor. Rofecoxib (**35c**) has shown an

ED_{50} of about 1 mg/kg in different animal models, offering a remarkable therapeutic index of greater than 300. Additionally, rofecoxib (**35c**) showed admirable pharmacokinetics and dose proportionality in various animal species. The US FDA approved rofecoxib on May 20, 1999 and the drug was marketed under the brand names Vioxx, Ceoxx, and Ceeoxx. Soon after approval, rofecoxib got wide acknowledgment from the medical fraternity dealing with patients having arthritis and other acute or chronic pain causing conditions. On September 30, 2004 Merck pulled back rofecoxib as its long-term high-dosage use led to high risk of stroke and heart attack in patients. Disruption of the physiological balance in cyclooxygenase pathway by rofecoxib leads to decreased levels of anti-aggregatory and vasodilatory prostacyclin PGI_2 and concurrently increased the levels of prothrombotic thromboxane A_2 that increases the incidence of adverse cardiovascular events. Rofecoxib was a standout among the most generally utilized medications ever to be pulled back from the market.

Habeeb et al. reported rofecoxib analog **(36)** (Fig. 7.10), in which the methylsulfonyl group, the hydrogen-bonding pharmacophore, was substituted by a bioisosteric dipolar azido group (Habeeb et al., 2001). Compound (**36**) showed promising COX-2 inhibitory activity (COX-2, IC_{50} value of 0.196 μM, SI = 812). Compound **(36)** also showed remarkable oral anti-inflammatory activity (42.9 ± 1.0 % inhibition at 3 h and 27.5 ± 4.6% inhibition at 5 h) in carrageenan-induced rat paw edema assay after giving the test compound orally at a dose of 50 mg/kg and analgesic activity (46.7 ± 1.3% inhibition of pain at 30 min and 60.6 ± 1.6% inhibition of pain at 60 min) in 4% NaCl-induced abdominal constriction assay in rats after 50 mg/kg ip dose of the test compound.

Rahim et al. (2002) reported 2-, 3-, or 4-acetoxy analogs of rofecoxib (**37a–c**) (Fig. 7.10) as selective COX-2 inhibitors. These compounds (**37a–c**) exhibited poor COX-1 inhibitory activity with IC_{50} values of greater than 100 μM, but interestingly showed excellent COX-2 inhibition having IC_{50} values in the range of 0.00126–0.00350 μM relative to rofecoxib (COX-2, IC_{50} value of 0.4279 μM, SI > 1168). These data suggested that the compounds (**37a–c**) might inhibit the prostaglandins synthesis at the sites of inflammation via the cyclooxygenase pathway and due to their poor COX-1 inhibitory activity, these compounds could be free from ulcerogenic side effects.

Black et al. (2003) introduced the hydroxyl group on the fifth position of the diaryl furanone. These compounds (**38**) (Fig. 7.11) have shown high selectivity for COX-2 and were lacking potency against COX-1. The aqueous solubility of most of the furanone derivatives was observed to be very low; these hydroxyl furanones showed excellent solubility in alkaline solution due to the formation of open chain isomer salts. In animal studies, the oral dosing of sodium salts of these compounds showed equivalent efficacy compared with the neutral

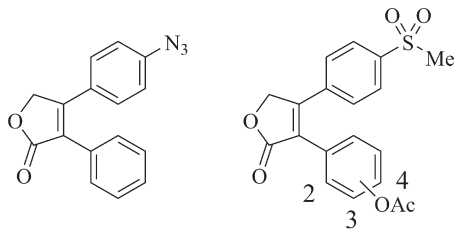

36 **(37a–c)**

FIG. 7.10 Rofecoxib analogs (**36**, **37**) as COX inhibitors.

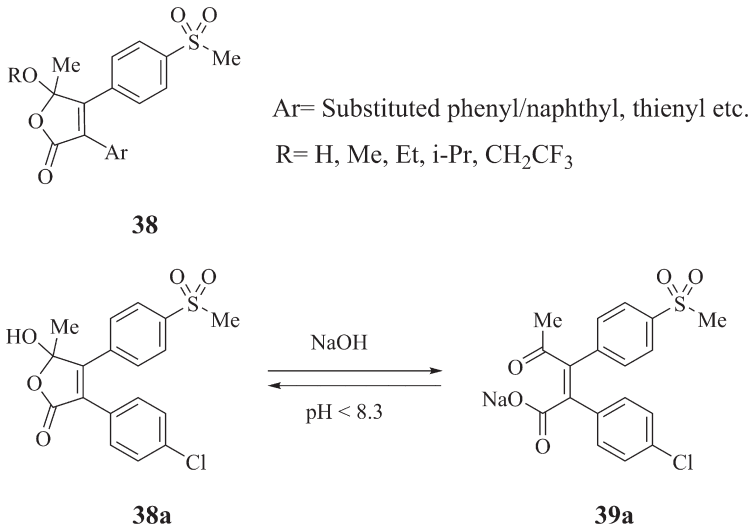

38 **38a** **39a**

FIG. 7.11 3,4-Diaryl hydroxyfuranones (**38**) as selective COX-2 inhibitors.

cyclic form. Compound (**39a**) showed good efficacy in rat paw edema assay with an ED_{50} value of 1.8 mg/kg, in rat pyresis model with an ED_{50} value of 0.7 mg/kg, in rat hyperalgesia model with an ID_{50} value of 0.8 mg/kg and in rat adjuvant arthritis model with an ID_{50} value of 0.6 mg/kg. The GI toxicity of the compound was studied by ^{51}Cr assay in rats wherein it showed that after dosing of 100 mg/kg for 10 days, there was no loss in the integrity of GI tract.

Zarghi et al. (2004) reported a series of rofecoxib analogs having *p*-substituted phenyl rings at C-3 and C-4 positions of the central furan-2-one scaffold (**40a–h**) (Fig. 7.12). Various substituents such as sulfonamido, azidosulfonyl, or *N*-acetylsulfonamido were tried and investigated the impact of these substituents on the potency and selectivity of COX isozymes. In vitro studies exhibited that the compounds (**40c** and **40d**) having an additional sulfonamido group were inactive COX inhibitors with IC_{50} values greater than 100 μM. In contrast, compound (**40g**) having a 4-azidosulfonylphenyl substituent showed modest inhibition of COX-1 and COX-2 with IC_{50} values of 31.5 μM and 11 μM, respectively. On the contrary, the corresponding regioisomer (**40h**) was not a potent COX-2 inhibitor (an IC_{50} value of

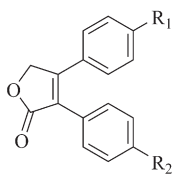

(40a–h)

Comp	R_1 =	R_2 =
40a	SO_2Me	H
40b	H	SO_2Me
40c	SO_2Me	SO_2NH_2
40d	SO_2NH_2	SO_2Me
40e	SO_2Me	$SO_2NHCOMe$
40f	$SO_2NHCOMe$	SO_2Me
40g	SO_2Me	SO_2N_3
40h	SO_2N_3	SO_2Me

FIG. 7.12 Rofecoxib analogs (**40a–h**) reported by Zarghi et al.

3.15 μM), but selectivity for COX-2 (SI > 31) was notable. The *N*-acetylsulfonamide-containing compounds (**40e** and **40f**) brought about the acetylation of the COX-2 enzyme, providing a new class of acetylating COX-2 inhibitors. Compound (**40e**) showed approximately comparable inhibition of COX-1 and COX-2 isozymes with IC_{50} values of 3.1 μM and 4.6 μM, respectively. On the other hand, the corresponding regioisomer compound (**40f**) was a potent and selective COX-2 inhibitor (IC_{50} value of 0.05 μM, SI > 2000) compared with rofecoxib (COX-2, with an IC_{50} value of 0.05 μM, SI > 1162), and was not ulcerogenic as it showed the least COX-1 inhibition (IC_{50} > 100 μM).

Shin et al. (2004) designed and synthesized some novel 2,2-dialkyl-4,5-diaryl-3(2*H*)-furanone derivatives. Compound (**41a**) (Fig. 7.13) showed good COX-2 inhibitory activity (IC_{50} value of 0.05 μg/mL) and COX-2 selectivity (SI = 400) comparable to celecoxib. Replacement of the 4-phenyl ring of the furanone with heterocyclic rings led to significant decrease in COX-2 inhibition. Compound (**41b**) (Fig. 7.13) having a spirocyclopentyl moiety showed COX-2 inhibitory activity (IC_{50} value of 0.03 μg/mL) better than the corresponding 2,2-diethyl-3(2*H*)-furanone derivative (IC_{50} value of 5 μg/mL) and equal to the 2, 2-dimethyl-3(2*H*)-furanone derivative (IC_{50} value of 0.05 μg/mL). The spirocyclopentyl moiety of compound (**41b**) occupies a lesser space compared with the diethyl moiety, which could be responsible for improved COX-2 inhibitory potency of compound (**41b**). Compounds having spirocyclohexyl moiety at this point showed poor COX-2 inhibitory activities due to the size limitation near the access of the COX-2 active site. When the methylsulfone group was replaced with the sulfonamide group, the selectivity for COX-2 decreased but COX-2 inhibitory activity got improved appreciably. Compound (**41d**) (Fig. 7.13) showed sevenfold better

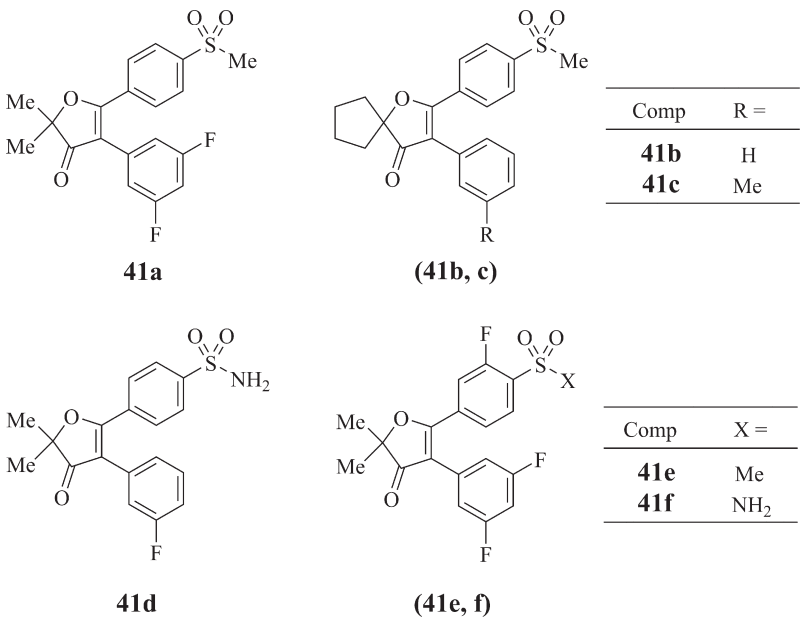

FIG. 7.13 2-Substituted 4,5-diaryl-3(2*H*)-furanone derivatives (**41a–f**) as COX-2 inhibitors reported by Shin et al.

COX-2 inhibitory activity (IC_{50} value of 0.003 μg/mL) than the corresponding methylsulfonyl derivative (IC_{50} value of 0.02 μg/mL).

To enhance the COX-2 selectivity of these compounds, a halide substituent was incorporated into the phenyl ring having a sulfonamide/methylsulfone group. Substitution with a halide next to these groups in compounds (**41e** and **41f**) (Fig. 7.13) increased the selectivity for COX-2 from 250 to 6667 and from 100 to 167, respectively, compared with the corresponding compounds without the halide substituent. The most potent compound (**41d**) showed a powerful anti-inflammatory activity in adjuvant-induced arthritis preventive model with an ED_{50} value of 0.1 mg/kg/day and strong analgesic activity in carrageenan-induced thermal hyperalgesia with an ED_{50} value of 0.25 mg/kg. On 7-day repeat dosing, these compounds exhibited reduced or no gastric side effects similar to selective COX-2 inhibitors. Although 2,2-dimethyl-4-phenyl-5-{4-(methylsulfonyl)phenyl}-3(2*H*)-furanone derivatives were powerful anti-inflammatory agents and potent selective COX-2 inhibitors, their poor bioavailability in dogs raised a question on their oral bioavailability in humans.

The sulfoxide moiety is an effective functionality to promote the transdermal penetration, which then get converted enzymatically into the corresponding sulfone. Sulfoxide analog as a prodrug could be utilized for improving oral bioavailability of the corresponding sulfone analog having bioavailability issues. Moh et al. used this strategy for improving the oral bioavailability of lipophilic selective COX-2 inhibitor with a methylsulfone moiety (Moh et al., 2004). The pharmacokinetics data for the sulfone analog (**42b**) (Fig. 7.14) after oral administration of the corresponding sulfoxide analog (**42a**) (Fig. 7.14) was C_{max} = 2.6 mg/mL, T_{max} = 2 h, and AUC_{0_24h} = 23.1 h mg/mL (10 mg/kg). Compound (**42b**) when given orally showed about 3.5-fold reduction in the systemic exposure of compound (**42b**) as shown by its pharmacokinetics parameters [C_{max} = 0.64 mg/mL, T_{max} = 4.3 h and AUC_{0_24h} = 6.6 h mg/mL (10 mg/kg)]. The concept of the sulfoxide analog as a prodrug was further justified by evaluating another set of sulfone analog (**42d**) (Fig. 7.14) and the corresponding sulfoxide prodrug (**42c**) (Fig. 7.14). The sulfoxide analogs (**42a** and **42c**) exhibited less COX-2 inhibition in comparison to their corresponding sulfone analogs (**42b** and **42d**). The sulfoxide prodrugs also have low COX-1 inhibitory activity. As the sulfoxide analogs exhibited weaker COX-1 and COX-2 inhibitory activities compared with the corresponding sulfone analogs, the sulfoxide analogs as

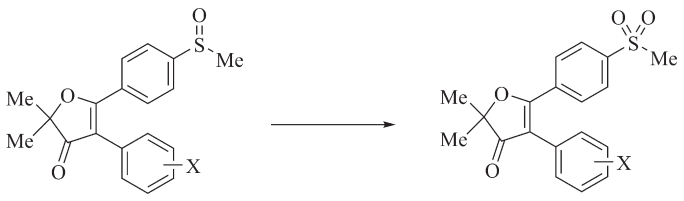

(42a, c) **(42b, d)**

Comp	X	IC_{50} mg/mL	
		COX-2	COX-1
42a	3-F,5-F	1	10
42c	3-Cl	0.3	5

Comp	X	IC_{50} mg/mL	
		COX-2	COX-1
42b	3-F,5-F	0.02	5
42d	3-Cl	0.01	2

FIG. 7.14 Vicinal diarylfuranone derivatives (**42a–d**) as reported by Moh et al.

prodrugs could offer an appropriate way out to lessen the GI side effects of COX-2 inhibitors having a methylsulfone grouping.

Zarghi et al. (2007) reported methanesulfonamido analogs of rofecoxib (**43a-f**) (Fig. 7.15) in which various substitutents (H, F, Cl, Me, OMe) were introduced into the lower phenyl ring (at C-3 position) to understand the cumulative steric and electronic effects of the substituents on the selectivity and inhibitory potencies for COX isozymes. Compounds **(43a–d)** having a phenyl or 4-halo-substituted phenyl ring at C-3 position exhibited dual COX-1 and COX-2 inhibition with COX-2 selectivity indices in the range of 3.1–39.4; whereas the compounds (**43e** and **43f**) possessing an electron-donating methyl or methoxy group were more selective COX-2 inhibitors having COX-1 IC_{50} values of greater than 100 μM. Among all of the reported compounds, compound (**43c**) showed the highest selective COX-2 inhibition with an IC_{50} value of 0.8 μM.

Considering the flexibility and chiral nature of COX-2 active site, Singh et al. designed a series of 5-substituted 2,3-diaryl-tetrahydrofuran-3-ol derivatives having substituted aryl moieties at C-2 and C-3 positions of the central tetrahydrofuran scaffold. The tetrahydrofurans with 5-hydroxymethyl (**44**) or 5-carboxylic acid (**45**) groups and different substituents on the aryl rings were evaluated for their COX inhibitory activities (Singh et al., 2008b). The presence of substituted aryl moieties in compounds (**44a–f**) (Fig. 7.16) not only affects the

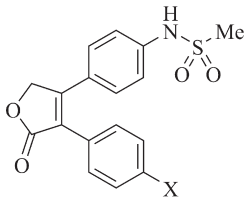

(43a–f)

Comp	X =
43a	H
43b	F
43c	Cl
43d	Br
43e	Me
43f	OMe

FIG. 7.15 Methanesulfonamido analogs of rofecoxib (**43a–f**) as reported by Zarghi et al.

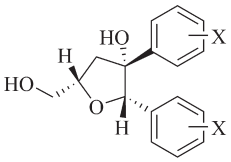

(44a–f)

Comp	X =
44a	H
44b	4-Cl
44c	2-Cl
44d	4-F
44e	4-OMe
44f	4-SO_2Me

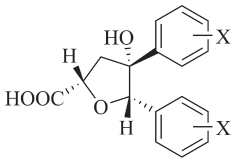

(45a–c)

Comp	X =
45a	H
45b	2-Cl
45c	4-F

FIG. 7.16 5-Substituted 2,3-diaryl-tetrahydrofuran-3-ols (**44a–f** and **45a–c**) as selective COX-2 inhibitors.

inhibitory activities but also govern the selectivity toward COX-2 enzyme. Compounds (**44b** and **44f**) showed almost comparable COX-2 (43% and 40% at 10^{-6} M concentration, respectively) and COX-1 (56% and 55% at 10^{-5} M concentration, respectively) inhibition. Compound (**44c**) exhibited moderate COX-2 (67% and 68% at 10^{-6} M and 10^{-5} M concentrations, respectively) and COX-1 (73% at 10^{-5} M concentration) inhibition. Compounds (**44d** and **44e**) showed notable COX-2 inhibition (88% and 65% at 10^{-6} M concentration, respectively) as well as a selectivity index of greater than 10 for COX-2. Compound (**45a**) (Fig. 7.16) displayed average COX-2 inhibition (69% and 68% at 10^{-5} M and 10^{-6} M concentrations, respectively) with a selectivity index of greater than 10 for COX-2. Compounds (**45b** and **45c**) (Fig. 7.16) showed 82% and 90% COX-2 inhibition, respectively, at 10^{-5} M concentration. These compounds showed considerable COX-2 inhibition, even better than celecoxib (50% at 10^{-6} M concentration) and are comparable to rofecoxib (75% at 10^{-6} M concentration). These compounds get relucted in air providing a benefit over rofecoxib which is prone to exert toxicity owing to its oxidative degration to maleic anhydride derivative (Reddy and Corey, 2005).

Several 2-oxo-3*H*-benzoxazole derivatives have shown potent analgesic and anti-inflammatory activity and some of them have additionally shown inhibitory activity for PGE_2 formation (Renard et al., 1981; Okçelik et al., 2003; Abdel-Azeem et al., 2009). Eren et al. incorporated a substituted benzoxazole moiety in place of one of the aryl rings in the diaryl furan for obtaining better COX-2 inhibitors (Eren et al., 2010). Only compound (**46**) (Fig. 7.17) from the series showed significant inhibition of COX isozymes at 10 μM concentration. The IC_{50} values of compound (**46**) for COX-1 and COX-2 were 0.061 μM and 0.325 μM, respectively. Compound (**46**) showed a selectivity index (COX-1/COX-2) of 0.19 relative to rofecoxib (SI = 250) and indomethacin (SI = 0.13).

Macrophages play a crucial role in inflammation as they produce numerous proinflammatory molecules including PGE_2. PGE_2 has been considered as an important prostaglandin involved in the pathophysiology of inflammation and inflammation-mediated disorders. So the pharmacological intervention of PGE_2 production has been assumed to diminish symptoms of diseases caused by excessive and/or extensive macrophage activation. Moon et al. reported vicinal diaryl furan-2,5-dione derivatives having a broad inhibitory spectrum against PGE_2 production in macrophage cells (Moon et al., 2010). Compound (**47**) having the sulfide moiety on the phenyl ring was reported to give better activity than those with sulfoxide or sulfone moieties. Among these derivatives, compound (**47**) (Fig. 7.17) showed good inhibitory activity (IC_{50} value of 3.58 μM) for PGE_2 production as well as COX-2 inhibition (IC_{50} value of 18.45 μM).

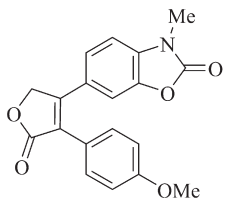

46

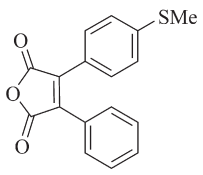

47

FIG. 7.17 Structures of compounds reported by Eren et al. (**46**) and Moon et al. (**47**).

7.3 VICINAL DIARYL FURANS AS ANTICANCER AGENTS

The three interacting moieties on a central scaffold like pyrazole in celecoxib and furanone in rofecoxib are the important structural features of diaryl-based COX-2 inhibitors. Singh et al. reported tetrahydrofuran as the central scaffold having substituted aryl moieties at the second and the third position and hydroxymethyl group at the fifth position (Singh et al., 2007). The tetrahydrofuran is structurally identical to the central scaffold of rofecoxib; nevertheless; it is lacking in the oxidation tendency of furanone. The substituents present on the two-phenyl rings have high impact on the anticancer activities of the compounds. Compounds (**48b** and **48c**) (Fig. 7.18) with chloro groups on the fourth and second positions of the phenyl rings showed excellent anticancer activities having an average GI_{50} value of 1.99×10^{-5} M and 2.20×10^{-5} M, respectively, for all the cell lines tested. Interestingly, these inhibitory activity values are in tune with the average GI_{50} value of 5-fluorouracil (5-FU) (1.77×10^{-5} M). Compound (**48b**) inhibited the growth of tumor cells showing 71% and 87% inhibition in CCRF-CEM and SR cell lines, respectively, at 10^{-6} M concentration. Replacement of the chloro group with the fluoro or methoxy groups as in compounds (**48d** and **48e**) (Fig. 7.18) offered poor average GI_{50} values for these compounds at concentrations of 9.50×10^{-5} M and 9.33×10^{-5} M, respectively.

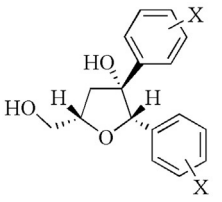

(48a–f)

Comp	X =
48a	H
48b	4-Cl
48c	2-Cl
48d	4-F
48e	4-OMe
48f	4-SO_2Me

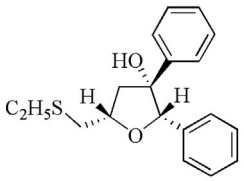

49a

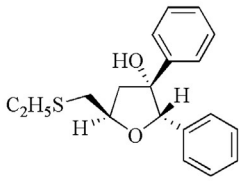

49b

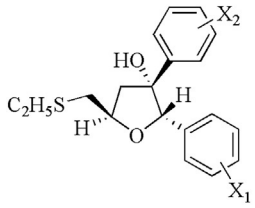

(49c–j)

Comp	X_1 =	X_2 =
49c	2-Cl	2-Cl
49d	4-Cl	4-Cl
49e	4-F	4-F
49f	4-OMe	4-OMe
49g	4-SO_2Me	4-SO_2Me
49h	H	4-SMe
49i	H	4-SO_2Me
49j	H	4-OMe

FIG. 7.18 Diaryl tetrahydrofuran derivatives (**48a–f** and **49a–j**) reported by Singh et al. as anticancer agents.

In the HOP-92 cell line of NSCLC and HS 578T cell line of breast cancer, compound (**48d**) showed 13% (at 10^{-5} M concentration) and 29% (at 10^{-7} M concentration) growth inhibition, respectively. In CCRF-CEM and SR cell lines of leukemia, compound (**48e**) showed 46% and 36% (at 10^{-6} M concentration) growth inhibition, respectively. Replacement of chloro with the methylsulfonyl group as in compound (**48f**) (Fig. 7.18) caused a decrease in activity with average the GI_{50} value being 1.0×10^{-4} M.

The authors also reported a series of diaryl tetrahydrofuran derivatives in which the hydroxymethyl group was substituted by ethylsulfanylmethyl group and evaluated the resulting derivatives for the COX-2 inhibitory activity (Singh et al., 2008a). The two diastereomers were well discriminated by COX-2 enzyme. Compound (**49b**) (Fig. 7.18) with 5*S** configuration showed good inhibition of COX-2 (IC_{50} value of 0.25 μM) while compound (**49a**) (Fig. 7.18) with 5*R** configuration showed relatively poor inhibition of COX-2 (IC_{50} value of 7.56 μM). Among the reported compounds, compound (**49c**) (Fig. 7.18) exhibited high COX-2 inhibition with $IC_{50} < 0.01$ μM, which was superior to that of rofecoxib and celecoxib.

Many COX inhibitors such as aspirin, rofecoxib, celecoxib, and so forth have been used as lead to exploit their potential as potent therapeutic agents in cancer chemotherapy along with other cytotoxic drugs after the connection of COX-2 enzyme in the advancement of cancer was well established (Meric et al., 2006). As the tetrahydrofuran derivatives were reported to have good COX-2 inhibitory activities, these derivatives were evaluated further for their growth inhibitory activities in several cancer cell lines. Compound (**49b**) (Fig. 7.18) showed an average GI_{50} value of 5.49×10^{-5} M for all the cell lines tested. In the SR cell line of leukemia, it exhibited a GI_{50} value of less than 1.00×10^{-8} M, showed 51% (at 10^{-7} M concentration) and 60% (at 10^{-8} M concentration) growth inhibition of tumor cells. Compounds (**49d** and **49e**) (Fig. 7.18) showed appreciable average GI_{50} values of 1.73×10^{-5} M and 1.31×10^{-5} M, respectively, for all the cell lines tested. Compound (**49e**) showed GI_{50} values of 3.65×10^{-8} M (CCRF-CEM cell line) and $<1.00\times10^{-8}$ M (SR cell lines). In the PC3 cell line of prostate cancer, compounds (**49d** and **49e**) showed better growth inhibitory activities than celecoxib. High LC_{50} values of compounds (**49b**, **49d**, and **49e**) indicated poor toxicity of these compounds.

Kim et al. (2002b) reported a diaryl oxazolone derivative (**52**) (Fig. 7.19) having potent cytotoxicity and antitumor activity (Nam et al., 2001). These derivatives were structurally similar to deoxypodophyllotoxin (DPT) (**50**) (Fig. 7.19), a potent cytotoxic compound obtained from the plant *Pulsatilla koreana* (Kim et al., 2002a). Combretastatin A4 (**51**) (Fig. 7.19) is a potent antimitotic and cytotoxic agent obtained from the plant *Combretum caffrum* (Pettit et al., 1989). The double bond with *cis* configuration and the 3,4,5-trimethoxy groups on ring A are the fundamental requirements for its antitumor action. The *cis* double bond is subject to rapid *cis–trans* isomerization in the presence of light, heat, and protic media. From this observation, to make the compound more stable, numerous *cis*-restricted analogs were prepared which showed a biological profile comparable to combretastatin A4. By taking the above inputs, Kim et al. have designed diaryl furanones having two aromatic moieties linked directly to the furan ring. This research group was the first to report 3,4-diaryl-2(5*H*)-furanones, a group of compounds recognized previously as selective COX-2 inhibitors, with admirable anticancer activity. In cell line study, compounds (**53a–d**) (Fig. 7.19) exhibited noteworthy cytotoxic activities ($ED_{50} < 20$ nM).

The neovasculature is a potential target for the discovery of new anticancer agents. A number of potential candidates that interacted with α-tubulin and disrupt the microtubule complex

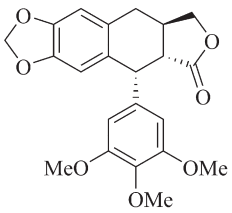

50, DPT

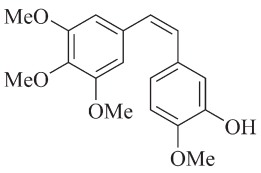

51, Combretastatin A4

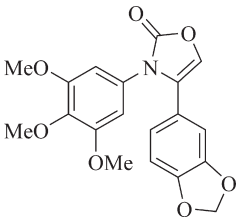

52

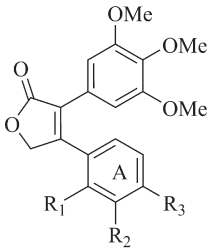

(53a–d)

Comp	R_1 =	R_2 =	R_3 =
53a	H	H	OMe
53b	H	OH	OMe
53c	H	NH_2	OMe
53d	A-ring ; 2-Naphthyl		

FIG. 7.19 Structures of deoxypodophyllotoxin (DPT) (**50**), combretastatin A4 (**51**), diaryl oxazolone derivative (**52**), and diaryl furanone derivatives (**53a–d**).

have already been studied in clinical trials (Jordan and Wilson, 2004; Neri and Bicknell, 2005). Combretastatin A4 (**51**) is reported to have neovasculature specificity and interacts with α-tubulin (Young and Chaplin, 2004). Pirali et al. reported replacement of the olefinic bridge present in combretastatin A4 (**51**) with a furan ring, by keeping in mind that the furan ring could be readily functionalized by electrophilic aromatic substitution reaction. In neuroblastoma cells, these rigid analogs showed potent cytotoxic activity at nanomolar concentrations and showed a structure–activity relationship comparable to combretastatin A4 (Pirali et al., 2006). Compound (**54a**) (Fig. 7.20) showed an IC_{50} of 39 ± 8.9 nM for cell growth. The hydroxyl group containing compound (**54d**) (Fig. 7.20) was the most potent one having an IC_{50} value of 2.9 ± 0.33 nM; compound (**54c**) (Fig. 7.20) having an amino group showed a slightly poor IC_{50} value (5.1 ± 0.7 nM); and compound (**54b**) (Fig. 7.20) having a nitro group exhibited an

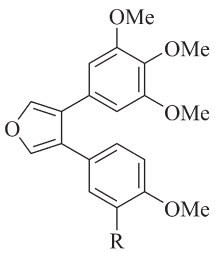

(54a–d)

Comp	R_1 =
54a	H
54b	NO_2
54c	NH_2
54d	OH

FIG. 7.20 3,4-Diarylfurans (**54a–d**) reported by Pirali et al. as anticancer agents.

IC_{50} value of between 100 nM and 1 μM. In the in vivo tubulin polymerization assay, these compounds behaved identically to combretastatin A4 (**51**) and inhibited the polymerization of tubulin but at the same time, in a cell cycle analysis these compounds did not show the G2/M blockage as combretastatin A4, thereby indicating a different mechanism of action that might or might not depend on tubulin polymerization.

7.4 VICINAL DIARYL FURANS AS ANTIOXIDANTS AND ANTI-INFLAMMATORY AGENTS

Medical conditions such as myocardial infarction, neurologic trauma, and carcinogenesis could be aggravated by the presence of free radicals (Gutteridge and Halliwell, 1993). Free radicals are toxic mainly because they initiate a chain reaction of lipid peroxidation and could split DNA, RNA, proteins, cellular membranes, and cellular organization. Free radicals are reported to have a crucial role in the pathophysiology of inflammation and airway obstruction in asthma. Under normal conditions, to offset the harmful effects of free radicals, aerobic organisms have their own defense systems such as glutathione peroxidase, superoxide dismutase, certain antioxidants, and free radical scavengers such as ascorbic acid (**55**) (Fig. 7.21), α-tocopherol, glutathione, and β-carotene (Halliwell, 1991). Ascorbate is a potent naturally occurring antioxidant working by reacting with aqueous peroxy radicals as well as by reviving the antioxidant properties of α-tocopherol (Bendich et al., 1986). However, it has low solubility in lipophilic environment and is susceptible to thermal and oxidative degradation, so there is a need of stable ascorbate derivatives with better lipophilicity (Kato et al., 1988; Nihro et al., 1991, 1992).

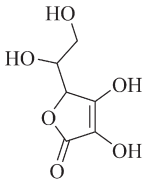

55, Ascorbic acid

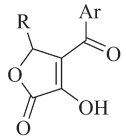

56a R= H, Ar

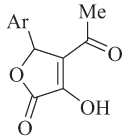

56b

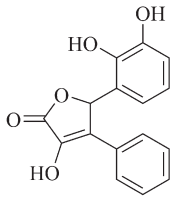

57

FIG. 7.21 Structures of ascorbic acid (**55**), ascorbic acid analogs (**56a, b**), and vicinal diaryl hydroxyfuranone (**57**).

Weber et al. (2000) reported antioxidant properties of lipophilic ascorbic acid analogs (**56a** and **56b**) (Fig. 7.21). These furanone derivatives were more effective than ascorbic acid, although substitution at fourth position of the furan ring by a benzoyl or an acetyl group enhanced their toxicity compared with ascorbic acid (Coudert et al., 1996; Weber et al., 2000). The authors also synthesized a series of novel 3-hydroxyfuranone derivatives having aromatic substituents directly linked to the furan ring in the fourth and fifth positions to identify suitable features for better activity with minimal toxicity (Weber et al., 2002). Among the reported compounds by the authors, compound (**57**) (Fig. 7.21) having a 2,3-dihydroxyphenyl ring on the fifth position of the furan ring was the most powerful antioxidant compound with superoxide anion quenching capacity (IC_{50} value of 0.187 μM), DPPH radical scavenging activity (IC_{50} value of 10.3 μM), and lipid peroxidation inhibitory effect (IC_{50} value of 0.129 μM). Anti-inflammatory activity of the compound was investigated in carrageenan-induced paw edema in rat and phorbol ester-induced ear edema in mice (TPA-test). In the TPA-test, the test compound at an i.p. dose of 100 mg/kg showed more potent anti-inflammatory activity compared with indomethacin and ketorolac as standard drugs.

In continuation of their earlier work on 4,5-diaryl-3-hydroxy-2(5*H*)-furanones possessing good antioxidant and anti-inflammatory activities, Weber et al. designed and synthesized new furanone derivatives having methylsulfonylphenyl or methylsulfonamidophenyl moieties, as present in potent NSAIDs such as nimesulide (**58**) (Fig. 7.22), celecoxib, and rofecoxib. Among these, compound (**59**) (Fig. 7.22) was found to be the most potent compound with DPPH radical scavenging activity (an IC_{50} value of 1779 μM), superoxide anion radical scavenging capacity (IC_{50} value of 511 μM), inhibition of lipid peroxidation (IC_{50} value of 123 μM), and anti-inflammatory activity (65% inhibition of edema at 200 mg/kg i.p.).

7.5 VICINAL DIARYL FURANS AS DUAL COX-2 AND LOX INHIBITORS

Cyclooxygenase (COX) and lipoxygenase (LOX) enzymes mediate the conversion of arachidonic acid into prostanoids and leukotrienes, respectively (Funk, 2001). LTs are important in the pathogenesis of inflammation. LOX is known to be associated with metabolism of low-density lipoproteins which leads to atherosclerosis and other cardiovascular complications (Zhao and Funk, 2004). Due to the blockage of COX pathway, the LOX pathway is upregulated and gastrotoxic leukotrienes get accumulated. So synergistic blocking of both COX- and LOX-mediated metabolic pathways of arachidonic acid for better

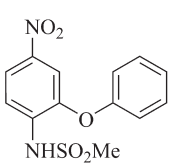

58, Nimesulide

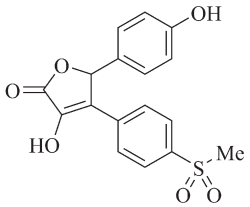

59

FIG. 7.22 Structures of nimesulide (**58**) and compound (**59**).

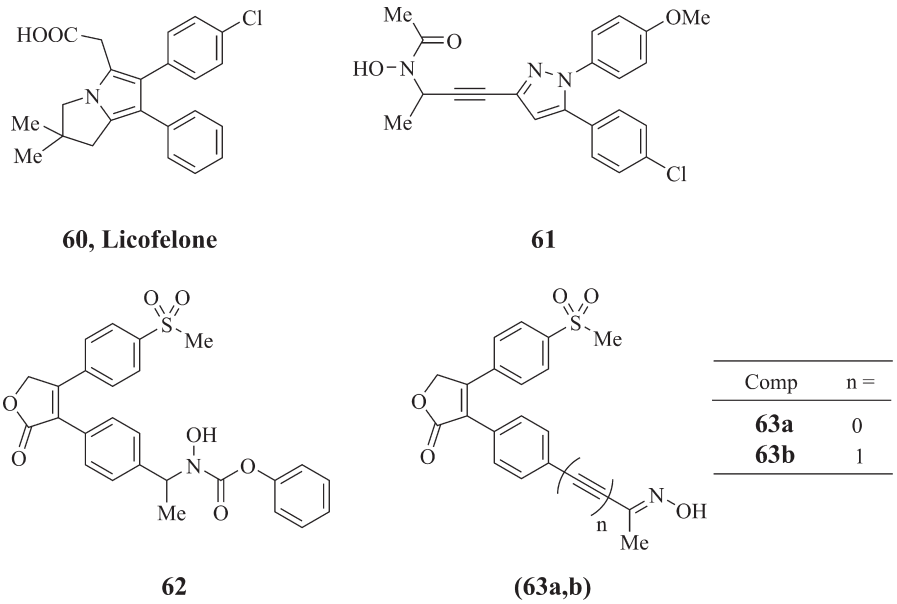

60, Licofelone **61**

62 **(63a,b)**

Comp	n =
63a	0
63b	1

FIG. 7.23 Structures of some dual COX and LOX inhibitors (**60–63**).

anti-inflammatory activity, emerged to be a safer alternative to selective inhibition of COX-2 (Fiorucci et al., 2001). Licofelone (**60**) (Fig. 7.23), a dual COX and LOX inhibitor was developed by Merckle GmbH, Germany. It was stated to have reduced GI toxicity relative to the conventional NSAIDs (Bias et al., 2004).

Arachidonoyl hydroxamate is reported to be a potent 5-LOX enzyme inhibitor, presumably due to chelation of iron in the catalytic site of 5-LOX-enzyme (Corey et al., 1984). This has provided an important clue for the designing of *N*-hydroxyurea and hydroxamic acid-based 5-LOX enzyme inhibitors (Carter et al., 1991). Using this rationale, dual inhibitors, such as compound (**61**) (Fig. 7.23) having a diarylpyrazole scaffold from celecoxib, a selective COX-2 inhibitor and an iron chelating hydroxamic acid moiety from 5-LOX inhibitors, were synthesized and evaluated. Taking inputs from this work, Chen et al. designed a series of hybrid compounds, in which rofecoxib was coupled to *N*-hydroxycarbamate moiety or an oxime group as dual COX/LOX inhibitors (Chen et al., 2006). In vitro enzyme inhibition studies revealed that compound (**62**) (Fig. 7.23) showed good COX-1, COX-2, and 15-LOX inhibition with IC_{50} values of 1 μM, 1.1 μM, and 3.4 μM, respectively. Compound **(63a)** (Fig. 7.23) showed an ideal combination of COX-2, 5-LOX and 15-LOX inhibitory activities with IC_{50} values of 1.4 μM, 0.28 μM, and 0.32 μM, respectively. Compound (**63b**) (Fig. 7.23) showed dual COX-2 and 5-LOX inhibitory activities with IC_{50} values of 2.7 μM and 0.30 μM, respectively. In carrageenan-induced rat paw edema assay, compounds (**63a** and **63b**) exhibited good anti-inflammatory activity relative to caffeic acid and nordihydroguaiaretic acid (NDGA) which are 5-LOX and 15-LOX inhibitors, respectively. However, these compounds (**63a** and **63b**) were found to be less potent than celecoxib (ED_{50} value of 10.8 mg/kg).

7.6 VICINAL DIARYL FURANS AS ANTIFUNGAL AGENTS

Immunocompromised patients, for example, those having HIV infection, cancer chemotherapy, or organ transplantation need to undergo long-term antifungal treatment to circumvent the opportunistic fungal infections. In spite of the fact that potent antifungal agents are there in the market, they are still suffering from some limitations like definite range of activity against various fungal strains or limited CNS penetration and toxicities. The problem is further complicated by extensive use of antifungal agents that leads to increased resistant in fungi. So, there is an urgent requirement of potential therapeutics that can effectively replace the currently used antifungal agents. There are some research groups reporting various antifungal furanones, based on the structural features of incrustoporin (**65**) (Fig. 7.24) (Pour et al., 2000, 2001; Vale-Silva et al., 2006). Pour et al. described 5-alkyl-3-aryl-2,5-dihydrofuran-2-ones as antifungal agents (Senel et al., 2010).

Borate et al. (2011) reported the hybrid compounds containing the pharmacophores present in furanones and fluconazole (**64**) as antifungal agents. Compound (**66**) (Fig. 7.24) showed very potent antifungal activity against *C. albicans* ATCC 24433 (MIC_{50} value of 0.5 μg/mL), *C. glabrata* ATCC 90030 (MIC_{50} value of 0.5 μg/mL), also a notable antifungal activity against *C. tropicalis* ATCC 750 (MIC_{50} value of 2 μg/mL). In compound (**66**), the substituent present on the phenyl ring (A) (Fig. 7.24) governed the antifungal activity of compounds. The presence of 2,4-difluoro and 4-fluoro groups were acceptable, while the 4-bromo, 4-methyl or 4-methoxy substituents diminished the antifungal activity marginally. When the 4-phenyl ring was replaced with a thiophene ring, there was not any observable change in the antifungal activity.

7.7 VICINAL DIARYL FURANS AS NO DONORS

Nitric oxide (NO) has a critical role of cytoprotection in GI homeostasis by promoting blood flow to mucosa, inhibiting platelet aggregation and inflammatory-cell activation (Wallace et al., 1994). These constructive actions of NO could complement the gastroprotective character of selective COX-2 inhibitors, and also induced the peripheral vasodilation to lower the blood pressure upsurge which was caused by diminished physiological

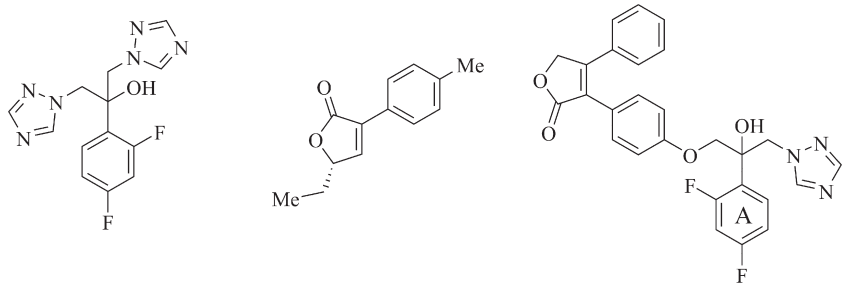

64, Fluconazole **65, Incrustoporin** **66**

FIG. 7.24 Structures of some antifungal agents (**64–66**).

levels of PGI_2 by selective COX-2 inhibitors (Elliott et al., 1995; Muscará et al., 1998). Hybrid compounds having an NO-donor moiety in their structures (NO-coxibs) have been explored to provide clinically safer COX-2 inhibitors. Compound (**67**) (Fig. 7.25) having NO donor moiety linked to the isoxazole ring showed anti-inflammatory activity comparable to valdecoxib having additional antithrombotic activity at a higher dose (Dhawan et al., 2005). Compound (**68**) (Fig. 7.25) having an NO-donor moiety was efficiently cleaved by esterases and released the parent anti-inflammatory agent indomethacin and NO (Velázquez et al., 2008).

Abdellatif et al. (2011) reported a novel hybrid prodrug (**69**) (Fig. 7.25) wherein the NO-donor moiety was attached to the parent compound (**70**). The authors designed a novel hybrid prodrug with the hope that the NO, released from the prodrug might show antihypertensive and antiplatelet aggregation actions, which would prevent the adverse hypertensive and thrombotic effects of the parent drug rofecoxib. On incubating the prodrug with phosphate buffer having pH of 7.4, a low amount of NO (4.2%) was released which was substantially increased in presence of rat serum. The incubation studies suggested that the prodrug (**69**) released both NO and the parent compound (**70**) in vivo after cleavage by nonspecific serum esterases (Fig. 7.26). Compound (**69**) was a selective COX-2 inhibitor showing marked anti-inflammatory activity with a ED_{50} value (72.2 μmol/kg) in between the values offered by the standard drugs celecoxib (30.9 μmol/kg) and ibuprofen (327 μmol/kg).

7.8 CONCLUSION

Over the last 2 decades, a good amount of research has been done for the synthesis and biological evaluation of vicinal diaryl furan derivatives. In this chapter, an attempt has been made to cover all the important perspectives of diaryl furans as medicinal agents. The general

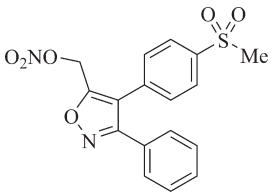

67, NMI-1093

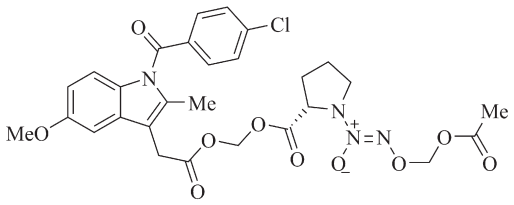

68

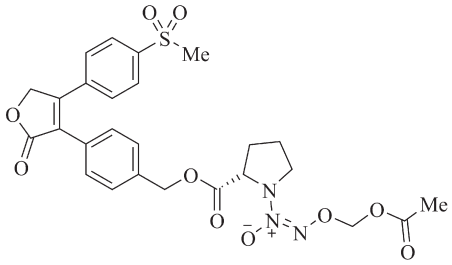

69

FIG. 7.25 Structures of compounds (**67–69**).

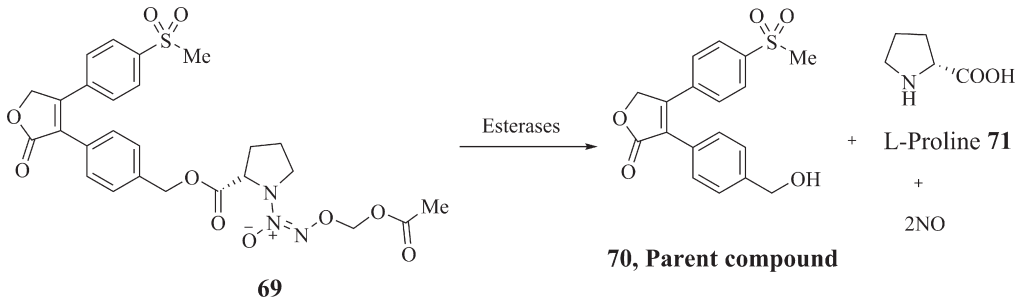

FIG. 7.26 Compound (**69**) released NO and the parent compound (**70**) after cleavage by nonspecific serum esterases.

methods of synthesis of diaryl furans have been schematically delineated. Various biological activities such as anti-inflammatory, anticancer, antioxidant, antifungal, and NO releasing activities of diaryl furans have been discussed.

Early efforts for finding a safer alternative to the traditional NSAIDs from the Merck Lab resulted into the discovery of rofecoxib, which gained FDA approval for osteoarthritis and other acute pain conditions but just after five years, Merck pulled back the drug due to enhanced risk of cardiovascular complications in patients using the drug. Various authors reported a number of rofecoxib analogs such as azido analog (**36**), acetoxy analogs (**37a-c**), *N*-acetylsulfonamideanalogs (**40e**, **40f**), and methanesulfonamido analogs (**43a-f**) with good anti-inflammatory activities. Shin et al. reported dialkyl diarylfuranones, among which the most potent compound (**41d**) showed good analgesic and anti-inflammatory activities. Moh et al. used the prodrug approach to improve the poor bioavailability of lipophilic selective COX-2 inhibitors having methylsulfone moiety. As the compounds (**42a**, **42c**) having sulfoxide moiety exhibited lower COX-1/COX-2 inhibition compared with the compounds (**42b**, **42d**) having sulfone moiety, the sulfoxide prodrugs could be beneficial in the reduction of the GI burden of the parent molecules. Moon et al. reported diaryl furandione (**47**) which showed good PGE_2 production inhibition as well as COX-2 inhibition.

The furanone ring present in rofecoxib was susceptible to oxidation to maleic anhydride derivative which could show toxicity. Singh et al. reported diaryl tetrahydrofurans which get relucted in the air providing an advantage for such compounds over rofecoxib. Compounds (**44d**, **44e**) showed good COX-2 inhibitory activity. Singh et al. also reported compounds (**48b, 48c**) with good anti-cancer activity. Compounds (**49b**, **49d**, and **49e**) showed significant growth inhibitory activity over all 59 cancer cell lines. The *cis*-restricted analogs of combretastatin A4 have been reported by various groups. These combretafurans (**53a-d** and **54a-d**) showed good anticancer activity.

Weber et al. reported the 5-hydroxyfuranone derivatives, among which compounds (**57**, **59**) showed potent anti-inflammatory and antioxidant activities. Chen et al. reported rofecoxib analogs with *N*-hydroxycarbamate moiety, as in compounds (**63a**, **b**) with dual COX and LOX inhibitory activity.

A hybrid molecule (**66**) containing furanone and fluconazole pharmacophores was reported by Borate et al., which has shown good antifungal activity against various fungal strains. Abdeallahatif et al. reported a hybrid compound (**69**) having NO donor moiety attached to hydroxymethyl group of rofecoxib analog. This prodrug showed good anti-inflammatory activity as well as inhibition of phenylephrine-induced vasoconstriction.

Thus, the diarylfuran motif has the potential for further exploration as an important scaffold for different therapeutic purposes.

References

Abdel-Azeem, A.Z., Abdel-Hafez, A.A., El-Karamany, G.S., Farag, H.H., 2009. Chlorzoxazone esters of some non-steroidal anti-inflammatory (NSAID) carboxylic acids as mutual prodrugs: design, synthesis, pharmacological investigations and docking studies. Bioorg. Med. Chem. 17, 3665–3670.

Abdellatif, K.R., Huang, Z., Chowdhury, M.A., Kaufman, S., Knaus, E.E., 2011. A diazen-1-ium-1, 2-diolated nitric oxide donor ester prodrug of 3-(4-hydroxymethylphenyl)-4-(4-methanesulfonylphenyl)-5*H*-furan-2-one: synthesis, biological evaluation and nitric oxide release studies. Bioorg. Med. Chem. Lett. 21, 3951–3956.

Bailly, F., Maurin, C., Teissier, E., Vezin, H., Cotelle, P., 2004. Antioxidant properties of 3-hydroxycoumarin derivatives. Bioorg. Med. Chem. 12, 5611–5618.

Bendich, A., Machlin, L., Scandurra, O., Burton, G., Wayner, D., 1986. The antioxidant role of vitamin C. Adv. Free Rad. Biol. Med. 2, 419–444.

Bias, P., Buchner, A., Klesser, B., Laufer, S., 2004. The gastrointestinal tolerability of the LOX/COX inhibitor, licofelone, is similar to placebo and superior to naproxen therapy in healthy volunteers: results from a randomized, controlled trial. Am. J. Gastroenterol. 99, 611–618.

Black, W.C., Brideau, C., Chan, C.C., Charleson, S., Cromlish, W., Gordon, R., Grimm, E.L., Hughes, G., Leger, S., Li, C.-S., 2003. 3,4-Diaryl-5-hydroxyfuranones: highly selective inhibitors of cyclooxygenase-2 with aqueous solubility. Bioorg. Med. Chem. Lett. 13, 1195–1198.

Borate, H.B., Sawargave, S.P., Chavan, S.P., Chandavarkar, M.A., Iyer, R., Tawte, A., Rao, D., Deore, J.V., Kudale, A.S., Mahajan, P.S., 2011. Novel hybrids of fluconazole and furanones: design, synthesis and antifungal activity. Bioorg. Med. Chem. Lett. 21, 4873–4878.

Cannon, G.W., Breedveld, F.C., 2001. Efficacy of cyclooxygenase-2-specific inhibitors. Am. J. Med. 110, 6–12.

Carter, G.W., Young, P.R., Albert, D.H., Bouska, J., Dyer, R., Bell, R.L., Summers, J.B., Brooks, D., 1991. 5-Lipoxygenase inhibitory activity of zileuton. J. Pharmacol. Exp. Ther. 256, 929–937.

Chen, Q.H., Rao, P.P., Knaus, E.E., 2006. Synthesis and biological evaluation of a novel class of rofecoxib analogues as dual inhibitors of cyclooxygenases (COXs) and lipoxygenases (LOXs). Bioorg. Med. Chem. 14, 7898–7909.

Corey, E., Cashman, J.R., Kantner, S.S., Wright, S.W., 1984. Rationally designed, potent competitive inhibitors of leukotriene biosynthesis. J. Am. Chem. Soc. 106, 1503–1504.

Coudert, P., Fernand, L., Duroux, E., Rubat, C., Couquelet, J., 1996. Effect on free radical processes of some ascorbic acid analogues. Biol. Pharm. Bull. 19, 220–223.

Dannhardt, G., Kiefer, W., 2001. Cyclooxygenase inhibitors–current status and future prospects. Eur. J. Med. Chem. 36, 109–126.

Dhawan, V., Schwalb, D.J., Shumway, M.J., Warren, M.C., Wexler, R.S., Zemtseva, I.S., Zifcak, B.M., Janero, D.R., 2005. Selective nitros (yl) action induced in vivo by a nitric oxide-donating cyclooxygenase-2 inhibitor: a nobonomic analysis. Free Radic. Biol. Med. 39, 1191–1207.

Dubois, R.N., Abramson, S.B., Crofford, L., Gupta, R.A., Simon, L.S., Van De Putte, L.B., Lipsky, P.E., 1998. Cyclooxygenase in biology and disease. FASEB J. 12, 1063–1073.

Elliott, S.N., Mcknight, W., Cirino, G., Wallace, J.L., 1995. A Nitric oxide-releasing nonsteroidal anti-inflammatory drug accelerates gastric ulcer healing in rats. Gastroenterology 109, 524–530.

Eren, G., Unlu, S., Nunez, M.T., Labeaga, L., Ledo, F., Entrena, A., Banoglu, E., Costantino, G., Sahin, M.F., 2010. Synthesis, biological evaluation, and docking studies of novel heterocyclic diaryl compounds as selective COX-2 inhibitors. Bioorg. Med. Chem. 18, 6367–6376.

Fields, E. K., Behrend, S., Meyerson, S., Winzenburg, M., Ortega, B. & Hall Jr, H. 1990. Diaryl-substituted maleic anhydrides. J. Org. Chem., 55, 5165-5170.

Fiorucci, S., Meli, R., Bucci, M., Cirino, G., 2001. Dual inhibitors of cyclooxygenase and 5-lipoxygenase. A new avenue in anti-inflammatory therapy? Biochem. Pharmacol. 62, 1433–1438.

Fu, J.Y., Masferrer, J., Seibert, K., Raz, A., Needleman, P., 1990. The induction and suppression of prostaglandin H_2 synthase (cyclooxygenase) in human monocytes. J. Biol. Chem. 265, 16737–16740.

Funk, C.D., 2001. Prostaglandins and leukotrienes: advances in eicosanoid biology. Science 294, 1871–1875.

Gans, K.R., Galbraith, W., Roman, R.J., Haber, S.B., Kerr, J.S., Schmidt, W.K., Smith, C., Hewes, W.E., Ackerman, N.R., 1990. Anti-inflammatory and safety profile of Dup 697, a novel orally effective prostaglandin synthesis inhibitor. J. Pharmacol. Exp. Ther. 254, 180–187.

Gauthier, J.Y., Leblanc, Y., Black, W.C., Chan, C.-C., Cromlish, W.A., Gordon, R., Kennedey, B.P., Lau, C.K., Léger, S., Wang, Z., 1996. Synthesis and biological evaluation of 2,3-diarylthiophenes as selective COX-2 inhibitors. Part II: replacing the heterocycle. Bioorg. Med. Chem. Lett. 6, 87–92.

Gutteridge, J.M., Halliwell, B., 1993. Invited review free radicals in disease processes: a compilation of cause and consequence. Free Radic. Res. Commun. 19, 141–158.

Habeeb, A.G., Praveen Rao, P., Knaus, E.E., 2001. Design and synthesis of celecoxib and rofecoxib analogues as selective cyclooxygenase-2 (COX-2) inhibitors: replacement of sulfonamide and methylsulfonyl pharmacophores by an azido bioisostere. J. Med. Chem. 44, 3039–3042.

Halliwell, B., 1991. Drug antioxidant effects. Drugs 42, 569–605.

Jordan, M.A., Wilson, L., 2004. Microtubules as a target for anticancer drugs. Nat. Rev. Cancer 4, 253–265.

Kato, K., Terao, S., Shimamoto, N., Hirata, M., 1988. Studies on scavengers of active oxygen species. 1. Synthesis and biological activity of 2-O-alkylascorbic acids. J. Med. Chem. 31, 793–798.

Kim, Y., Kim, S.B., You, Y.J., Ahn, B.Z., 2002a. Deoxypodophyllotoxin; the cytotoxic and antiangiogenic component from pulsatilla koreana. Planta Med. 68, 271–274.

Kim, Y., Nam, N.H., You, Y.J., Ahn, B.Z., 2002b. Synthesis and cytotoxicity of 3,4-diaryl-2 (5*H*)-furanones. Bioorg. Med. Chem. Lett. 12, 719–722.

Leblanc, Y., Gauthier, J., Ethier, D., Guay, J., Mancini, J., Riendeau, D., Tagari, P., Vickers, P., Wong, E., Prasit, P., 1995. Synthesis and biological evaluation of 2, 3-diarylthiophenes as selective COX-2 and COX-1 inhibitors. Bioorg. Med. Chem. Lett. 5, 2123–2128.

Mancini, J.A., O'neill, G.P., Bayly, C., Vickers, P.J., 1994. Mutation of serine-516 in human prostaglandin G/H synthase-2 to methionine or aspirin acetylation of this residue stimulates 15-r-hete synthesis. FEBS Lett. 342, 33–37.

Méric, J.B., Rottey, S., Olaussen, K., Soria, J.C., Khayat, D., Rixe, O., Spano, J.P., 2006. Cyclooxygenase-2 as a target for anticancer drug development. Crit. Rev. Oncol. Hematol. 59, 51–64.

Moh, J.H., Choi, Y.H., Lim, K.M., Lee, K.W., Shin, S.S., Choi, J.K., Koh, H.J., Chung, S., 2004. A prodrug approach to COX-2 inhibitors with methylsulfone. Bioorg. Med. Chem. Lett. 14, 1757–1760.

Moon, J.T., Jeon, J.Y., Park, H.A., Noh, Y.S., Lee, K.T., Kim, J., Choo, D.J., Lee, J.Y., 2010. Synthesis and PGE_2 production inhibition of 1*H*-furan-2,5-dione and 1*H*-pyrrole-2, 5-dione derivatives. Bioorg. Med. Chem. Lett. 20, 734–737.

Muscará, M.N., Mcknight, W., Del Soldato, P., Wallace, J.L., 1998. Effect of a nitric oxide-releasing naproxen derivative on hypertension and gastric damage induced by chronic nitric oxide inhibition in the rat. Life Sci. 62, Pl235–Pl240.

Nam, N.-H., Kim, Y., You, Y.-J., Hong, D.-H., Kim, H.-M., Ahn, B.-Z., 2001. Combretoxazolones: synthesis, cytotoxicity and antitumor activity. Bioorg. Med. Chem. Lett. 11, 3073–3076.

Namiki, T., Baba, Y., Suzuki, Y., Nishikawa, M., Sawada, K., Itoh, Y., Oku, T., Kitaura, Y., Hashimoto, M., 1988. Synthesis and aldose reductase-inhibitory activities of structural analogues of WF-3681, a novel aldose reductase inhibitor. Chem. Pharm. Bull. 36, 1404–1414.

Neri, D., Bicknell, R., 2005. Tumour vascular targeting. Nat. Rev. Cancer 5, 436–446.

Nihro, Y., Miyataka, H., Sudo, T., Matsumoto, H., Satoh, T., 1991. 3-O-alkylascorbic acids as free-radical quenchers: synthesis and inhibitory effect on lipid peroxidation. J. Med. Chem. 34, 2152–2157.

Nihro, Y., Sogawa, S., Izumi, A., Sasamori, A., Sudo, T., Miki, T., Matsumoto, H., Satoh, T., 1992. 3-O-Alkylascorbic acids as free radical quenchers. 3. Protective effect on coronary occlusion-reperfusion induced arrhythmias in anesthetized rats. J. Med. Chem. 35, 1618–1623.

Ökçelik, B., Ünlü, S., Banoglu, E., Küpeli, E., Yeşilada, E., Şahin, M.F., 2003. Investigations of new pyridazinone derivatives for the synthesis of potent analgesic and anti-inflammatory compounds with cyclooxygenase inhibitory activity. Arch. Pharm. 336, 406–412.

Pettit, G., Singh, S., Hamel, E., Lin, C.M., Alberts, D.S., Garcia-Kendal, D., 1989. Isolation and structure of the strong cell growth and tubulin inhibitor combretastatin A-4. Experientia 45, 209–211.

Pirali, T., Busacca, S., Beltrami, L., Imovilli, D., Pagliai, F., Miglio, G., Massarotti, A., Verotta, L., Tron, G.C., Sorba, G., 2006. Synthesis and cytotoxic evaluation of combretafurans, potential scaffolds for dual-action antitumoral agents. J. Med. Chem. 49, 5372–5376.

Pour, M., Spulak, M., Balsanek, V., Kunes, J., Buchta, V., Waisser, K., 2000. 3-Phenyl-5-methyl-2*H*,5*H*-furan-2-ones: tuning antifungal activity by varying substituents on the phenyl ring. Bioorg. Med. Chem. Lett. 10, 1893–1895.

Pour, M., Spulak, M., Buchta, V., Kubanova, P., Voprsalova, M., Wsol, V., Fakova, H., Koudelka, P., Pourová, H., Schiller, R., 2001. 3-Phenyl-5-acyloxymethyl-2*H*, 5*H*-furan-2-ones: synthesis and biological activity of a novel group of potential antifungal drugs. J. Med. Chem. 44, 2701–2706.

Rahim, M.A., Rao, P.P., Knaus, E.E., 2002. Isomeric acetoxy analogues of rofecoxib: a novel class of highly potent and selective cyclooxygenase-2 inhibitors. Bioorg. Med. Chem. Lett. 12, 2753–2756.

Reddy, L.R., Corey, E., 2005. Facile air oxidation of the conjugate base of rofecoxib (vioxx™), a possible contributor to chronic human toxicity. Tetrahedron Lett. 46, 927–929.

Renard, P., Lesieur, D., Lespagnol, C., Cazin, M., Brunet, C., Cazin, J.C., 1981. 6-Acylbenzoxazolinones and 6-acyl-2-oxo-3-benzoxazolinyl alkanoic acids. Chemical and pharmacological study. ChemInform 12.

Šenel, P., Tichotová, L., Votruba, I., Buchta, V., Špulák, M., Kuneš, J., Nobilis, M., Krenk, O., Pour, M., 2010. Antifungal 3,5-disubstituted furanones: from 5-acyloxymethyl to 5-alkylidene derivatives. Bioorg. Med. Chem. 18, 1988–2000.

Shin, S.S., Byun, Y., Lim, K.M., Choi, J.K., Lee, K.W., Moh, J.H., Kim, J.K., Jeong, Y.S., Kim, J.Y., Choi, Y.H., 2004. In vitro structure-activity relationship and in vivo studies for a novel class of cyclooxygenase-2 inhibitors: 5-aryl-2,2-dialkyl-4-phenyl-3(2*H*) furanone derivatives. J. Med. Chem. 47, 792–804.

Shin, S.S., Noh, M.S., Byun, Y.J., Choi, J.K., Kim, J.Y., Lim, K.M., Ha, J.Y., Kim, J.K., Lee, C.H., Chung, S., 2001. 2,2-Dimethyl-4,5-diaryl-3(2*H*) furanone derivatives as selective cyclo-oxygenase-2 inhibitors. Bioorg. Med. Chem. Lett. 11, 165–168.

Singh, P., Mittal, A., Kaur, S., Holzer, W., Kumar, S., 2008a. 2,3-Diaryl-5-ethylsulfanylmethyltetrahydrofurans as a new class of COX-2 inhibitors and cytotoxic agents. Org. Biomol. Chem. 6, 2706–2712.

Singh, P., Mittal, A., Kaur, S., Kumar, S., 2008b. 2,3,5-Substituted tetrahydrofurans: COX-2 inhibitory activities of 5-hydroxymethyl-/carboxyl-2,3-diaryl-tetrahydro-furan-3-ols. Eur. J. Med. Chem. 43, 2792–2799.

Singh, P., Mittal, A., Kumar, S., 2007. 2,3,5-Substituted tetrahydrofurans as cancer chemopreventives. part 1: synthesis and anti-cancer activities of 5-hydroxymethyl-2,3-diaryl-tetrahydrofuran-3-ols. Bioorg. Med. Chem. 15, 3990–3996.

Smith, W.L., Dewitt, D.L., 1996. Prostaglandin endoperoxide H synthases-1 and-2. Adv. Immunol. 62, 167–215.

Stetter, H., Kuhlmann, H., 2004. The catalyzed nucleophilic addition of aldehydes to electrophilic double bonds. Org. React. 40, 407–496.

Vale-Silva, L.A., Buchta, V., Vokurková, D., Pour, M., 2006. Investigation of the mechanism of action of 3-(4-bromophenyl)-5-acyloxymethyl-2,5-dihydrofuran-2-one against *candida albicans* by flow cytometry. Bioorg. Med. Chem. Lett. 16, 2492–2495.

Vane, J.R., 1971. Inhibition of prostaglandin synthesis as a mechanism of action for aspirin-like drugs. Nature 231, 232–235.

Velázquez, C.A., Chen, Q.-H., Citro, M.L., Keefer, L.K., Knaus, E.E., 2008. Second-generation aspirin and indomethacin prodrugs possessing an o 2-(acetoxymethyl)-1-(2-carboxypyrrolidin-1-yl) diazenium-1,2-diolate nitric oxide donor moiety: design, synthesis, biological evaluation, and nitric oxide release studies. J. Med. Chem. 51, 1954–1961.

Wallace, J.L., Reuter, B., Cicala, C., Mcknight, W., Grisham, M.B., Cirino, G., 1994. Novel nonsterodial anti-inflammatory drug derivatives with markedly reduced ulcerogenic properties in the rat. Gastroenterology 107, 173–179.

Weber, V., Coudert, P., Rubat, C., Duroux, E., Leal, F., Couquelet, J., 2000. Antioxidant properties of novel lipophilic ascorbic acid analogues. J. Pharm. Pharmacol. 52, 523–530.

Weber, V., Coudert, P., Rubat, C., Duroux, E., Vallée-Goyet, D., Gardette, D., Bria, M., Albuisson, E., Leal, F., Gramain, J.-C., 2002. Novel 4,5-diaryl-3-hydroxy-2(5*H*)-furanones as anti-oxidants and anti-inflammatory agents. Bioorg. Med. Chem. 10, 1647–1658.

Young, S.L., Chaplin, D.J., 2004. Combretastatin A4 phosphate: background and current clinical status. Expert Opin. Investig. Drugs 13, 1171–1182.

Zarghi, A., Rao, P.P., Knaus, E.E., 2004. Sulfonamido, azidosulfonyl and *N*-acetylsulfonamido analogues of rofecoxib: 4-[4-(*N*-acetylsulfonamido)phenyl]-3-(4-methanesulfonylphenyl)-2(5*H*)-furanone is a potent and selective cyclooxygenase-2 inhibitor. Bioorg. Med. Chem. Lett. 14, 1957–1960.

Zarghi, A., Rao, P.P., Knaus, E.E., 2007. Synthesis and biological evaluation of methanesulfonamide analogues of rofecoxib: replacement of methanesulfonyl by methanesulfonamido decreases cyclooxygenase-2 selectivity. Bioorg. Med. Chem. 15, 1056–1061.

Zhao, L., Funk, C.D., 2004. Lipoxygenase pathways in atherogenesis. Trends Cardiovasc. Med. 14, 191–195.

Vicinal Diaryl Thiazoles and Thiadiazoles

Chapter · January 2018

DOI: 10.1016/B978-0-08-102237-5.00008-0

2 authors:

Dushyant Patel
The Maharaja Sayajirao University of Baroda
10 PUBLICATIONS **28** CITATIONS
SEE PROFILE

Nirav R. Patel
11 PUBLICATIONS **28** CITATIONS
SEE PROFILE

CHAPTER

8

Vicinal Diaryl Thiazoles and Thiadiazoles

Dushyant V. Patel, Nirav R. Patel

The Maharaja Sayajirao University of Baroda, Vadodara, India

Abstract

Azoles are a broad class of five-membered nitrogen containing heterocyclic ring systems that may contain other non-carbon atom(s) such as sulfur or oxygen. They are important heterocycles to develop novel therapeutic agents. Several nitrogen–sulfur containing azoles such as thiazoles, thiazolines, thiazolidinones, and thiadiazoles have been extensively investigated and reported to possess a diversified spectrum of biological activities. Some of the vicinal diaryl thiazoles, thiazolines, thiazolidinones, and thiadiazoles demonstrated anticancer, anti-HIV, and anti-inflammatory activities. This chapter describes general synthetic schemes, designing, and biological profiles of various vicinal diaryl thiazoles, thiazolines, thiazolidinones, and thiadiazoles.

Keywords: Vicinal diaryl thiazoles, Thiazolines, Thiazolidinones, Thiadiazoles, Anti-HIV, Anticancer, Anti-inflammatory, COX-2 inhibitors, Anti-Alzheimer, ACAT/SOAT inhibitors

Medicinal chemists are fascinated by heterocyclic compounds due to their diversified pharmaceutical and medicinal applications. Azoles are a class of five-membered heterocyclic compounds containing a nitrogen atom that may contain additional heteroatom (nitrogen, sulfur, or oxygen) in the ring (Turchi and Dewar, 1975). The presence of azoles in many biologically active natural and synthetic compounds has proved its medicinal importance. Heterocycles of this class including tetrazoles (Ostrovskii et al., 2012), pyrazoles (Kumar et al., 2013), thiazoles (Rouf and Tanyeli, 2015), oxazoles (Ghani et al., 2016), isoxazoles (Barmade et al., 2016), etc., have motivated many researchers throughout the world to exploit their biological potential to design and develop newer therapeutic agents. A large number of nitrogen–sulfur containing azoles such as thiazoles, thiazolines, thiazolidinones, and thiadiazoles have been extensively investigated for their widespread biological activities. This chapter will cover synthesis, designing, and biological profile of vicinal diaryl thiazoles (**1**), thiazolines (**2**), thiazolidinones (**3**), and thiadiazoles (**4**) (Fig. 8.1).

https://doi.org/10.1016/B978-0-08-102237-5.00008-0

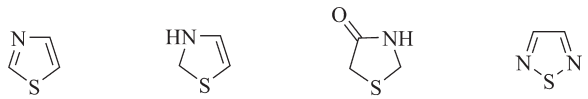

1 **2** **3** **4**

FIG. 8.1 Nitrogen–sulfur containing ring systems.

8.1 THIAZOLES

Thiazoles are a class of five-membered heterocyclic compounds featuring both nitrogen and sulfur atoms as part of aromatic ring system. On the basis of the positions of nitrogen and sulfur atoms in the ring this heterocycle can acquire two isomeric forms 1,3-thiazole (**1**; called as thiazole) or 1,2-thiazole (**5**) also known as isothiazole (Fig. 8.2). The thiazole ring has been found to be a prime component of vitamin B1 (thiamine), a vitamin essential for our body.

Thiazoles are widely used in the manufacture of fungicides, dyes, cosmetics (Bach and Heuser, 2000), sensors, molecular switches, and preparation of liquid crystals (Frija et al., 2016). In addition, they have also been utilized in medicinal chemistry to develop bioactive molecules and drugs. Thiazole has been frequently used either as a scaffold or an important pharmacophoric moiety in several drug molecules (**6–10**) (Fig. 8.3).

Apart from some interesting biological activities shown by thiazole derivatives, the thiazole ring has been exploited by medicinal chemists to develop some novel therapeutic agents for the treatment of hypertension, schizophrenia, thrombosis, inflammation, bacterial and HIV infections, allergies, and more recently in the management of pain (Siddiqui et al., 2009). As a result of its great significance, thiazole ring has been considered as a versatile scaffold in the field of medicinal chemistry (Chhabria et al., 2016).

Vicinal diaryl thiazoles have also shown interesting pharmacological profile. In the following section, some of the general synthetic routes and biological activities of vicinal diaryl thiazoles are systematically discussed.

8.1.1 Synthesis of Vicinal Diaryl Thiazoles

8.1.1.1 Hantzsch Synthesis

This is the oldest and the most widely used straightforward method for the synthesis of thiazole derivatives (**13**). This involves one-pot condensation of α-haloketones (**11**) and thioamides (**12**) in refluxing alcohol. General synthetic route is depicted in Fig. 8.4.

In another method (Fig. 8.5), diazocarbonyl compounds (**14**) were reacted with primary amides (**15**) to form α-acylaminoketones (**16**) in the presence of dirhodium tetraacetate. The 1,4-dicarbonyl intermediates (**16**) are then subsequently cyclized into thiazole derivatives (**17**) with the treatment of Lawesson's reagent (Davies et al., 2004).

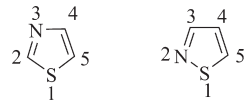

1 **5**

FIG. 8.2 Structures of thiazole (**1**) and isothiazole (**5**).

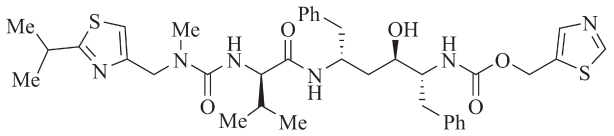

6, Ritonavir

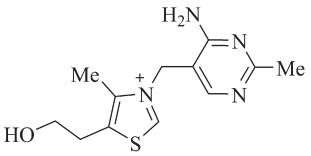

7, Vitamin B1

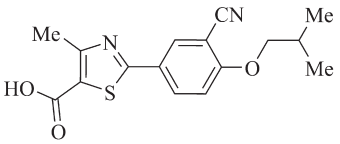

8, Febuxostat

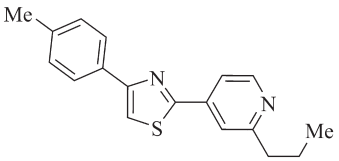

9, Fatostatin

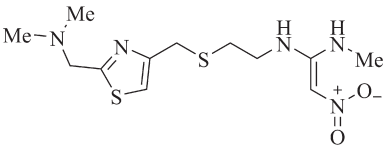

10, Nizatidine

FIG. 8.3 Some well-known drugs (**6–10**) having thiazole ring.

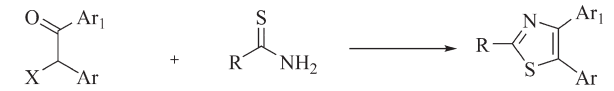

X = Cl, Br, OTs, OMs

11 **12** **13**

FIG. 8.4 Hantzsch synthesis for vicinal diaryl thiazoles (**13**).

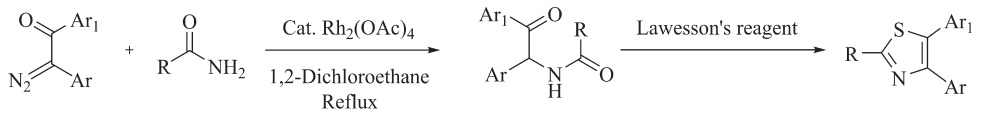

14 **15** **16** **17**

FIG. 8.5 Synthesis for vicinal diaryl thiazoles (**17**) using Lawesson's reagent.

4,5-Disubstituted 2-aminothiazoles (**20**) were synthesized via the copper-catalyzed coupling of oxime acetates (**18**) with isothiocyanates (**19**) as depicted in Fig. 8.6 (Tang et al., 2016).

Lingaraju et al. reported an efficient method (Fig. 8.7) to synthesize 4,5-disubstituted thiazoles (**23**) from aryl methyl isocyanides (**22**) and methyl or hetero arene-carbodithioates (**21**) in the presence of sodium hydride (Lingaraju et al., 2012).

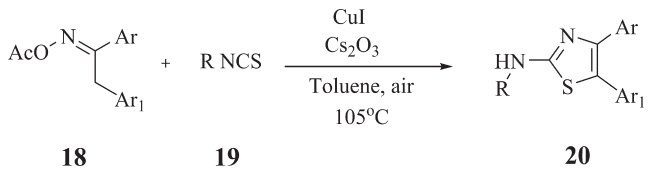

18 **19** **20**

FIG. 8.6 Synthesis of 4,5-diaryl 2-aminothiazoles (**15**).

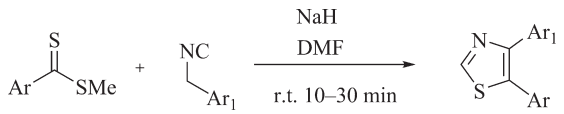

21 **22** **23**

FIG. 8.7 Synthesis of 4,5-diaryl thiazoles (**23**).

8.1.2 Biological Properties of Vicinal Diaryl Thiazoles and Isothiazoles

Most of the vicinal diaryl thiazole derivatives have been reported as anti-inflammatory, analgesic, and anticancer agents. The following section will cover biological spectrum of thiazoles and their isomeric isothiazoles.

8.1.2.1 Anti-Inflammatory Activity

The anti-inflammatory activity of conventional NSAIDs is due to the inhibition of cyclooxygenases (COXs). Two isoenzymes, COX-1 and COX-2, are responsible for the formation of prostaglandins from arachidonic acid. The constitutive COX-1 maintains important physiological processes like vascular hemostasis and gastroprotection. On the other side, COX-2 is inducible, having a significant role in inflammation. Thus, selective inhibition of COX-2 has been considered as a more effective strategy to treat inflammation and related disorders with reduced gastrointestinal (GI) side effects than NSAIDs. To overcome the limitations of the current anti-inflammatory drugs, COX-2 as a target attracted the attention of medicinal chemists in the last 2 decades. The vicinal diaryl carbo/heterocyclic scaffold received widespread popularity among the researchers for the advancement of selective COX-2 inhibitors. Several substituted diaryl heterocycles have been successfully reported as selective COX-2 inhibitors (**24–28**) (Fig. 8.8) (Dannhardt and Kiefer, 2001).

In their efforts for developing selective COX-2 inhibitors, Tanaka et al. designed compound (**31**) from the structural analysis of itazigrel (**29**) and timegadine (**30**) (Fig. 8.9). Compound (**31**) inhibited the production of malondialdehyde (MDA) ($IC_{50} = 31\,\mu M$) with vasodilatory activity ($ED_{50} = 2\,\mu M$). MDA is produced from the metabolism of arachidonic acid in the synthesis of prostaglandins in platelets, so inhibition of its production is considered to be in tune with COX inhibitory activity. Further structural modifications of the lead compound (**31**) were carried out to design a novel series of 4,5-*bis*(4-methoxyphenyl)-2-substituted thiazoles. Among the series, compound (**32**) was identified as the most potent selective COX-2 inhibitor (Fig. 8.9). Biological data demonstrated that compound (**32**) exhibited potent inhibitory activity against MDA ($IC_{50} = 0.088\,\mu M$) and ex vivo antiplatelet activity (100% inhibition, 6 h after 1 mg/kg administration) with in vitro vasodilation ($ED_{50} = 6.2\,\mu M$). Although compound (**32**)

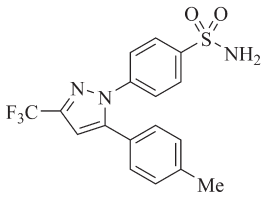

24, Celecoxib

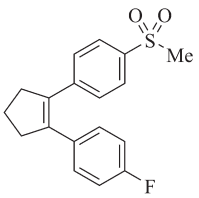

25, SC57666

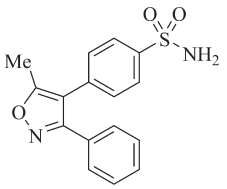

26, Valdecoxib

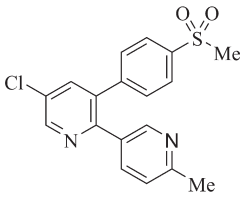

27, Etoricoxib

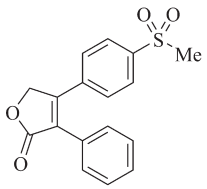

28, Rofecoxib

FIG. 8.8 Some selective COX-2 inhibitors (**24–28**).

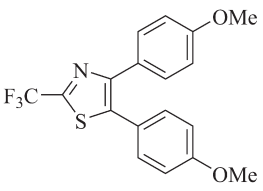

29, Itazigrel

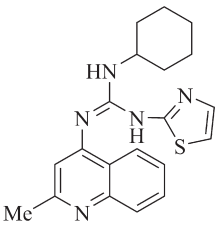

30, Timegadine

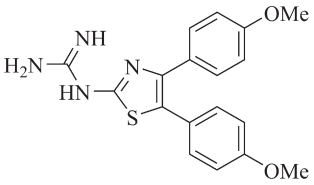

31

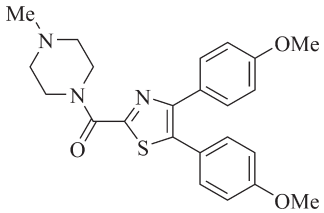

32

FIG. 8.9 Some vicinal diaryl thiazoles (**29, 31,** and **32**) reported by Tanaka et al.

showed the most potent cyclooxygenase inhibition ($IC_{50} = 0.43\,\mu M$), it manifested no ulcerogenesis in rats unlike aspirin (Tanaka et al., 1994).

Carter et al. reported a series of sulfonyl-substituted 4,5-diaryl thiazoles (**34**, **36**, and **37**) (Fig. 8.10) which were evaluated for their COX inhibitory activity. On the basis of the lead molecule SC-58125 (**33**), sulfonyl moiety was retained for optimal selectivity to obtain 4,5-diaryl thiazole derivative (**34**). Compound (**34**) was the most potent selective COX-2 inhibitor

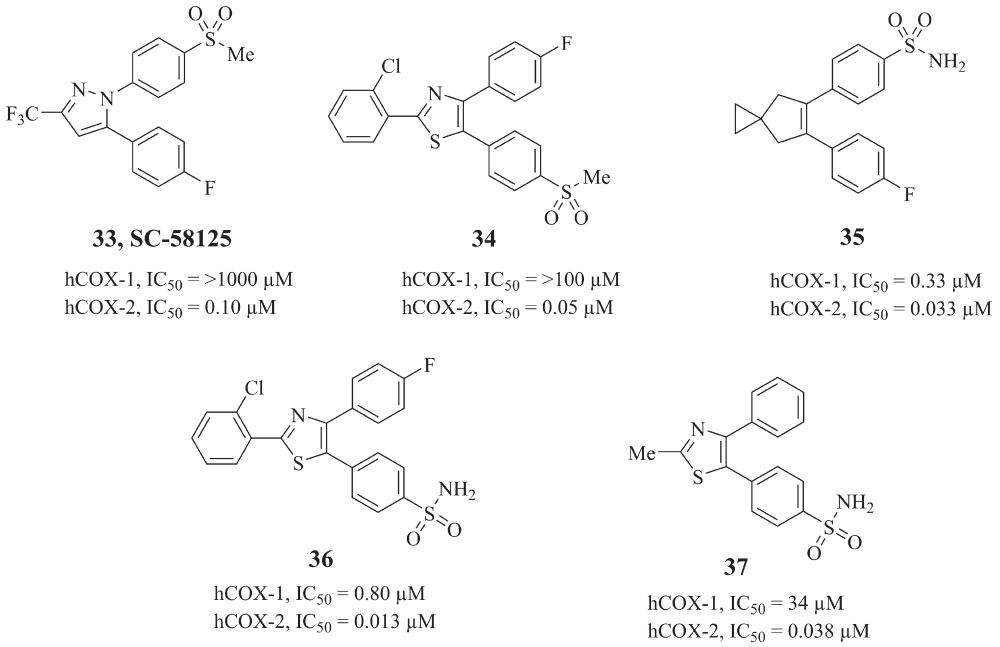

FIG. 8.10 Structures of SC58125 (**33**), **35**, and some vicinal diaryl thiazoles (**34, 36,** and **37**).

with good activity in carrageenan-induced rat paw edema assay (27% inhibition at 20 mg/kg). Inspired from the selective COX-2 inhibitor celecoxib (**24**) and **35**, sulfonylmethyl moiety of compound (**34**) was replaced by sulfonamide group to obtain compound (**36**) which showed enhanced inhibitory activity against COX-1. Compound (**36**) also showed good in vivo activity (50% inhibition at 2 mg/kg) as examined by rat air pouch assay (AP). Further modifications at C-2 position of the thiazole ring and minimal/no substitution on non-sulfonamide phenyl ring resulted in compound (**37**) with improved in vivo activity (59% inhibition in AP at 2 mg/kg) and in vitro inhibition of COX-2 (Carter et al., 1999).

On the basis of the previously reported 3,4-diaryl oxazol-2-ones (**38**), Emami et al. synthesized 3,4-diaryl-2(3*H*)-thiazolethiones (e.g., **39**) (Fig. 8.11) as potential selective COX-2 inhibitors (Emami and Foroumadi, 2006).

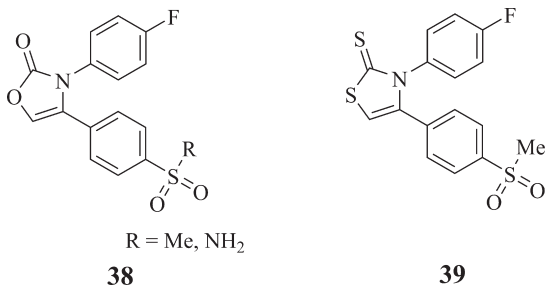

FIG. 8.11 Some selective COX-2 inhibitors (**38, 39**) reported by Emami et al.

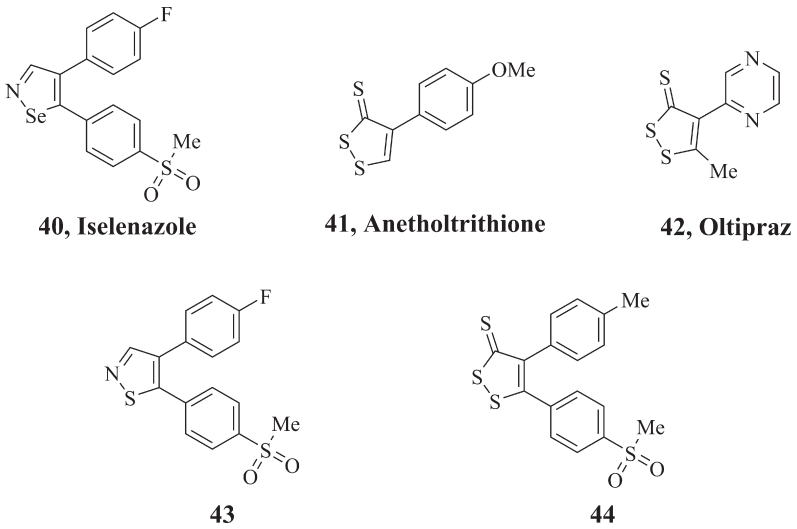

FIG. 8.12 Structures of iselenazole (**40**), anetholtrithione (**41**), oltipraz (**42**), vicinal diaryl isothiazole (**43**), and dithiolane (**44**).

Scholz et al. discovered isothiazoles (e.g., **43**) and dithiolanes (e.g., **44**) (Fig. 8.12) as COX/5-LOX inhibitors for anti-inflammatory, hydroxyl radical (OH)-scavenging, and anti-adhesive activities. Initially the isoselenazole ring of the existing COX/5-LOX inhibitor iselenazole (**40**) (Fig. 8.12) was exchanged by isothiazole ring with the logic to develop compounds retaining COX/5-LOX inhibitory activities and additionally to possess hydroxyl radical scavenging potential. Unfortunately, compound (**43**) having the isothiazole ring did not show any improvement in the hydroxyl radical scavenging activity. Further modifications were carried out by incorporating the dithiothione heterocycle present in anetholtrithione (**41**) or oltipraz (**42**), which was expected to infuse hydroxyl radical scavenging activity into the vicinal diaryl system. Compound (**44**) was found to be the most favorable hit with a balanced inhibition of all four targets (COX-1, $IC_{50} = 7\,\mu M$; COX-2, $IC_{50} = 9\,\mu M$; 5-LOX, IC_{50} ~$10\,\mu M$, and hydroxyl radical scavenging activity, $IC_{50} = 9\,\mu M$). Compound (**44**) was also found to inhibit the expression of Mac-1, and adhesion and infiltration of leukocytes in vitro and in vivo (Scholz et al., 2009).

8.1.2.2 Anticancer Activity

Cancer is a multifactorial disease, medically called as malignant neoplasm. Carcinogenesis appears with many abnormal physiological changes such as apoptosis, uncontrolled cell growth, cell adherence, tumor acidity (pH reduction), hypoxia, metastasis, and angiogenesis (Chowdhury et al., 2012; Pinto et al., 2009; Subramanian et al., 2004; Weinmann et al., 2004; Zhang et al., 2010).

Antitumor agents that bind to colchicine site of tubulin and prevent polymerization of microtubules have fascinated many researchers in the last decade. Combretastatin A-4 (**45**) (Fig. 8.13) has been reported as a standout among the most active antimitotic agents derived from *Combretum caffrum*, the African bushwillow tree. Although CA-4 (**45**) has proved its strong cytotoxic effect against different human cancer cell lines, it was found to be inactive

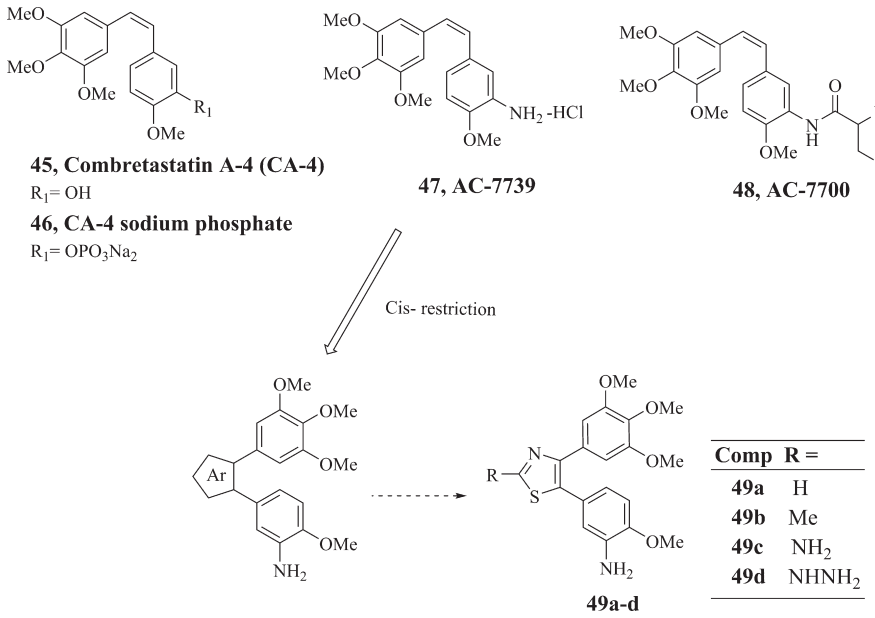

FIG. 8.13 Structures of combretastatin A-4 (**45, 46**), AC-7739 (**47**), AC-7700 (**48**), and vicinal diaryl thiazole analogs (**49a–d**).

in in vivo studies due to its low aqueous solubility. Initially prodrug approach was adopted for improvement in the aqueous solubility of combretastatin A-4 (**45**) to obtain compounds (**46–48**) (Fig. 8.13) (Ohsumi et al., 1998; Pettit et al., 1995). However, these compounds showed greater cytotoxicity and caused hemorrhagic necrosis within tissue by arresting the blood flow at the site of tumor. In addition, it was found that *cis*-combretastatin analogs easily isomerize into *trans*-forms showing dramatic reduction in antitumor activity. Thus, to develop chemically stable *cis*-restricted combretastatins with suitable geometry of the neighboring aryl groups required for the potency, derivatives were obtained by introducing various five-membered heterocycles such as pyrazole, tetrazole, imidazole, furazan (1,2,5-oxadiazole), oxazole, isoxazole, triazole, 1,2,5-thiadiazole, and thiazole.

Ohsumi et al. reported a small series of thiazole derivatives (**49a–d**) (Fig. 8.13) with substitutions at the 2-position with hydrogen (**49a**), methyl (**49b**), amino (**49c**), and hydrazino (**49d**) groups. Among these, compound (**49c**) showed potent antitubulin (IC_{50} = 1 μM) activity and cytotoxicity (IC_{50} = 57.5 nM) with in vivo antitumor activity (inhibition ratio = 75%, 40 mg/kg) which was comparable to that of AC-7739 (**47**) (inhibition ratio = 73%, 40 mg/kg). Compound (**49c**) was reported to have lesser antiproliferative activity than that of CA-4 (Ohsumi et al., 1998).

Romagnoli et al. designed a novel series of 2-amino-4,5-diaryl thiazole (**50a–e**) (Fig. 8.14) by retaining trimethoxyphenyl moiety similar to CA-4 (**45**), which was thought to show maximal tubulin binding affinity. Modifications were carried out on the phenyl ring of C-5 position of the thiazole scaffold by incorporating electron withdrawing (CF_3) and electron releasing substituents (Me, Et, OMe, and OEt). All the synthesized compounds were assessed for their antiproliferative actions against seven human tumor cell lines (HeLa, A549, K562,

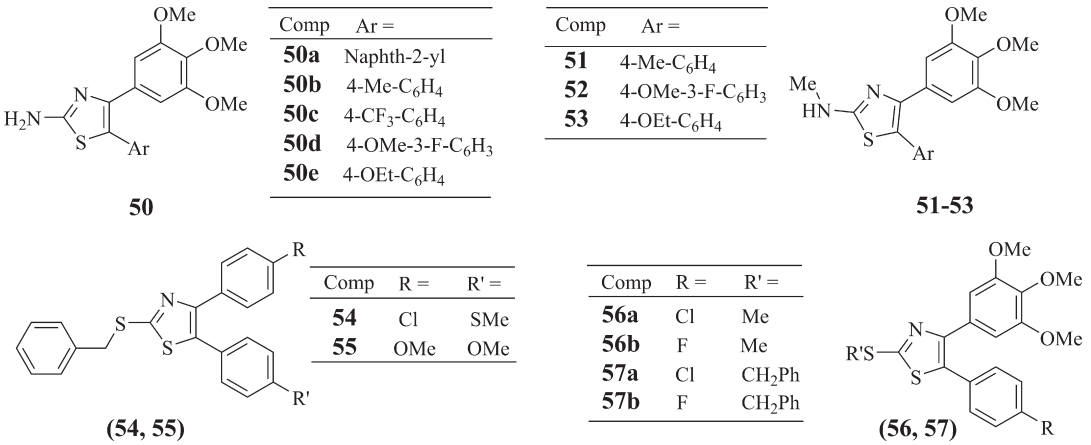

FIG. 8.14 Vicinal diaryl thiazole derivatives (**50–57**) as anticancer agents.

HT-29, MCF-7, HL-60, and Jurkat). Compounds (**50a**; 2-naphthyl) and (**50b**; 4-methylphenyl) showed higher antiproliferative activity than CA-4 (**45**) against five of the seven cell lines. Compound (**50e**) was found to show the most potent inhibitory activity with IC_{50} values varying from 0.03 to 0.9 nM against all the seven cancer cell lines except HT-29 and MCF-7. Compound (**50c**; 4-CF_3 substituent) having IC_{50} value of 0.4 nM was found to be the most active in MCF-7 cells. Compound (**50d**; 4-OMe and 3-F substituents) was identified as the most active derivative against HT-29 cells with an IC_{50} value of 5.7 nM. By considering these results, the authors made further modifications in compounds (**50a–e**) at C-2 position of the thiazole ring by replacing the amino group with different moieties such as *N*-methylamino, *N*,*N*-dimethylamino, and methyl groups. Compounds (**51–53**) (Fig. 8.14) having *N*-methylamino moiety at C-2 were the most active as antiproliferative agents. Compound (**53**) showed the highest inhibition of tubulin polymerization ($IC_{50} = 0.89\,\mu M$) and it also inhibited the binding of colchicine with tubulin (80% inhibition) (Romagnoli et al., 2012).

Salehi et al. also replaced the *cis*-olefinic bond by a thiazole ring to develop a series of 4,5-diaryl-thiazol-2-thioalkyl analogs (e.g., **54**, **55**) (Fig. 8.14) of CA-4 (**45**). Compounds were tested against the cancer cell lines (HT-29, MCF-7, and AGS) and the fibroblastic cell line (NIH-3T3) utilizing MTT test. In biological testing, all the compounds were found inactive against HT-29 cell line except for compound (**54**) which exhibited a low cytotoxicity. Compound (**54**) containing 4-chloro and 4-thiomethyl substituents on the phenyl rings was found to have higher cytotoxicity ($IC_{50} = 7.1\,\mu M$) against MCF-7 cell line than rest of the compounds. Interestingly, compound (**54**) showed very low toxicity against NIH-3T3 cells as compared to CA-4 (**45**). Compound (**55**) with methoxy group on the two phenyl rings displayed moderate cytotoxicity against MCF-7 ($IC_{50} = 23.8\,\mu M$) and AGS ($IC_{50} = 23.9\,\mu M$) cell lines. Docking studies of compounds (**54** and **55**) in the colchicine binding site of tubulin revealed that the phenyl group on the 4th position of the thiazole ring resembled the trimethoxyphenyl moiety of the colchicine and was accommodated near Cys249 in α, β-tubulin structure. The phenyl ring on the 5th position of the thiazole ring builds up a π–π interaction with Asn258 and a progression of hydrophobic interactions with Met259 and Lys352. Moreover, the authors have also reported a series of 2-alkylthio-4-(2,3,4-trimethoxyphenyl)-5-arylthiazole derivatives (**56**, **57**)

and evaluated them for their antiproliferative activity. Biological data demonstrated that a benzylthio group (**57a, b**; IC_{50} = 8–20 μM) on C-2 position of the thiazole nucleus resulted in the significant improvement in cytotoxicity as compared to the 2-methylthio substituted derivatives (**56a, b**; IC_{50} = 95–100 μM) (Salehi et al., 2013).

8.1.2.3 Anti-Alzheimer Activity

In the contemporary advancements of therapeutics, Alzheimer disease (AD) has emerged as a demanding disease to be taken care of among the neurodegenerative diseases (Kumar et al., 2015). In spite of the fact that the correct reason(s) for the AD is not yet completely known, reports figure out several factors like reduction of acetylcholine (ACh) levels in the brain, neurofibrillary tangles and amyloid β (Aβ) plaque formation, and oxidative stress (Goedert and Spillantini, 2006). Several preclinical studies suggested that acetylcholinesterase (AChE) and butyrylcholinesterase (BuChE) are responsible for the hydrolysis of ACh in the brain. Inhibition of these two enzymes is considered as a potential strategy to enhance the cholinergic transmission in AD (Mesulam et al., 2002). A multi-target directed drug development approach has been currently utilized by various researchers as such drugs have shown better efficacy and safety profile (Cavalli et al., 2008). Some vicinal diaryl heterocycles have been reported to possess neuroprotective activity.

Inspired from some previously reported vicinal diaryltriazines (Sinha et al., 2015) exhibiting AChE inhibitory activity, Shidore et al. extended the multi-target directed drug design concept by developing a novel series of hybrid molecules for the treatment of AD (Shidore et al., 2016). The authors designed hybrid molecules by using pharmacophoric moiety of donepezil (AChE inhibitor) and diarylthiazole as multi-target directed ligands. The diarylthiazole–benzylpiperidine hybrid molecules (**58–61**) (Fig. 8.15) were synthesized and investigated for their anti-Alzheimer activity. Biological data revealed that compounds having benzylpiperidine and 4,5-disubstituted thiazolyl-2-amine linked with aminomethylene spacer (**58** and **59**) and without carbon spacer (**60**) possessed higher AChE and BuChE inhibitory activity than compounds (e.g., **61**) linked with carboxamide group. Among the se-

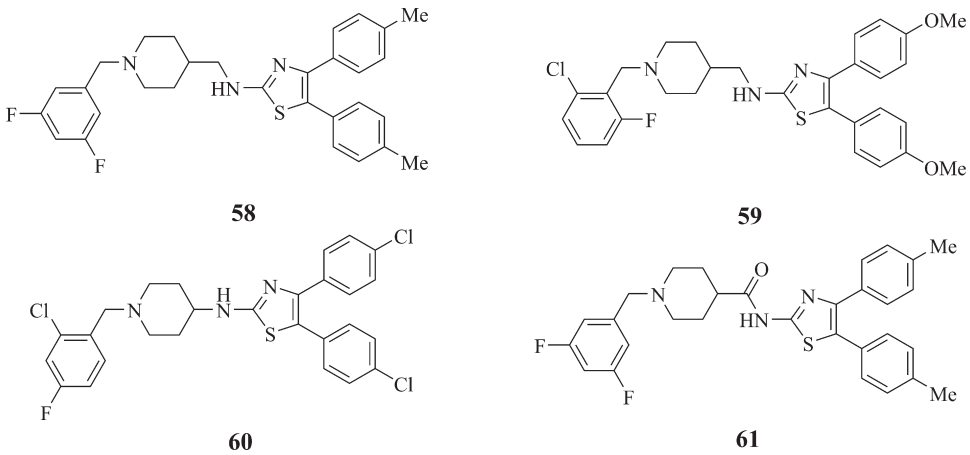

FIG. 8.15 Vicinal diaryl thiazoles (**58–61**) as multi-target directed ligands.

ries, compound (**58**) demonstrated the most potent inhibitory activity against AChE (IC_{50} value of 0.30 μM) and BuChE (IC_{50} value of 1.84 μM). Compounds (**58–60**) showed moderate to high inhibition of AChE-induced $A\beta_{1-42}$ aggregation and detectable in vitro antioxidant and antiapoptotic properties. Compound (**58**) exhibited remarkable in vivo anti-ChE and antioxidant activities. Besides, compound (**58**) exhibited in vivo neuroprotective action by diminishing $A\beta_{1-42}$-induced toxicity by reducing abnormal levels of $A\beta_{1-42}$, p-Tau, cleaved caspase-3, and cleaved PARP proteins. Compound (**58**) also indicated good oral absorption and was well tolerated up to 2000 mg/kg, p.o., dose without demonstrating any toxic effect (Shidore et al., 2016).

8.1.2.4 Cholesterol Lowering Agents

Atherosclerosis promoting cardiovascular disease (CVD) is one of the major causes for high morbidity and mortality in the industrialized world (Grundy et al., 1997). Decreasing the elevated lipid and cholesterol levels in serum is considered as one of the preventive measures of atherosclerosis. Inhibition of endogenous cholesterol biosynthesis and absorption of dietary cholesterol from the intestine have become a point of focus to reduce serum cholesterol levels (Kannel et al., 1971). Esterification of cholesterol in intestine is the rate-limiting step for the absorption of dietary cholesterol. Sterol O-acyltransferase (SOAT) also known as acyl-CoA: cholesterol acyltransferase (ACAT) is a group of enzymes responsible for the formation and deposition of cholesteryl esters as the plaque in atherosclerosis (Norum et al., 1979). Over the last few years, various SOAT inhibitors and cholesterol absorption inhibitors have been explored to control serum cholesterol (Bell et al., 2006; Pal et al., 2013).

Pal et al. synthesized some novel vicinal diaryl thiazole-urea derivatives as cholesterol-lowering agents (Pal et al., 2017). All of the reported compounds were screened for SOAT enzyme inhibitory activity. Among the series, compound (**62**) (Fig. 8.16) showed the most remarkable activity with an IC_{50} value of 2.43 μM. Compound (**62**) exhibited reduction of in vivo triglyceride turnover in polaxamer-407-induced lipoprotein lipase inhibition model. Compound (**62**) additionally exhibited dose-dependent inhibition of serum total cholesterol and avoidance of LDL-C rise at a dose of 30 mg/kg. Moreover, compound (**62**) dose-dependently demonstrated its potential to prevent decreasing levels of serum HDL-C, and enhanced the atherogenic index. Toxicological investigation of compound (**62**) suggested that a dose of 2000 mg/kg of (**62**) did not indicate any toxic effect or mortality (Pal et al., 2017).

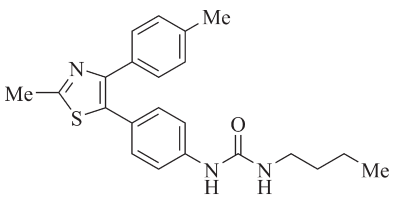

62

FIG. 8.16 Vicinal diaryl thiazole (**62**) as cholesterol lowering agent.

8.2 THIAZOLINES

Thiazolines are a group of positional isomers having nitrogen and sulfur in the five-membered heterocyclic ring system. They are also called as dihydrothiazoles. Different isomeric forms of thiazolines such as 4-thiazoline (**63**), 3-thiazoline (**64**), and 2-thiazoline (**65**) are shown in Fig. 8.17.

8.2.1 Synthesis of Vicinal Diaryl Thiazolines

Synthesis of 3,4-diaryl-2-imino-4-thiazolines (**68**) was reported wherein condensation of the corresponding amine hydrochloride (**66**) was carried out with phenacyl thiocyanate (**67**) (Fig. 8.18) (Mahajan et al., 1972).

3,4-Diaryl-2-imino-4-thiazolines (**68**) were also synthesized by treatment of the substituted phenacyl bromides (**69**) with arylthiosemicarbazides (**70**) (Fig. 8.18) (Liu et al., 2009).

Liu et al. synthesized 3,4-diarylthiazolones (**74**) from acetophenones (**71**) and anilines (**72**) as shown in Fig. 8.19. The ketimines (**73**) as intermediates obtained from dehydration of acetophenones (**71**) and anilines (**72**) were further treated with chlorocarbonylsulfenyl chloride in the presence of pyridine to get the final compounds (**74**) (Liu et al., 2009).

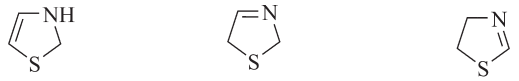

63 **64** **65**

FIG. 8.17 Isomeric forms of thiazolines (**63–65**).

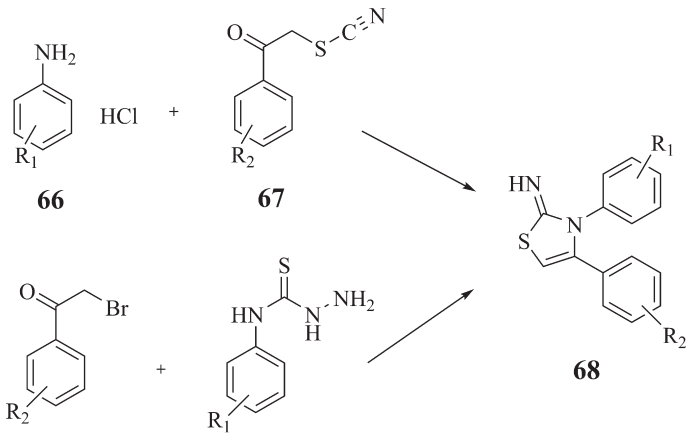

66 **67** **68** **69** **70**

FIG. 8.18 Synthesis of vicinal diaryl 4-thiazolines (**68**).

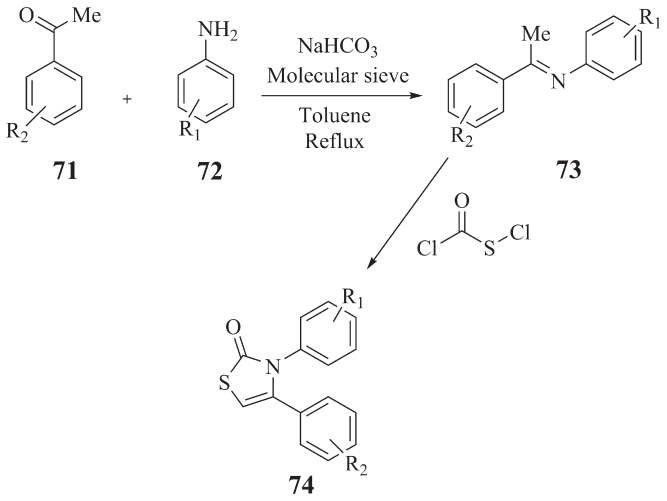

FIG. 8.19 Synthesis of 3,4-diarylthiazolones (**74**).

8.2.2 Biological Activities of Vicinal Diaryl Thiazolines

Vicinal diaryl thiazolines reported as anti-inflammatory, analgesic, and anticancer agents are described in the following section.

8.2.2.1 Anticancer, Analgesic, and Anti-Inflammatory Activities

Various 3,4-diaryl-2-imino-4-thiazolines (**68**) were condensed with 4-cyanopyridine and 2-cyanopyrazine to obtain the corresponding 3,4-diaryl-2-imino-*N*-(4′-pyridyliminomethyl)-4-thiazolines (**75a–d**) and 3,4-diaryl-2-imino-*N*-(2′-pyrazinyliminomethyl)-4-thiazolines (**76a–d**) (Fig. 8.20). During column chromatography over silica gel some of these compounds got hydrolyzed into the corresponding 3,4-diaryl-2-imino-*N*-(4′-carbonylpyridyl)-4-thiazolines (e.g., **75e**) and 3,4-diaryl-2-imino-*N*-(2'-carbonylpyrazinyl)-4-thiazolines (e.g., **76e**) (Fig. 8.20). During the screening for anticancer activity against six human cancer cell lines including prostate (DU 145), colon (HT 29), breast (MCF 7/ADR), CNS (U 251), and lung large tumors (NCIH 460), the best IC_{50} values were shown for **75e** (4.8 μM, breast tumor, cell line MCF 7/ADR), **75e** (6.3 μM, CNS tumor, cell line U 251), **75d** (6.2 μM, breast tumor, cell line MCF 7), **76b** (11.5 μM, prostate tumor, cell line DU 145), **76b** (1.0 μM, colon tumor, cell line HT 29), and **76b** (0.9 μM, lung large carcinoma, cell line NCIH 460, CNS, cell line U 251). Compounds (**75a**, **b**, **76a**) also exhibited anti-inflammatory activity (100 mg/kg p.o.) in carrageenan-induced rat paw edema model. Compounds (**75b**, **75c**, **75e**, **76c**, **76d** and **76e)** have been reported to possess strong analgesic activity (Sondhi et al., 2005b).

Sondhi et al. also performed condensation of 3,4-diaryl-2-imino-4-thiazolines (**68**) with acridine derivatives to get acridinyl-thiazolino derivatives (**77a–c** and **78a**, **b**) (Fig. 8.20). The compounds were evaluated for anti-inflammatory, analgesic, and kinase inhibition activities. Compounds (**77a**, **b** and **78b**) having methoxy group of the acridine ring and methoxy, nitro and hydrogen, respectively, at ortho positions of the phenyl ring attached to the nitrogen showed good anti-inflammatory activity (>30%). Compounds (**77c** and **78a**) also showed good analgesic activity (>50%). Compound (**77c**) exhibited moderate activity against CDK1

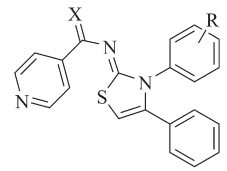

75a-e

Comp	R =	X =
75a	2-Me	NH
75b	2-OMe	NH
75c	4-Me	NH
75d	2-NO_2-6-Me	NH
75e	2,3-diMe	O

Comp	R =	X =
76a	2-OMe	NH
76b	4-Me	NH
76c	3-NO_2	NH
76d	2,3-diMe	NH
76e	4-NO_2	O

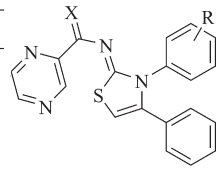

76a-e

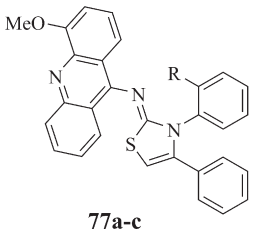

77a-c

Comp	R =
77a	4-OMe
77b	4-NO_2
77c	H

Comp	R =	R_1 =	R_2 =
78a	Me	Me	H
78b	H	H	OMe

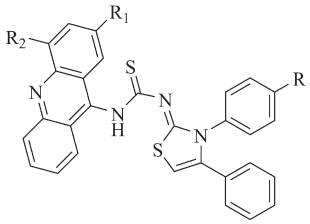

78a, 78b

FIG. 8.20 Vicinal diaryl 4-thiazolines (**75–78**) reported by Sondhi et al.

(IC_{50} = 8.5 μM). This data offers an opportunity for researchers to explore novel analogs of this class of compounds as potential CDK1 inhibitors (Sondhi et al., 2005a).

In continuation of their efforts, the same research group carried out condensation of 3,4-diaryl-2-imino-4-thiazolines (**68**) with 2-cyanopyridine and hydantoin-5-acetic acid to get compounds (**79a–c, d**) (Fig. 8.21). Compounds (**79a,d**) have been reported to possess anti-inflammatory activity with 49% and 34% inhibition, respectively, at 50 mg/kg p.o. dose. Compounds (**79b, c**) showed good analgesic activity (with 50% inhibition) (Sondhi et al., 2009b).

The authors have synthesized and investigated methanesulfonamide (**80a**, **b**) (Fig. 8.21) and amidine (**81** and **82**) (Fig. 8.21) derivatives of 3,4-diaryl-2-imino-4-thiazolines (**68**) for their anti-inflammatory and anticancer activities. Compounds (**80a** and **81)** showed good anticancer activity against colon cancer cell line (COLO-205). Compound (**82)** was found to have good anticancer activity against liver (HEP-2; 32%) and neuroblastoma cell lines (IMR-32; 47%). Compound (**80b**) demonstrated good anti-inflammatory activity (34.7%) at 50 mg/kg p.o. dose which was equivalent to the standard drug phenylbutazone (37%) (Sondhi et al., 2009a).

Lui et al. designed and synthesized two series of *cis*-restricted analogs of CA-4 (**45**) using thiazolimines (**83**) and thiazolones (**84**) (Fig. 8.22) as a replacement of olefinic group in CA-4 (**45**). All the synthesized compounds were tested for their anticancer activity against human CEM leukemia cells. Compound (**83a**; IC_{50} = 1.5 μM) showed higher cytotoxicity than compound (**83b**; IC_{50} = 13.2 μM) which indicated that 3,4,5-trimethoxyphenyl moiety on the *N*-3 position of the thiazoline ring was more favorable for cytotoxicity. In second series, the authors synthesized 3,4-diaryl thiazolones (**84**) by utilizing the same substitution pattern of both the essential 3,4,5-trimethoxyphenyl and 4-methoxyphenyl groups. Compound (**84a;** IC_{50} = 1.8 μM) showed higher cytotoxicity than its isomeric derivative (**84b**; IC_{50} = 14.9 μM). Introduction of 3-amino group on 4-methoxyphenyl moiety in compound (**84a**) resulted in compound (**84c**; IC_{50} = 0.24 μM) with improved cytotoxicity. Replacement of 4-H of thiazolone ring of compound (**84c**) with chloro group resulted in compound (**84d**; IC_{50} = 0.12 μM) with twofold increase in activity.

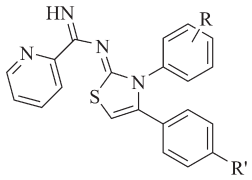

79a-c

Comp	R =	R' =
79a	2-NO_2	H
79b	H	OEt
79c	2-Me	H

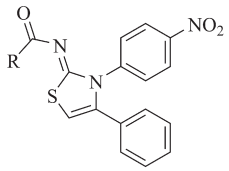

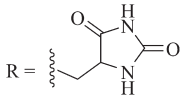

79d

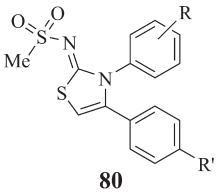

80

Comp	R =	R' =
80a	4-NO_2	Cl
80b	2-NO_2	OMe

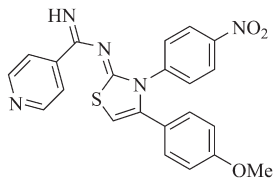

81

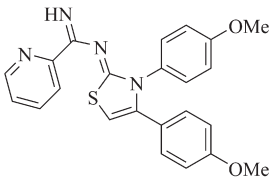

82

FIG. 8.21 Vicinal diaryl 4-thiazolines (**79–82**) reported by Sondhi et al.

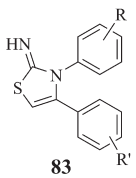

83

Comp	R =	R' =
83a	3,4,5-$(OMe)_3$	4-OMe
83b	4-OMe	3,4,5-$(OMe)_3$

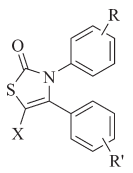

84

Comp	R =	R' =	X =
84a	3,4,5-$(OMe)_3$	4-OMe	H
84b	4-OMe	3,4,5-$(OMe)_3$	H
84c	3,4,5-$(OMe)_3$	3-NH_2-4-OMe	H
84d	3,4,5-$(OMe)_3$	3-NH_2-4-OMe	Cl

FIG. 8.22 Vicinal diaryl thiazolimines (**83**) and thiazolones (**84**) as anticancer agents.

8.3 THIAZOLIDINONES

The five-membered heterocycle thiazolidinone is a saturated form of thiazole ring having a carbonyl group at positions 2, 4, or 5. Availability of more sites (2, 3, and 5) for substitution and two important hetero atoms (N and S) make thiazolidinone ring an attractive moiety to the medicinal chemists. The 1,3-thiazolidin-4-one scaffold (**85**) having a carbonyl group at position 4, sulfur and nitrogen atoms at positions 1 and 3, respectively, has been exploited

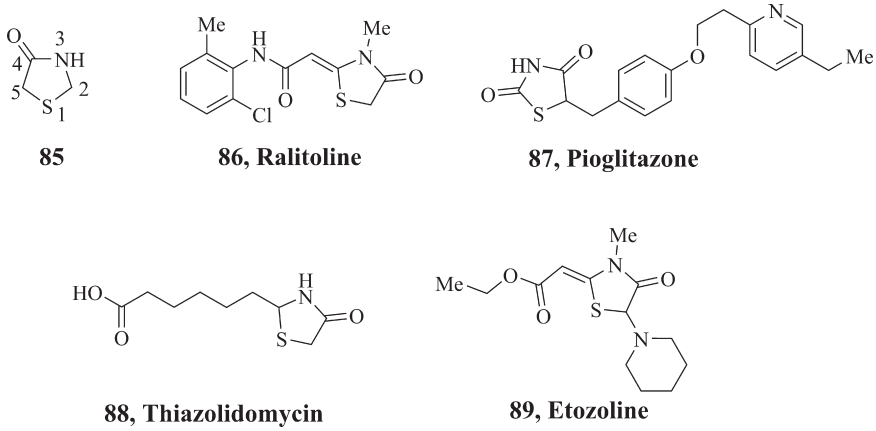

FIG. 8.23 Structures of 4-thiazolidinone (**85**) and some drugs (**86–89**) containing thiazolidinone moiety.

for its biological potential. Owing to the combination of molecular flexibility and presence of elementary heteroatoms, 4-thiazolidinone scaffold has been known to show a diversified range of biological activities. An impressive pharmacological profile of ralitoline (**86**) as anticonvulsant, pioglitazone (**87**) as antidiabetic, thiazolidomycin (**88**) as bactericidal agent, and etozoline (**89**) as antihypertensive demonstrated the potential of thiazolidinone moiety (Fig. 8.23) (Devinyak et al., 2012; Tripathi et al., 2014; Verma and Saraf, 2008). As a result of the biological importance attached to 4-thiazolidinone, substantial efforts have been made to exploit its medicinal potential.

Further, vicinal diaryl-substituted thiazolidin-4-ones have generated enormous interest in the drug discovery field among the researchers due to their multifarious biological potential. Intensive research endeavors have been made on the synthesis and biological activities of vicinal diaryl-substituted thiazolidin-4-ones. Its remarkable pharmacological profile motivated many researchers to carry out changes at *N*-3 and C-2 positions of thiazolidin-4-one (**85**) with different aryl or heteroaryl substituents.

8.3.1 Synthesis of Vicinal Diaryl Thiazolidinones

Several approaches have been reported for the synthesis of vicinal diaryl-substituted thiazolidin-4-ones. The basic synthetic routes required three segments, that is, a carbonyl compound, an amine, and thioglycolic acid. The typical synthetic process reported is suitable either with a one-pot three components condensation or a two-step process (Fig. 8.24). The formation of an imine (**92**) by the attack of nitrogen of an amine (**91**) on the carbonyl of aldehyde or ketone (**90**) initiates the reaction. Nucleophilic attack of sulfur on imine

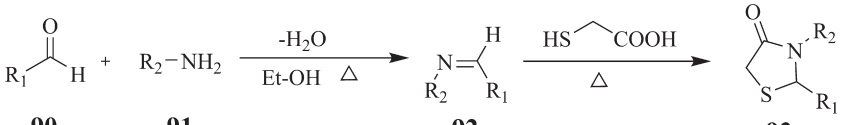

FIG. 8.24 General synthetic route for 4-thiazolidinone scaffold (**93**).

preceded by intramolecular cyclization and elimination of H_2O resulted in the formation of thiazolidin-4-one (**93**).

Several synthetic reports promote the above cyclocondensation using catalysts such as *N,N′*-dicyclohexylcarbodiimide (DCC) (Srivastava et al., 2002), $ZnCl_2$ (Desai and Desai, 2006), 2-(*1H*-benzotriazol-1-yl)-1,1,3,3-tetramethyluronium hexafluorophosphate (HBTU), sodium sulfate, ferrite, ionic liquids ([bmim][PF_6] (Yadav et al., 2009), *N*-methylpyridinium tosylate (Lingampalle et al., 2010)), silica gel (Thakare et al., 2014), nano-Fe_2O_3/SiO_2 (Azgomi and Mokhtary, 2015), yttrium triflate Y(OTf)$_3$ (Luo et al., 2016), and activated fly ash (Shanti et al., 2013). The use of solid-phase systems, microwave heating, and polymer supported systems to synthesize 2,3-disubstitiuted 4-thiazolidinones (**93**) have also been reported (Subhedar et al., 2016).

In another method (Fig. 8.25A), Bolognese et al. reported microwave-assisted synthesis of 1,3-thiazolidin-4-one derivatives (**95**) from benzylidene-anilines (**94**) and thioglycolic acid in benzene (Bolognese et al., 2004).

Pratap et al. explored *Saccharomyces cerevisiae* as biocatalyst to accelerate the formation of imines along with cyclocondensation of aldehydes (**96**), amines (**97**), and thioglycolic acid in formation of the final product 2,3-diaryl thiazolidinones (**98**) (Fig. 8.25B) (Pratap et al., 2011).

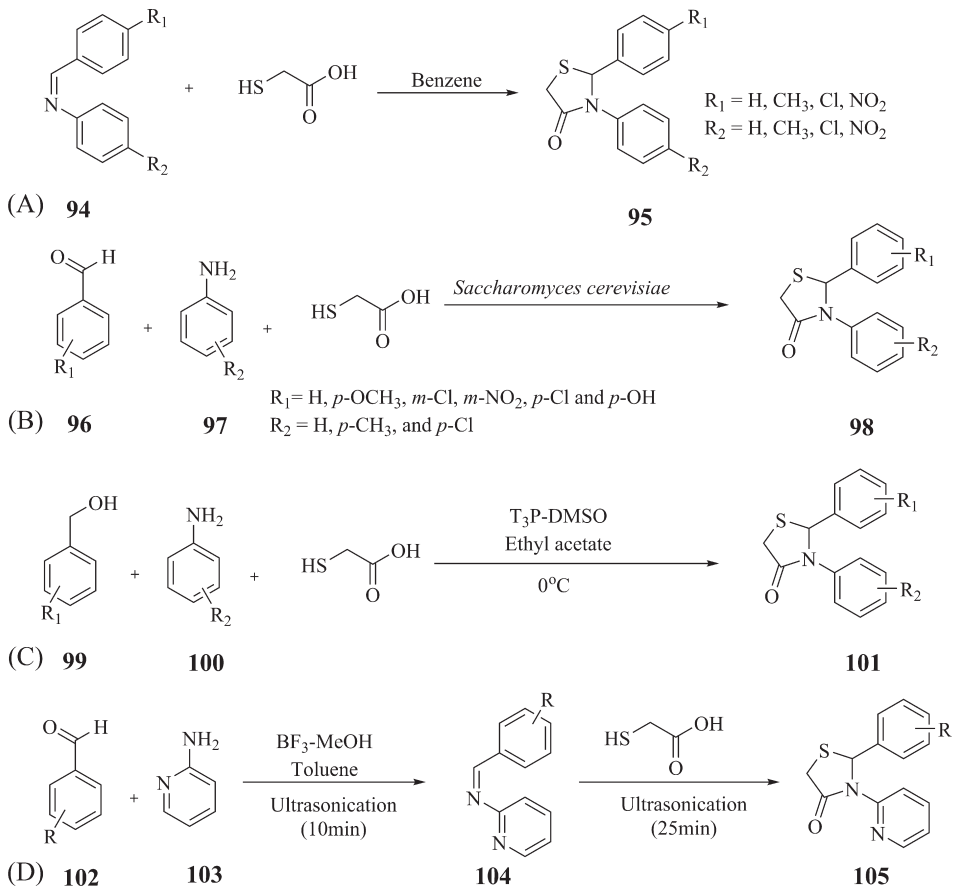

FIG. 8.25 Synthesis of vicinal diaryl thiazolidin-4-ones using (A) microwave heating, (B) *S. cerevisiae* as biocatalyst, (C) propylphosphonic anhydride (T_3P)-DMSO, and (D) ultrasonication.

Kumar et al. synthesized 2,3-disubstituted 4-thiazolidinones (**101**) from substituted benzyl alcohols (**99**) (Fig. 8.25C). This method involved propylphosphonic anhydride (T_3P)-DMSO assisted oxidation of alcohols (**99**) to aldehydes or keto compounds and their further cyclization with anilines (**100**) and thioglycolic acid to afford 4-thiazolidinones (**101**) (Sharath Kumar et al., 2012).

Gouvea et al. synthesized thiazolidinones from the reaction of arene aldehydes (**102**), 2-aminopyridine (**103**), and thioglycolic acid under ultrasonication (Fig. 8.25D). The reaction of the aldehyde (**102**) with 2-aminopyridine (**103**) requires a Lewis acid (BF_3: MeOH 50 %) catalyst to form the corresponding imine (**104**). The intermediate imine (**104**) then reacted with thioglycolic acid in the presence of ultrasound irradiation (25 min) to afford 2-aryl-3-(pyridin-2-yl)-1,3-thiazolidin-4-ones (**105**) (Gouvêa et al., 2012).

8.3.2 Biological Activity of 1,3-thiazolidin-4-ones

A diversified spectrum of biological activities, mainly antiviral (anti-HIV), antiproliferative, anti-inflammatory, and analgesic activities exhibited by vicinal diaryl-substituted thiazolidin-4-ones have been described in the following section.

8.3.2.1 Antiviral Activity

2,3-Diaryl-1,3-thiazolidin-4-one analogs turned out to be a novel class of HIV-1 non-nucleoside reverse transcriptase inhibitors (NNRTIs). On the basis of structure–activity relationship (SAR) and molecular modeling studies, different structural modifications were performed on almost all the positions of the thiazolidin-4-one scaffold (Barreca et al., 1999). In their continuous efforts to develop potent NNRTIs, Barreca et al. designed and synthesized 2,3-diaryl-1,3-thiazolidin-4-ones on the basis of their previously reported thiazolobenzimidazoles (TBZs) (**106** and **107**) (Fig. 8.26) as NNRTIs (Barreca et al., 2001). The targeted compounds were designed by the ring opening of imidazole nucleus of TBZs and keeping the π-system and nitrogen atom intact. Introduction of phenyl or 2-pyridinyl ring at *N*-3 position of the thiazolidinone with dihalo-substituted phenyl ring at C-2 position offered compounds (**108–120**) (Fig. 8.26). From the SAR study, it has been observed that compounds with 2-pyridinyl substituent at *N*-3 position and two chloro groups at 2nd and 6th positions of the phenyl ring of C-2 position enhanced the potency. Incorporation of methyl group at the C-6 position of pyridin-2-yl ring resulted in compounds (**112–114**) with EC_{50} values of 44, 82, and 53 nM, respectively. Moreover, the introduction of more lipophilic substituents at 6-postion of 2-pyridinyl group resulted in additional compounds (**115–119**) with higher antiviral activity and low toxicity (Barreca et al., 2002). Sriram et al. also synthesized and evaluated some compounds by utilizing the same approach of substitution at phenyl ring of C-2 and *N*-3 positions of thiazolidinone. The compound (**120**) (Fig. 8.26) has been reported as a potent inhibitor of HIV-1 replication with EC_{50} value of 10 μM and CC_{50} of 120 μM. (Sriram et al., 2005).

Rao et al. also made extensive efforts toward the development of 2,3-diaryl-1,3-thiazolidin-4-ones (**121–127**) (Fig. 8.26) as anti-HIV agents (Rao et al., 2002; Rao et al., 2003). To have more understanding of the SARs of 1,3-thiazolidin-4-ones exhibiting anti-HIV-1 activity, the pyridine ring was strategically replaced by suitably substituted pyrimidine ring and retaining the 2,6-disubstituted phenyl ring at C-2 position (Rao et al., 2004). The synthesized compounds were tested for reduction in cytopathic effects of HIV-1 (IIIb) and HIV-2 (ROD) in MT-4 cells.

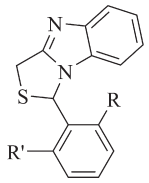

Comp	R =	R' =	EC_{50} (nM)
106	F	F	352
107	Cl	Cl	589

106, 107

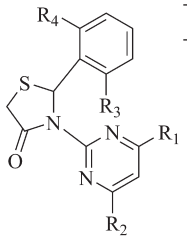

Comp	R_1=	R_2 =	R_3 =	R_4 =
121	H	H	Cl	Cl
122	H	H	F	Cl
123	H	H	F	F
124	Me	H	Cl	Cl
125	Me	Me	Cl	Cl
126	Me	OMe	Cl	Cl
127	Me	OH	Cl	Cl

(121–127)

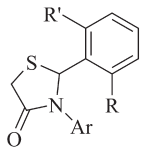

108–120

Comp	Ar =	R =	R' =	EC_{50} (nM)
108	4-Ph	F	F	2300
109	4-Ph	Cl	Cl	401
110	2-Pyr	F	F	855
111	2-Pyr	Cl	Cl	178
112	6-Me-2-Pyr	F	F	44
113	6-Me-2-Pyr	Cl	Cl	82
114	6-Me-2-Pyr	Cl	F	53
115	6-Br-2-Pyr	Cl	F	64
116	6-Br-2-Pyr	F	F	30
117	4,6-diMe-2-Pyr	Cl	F	90
118	4,6-diMe-2-Pyr	Cl	F	42
119	4,6-diMe-2-Pyr	F	F	59
120	2-Pyr	Cl	H	10000

FIG. 8.26 Structures of TBZs (**106, 107**) and vicinal diaryl thiazolidin-4-ones reported by Berreca et al. (**108–120**) and Rao et al. (**121–127**).

Most of the compounds exhibited high selectivity by showing more preventive effect on HIV-1 (IIIb) and were negligibly toxic to MT-4 cells. Compound (**121**; EC_{50} = 0.227 μM, CC_{50} = 173 μM, selectivity index (SI) = 758) possessing 2,6-dichlorophenyl at C-2 position was found to be more active than the corresponding 2-chloro-6-fluoro-substituted (**122**; EC_{50} = 0.581 μM, CC_{50} = 136 μM, SI = 234) and 2,6-difluoro-substituted (**123**; EC_{50} = 3.65 μM, CC_{50} = 426 μM, SI = 118) derivatives. Introduction of methyl group at C-4′ position of the pyrimidine ring in compound (**121**) resulted in compound (**124**) with enhanced activity (EC_{50} = 0.044 μM, CC_{50} = 180 μM, SI = 2454). Furthermore, to explore the importance of lipophilicity, a second methyl group was introduced at C-6′ position of pyrimidine ring in compound (**124**) to get the most active compound (**125**; EC_{50} = 0.017 μM, CC_{50} = 52.5 μM, SI = 9521) of the series. Replacement of methyl group at C-6′ position of pyrimidine ring with methoxy group led to the formation of compound (**126**; EC_{50} = 0.024 μM, CC_{50} = 161 μM, SI = 2187) having activity comparable to that of compound (**125**). Compound (**127**; EC_{50} = 32.84 μM, CC_{50} = 179 μM, SI = 5.5) having hydroxyl group at C-6′ position of the pyrimidine ring showed reduced activity due to low affinity toward hydrophobic site of NNRTIs (Rao et al., 2004).

Subsequently, 1,3-thiazolidin-4-one scaffold was also employed by Rawal et al. to examine the effect of changes at C-2 position of the thiazolidinone moiety. Initially, compounds were prepared by placing different substituents on the phenyl ring at C-2 and keeping the furfuryl moiety constant at the *N*-3 position (Rawal et al., 2005). Compound (**128**) (Fig. 8.27) having 2,6-dichlorophenyl at C-2 position was found to be the most active among the series with EC_{50} value of 0.204 μM (SI = 216). From molecular modeling and QSAR studies,

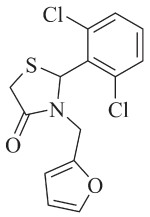

128

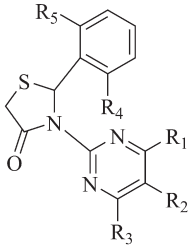

129–136

Comp	R_1=	R_2 =	R_3 =	R_4 =	R_5 =
129	Me	H	CF_3	Cl	Cl
130	Me	H	CF_3	Cl	F
131	Me	H	CF_3	F	F
132	Me	H	Ph	Cl	Cl
133	Ph	H	CF_3	Cl	Cl
134	Me	H	Ph	Cl	Cl
135	Me	Me	Me	Cl	Cl
136	Me	Me	Me	Cl	F

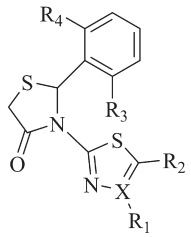

(137–143)

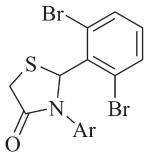

(144–151)

Comp	R_1=	R_2 =	X =	R_4 =	R_5 =
137	H	H	C	Cl	Cl
138	H	H	C	Cl	F
139	Me	Me	C	Cl	F
140	Me	Me	C	F	F
141	-	Et	N	Cl	Cl
142	-	Et	N	Cl	F
143	-	Et	N	F	F

Comp	Ar =
144	Furan-2ylmethyl
145	Pyridin-2-yl
146	6-Methylpyridin-2-yl
147	Pyrimidin-2-yl
148	4-Methylpyrimidin-2-yl
149	4,6-Dimethylpyrimidin-2-yl
150	4-Methyl-6-trifluoromethylpyrimidin-2-yl
151	4,5,6-Trimethylpyrimidin-2-yl

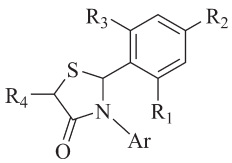

(152–155)

Comp	R_1=	R_2 =	R_3 =	R_4 =	Ar =
152	H	F	H	H	Pyridin-2-yl
153	H	NMe_2	H	H	6-Methylpyridin-2-yl
154	Cl	H	Cl	Me	Pyridin-3-ylmethyl
155	Cl	H	Cl	Me	Furan-2-ylmethyl

FIG. 8.27 Structures of thiazolidin-4-one derivatives (**128–155**) reported by Rawal et al.

compounds with the overall high hydrophobicity were predicted to show better HIV-1 RT inhibitory activity. Modifications were carried out by incorporating different substituents in the pyrimidine ring at *N*-3 position of the thiazolidinone moiety to increase hydrophobicity. Compounds (**129–131**) (Fig. 8.27) having 4-methyl-6-trifluoromethylprimidin-2-yl at *N*-3 position showed moderate activity. Introduction of the 4-methyl-6-phenylprimidin-2-yl (**132**; $EC_{50} = 6.1\,\mu M$) (Fig. 8.27), 4-phenyl-6-trifluoromethylprimidin-2-yl (**133**; $EC_{50} \geq 80\,\mu M$),

and 4,6-diphenylprimidin-2-yl (**134**; $EC_{50} \geq 194\,\mu M$) led to decrease in HIV-1 RT inhibitory activity. Further modification by incorporating 4,5,6-trimethylprimidin-2-yl moiety resulted in the identification of the most active compounds (**135**; $EC_{50} = 30\,nM$ and **136**; $EC_{50} = 30\,nM$) with high selectivity indices of ≥10,000 and low toxicity in MT-4 as well as CEM cells. Compounds (**135** and **136)** were found to be more active in MT-4 (10-fold) and CEM cells (50-fold) than the TBZ derivative (**106**) (Rawal et al., 2007b).

The same research group designed and synthesized novel 1,3-thiazolidin-4-ones substituted with thiourea or isothiourea group at the *N*-3 position. Introduction of a thiazol-2-yl moiety at the *N*-3 position of the 1,3-thiazolidin-4-one scaffold resulted in the identification of compounds (**137–140**) (Fig. 8.27) with improved HIV-1 RT inhibitory activity. Compounds (**137**; $EC_{50} = 0.41\,\mu M$, SI > 893, **138**; $EC_{50} = 0.60\,\mu M$, SI = 72, and **140**; $EC_{50} = 0.37\,\mu M$, SI > 1001) showed higher activity than **TBZ** ($EC_{50} = 1.10\,\mu M$, SI = 45) in CEM cells with higher selectivity indices. Compound (**139**) was found to be the most potent in MT-4 cells ($EC_{50} = 0.26\,\mu M$, SI = 113) and CEM cells ($EC_{50} = 0.23\,\mu M$, SI = 138) in the series. Introduction of 5-ethyl[1,3,4] thiadiazol-2-yl (e.g., **141–143**) at *N*-3 resulted in decrease in the activity ($EC_{50} = 10$ to $50\,\mu M$) compared to the thiazol-2-yl containing compounds (Rawal et al., 2007a). The biological data of all these compounds revealed that the anti-HIV activity of 2,3-diaryl-1,3-thiazolidin-4-ones was greatly dependent on the nature of substituents at C-2 and *N*-3 positions of the thiazolidin-4-one ring. To support the inference, the authors employed 2,6-dibromophenyl substituent at C-2 and different heteroaryls at *N*-3 position of the thiazolidin-4-one. Compounds (**144–151**) (Fig. 8.27) were identified as the most active anti-HIV agents, inhibiting HIV-1 replication at 20–320 nM with negligible cytotoxicity and high selectivity (SI up to 7123 in MT-4 and 6726 in CEM cells). Moreover, in MT-4 cells (1- to 17.5-fold) and CEM cells (1.7- to 36.7-fold) these compounds exhibited activities higher than that in TBZ-1 (Rawal et al., 2008b).

The 4-thiazolidinone scaffold has also been focused for the advancement of inhibitors of hepatitis C virus NS5B polymerase. By taking a cue from the previously reported thiazolidin-4-ones, Rawal et al. also investigated a novel series of 2,3-diaryl-1,3-thiazolidin-4-ones for the same activity (Rawal et al., 2008a). Modifications at 2- and 3-positions of the thiazolidin- 4-one ring resulted in the identification of compounds (**152–155**) (Fig. 8.27) with promising anti-HCV activity (>85% and >60% inhibition of NS5B and NS5B RdRp, respectively). Among these, compounds (**152** and **155**) were observed to be the most potent with IC_{50} values of 31.9 μM and 32.2 μM, respectively (Rawal et al., 2008a).

In a slightly different manner, Murugesan et al. applied QSAR and bioisosterism-based drug design concept to develop a novel series of thiazolidin-4-ones having different aryl/heteroaryl groups at C-2 and *N*-3 positions (Murugesan et al., 2011). Compounds (**156**; 75% inhibition at 100 μg/mL and **157**; 95% inhibition at 100 μg/mL) (Fig. 8.28) containing

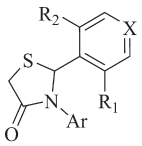

(156–159)

Comp	R_1=	R_2 =	X =	Ar =
156	Cl	Cl	CH	5-Methylisoxazol-3-yl
157	Cl	F	CH	5-Methylisoxazol-3-yl
158	Cl	F	CH	5-Bromo-4,6-dimethylpyridin-2-yl
159	Cl	Cl	N	4,6-Dimethylpyridin-2-yl

FIG. 8.28 Structure of vicinal diaryl thiazolidin-4-ones (**156–159**) reported by Murugesan et al.

5-methylisoxazol-3-yl moiety at *N*-3 showed good anti-HIV RT activity. Compound (**158**) (Fig. 8.28) bearing 5-bromo-4,6-dimethylpyridin-2yl at *N*-3 exhibited the highest inhibitory activity (98% inhibition). Bioisosteric replacement of the phenyl ring with pyridine ring at C-2 and introduction of 4,6-dimethylpyridin-2yl moiety at *N*-3 position of thiazolidin-4-one resulted in an active compound (**159**; 85% inhibition). In further cell-based biological studies, the compounds (**156–159**) showed potent activity against HIV-1 III_B (EC_{50} value of 0.09–0.8 μM with SI of 46–446) and HIV-1 ADA5 (EC_{50} value of 0.12–1.06 μM with SI of 36–335). These compounds were also active against HIV-1 UG070 (EC_{50} value of 0.10–1.55 μM with SI of 24–402) and HIV-1 VB59 (EC_{50} value of 0.07–1.1 μM with SI of 33.9–574). Docking studies indicated that the 2′,6′-dihalophenyl of compounds (**156–158**) and 3′,5′-dihalopyridyl moiety of compound (**159)** interacted through π–π interactions into hydrophobic pocket which was made up of aromatic amino acids such as Tyr181, Tyr188, and Trp229. The substituents (methyl/bromo) on heteroaryl ring at *N*-3 position show hydrophobic interactions with aromatic side chain of Tyr318. The carbonyl oxygen of thiazolidin-4-one and oxygen atom of isoxazolidine ring in compounds (**156** and **157)** form hydrogen bonds with N–H of Lys101 residue of the backbone (Murugesan et al., 2011).

8.3.2.2 Anti-Inflammatory and Analgesic Activities

During a search for selective COX-2 inhibitors, compound (**160**) (Fig. 8.29) was found with a significant anti-inflammatory activity against carrageenan-induced rat paw edema. Compound (**161**) showed 78% edema inhibition which was comparable to celecoxib (**24**) having 45% inhibition at the same dose (Vazzana et al., 2004). From the structure analysis of the available selective COX-2 inhibitors, it has been observed that 4-methylsulfonyl group on one of the phenyl rings is necessary for good COX-2 selectivity and potency. By keeping this in mind, Zarghi et al. have reported 2,3-diaryl-1,3-thiazolidin-4-ones having *p*-methylsulfonyl group on C-2 phenyl ring and different substituents (H, F, Me, and OMe) at *para* position of *N*-3 phenyl ring. Compound (**162**; $IC_{50} = 0.12$ μM and SI > 833) was found to be the most potent and selective COX-2 inhibitor of the series (Zarghi et al., 2007).

8.3.2.3 Anticancer Activity

Protein tyrosine kinases (PTKs) play a crucial role in cell growth and differentiation in all organisms and also show their participation in the development of neoplastic diseases. Small molecule inhibitors of tyrosine kinases have attracted more attention these days for developing anticancer agents due to their favorable safety profile and compatibility with

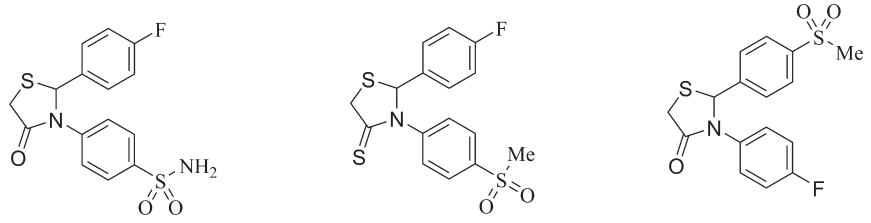

FIG. 8.29 Vicinal diaryl thiazolidin-4-ones (**160–162**) as selective COX-2 inhibitors.

other chemotherapeutic agents or radiation therapy. Several tyrosine kinase inhibitors such as gefitinib (Iressa), imatinib (Gleevec), erlotinib (Tarceva), and sorafenib (BAY 43-9006) have been successfully approved or are in clinical trials. Thus tyrosine kinase is considered as an important target for antitumor agents which interfere with specific cell signaling pathway that permits target specific therapy. There are several reports on the anticancer activity of vicinal diaryl thiazolidinones as discussed below.

Kamel et al. synthesized thiazolidin-4-ones and evaluated them for their cytotoxic activity. Compound (**163**) (Fig. 8.30) exhibited noteworthy cytotoxic effect against cervix cancer cell line HELA (IC_{50} = 1.95 μM) and breast cancer cell line MCF7 (IC_{50} = 1.07 μM). It was noted that the activity was mainly attributed to 4-[(pyridin-2ylamino)sulfonyl]phenyl moiety rather than the thiazolidin-4-one ring attached to this moiety that played a subsidiary role (Kamel et al., 2010).

A number of analogs of compounds (**164** and **165**) (Fig. 8.30) were synthesized and investigated for their anticancer activity against cell lines of lung cancer (A549) and breast cancer (MB-231) (Wu et al., 2014). Initial modifications with the two aromatic rings of **164** and **165** identified compound (**166**) with good activity (IC_{50} values of 1.87 μM and 4.57 μM for A549 and MB-231, respectively). Replacement of the bromo substituent of compound (**166**) with the ester group resulted in compound (**167**; IC_{50} values of 0.29 μM and 23.07 μM for A549 and MB-231, respectively) with enhanced anticancer activity. Further modifications with arylalkyl aminocarbonyl groups in the 3rd position of the 2-aryl ring led to the discovery of compounds (**168**; IC_{50} values of 0.21 μM and 0.23 μM for A549 and MB-231, respectively, and **169**; IC_{50} values of 0.16 μM and 0.18 μM for A549 and MB-231, respectively) with dramatically improved cytotoxic effects. Compounds (**168** and **169**) exhibited good anti-migration activities (IC_{50} = 0.01–0.05 μM) in wound healing and transwell migration models. Compound

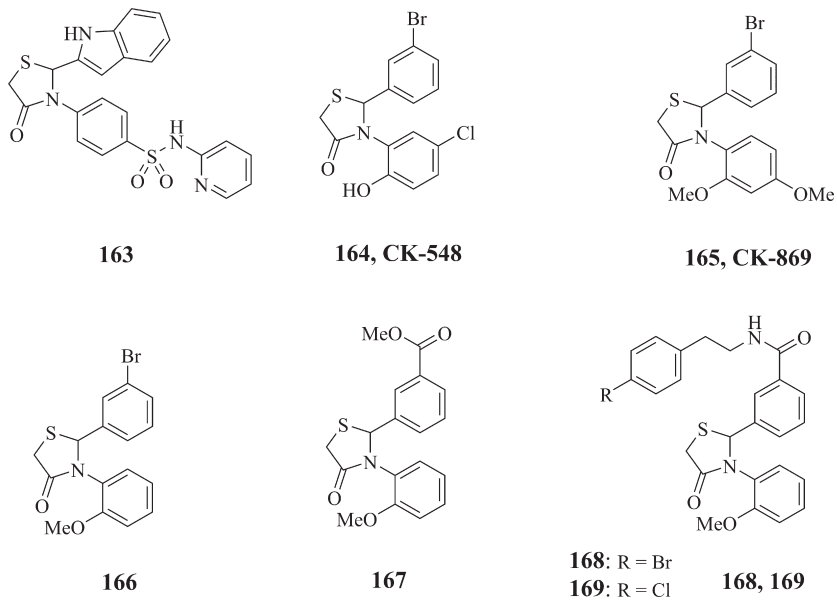

163 **164, CK-548** **165, CK-869**

166 **167** **168**: R = Br **169**: R = Cl **168, 169**

FIG. 8.30 Vicinal diaryl thiazolidin-4-one derivatives (**163–169**) as anticancer agents.

(**168**) also showed in vivo inhibition of tumor growth and metastasis in animal models (Wu et al., 2014).

8.3.2.4 Antibacterial and Antifungal Activities

A substantial growth in the cases of multidrug-resistant bacterial infections over the years has turned into a point of concern across the globe. All the positions in thiazolidin-4-one scaffold have been investigated to enhance the antibacterial and antifungal activities. It has been successfully reported that the arylazo (Labouta et al. 1987), sulfamoylphenylazo, and phenylhydrazono groups at different positions of the thiazolidinone ring improved antibacterial activity (Mandlik and Patwardham, 1966). The antibacterial activity of these compounds could be due to the effect of inhibition of Mur B enzyme which acted on the precursor of the biosynthesis of peptidoglycans (Bronson et al., 2003). The C-2 and *N*-3 substituted thiazolidinones have mostly been reported to possess broad range of inhibition against bacteria and fungi. The SAR analysis indicated that thiazolidinone derivatives were more active against Gram-negative bacteria than Gram-positive bacteria (Jain et al., 2012).

The effect of various substituents on C-2 and *N*-3 positions of 1,3-thiazolidin-4-one was studied by Sayyed e*t al*. All the synthesized 2,3-diaryl-1,3-thiazolidin-4-one derivatives containing 2,6-dichlorophenyl, 1,2,4-triazolyl, or antipyrine ring at *N*-3 and differently substituted 3-iodo-or 3-bromo-phenyl rings at C-2 showed good antimicrobial activity at a concentration of 50 μg/mL. Compound (**170**) (Fig. 8.31) exhibited zone of inhibition of 24, 25, and 27 mm against *Bacillus subtilis*, *Salmonella typhi*, and *Escherichia coli*, respectively, at this concentration (Sayyed et al., 2006).

Gopalakrishnan et al. reported the synthesis and evaluation of 2-phenyl-3-(4, 6-diarylpyrimidin-2-yl)thiazolidin-4-ones (**171**) (Fig. 8.31) for their antibacterial activity (Gopalakrishnan et al., 2009). All the synthesized compounds were screened for their antibacterial activity against *Staphylococcus aureus*, β-hemolytic *Streptococcus*, *Vibrio cholera*, *S. typhi*, *Shigella flexneri*, *E. coli*, *Klebsiella pneumonia,* and *Pseudomonas aeruginosa*. Generally, compounds having electron-donating groups showed good antibacterial activity. Compounds containing electron-donating groups (OMe and Me) at different positions of the phenyl ring linked to the pyrimidine ring demonstrated good activity against *S. aureus*, *S. typhi*, and *E. coli*. Compounds having both electron-withdrawing (Cl, F) and electron-donating (Me) groups exhibited low antibacterial activity but potent activity against *Aspergillus flavus* and *Rhizopus* (Gopalakrishnan et al., 2009).

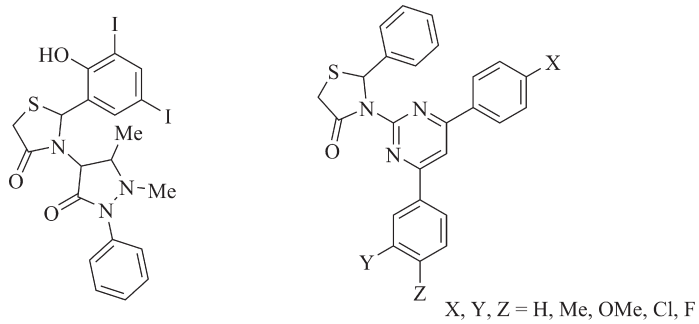

170 **171**

FIG. 8.31 Vicinal diaryl thiazolidin-4-one derivatives (**170**, **171**) as antibacterial agents.

8.4 THIADIAZOLES

Thiadiazole is a member of azole class of heterocycles containing two carbons, two nitrogens, and one sulfur atom. According to the position of the nitrogen and sulfur atoms in the ring, thiadiazoles are classified as 1,2,3-thiadiazole (**172**), 1,2,4-thiadiazole (**173**), 1,2,5-thiadiazole (**174**), and 1,3,4-thiadiazole (**175**) (Fig. 8.32) (Kushwaha et al., 2012).

Some of the drug molecules that contain thiadiazole ring are sulfamethizole (**176**), acetazolamide (**177**), cefazolin (**178**), xanomeline (**179**), timolol (**180**), and recently developed SCH-202676 (**181**) (Fig. 8.33). Thiadiazoles are used as bioisosteres of thiazole, oxazole, oxadiazole, and benzene for the development of analogs with improved biological profiles. 1,2,4-Thiadiazoles and 1,3,4-thiadiazoles have been widely used by researchers due to their diverse chemical and biological potential (Hu et al., 2014; Li et al., 2013).

Vicinal diaryl thiadiazoles have been reported to offer interesting biological profile. In the following section, some of the general methods of synthesis and biological activities of vicinal diaryl thiadiazoles are discussed.

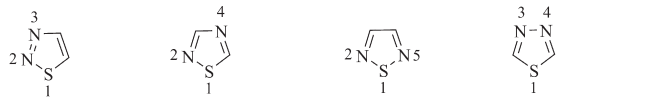

1,2,3-Thiadiazole **172** 1,2,4-Thiadiazole **173** 1,2,5-Thiadiazole **174** 1,3,4-Thiadiazole **175**

FIG. 8.32 Isomers of thiadiazole (**172–175**).

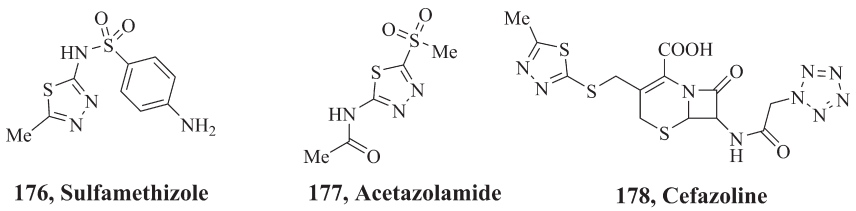

176, Sulfamethizole **177, Acetazolamide** **178, Cefazoline**

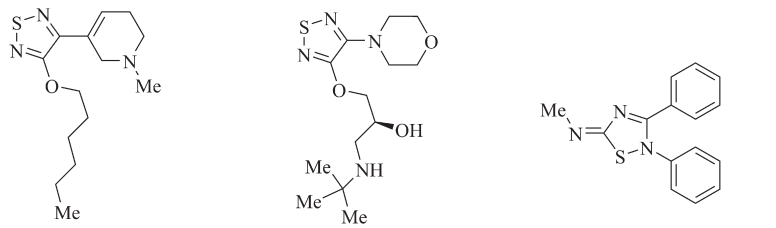

179, Xanomeline **180, Timolol** **181, SCH-202676**

FIG. 8.33 Thiadiazole ring containing drugs (**176–181**).

8.4.1 Synthesis of Vicinal Diaryl Thiadiazoles

A series of 2,3,5-substituted [1,2,4]thiadiazoles (**186**) was reported to be prepared via synthetic routes as shown in Fig. 8.34. Substituted anilines (**182**) were reacted with benzonitriles (**183**) to form *N*-arylbenzamidines (**184**) which were further reacted with substituted isothiocyanates to obtain imidoylthioureas (**185**). The intermediates (**185**) upon oxidation with bromine afforded the final compounds (**186**) (Pan et al., 2003).

Goblyos et al. also reported synthesis of 2,3,5-substituted[1,2,4]thiadiazoles (**186**) by using benzamides (**187**) as the starting material which was initially converted into benzimidoyl chlorides (**188**). Substitution of chloro by NCS followed by the addition of amine formed the thioureas (**185**) which were further oxidized by bromine to obtain the final products (**186**) as depicted in Fig. 8.34 (Göblyös et al., 2005).

8.4.2 Biological Activity of Vicinal Diaryl Thiadiazoles

Melanocortin-4 receptor (MC4) plays a vital role in the modulation of feeding behavior, nerve recovery, nociception, sexual function, energy homeostasis, stress responses, and drug addiction. To develop selective receptor agonists, Pan et al. identified 2,3-diaryl-5-anilino[1,2,4]thiadiazole derivatives (**189a–c**) (Fig. 8.35) as selective MC4 agonists by using

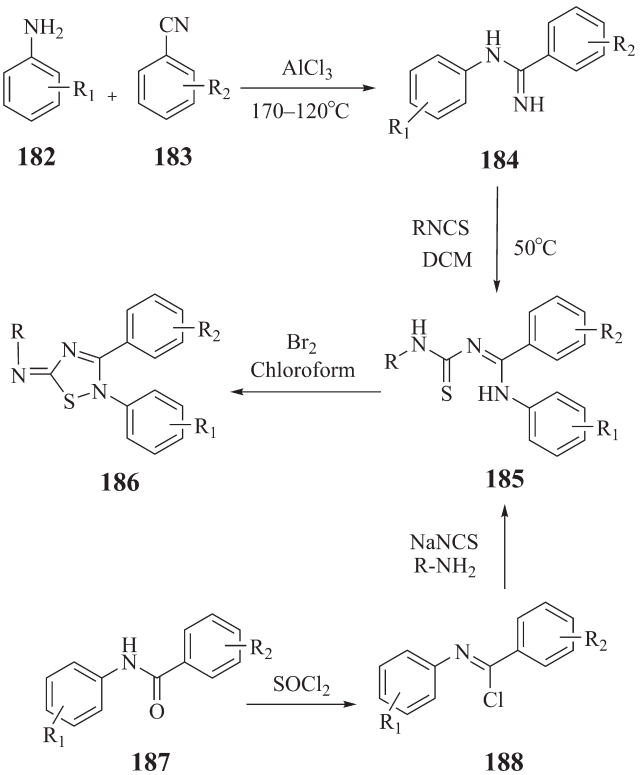

FIG. 8.34 Synthesis of vicinal diaryl 1,2,4-thiadiazoles (**186**).

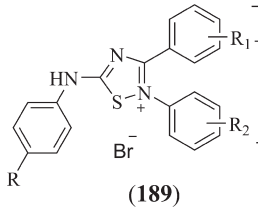

(**189**)

Comp	R =	R_1 =	R_2 =
189a	OMe	H	4-Me
189b	Me	H	2-OMe
189c	Me	2-OMe	2-OMe

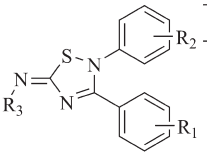

(**190–194**)

Comp	R_1 =	R_2 =	R_3 =
190	H	H	Me
191	H	3-Me	Me
192	H	4-OMe	Me
193	4-Me	4-Me	Et
194	H	H	*c*Pentyl

FIG. 8.35 Structures of some vicinal diaryl 1,2,4-thiadiazoles (**189–194**).

high throughput screening (Pan et al., 2003). Further modifications were carried out on the three aryl rings of **189a** (IC_{50} value of 174 nM) resulted in some active compounds (**189b**, **c**) with improved binding affinity (IC_{50} value of 22 nM and 4.4 nM, respectively). When administered intraperitoneally, compounds **(189a–c)** caused significant reduction in food intake in a fasting-instigated feeding model in rats. When fed orally, **189a–c** lost activity, mainly because of quick conversion to the inactive imidoylthiourea reduction products (Pan et al., 2003).

SCH-202676 (**190**) (Fig. 8.35) has been reported as an effective modulator of G-protein coupled receptors (GPCRs) such as muscarinic, dopaminergic, adrenergic, and opioid. Nieuwendijk et al. synthesized analogs (**190–194**) and tested them for their modulatory properties on adenosine receptors (van den Nieuwendijk et al., 2004). Compounds (**190–192**; methyl substituted and **193**; ethyl substituted) (Fig. 8.35) have been reported to have good modulatory activity on A_1 receptor. Further biological studies demonstrated that compounds (**190–193**) were allosteric inhibitors. Compound (**192**) has been found to be the most active with an EC_{50} value of 0.64 μM which is four times more potent than SCH-201676 (**190**; EC_{50} value of 2.8 μM). Compounds (**190** and **191**) displayed peculiar displacement characteristics of both radiolabeled agonists and antagonists binding to the A_{2A} receptors, and compound (**190**) showed some activity on A_3 receptors (van den Nieuwendijk et al., 2004).

Goblyos et al. thought to carry out variations at *N*-imino substituent of compound (**190**) to develop a novel series of 2,3,5-substituted [1,2,4]thiadiazoles (Göblyös et al., 2005). All the compounds containing alkyl groups on imine nitrogen showed significant inhibition of binding of [^{3}H]CCPA (2-chloro-N^6-cyclopentyladenosine) to human A_1 adenosine receptors. Introduction of phenyl and benzyl substituents resulted in slightly decreased inhibition of binding of [^{3}H]CCPA. Most of the compounds were also reported to increase [^{3}H]DPCPX (1,3-dipropyl-8-cyclopentylxanthine) antagonist binding. Further investigation of **190** and **194** by bioanalytical procedures demonstrated unusual receptor binding due to conversion of **190** and **194** into the corresponding thioureas. It is also stated that thiadiazoles are sulfhydryl modifying operators instead of allosteric modulators, as they reversibly alter the sulfhydryl groups of cysteine residues in cell membrane preparations (Göblyös et al., 2005).

8.5 CONCLUSION

This chapter emphasized the general synthetic methods, design, and biological profiles of vicinal diaryl substituted thiazoles, thiazolines, thiazolidinones, and thiadiazoles. It has been

revealed that these vicinal diaryl-substituted heterocycles provide the structural framework for the development of new therapeutic agents having diversified pharmacological potential. Vicinal diaryl thiazoles and thiazolidinones have been more widely explored compared to thiazolines and thiadiazole. Most of the thiazole derivatives showed anticancer and COX-2 inhibitory activities. A few of them (**36** and **37**) showed more significant COX-2 inhibitory activity than celecoxib. Thiazole has also been used as a pharmacophoric moiety in the development of various therapeutic agents for the treatment of hyperlipidemia and Alzheimer disease. Thiazolidin-4-one scaffold, having vacant C-2 and *N*-3 positions, has been exploited more by various research groups for different biological activities such as antiviral (anti-HIV), antiproliferative, anti-inflammatory, analgesic, antibacterial, and antifungal. Biological potential of vicinal diaryl-substituted thiazolines and thiadiazoles has not been still fully utilized which creates an opportunity for medicinal chemists to develop novel drug molecules for newer targets.

References

Azgomi, N., Mokhtary, M., 2015. Nano-Fe_3O_4@SiO_2 supported ionic liquid as an efficient catalyst for the synthesis of 1,3-thiazolidin-4-ones under solvent-free conditions. J. Mol. Catal. A Chem. 398, 58–64.

Bach, T., Heuser, S., 2000. Synthesis of 2-(o-hydroxyaryl)-4-arylthiazoles by regioselective Pd(0)-catalyzed cross-coupling. Tetrahedron Lett. 41, 1707–1710.

Barmade, M., Murumkar, P., Sharma, M., Yadav, M., 2016. Medicinal chemistry perspective of fused isoxazole derivatives. Curr. Top. Med. Chem. 16, 2863–2883.

Barreca, M.L., Carotti, A., Carrieri, A., Chimirri, A., Monforte, A.M., Pellegrini Calace, M., Rao, A., 1999. Comparative molecular field analysis (CoMFA) and docking studies of non-nucleoside HIV-1 RT inhibitors (NNIs). Bioorg. Med. Chem. 7, 2283–2292.

Barreca, M.L., Chimirri, A., De Luca, L., Monforte, A.M., Monforte, P., Rao, A., Zappalà, M., Balzarini, J., De Clercq, E., Pannecouque, C., Witvrouw, M., 2001. Discovery of 2,3-diaryl-1,3-thiazolidin-4-ones as potent anti-HIV-1 agents. Bioorg. Med. Chem. Lett. 11, 1793–1796.

Barreca, M.L., Balzarini, J., Chimirri, A., Clercq, E.D., Luca, L.D., Höltje, H.D., Höltje, M., Monforte, A.M., Monforte, P., Pannecouque, C., Rao, A., Zappalà, M., 2002. Design, synthesis, structure−activity relationships, and molecular modeling studies of 2,3-diaryl-1,3-thiazolidin-4-ones as potent anti-HIV agents. J. Med. Chem. 45, 5410–5413.

Bell, T.A., Brown, J.M., Graham, M.J., Lemonidis, K.M., Crooke, R.M., Rudel, L.L., 2006. Liver-specific inhibition of acyl-coenzyme A: cholesterol acyltransferase 2 with antisense oligonucleotides limits atherosclerosis development in apolipoprotein B100–only low-density lipoprotein receptor−/− mice. Arterioscler. Thromb. Vasc. Biol. 26, 1814–1820.

Bolognese, A., Correale, G., Manfra, M., Lavecchia, A., Novellino, E., Barone, V., 2004. Thiazolidin-4-one formation: mechanistic and synthetic aspects of the reaction of imines and mercaptoacetic acid under microwave and conventional heating. Org. Biomol. Chem. 2, 2809–2813.

Bronson, J.J., Denbleyker, K.L., Falk, P.J., Mate, R.A., Ho, H.T., Pucci, M.J., Snyder, L.B., 2003. Discovery of the first antibacterial small molecule inhibitors of MurB. Bioorg. Med. Chem. Lett. 13, 873–875.

Carter, J.S., Rogier, D.J., Graneto, M.J., Seibert, K., Koboldt, C.M., Zhang, Y., Talley, J.J., 1999. Design and synthesis of sulfonyl-substituted 4,5-diarylthiazoles as selective cyclooxygenase-2 inhibitors. Bioorg. Med. Chem. Lett. 9, 1167–1170.

Cavalli, A., Bolognesi, M.L., Minarini, A., Rosini, M., Tumiatti, V., Recanatini, M., Melchiorre, C., 2008. Multi-target-directed ligands to combat neurodegenerative diseases. J. Med. Chem. 51, 347–372.

Chowdhury, R., Godoy, L.C., Thiantanawat, A., Trudel, L.J., Deen, W.M., Wogan, G.N., 2012. Nitric oxide produced endogenously is responsible for hypoxia-induced HIF-1α stabilization in colon carcinoma cells. Chem. Res. Toxicol. 25, 2194–2202.

Chhabria, M.T., Patel, S., Modi, P., Brahmkshatriya, P.S., 2016. Thiazole: a review on chemistry, synthesis and therapeutic importance of its derivatives. Curr. Top. Med. Chem. 16, 2841–2862.

Dannhardt, G., Kiefer, W., 2001. Cyclooxygenase inhibitors-current status and future prospects. Eur. J. Med. Chem. 36, 109–126.
Davies, J.R., Kane, P.D., Moody, C.J., 2004. N–H insertion reactions of rhodium carbenoids. part 5: a convenient route to 1,3-azoles. Tetrahedron 60, 3967–3977.
Desai, K.G., Desai, K.R., 2006. A facile microwave enhanced synthesis of sulfur-containing 5-membered heterocycles derived from 2-mercaptobenzothiazole over $ZnCl_2$/DMF and antimicrobial activity evaluation. J. Sulfur Chem. 27, 315–328.
Devinyak, O., Zimenkovsky, B., Lesyk, R., 2012. Biologically active 4-thiazolidinones: a review of QSAR studies and QSAR modeling of antitumor activity. Curr. Top. Med. Chem. 12, 2763–2784.
Emami, S., Foroumadi, A., 2006. Synthesis of 4-(4-methylsulfonylphenyl)-3-phenyl-2(3*H*)-thiazole thione derivatives as new potential cox-2 inhibitors. Chin. J. Chem. 24, 791–794.
Frija, L.M.T., Pombeiro, A.J.L., Kopylovich, M.N., 2016. Coordination chemistry of thiazoles, isothiazoles and thiadiazoles. Coord. Chem. Rev. 308, 32–55.
Ghani, A., Hussain, E.A., Sadiq, Z., Naz, N., 2016. Advanced synthetic and pharmacological aspects of 1, 3-oxazoles and benzoxazoles. Indian J. Chem. 55B, 833–853.
Göblyös, A., De Vries, H., Brussee, J., Ijzerman, A.P., 2005. Synthesis and biological evaluation of a new series of 2,3,5-substituted [1,2,4]thiadiazoles as modulators of adenosine A_1 receptors and their molecular mechanism of action. J. Med. Chem. 48, 1145–1151.
Goedert, M., Spillantini, M.G., 2006. A century of Alzheimer's disease. Science 314, 777–781.
Gopalakrishnan, M., Thanusu, J., Kanagarajan, V., 2009. Design, synthesis, spectral analysis and in vitro microbiological evaluation of 2-phenyl-3-(4, 6-diarylpyrimidin-2-yl) thiazolidin-4-ones. J. Enzyme Inhibit. Med. Chem. 24, 1088–1094.
Gouvêa, D.P., Bareño, V.D.O., Bosenbecker, J., Drawanz, B.B., Neuenfeldt, P.D., Siqueira, G.M., Cunico, W., 2012. Ultrasonics promoted synthesis of thiazolidinones from 2-aminopyridine and 2-picolilamine. Ultrason. Sonochem. 19, 1127–1131.
Grundy, S.M., Balady, G.J., Criqui, M.H., Fletcher, G., Greenland, P., Hiratzka, L.F., Houston-Miller, N., Kris-Etherton, P., Krumholz, H.M., Larosa, J., 1997. Guide to primary prevention of cardiovascular diseases. Circulation 95, 2329–2331.
Hu, Y., Li, C.Y., Wang, X.M., Yang, Y.H., Zhu, H.L., 2014. 1,3,4-Thiadiazole: synthesis, reactions, and applications in medicinal, agricultural, and materials chemistry. Chem. Rev. 114, 5572–5610.
Jain, A.K., Vaidya, A., Ravichandran, V., Kashaw, S.K., Agrawal, R.K., 2012. Recent developments and biological activities of thiazolidinone derivatives: a review. Bioorg. Med. Chem. 20, 3378–3395.
Kamel, M.M., Ali, H.I., Anwar, M.M., Mohamed, N.A., Soliman, A.M., 2010. Synthesis, antitumor activity and molecular docking study of novel sulfonamide-Schiff's bases, thiazolidinones, benzothiazinones and their C-nucleoside derivatives. Eur. J. Med. Chem. 45, 572–580.
Kannel, W.B., Castelli, W.P., Gordon, T., Mcnamara, P.M., 1971. Serum cholesterol, lipoproteins, and the risk of coronary heart disease: the framingham study. Ann. Intern. Med. 74 (1), 12.
Kumar, A., Singh, A., Ekavali, 2015. A review on Alzheimer's disease pathophysiology and its management: an update. Pharmacol. Rep. 67, 195–203.
Kumar, V., Kaur, K., Gupta, G.K., Sharma, A.K., 2013. Pyrazole containing natural products: synthetic preview and biological significance. Eur. J. Med. Chem. 69, 735–753.
Kushwaha, N., Kushwaha, S.K., Rai, A., 2012. Biological activities of thiadiazole derivatives: a review. Int. J. ChemTech. Res. 4, 517–531.
Labouta, I.M., Salama, H.M., Eshba, N.H., Kader, O., El-Chrbini, E., 1987. Potential anti-microbial: syntheses and *in vitro* anti-microbial evaluation of some 5-arylazo-thiazolidones and related compounds. Eur. J. Med. Chem. 22 (6), 485–489.
Li, Y., Geng, J., Liu, Y., Yu, S., Zhao, G., 2013. Thiadiazole-a promising structure in medicinal chemistry. ChemMedChem 8, 27–41.
Lingampalle, D., Jawale, D., Waghmare, R., Mane, R., 2010. Ionic liquid–mediated, one-pot synthesis for 4-thiazolidinones. Synth. Commun. 40, 2397–2401.
Lingaraju, G.S., Swaroop, T.R., Vinayaka, A.C., Sharath Kumar, K.S., Sadashiva, M.P., Rangappa, K.S., 2012. An easy access to 4,5-disubstituted thiazoles via base-induced click reaction of active methylene isocyanides with methyl dithiocarboxylates. Synthesis 44, 1373–1379.
Liu, Z.Y., Wang, Y.M., Li, Z.R., Jiang, J.D., Boykin, D.W., 2009. Synthesis and anticancer activity of novel 3, 4-diarylthiazol-2(3*H*)-ones (imines). Bioorg. Med. Chem. Lett. 19, 5661–5664.

Luo, J., Zhong, Z., Ji, H., Chen, J., Zhao, J., Zhang, F., 2016. A facile and effective procedure for the synthesis of 4-thiazolidinone derivatives using $Y(OTf)_3$ as catalyst. J. Sulfur Chem. 37, 438–449.

Mahajan, M., Vasudeva, S., Ralhan, N., 1972. Synthesis of 2-iminothiazolines. Indian J. Chem. 10, 318.

Mandlik, J., Patwardham, V., Nargund, K.S., 1966. Synthesis of 2-substituted thiazolidinones and their antibacterial activity. J. Univ. Poona. Sci. Technol. 32, 39.

Mesulam, M.M., Guillozet, A., Shaw, P., Levey, A., Duysen, E.G., Lockridge, O., 2002. Acetylcholinesterase knockouts establish central cholinergic pathways and can use butyrylcholinesterase to hydrolyze acetylcholine. Neuroscience 110, 627–639.

Murugesan, V., Tiwari, V.S., Saxena, R., Tripathi, R., Paranjape, R., Kulkarni, S., Makwana, N., Suryawanshi, R., Katti, S.B., 2011. Lead optimization at C-2 and *N*-3 positions of thiazolidin-4-ones as HIV-1 non-nucleoside reverse transcriptase inhibitors. Bioorg. Med. Chem. 19, 6919–6926.

Norum, K.R., Lilljeqvist, A.-C., Helgerud, P.E.R., Normann, E.R., Mo, A., Selbekk, B., 1979. Esterification of cholesterol in human small intestine: the importance of acyl-CoA: cholesterol acyltransferase. Eur. J. Clin. Investig. 9, 55–62.

Ohsumi, K., Hatanaka, T., Fujita, K., Nakagawa, R., Fukuda, Y., Nihei, Y., Suga, Y., Morinaga, Y., Akiyama, Y., Tsuji, T., 1998. Synthesis and antitumor activity of *cis*-restricted combretastatins: 5-membered heterocyclic analogues. Bioorg. Med. Chem. Lett. 8, 3153–3158.

Ostrovskii, V., Trifonov, R., Popova, E., 2012. Medicinal chemistry of tetrazoles. Russ. Chem. Bull. 61, 768–780.

Pal, P., Gandhi, H., Giridhar, R., Yadav, M.R., 2013. ACAT inhibitors: the search for novel cholesterol lowering agents. Mini. Rev. Med. Chem. 13 (8), 1195–1219.

Pal, P., Gandhi, H.P., Kanhed, A.M., Patel, N.R., Mankadia, N.N., Baldha, S.N., Barmade, M.A., Murumkar, P.R., Yadav, M.R., 2017. Vicinal diaryl azole-based urea derivatives as potential cholesterol lowering agents acting through inhibition of SOAT enzymes. Eur. J. Med. Chem. 130, 107–123.

Pan, K., Scott, M.K., Lee, D.H., Fitzpatrick, L.J., Crooke, J.J., Rivero, R.A., Rosenthal, D.I., Vaidya, A.H., Zhao, B., Reitz, A.B., 2003. 2,3-Diaryl-5-anilino[1,2,4]thiadiazoles as melanocortin MC4 receptor agonists and their effects on feeding behavior in rats. Bioorg. Med. Chem. 11, 185–192.

Pettit, G.R., Temple Jr., C., Narayanan, V.L., Varma, R., Simpson, M.J., Boyd, M.R., Rener, G.A., Bansal, N., 1995. Antineoplastic agents 322. synthesis of combretastatin A-4 prodrugs. Anticancer Drug Des. 10, 299–309.

Pinto, F.C., Menezes, G.B., Moura, S.A., Cassali, G.D., Teixeira, M.M., Cara, D.C., 2009. Induction of apoptosis in tumor cells as a mechanism of tumor growth reduction in allergic mice. Pathol. Res. Pract. 205, 559–567.

Pratap, U.R., Jawale, D.V., Bhosle, M.R., Mane, R.A., 2011. *Saccharomyces Cerevisiae* catalyzed one-pot three component synthesis of 2,3-diaryl-4-thiazolidinones. Tetrahedron Lett. 52, 1689–1691.

Rao, A., Carbone, A., Chimirri, A., De Clercq, E., Monforte, A.M., Monforte, P., Pannecouque, C., Zappalà, M., 2002. Synthesis and anti-HIV activity of 2,3-diaryl-1,3-thiazolidin-4-(thi)one derivatives. Il Farmaco 57, 747–751.

Rao, A., Carbone, A., Chimirri, A., De Clercq, E., Monforte, A.M., Monforte, P., Pannecouque, C., Zappalà, M., 2003. Synthesis and anti-HIV activity of 2,3-diaryl-1,3-thiazolidin-4-ones. Il Farmaco 58, 115–120.

Rao, A., Balzarini, J., Carbone, A., Chimirri, A., De Clercq, E., Monforte, A.M., Monforte, P., Pannecouque, C., Zappalà, M., 2004. 2-(2,6-Dihalophenyl)-3-(pyrimidin-2-yl)-1,3-thiazolidin-4-ones as non-nucleoside HIV-1 reverse transcriptase inhibitors. Antivir. Res. 63, 79–84.

Rawal, R.K., Prabhakar, Y.S., Katti, S.B., De Clercq, E., 2005. 2-(Aryl)-3-furan-2-ylmethyl-thiazolidin-4-ones as selective HIV-RT Inhibitors. Bioorg. Med. Chem. 13, 6771–6776.

Rawal, R.K., Tripathi, R., Katti, S.B., Pannecouque, C., De Clercq, E., 2007a. Design, synthesis, and evaluation of 2-aryl-3-heteroaryl-1,3-thiazolidin-4-ones as anti-HIV agents. Bioorg. Med. Chem. 15, 1725–1731.

Rawal, R.K., Tripathi, R., Katti, S.B., Pannecouque, C., De Clercq, E., 2007b. Synthesis and evaluation of 2-(2,6-dihalophenyl)-3-pyrimidinyl-1,3-thiazolidin-4-one analogues as anti-HIV-1 agents. Bioorg. Med. Chem. 15, 3134–3142.

Rawal, R.K., Katti, S.B., Kaushik-Basu, N., Arora, P., Pan, Z., 2008a. Non-Nucleoside inhibitors of the hepatitis C virus NS5B RNA-dependant RNA polymerase: 2-aryl-3-heteroaryl-1,3-thiazolidin-4-one derivatives. Bioorg. Med. Chem. Lett. 18, 6110–6114.

Rawal, R.K., Tripathi, R., Katti, S.B., Pannecouque, C., De Clercq, E., 2008b. Design and synthesis of 2-(2,6-dibromophenyl)-3-heteroaryl-1,3-thiazolidin-4-ones as anti-HIV agents. Eur. J. Med. Chem. 43, 2800–2806.

Romagnoli, R., Baraldi, P.G., Salvador, M.K., Camacho, M.E., Preti, D., Tabrizi, M.A., Bassetto, M., Brancale, A., Hamel, E., Bortolozzi, R., Basso, G., Viola, G., 2012. Synthesis and biological evaluation of 2-substituted-4-(3′,4′,5′-trimethoxyphenyl)-5-aryl thiazoles as anticancer agents. Bioorg. Med. Chem. 20, 7083–7094.

Rouf, A., Tanyeli, C., 2015. Bioactive thiazole and benzothiazole derivatives. Eur. J. Med. Chem. 97, 911–927.
Salehi, M., Amini, M., Ostad, S.N., Riazi, G.H., Assadieskandar, A., Shafiei, B., Shafiee, A., 2013. Synthesis, cytotoxic evaluation and molecular docking study of 2-alkylthio-4-(2,3,4-trimethoxyphenyl)-5-aryl-thiazoles as tubulin polymerization inhibitors. Bioorg. Med. Chem. 21, 7648–7654.
Sayyed, M., Mokle, S., Bokhare, M., Mankar, A., Surwase, S., Bhusare, S., Vibhute, Y., 2006. Synthesis of some new 2, 3-diaryl-1, 3-thiazolidin-4-ones as antibacterial agents. ARKIVOC (2)187–192.
Scholz, M., Ulbrich, H.K., Soehnlein, O., Lindbom, L., Mattern, A., Dannhardt, G., 2009. Diaryl-dithiolanes and -isothiazoles: COX-1/COX-2 and 5-LOX-inhibitory, OH scavenging and anti-adhesive activities. Bioorg. Med. Chem. 17, 558–568.
Shanti, M.D., Shanti, K., Meshram, J., 2013. Activated fly ash catalyzing the synthesis of novel potent 4-thiazolidinones of 4-amino antipyrine anils using CEM discover microwave methodology and their virtual screening. Phosphorus Sulfur Silicon Relat. Elem. 188, 1351–1360.
Sharath Kumar, K.S., Swaroop, T.R., Harsha, K.B., Narasimhamurthy, K.H., Rangappa, K.S., 2012. T_3P®-DMSO mediated one pot cascade protocol for the synthesis of 4-thiazolidinones from alcohols. Tetrahedron Lett. 53, 5619–5623.
Shidore, M., Machhi, J., Shingala, K., Murumkar, P., Sharma, M.K., Agrawal, N., Tripathi, A., Parikh, Z., Pillai, P., Yadav, M.R., 2016. Benzylpiperidine-linked diarylthiazoles as potential anti-Alzheimer's agents: synthesis and biological evaluation. J. Med. Chem. 59, 5823–5846.
Siddiqui, N., Arshad, M.F., Ahsan, W., Alam, M.S., 2009. Thiazoles: a valuable insight into the recent advances and biological activities. Int. J. Pharm. Sci. Drug Res. 1, 136–143.
Sinha, A., Tamboli, R.S., Seth, B., Kanhed, A.M., Tiwari, S.K., Agarwal, S., Nair, S., Giridhar, R., Chaturvedi, R.K., Yadav, M.R., 2015. Neuroprotective role of novel triazine derivatives by activating Wnt/Beta catenin signaling pathway in rodent models of alzheimer's disease. Mol. Neurobiol. 52, 638–652.
Sondhi, S.M., Singh, N., Lahoti, A.M., Bajaj, K., Kumar, A., Lozach, O., Meijer, L., 2005a. Synthesis of acridinyl-thiazolino derivatives and their evaluation for anti-inflammatory, analgesic and kinase inhibition activities. Bioorg. Med. Chem. 13, 4291–4299.
Sondhi, S.M., Singh, N., Rajvanshi, S., Johar, M., Shukla, R., Raghubir, R., Dastidar, S.G., 2005b. Synthesis, hydrolysis over silica column, anticancer, anti-inflammatory and analgesic activity evaluation of some pyridine and pyrazine derivatives. Indian J. Chem. 44B, 387–399.
Sondhi, S.M., Rani, R., Gupta, P., Agrawal, S., Saxena, A., 2009a. Synthesis, anticancer, and anti-inflammatory activity evaluation of methanesulfonamide and amidine derivatives of 3, 4-diaryl-2-imino-4-thiazolines. Mol. Divers. 13, 357–366.
Sondhi, S.M., Singh, J., Kumar, A., Jamal, H., Gupta, P., 2009b. Synthesis of amidine and amide derivatives and their evaluation for anti-inflammatory and analgesic activities. Eur. J. Med. Chem. 44, 1010–1015.
Srivastava, T., Haq, W., Katti, S.B., 2002. Carbodiimide mediated synthesis of 4-thiazolidinones by one-pot three-component condensation. Tetrahedron 58, 7619–7624.
Sriram, D., Yogeeswari, P., Kumar, T.A., 2005. Microwave-assisted synthesis, and anti-HIV activity of 2,3-dairyl-1, 3-thiazolidin-4-ones. Indian J. Pharm. Sci. 67, 496.
Subhedar, D.D., Shaikh, M.H., Arkile, M.A., Yeware, A., Sarkar, D., Shingate, B.B., 2016. Facile synthesis of 1, 3-thiazolidin-4-ones as antitubercular agents. Bioorg. Med. Chem. Lett. 26, 1704–1708.
Subramanian, L., Crabb, J.W., Cox, J., Durussel, I., Walker, T.M., Van Ginkel, P.R., Bhattacharya, S., Dellaria, J.M., Palczewski, K., Polans, A.S., 2004. Ca^{2+} binding to EF hands 1 and 3 is essential for the interaction of apoptosis-linked gene-2 with Alix/Aip1 in ocular melanoma. Biochemistry 43, 11175–11186.
Tanaka, A., Sakai, H., Motoyama, Y., Ishikawa, T., Takasugi, H., 1994. Antiplatelet agents based on cyclooxygenase inhibition without ulcerogenesis. evaluation and synthesis of 4,5-bis(4-methoxyphenyl)-2-substituted-thiazoles. J. Med. Chem. 37, 1189–1199.
Tang, X., Zhu, Z., Qi, C., Wu, W., Jiang, H., 2016. Copper-catalyzed coupling of oxime acetates with isothiocyanates: a strategy for 2-aminothiazoles. Org. Lett. 18, 180–183.
Thakare, M.P., Kumar, P., Kumar, N., andey, S.K., 2014. Silica gel promoted environment-friendly synthesis of 2,3-disubstituted 4-thiazolidinones. Tetrahedron Lett. 55, 2463–2466.
Tripathi, A.C., Gupta, S.J., Fatima, G.N., Sonar, P.K., Verma, A., Saraf, S.K., 2014. 4-Thiazolidinones: the advances continue. Eur. J. Med. Chem. 72, 52–77.
Turchi, I.J., Dewar, M.J., 1975. Chemistry of oxazoles. Chem. Rev. 75, 389–437.
Van Den Nieuwendijk, A.M., Pietra, D., Heitman, L., Goblyos, A., Ap, I.J., 2004. Synthesis and biological evaluation of 2,3,5-substituted [1,2,4]thiadiazoles as allosteric modulators of adenosine receptors. J. Med. Chem. 47, 663–672.

Vazzana, I., Terranova, E., Mattioli, F., Sparatore, F., 2004. Aromatic Schiff bases and 2, 3-disubstituted-1, 3-thiazolidin-4-one derivatives as antiinflammatory agents. ARKIVOC 2004 (5), 364–374.
Verma, A., Saraf, S.K., 2008. 4-Thiazolidinone—a biologically active scaffold. Eur. J. Med. Chem. 43, 897–905.
Weinmann, M., Marini, P., Jendrossek, V., Betsch, A., Goecke, B., Budach, W., Belka, C., 2004. Influence of hypoxia on TRAIL-induced apoptosis in tumor cells. Int. J. Radiat. Oncol. Biol. Phys. 58, 386–396.
Wu, J., Yu, L., Yang, F., Li, J., Wang, P., Zhou, W., Qin, L., Li, Y., Luo, J., Yi, Z., Liu, M., Chen, Y., 2014. Optimization of 2-(3-(arylalkyl amino carbonyl)phenyl)-3-(2-methoxyphenyl)-4-thiazolidinone derivatives as potent antitumor growth and metastasis agents. Eur. J. Med. Chem. 80, 340–351.
Yadav, A.K., Kumar, M., Yadav, T., Jain, R., 2009. An ionic liquid mediated one-pot synthesis of substituted thiazolidinones and benzimidazoles. Tetrahedron Lett. 50, 5031–5034.
Zarghi, A., Najafnia, L., Daraee, B., Dadrass, O.G., Hedayati, M., 2007. Synthesis of 2,3-diaryl-1,3-thiazolidine-4-one derivatives as selective cyclooxygenase (COX-2) inhibitors. Bioorg. Med. Chem. Lett. 17, 5634–5637.
Zhang, C.Z., Chen, G.G., Lai, P.B., 2010. Transcription factor ZBP-89 in cancer growth and apoptosis. Biochim. Biophys. Acta 1806, 36–41.

Further Reading

Pal, P., Gandhi, H.P., Giridhar, R., Yadav, M.R., 2013. ACAT inhibitors: the search for novel cholesterol lowering agents. Mini-Rev. Med. Chem. 13, 1195–1219.